Naval Facilities Engineering Systems Command Hawaii

Groundwater Model Report
Red Hill Bulk Fuel Storage Facility
JBPHH, O‘ahu, Hawai‘i

Volume 1: Main Report, Appendixes A–C

September 24, 2024;
Revised September 26, 2024

Distribution Statement F: Further distribution only as directed by NAVFAC Hawaii, July 26, 2024, or higher DoD authority.
Draft / Deliberative Process Not Subject to FOIA.

2024-09-26: Figures 5-8 through 5-17 and Section 5.4.2 Predictive Simulation Results were revised to correct a geographic projection issue.

Naval Facilities Engineering Systems Command Hawaii

Groundwater Model Report
Red Hill Bulk Fuel Storage Facility
JBPHH, O‘ahu, Hawai‘i

Volume 1: Main Report, Appendixes A–C

September 24, 2024;
Revised September 26, 2024

Prepared for NAVFAC Hawaii by
AECOM Technical Services Inc
1001 Bishop Street Suite 1600
Honolulu HI 96813-3698

N62742-17-D-1800
CTO N6274218F0106

Executive Summary

The modeling study documented in this report is intended to be responsive to the Regulatory Agency (RA) concerns outlined in their March 2022 Groundwater Flow Model (GWFM) Report disapproval letter. In addition, this study should improve the understanding of the direction and rate of groundwater flow within the aquifers around the Facility in support of long-term site management and support risk evaluation based on Contaminant Fate and Transport (CF&T) models. Key components of the model that have been added or updated include regional water budget calculations to inform model boundary conditions; revisions to model grids and layers; use of temperature and chloride data to evaluate source water contributions to (b) (b)(3) ((b)) and Hālawa Shaft; revisions to the model calibration approach that focuses on matching water levels and gradients; and implementation of lava flow structure-imitating heterogeneous basalt. The models also provide a framework where concepts can continue to be tested as new information becomes available.

The GWFM and CF&T models documented in this report used the MODFLOW-USG Transport (Panday 2022; Panday et al. 2013) code to simulate groundwater flow and contaminant transport, as well as mod-PATH3DU (SSPA 2022) for particle tracking. Model calibration at various stages was conducted using the PEST software (Doherty 2015). A novel approach for generating structure imitating heterogeneity of basalt was developed using the lava flow simulator MrLavaLoba (Vitturi and Tarquini 2018) and the sequential indicator simulation software SISIM (Deutsch and Journel 1997). Additionally, a spreadsheet-based vadose zone model (VZM) was developed, consisting of calculations to estimate light nonaqueous-phase liquid (LNAPL) distribution and chemical partitioning following a release. The modeling was conducted in several stages, including regional groundwater flow model development and calibration, incorporation of basalt heterogeneity into a refined area of the regional model, simulation of a historical release to calibrate transport parameters, predictive particle tracking, predictive CF&T simulations, and a sensitivity analysis. Fifty realizations of basalt heterogeneity were generated and carried through each step of the modeling process.

The model was calibrated by minimizing the difference between simulated results and observed results for the following parameters: groundwater heads, drawdowns, gradients down Red Hill ridge, horizontal head differences, vertical head differences, observed flow distribution along (b) , conceptual water budget estimates, and chloride concentrations and temperature of water from (b) and Hālawa Shaft. Transport parameters including effective porosity and dispersivity were calibrated through simulation of the May 2021 release.

After model calibration was complete, forward particle tracking from the water table beneath the tank farm was conducted to estimate groundwater flow patterns under multiple pumping configurations. Results generally showed particles migrating to (b) with upwards of 90% capture when pumping at either (or (b million gallons per day (mgd), which was largely independent of conditions at other pumping wells. With (b) off, particles generally discharge to the Kalauao Springs, Pearl Harbor, or out of the northwest boundary of the model, with few particles migrating to other water supply wells including Hālawa Shaft. It is important to recognize that the "particle tracking" represents potential *groundwater* flow and does not necessarily suggest transport of petroleum hydrocarbons to particular receptors, which is affected by many more natural factors in addition to groundwater flow.

Predictive transport simulations were conducted using two source scenarios: the current concentrations near RHM(b) , which represents the most persistent location of dissolved fuel constituents, and the maximum historical concentrations near both RHM(b) and RHM(b) . In these simulations, source concentrations were kept constant with no degradation and run until steady state conditions were reached. Similarly, natural decay processes that are known to operate on petroleum hydrocarbons during transport were not modeled (but may be considered in future modeling efforts). The second scenario in particular is not representative of actual or anticipated site conditions, but these hypothetical source terms may help inform decision-making. Simulation results were compared both to the total petroleum hydrocarbon – diesel range organics (TPH-d) Groundwater Screening Criterion (GWSC) of 400 micrograms per liter (µg/L) from the Consolidated Groundwater Sampling Program (DOH 2024) and to 100 µg/L, which is a round number close to the lower limits of most laboratory reporting levels and the current Environmental Action Level. Most of the modeling realizations showed some simulated GWSC exceedances at monitoring wells near the source zones, including RHM(b) , RHM(b) , and RHM(b) , but the exceedance frequency at (b) across all realizations was less than 12%. An exception is the scenario with maximum historical concentrations and (b) pumping at (b mgd, where 35% of realizations resulted in GWSC exceedances at (b) .

Table of Contents

Volume 1 (Main Report, Appendixes A–C):

Executive Summary ii
Table of Contents iv
Acronyms and Abbreviations xii
1.0 Introduction 1-1
1.1 2021 Releases 1-2
1.2 Regulatory Response to the 2020 Groundwater Flow Model Report 1-3
1.3 Best Available GWFM Results 1-4
1.4 (b)(3)(b)(3) Flow Optimization Study 1-5
1.5 Study Objectives 1-5
2.0 Regional Homogeneous Groundwater Flow Model 2-1
2.1 Numerical Groundwater Flow Model 2-1
2.1.1 Approach 2-1
2.1.2 Geological Conceptual Site Model Update 2-2
2.1.3 Hydrogeological Conceptual Model Update 2-2
2.2 Numerical Model Development 2-13
2.2.1 Numerical Code Selection 2-13
2.2.2 Model Grid 2-13
2.2.3 Boundary Conditions 2-14
2.3 Regional GWFM Calibration 2-16
2.3.1 Approach 2-16
2.3.2 Steady State Model Calibration 2-19
2.3.3 Transient Calibration Model Setup 2-19
2.3.4 Model Parameterization for Regional GWFM 2-25
2.3.5 Evaluation of Model Calibration 2-32
2.3.6 Evaluation of Source Water with Chloride and Temperature Data 2-50
2.4 Particle Tracking Simulations 2-55
2.5 Sensitivity Analysis 2-56
2.5.1 Scenario 1 – K_x fixed at 4,500 ft/d 2-60
2.5.2 Scenario 2 – Horizontal Anisotropy Fixed at 3:1 2-60
2.5.3 Scenario 3 – Vertical Anisotropy Fixed at 200:1 2-61
2.5.4 Scenario 4 – No Dike Region Flux 2-61
2.5.5 Scenario 5 – Northwest Flow Direction Scenario 2-62
2.5.6 Scenario 6 – 2-Degree Dip of Basalt 2-62
2.5.7 Scenario 7 – 7-Degree Dip of Basalt 2-63
2.5.8 Scenario 8 – Horizontally Isotropic Model 2-63
2.5.9 Sensitivity Analysis Summary 2-64
3.0 Heterogeneous Basalt Models 3-1
3.1 Generation of Basalt Realizations 3-1
3.1.1 Introduction 3-1

3.1.2 Site Data Statistical Analysis 3-2
3.1.3 Monte Carlo Lava Flow Model Simulation 3-3
3.1.4 Monte Carlo Simulation of Clinker Presence 3-3
3.1.5 Clinker Data Interpretation 3-4
3.1.6 Digital Elevation Model Generation 3-9
3.1.7 Lava Flow Parameter Calibration 3-11
3.1.8 Lava Flow Simulation 3-11
3.1.9 Horizontal Variogram Calculation 3-12
3.1.10 Clinker Heterogeneity Simulation 3-13
3.2 Hydraulic Properties 3-14
3.3 Comparison of Model Calibration 3-19
3.4 Particle Tracking Results 3-23
4.0 Vadose Zone Model 4-1
4.1 Introduction and Summary 4-1
4.2 Model Conceptualization and Key Assumptions 4-3
4.3 Model Input 4-5
4.3.1 Main Tab 4-5
4.3.2 Release Info Tab 4-6
4.3.3 Location Info Tab 4-6
4.3.4 Hydrogeologic Info Tab 4-6
4.3.5 Fuel Info Tab 4-6
4.3.6 Partitioning Tab 4-6
4.3.7 Chem Props Tab 4-7
4.4 Model Calculations 4-7
4.4.1 LNAPL Retained in the Vadose Zone 4-9
4.4.2 LNAPL Lens Size on the Water Table 4-10
4.4.3 Partitioning of LNAPL Constituents into Groundwater 4-10
4.5 Results 4-12
4.6 Model Limitations 4-13
5.0 Contaminant Fate and Transport Model 5-1
5.1 Introduction 5-1
5.2 Forensic Analysis of TPH Data 5-2
5.2.1 Special Purpose Meetings on CF&T Modeling and Interpretation of TPH Data for Use in Model Calibration 5-2
5.2.2 General Considerations for CF&T Constituents at Red Hill 5-2
5.2.3 Characteristics of TPH and TPH Analysis 5-4
5.2.4 Forensic Analysis of TPH-d in Tank Farm Wells RHM(b) , RHM(b) , and RHM(b) 5-6
5.2.5 Forensic Analysis of TPH-d in Perimeter Wells 5-11
5.3 History Matching 5-11
5.3.1 Approach 5-11
5.3.2 Results 5-13
5.4 Predictive Simulations 5-20

5.4.1 Approach 5-20
5.4.2 Results 5-21
5.4.3 Evaluation of Hālawa Shaft 5-36
5.5 Travel Times to (b)(3)(b)(3) 5-37
5.6 Sensitivity Analysis 5-39
6.0 Summary and Conclusions 6-1
7.0 Model Limitations 7-1
8.0 Path Forward 8-1
9.0 References 9-1

APPENDIXES

A Navy Groundwater Modeling Meetings and Calls with Regulators and SMEs Since Submittal of March 2020 GWFM Report
B Summary of Regulator 2022 GWFM Comments and Approach
C Responses to Regulator Comments and from Correspondence from Regulators

Volume 2 (Appendixes D–H):

D Documentation of Regional Model Calibration
E Documentation of Sensitivity Analysis Model Calibration
F Basalt Lithologic Data
G Documentation of Calibration for Realizations
H History Matching Time Series Plots

FIGURES (compiled after Section 9.0 References)

1-1 Groundwater Flow Model Domain and Study Area
2-1 Anisotropy Evaluation - Drawdown with Pumping at 4.3 mgd after 18 Days
2-2 Cross Section B-B' (View Looking East)
2-3 Water Budget Watersheds Analysis Area
2-4 Water Budget Watersheds Including Model Domain Budget
2-5 Spatial Distribution of Recharge
2-6 Caprock Flux Estimation
2-7 Water Budge for Watersheds in the Model Domain HUC12 Watersheds
2-8 Water Budget for Average Conditions – Model Domain
2-9 Model Grid and Domain
2-10 Freshwater/Saltwater Interface (Model Bottom)
2-11 Cross Section of Model Grid
2-12 Model Boundary Conditions
2-13 Model Hydrogeological Unit Parameterization
2-14 Model Hydrogeological Unit Parameterization Cross Sections
2-15 Average Residuals for Basal Aquifer Wells
2-16 Recharge Zones for Unit Source Simulations
2-17 Simulation of Upconing from the Saltwater Interface

2-18 Forward Particle Tracking from Tank Farm – (b)(3)(b)(3) Pumping at (mgd, Hālawa Shaft Pumping at 12 mgd, (b)(3)(b)(3)(b)(3) Pumping at (b) mgd
2-19 Forward Particle Tracking from Tank Farm – (b)(3)(b)(3) Pumping at (mgd, Hālawa Shaft Off, N(b)(3)(b)(3)(b)(3) (b)
2-20 Forward Particle Tracking from Tank Farm – (b)(3)(b)(3) Pumping(b) Hālawa Shaft Pumping Off, N(b)(3)(b)(3)(b)(3) Pumping (b)
2-21 Forward Particle Tracking from Tank Farm – (b)(3)(b)(3) Pumping (b), Hālawa Shaft Pumping at 12 mgd, (b)(3)(b)(3)(b)(3) Pumping (b)
2-22 Forward Particle Tracking from Tank Farm – (b)(3)(b)(3) Pumping at (b mgd, Hālawa Shaft Pumping Off,(b)(3)(b)(3)(b)(3) Pumping (b)
2-23 Sensitivity Analysis Particle Tracking – (b)(3)(b)(3) Pumping at(b mgd, Hālawa Shaft Pumping at 12 mgd, (b)(3)(b)(3)(b)(3) Pumping at (b) mgd
2-24 Sensitivity Analysis Particle Tracking – (b)(3)(b)(3) Pumping at(mgd, Hālawa Shaft Off,(b)(3)(b)(3)(b)(3)(b)(3)
2-25 Sensitivity Analysis Particle Tracking – (b)(3)(b)(3) Pumping (b) Hālawa Shaft Pumping Off, (b)(3)(b)(3)(b)(3) Pumping (b)
2-26 Sensitivity Analysis Particle Tracking – (b)(3)(b)(3) Pumping (b) Hālawa Shaft Pumping at 12 mgd, (b)(3)(b)(3)(b)(3) Pumping (b)
2-27 Sensitivity Analysis Particle Tracking – (b)(3)(b)(3) Pumping at (b mgd, Hālawa Shaft Pumping Off, (b)(3)(b)(3)(b)(3) Pumping(b)
3-1 Available Geology Data for Use in Developing Basalt Realizations
3-2 Box Model Example – Realization 10
3-3 Compartmentalization Groups
3-4 (b)(3)(b)(3) Flow Distribution
3-5 Regional Model with Example Realization
3-6 Particle Tracking Results Example – Realization 10 (b)(3)(b)(3) Pumping at (mgd, Hālawa Shaft Pumping at 12 mgd,(b)(3)(b)(3)(b)(3) Pumping at(b) mgd
3-7 Particle Tracking Results Example – Realization 10 (b)(3)(b)(3) Pumping a(b) mgd, (b)(3)(b)(3) , (b)(3)(b)(3)(b)(3) (b)
3-8 Particle Tracking Results Example – Realization 10 (b)(3)(b)(3) Pumping (b), Hālawa Shaft Pumping Off, (b)(3)(b)(3)(b)(3)(b)(3)(b)(3)
3-9 Particle Tracking Results Example – Realization 10 (b)(3)(b)(3) Pumping(b) Hālawa Shaft Pumping at 12 mgd, (b)(3)(b)(3)(b)(3) Pumping (b)
3-10 Particle Tracking Results Example – Realization 10 (b)(3)(b)(3) Pumping at (b mgd, Hālawa Shaft Pumping Off, (b)(3)(b)(3)(b)(3) Pumping (b)
3-11 Particle Tracking Results for All Realizations – (b)(3)(b)(3) Pumping at (mgd, Hālawa Shaft Pumping at 12 mgd,(b)(3)(b)(3)(b)(3) Pumping at(b) mgd
3-12 Particle Tracking Results for All Realizations – (b)(3)(b)(3) Pumping at(b mgd, Hālawa Shaft Off, (b)(3)(b)(3)(b)(3) Pumping at (b) mgd
3-13 Particle Tracking Results for All Realizations – (b)(3)(b)(3) Pumping (b), Hālawa Shaft Pumping Off, (b)(3)(b)(3)(b)(3) Pumping (b)
3-14 Particle Tracking Results for All Realizations – (b)(3)(b)(3) Pumping (b), Hālawa Shaft Pumping at 12 mgd,(b)(3)(b)(3)(b)(3) Pumping(b)

3-15 Particle Tracking Results for All Realization – (b)(3)(b)(3) Pumping at (b mgd, Hālawa Shaft Pumping Off, (b)(3)(b)(3)(b)(3) Pumping (b)
4-1 Main Tab of the Heuristic Model
4-2 Release Info Tab of the Heuristic Model
4-3 Location Info Tab of the Heuristic Model
4-4 Hydrogeologic Info Tab of the Heuristic Model
4-5 Fuel Info Tab of the Heuristic Model
4-6 Partitioning Tab of the Heuristic Model
4-7 VZM Partitioning Module Output Compared to the AGU Model of Mayer and Hassanizadeh (2005)
4-8 VZM Conceptual Model
5-1 Sampling Locations with TPH-d Exceedances
5-2 May 2021 Release Conceptual Model – One Source
5-3 May 2021 Release Conceptual Model – Two Sources
5-4 May 2021 Release Results for Example Realization – One Source
5-5 May 2021 Release Results for Example Realization – Two Sources
5-6 Predictive Simulation Results – Scenario 1 (example realization)
5-7 Predictive Simulation Results – Scenario 2 (example realization)
5-8 Predictive Simulation Results – Scenario 1 – Average Simulated TPH-d Concentrations Across All Calibrated Realizations – (b)(3)(b)(3) Pumping at 4 mgd, Hālawa Shaft Pumping at 12 mgd, Navy(b)(3)(b)(3)(b)(3) Pumping at(b) mgd
5-9 Predictive Simulation Results – Scenario 1 – Average Simulated TPH-d Concentrations Across All Calibrated Realizations – (b)(3)(b)(3) Pumping at (mgd, Hālawa Shaft Off, (b)(3)(b)(3)(b)(3) (b)
5-10 Predictive Simulation Results – Scenario 1 – Average Simulated TPH-d Concentrations Across All Calibrated Realizations – (b)(3)(b)(3) Pumping (b) Hālawa Shaft Pumping Off, (b)(3)(b)(3)(b)(3) Pumping (b)
5-11 Predictive Simulation Results – Scenario 1 – Average Simulated TPH-d Concentrations Across All Calibrated Realizations – (b)(3)(b)(3) Pumping (b) (b)(3)(b)(3) Pumping at(b) mgd(b)(3)(b)(3)(b)(3) Pumping (b)
5-12 Predictive Simulation Results – Scenario 1 – Average Simulated TPH-d Concentrations Across All Calibrated Realizations – (b)(3)(b)(3) Pumping at (b mgd, Hālawa Shaft Pumping Off, (b)(3)(b)(3)(b)(3) Pumping (b)
5-13 Predictive Simulation Results – Scenario 2 – Average Simulated TPH-d Concentrations Across All Calibrated Realizations – (b)(3)(b)(3) Pumping at(mgd, (b)(3)(b)(3) Pumping at (b mgd, (b)(3)(b)(3)(b)(3) Pumping at (b) mgd
5-14 Predictive Simulation Results – Scenario 2 – Average Simulated TPH-d Concentrations Across All Calibrated Realizations – (b)(3)(b)(3) Pumping at (mgd, Hālawa Shaft Off, (b)(3)(b)(3)(b)(3)(b)(3)
5-15 Predictive Simulation Results – Scenario 2 – Average Simulated TPH-d Concentrations Across All Calibrated Realizations – (b)(3)(b)(3) Pumping (b) Hālawa Shaft Pumping Off,(b)(3)(b)(3)(b)(3) t Pumping (b)

5-16 Predictive Simulation Results – Scenario 2 – Average Simulated TPH-d Concentrations Across All Calibrated Realizations – (b)(3)(b)(3) Pumping (b) Hālawa Shaft Pumping at 12 mgd, (b)(3)(b)(3)(b)(3) Pumping (b)
5-17 Predictive Simulation Results – Scenario 2 – Average Simulated TPH-d Concentrations Across All Calibrated Realizations – (b)(3)(b)(3) Pumping at (b mgd, Hālawa Shaft Pumping Off, (b)(3)(b)(3)(b)(3) Pumping (b)
5-18 Homogeneous vs Heterogeneous Particle Tracking Results

CHARTS

2-1 Percentage of Weathered Basalt Under Stream Valleys and Ridges 2-7
2-2 Calculation of Weathered Basalt Hydraulic Conductivity Beneath Stream Valleys (top) and Beneath Caprock (bottom) 2-31
2-3 Residual Statistic Charts 2-36
2-4 Simulated and Observed Water Levels During the Flow Optimization Study at RH(b) (top), and RH(b) (bottom) Showing a Lack of Full Recovery Between Pump Cycles 2-38
2-5 Simulated and Observed Water Levels During the Flow Optimization Study at RHP(b) (top) and RHMW(b)(9) (bottom) Showing an Example of a Well with Full Recovery Between Pump Cycles 2-38
2-6 Simulated and Observed Heads for 2017/2018 Data 2-40
2-7 Simulated and Observed Heads for 2021/2022 Data 2-41
2-8 Simulated and Observed Heads for FOS 2-42
2-9 Simulated and Observed Heads for All Time Periods 2-43
2-10 Examples of Hydraulic Gradients Along Red Hill Ridge 2-44
2-11 Hydraulic Gradients Northwest of Red Hill Ridge 2-45
3-1 Clinker Heterogeneity Simulation Flow Chart (report section number in parenthesis) 3-2
3-2 Occurrence of Clinker Map (left) and Horizontal Cross Section of Clinker (green) / Non-Clinker (blue) Distribution Around (b)(3)(b)(3) (right) 3-6
3-3 Probability Density Functions of A‘ā (left) and Pāhoehoe (right) Flow Thicknesses (log scale base 10, ft) 3-7
3-4 Histograms of Top (left) and Bottom (right) Clinker Fraction of Total A‘ā Flow Thickness 3-7
3-5 Semi-variograms of Clinker Occurrence in Vertical Direction, from Boring Log Data (left) 3-8
3-6 Semi-variograms of Clinker Occurrence in Horizontal Directions. General dip direction (left), strike direction (right) from barrel log (top) and boring log data (bottom) 3-8
3-7 Topography in Red Hill GWFM Area 3-9
3-8 Topography Area Used for Variogram Calculation (left) and Approximate Extent of Topography Area on Map (right) 3-9
3-9 Semi-variogram of Topography Elevation Deviation from Longitudinal Base Plane in Dip Direction (left) and Transverse Strike Direction (right). Lag distance is shown on the x-axis with the variogram value shown on the y-axis. 3-10
3-10 Example of Simulated DEM Realization 3-10
3-11 CDFs of MrLavaLoba Flow Thicknesses for A‘ā (left) and Pāhoehoe Flows (right) 3-11
3-12 Examples of Simulated A‘ā (left) and Pāhoehoe Flows (right) 3-12

3-13 Average Semi-variogram (solid line) in Dip Direction (left) and Strike Direction (right). The dashed lines indicate the standard deviation from the average based on the 40 MrLavaLoba simulations. 3-13
3-14 Example Realization of Clinker Occurrence. 1 is clinker and 0 is massive basalt. 3-14
3-15 Histogram of Clinker Percentage 3-15
3-16 Histogram of Hydraulic Conductivity Values 3-16
3-17 Histogram of Horizontal Anisotropy Values 3-17
3-18 Histogram of Vertical Anisotropy Values 3-18
3-19 Histogram of Specific Yield Values 3-19
5-1 TPH Ranges Corresponding to Petroleum Fuel Types and Effective Carbon Numbers 5-6
5-2 Comparison of Raw and Normalized TPH-d in Groundwater from Wells RHM(b) , RHM(b) , and RHM(b) 5-7
5-3 Normalized TPH-d Groundwater Concentrations in RHM(b) , RHM(b) , and RHM(b) Smoothed by Calculating an 11-Point Moving Average 5-8
5-4 TPH-d Concentrations at RHM(b) , RHM(b) and RHM(b) Following May 2021 Release with 11-Point Moving Average Used for PEST Simulations as Target Data 5-9
5-5 Histogram of Median Travel Times to (b) for Calibrated Realizations 5-39

TABLES

2-1 Summary of Anisotropy Evaluation 2-5
2-2 Caprock Discharge Estimates by HUC12 Watershed 2-10
2-3 Average Water Budget for HUC12 Watersheds 2-12
2-4 Water Budget Calculations for Average Conditions Within GWFM Domain 2-12
2-5 Well Group Designations 2-17
2-6 Summary of Model Calibration Target Data 2-18
2-7 GWFM Stress Period Setup 2-20
2-8 Individual Water Supply Well Pumping Rates by Stress Period 2-22
2-9 Conceptual Water Budget for GWFM Domain by Stress Period 2-23
2-10 Model Parameterization 2-26
2-11 Preferred Values for Parameter Regularization 2-32
2-12 Summary of GWFM Calibration Statistics 2-34
2-13 Summary of Simulated and Observed Vertical Head Differences 2-46
2-14 Comparison of Conceptual and Simulated Water Budgets 2-48
2-15 Simulated (b) Source Water Contribution 2-53
2-16 Simulated Hālawa Shaft Source Water Contribution 2-53
2-17 Comparison of Observed and Simulated Chloride Concentration and Temperature 2-53
2-18 Summary of Sensitivity Analysis Results – Statistics 2-58
2-19 Summary of Sensitivity Analysis Results – Particle Tracks 2-59
3-1 Boring Log Data Summary 3-5
3-2 Transitional Probabilities of Eruptions by Lava Flow Type 3-7
3-3 Comparison of Realizations 3-21
3-4 Summary of Particle Destinations for (b) Pumping at (b) mgd, Hālawa Shaft Pumping at 12 mgd, (b)(3) Pumping at (b) mgd 3-24

3-5 Summary of Particle Destinations for (b) Pumping at (mgd, Hālawa Shaft Off, (b)(3) Off 3-26
3-6 Summary of Particle Destinations for (b) (b) Hālawa Shaft Off, (b)(3) Pumping (b) 3-28
3-7 Summary of Particle Destinations for (b) (b), Hālawa Shaft Pumping at 12 mgd, (b)(3) Pumping (b) 3-30
3-8 Summary of Particle Destinations for (b) Pumping at (b mgd, Hālawa Shaft Off, (b)(3) (b) 3-32
4-1 Simulated Release Scenarios and Heuristic Model Results 4-2
4-2 Definitions of Variables Used in VZM Calculations 4-8
5-1 Detection Frequency of Analytes Associated with Petroleum Fuels in Groundwater 5-3
5-2 Detection of Analytes Associated with Petroleum Fuels in Groundwater by Location 5-4
5-3 History Matching Model Stress Period Setup 5-12
5-4 PEST Input Parameters for History Matching 5-13
5-5 History Matching Results for One-Source Conceptual Model 5-15
5-6 History Matching Results for Two-Source Conceptual Model 5-17
5-7 Realizations Below Calibration Threshold 5-19
5-8 Average Calibrated Model Parameter Values 5-20
5-9 Simulated TPH-d Concentrations at Monitoring Wells and Water Supply Wells in Scenario 1 5-23
5-10 Simulated TPH-d Concentrations at Monitoring Wells and Water Supply Wells in Scenario 2 5-30
5-11 Calculated TPH-d Concentrations at Hālawa Shaft Pumping at 8 mgd, by Percentage of Tank Farm Groundwater Captured by Hālawa Shaft 5-37
5-12 Summary of Particle Track Travel Times 5-38
5-13 Sensitivity Analysis Results 5-41

Acronyms and Abbreviations

σ	standard deviation
%	percent
°C	degree Celsius
µg/L	micrograms per liter
AGU	American Geophysical Union
AOC	Administrative Order on Consent
BAM	best available model
bgs	below ground surface
BWS	Board of Water Supply, City and County of Honolulu
CA	cellular automata
CDF	cumulative density function
CF&T	contaminant fate and transport
CFD	computational fluid dynamics
CLEAN	Comprehensive Long-Term Environmental Action Navy
CLN	connected linear network
CSM	conceptual site model
CUDEM	Continuously Updated Digital Elevation Model
CUI	Controlled Unclassified Information
DDF	Density Dependent Flow
DEM	digital elevation model
Det %	percent detected
DLA	Defense Logistics Agency
DLNR	Department of Land and Natural Resources, State of Hawai‘i
DOH	Department of Health, State of Hawai‘i
DRO	diesel range organics
EPA	Environmental Protection Agency, United States
EVS	Earth Volumetric Studio
FOS	Flow Optimization Study
ft	foot/feet
ft/d	feet per day
ft/ft	feet per foot
ft^2	square feet
ft^3	cubic feet
ft^3/d	cubic feet per day
GHB	general head boundary
GRO	gasoline range organics
GUI	graphical user interface
GWFM	groundwater flow model
GWSC	Groundwater Screening Criterion
HDMW	Hālawa Deep Monitor Well
HUC	Hydrologic Unit Code

HVO	Hawaii Volcano Observatory
ID	identifier
JBPHH	Joint Base Pearl Harbor-Hickam
(b	(b)(3)
Kh	horizontal hydraulic conductivity
km	kilometer
K_v	vertical hydraulic conductivity
K_x	hydraulic conductivity in the down-dip direction
K_y	hydraulic conductivity in the cross-dip direction
K_z	hydraulic conductivity in the vertical direction
LiDaR	light detection and ranging
LNAPL	light nonaqueous-phase liquid
m	meter
mg/L	milligrams per liter
mgd	million gallons per day
MPG	Multiple Point Geostatistics
msl	mean sea level
MW	monitoring well
(b)(3)	(b)(3)(b)(3)(b)(3)(b)(3)
NSZD	natural source-zone depletion
OWDF	Oily Waste Disposal Facility
PCB	Prescribed Concentration Boundary
RA	Regulatory Agency
(b)	(b)(3)(b)(3)
RMSE	root mean squared error
SGSIM	Sequential Gaussian Simulation
SIS	Sequential Indicator Simulation
SISIM	sequential indicator simulation software
SME	subject matter expert
SOW	Statement of Work
SPM	Special Purpose Meeting
SR	stochastic routing
TPH	total petroleum hydrocarbons
TPH-d	total petroleum hydrocarbons – diesel range organics
TPH-g	total petroleum hydrocarbons – gasoline range organics
TPH-o	total petroleum hydrocarbons – residual oil range organics
TRRP	Texas Risk Reduction Program
U.S.	United States
USGS	United States Geological Survey
VZM	vadose zone model
WS	water supply well

1.0 Introduction

This report presents the new groundwater models developed for the Red Hill Bulk Fuel Storage Facility (the Facility) to fulfill the requirements of the 2015 Red Hill Administrative Order on Consent (AOC) (EPA Region 9 and DOH 2015). The new models include a saturated-zone groundwater flow model (GWFM), limited vadose zone model (VZM), and contaminant fate and transport (CF&T) model. The foundation of these new groundwater models is the Navy's best available models (BAMs) (DON 2023d; 2023e; 2023b) and the new geological conceptual site model (CSM) addendum developed in 2023 (DON 2023a). The BAMs were previously used to support hypothetical release scenarios that could have occurred, but did not, during the Facility tank defueling effort, which was completed in February 2024.

These new models were constructed using completely new grids and conceptual models, and supersede both the 2019 Red Hill (CSM) (DON 2019) and the 2020 GWFM (DON 2020). The new models are based on comments and suggestions that the Regulatory Agencies (RAs; U.S. Environmental Protection Agency [EPA] Region 9 and Hawai'i State Department of Health [DOH]) and their subject matter experts (SMEs) made after reviewing the 2020 GWFM (Appendix B), and during subsequent special purpose meetings, as well as new data that has been gathered over the past several years. The models presented in this report will be used to evaluate potential risks during long-term management of the Facility now that fuel is no longer stored in the tank system.

This document is provided as part of the Comprehensive Long-Term Environmental Action Navy (CLEAN) V Program under contract number N62742-17-D-1800, contract task order N6274222F0106. The Facility is located along Red Hill ridge between South Hālawa Valley to the northwest and Moanalua Valley to the southeast on the island of O'ahu, Hawai'i. The study area is shown on Figure 1-1.[1] The Facility includes 20 steel-lined concrete underground tanks that used to store petroleum fuel located in the unsaturated (vadose) zone above the basal water table. These tanks were defueled between September 2023 and March 2024.The tanks formerly stored various fuels (e.g., jet fuel, diesel) as described in the Red Hill CSM report (DON 2019). Previous investigations have identified petroleum hydrocarbons in the rock beneath the tanks and in the underlying aquifer. Groundwater levels in the aquifer are approximately 100 feet (ft) below the bottom of the tanks, and supplies drinking water to the Navy, other military branches, and the community via Navy water supply wells (b)(9) ((b)(3)(b)(3) [(b)]), (b)(9) ((b)(3)), City and County of Honolulu Board of Water Supply (BWS) municipal water supply wells, 3-2354-001 Hālawa Shaft, Moanalua Wells (3-2153-002, 3-2153-010, 3-2153-011, 3-2153-012), and other wells.

On January 23, 2014, the Navy reported a fuel release of an estimated 27,000 gallons of Jet Fuel Propellant (b)(3) from (b)(3) of the Facility's underground fuel storage tanks to DOH. The release occurred in December 2013 when placing the tank back in service following a 3-year tank inspection and refurbishment process.

[1] Report figures are compiled after Section 9.0.

The Administrative Order of Consent (AOC) in the Matter of the Red Hill Bulk Fuel Storage Facility (EPA Region 9 and DOH 2015) was issued in September 2015 following the (b)(3) release. The AOC requires the United States (U.S.) Department of the Navy and Defense Logistics Agency (DLA) to take actions, subject to EPA and DOH approval, to address potential future fuel releases from the former fuel storage system and to implement infrastructure improvements to protect human health and the environment.

Sections 6 and 7 of the AOC Statement of Work (SOW) require environmental investigations to characterize the subsurface pursuant to addressing current and future environmental risk concerns. Several completed and ongoing environmental investigations have been and continue to be conducted to fulfill the requirements of Sections 6 and 7 of the AOC SOW:

- AOC SOW Section 7.1 requires developing a GWFM report that will "refine the existing groundwater flow model and improve the understanding of the direction and rate of groundwater flow within the aquifers around the Facility."
- AOC SOW Section 7.2 requires developing a CF&T model report that will "utilize the Groundwater Flow Model to improve the understanding of the potential fate and transport, degradation, and transformation of contaminants that have been and could be released from the Facility."

An interim GWFM was developed (DON 2018, Appendix A) to meet the AOC requirement to address current and future environmental risks. Further investigation (including but not limited to: completing detailed geologic and geophysical logging, groundwater sampling, and transducer studies) and modeling analysis were conducted to address data gaps in the 2018 interim model. The resulting groundwater flow model was published in the 2020 GWFM Report (DON 2020), which incorporated data and concepts from the RAs and other SMEs during meetings listed in Appendix A. The goals of the 2020 GWFM Report were to evaluate capture zones of various water supply wells and serve as the flow modeling foundation for CF&T modeling (as required by AOC SOW Section 7.2.2). According to the AOC, development of the CF&T model is to occur after the GWFM is approved. On March 17, 2022, the Navy received a letter from EPA and DOH disapproving the GWFM Report, citing deficiencies identified by the RAs' SMEs, and including a suggested methodology to model site heterogeneity.

1.1 2021 Releases

In 2021, two additional releases from the Facility were documented:

- May 2021 Release: On May 6, 2021, a (b) pipeline near Red Hill (b)(3)(b)(3) was damaged during a fuel transfer procedure. (b) was released to the tunnel floor, and attempts were made to recover the fuel. It was later determined that a small amount of fuel escaped into the subsurface, and that some fuel that was not recovered was pumped from a fire suppression retention system into a fire suppression recovery drain line. The fuel remained contained in the drain line until the drain line was damaged on November 20, 2021.
- November 2021 Release: On November 20, 2021, (b) was released from the fire suppression recovery drain line, traveled along the concrete tunnel floor toward Adit 3, and collected in a groundwater sump and a sanitary sewer tank near Adit 3 (Adit 3 Sump). The fuel was transported

via automated pumping systems to exterior holding tanks and a leach tank system where some of the fuel was released to the environment. A portion of the fuel was recovered from Adit 3, the sump, and the external tanks. The remainder of the fuel entered the soil and volcanic bedrock near U.S. Department of the Navy Well 3-(b)(9) ((b)), from which some of the fuel entered the Joint Base Pearl Harbor-Hickam (JBPHH) Water Distribution System. (b) ceased pumping and was isolated from the JBPHH Water Distribution System on November 28, 2021. BWS Hālawa Shaft and (b)(3) did not have evidence of impacts but ceased pumping on December 3, 2021 as a precautionary measure, which isolated public water systems from the releases. Initial site characterization of the release areas has been completed; additional characterization, monitoring, and remediation efforts continue.

Previous groundwater flow models and groundwater protection plans developed by the Navy identified the pumping capability of (b) as an important factor to be considered if a large fuel release from the Facility were to occur. These studies indicated that the flow of adjacent groundwater, including potentially dissolved fuel and floating fuel product in the study area, could be captured by the (b) pump and increasing or decreasing the pumping rate would have a direct effect on potential containment. The degree of the containment is demarcated by a capture zone, the part of the aquifer in which groundwater flows to the (b) pump and associated water development tunnel. The size of the capture zone is expected to be directly related to the pumping rate of the (b) system.

At the time of the November 2021 Release, (b) was pumping at a rate of approximately 4.3 million gallons per day (mgd) to meet public drinking water needs. Following the November 2021 Release, (b) continued to pump at 4.3 mgd to induce drawdown in the aquifer in the vicinity of (b) water development tunnel. This pumped water is treated through a granular activated carbon treatment system, then discharged under a National Pollution Discharge Elimination System permit to South Hālawa Stream.

The GWFM is an important tool in evaluating the effect of increasing or decreasing the pumping rate at (b) . Decreasing the pumping rate too much may allow fuel-impacted water to migrate away from the Facility, and increasing the pumping too much may have a detrimental effect on the long-term sustainability of the basal aquifer, which is an important source of drinking water to the island.

In response to these releases and associated potential risks, the Secretary of Defense made the decision to defuel and close the Facility (DoD 2022), and defueling was completed in March 2024. Defueling refers to the removal of stored flowable fuel from all fuel tanks and supply lines within the Facility.

1.2 Regulatory Response to the 2020 Groundwater Flow Model Report

In March 2022, the RAs submitted their comments on the 2020 GWFM Report to the Navy in a joint letter. Their comments cited a number of technical concerns that needed to be addressed before the Navy AOC modeling requirement would be considered complete. A matrix developed from and summarizing their comments is included as Appendix B along with the RAs' March 2022 disapproval letter. RA comments were provided to the Navy in the following documentation:

- EPA and DOH letter to US Navy, Subject: Disapproval of the Groundwater Flow Model Report, dated March 17, 2022

- Attachment A: Joint Agency Deficiencies on the Groundwater Flow Model Report for the Red Hill Bulk Fuel Storage Facility, dated March 25, 2020, delivered to Navy March 17, 2022
- Attachment B: Hawaii DOH SME Deficiencies Identified, Red Hill Groundwater Flow Model Report, dated December 3, 2020, delivered to Navy March 17, 2022
- Attachment C: EPA SME Deficiencies Identified, Red Hill Groundwater Flow Model Report, dated November 10, 2021, delivered to Navy March 17, 2022
- Attachment D: DOH Review: Navy Groundwater Flow Models & Related Issues with the Navy CSM for the Red Hill Facility, dated October 19, 2021, delivered to Navy March 17, 2022

1.3 Best Available GWFM Results

To meet the Navy's internal requirements to evaluate risks that they might encounter during defueling and to assist in decision-making that would be protective of human health and the environment during associated activities, the Navy developed the Best Available GWFM, along with related vadose zone and CF&T models (BAMs). On June 30, 2023, the Navy submitted to the RAs the GWFM, VZM, and CF&T Model Technical Memoranda (DON 2023d; 2023e; 2023b) that were responsive to many of the RA concerns outlined in their March 2022 disapproval letter. Several key issues were addressed, including:

- Revision of the regional water budget calculations to inform model boundary conditions
- Revision of the model gridding and layering
- Use of temperature and chloride to inform source water contributions to (b) and Hālawa Shaft
- Revision of the model calibration approach that focuses on matching water levels and gradients

The BAMs did not address concerns related to local-scale heterogeneity of the basalt. Appendix B summarizes the main groups of RA comments and outlines how each will be addressed in the model discussed herein.

The following Special Purpose Meetings (SPMs) were held among the Navy and RAs to discuss various aspects of the BAMs that were carried through to the current modeling efforts:

- SPM #3 on September 14, 2022, *Confining Unit*
- SPM #5 on September 21, 2022, Stochastic Basalt Subtype Generation using a Geologic Fabric Exploration Tool
- SPM #6 on September 28, 2022, *MODFLOW Model Setup*
- SPM #9 on December 17, 2022, Geologic Fabric Explorer Technical Support Session Meeting 1
- SPM #10 on December 15, 2022, Geologic Modeling Framework Conceptional Site Model
- SPM #11 on January 10, 2023, *Strike and Dip*
- SPM #13 on January 13, 2023, Geologic Fabric Explorer Technical Support Session Meeting 2
- SPM #16 on February 14, 2023, *Modeling Schedule Update*

- SPM #20 on March 15, 2023, Modeling – RA SME Perspective and Questions
- SPM #21 on April 5, 2023, Approach to Vadose Zone Modeling
- SPM #25 on May 17, 2023, RA Comments on the Groundwater Flow Model
- SPM #27 on May 31, 2023, Contaminant Fate and Transport Modeling Approach
- SPM #28 on August 19, 2023, Representation of Basalt Heterogeneity

Prior to June 30, 2023 submittal of the BAMs, interim work products and model files had been submitted for RA review. RA comments on the BAMs were discussed in SPM #31 on January 31, 2024.

1.4 (b)(3)(b)(3) Flow Optimization Study

From April 7 to July 17, 2023, the (b) Flow Optimization Study (FOS) was conducted to gather data to evaluate the hydrogeological impacts of pumping (b) at different flow rates. The purpose was to use the data in increasingly complex models to optimize the flow of basal water to South Hālawa Stream while maintaining a sufficient capture zone to mitigate the migration of fuel-impacted water off site should a potential release occur during defueling operations. During the data-gathering portion of the study, groundwater levels were recorded at 10-minute intervals throughout the Red Hill monitoring well network and at some offsite wells while different pumping scenarios (trial periods) were implemented at (b). These data were used to further the understanding of geological, hydrogeological, and geochemical aspects of the Red Hill CSM. Data collected for the study were analyzed in a manner consistent with the procedure outlined in EPA documentation entitled *A Systematic Approach for Evaluation of Capture Zones at Pump and Treat Systems* (EPA 2008). Several lines of evidence were evaluated to estimate the capture zone of (b), including water level mapping with particle tracking, analytical calculations, an analytic element model, and the BAMs. The Navy submitted the FOS report (DON 2023c) to the RAs on September 19, 2023. The conclusions of the study indicated that pumping (b) at (b) and (b) mgd likely captures much of the shallow groundwater beneath the tank farm, whereas pumping at (b) mgd reduces the likelihood of capture of all groundwater beneath the tank farm.

Regulatory Agencies' Comments. The RAs issued a letter on September 29, 2023 that provided some general feedback related to both the Navy's FOS report and BAMs but indicated that additional technical comments will be provided under a separate cover at a later date. To date, the Navy has not received additional technical comments for incorporation into the models.

The RAs also issued letters on November 1 and November 15, 2023 in response to the Navy's Proposal to reduce the (b)(3)(b)(3) Pumping Rate. These letters did include some comments on the best available GWFM. Comments that had been received prior to submittal of this report are addressed herein.

1.5 Study Objectives

The objectives of the three modeling components stated in the AOC are as follows:

- GWFM: AOC SOW Section 7.1 indicates that the flow model should improve the understanding of the direction and rate of groundwater flow within the aquifers around the Facility.

- VZM: The vadose zone modeling, which is not required by the AOC, will inform source-term conditions for the CF&T model.
- CF&T Modeling: AOC SOW Section 7.2 specifies that the purpose of the Contaminant Fate and Transport Model Report is to utilize the Groundwater Flow Model to improve the understanding of the potential fate and transport, degradation, and transformation of contaminants that have been and could be released from the Facility.

Modeling work will build upon these general objectives and other specific objectives identified in the AOC. The study incorporates previous modeling studies and comments from RAs, improving previous models and incorporating heterogeneity in response to key RA comments from their GWFM Disapproval Letter. In accordance with the AOC, this study will provide information, data, and conclusions that can be used to update the existing Groundwater Protection Plan (DON 2014) to include response procedures and trigger points in the event that contamination from the Facility shows movement toward any drinking water well.

Finally, the modeling study may be used to guide and inform the number and placement of groundwater monitoring wells required to adequately identify possible contaminant migration (AOC SOW Section 7.3), installation of which is already underway prior to approval of the models.

2.0 Regional Homogeneous Groundwater Flow Model

2.1 Numerical Groundwater Flow Model

2.1.1 Approach

The objective of the numerical groundwater flow modeling task is to develop a tool to simulate groundwater flow under historical, current, and hypothetical future conditions. The model results are intended to improve the understanding of the direction and rate of groundwater flow within the aquifers around the Facility to support CF&T modeling. The GWFM is a hybrid model that simulates regional hydrogeological processes at a coarse spatial resolution and localized hydrogeological processes at a finer resolution in a nested grid surrounding the areas of interest within the larger regional model. The GWFM is calibrated to observed conditions in the study area.

In the first phase of the flow modeling task, the regional GWFM was developed both to meet the objectives of simulating observed historical conditions, including groundwater elevations, drawdowns, gradients, and estimated water budget at the scale of the full model domain and to ensure consistency with the CSM for regional groundwater flow. The extent of the model domain remains the same as that of the 2020 GWFM and is shown on Figure 1-1, while significant changes were made to the grid structure and boundary condition setup. The regional GWFM was calibrated by modifying hydrogeological parameters and boundary conditions to match the transient water levels, drawdowns, gradients, and head differences as well as to demonstrate consistency with the conceptual water budget and with measured temperature and chloride concentrations at (b) and Hālawa Shaft. The term gradient is used throughout this report referring to the direction and magnitude of head decrease over distance in the specified plane. Typically, this aligns with the direction of groundwater flow; however, in the subsurface at the site, dipping layers and three-dimensional anisotropy draw groundwater flow to some degree toward the direction of maximum hydraulic conductivity. Transient water levels used in model calibration included those collected in the 2017/2018 Synoptic Survey (USGS 2017), between the November 2021 release and the end of March 2022 (USGS 2022a; 2022b), and during the 2023 FOS (DON 2023c). The regional GWFM was calibrated with homogeneous anisotropic hydraulic parameters for the basal aquifer with the exception of decreased hydraulic conductivity beneath stream valleys and caprock where weathering of the basalt is present.

The second phase of the flow modeling task incorporated a nested grid with finer resolution within the regional GWFM to encompass prominent features of the Facility and BWS' Hālawa Shaft (Figure 1-1). The purposes of the grid refinement are to increase spatial resolution in the area where the most data are available and to provide detailed calculations at the scale of the Facility. Specifically, the grid refinement can represent site-specific geologic and hydrogeologic information at a finer scale than is possible with the regional flow model. Basalt heterogeneity was modeled within the nested grid area and is discussed further in Section 3.0.

This numerical GWFM study is generally consistent with the following ASTM International standards:

- D5447-17 Standard Guide for Application of a Numerical Groundwater Flow Model to a Site-Specific Problem (2017)

- D5609-16 Standard Guide for Defining Boundary Conditions in Groundwater Flow Modeling (2016b)
- D5981M-18 Standard Guide for Calibrating a Groundwater Flow Model Application (2018)
- D5611-94 Standard Guide for Conducting a Sensitivity Analysis for a Groundwater Flow Model Application (2016a)

2.1.2 Geological Conceptual Site Model Update

In January 2023, the Navy prepared an updated geological CSM addendum (DON 2023a) with revisions to the prior geologic framework. In that Technical Memorandum, revisions to the prior geologic framework originally presented in the 2019 CSM report (DON 2019) and the 2020 GWFM Report (DON 2020) were based on newly available data described below. These additional geologic data were incorporated into the 2024 GWFM. Revisions made to the geological CSM were based on data gathered during additional drilling activities through January 1, 2024.

2.1.3 Hydrogeological Conceptual Model Update

Additional hydrogeological data collected since the submittal of the 2019 CSM report (DON 2019) include the following:

- Synoptic groundwater elevations collected between December 2021 and February 2022 (USGS 2022a)
- Groundwater elevations collected during the restart of (b) in January 2022 through April 2022, per the (b)(3)(b)(3) Recovery and Monitoring Plan (IDWST 2022)
- Synoptic groundwater elevations collected at the Oily Waste Disposal Facility (OWDF) from August 2022 to present per the Draft Summary of Groundwater Transducer Study (DON 2022c) and the Site Assessment Work Plan (DON 2021)

Future planned data gathering events include the following:

1) Groundwater elevation data collected using pressure transducers to monitor aquifer response to revised (b) pumping in both existing and newly complete wells, which is anticipated to begin in July 2024
2) Geophysical surveying to be conducted by the University of Hawai‘i under the Navy’s Office of Naval Research program
3) In-well and tracer testing to be conducted by the Navy and the U.S. Geological Survey (USGS) per the Draft Groundwater Flow and Velocity Evaluation Work Plan (DON 2022a) in concert with the University of Hawai‘i
4) Groundwater elevations, cores, and water quality data gathered from new monitoring wells during the ongoing network expansion (DON 2022b)

2.1.3.1 EVALUATION OF ANISOTROPY

Drawdown data collected during the FOS were used to estimate the aquifer anisotropy based on the shape and orientation of the inferred drawdown cone. In an infinite and anisotropic aquifer with homogeneous hydraulic conductivities in the primary (K_x) and secondary (K_y) directions, the drawdown cone will form an ellipse with the long axis oriented along the axis of K_x with an aspect ratio equivalent to the square root of K_x divided by the square root of K_y (Freeze and Cherry 1979; Mutch, Jr. 2005).

To provide an estimate of anisotropy, an idealized ellipse was fit to the 0.3-ft drawdown contour (derived from water levels collected during the FOS) with the ellipse oriented at the dip azimuth of (b)(3) agreed to in SPM #11 on January 10, 2023. Ellipses at various other drawdowns (0.1, 0.2, 0.4 ft) were attempted at multiple orientations; however, drawdown ellipses below 0.3 ft were not as well constrained, and the 0.4 drawdown ellipse contained several wells that were not consistent with the contour value.

This methodology is intended for vertical pumping wells where the center of the ellipse is at the pumping well. Because the (b) water development tunnel is a horizontal feature approximately (b)(3) placement of the ellipse center point is subject to interpretation. The horizontal nature of (b) and its orientation mainly in the cross-dip transverse direction would lead to a widened ellipse compared to a vertical well pumping at the same rate. Two alternative alignments of the ellipse were evaluated, as shown on Figure 2-1. The top ellipse in the figure orients the ellipse on the 200 ft of clinker at the eastern end of (b) and the ellipse on the bottom of the figure shows the ellipse oriented at the midpoint along (b).

To better understand the variability associated with the deviation from initial ellipse center placement, six interpretations for each of the two ellipse orientations resulting in a different longitudinal distance (*a*) and transverse distance (*b*) from (b) to the drawdown ellipse were explored. For each of these orientations, the *a* and *b* distances were calculated both to the center point and from the orthogonal distance from the nearest point on (b) to each end of the oval. The final result are the twelve total interpretations of the longitudinal (*a*) and transverse (*b*) distances shown on Figure 2-1.

Although wells are not distributed around (b) evenly enough to depict a symmetric drawdown ellipse in all directions, the analysis does provide added confidence that anisotropy does generally occur along the assumed dip azimuth of (b)(3) with some potential local variation. The calculated anisotropy ratio values range from 5.3 to 25.8 with an average of 14.2, as shown on Table 2-1. Other factors that are not accounted for in the analysis include the effects of valley fill, dipping lava flows, and local heterogeneity. Estimates of the drawdown ellipse orientation and anisotropy ratios were carried forward for use in aquifer test analysis and as a guideline for model calibration parameters.

2.1.3.2 ANISOTROPIC HYDRAULIC CONDUCTIVITY EVALUATION

Two peer-reviewed methods of aquifer test evaluation that account for areal anisotropy of the aquifer were used in the analysis: Hantush and Thomas (1966) and Mutch Jr. (2005). Both methods rely on the assumption that an elliptical drawdown contour can be clearly delineated to make a determination of the major and minor axes as well as the aspect ratio of the ellipse. The twelve alternative interpretations of the drawdown ellipse and their corresponding anisotropy values were included in the analysis for both methods.

These calculations were carried out only for Trial Period 1 of the FOS data because it was the only period with consistent pumping.

The Hantush and Thomas method uses transmissivity (T_r) along a ray estimated through the Cooper-Jacob distance-time method and the aspect ratio of the drawdown ellipse to calculate the transmissivity in the major and minor axis directions:

$$\boldsymbol{T_e = \frac{T_r \times a \times b}{r^2}}$$

$$\boldsymbol{T_x = \frac{a}{b} T_e}$$

$$\boldsymbol{T_y = \frac{b}{a} T_e}$$

Where:

T_e = Effective transmissivity (ft^2/day), estimated from distance drawdown, equivalent to the geometric mean of the principal components

T_r = Transmissivity along a ray (ft^2/day)

r = the distance between each monitoring well and the ellipse center point

a/b = Aspect ratio of the drawdown ellipse along the major axis, equivalent to $\sqrt{K_x / K_y}$

b/a = Aspect ratio of the drawdown ellipse along the minor axis, equivalent to $\sqrt{K_y / K_x}$

T_x = Transmissivity along the major axis (ft^2/day)

T_y = Transmissivity along the minor axis (ft^2/day)

The Mutch method applies a coordinate transformation technique to the distance drawdown method, allowing for estimation of transmissivity along the major and minor axes as an equivalent isotropic aquifer. In this method, *x* and *y* distance from the pumping well are calculated with respect to the orientation of the major axis. The *y* distance is then expanded by the aspect ratio of the drawdown ellipse along the major axis (*a/b*). The Cooper-Jacob distance drawdown analysis is then applied to estimate the effective transmissivity, and the transmissivity along each axis is calculated using the same method as applied above.

Calculation results are presented in Table 2-1. The resulting hydraulic conductivity calculations are dependent upon the assumption that water is derived from the upper 150 ft of aquifer. While this assumption is difficult to verify and simplifies a complex flow system, it allows for a reasonable estimate of expected hydraulic conductivity values to be derived from model calibration.

Mutch (2005) states that when multiple interpretations of the drawdown cone are made, the most appropriate practice is to use the average of the values. The minimum and maximum values in Table 2-1 were used as bounds for model calibration, whereas the average value for hydraulic conductivity and

horizontal anisotropy were used as preferred values in parameter regularization with the PEST software, which is discussed further in Section 2.3.4.

Table 2-1: Summary of Anisotropy Evaluation

Description	Aniso-tropy Ratio	Major Axis		Minor Axis	
		Transmissivity (ft^2/d)	Hydraulic Conductivity (ft/d) if b = 150 ft	Transmissivity (ft^2/d)	Hydraulic Conductivity (ft/d) if b = 150 ft
Hantush and Thomas (1966) Method Calculations					
Centered on clinker on SE end of [redacted]	5.3	1,529,124	10,194	289,993	1,933
Centered on clinker, off SW edges of box	6.3	1,665,300	11,102	266,279	1,775
Centered on clinker, off NW edges of box	25.8	3,384,233	22,562	131,030	874
Centered on midpoint of [redacted]	8.5	1,945,437	12,970	227,936	1,520
Centered on midpoint of [redacted], off SW edges of box	19.8	2,960,158	19,734	149,801	999
Centered on midpoint of [redacted], off NW edges of box	19.4	2,933,409	19,556	151,167	1,008
Mutch Jr. (2005) Method Calculations					
Centered on clinker on SE end of [redacted]	5.3	929,264	6,195	176,231	1,175
Centered on clinker, off SW edges of box	6.3	1,012,020	6,747	161,821	1,079
Centered on clinker, off NW edges of box	25.8	2,056,632	13,711	79,628	531
Centered on midpoint of [redacted]	8.5	1,182,262	7,882	138,519	923
Centered on midpoint of [redacted], off SW edges of box	19.8	1,798,917	11,993	91,036	607
Centered on midpoint of [redacted], off NW edges of box	19.4	1,782,662	11,884	91,866	612
Summary					
Average	14.2	1,931,618	12,878	162,942	1,086
Minimum	5.3	929,264	6,195	79,628	531
Maximum	25.8	3,384,233	22,562	289,993	1,933

Notes:
ft/d feet per day
ft^2/d square feet per day

2.1.3.3 WEATHERING OF BASALT

The regional GWFM utilizes the assumption of uniform anisotropic hydraulic properties across the model domain. In reality, hydraulic properties of the aquifer vary spatially at both the micro- and macro-scales, which include a greater degree of weathering of bedrock near the ground surface and below stream valleys. These effects are expected to result in decreased weathering with depth and consequently reduced hydraulic conductivity of the basalt with increasing depth. Hunt (1996) and Oki (2005) discuss weathering of the basalt, stating that saprolite thickness and degree of weathering are functions of annual precipitation. According to these authors, where rainfall is less than 50 in/year, which is true for most of the model domain, saprolite is generally less than 100 ft thick, whereas in areas with precipitation greater than 50 in/yr, saprolite is generally 100 to 300 ft thick. Beneath stream channels where percolating water is almost always present, the thickness of saprolite and degree of basalt weathering may be significantly greater.

During coring for monitoring well NM(b) , located near the confluence of the North and South Hālawa Stream Valleys, weathering was observed to a depth of greater than 700 ft bgs, which included approximately 145 ft of valley fill above the basalt. Weathering at depths in this borehole was most prevalent within clinker sections where significant groundwater flow often occurs. Construction of NM(b) was not complete at the time of the groundwater flow modeling but was completed by the time of final report issuance. These and other data available after the modeling data-cutoff dates can be considered in future modeling efforts.

Figure 2-2 illustrates a schematic depiction of saprolite and bedrock weathering in cross section across a ridge and stream valley, showing the degree of weathering. The figure generally shows that weathering decreases with depth and occurs to greater depths below stream valleys. Chart 2-1 presents the percentage of weathered material based on boring logs in 25-ft intervals. Data from boreholes located within stream valleys are shown separately from and boreholes under ridges. Valley fill and saprolite were grouped with weathered basalt, as was basalt with any degree of weathering. Because NM(b) was not completed at the time this report was being finalized, it was not included in the chart, and no completed wells located in valleys had yet extended beyond 500 ft bgs.

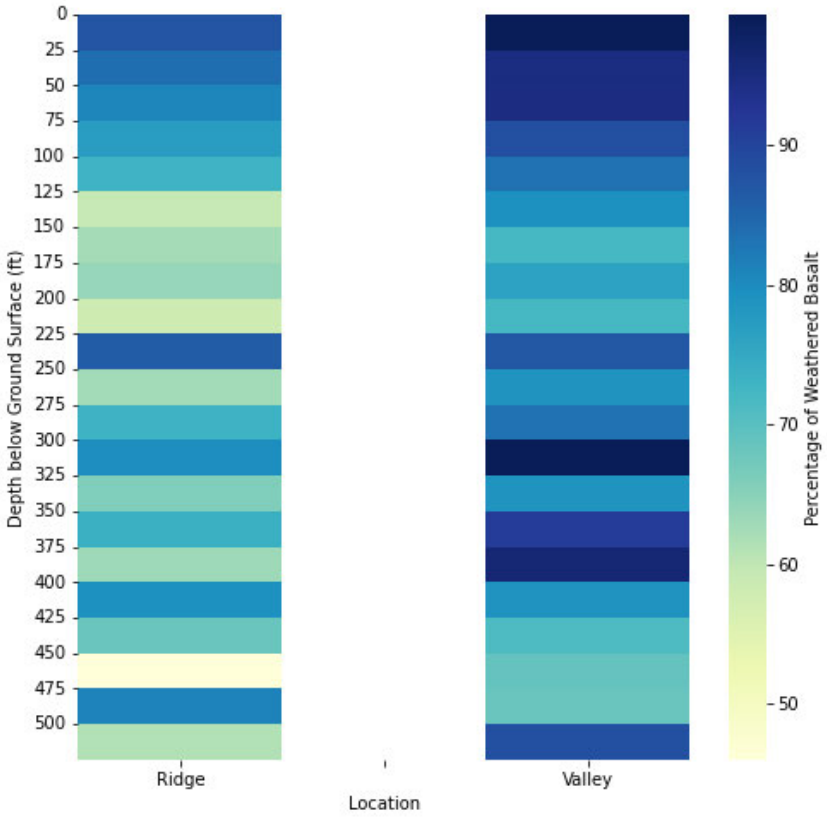

Chart 2-1: Percentage of Weathered Basalt Under Stream Valleys and Ridges

Infiltration through the saprolite and weathered basalt is impeded by the lower hydraulic conductivities, resulting in elevated groundwater levels in the areas surrounding stream valleys; consequently, downward vertical gradients occur from the valley fill and saprolite to the basalt, as well as within the basalt. This generally downward vertical gradient is apparent in water levels measured in the multilevel wells located within the stream valleys, including RHM(b) and RHM(b).

The BAM study demonstrated that through the assumption of uniform isotropic parameters, the high uniform transmissivity of the simulated aquifer led to a general lack of vertical hydraulic gradients within the basalt simulated in the model. Simulated vertical gradients were flat or upward within the basalt, but still downward from the saprolite to the basalt. To better simulate vertical gradients within these areas, the degree of basalt weathering was incorporated into the conceptual model where weathering is a function of depth from the ground surface, using an exponential relationship with depth from ground surface combined with a final extinction depth below the streams and under the caprock. No weathering was included outside of stream valleys and caprock because it is assumed that weathering does not extend to the water table. Implementation of the basalt weathering model in the numerical model is discussed further in Section 2.3.4.

2.1.3.4 CONCEPTUAL WATER BUDGET – HUC 12 WATERSHEDS

Approach

A conceptual regional water budget analysis was conducted to address RA comments regarding water budget calculations in development of GWFM boundary conditions. The analysis covered the five

watersheds surrounding Pearl Harbor as established by 12-digit Hydrologic Unit Code (HUC-12) watersheds from the National Hydrography Dataset (USGS 2022a) (Figure 2-3). The analysis area was based on conceptualized regional groundwater flow patterns (Oki 1998) and was selected assuming that recharge from precipitation is the only source of water over the entire area, with no groundwater flow occuring across its outer extents. The methodology includes summing the sources and sinks of groundwater within each HUC-12 watershed and over the entire five-watershed analysis area.[2] The GWFM domain lies within the area shown on Figure 2-3. The goal of the water budget calculations is to estimate inflows and outflows from the model domain and across the model domain boundaries.

Groundwater sinks (i.e., groundwater discharge from the analysis area) include spring flows, water supply wells, and discharge to Pearl Harbor or the Pacific Ocean. Interactions between streams and groundwater were assumed to be negligible because stream beds above the basalt aquifer are generally much higher than the water table, and downward seepage from the streams is impeded by highly weathered old alluvium and weathered basalt (Oki 1998), as well as concrete-lined channels in some areas.

Results of the initial analysis demonstrated a reasonable water budget without a significant surplus or deficit over the entire area but significant surpluses and deficits within individual HUC-12 watersheds, indicating flow across the interior HUC-12 watershed boundaries. The next step in the analysis included incorporation of the GWFM domain, which split some HUC-12 boundaries into partial watersheds and accounted for flow across watershed boundaries, shown on Figure 2-4. This step allowed for estimation of inflows and outflows across the GWFM domain boundary.

Recharge

The spatial distribution of rainfall recharge to groundwater was assigned using USGS estimated values for average conditions from 1978 to 2007 (Engott et al. 2017). Figure 2-5 shows the distribution of recharge established by the USGS. Water budget calculations were performed for average conditions. Recharge was divided into two categories: recharge to the basal aquifer and recharge to the caprock.

Spring Discharge

Spring locations in the study area are shown on Figure 2-3 and Figure 2-4. Spring discharge was estimated using linear regression equations developed by Oki (1998) to correlate water levels in Well 3-2256-010 (‘Aiea Bay Well) and spring discharges near Pearl Harbor. The average water level in Well 3-2256-010 (16.45 ft mean sea level [msl]) was used to estimate spring discharges for the water budget calculations. The average water level was estimated for the same time period as the average recharge calculations.

Water Supply Well Discharge

The Hawai‘i State Department of Land and Natural Resources (DLNR) provided average water supply well pumping rates as of 2017, which were used for water budget calculations. Updated water supply well

[2] Because the first nine digits of the HUC12 boundaries are the same (i.e., 200600000), the codes are hereafter referred to by only the last three digits.

pumping rates for time periods of water level data were also provided and used later in the GWFM water budget development, discussed further in Section 2.3.3. Figure 2-3 and Figure 2-4 show the water supply wells that were included in the calculations, with symbol scaling proportional to pumping rates, and larger symbols corresponding to higher pumping rates.

Ocean and Pearl Harbor Discharge

Discharge of groundwater through the caprock to Pearl Harbor and the Pacific Ocean was estimated based on a Darcy-flux calculation:

$$Q = KiA$$

Where:

Q = discharge rate (cubic ft per day [ft^3/d])

K = hydraulic conductivity (ft/d)

i = hydraulic gradient (ft per ft [ft/ft])

A = area (ft^2)

To estimate caprock flux, a line was drawn along the extent of the caprock across the water budget area, as shown as the pink line labeled as Caprock Extent on Figure 2-6. A point was placed every 50 ft along the line, then additional flow lines were drawn from these points to the nearest point on Pearl Harbor or the Pacific Ocean. Along each flow line, the Darcy flux calculation was performed, then the discharge rate for each segment was summed within each watershed. The caprock was assigned a value of 0.2 ft/d. Literature values for effective hydraulic conductivity of the caprock generally range from 0.02 ft/d (Oki 1998) to 0.15 ft/d (Souza and Voss 1987). The resulting fluxes presented on Table 2-2 show that the flux through the caprock is relatively small and variations in the assumption for caprock hydraulic conductivity do not substantially affect the overall water budget.

Figure 2-6 presents a visualization of the cross section through which groundwater flows to Pearl Harbor or the Pacific Ocean. The simplified cross section schematic represents the assumptions used for the Pacific Ocean and Pearl Harbor discharge calculations. Hydraulic gradient was calculated by subtracting an assumed head in the aquifer that varies by watershed from a head of 0 ft msl in Pearl Harbor or the Pacific Ocean divided by the distance between the caprock extent and the discharge point along the flow path. The area through which flow occurs was calculated as having a width of 50 ft, representing the distance between points and an assumed depth of 800 ft, which is the assumed approximate depth to the freshwater/saltwater interface. This calculation was completed for each segment and summed over all segments and for each watershed. The total groundwater discharging through caprock to surface water for each watershed is shown in Table 2-2.

Table 2-2: Caprock Discharge Estimates by HUC12 Watershed

HUC12 Watershed ID	Total Caprock Discharge (mgd)
303	0.01
304	0.01
305	0.03
401	0.01
402	0.03
403	0.00
404	0.05
Total	0.14

Uncertainty in this calculation is primarily related to simplifying assumptions of the geometry, depth to the freshwater/saltwater interface, and the hydraulic conductivity of the caprock. However, the objective of this calculation is to constrain the water budget estimates for modeling purposes, and the analysis demonstrated that discharge to surface water through caprock is small, through a reasonable range of input assumptions, relative to the spring flows and groundwater extraction. Therefore, the relative accuracy of spring and well flows is more important to the model predictions than groundwater flow through the caprock to Pearl Harbor and the Pacific Ocean. Variations in caprock discharge estimates across the range of literature values for effective hydraulic conductivity will result in only minor changes to the overall water budget.

Analysis of HUC12 Regional Water Budget

Table 2-3 tabulates the in- and out-flows for each HUC12 watershed. The calculations indicate that several watersheds have inflows that are greater than outflows (shown in Table 2-3 as a surplus with a positive value). However, when summing over all the contributing watersheds, the inflows and outflows approach balance. This is due to flow between adjacent watersheds. The largest deficit of water (indicated as a negative value in Table 2-3), HUC-12 401, appears to be driven primarily by spring outflows, totaling approximately 32 mgd. The caprock is also thinnest in this area, resulting in a higher estimated caprock discharge compared to adjacent watersheds, though it is still a relatively small portion of the water budget. Groundwater outflow to Pearl Harbor and the Pacific Ocean is limited by the relatively low hydraulic conductivity of the caprock compared to the basalt aquifer and composes only about 0.1% of the total water budget. In comparison, approximately 66% of aquifer discharge occurs through water supply wells, and the remaining approximately 34% of discharge occurs through springs. The conclusion is that groundwater flow occurs laterally from one watershed to the next converging on the springs around Pearl Harbor.

The conclusions of the water budget calculations are that 1) groundwater converges regionally into HUC12 401, where the caprock is thin and the largest spring flows occur, and 2) that spring outflows and groundwater extraction for water supply are significantly larger components of the water budget than direct groundwater discharge to the Pacific Ocean and Pearl Harbor. Representation of the water budget for average conditions is shown on Figure 2-7.

2.1.3.5 CONCEPTUAL WATER BUDGET – GWFM DOMAIN

Similar water budget calculations were performed using the GWFM domain where it intersects the watersheds analyzed for water budget. Watersheds intersecting the GWFM domain were split as shown on Figure 2-4. Sinks and sources to each watershed were recalculated based on spatial location. Similar to the water budget calculations by HUC-12 watershed, a deficit of water resulted in the partial watershed for HUC-12 401 and surpluses resulted in the surrounding watersheds, including the GWFM domain, further supporting the conclusion that that groundwater converges on the springs to the northwest of the GWFM domain. Additionally, this implies that there is a component of groundwater flow that enters from the southeast and a component that exits northwest of the GWFM domain. The water budget was then recalculated passing the surplus of water from one watershed to the next toward partial HUC-12 401. The result is a discrepancy of in- and out-flows of 5.4 mgd, or an error of 3.0%. The results of the calculation are shown in Table 2-4. Figure 2-8 shows the model domain and inflows and outflows for average conditions. These water budget calculations provide a conceptual framework for groundwater flow and a foundation for subsequent calculations of water budget during each GWFM stress period, accounting for changes in stresses over time such as variations in pumping. This topic is discussed further in Section 2.3.3. These numbers provide a foundation for constraining the water budget in the GWFM.

Table 2-3: Average Water Budget for HUC12 Watersheds

HUC12 ID	Recharge - Basal Aquifer		Total Inflow to Basal Aquifer (mgd)	Recharge - Caprock		Total Inflow to Caprock (mgd)	Spring Discharge		Well Discharge		Discharge from Basal Aquifer to Caprock		Total Outflow (mgd)
	Rate (mgd)	Percent of Total		Rate (mgd)	Percent of Total		Rate (mgd)	Percent of Total	Rate (mgd)	Percent of Total	Rate (mgd)	Percent of Total	
304	21.9	100%	21.9	0.6	97.8%	0.6	0.0	0.0%	22.9	99.9%	0.01	0.1%	23.0
305	14.7	100%	14.7	2.5	99.6%	2.5	0.0	0.0%	4.1	99.7%	0.01	0.3%	4.2
401	38.7	100%	38.7	1.1	94.2%	1.2	34.7	42.0%	48.0	58.0%	0.07	0.1%	82.8
402	49.5	100%	49.5	0.4	98.4%	0.4	16.7	49.1%	17.2	50.8%	0.01	0.0%	33.9
403	57.1	100%	57.1	1.0	97.4%	1.0	13.9	30.1%	32.4	69.9%	0.03	0.1%	46.4
Total	181.9	100%	181.9	5.6	97.8%	5.7	65.3	34.4%	124.7	65.6%	0.1	0.1%	190.2

Note: Inflows to caprock include calculated discharge to caprock from basal aquifer.

Table 2-4: Water Budget Calculations for Average Conditions Within GWFM Domain

HUC12 ID	Year/ Scenario	Recharge (mgd) - Basal Aquifer	Recharge (mgd) - Caprock	Dike Region Inflow (mgd)	Spring Discharge (mgd)	Well Discharge (mgd)	Diffuse Submarine Discharge/ Caprock Seepage (mgd)	Inflow from Adjacent Watershed - Basal Aquifer	Flow to Adjacent Watershed (mgd) - Basal Aquifer	Total Inflow (mgd) - All	Total Outflow (mgd) - All
Data Source	—	Engott et al. (2017)	Engott et al. (2017)	Engott et al. (2017)	Oki (1998)	DLNR Data, 2021	Calculated	Calculated	Calculated	Calculated	Calculated
304 (Partial)	Average	16.6	0.5	—	0.0	15.0	0.01	0.0	2.1	17.1	17.1
Model Domain	Average	30.1	2.3	26.1	13.3	38.2	0.05	2.1	9.0	60.6	60.6
401 (Partial)	Average	2.5	0.0	—	21.4	21.9	0.03	36.7	—	39.2	43.3
402	Average	49.5	0.4	—	16.7	17.2	0.01	11.7	27.7	61.2	61.2
403	Average	57.1	1.0	—	13.9	32.4	0.03	0.0	11.7	57.1	57.1
Total	Average	155.8	4.2	26.1	65.3	124.7	0.13	—	—	235.3	239.3

2.2 Numerical Model Development

2.2.1 Numerical Code Selection

Several criteria were considered in selection of the groundwater modeling software. First, the software needed to be capable of meeting project objectives and handling site-related complexities. Of particular importance was the ability of the model code to handle complex geometry with dipping and pinched discontinuous geologic layers to accommodate incision of saprolite and valley fill into dipping basalt. The modeling code needed to be robust enough to handle extreme parameter values that may be used to examine model sensitivity or extreme stresses that may be simulated to evaluate solute migration or influence zones of wells under reasonably conservative conditions. A robust simulator allows focus on hydrogeology, calibration, and understanding model behavior rather than on evaluating/correcting for convergence or dry cell issues. Furthermore, the code needed to efficiently enable multiple simulations within a reasonable time period as required for model calibration and application. Finally, the model needed to be easy to access, develop, and process. A graphical user interface (GUI) that works with the model code greatly facilitates input and output of complex spatial and temporal information.

The MODFLOW-USG groundwater modeling code (Panday 2022; Panday et al. 2013) was selected to develop the numerical groundwater flow model. MODFLOW-USG is an open-source, public-domain groundwater flow modeling code released by USGS in 2013 to accommodate the flexibility of unstructured grids. The code can meet all study objectives and can accommodate the relevant features, events, and processes identified in the CSM. The upstream weighting formulation with Newton Raphson linearization provides robustness available in the MODFLOW-NWT (Niswonger, Panday, and Ibaraki 2011) version of the MODFLOW suite of codes. An unstructured discretization accommodates nested grids and quad-tree grid-block refinement, providing resolution only where required for optimal simulation efficiency. A public-domain particle tracking routine, mod-PATH3DU, for MODFLOW-USG available from S.S. Papadopulos & Associates, Inc. (SSPA)[3] (2022) was used to evaluate migration pathways or well capture zones via forward and reverse particle tracking.

Transport simulations used the USG-Transport code, which is also available as an open-source, public domain software from the GSI Environmental website.[4] The simulation software interfaces with the autocalibration software PEST (Doherty 2015), which was used to assist with model calibration. Groundwater Vistas Version 8 (Rumbaugh and Rumbaugh 2020) was used as a GUI.

2.2.2 Model Grid

The numerical model domain remained the same as the domain of the 2020 GWFM. In the horizontal plane, uniform grid cells of 250 ft × 250 ft were used. The areas encompassing the tank farm, (b) , and Hālawa Shaft were refined with a nested grid of 25 ft × 25 ft, in accordance with suggestions made by the Regulators' SMEs. The domain grid cells were rotated from orthogonal to align with the dip azimuth and

[3] http://mp3du.sspa.com/
[4] https://www.gsienv.com/software/modflow-usg/modflow-usg/

magnitude of the basalt, with a dip azimuth of 246 degrees and a dip magnitude of 4 degrees, which was agreed to with the Regulators and their SMEs in SPM #11 on January 10, 2023. The model domain and horizontal gridding are shown on Figure 2-9 with the nested grid shown in the inset. The top of the model grid is the ground surface topography, from a combination of light detection and ranging (LiDaR) imagery and the Continuously Updated Digital Elevation Model (CUDEM) (CIRES 2014). The bottom of the model domain is a no-flow boundary positioned near the assumed freshwater/saltwater interface, corresponding to the 50% seawater concentration of chloride as simulated by Oki (2005), which is approximately 650–900 ft below the water table throughout much of the model domain, thinning in areas closest to Pearl Harbor and the Pacific Ocean. The freshwater/saltwater interface and model bottom elevations are depicted on Figure 2-10. Negative elevations indicate values below msl.

The GWFM is discretized into 36 layers, which represent stratigraphic layering through the first four layers, and dipping basalt in the remaining layers. Layers 1 and 2 represent valley fill, alluvium, and caprock, then Layers 3 and 4 represent saprolite. Layers 5 through 36 represent basalt where each layer dips at 4 degrees. Thicknesses of the basalt layers generally vary from 25 to 200 ft thick, with the finest vertical discretization beneath the Facility, (b) , and Hālawa Shaft. Basalt model layers pinch out when rising above 22 ft msl, just above the water table, to eliminate unnecessary cells within the unsaturated zone. Basalt model layers also pinch out below the freshwater/saltwater interface. Cross sections of the numerical model grid setup are shown on Figure 2-11. The model grid setup includes 204,344 active cells before the addition of nested grid refinement, and 1,473,039 active cells with the nested grid refinement.

2.2.3 Boundary Conditions

Several boundary condition types were used to represent hydrogeological stresses in the GWFM, including constant heads, specified fluxes, general head boundaries (GHBs), wells represented as vertical connected linear networks (CLNs), and horizontal water production shafts represented as CLN polylines. Descriptions of each boundary condition implementation are provided below. Figure 2-12 shows the model boundary condition layout in plan view.

2.2.3.1 CONSTANT HEADS

A constant head boundary was applied using the MODFLOW CHD package to Pearl Harbor and the Pacific Ocean (makai). To correct for the effect of water density on piezometric head, equivalent freshwater head was calculated by subtracting the CUDEM bathymetry (CIRES 2014) from the average head value of 0 ft msl, then dividing by 40, assuming that seawater is 1.025 times the density of freshwater. Constant head cells are present only in Layer 1. Figure 2-12 shows the constant head boundary cells in dark blue.

2.2.3.2 SPECIFIED FLUX

The northeast (mauka) model boundary is set to align with the boundary of the dike region, located to the northwest of the model domain, which is a low-permeability area with significantly elevated heads (Oki 1998). Inflow from the northeast dike region boundary of the Koʻolau Range is represented as a specified flux using the WEL package. The inflow from the dike region was calculated as the sum of average recharge within the contributing topographic area to the northeast of the dike region boundary and outside the model boundary, totaling (b) mgd. Figure 2-12 shows specified flux boundary cells in red.

2.2.3.3 GENERAL HEAD BOUNDARIES

GHBs represent groundwater flow to and from the basalt aquifer across lateral model boundaries to the southeast and northwest of the model domain. The GHB package requires groundwater elevations and conductance as inputs. The GHB setup was generated through the calibration process, using the head magnitude and gradient along the boundaries as modifiable parameters to match water levels, as discussed further in Section 2.3.3. Gradients along each GHB reach and the gradients between the reaches were held constant through the simulation, while the magnitude of the heads was modified for each of the three study periods. Reported hydraulic gradients were approximately 1 ft per mile (Oki 1998). Conductance for the GHBs was set sufficiently high as to not restrict flow. Figure 2-12 shows GHB cells in light blue.

2.2.3.4 RECHARGE

Recharge is represented as a specified flux using the RCH package. Recharge values at each model cell were calculated using a weighted volumetric average over each model cell based on average conditions recharge distribution over the period from 1978 to 2007 (Engott et al. 2017), as shown on Figure 2-5. Areal recharge into the model domain totaled (b) mgd, consistent with the water budget analysis discussed in Section 2.0. Transient recharge based on recent precipitation was evaluated. Results showed that water level responses to precipitation events were relatively muted. This response may be indicative of either a more diffuse process of the majority of the recharge entering the aquifer, or the high transmissivity of the aquifer that redistributes recharge horizontally before well water levels rise in response to precipitation. Scaling of recharge values did not result in improvements in model behavior or calibration and was therefore held constant at the average value through all stress periods. Recharge was applied throughout the horizontal extent of the model domain and is therefore not depicted on Figure 2-12.

2.2.3.5 CONNECTED LINEAR NETWORKS

CLNs were used to represent water supply wells and tunnels. The advantage of the CLN package is in its simulation of vertical and horizontal conduit features such as wells and shafts. The simulated well may be screened in multiple groundwater model layers, and simulated shafts may cross multiple groundwater model cells in both the horizontal and vertical direction. Withdrawals are then applied to the CLN cell using the WEL package of MODFLOW to allow for appropriate distribution of flow through various model layers.

Twenty vertical wells were included, while (b) and Hālawa Shaft were implemented using CLN polylines. The (b) water development tunnel was divided into three connected polylines, shown on Figure 2-12. The pumping rate is defined by a well boundary condition located in the western wing, consistent with the actual location of the (b) pumps. During construction, Stearns (1943) noted that much of the flow entered the shaft through the clinker section in the easternmost 200 ft. This is discussed further in Section 3.3. Hālawa Shaft was simulated as one CLN polyline. Although (b)(3) is known to also be of shaft type construction (i.e., Maui-type well), the exact dimensions and orientation were not available. Due to its distance from the Facility and relatively low pumping capacity (compared to (b) and Hālawa Shaft), it is simulated simply as a vertical CLN well. Flow rates for the pumping wells were assigned average values during each stress period based on data provided by DLNR, presented in Section 2.3.3. Wells and water supply tunnels represented by CLNs are shown on Figure 2-12.

2.3 Regional GWFM Calibration

2.3.1 Approach

Model calibration was conducted using the PEST software (Doherty 2015). PEST is a non-linear inverse modeling program that automatically runs the MODFLOW-USG model multiple times, varying selected input parameters for each run until the difference between the model outputs and the site-specific observation targets is minimized (a process called optimization). Model calibration was conducted in two stages: a steady state calibration for caprock, valley fill, and saprolite parameters, and then a more detailed transient calibration focused on water levels in the basal aquifer. This two-stage approach was adopted because water levels in the caprock, valley fill, and saprolite do not respond to transient aquifer stresses in the basal aquifer and thus could be calibrated separately. PEST targets included water levels, drawdowns in response to pumping rate changes, flows to springs, flows to Pearl Harbor and the Pacific Ocean, hydraulic gradients along Red Hill ridge, horizontal head differences, and vertical head differences. Water level and flow rate information provide the model with the appropriate water budget. Water levels help to evaluate hydraulic gradients, which provide the model with information critical to the objectives of evaluating migration behavior of groundwater from beneath the Facility. Drawdown responses to changes in pumping provide the model with information useful for determining the hydrogeologic parameters (transmissivity, anisotropy, specific yield, and specific storage) of the basalt, which are critical for evaluating flow velocity and direction.

Water level and drawdown data were broken into several groups: local Red Hill monitoring wells, regional monitoring wells, transitional wells, down-weighted wells, and elevated head/confining unit wells. Red Hill (Group 1) monitoring wells include wells with the prefix RHMW, OWDF, and RHP; exceptions include wells in Group 3, described below. Regional (Group 2) monitoring wells include all other wells outside of the Red Hill wells that are screened in the basal aquifer.

Transitional (Group 3) wells are basal aquifer wells that are in proximity to the interpreted confining unit where the top of the basal aquifer was encountered at depths lower than the elevation of the water table, or where heads were slightly above those in the nearby basal aquifer, and at wells that responded more slowly to pumping influences than other basal aquifer wells. These wells are hypothesized to be affected by weathering of the basalt beneath stream valleys or local small-scale heterogeneity.

Down-weighted (Group 4) wells include wells with unconventional or unknown construction in addition to wells screened near the salt-water interface where density may be affecting the measured water level, including (b)(9) is cased to a depth of 250 ft below ground surface (bgs), then is an open (uncased) borehole below that to the freshwater/saltwater interface. (b)(9) is also an open borehole to the freshwater/saltwater interface. (b)(9) is an unscreened and unslotted pipe located next to (b)(9) (b)(9) which extends to a depth of 215 ft bgs. Well construction information for (b) is not available. Video survey of the well showed a solid casing with no slots or screen to a depth of 244 ft bgs, where the camera was blocked by an obstruction (Juturna LLC 2014). A water level meter was either obstructed or reached the bottom of the borehole at a depth of 275.46 ft bgs. These wells were grouped together due to similar behavior and lower confidence in their representativeness of conditions in the basal aquifer.

Group 5 includes wells that are screened above the basal aquifer in either saprolite or highly weathered bedrock where minimal hydraulic connection to the basal aquifer is indicated, and minimal responses to pumping stresses from [redacted] are evident.

Monitoring wells with perched conditions were not included because the simulation is not designed to account for perched conditions. Moreover, there are no indications of hydraulic communication between the basalt aquifer and perched water due to the presence of unsaturated rock between those zones and the water table. Each group of wells is further discussed in Section 2.3.5.1. Wells assigned to each group designation are presented in Table 2-5.

Table 2-5: Well Group Designations

Group	Description	Well Names		
1	Red Hill Basal Aquifer Monitoring Wells	OWDFMW[redacted] OWDFM[redacted] RHM[redacted] RHM[redacted] RHM[redacted] RHM[redacted] RHM[redacted] RHM[redacted] RHM[redacted] RHM[redacted] RHM[redacted] RHM[redacted]	RHM[redacted] RHM[redacted]3 RHM[redacted] RHM[redacted] RHMW[redacted] RHM[redacted] RHM[redacted] RHM[redacted] RHM[redacted] RHM[redacted] RHM[redacted]	RHM[redacted] RHM[redacted] RHM[redacted] RHM[redacted] RHM[redacted] RHM[redacted] RHMW[redacted] RH[redacted] RHP[redacted] RHP[redacted] RH[redacted]
2	Regional Basal Aquifer Monitoring Wells	[redacted]	[redacted]	[redacted]
3	Transitional Wells	OWDFM[redacted] OWDFM[redacted] OWDFM[redacted] OWDFM[redacted]	OWDFM[redacted] OWDFM[redacted] RHM[redacted] RHM[redacted]	RH[redacted] RH[redacted] RHP[redacted] RH[redacted]
4	Deep or Un-conventional Wells	[redacted]	[redacted]	[redacted]

Group	Description	Well Names		
5	Elevated Head/ Confining Unit Wells	OWDFM(b)	RHM (b)(9)	RHM (b)(9)
		RHM(b)	RHMW(b)	RHM (b)(9)
		RHM (b)(9)	RHM (b)(9)	RHM(b)(3)
		RHM (b)(9) 7	RHM (b)(9)	

Table 2-6 summarizes the target data used during the calibration process, as well as weighting and contribution to the overall objective function minimized by the PEST software. The objective function is the sum of the weighted squared residuals from all target groups. Water level and drawdown data were parsed into daily averages. Water level data from three study periods were included: the 2017/2018 synoptic survey, the 2021/2022 survey, and the 2023 FOS. Drawdowns were calculated based on the starting and ending elevations of each study period. Time periods for reference water levels are discussed in Section 2.3.3. Flux targets were derived from the water budget calculations described in Section 2.1.3.1.

Table 2-6: Summary of Model Calibration Target Data

Parameter Type	Number of Target Data Points	Group	Weight per Target	Weighted Sum of Square Residuals	Rank of Final Contribution to the Objective Function
Vertical head differences	1,291	vdiff	22	71,838	1
Spring/southeast GHB fluxes	88	flux	1.60E-05	31,180	2
Ridgeline gradients	72	grad	8.00E+05	26,518	3
Transitional well heads	1,175	3	0.1	17,029	4
Red Hill basal aquifer drawdowns	3,509	1	15	11,245	5
Red Hill basal aquifer heads	3,934	1	6	8,200	6
Horizontal head differences	1,867	hdiff	9	6,549	7
CLN drawdowns [a]	159	1–2	15	5996	8
Saprolite/confining unit heads	252	5	0.025[b]	4706	9
CLN heads [a]	254	1–2	6	2,542	10
Regional basal aquifer heads	1,123	2	6	1,420	11
Regional basal aquifer drawdowns	842	2	15	1050	12
Unconventional/down-weighted wells	125	4	10	160	13

Notes:
[a] Connected linear network (CLN) heads and drawdowns include those for (b) and Hālawa Shaft.
[b] These targets were used in separate steady state calibration, then down-weighted in transient calibration because targets are not sensitive to basal aquifer parameters modified in transient calibration.

2.3.2 Steady State Model Calibration

A steady state model was used to calibrate the valley fill, caprock, saprolite/confining unit parameters utilizing the Group 5 wells which exhibit heads elevated above the basal aquifer and generally do not respond to transient stresses in the basal aquifer. Average values were used for the Group 5 heads. Additionally, five censor targets were placed in Layer 1 of the caprock and three censor targets were placed in Layer 1 of the valley fill. These targets were imposed to prevent simulated flooding of the model cell, assigning a maximum head of 10 ft below ground surface at each location. When the simulated head is below the censor target value, then no penalty was applied in calibration. The results of the BAM study and estimated water budget suggest that the basal aquifer has little interaction with the caprock and saprolite. The primary behavior of these units is that they act essentially as vertical no-flow boundaries to the aquifer, imposing vertical gradients from the saprolite to the caprock. While some recharge does enter the basal aquifer through the saprolite, it is expected to be insignificant in comparison to the flow in the basal aquifer. An additional function of the deep caprock in Layer 2, along with the saprolite, is that it acts as a flow barrier between the shallow groundwater in the caprock and the confined basal aquifer. Parameters from this unit were carried over from the BAM study as there are no water levels available in the deep caprock.

2.3.3 Transient Calibration Model Setup

Regional GWFM calibration matched target data through adjustment of basalt hydraulic properties, GHB heads, and spring heads. The GWFM was assigned 44 stress periods, encompassing the water level and drawdown data collected during the 2017/2018 synoptic monitoring (Mitchell and Oki 2018), the synoptic groundwater level survey from December 2021 (USGS 2022a), the groundwater level monitoring from January to March 2022 (USGS 2022b), and the 2023 FOS (DON 2023c). The stress periods are tabulated in Table 2-7. GHB heads were modified where noted in Table 2-7; however, inter- and intra-boundary gradients were maintained through all stress periods. GHB heads were adjusted at the start of each study period as well as during two stress periods prior to the start of the 2022 water level measurements when several rainfall events caused significant increases in regional heads. A statistical summary of pumping rates defined for other water supply wells are shown in Table 2-8.

Water budget calculations as described in Section 2.1.3.1 were performed with updated pumping rates for each stress period. The results are shown in Table 2-9. The average water budget estimates described in Section 2.1.3 resulted in a relatively small error, or difference between the sum of inflows and sum of outflows of 2 mgd, or about 1% of the total water budget. When adjusting the water budget by stress period to account for pumping changes for these specific time periods, the error ranged from approximately 2–25 mgd surplus of water, or approximately 2–14% of the total 181.9 mgd accounted for in the water budget. The water budget calculations are generally intended to guide model behavior, but exact adherence to the estimated values is not necessary. Uncertainty related to many boundary fluxes can be considered epistemic (uncertainty resulting from a lack of knowledge (Beven 2002; 2019) and the error associated with these calculations is considered acceptable.

Targets for model calibration included inflows to the southeast GHB and discharge from the springs. All other inflows and well pumping rates were fixed. Caprock discharge was not sensitive to the calibrated model parameters, leaving only the northwest GHB, which discharges the remainder of groundwater; therefore, these two targets sufficiently constrained the model water budget.

Table 2-7: GWFM Stress Period Setup

Stress Period	Type	Description	Start Date	End Date	Duration (days)	Number of Time Steps
1 [a,b]	Steady State	(b) - (b)(3) gd, Hālawa Shaft - 6.3 mgd	1/9/2018 9:00	1/10/2018 9:00	1.00	1
2	Transient	(b) (b) Hālawa Shaft - 6.3 mgd	1/10/2018 9:00	1/15/2018 12:00	5.13	10
3	Transient	(b) -(b) mgd, Hālawa Shaft - 6.3 mgd	1/15/2018 12:00	1/20/2018 12:00	5.00	7
4	Transient	(b) - (b) mgd, Hālawa Shaft - 6.2 mgd	1/20/2018 12:00	1/27/2018 12:10	7.01	5
5	Transient	(b) -(b) mgd, Hālawa Shaft off	1/27/2018 12:10	2/2/2018 7:05	5.79	10
6	Transient	(b) -(b) mgd, Hālawa Shaft off	2/2/2018 7:05	2/4/2018 20:20	2.55	6
7	Transient	(b) - (b) mgd, Hālawa Shaft off	2/4/2018 20:20	2/6/2018 12:10	1.66	4
8	Transient	(b) - (b) mgd, Hālawa Shaft - 12.1 mgd	2/6/2018 12:10	2/14/2018 7:00	7.78	15
9	Transient	(b) - (b) mgd, Hālawa Shaft - 12.1 mgd	2/14/2018 7:00	2/16/2018 14:00	2.29	3
10	Transient	(b) -(b) mgd, Hālawa Shaft - off	2/16/2018 14:00	2/19/2018 0:00	2.42	3
11 [a,b]	Steady State	(b) - (b) mgd, Hālawa Shaft - 8.1 mgd	2/19/2018 0:00	11/28/2021 12:00	1378.50	1
12	Transient	(b) (b) Hālawa Shaft - 8.1 mgd	11/28/2021 12:00	12/2/2021 12:00	4.00	8
13	Transient	(b) (b) Hālawa Shaft off	12/2/2021 12:00	12/6/2021 0:00	3.50	5
14 [b]	Transient	Significant Precipitation Event	12/6/2021 0:00	12/29/2021 0:00	23.00	10
15 [b]	Transient	Significant Precipitation Event	12/29/2021 0:00	1/29/2022 14:00	31.58	10
16	Transient	(b) - (b) mgd, Hālawa Shaft off	1/29/2022 14:00	3/5/2022 0:00	34.42	15
17 [a,b]	Steady State	(b) - (b) mgd, Hālawa Shaft off	3/5/2022 0:00	4/7/2023 9:00	398.38	1
18	Transient	(b) (b) Hālawa Shaft off	4/7/2023 9:00	4/10/2023 9:00	3.00	6
19	Transient	(b) -(b) mgd, Hālawa Shaft off	4/10/2023 9:00	4/28/2023 9:00	18.00	10
20	Transient	(b) (b) Hālawa Shaft off	4/28/2023 9:00	5/1/2023 9:00	3.00	6
21	Transient	(b) - (b) mgd, Hālawa Shaft off	5/1/2023 9:00	5/6/2023 9:00	5.00	10
22	Transient	(b) (b) Hālawa Shaft off	5/6/2023 9:00	5/8/2023 9:00	2.00	4
23	Transient	(b) -(b) mgd, Hālawa Shaft off	5/8/2023 9:00	5/10/2023 0:00	1.63	4
24	Transient	(b) - (b) mgd, Hālawa Shaft off	5/10/2023 0:00	5/12/2023 0:00	2.00	4
25	Transient	(b) - (b) mgd, Hālawa Shaft off	5/12/2023 0:00	5/13/2023 9:00	1.38	3
26	Transient	(b) (b) Hālawa Shaft off	5/13/2023 9:00	5/15/2023 9:00	2.00	4

Stress Period	Type	Description	Start Date	End Date	Duration (days)	Number of Time Steps
27	Transient	(b) - (b) mgd, Hālawa Shaft off	5/15/2023 9:00	5/20/2023 9:00	5.00	10
28	Transient	(b) (b) Hālawa Shaft off	5/20/2023 9:00	5/23/2023 9:00	3.00	6
29	Transient	(b) - (b) mgd, Hālawa Shaft off	5/23/2023 9:00	5/25/2023 9:00	2.00	4
30	Transient	(b) (b) Hālawa Shaft off	5/25/2023 9:00	5/26/2023 9:00	1.00	3
31	Transient	(b) -(b) mgd, Hālawa Shaft off	5/26/2023 9:00	5/27/2023 9:00	1.00	3
32	Transient	(b) (b) Hālawa Shaft off	5/27/2023 9:00	5/30/2023 9:00	3.00	6
33	Transient	(b) - (b) mgd, Hālawa Shaft off	5/30/2023 9:00	6/1/2023 9:00	2.00	4
34	Transient	(b) (b), Hālawa Shaft off	6/1/2023 9:00	6/2/2023 9:00	1.00	3
35	Transient	(b) -(b) mgd, Hālawa Shaft off	6/2/2023 9:00	6/3/2023 9:00	1.00	3
36	Transient	(b) (b), Hālawa Shaft off	6/3/2023 9:00	6/6/2023 9:00	3.00	6
37	Transient	(b) -(b) mgd, Hālawa Shaft off	6/6/2023 9:00	6/8/2023 9:00	2.00	4
38	Transient	(b) (b) Hālawa Shaft off	6/8/2023 9:00	6/9/2023 9:00	1.00	3
39	Transient	(b) - (b) mgd, Hālawa Shaft off	6/9/2023 9:00	6/10/2023 9:00	1.00	3
40	Transient	(b) (b) Hālawa Shaft off	6/10/2023 9:00	6/13/2023 9:00	3.00	6
41	Transient	(b) - (b) mgd, Hālawa Shaft off	6/13/2023 9:00	6/15/2023 9:00	2.00	4
42	Transient	(b) (b), Hālawa Shaft off	6/15/2023 9:00	6/16/2023 9:00	1.00	3
43	Transient	(b) -(b) mgd, Hālawa Shaft off	6/16/2023 9:00	6/17/2023 9:00	1.00	3
44	Transient	(b) (b) Hālawa Shaft off	6/17/2023 9:00	6/20/2023 9:00	3.00	6

Notes:
[a] Indicates that last water level in stress period was used as reference elevation for drawdown calculations in subsequent stress periods.
[b] Indicates stress period where GHB elevations were adjusted.

Table 2-8: Individual Water Supply Well Pumping Rates by Stress Period

Well Number	Well Name	Longitude	Latitude	Top of Well Screen (ft msl)	Flow Rate Statistics During Model Stress Periods (mgd)				
					Bottom of Well Screen (ft msl)	Average (arithmetic mean)	Minimum	Maximum	Standard Deviation
3-2355-006	Aiea 1	-157.924	21.383	-32	-102	0.29	0.00	1.10	0.47
3-2355-003	Aiea Gulch 1	-157.915	21.386	16	-38	0.34	0.20	1.61	0.36
3[redacted]									
(b)(9)									
3-2255-037	Hālawa 2	-157.919	21.381	-29	-78	0.25	0.00	1.01	0.42
3-2154-001	Honolulu International Country Club	-157.901	21.354	-89	-280	0.30	0.19	0.43	0.04
3-2356-058	Ka‘amilo 1	-157.932	21.385	-43.3	-192.3	0.59	0.00	0.97	0.34
3-2355-009	Kalauao P1	-157.929	21.391	-61	-253.42	7.90	3.54	9.07	1.41
3-2052-008	Kalihi Shaft	-157.874	21.344	51.95	-4.86	8.32	3.92	8.70	0.73
3-2356-055	Kaonohi I-2	-157.937	21.394	-37	-290.89	1.41	0.79	1.71	0.28
3-2356-065	Kaonohi II-3	-157.944	21.388	-83	-223	0.00	0.00	0.00	0.00
3-2356-070	Lau Farm	-157.941	21.384	39.65	-249.5	0.00	0.00	0.05	0.01
3-2153-002	Moanalua	-157.891	21.349	-59	-269	0.01	0.01	0.02	0.00
3-2153-010	Moanalua 1	-157.896	21.353	-114	-264	1.41	0.39	2.21	0.53
3-2356-054	Pearl C C Golf	-157.932	21.396	-21	-178	0.13	0.00	0.25	0.11
3[redacted]									
3-2455-002	Waimalu	-157.929	21.400	-12	-78	0.00	0.00	0.00	0.00
3-2455-003	Waimalu	-157.929	21.399	-80	-120	0.00	0.00	0.00	0.00
3-2356-060	Waimalu II-1	-157.946	21.390	-77	-217	0.00	0.00	0.00	0.00
3-2355-016	WG Minami 2007	-157.929	21.399	-101.73	-202.17	0.00	0.00	0.01	0.00

Source: Various DLNR email communications with AECOM in 2023

Table 2-9: Conceptual Water Budget for GWFM Domain by Stress Period

Stress Period	Caprock Recharge (mgd)	Basalt Recharge (mgd)	Dike Region Inflows (mgd)	Well Discharge (mgd)	Spring Discharge (mgd)	Caprock Discharge (mgd)	Inflow from Adjacent Watershed (mgd)	Outflow to Adjacent Watershed (mgd)	Total Inflows (mgd)	Total Outflows (mgd)
1	2.3	30.1	26.1	33.4	13.6	2.3	3.0	12.2	61.5	61.5
2	2.3	30.1	26.1	28.5	13.6	2.3	3.0	17.1	61.5	61.5
3	2.3	30.1	26.1	36.1	13.5	2.3	3.0	9.5	61.5	61.5
4	2.3	30.1	26.1	32.4	13.5	2.3	3.0	13.2	61.5	61.5
5	2.3	30.1	26.1	25.8	13.7	2.3	4.9	21.6	63.4	63.4
6	2.3	30.1	26.1	22.8	13.8	2.3	4.9	24.5	63.4	63.4
7	2.3	30.1	26.1	26.2	13.9	2.3	4.9	21	63.4	63.4
8	2.3	30.1	26.1	37.3	13.6	2.3	4.9	10.2	63.4	63.4
9	2.3	30.1	26.1	36.0	13.6	2.3	4.9	11.4	63.4	63.4
10	2.3	30.1	26.1	31.2	13.7	2.3	4.9	16.2	63.4	63.4
11	2.3	30.1	26.1	31.7	13.9	2.3	4.2	14.8	62.7	62.7
12	2.3	30.1	26.1	33.1	12.6	2.3	2.9	13.5	61.4	61.4
13	2.3	30.1	26.1	21.4	12.9	2.3	2.9	24.9	61.4	61.4
14	2.3	30.1	26.1	21.4	13.4	2.3	2.9	24.4	61.4	61.4
15	2.3	30.1	26.1	21.6	13.9	2.3	2.8	23.5	61.3	61.3
16	2.3	30.1	26.1	14.4	13.9	2.3	3.8	31.7	62.3	62.3
17	2.3	30.1	26.1	23.3	13.6	2.3	4.5	23.8	63.0	63.0
18	2.3	30.1	26.1	21.5	13.5	2.3	4.1	25.3	62.6	62.6
19	2.3	30.1	26.1	25.8	13.4	2.3	4.1	21.1	62.6	62.6
20	2.3	30.1	26.1	22.4	13.4	2.3	3.8	24.1	62.3	62.3
21	2.3	30.1	26.1	26.7	13.5	2.3	3.8	19.8	62.3	62.3
22	2.3	30.1	26.1	22.4	13.4	2.3	3.8	24.2	62.3	62.3
23	2.3	30.1	26.1	26.6	13.4	2.3	3.8	20	62.3	62.3
24	2.3	30.1	26.1	26.6	13.4	2.3	3.8	20	62.3	62.3

Stress Period	Caprock Recharge (mgd)	Basalt Recharge (mgd)	Dike Region Inflows (mgd)	Well Discharge (mgd)	Spring Discharge (mgd)	Caprock Discharge (mgd)	Inflow from Adjacent Watershed (mgd)	Outflow to Adjacent Watershed (mgd)	Total Inflows (mgd)	Total Outflows (mgd)
25	2.3	30.1	26.1	26.6	13.4	2.3	3.8	20	62.3	62.3
26	2.3	30.1	26.1	22.4	13.4	2.3	3.8	24.2	62.3	62.3
27	2.3	30.1	26.1	26.6	13.4	2.3	3.8	20.0	62.3	62.3
28	2.3	30.1	26.1	22.4	13.4	2.3	3.8	24.2	62.3	62.3
29	2.3	30.1	26.1	26.6	13.4	2.3	3.8	20.0	62.3	62.3
30	2.3	30.1	26.1	22.4	13.4	2.3	3.8	24.2	62.3	62.3
31	2.3	30.1	26.1	26.6	13.4	2.3	3.8	20.0	62.3	62.3
32	2.3	30.1	26.1	22.4	13.4	2.3	3.8	24.1	62.3	62.3
33	2.3	30.1	26.1	27.1	13.4	2.3	2.0	17.6	60.5	60.5
34	2.3	30.1	26.1	22.9	13.4	2.3	2.0	21.8	60.5	60.5
35	2.3	30.1	26.1	27.1	13.4	2.3	2.0	17.7	60.5	60.5
36	2.3	30.1	26.1	22.9	13.4	2.3	2.0	21.8	60.5	60.5
37	2.3	30.1	26.1	27.1	13.4	2.3	2.0	17.7	60.5	60.5
38	2.3	30.1	26.1	22.9	13.4	2.3	2.0	21.9	60.5	60.5
39	2.3	30.1	26.1	27.1	13.4	2.3	2.0	17.7	60.5	60.5
40	2.3	30.1	26.1	22.9	13.4	2.3	2.0	21.8	60.5	60.5
41	2.3	30.1	26.1	27.0	13.4	2.3	2.0	17.8	60.5	60.5
42	2.3	30.1	26.1	22.9	13.4	2.3	2.0	21.9	60.5	60.5
43	2.3	30.1	26.1	27.1	13.4	2.3	2.0	17.7	60.5	60.5
44	2.3	30.1	26.1	22.9	13.4	2.3	2.0	21.9	60.5	60.5

2.3.4 Model Parameterization for Regional GWFM

As discussed in Section 2.2.2, there are 36 model layers representing many distinct hydrogeologic units. The major hydrogeologic units delineated within the model include the caprock, valley fill, volcanic tuff, saprolite, basalt, and basalt behaving as a confining unit. Details about the geologic setting are presented in the CSM report (DON 2019) and updated in the 2023 CSM Appendix E Addendum (DON 2023a), with newly collected data summarized in Section 2.1.2.

The three-dimensional geological model constructed in Earth Volumetric Studio (EVS) version 2022.10.2 (C Tech 2022) was used to interpolate observed geologic data across the flow model domain to construct hydrogeological units. Data from the EVS model were transferred to the MODFLOW-USG grid by sampling the EVS model for each model cell. During the model calibration process, the caprock was further divided into alluvium and marine sediments, each of which consists of two layers: 1) shallow with high permeability to match shallow heads, and 2) deep with lower hydraulic conductivity to limit outflow through the caprock. Figure 2-13 and Figure 2-14 show the model parameterization in plan view and cross section, respectively.

The model was calibrated such that the hydrogeologic properties are constrained by reasonable ranges interpreted from field measurements, past studies, and consensus of experienced professional judgment among the project team. These values are shown in Table 2-10. Parameter ranges were derived from the 2023 geological CSM addendum Table 3 (DON 2023a). Parameter ranges were often narrowed from previously published values to align with the CSM and anticipated behavior of the hydrogeologic system based on the CSM. Insensitive parameters, meaning parameters that do not affect simulated targets that are compared to observations, were not calibrated. Several parameters pertaining to the caprock, saprolite, and tuff are insensitive to basal aquifer heads within parameter ranges that maintain an effective hydraulic disconnection to the basal aquifer, which is consistent with the hydrogeological conceptual model and water budget analysis discussed in Section 2.1.3. Those parameters were either estimated in steady state model calibration of Group 5 water levels or values were carried through from those estimated in the BAM study.

Table 2-10: Model Parameterization

Geologic Material/Feature	Parameter	Unit	Layer(s)	Minimum Value for PEST Bounds	Maximum Value for PEST Bounds	Calibrated/ Assigned Value	Literature/Field Data Value Range (Source)
Caprock - Marine Sediments	Kh	ft/d	1	1	500	145	• 0.01 – 2,500 (Oki 2005) • 115 (Rotzoll and El-Kadi 2007) • 0.03 – 330 (Souza and Voss 1987)
Caprock - Marine Sediments	Kh:Kv Ratio	—	1	Not Calibrated		10	• 1 – 10 (Oki et al. 1996) • 1 – 100 (Oki 2005)
Caprock - Marine Sediments	Kh	ft/d	2	Not Calibrated [a]		0.1	• 0.01 – 2,500 (Oki 2005) • 115 (Rotzoll and El-Kadi 2007) • 0.03 – 330 (Souza and Voss 1987)
Caprock - Marine Sediments	Kh:Kv Ratio	—	2	Not Calibrated [a]		10	• 1 – 10 (Oki et al. 1996) • 1 – 100 (Oki 2005)
Caprock - Marine Sediments	Specific Storage	ft[1]	1–2	Insensitive Parameter, Not Calibrated		5.0E-05	• 4E-05 – 6E-05 [b] (Domenico and Mifflin 1965)
Caprock - Marine Sediments	Specific Yield	%	1–2	Insensitive Parameter, Not Calibrated		15%	• 0.2 (Oki 2005) • 0.1 (Rotzoll and El-Kadi 2007)
Caprock - Marine Sediments	Effective Porosity	%	1–2	Insensitive Parameter, Not Calibrated		15%	• 0.2 (Oki 2005) • 0.1 (Rotzoll and El-Kadi 2007)
Caprock - Alluvium	Kh	ft/d	1	1	500	71	• <1 – 500 (Hunt Jr. 1996) • 0.058 (Oki 2005)
Caprock - Alluvium	Kh:Kz Ratio	—	1	Not Calibrated [a]		10	• 1 (Oki 2005)
Caprock - Alluvium	Kh	ft/d	2	Not Calibrated [a]		0.1	• <1 – 500 (Hunt Jr. 1996) • 0.01 – 0.6 (Oki 2005)
Caprock - Alluvium	Kh:Kz Ratio	—	2	Not Calibrated [a]		10	• 2 – 100 (Todd 1980)
Caprock - Alluvium	Specific Storage	—	1–2	Insensitive Parameter, Not Calibrated		5.0E-05	• 4E-5 – 6E-5 [b] (Domenico and Mifflin 1965)
Caprock - Alluvium	Specific Yield	%	1–2	Insensitive Parameter, Not Calibrated		15%	• 0.1 (Oki 2005) • 0.1 (Rotzoll and El-Kadi 2007)

Geologic Material/Feature	Parameter	Unit	Layer(s)	Minimum Value for PEST Bounds	Maximum Value for PEST Bounds	Calibrated/ Assigned Value	Literature/Field Data Value Range (Source)
Caprock - Alluvium	Effective Porosity	%	1–2	Insensitive Parameter, Not Calibrated		15%	• 0.15 (Oki 2005) • 0.1 (Rotzoll and El-Kadi 2007)
Valley Fill	Kh	ft/d	1	1	500	71	• <1 – 500 (Hunt Jr. 1996) • 0.058 (Oki 2005)
Valley Fill	Kh:Kz Ratio	—	1	Not Calibrated [a]		10	• 1 (Oki 2005)
Valley Fill	Specific Storage	—	1–2	Insensitive Parameter, Not Calibrated		5.0E-05	• <1 – 500 (Hunt Jr. 1996) • 0.058 (Oki 2005)
Valley Fill	Specific Yield	%	1–2	Insensitive Parameter, Not Calibrated		15%	• 1 (Oki 2005)
Valley Fill	Effective Porosity	%	1–2	Insensitive Parameter, Not Calibrated		15%	• 4E-5 – 6E-5 (Domenico and Mifflin 1965)
Volcanic Tuff	Kh	ft/d	1–36	Not Calibrated [a]		1.0E-03	• <1 – 100 ((Eyre, Ewart, and Shade 1986) • <1 – 45 ((Belcher, Elliot, and Geldon 2001) • 3E-06 – 6E-04 (Lahoud, Lobmeyer, and Whitfield 1984)
Volcanic Tuff	Kh:Kz Ratio	—	1–36	Not Calibrated [a]		1	• No literature values available, assumed isotropic
Volcanic Tuff	Specific Storage	—	1–36	Insensitive Parameter, Not Calibrated		1.0E-05	• 1E-06 – 1E-04 [c] (Domenico and Mifflin 1965)
Volcanic Tuff	Specific Yield	%	1–36	Insensitive Parameter, Not Calibrated		5%	• 1E-06 – 1E-04 [c] (Domenico and Mifflin 1965)
Volcanic Tuff	Effective Porosity	%	1–36	Insensitive Parameter, Not Calibrated		5%	• ~5 – 20% (Lahoud, Lobmeyer, and Whitfield 1984) • 6 – 21% (Morris and Johnson 1967)
Saprolite	Kh	ft/d	1–35	1.0E-04	1.0	7.8E-03	• 0.0028 – 283 (Miller 1987) • <1 (Hunt Jr. 1996) • 0.058 (Oki 2005) • 0.0033 – 0.026 (slug test) (DON 2023a) • 7.99E-06 – 8.50E-05 (laboratory test)
Saprolite	Kh:Kz Ratio	—	1–35	Not Calibrated [a]		1	• No literature values available
Saprolite	Specific Storage	—	1–36	Insensitive Parameter, Not Calibrated		1.0E-05	• No literature values available, assumed to be similar to clay • 1E-06 – 1E-04 (Domenico and Mifflin 1965)

Geologic Material/Feature	Parameter	Unit	Layer(s)	Minimum Value for PEST Bounds	Maximum Value for PEST Bounds	Calibrated/ Assigned Value	Literature/Field Data Value Range (Source)
Saprolite	Specific Yield	%	1–36	Insensitive Parameter, Not Calibrated		5%	• No literature values available, assumed to be similar to clay • 2% (Heath 1993) • 6% (Morris and Johnson 1967)
Saprolite	Effective Porosity	%	1–36	Insensitive Parameter, Not Calibrated		5%	• No literature values available, assumed to be similar to clay • 2% (Heath 1993) • 6% (Morris and Johnson 1967)
Confining Unit (Basalt)	Kh	ft/d	8–26	1.0E-04	1	1.6E-02	• No literature values, assumed to be similar to saprolite • 0.0028 – 283 (Miller 1987) • <1 (Hunt Jr. 1996) • 0.058 (Oki 2005) • 0.0033 – 0.026 (slug test) (DON 2023a) 7.99E-06 – 8.50E-05 (laboratory test)
Confining Unit (Basalt)	Kh:Kz Ratio	—	11–25	Not Calibrated		1	• No literature values available, assumed be isotropic
Confining Unit (Basalt)	Specific Storage	—	1–36	Insensitive Parameter, Not Calibrated		1.0E-05	• No literature values available, assumed be similar to saprolite
Confining Unit (Basalt)	Specific Yield	%	1–36	Insensitive Parameter, Not Calibrated		5%	• No literature values available, assumed be similar to saprolite
Confining Unit (Basalt)	Effective Porosity	%	1–36	Insensitive Parameter, Not Calibrated		5%	• No literature values available, assumed be similar to saprolite
Basalt	Kh	ft/d	1–36	4,000	15,000	18,546	• 4,500 (Oki 2005) • 500 – 5,000 (Hunt Jr. 1996) • 6,195 – 22,562 (Evaluation of field data, Section 2.1.3.2)
Basalt	Kx:Ky (Horizontal Anisotropy Ratio)	—	1–36	2	10	14	• 3 (Oki 2005) • 5.3 – 25.8 (Evaluation of field data, Section 2.1.3.2)
Basalt	Kh:Kz Ratio	—	1–36	50	200	50	• 600 (Oki 2005) • 200 (Rotzoll 2012) • 10 (Rotzoll and El-Kadi 2007)

Geologic Material/Feature	Parameter	Unit	Layer(s)	Minimum Value for PEST Bounds	Maximum Value for PEST Bounds	Calibrated/ Assigned Value	Literature/Field Data Value Range (Source)
Basalt	Specific Storage	—	1–36	Insensitive Parameter, Not Calibrated		1.0E-06	• 1E-07 – 1E-04 (Oki 2005)
Basalt	Specific Yield	%	1–36	1%	15%	7.4%	• 0.04 (Oki 2005) • 0.3 (Rotzoll and El-Kadi 2007)
Basalt	Effective Porosity	%	1–36	Insensitive Parameter, Not Calibrated [d]		11.0%	• 0.04 (Oki 2005) • 0.3 (Rotzoll and El-Kadi 2007)
GHB - Southeast	Maximum Head	ft msl	35–36	18	25	20.4 to 21.2	• Calibrated based on measured water levels [e]
GHB - Southeast	Gradient	ft/ft	36	1.0E-5	1.0E-3	2.0E-04	• Calibrated based on measured water levels
GHB - Northwest	Maximum Head	ft msl	5–36	13	22	18.1 to 18.9	• Calibrated based on measured water levels [e]
GHB - Northwest	Gradient	ft msl	5–36	2.0E-5	2.0E-3	2.2E-04	• Calibrated based on measured water levels
Spring	Head	ft msl	1–5	7	18	14.9	• Calibrated based on measured spring fluxes
Spring	Conductance	ft^2/d	1–5	Not Calibrated		6.25E08	• No literature values available, set not to limit flow
Basalt	Weathering Depth	ft	1-36	300	900	736	• > 700 Weathering depth at NM[redacted] • >>300 (Oki 2005)
Basalt	Weathering Factor (beneath Streams)	-	1-36	1	1.0E5	6,624	• 0.0028 to 283 - Hydraulic conductivity of weathered basalt (Miller 1987)
Basalt	Weathering Factor (beneath caprock)	-	1-36	1	1.0E-5	2.6	• 0.0028 to 283 - Hydraulic conductivity of weathered basalt (Miller 1987)

Notes:
Effective porosity of basalt adjusted based on estimated groundwater velocities.
K_h horizontal conductivity
K_v vertical conductivity
K_x hydraulic conductivity in the down-dip direction
K_y hydraulic conductivity in the cross-dip direction

[a] Basal aquifer flow is insensitive to these parameters because of a hydraulic disconnection between the basal aquifer and caprock. The BAM study demonstrated parameter insensitivity below a threshold that was dictated by the water budget (DON 2023d).

[b] Generic value for dense sand

[c] Generic values ranging from loose sand to fissured rock

[d] Calibration of effective porosity performed in CF&T modeling (Section 5.0)

[e] Maximum head values vary by stress period as indicated in Table 2-7.

2.3.4.1 WEATHERING OF BASALT

Weathering of the basalt was implemented using an exponential relationship between hydraulic conductivity and ground surface. A maximum reduction factor for hydraulic conductivity of the weathered basalt and a maximum depth of weathering were implemented beneath stream valleys. The equation applied to calculate the hydraulic conductivity as a function of depth below ground surface was defined as:

$$K_{weathered} = K_{unweathered} * WFactor^{\frac{(depth - depth_{max})}{depth_{max}}}$$

Where:

$K_{weathered}$ = Calculated hydraulic conductivity of weathered basalt (ft/d)

$K_{uweathered}$ = Hydraulic conductivity of unweathered basalt (ft/d)

$WFactor$ = Weathering factor for reduction in basalt hydraulic conductivity (unitless)

$depth$ = Depth below ground surface of model cell (ft bgs)

$depth_{max}$ = Maximum depth of weathering (ft bgs)

Chart 2-2 illustrates the hydraulic conductivity calculation for weathered basalt both under stream valleys and beneath the caprock as an exponential function of depth below ground surface for a hydraulic conductivity of unweathered basalt of 18,600 ft/d, a weathering factor of 6,624 for stream valleys and 2.6 for caprock, and a maximum weathering depth of 736 ft. As discussed in Section 2.1.3.3, weathering depth under ridges is expected to be generally less than 100 ft bgs, well above the depth to water in most areas; therefore, no weathering was applied. Weathering beneath the caprock was applied in the same manner with the same depth as below stream segments; however, the separate caprock weathering factor was applied. The depth of weathering, weathering factor for stream segments, and weathering factor for beneath the caprock were calibrated parameters by PEST.

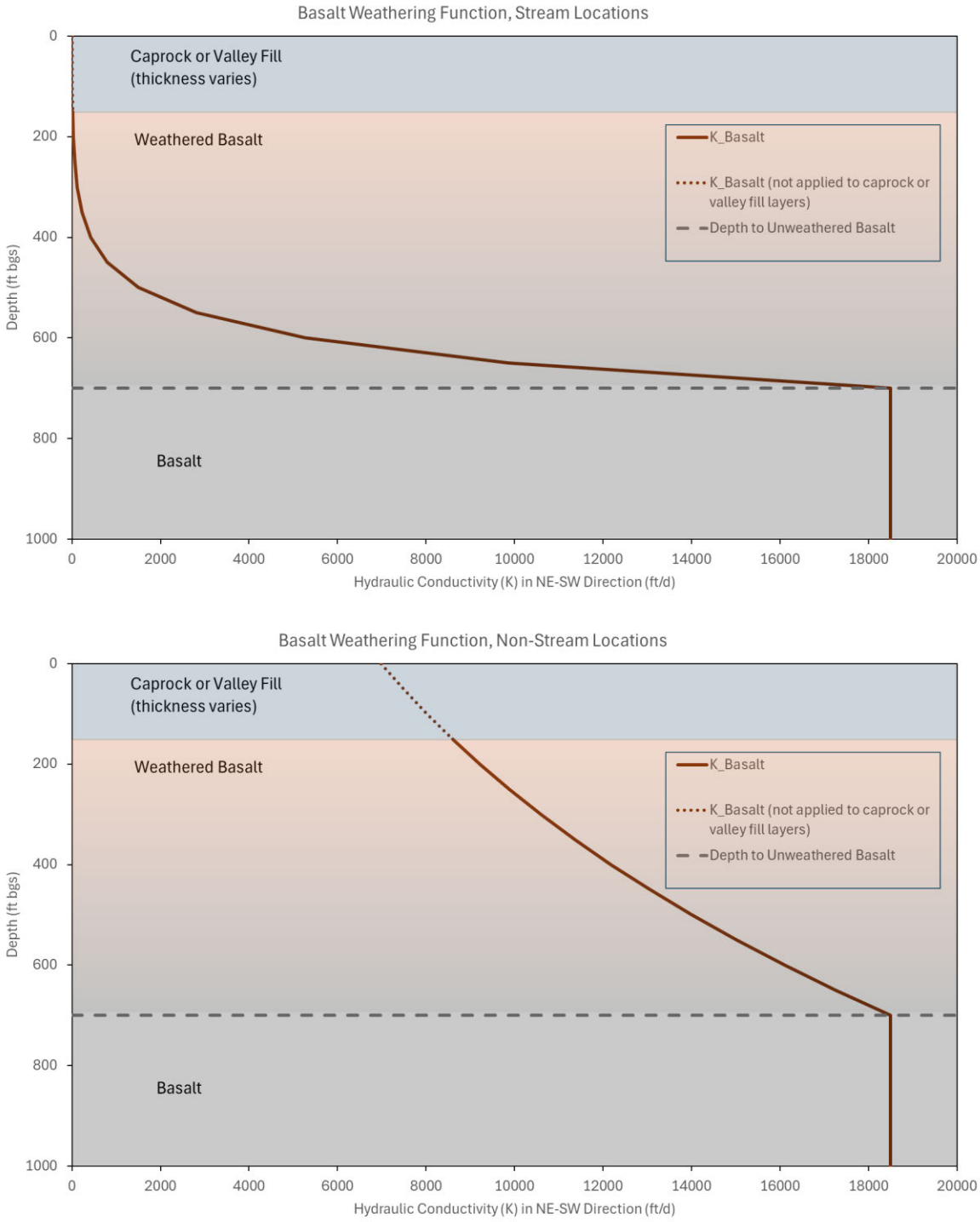

Chart 2-2: Calculation of Weathered Basalt Hydraulic Conductivity Beneath Stream Valleys (top) and Beneath Caprock (bottom)

2.3.4.2 REGULARIZATION OF MODEL PARAMETERS

The PEST software suite allows for regularization of estimated model parameters to prevent overfitting and favor preferred values based on previous knowledge of the flow system. Regularization was implemented

by testing the model calibration without regularization constraints for an estimate of the optimal objective function (phi) value, which is the optimum sum of weighted squared residuals from all target groups. This optimal phi value plus one percent was set as the target phi value, then an acceptable phi value of the target phi value plus three percent was established as a calibration goal. The PEST software calibrated the model to the target phi, then allowed the phi value to increase to the acceptable phi using a second regularization objective function to adjust parameter values back toward their preferred values. The preferred values set for calibration are presented in Table 2-11.

Table 2-11: Preferred Values for Parameter Regularization

Parameter	Preferred Value	Unit	Source
Hydraulic Conductivity (longitudinal)	12,878	ft/d	Average value from Section 2.1.3
Horizontal Anisotropy Ratio	14	-	Average value from Section 2.1.3
Vertical Anisotropy Ratio	200	-	Rotzoll (2012)
Specific Yield	8%	-	Heath (1993)
Weathering Depth for valleys and caprock	700	ft	Weathering Depth at NM[redacted] (> 700 ft) Oki (2005) (>>300 ft)

2.3.5 Evaluation of Model Calibration

The regional homogeneous-anisotropic GWFM calibration was evaluated using multiple lines of evidence with both quantitative and qualitative approaches. Adequacy of model calibration is defined only in part by statistical metrics; other metrics are also important to the conclusions, predictions, and decisions derived from model results. Of particular importance are the accuracy of rates and directions of groundwater flow beneath the Facility, as well as the capture zones and water sources to (b) and Hālawa Shaft. Hydraulic gradients along Red Hill ridge are significant for assessing the potential capture of groundwater from beneath the Facility by (b) and were compared using plots of simulated versus observed values against distance from (b). Horizontal head differences between monitoring wells under the tank farm and other local wells as well as vertical head differences at West Bay and nested wells were also evaluated comparing simulated and observed differences. Hydrographs at each well were evaluated to compare the simulated and observed heads over time. Heads were converted to drawdown and compared to observed drawdowns for better estimation of hydraulic properties.

The overall model water budget was compared to the estimated water budget presented in Table 2-9 to ensure consistency with the hydrogeological conceptual model. Chloride and temperature data were used to evaluate the source water to (b) and Hālawa Shaft with simulated concentrations using unit concentration source simulations. The groundwater inflow distribution along (b) water development tunnel was considered; however, the distribution was not expected to be replicated in the regional homogeneous model. The flow distribution along (b) is further discussed in Section 3.3 from homogeneous models where the distribution of flow is better represented. Documentation of the data associated with evaluation of the model calibration, including calibration statistics, scatter plots, gradient plots, head difference plots, and hydrographs, are presented in Appendix D.

2.3.5.1 CALIBRATION STATISTICS

Summary calibration statistics comparing observed and model-simulated values were evaluated to initially assess the model calibration. Heads were divided into the five groups identified previously:

- Group 1: local Red Hill wells in the basal aquifer
- Group 2: regional wells
- Group 3: transitional wells
- Group 4: wells that include deep wells that may be affected by density effects from the freshwater-saltwater interface, and wells with unconventional construction
- Group 5: wells screened in the confining unit or saprolite with elevated heads

The primary focus of the calibration is on the basal aquifer wells in groups 1 and 2. Heads from group 3 have slightly greater residuals compared to those in Groups 1 and 2. The largest residuals are associated with wells RHM(b) , RH(b) , and RH(b) . Group 4 was down-weighted and therefore did not achieve similar levels of correspondence between observed and simulated values. Group 5 wells include water levels in saprolite and valley fill which do not respond to stresses within the basal aquifer and were calibrated using a steady state model and average water levels as described above. These water levels are often simulated lower than observed; however, they do still form downward gradients from the saprolite to the basal aquifer and, where present below the water table, were generally assigned hydraulic conductivities that form effective flow barriers consistent with the CSM.

The calibration statistics are summarized in Table 2-12 and in Appendix D. Basal aquifer heads are further divided into three categories: heads from the 2017/2018 study, those from the 2021/2022 study, and those from the 2023 FOS. Cumulative statistics over all transient stress periods are presented for the basal aquifer as well.

Late in the modeling stage, leading up to preparation of this report, data became available from coring for a new monitoring well, NM(b) , installed near the confluence of the North and South Hālawa stream valleys. While water quality and precise water level data were not available from the completed well, data available from the corehole for this well indicated the following: 1) valley fill was observed down to a depth of approximately 145 ft bgs (-18 ft msl); 2) heads within the valley fill and upper portion of the basalt (to a depth of about 215 ft bgs, -88 ft msl) were approximately 70 ft bgs (57 ft msl); 3) below a depth of about 245 ft bgs the heads dropped to about (b) ft bgs (approximately 19 ft msl); and 4) below that depth a weak hydraulic connection was observed down to the upper portion transition zone above the freshwater/saltwater interface. Based on unpublished preliminary data, provided from the University of Hawaii's colloidal borescope work, the strongest connection to the basal aquifer occurred at a depth of about 585 to 605 ft bgs. That zone was targeted for screen installation. Above and below that depth, the water was essentially horizontally stagnant or moving vertically.

Table 2-12: Summary of GWFM Calibration Statistics

	Red Hill Wells (Group 1)				Regional Wells (Group 2)	All Basal Wells (Groups 1 and 2)	Transition-al Wells (Group 3)	Down-weighted Wells (Group 4)	Elevated Head/ Confining Unit (Group 5)	All Wells
Time Period:	**2017/2018**	**2021/2022**	**FOS**	**All Time Periods**	**All Time Periods**	**All Time Periods**	**All Time Periods**	**All Time Periods**	**All Time Periods**	**All Time Periods**
Residual Mean (ft)	0.03	-0.11	-0.17	-0.12	-0.09	-0.11	0.16	1.11	41.49	1.48
Absolute Residual Mean (ft)	0.13	0.20	0.19	0.19	0.20	0.19	0.24	1.11	41.53	1.73
Residual Standard Deviation (ft)	0.17	0.24	0.20	0.22	0.23	0.22	0.32	0.15	30.54	9.76
Sum of Squared Residuals (ft^2)	18.14	73.55	160.53	252.77	76.47	329.24	147.87	156.14	667870.23	668503.48
RMSE Error (ft)	0.18	0.26	0.26	0.25	0.25	0.25	0.35	1.12	51.48	9.87
Minimum Residual (ft)	-0.79	-0.88	-0.88	-0.88	-2.10	-2.10	-0.46	0.79	-0.65	-2.10
Maximum Residual (ft)	0.28	0.42	0.36	0.42	1.20	1.20	1.07	1.37	90.58	90.58
Number of Observations	592	1077	2357	4040	1271	5311	1175	125	252	6863
Range in Observations	2.14	1.80	1.46	2.64	7.19	7.19	1.71	0.87	97.72	104.53
Scaled Residual Standard Deviation (%)	8.05%	13.29%	13.70%	8.30%	3.16%	3.08%	18.62%	17.00%	31.26%	9.34%
Scaled Absolute Residual Mean (%)	6.29%	11.05%	13.19%	7.04%	2.76%	2.63%	13.89%	127.23%	42.50%	1.66%
Scaled RMSE Error (%)	8.19%	14.56%	17.84%	9.48%	3.41%	3.46%	20.75%	128.35%	52.68%	9.44%
Scaled Residual Mean (%)	1.54%	-5.96%	-11.43%	-4.58%	-1.29%	-1.59%	9.18%	127.23%	42.46%	1.42%
Correlation Coefficient	0.86	0.59	0.55	0.74	0.98	0.96	0.42	0.87	0.57	0.83

Although heads measured while coring below 245 ft bgs (100 ft msl) were all approximately at 108 ft bgs (-37 ft msl), it should be noted that these measurements were composite heads resulting from having the corehole essentially open from the then-current bottom of the corehole up to the bottom of the conductor casing at 215 ft bgs (70 ft msl). This is because the core bit creates a hole that is larger in diameter than the core pipe. That zone cannot be hydraulically isolated from section at the bottom where the core barrel is lifted (typically about 5 ft off the bottom) during testing. Following completion, development, monitoring, and sampling of the monitoring well, it will be possible to measure a discrete head and collect discrete water quality field parameters and samples for laboratory testing for the screened interval. Following receipt of those data, as well as results of future UH testing, it will be possible to make further judgements about the effects of the deep low permeability weathered basalt. Those results may be utilized in future model updates. These iterative improvements as data become available are typical in complex geologic settings and dynamic investigations. However, the preliminary data suggests the presence of a deep hydraulic barrier that may essentially isolate the North and South Hālawa Valleys. The effects of such a hydraulic barrier were evaluated in previous modeling conducted by Oki (2005),

Chart 2-3 shows graphical representation of head calibration statistics. Calibration statistics for the Red Hill basal aquifer wells in Group 1 meet generally acceptable criteria for a model calibration. The mean of all residuals (observed minus simulated) is -0.12 ft with a root mean squared error (RMSE) of 0.25 ft. When scaled over the range of observed heads of 2.64 ft, the scaled RMSE becomes 9.4%. The simulated match to the 2017/2018 observed heads is slightly better than that of the 2021/2022 heads and the FOS heads. Comparatively, the 2017/2018 water level targets have a 0.18-ft RMSE, versus the FOS water level targets with a 0.26-ft RMSE and a 0.26-ft RMSE for the 2021/2022 heads.

Calibration statistics for the regional basal aquifer wells in Group 2 have a similar residual mean of -0.09 ft but a slightly higher RMSE of 0.25 ft, similar to that of the Group 1 wells. The range of regional water level observations is 7.19 ft, resulting in a scaled RMSE of 3.4%. Cumulative statistics for both Group 1 and 2 heads, which include all basal aquifer monitoring wells results in an average residual of -0.11 ft with a RMSE of 0.25 ft. Scaled over the 7.19 ft range, the resulting scaled RMSE is 3.46%. Though no specific quantitative measure of acceptable model calibration exists, these statistics are consistent with acceptable error in typical groundwater model head comparisons.

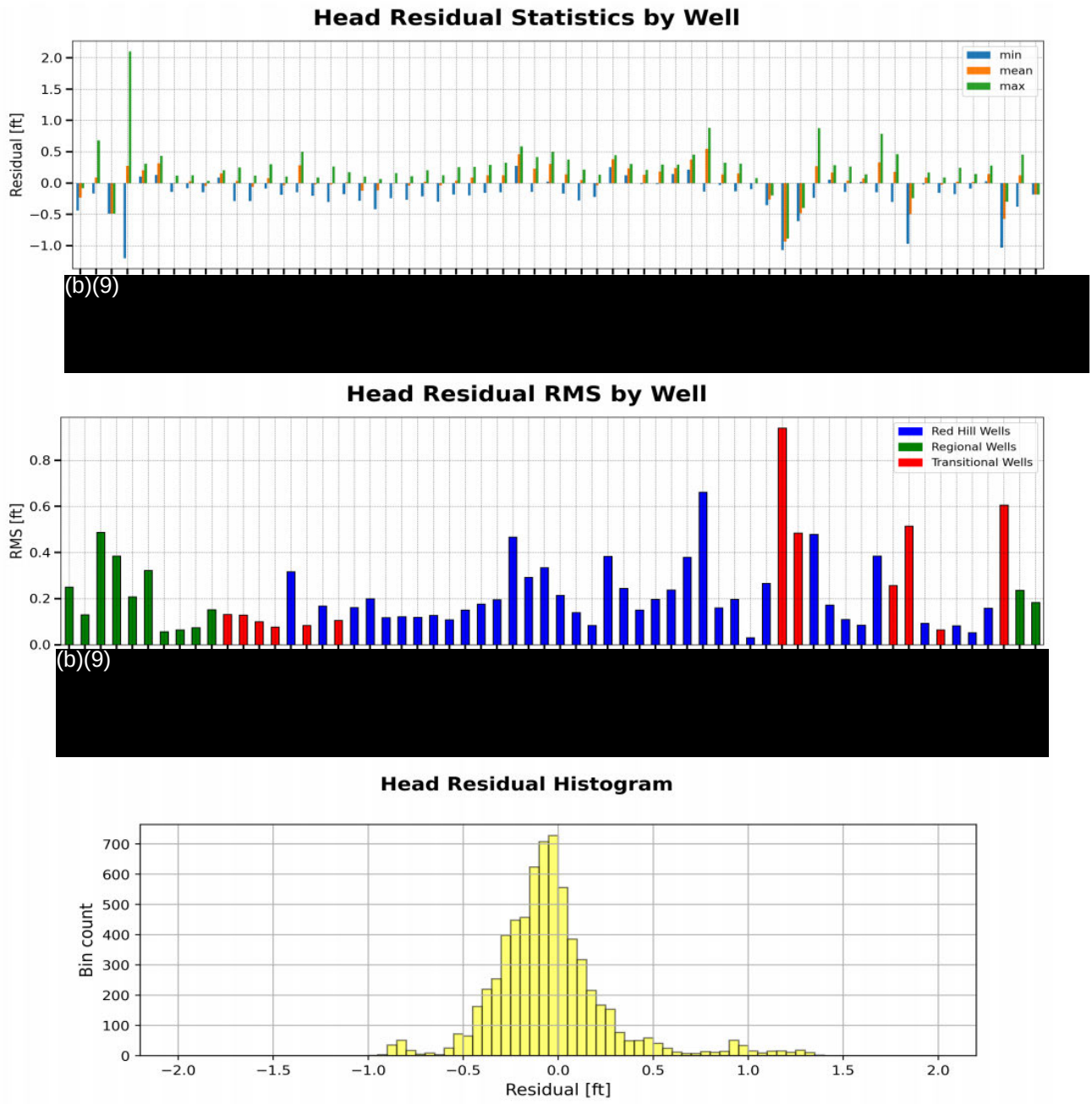

Chart 2-3: Residual Statistic Charts

Transitional wells in Group 3 represent monitoring wells screened near the interpreted confining unit. These wells have slightly elevated heads, and in some cases, recover more slowly than wells with a stronger connection to the basal aquifer. The confining unit represents portions of the aquifer with significantly elevated heads that did not appear to be hydraulically connected to the basal aquifer during drilling. It is presumed that the confining unit is part of a gradual transition from saprolite to weathered basalt to unweathered basalt. Heads in these wells are matched to a similar level as the Group 1 and 2 wells, with the exception of three outlier wells (RHM(b)(9), RH(b), and RH(b)). The result was a residual mean

of all Group 3 wells of 0.16 ft with a RMSE of 0.35 ft. Discrepancies at RHM(b))(3) are discussed in the context of vertical head differences in Section 2.3.5.4.

Observed water levels and drawdowns in RH(b) and RH(b) exhibit similar behavior in that they did not recover completely during the FOS compared to other basal aquifer wells. RHP01 also exhibits this behavior in conjunction with greater drawdown, though the residual is comparatively lower. Chart 2-4 shows the water levels during the flow optimization study at wells RH(b) (top), RH(b) (bottom). Chart 2-5 shows the water level at RHP(b) and in (b) measured at RHMW(b)(9) during the FOS study as an example of typical behavior where full or near full recovery is achieved between each cycle of the pumping schedule. Water levels in RH(b) and RH(b) decline approximately 0.45 and 0.35 ft over the course of the study, respectively, whereas RHP(b) and RHMW(b)(9) declined approximately 0.05 ft over the course of the study. The lack of full recovery at these three wells is indicative of a subdued hydraulic connection compared to wells with full recovery. It is likely that the lack of full recovery and higher heads are due to a local-scale heterogeneity. The connection is present, as exhibited by the drawdown responses to pumping stresses from (b) , but lack of full recovery is indicative of a slightly smaller degree of hydraulic connection that cannot be fully represented at the current resolution of the model grid. Consequently, the simulated water levels at these wells recover fully between pump cycles.

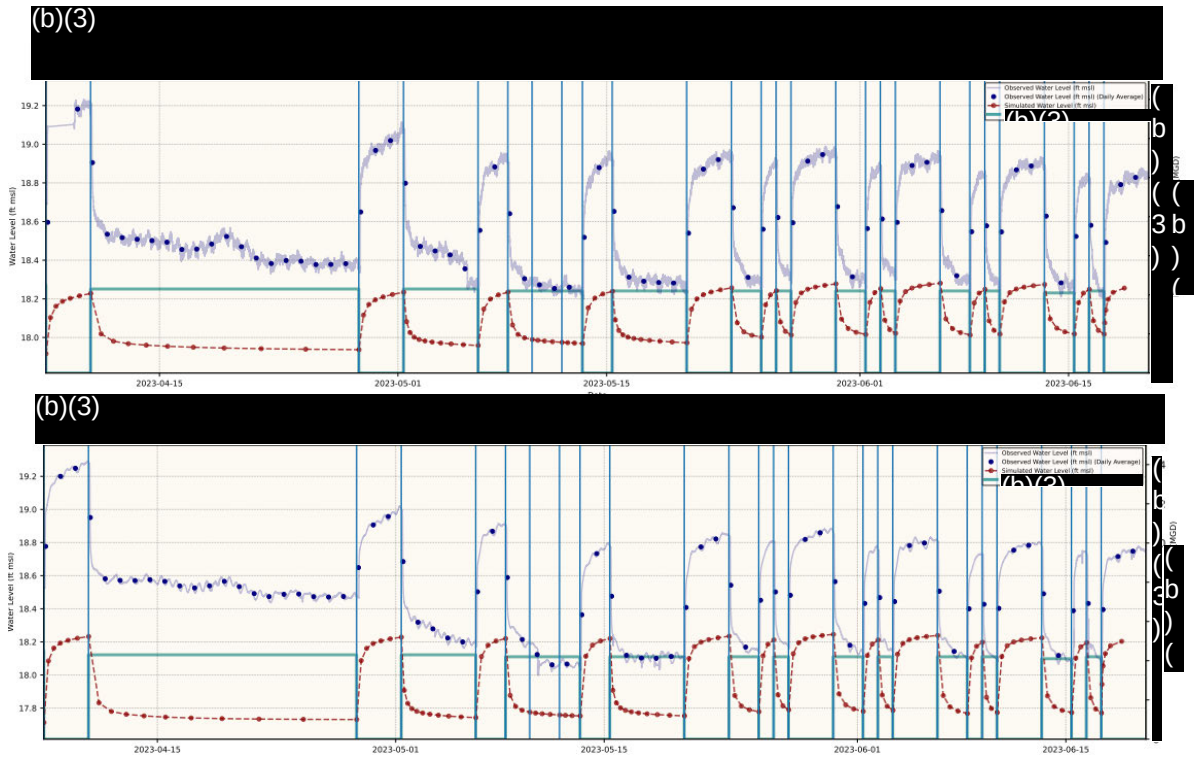

Chart 2-4: Simulated and Observed Water Levels During the Flow Optimization Study at RH(b) (top), and RH(b) (bottom) Showing a Lack of Full Recovery Between Pump Cycles

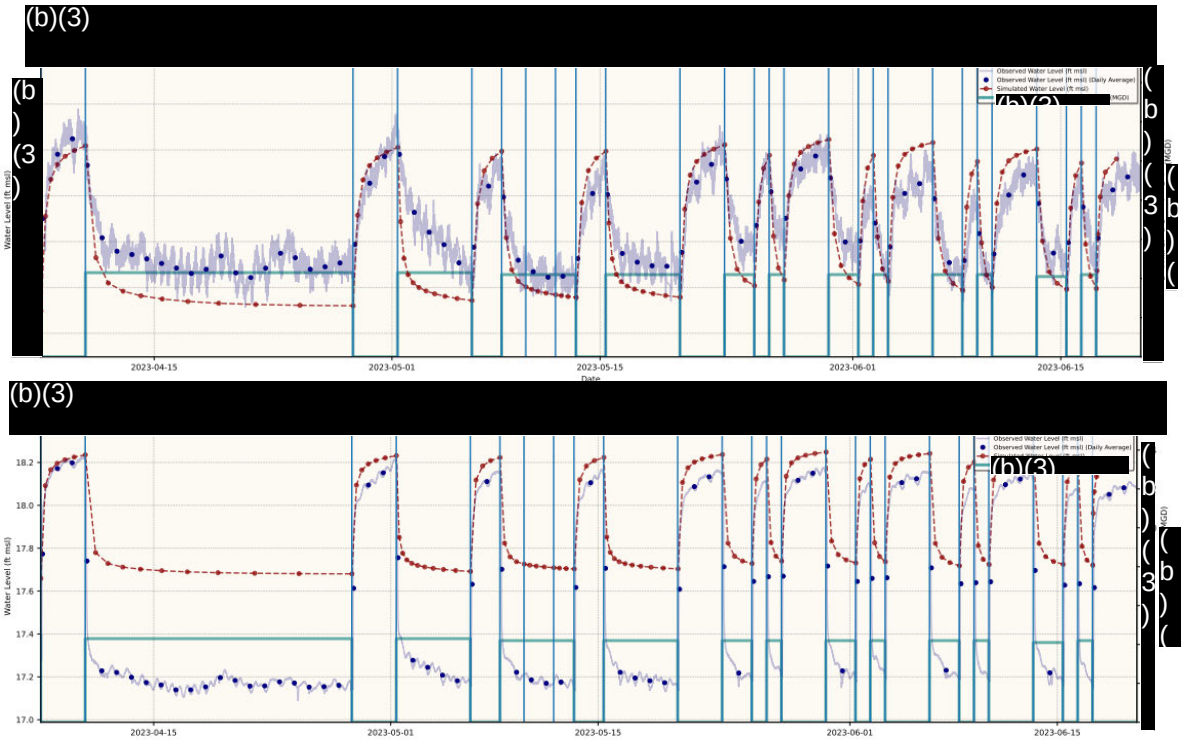

Chart 2-5: Simulated and Observed Water Levels During the Flow Optimization Study at RHP(b) (top) and RHMW(b)(9) (bottom) Showing an Example of a Well with Full Recovery Between Pump Cycles

Group 5 wells are wells screened in saprolite or in confining unit conditions with highly variable and significantly elevated heads; however, during drilling these wells did not appear to be perched above the water table. These wells did not appear to be in close hydraulic communication with the basal aquifer. An example of the lack of hydraulic connection is RHM(b) , which was believed during construction to be screened in the basal aquifer but maintains a head of approximately 4.5 ft higher than the underlying basal aquifer and exhibits a muted response to pumping rate changes at (b) compared to what would be expected if it were screened fully in the basal aquifer, as evidenced by responses at nearby RHM(b) . Other wells in this group generally have heads higher than at RHM(b) and exhibit similar muted or non-responses to pumping rate changes. Simulation of the saprolite and confining unit was considered to be more important conceptually as effectively a no-flow barrier adjacent to the basal aquifer. Accurate simulation of the highly variable heads in this unit would have required significant effort and finer grid discretization with little to no impact on groundwater flow in the basal aquifer. For Group 5 wells, the residual mean was 41.49 ft and the RMSE was 51.48 ft.

2.3.5.2 SCATTER PLOTS OF SIMULATED AND OBSERVED HEADS

Scatter plots comparing simulated groundwater elevations to observed elevations are often used as an assessment of model calibration. Where simulated elevations exactly match the observations, the point falls along a central diagonal line. If points deviate from the line, the plotted points should spread equally above and below the perfect match line with no apparent bias. The simulated versus observed heads are presented on scatter plots and divided into 2017/2018 basal aquifer heads (Chart 2-6), 2021/2022 basal aquifer heads (Chart 2-7), 2023 FOS basal aquifer wells (Chart 2-8), and combined basal aquifer heads (Chart 2-9).

Additional scatter plots are also included in Appendix D. In all plots, grayed-out heads belong to Group 3, blacked-out heads belong to Group 4, while Group 5 heads are not plotted because of their relatively lower importance and significantly greater ranges compared to the basal aquifer heads. Dashed lines show error of 0.3 ft (blue), 0.6 ft (yellow), and 0.9 ft (red).

Many of the plotted points on the four scatter plots fall around the idealized perfect match line without bias. The 2017/2018 heads on Chart 2-6 show good matches with most points falling between the lines of 0.3 ft residual except for several points at lower elevations, all of which correspond to the drawdown within Hālawa Shaft where observed drawdown was slightly greater than simulated. No other wells are in close proximity to this location, and limited geological information limits the ability to closely calibrate the model in this area, particularly with a homogeneous regional model. The 2021/2022 heads on Chart 2-7 exhibit a larger spread around the perfect match line, while the slope of the points is similar to the perfect match line, indicating that the drawdown responses are matching well, but the magnitude of the residuals is slightly larger as compared to the 2017/2018 data. The FOS heads (Chart 2-8) appear to show a more rounded cluster around the perfect match line, but this is primarily due to a larger number of wells in a smaller area compared to the other study periods.

Combining the data into a single scatter plot (Chart 2-9) demonstrates the same overall behavior as the individual plots, where the most significant outlier heads either in residual magnitude or behavior are those measured in Hālawa Shaft, which is not unexpected due to fewer data points in the area of Hālawa Shaft and uniform model parameters that are focused on matching local Red Hill wells.

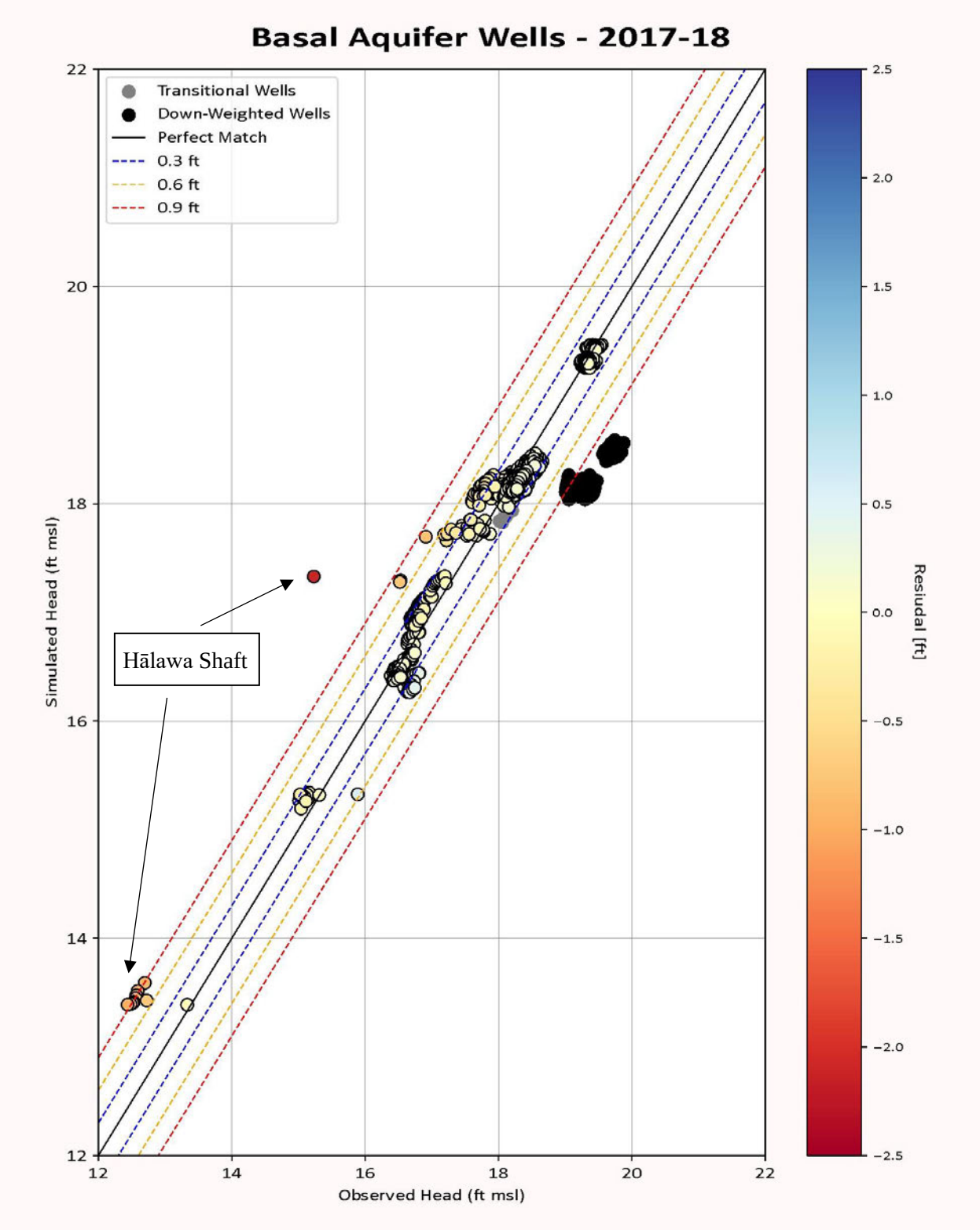

Chart 2-6: Simulated and Observed Heads for 2017/2018 Data

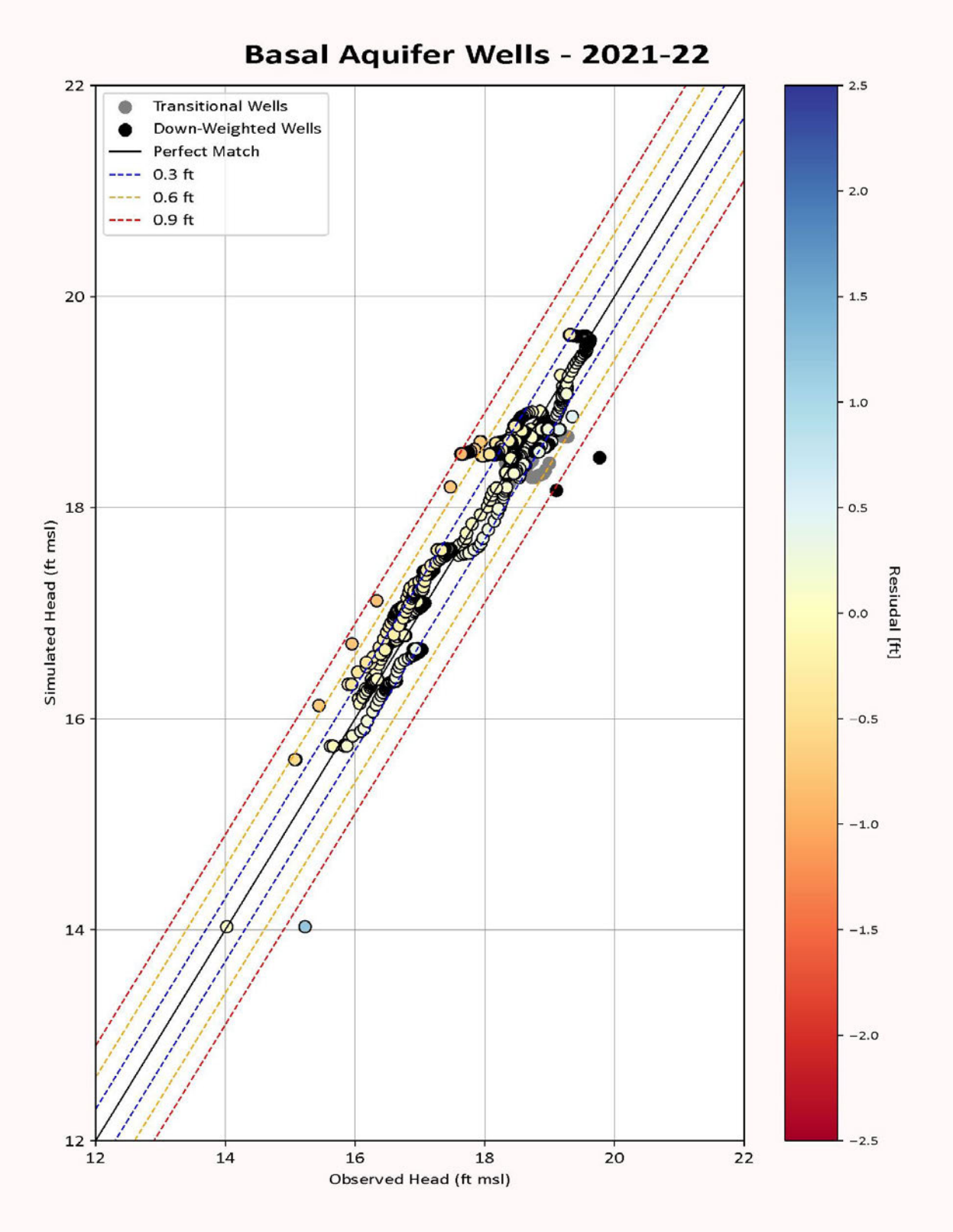

Chart 2-7: Simulated and Observed Heads for 2021/2022 Data

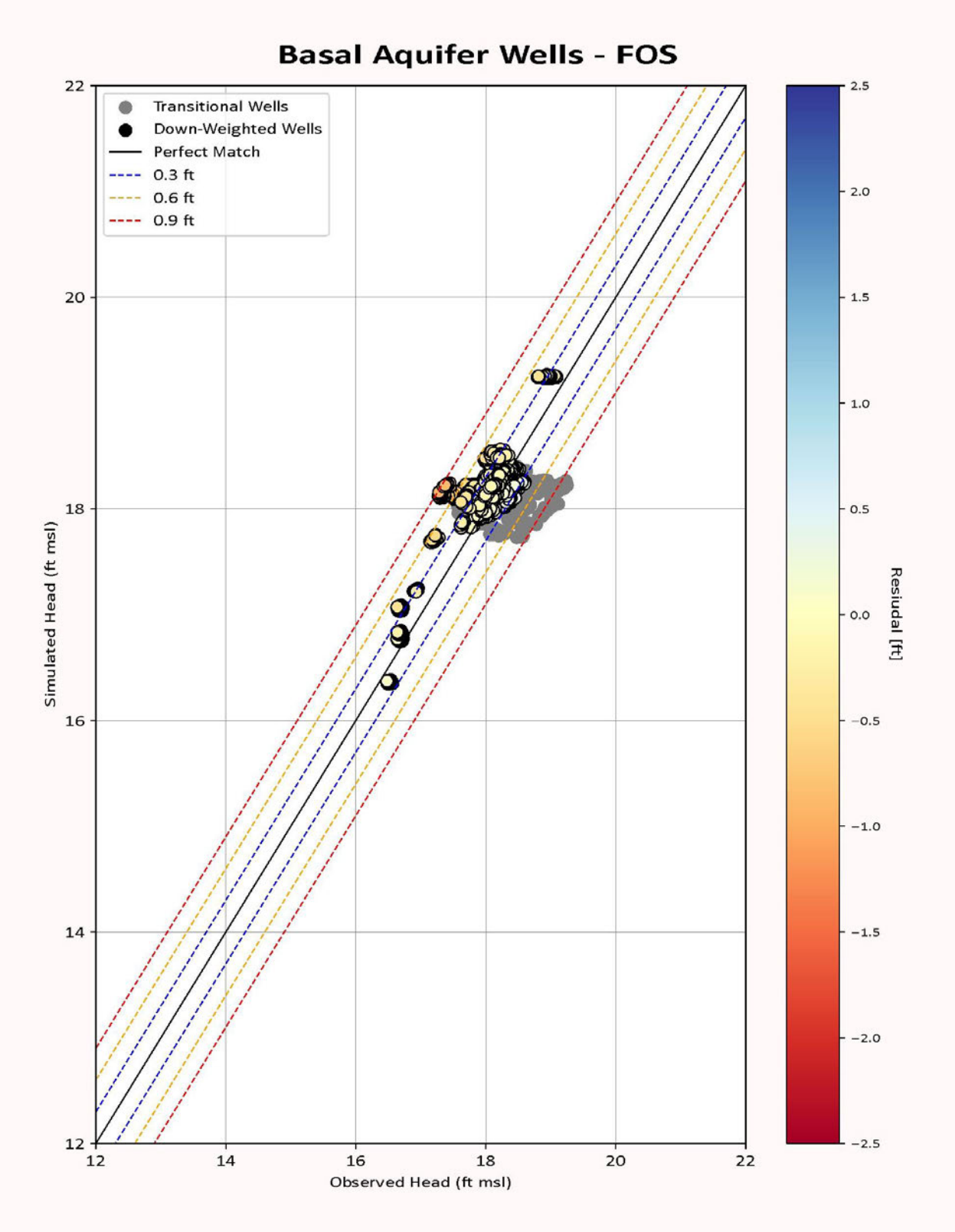

Chart 2-8: Simulated and Observed Heads for FOS

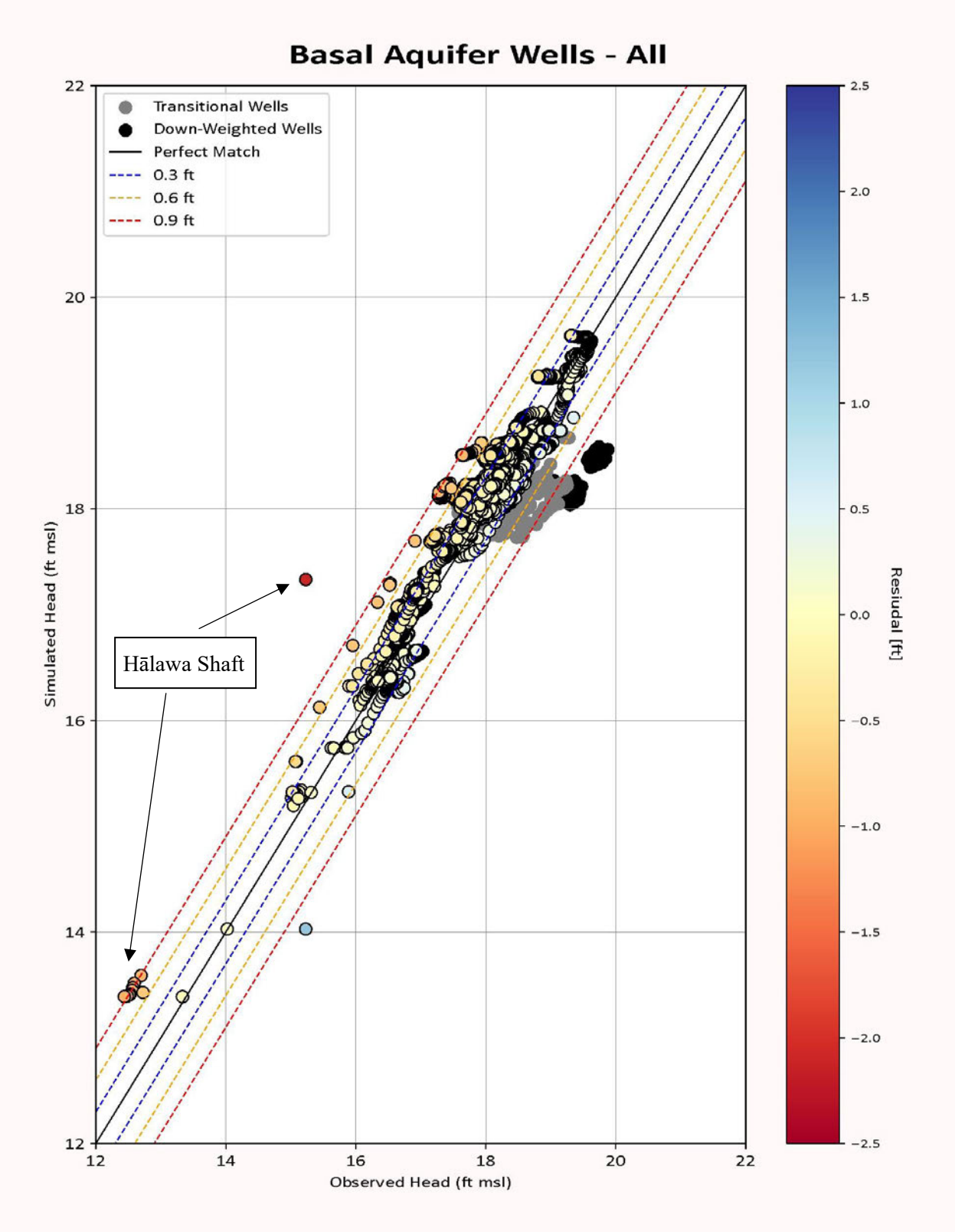

Chart 2-9: Simulated and Observed Heads for All Time Periods

2.3.5.3 GRADIENTS ALONG RED HILL RIDGE

Gradient magnitudes along Red Hill ridge were compared by plotting simulated and observed heads against distance from (b), which are presented in Appendix D. For each stress period, two sets of plots were constructed: 1) wells along Red Hill ridge, including RHM(b), RHM(b), RHM(b), RHM(b), and 2) RHM(b) and to the northwest of Red Hill ridge, including RHM(b), RHM(b)(9), RHM(b), and RHM(b). A separate plot was made for each of four stress periods and each plot uses the last water level measurement within the respective stress period for comparison. Only stress periods where enough data were available to construct the plots are presented, which included 35 of the 44 model stress periods. Linear regression trend lines were fit through the data points to compare simulated and observed gradient magnitudes. Gradient magnitudes from two example stress periods are shown in Chart 2-10 and Chart 2-11. This calibration metric focuses on the component of the gradient along a fixed direction (down the ridge, aligned with the dip azimuth) that does not represent the primary direction of the hydraulic gradient, which is generally to the northwest.

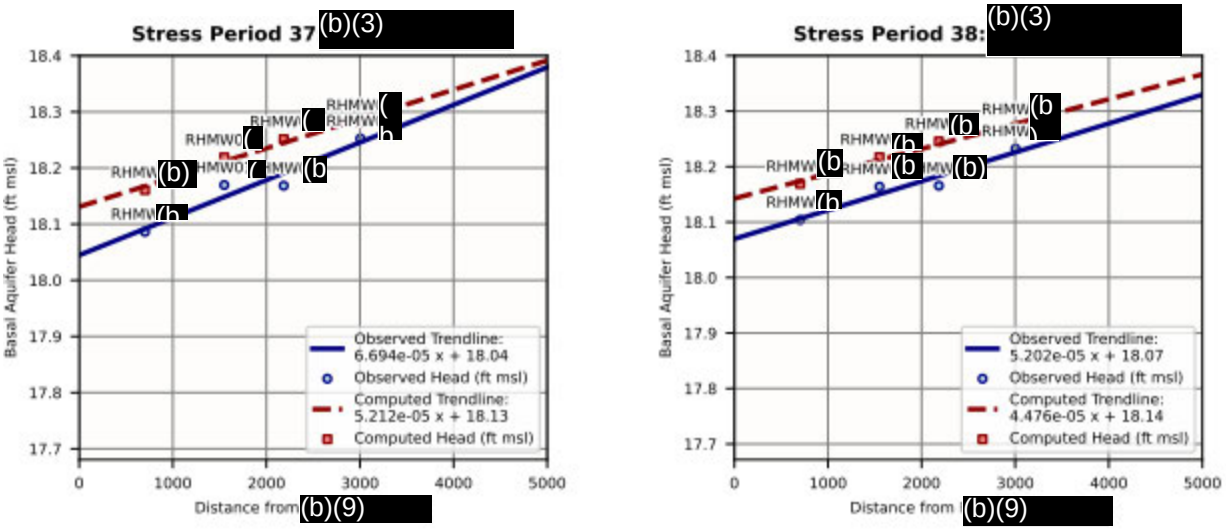

Chart 2-10: Examples of Hydraulic Gradients Along Red Hill Ridge

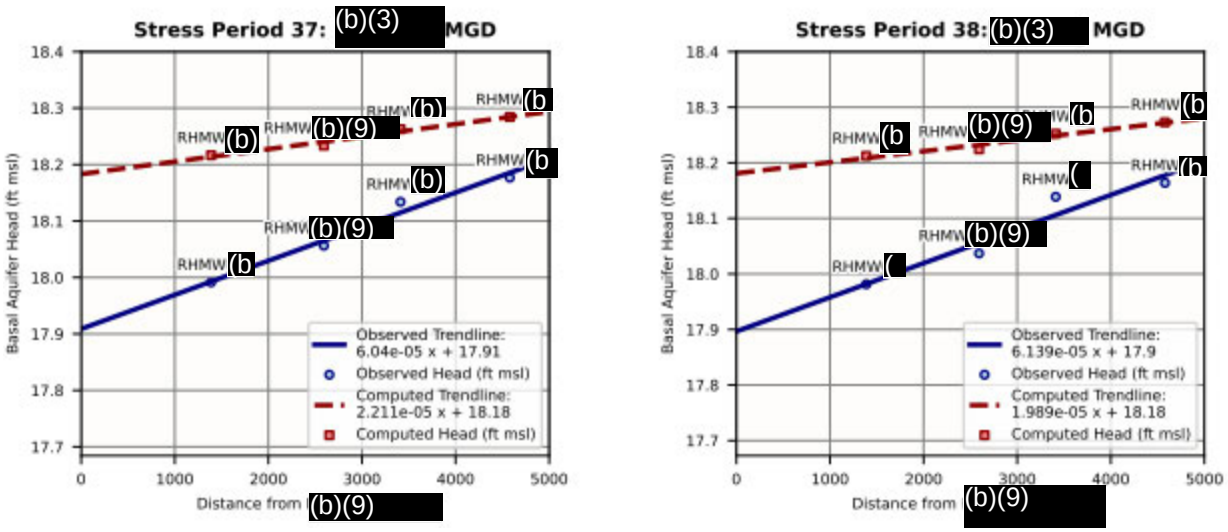

Chart 2-11: Hydraulic Gradients Northwest of Red Hill Ridge

Gradient magnitudes along Red Hill ridge were simulated to match the observed gradient magnitudes relatively well or were slightly steeper down the ridge than observed. Gradient magnitudes calculated from measured heads ranged from 5.7×10^{-6} to 6.7×10^{-5} ft/ft, and simulated gradient magnitudes ranged from 2.2×10^{-5} to 8.0×10^{-4} ft/ft. Average simulated and observed gradient magnitudes were 3.1×10^{-5} and 4.1×10^{-5}, respectively.

Gradient magnitudes northwest of Red Hill ridge were simulated to match the observed gradient magnitudes very closely, or were slightly flatter down the ridge than observed except in three Stress Periods 2, 18, and 28, where observed gradient magnitudes appeared to reverse up the ridge, which was not captured by the simulations. Gradient magnitudes calculated from measured heads ranged from -1.2×10^{-5} to 8.3×10^{-5} ft/ft, and simulated gradient magnitudes ranged from 7.5×10^{-6} to 3.3×10^{-5} ft/ft. Average simulated and observed gradient magnitudes were 3.8×10^{-5} and 1.8×10^{-5}, respectively.

2.3.5.4 HEAD DIFFERENCE TARGETS

Horizontal head difference targets were calculated between three wells along the axis of the tank farm including RHM(b) , RHM(b) , RHM(b) and other combinations of monitoring wells. The mean residual between simulated and observed head differences was 0.08 ft with an RMSE of 0.23 ft. The scaled root mean square error was 3.2%, with a correlation coefficient of 0.95. Plots for each well by stress period are located in Appendix D. The plots generally follow the trend of the perfect match line, with some variability due to the small differences in heads.

Vertical head difference targets were evaluated by comparing the uppermost basal aquifer well within West Bay wells and other nested wells to each successive lower well. Table 2-13 summarizes the average simulated and observed differences at each monitoring well over the 44 stress periods of the calibration model. At locations RHM(b) , RHM(b) , and RHM(b) , the direction of the vertical head differences is matched correctly, although the computed model magnitudes of the differences are generally smaller than the observed values. Observed vertical head differences at RHM(b) exhibit a varying pattern with upward gradient from Zone (to Zone(b) with a 0.5-ft head difference, but downward gradient from Zone(b) to the

three lowest zones. Computed vertical differences show a consistent, but small, upward gradient in between each zone. Because the model was unable to replicate the varying pattern of the head differences, the calibration resulted in head differences that balanced the upward and downward gradients. Vertical head differences at RHP(b), (and (b were very small, which was generally well simulated; however, the observed direction was nearly neutral at 0.01 ft downward, whereas the computed direction was slightly upward at 0.04 to 0.05 ft. Plots of vertical head differences are presented in Appendix D. Additional vertical head data will become available following installation of the RHP(b/RHP(b) /RHP(b) cluster. Data from this cluster (being installed at this time of this report) may be useful in future modeling.

Table 2-13: Summary of Simulated and Observed Vertical Head Differences

Upper Well	Lower Well	Observed (ft)	Observed Direction	Computed (ft)	Computed Direction	Residual (ft)	Direction Match
RHM[redacted]-(b)(9)	RHM[redacted]	0.11	↓	0.05	↓	0.06	Yes
	RHM[redacted]	0.29	↓	0.07	↓	0.22	Yes
	RHM[redacted]	0.23	↓	0.09	↓	0.15	Yes
	RHM[redacted]	0.47	↓	0.1	↓	0.38	Yes
RHM[redacted](b)(9)	RHM[redacted]	0	↑	-0.01	↑	0.01	Yes
	RHM[redacted]	0.04	↓	0.01	↓	0.03	Yes
	RHM[redacted]	0.15	↓	0.02	↓	0.13	Yes
	RHM[redacted]1	0.3	↓	0.02	↓	0.27	Yes
RHM[redacted]-(b)(9)	RHM[redacted]	0.47	↓	0.08	↓	0.39	Yes
	RHM[redacted]	0.31	↓	0.08	↓	0.22	Yes
RHM[redacted]-(b)(9)	RHM[redacted]	-0.5	↑	-0.01	↑	-0.48	Yes
	RHM[redacted]	0.13	↓	-0.06	↑	0.19	No
	RHM[redacted]	0.39	↓	-0.07	↑	0.46	No
	RHM[redacted]1	0.52	↓	-0.11	↑	0.63	No
RHP[redacted]	RHP[redacted]	0.04	↓	-0.01	↑	0.04	No
	RHP[redacted]	0.04	↓	-0.01	↑	0.05	No

2.3.5.5 COMPARISON TO WATER LEVEL AND DRAWDOWN HYDROGRAPHS

Appendix D presents hydrographs of simulated and observed hydrographs over time. A good model calibration is indicated when the simulated heads over time (represented by the red dashed line) approximate observed water level data (represented by the solid light blue line). Blue dots represent daily averaged heads used as calibration targets. Matching heads helps ensure that the model reasonably represents flow directions and gradients over time. Drawdown plots illustrate the aquifer responses to pumping rate changes. Drawdown was calculated by subtracting the initial simulated head at the reference stress periods indicated in Table 2-7 from the simulated head at subsequent time steps until the next drawdown reference head. Matching drawdown values helps demonstrate that the estimated hydrogeologic properties of the basal aquifer are representative.

Most of calibration assessment focuses on heads in wells near the Facility; however, reasonable representation of gradients is also necessary to reproduce the regional and local groundwater flow fields and water budget. Regional monitoring wells include Manaiki T24, Moanalua Deep, TAMC MW2, Hālawa TZ, ʻAiea Bay, Kaʻāmilo Deep, Hālawa T45, [redacted] Regional monitoring wells generally show muted responses to pumping, which is generally well represented in the model as evidenced by the hydrographs in Appendix D. Also, the average residual at each monitoring well plotted on Figure 2-15 shows no significant bias or trend in average residuals across the domain.

Heads at wells within the vicinity of the Facility generally match the magnitude and trend of the heads and drawdown plots, although the average drawdown residual is approximately 0.09 ft smaller than observed. Heads within (b) itself fluctuate significantly due to cyclic pumping; therefore, daily averages were used in the calibration.

2.3.5.6 Comparison to Conceptual Water Budget

The simulated water budget at the end of each stress period was compared to the conceptual water budget calculations, as shown in Table 2-14. Both the conceptual and simulated water budgets are presented for the last time step of each stress period along with the difference between the two. Values highlighted in blue indicate simulated values lower than conceptual estimates, and values highlighted in orange indicate simulated values higher than conceptual estimates. Cells highlighted in gray are intended to indicate transition from the block of cells associated with a specific stress period compared to another. All results fall within approximately ±5%, which can be calculated by dividing the "Difference" row of the "Total Outflows (mgd)" column for each stress period by the "Conceptual" row. The most significant exceptions include Stress Periods 3 and 16, which have a discrepancy of 8.8%. This is within the accuracy of the water budgets' estimate and aligns the flow model with the conceptual model.

Table 2-14: Comparison of Conceptual and Simulated Water Budgets

Type	Stress Period	Recharge (mgd)	Dike Region Inflows (mgd)	Well Discharge (mgd)	Spring Discharge (mgd)	Caprock Discharge (mgd)	Inflow from Adjacent Watershed (mgd)	Outflow to Adjacent Watershed (mgd)	Storage (mgd)	Total Inflows (mgd)	Total Outflows (mgd)
Conceptual	1	32.4	26.1	33.4	13.6	2.3	3	12.2	-	61.5	61.5
Simulated	1	32.3	26.1	33.4	13.5	3.7	6.3	14.1	0.0	64.7	64.7
Difference	1	-0.1	0.0	0.0	-0.1	1.4	3.3	1.9	-	3.2	3.2
Conceptual	2	32.4	26.1	28.5	13.6	2.3	3.0	17.1	-	61.5	61.5
Simulated	2	32.3	26.1	28.5	14.1	3.7	4.6	15.1	-1.6	63.0	63.0
Difference	2	-0.1	0.0	0.0	0.5	1.4	1.6	-2.0	-	-1.5	-1.5
Conceptual	3	32.4	26.1	36.1	13.5	2.3	3	9.5	-	61.5	61.4
Simulated	3	32.3	26.1	36.1	13.4	3.7	6.7	14.0	2.1	67.3	67.3
Difference	3	-0.1	0.0	0.0	-0.1	1.4	3.7	4.5	-	5.8	5.9
Conceptual	4	32.4	26.1	32.4	13.5	2.3	3.0	13.2	-	61.5	61.4
Simulated	4	32.3	26.1	32.4	13.6	3.7	6.1	14.3	-0.4	64.5	64.5
Difference	4	-0.1	0.0	0.0	0.1	1.4	3.1	1.1	-	-3.0	-3.1
Conceptual	5	32.4	26.1	25.8	13.7	2.3	4.9	21.6	-	63.4	63.4
Simulated	5	32.3	26.1	25.8	15.2	3.7	5.3	17.3	-1.7	63.7	63.7
Difference	5	-0.1	0.0	0.0	1.5	1.4	0.4	-4.3	-	0.3	0.3
Conceptual	6	32.4	26.1	22.8	13.8	2.3	4.9	24.5	-	63.4	63.4
Simulated	6	32.3	26.1	22.8	15.5	3.7	4.3	18.0	-2.7	62.8	62.8
Difference	6	-0.1	0.0	0.0	1.7	1.4	-0.6	-6.5	-	0.6	0.6
Conceptual	7	32.4	26.1	26.2	13.9	2.3	4.9	21	-	63.4	63.4
Simulated	7	32.3	26.1	26.2	15.5	3.7	4.4	18.1	0.8	63.6	63.6
Difference	7	-0.1	0.0	0.0	1.6	1.4	-0.5	-2.9	-	0.2	0.2
Conceptual	8	32.4	26.1	37.3	13.6	2.3	4.9	10.2	-	63.4	63.4
Simulated	8	32.3	26.1	37.3	13.0	3.7	7.0	13.1	1.8	67.2	67.2
Difference	8	-0.1	0.0	0.0	-0.6	1.4	2.1	2.9	-	-3.8	-3.8
Conceptual	9	32.4	26.1	36	13.6	2.3	4.9	11.4	-	63.4	63.3
Simulated	9	32.3	26.1	36.0	13.0	3.7	7.1	12.9	0.2	65.7	65.7
Difference	9	-0.1	0.0	0.0	-0.6	1.4	2.2	1.5	-	2.3	2.4
Conceptual	10	32.4	26.1	31.2	13.7	2.3	4.9	16.2	-	63.4	63.4
Simulated	10	32.3	26.1	31.2	13.6	3.7	6.9	13.9	-2.8	65.3	65.3
Difference	10	-0.1	0.0	0.0	-0.1	1.4	2.0	-2.3	-	-1.9	-1.9
Conceptual	11	32.4	26.1	31.7	13.9	2.3	4.2	14.8	-	62.7	62.7
Simulated	11	32.3	26.1	31.7	1.3	3.7	2.9	24.6	0.0	61.3	61.3
Difference	11	-0.1	0.0	0.0	-12.6	1.4	-1.3	9.8	-	-1.4	-1.4
Conceptual	12	32.4	26.1	33.1	12.6	2.3	2.9	13.5	-	61.4	61.5
Simulated	12	32.3	26.1	33.1	1.1	3.7	3.0	23.4	-0.2	61.4	61.4
Difference	12	-0.1	0.0	0.0	-11.5	1.4	0.1	9.9	-	0.0	0.1
Conceptual	13	32.4	26.1	21.4	12.9	2.3	2.9	24.9	-	61.4	61.5
Simulated	13	32.3	26.1	21.4	1.8	3.7	1.7	27.5	-5.7	60.1	60.1
Difference	13	-0.1	0.0	0.0	-11.1	1.4	-1.2	2.6	-	-1.3	-1.4
Conceptual	14	32.4	26.1	21.4	13.4	2.3	2.9	24.4	-	61.4	61.5
Simulated	14	32.3	26.1	21.4	11.8	3.7	1.2	22.2	-0.5	59.6	59.6
Difference	14	-0.1	0.0	0.0	-1.6	1.4	-1.7	-2.2	-	1.8	1.9
Conceptual	15	32.4	26.1	21.6	13.9	2.3	2.8	23.5	-	61.3	61.3
Simulated	15	32.3	26.1	21.6	20.8	3.7	2.5	14.5	-0.3	60.9	60.9
Difference	15	-0.1	0.0	0.0	6.9	1.4	-0.3	-9.0	-	-0.4	-0.4
Conceptual	16	32.4	26.1	14.4	13.9	2.3	3.8	31.7	-	62.3	62.3
Simulated	16	32.3	26.1	15.4	21.8	3.7	-1.2	16.2	-0.1	57.2	57.2
Difference	16	-0.1	0.0	1.0	7.9	1.4	-5.0	-15.5	-	5.1	5.1
Conceptual	17	32.4	26.1	23.3	13.6	2.3	4.5	23.8	-	63	63
Simulated	17	32.3	26.1	24.5	12.1	3.7	2.2	20.3	0.0	60.7	60.7
Difference	17	-0.1	0.0	1.2	-1.5	1.4	-2.3	-3.5	-	-2.3	-2.3
Conceptual	18	32.4	26.1	21.5	13.5	2.3	4.1	25.3	-	62.6	62.6
Simulated	18	32.3	26.1	21.5	12.1	3.7	1.2	20.2	-2.2	59.6	59.6
Difference	18	-0.1	0.0	0.0	-1.4	1.4	-2.9	-5.1	-	3.0	3.0
Conceptual	19	32.4	26.1	25.8	13.4	2.3	4.1	21.1	-	62.6	62.6
Simulated	19	32.3	26.1	25.8	11.7	3.7	2.3	19.6	0.1	60.8	60.8
Difference	19	-0.1	0.0	0.0	-1.7	1.4	-1.8	-1.5	-	-1.8	-1.8
Conceptual	20	32.4	26.1	22.4	13.4	2.3	3.8	24.1	-	62.3	62.2
Simulated	20	32.3	26.1	22.4	12.0	3.7	2.0	20.0	-2.3	60.4	60.4
Difference	20	-0.1	0.0	0.0	-1.4	1.4	-1.8	-4.1	-	1.9	1.8
Conceptual	21	32.4	26.1	26.7	13.5	2.3	3.8	19.8	-	62.3	62.3
Simulated	21	32.3	26.1	26.7	11.8	3.7	2.7	19.8	0.8	61.9	61.9
Difference	21	-0.1	0.0	0.0	-1.7	1.4	-1.1	0.0	-	-0.4	-0.4
Conceptual	22	32.4	26.1	22.4	13.4	2.3	3.8	24.2	-	62.3	62.3
Simulated	22	32.3	26.1	22.4	12.0	3.7	2.2	20.0	-2.6	60.6	60.6
Difference	22	-0.1	0.0	0.0	-1.4	1.4	-1.6	-4.2	-	1.7	1.7
Conceptual	23	32.4	26.1	26.6	13.4	2.3	3.8	20	-	62.3	62.3
Simulated	23	32.3	26.1	26.6	11.9	3.7	2.3	20.0	1.5	62.2	62.2
Difference	23	-0.1	0.0	0.0	-1.5	1.4	-1.5	0.0	-	-0.1	-0.1

Type	Stress Period	Recharge (mgd)	Dike Region Inflows (mgd)	Well Discharge (mgd)	Spring Discharge (mgd)	Caprock Discharge (mgd)	Inflow from Adjacent Watershed (mgd)	Outflow to Adjacent Watershed (mgd)	Storage (mgd)	Total Inflows (mgd)	Total Outflows (mgd)
Conceptual	24	32.4	26.1	26.6	13.4	2.3	3.8	20.0	-	62.3	62.3
Simulated	24	32.3	26.1	26.6	11.8	3.7	2.6	19.9	0.9	62.0	62.0
Difference	24	-0.1	0.0	0.0	-1.6	1.4	-1.2	-0.1	-	0.3	0.3
Conceptual	25	32.4	26.1	26.6	13.4	2.3	3.8	20	-	62.3	62.3
Simulated	25	32.3	26.1	26.6	11.8	3.7	2.7	19.8	0.7	61.8	61.8
Difference	25	-0.1	0.0	0.0	-1.6	1.4	-1.1	-0.2	-	-0.5	-0.5
Conceptual	26	32.4	26.1	22.4	13.4	2.3	3.8	24.2	-	62.3	62.3
Simulated	26	32.3	26.1	22.4	12.0	3.7	2.2	20.0	-2.6	60.6	60.6
Difference	26	-0.1	0.0	0.0	-1.4	1.4	-1.6	-4.2	-	1.7	1.7
Conceptual	27	32.4	26.1	26.6	13.4	2.3	3.8	20	-	62.3	62.3
Simulated	27	32.3	26.1	26.6	11.8	3.7	2.7	19.8	0.7	61.8	61.8
Difference	27	-0.1	0.0	0.0	-1.6	1.4	-1.1	-0.2	-	-0.5	-0.5
Conceptual	28	32.4	26.1	22.4	13.4	2.3	3.8	24.2	-	62.3	62.3
Simulated	28	32.3	26.1	22.4	12.0	3.7	1.9	20.1	-2.0	60.3	60.3
Difference	28	-0.1	0.0	0.0	-1.4	1.4	-1.9	-4.1	-	2.0	2.0
Conceptual	29	32.4	26.1	26.6	13.4	2.3	3.8	20	-	62.3	62.3
Simulated	29	32.3	26.1	26.6	11.9	3.7	2.2	20.1	1.8	62.3	62.3
Difference	29	-0.1	0.0	0.0	-1.5	1.4	-1.6	0.1	-	0.0	0.0
Conceptual	30	32.4	26.1	22.4	13.4	2.3	3.8	24.2	-	62.3	62.3
Simulated	30	32.3	26.1	22.4	12.0	3.7	2.1	20.1	-2.3	60.5	60.5
Difference	30	-0.1	0.0	0.0	-1.4	1.4	-1.7	-4.1	-	1.8	1.8
Conceptual	31	32.4	26.1	26.6	13.4	2.3	3.8	20	-	62.3	62.3
Simulated	31	32.3	26.1	26.6	11.9	3.7	2.1	20.1	1.8	62.3	62.3
Difference	31	-0.1	0.0	0.0	-1.5	1.4	-1.7	0.1	-	0.0	0.0
Conceptual	32	32.4	26.1	22.4	13.4	2.3	3.8	24.1	-	62.3	62.2
Simulated	32	32.3	26.1	22.4	12.1	3.7	1.6	20.4	-1.4	60.0	60.0
Difference	32	-0.1	0.0	0.0	-1.3	1.4	-2.2	-3.7	-	2.3	2.2
Conceptual	33	32.4	26.1	27.1	13.4	2.3	2	17.6	-	60.5	60.4
Simulated	33	32.3	26.1	27.1	12.0	3.7	2.6	20.5	2.4	63.4	63.4
Difference	33	-0.1	0.0	0.0	-1.4	1.4	0.6	2.9	-	2.9	3.0
Conceptual	34	32.4	26.1	22.9	13.4	2.3	2.0	21.8	-	60.5	60.4
Simulated	34	32.3	26.1	22.9	12.1	3.7	2.6	20.5	-1.8	61.0	61.0
Difference	34	-0.1	0.0	0.0	-1.3	1.4	0.6	-1.3	-	-0.5	-0.6
Conceptual	35	32.4	26.1	27.1	13.4	2.3	2	17.7	-	60.5	60.5
Simulated	35	32.3	26.1	27.1	12.0	3.7	2.7	20.4	2.2	63.3	63.3
Difference	35	-0.1	0.0	0.0	-1.4	1.4	0.7	2.7	-	2.8	2.8
Conceptual	36	32.4	26.1	22.9	13.4	2.3	2.0	21.8	-	60.5	60.4
Simulated	36	32.3	26.1	22.9	12.2	3.7	2.3	20.6	-1.2	60.7	60.7
Difference	36	-0.1	0.0	0.0	-1.2	1.4	0.3	-1.2	-	-0.2	-0.3
Conceptual	37	32.4	26.1	27.1	13.4	2.3	2	17.7	-	60.5	60.5
Simulated	37	31.7	26.1	27.1	12.0	3.7	2.8	20.4	2.7	63.3	63.3
Difference	37	-0.7	0.0	0.0	-1.4	1.4	0.8	2.7	-	2.8	2.8
Conceptual	38	32.4	26.1	22.9	13.4	2.3	2.0	21.9	-	60.5	60.5
Simulated	38	31.7	26.1	22.9	12.0	3.7	2.8	20.4	-1.5	60.6	57.5
Difference	38	-0.7	0.0	0.0	-1.4	1.4	0.8	-1.5	-	-0.1	3.0
Conceptual	39	32.4	26.1	27.1	13.4	2.3	2	17.7	-	60.5	60.5
Simulated	39	31.7	26.1	27.1	12.0	3.7	2.9	20.3	2.4	63.1	63.1
Difference	39	-0.7	0.0	0.0	-1.4	1.4	0.9	2.6	-	2.6	2.6
Conceptual	40	32.4	26.1	22.9	13.4	2.3	2.0	21.8	-	60.5	60.4
Simulated	40	31.7	26.1	22.9	12.1	3.7	2.4	20.4	-1.0	60.2	60.2
Difference	40	-0.7	0.0	0.0	-1.3	1.4	0.4	-1.4	-	0.3	0.2
Conceptual	41	32.4	26.1	27	13.4	2.3	2	17.8	-	60.5	60.5
Simulated	41	31.7	26.1	27.0	11.9	3.7	2.9	20.3	2.3	63.0	63.0
Difference	41	-0.7	0.0	0.0	-1.5	1.4	0.9	2.5	-	2.5	2.5
Conceptual	42	32.4	26.1	22.9	13.4	2.3	2.0	21.9	-	60.5	60.5
Simulated	42	31.7	26.1	22.9	12.0	3.7	2.9	20.3	-1.7	60.7	60.7
Difference	42	-0.7	0.0	0.0	-1.4	1.4	0.9	-1.6	-	-0.2	-0.2
Conceptual	43	32.4	26.1	27.1	13.4	2.3	2	17.7	-	60.5	60.5
Simulated	43	31.7	26.1	27.1	11.9	3.7	2.9	20.2	2.3	63.0	63.0
Difference	43	-0.7	0.0	0.0	-1.5	1.4	0.9	2.5	-	2.5	2.5
Conceptual	44	32.4	26.1	22.9	13.4	2.3	2.0	21.9	-	60.5	60.5
Simulated	44	31.7	26.1	22.9	12.1	3.7	2.5	20.4	-1.2	60.3	60.3
Difference	44	-0.7	0.0	0.0	-1.3	1.4	0.5	-1.5	-	0.2	0.2

Notes:

	Indicates transition from the block of cells associated with a specific stress period compared to another.
	Comparison of direct input values to model, always equal to zero.
	Simulated values are greater than conceptual estimates.
	Simulated values are less than conceptual estimates.

Several components of the water budget inform model boundary inputs, including recharge, dike region inflow, and well discharge. Changes in storage were not considered in the conceptual water budget calculations because they rely on water level changes over the entire domain, which are not easily estimated, and its interpretation is obscured by other stress changes. Overall storage changes are a relatively small component of the water budget and within the error bracketing the water budget estimates. The transient model simulations do include storage changes and confirm that they are a relatively small portion of the water budget by the end of each stress period.

Discharge to Pearl Harbor and the Pacific Ocean through the caprock was estimated to be 2.3 mgd, primarily due to recharge on the caprock in the conceptual water budget estimate, which is in close agreement with simulated values. Inflow from the southeast and outflow to the northwest were calculated during the simulation. Inflow from the southeast was estimated to range from 2.8 to 4.9 mgd, whereas simulated values ranged from -1.2 to 7.1 mgd. Such deviations from the conceptual water budget estimates were considered reasonable given the epistemic uncertainty in the assumptions associated with the water budget estimates. Also, the majority of calibration targets correspond to stress periods where the water budget is closely matched. Acceptance of these estimated water budget discrepancies allowed the model calibration process to reach better agreement with measured data such as heads and drawdowns in wells.

2.3.6 Evaluation of Source Water with Chloride and Temperature Data

Chloride concentration and temperature data were considered in evaluation of water sources to (b) and Hālawa Shaft. Generally, higher chloride concentrations and temperatures are attributed to source water in the region downslope of the Facility, whereas lower chloride concentrations and temperatures are attributed to source water from the upslope region including from the dike complex, although some basal wells, including RHM(b) , RHM(b) , RHM(b) , RH(b) , RHP(b) , RH(b) and RH(b) , typically see elevated chloride concentrations. The updated analysis presented here incorporates feedback included in DOH's letter of November 1, 2023, responding to the Navy's proposal to reduce the pumping rate at (b) .

To estimate the contribution from each source of water to the water supply shafts, simulations were conducted by assigning a hypothetical concentration value to each contributing source boundary condition in separate steady-state simulations. After post-processing of the results, the final concentration at each shaft in each simulation represents the percentage of water derived from each boundary condition. All unit source simulations were completed with (b) pumping at (mgd and Hālawa Shaft at 12 mgd. Sources of water in the model were recharge (divided into northern and southern zones), dike region inflow, the southeast GHB, and the freshwater/saltwater interface. Localized sources of higher chloride are not included.

The Prescribed Concentration Boundary (PCB) package in the MODFLOW-USG Transport code was used to assign the specified concentrations. The Density Dependent Flow (DDF) package in the MODFLOW-USG Transport code was used when performing all unit source simulations.

In post-processing of the model results, the percentage of water from each boundary condition was assigned an estimated chloride or temperature value based on available data. A weighted average concentration was calculated using the assigned value and percentage of contribution to estimate the chloride concentration

and temperature in both water supply shafts. Simulated values were then compared to measured chloride concentrations and temperature within each shaft.

The simulations that considered boundary contributions to the two water supply shafts required adjustments to the model setup to account for potential contributions from the freshwater/saltwater interface. In the calibration model, the freshwater/saltwater interface was assumed to be a no-flow boundary; however, for all unit source concentration simulations, an additional layer was added along the bottom of the model where GHBs were implemented. The GHB heads were assigned values equal to the simulated heads without the GHBs present. In the simulations, density-dependent flow was incorporated to improve the representation of the physics of high-salinity groundwater flow. The DDF package simulation parameters were assigned values that caused the GHB cells to emit simulated salty water, with a density halfway between fresh and sea water. This allowed for assessment of the significance of potential migration from near the freshwater/saltwater interface to the water development shafts.

Density-dependent flow from the bottom-layer GHBs was simulated during each unit source simulation. This was achieved by first assigning the freshwater/saltwater interface a concentration of 100, representing both 50% saltwater and a 100 percent contribution of source water to the shafts for the initial simulation. Test simulations in which density-dependent flow was deactivated for the freshwater/saltwater interface simulation resulted in substantial changes to the results, compared to when density-dependent flow was activated for the simulation. Density effects were included in the simulations for the other water sources by assuming that a density equal to 0.5% of seawater (i.e., 1% of the freshwater/saltwater interface density) would have a negligible impact on results, and sequentially assigning a concentration of 1 at those sources. The result of the initial freshwater/saltwater interface simulation was subtracted from the results of subsequent simulations, and those differences were multiplied by 100 to scale up to percent contribution to the shafts from the relevant water sources. Summing the simulated contributions from all water sources at each shaft resulted in a contribution of 100 percent, indicating that all simulated source water was accounted for in the unit source simulations.

Chloride

Chloride concentrations were estimated based on the rainfall, runoff, and recharge rates defined in the USGS recharge coverage for Oʻahu (Engott et al. 2017).Visher and Mink (1964) state that the chloride concentration in Honolulu coastal rainfall varied from 3.0 to 29 milligrams per liter (mg/L) for an average value of 16 mg/L. Average chloride concentration in the upland areas in the Kīpapa drainage basin, located to the northwest of the model domain, was 6.5 mg/L, making 11 mg/L a representative rainfall concentration. Assuming that chloride is a conservative species, the chloride concentration of the recharging water can be approximated by:

$$Chloride_{recharge}\left[\frac{mg}{l}\right] = 11\ \left[\frac{mg}{l}\right] * \frac{(rainfall\ \left[\frac{in}{yr}\right] - runoff\ \left[\frac{in}{yr}\right])}{recharge\left[\frac{in}{yr}\right]}$$

Where recharge is the difference between rainfall and runoff minus evapotranspiration, so that the calculated recharge chloride concentration is always greater than the rainfall chloride concentration. This method was applied to the USGS recharge, calculating an area-weighted average for northern and southern

zones at an elevation of approximately 500 ft msl (Figure 2-16), resulting in an average chloride concentrations in recharge of approximately 104 mg/L in the southern recharge area south of the Facility. Chloride concentrations in recharge gradually decrease in the northerly direction toward the dike region, resulting in average recharge chloride concentrations of approximately 25 mg/L for the northern zone. The dike region was assigned a chloride concentration of 15 mg/L, which results from application of this method to the rainfall concentration in the dike region. As recommended in the November 1, 2023 letter from DOH, the GHBs to the southeast were assigned a chloride concentration of 60 mg/L as the average of the Kamehameha School B Well (41.1 mg/L) and the Kalihi Pump Station (80.9 mg/L; Table D2 in Hunt Jr. 2004). The freshwater/saltwater interface representing the bottom of the model was derived from the 50% chloride concentration of seawater, or 9,500 mg/L, as simulated by Oki (2005). This value was assigned to the freshwater/saltwater interface.

Temperature

Temperature of water in the rainfall, infiltration, and groundwater flow cycle is generally the lowest in rainfall, and changes thereafter lead to higher temperatures (Visher and Mink 1964). Groundwater temperature is generally correlated to average atmospheric temperature, with groundwater coolest at higher elevations, and groundwater temperature gradually increasing as elevation decreases. The temperature of groundwater in the dike region is the coolest and was assigned a temperature of 19 degrees Celsius (°C) based on DLNR 2023 well data[5] and on average annual temperature. Average annual temperature at the Facility is approximately 24 °C. Given that much of the recharge and the southeast GHBs are located in the area between the dike region and the Facility, temperatures between the bounding values of 19 and 24 °C were assumed. The northern recharge zone was assigned a temperature of 20 °C, the southeast GHB was assigned 21 °C, and the southern recharge zone was assigned 22 °C. The freshwater/saltwater interface was assigned a temperature of 23 °C based on temperature profiles of HDMW2253-03.

Results

The resulting source contribution percentages from the unit concentration simulations, their associated chloride concentration and temperature assumptions, as well as the flow-weighted average of each, are shown in Table 2-15 and Table 2-16. The simulation demonstrates that chloride concentrations in either shaft can be dominated by a relatively small proportion (1.2% to 2.0%) of source water attributed to migration from near the freshwater/saltwater interface, while temperature is much less sensitive to freshwater/saltwater interface contributions and primarily is driven by the coolest water flowing into the model domain from the dike region and northern recharge zone. Figure 2-17 shows a plan view of the unit concentration source simulation for the freshwater/saltwater interface in Layer 18 where Hālawa Shaft is primarily located, demonstrating the effects of pumping on the potential chloride distribution in groundwater. Where no concentrations are shown to the southwest, Layer 18 has descended below the

[5] https://dlnr.hawaii.gov/cwrm/groundwater/wellinfo/

freshwater/saltwater interface and is inactive in the simulation. To the northeast of the color flood, percentage contribution from the unit concentration is below 1%.

Table 2-15: Simulated (b) Source Water Contribution

Source	% Contribution	Chloride (mg/L)	Temperature (°C)
Rainfall Recharge, North	8.2%	25	20
Rainfall Recharge, South	19.0%	104	22
GHB Southeast	71.2%	60	21
Dike Region	0.4%	30	19
Freshwater/saltwater interface	1.2%	9,500	23
	Weighted Average	179	21.1

Table 2-16: Simulated Hālawa Shaft Source Water Contribution

Source	% Contribution	Chloride (mg/L)	Temperature (°C)
Rainfall Recharge, North	33.8%	25	20
Rainfall Recharge, South	7.9%	104	22
GHB Southeast	25.3%	60	21
Dike Region	30.7%	30	19
Freshwater/saltwater interface	2.0%	9,500	23
	Weighted Average	226	20.2

Comparisons of observed and simulated chloride concentrations and temperature are shown in Table 2-17. The observed average chloride concentration at Hālawa Shaft is approximately 152 mg/L (EPA Region 9 and DOH 2023). Observed average temperatures at (b) and Hālawa Shaft are 20.9 °C and 20.3 °C, respectively.

Table 2-17: Comparison of Observed and Simulated Chloride Concentration and Temperature

	Chloride (mg/L)		Temperature (°C)	
Supply Well	Observed	Simulated	Observed	Simulated
(b)	98	179	20.9	21.1
Hālawa Shaft	152	226	20.3	20.2

Chloride concentrations at (b) were derived from 27 specific conductivity measurements collected while (b) was pumping. Specific conductivity measurements ranged from 500 µS/cm to 600 µS/cm, yielding chloride concentrations of 72 mg/L to 98 mg/L. Four of the 27 specific conductivity measurements (15%) shared the minimum value of 500 µS/cm and fourteen samples (52%) shared the maximum specific conductivity value of 600 µS/cm. This data distribution suggests that some as-yet-unknown mechanism

constrains the reported values to between 500 and 600 µS/cm. The maximum value (98 mg/L of chloride, or 600 µS/cm) was used when computing flow-weighted average chloride concentrations at (b) because that value represents over half of the measurements. The truncated data distribution suggests that the true average chloride value at (b) during pumping could be higher than 98 mg/L. The unusual statistical distribution of chloride and the possibility of a higher average value should be considered when interpreting the comparisons below.

Source water to Hālawa Shaft primarily comes from upslope regions, consistent with the colder temperatures seen in the shaft. A total of 64.5% of the water is simulated to come from either the dike region or the upslope region between the dike complex and the shaft itself. Furthermore, the 25.3 percent of water that enters from the southeast GHB comes mostly from the upslope region, because much of the model boundary flow is limited by valley fill and weathered basalt. Only in the most upslope regions are the weathering and valley fill not present or above the water table. In that upslope region, it is likely that much of the water originated from the dike complex just outside the model domain.

Field data from the two shafts show chloride at Hālawa Shaft roughly 55% higher than at (b)(3)(b)(3), despite being farther upslope and farther along dip from the freshwater/saltwater interface, with lower temperature. The influence of the freshwater/saltwater interface in unit source simulations is broadly distributed and impacts (b) and Hālawa Shaft in similar amounts: 1.2% to 2.0% of inflow. Figure 2-17 shows the results of the unit concentration source simulation, demonstrating migration from near the freshwater/saltwater interface along dip. Hālawa Shaft received a greater portion of its inflows from the dike region with 30.7%, compared to (b) with 0.4%, explaining the mechanism for cooler temperatures at Hālawa Shaft. Estimated temperatures at (b) and Hālawa Shaft compare well to observed data. Higher chloride at Hālawa Shaft is also achieved in the simulation, although both simulated values are higher than field results, and the simulated chloride at Hālawa Shaft is 27% higher, instead of the 55% observed in field measurements.

The measured chloride concentration at Hālawa Shaft cannot be computed from the field-measured (or estimated) source-water concentrations discussed above by any method, unless a) some contribution from the freshwater/saltwater interface is included, or b) some other mechanism of adding (or concentrating) chloride mass to the system is identified.

The unit source simulations demonstrate that only a very small amount of water of seawater origin (approximately 1% to 2%) is needed to explain the chloride concentrations at the shafts, but such a small volume would not have a significant overall effect on the model simulation results. This indicates that the assumption of no-flow at the freshwater/saltwater interface is a reasonable simplifying assumption for the overall model objectives. Explicit simulation of the freshwater/saltwater interface for all simulations would require significant structural changes to the GWFM, including addition of a significant number of layers and cells, which would increase computational requirements without impactful changes to the flow in and around the Facility.

Assumptions in this section and resulting estimates for chloride concentration and temperature are inherently epistemic and non-unique and do not account for all possible processes that may affect chloride concentrations and temperature, such as higher or potentially higher chloride concentrations at OWDF and

perched-zone groundwater, and potential impacts from quarry operations or natural source-zone depletion (NSZD). Although simplifying assumptions that do not account for all processes (such as those listed above) are made for these estimates, the simulations and subsequent calculations demonstrate an explanation for the patterns of chloride concentrations and temperature between (b) and Hālawa Shaft. Although the chloride concentrations were not matched exactly, minor changes to aquifer properties and boundary conditions could have large effects on the chloride concentrations at each shaft. The conclusion of this portion of the study is that of the boundary conditions that supply chloride sources to (b) and particularly Hālawa Shaft, only the freshwater-saltwater interface is likely to supply concentrations high enough to result in the observed chloride concentrations. Very small contributions from near the freshwater-saltwater interface are the most plausible explanation for the elevated chlorides in both water supply shafts. In contrast, temperature estimated from these simulations matched observations well because temperature is not sensitive to small contributions from the freshwater-saltwater interface. Despite the uncertainty in computing average chloride concentrations at (b), this evaluation adds confidence to the model calibration by explaining the mechanisms for two differing lines of evidence: elevated chloride is likely due to the influence of the freshwater/saltwater interface, and cooler water temperatures are likely caused by water sourced from the dike region.

2.4 Particle Tracking Simulations

Forward particle tracking was conducted with steady-state flow models under various pumping conditions from the water table beneath the tank farm to estimate the potential migration direction of hypothetical releases of solutes to groundwater beneath the tank farm. Particle tracking accounts only for advective groundwater flow and does not include the contaminant transport processes of dispersion, sorption, and degradation. Particles were released as a uniformly spaced grid throughout the tank farm area just below the water table to simulate movement of groundwater from this area, which could be impacted by a potential contaminant entering from the vadose zone. The four scenarios were constructed as follows:

- (b) pumping at (b) mgd, Hālawa Shaft pumping at 12 mgd, (b)(3) pumping at (b) mgd (Figure 2-18)
- (b) pumping at (b) mgd, Hālawa Shaft off, (b)(3) (b) (Figure 2-19)
- (b) (b) Hālawa Shaft off, (b)(3) (b) Figure 2-20)
- (b) (b), Hālawa Shaft pumping at 12 mgd, (b)(3) off (Figure 2-21)
- (b) pumping at (b) mgd, Hālawa Shaft off, (b)(3) off (Figure 2-22)

The first scenario represents (b) pumping at 4 mgd, Hālawa Shaft pumping at (b) mgd, and (b)(3) pumping at (b) mgd. Of the first three scenarios, this represents conditions where Hālawa Shaft is relatively more vulnerable to releases from the Facility, specifically where the significant pumping rate at Hālawa Shaft is mostly likely to extract groundwater from beneath the Facility. Figure 2-18 shows the simulation results for this scenario, including the potentiometric surface and particle tracking pathlines. Particles are simulated to originate from the Facility. From there they move with a small component of flow to the west-northwest before heading predominantly in the southwest direction, terminating at (b).

The second scenario simulates (mgd withdrawal from (b) and no withdrawals from Hālawa Shaft or (b)(3). This scenario demonstrates the maximum potential capture of groundwater from beneath the Facility by (b) because Hālawa Shaft is not pumping. Figure 2-19 shows the simulation results for this scenario, including the potentiometric surface and particle tracking pathlines. Particles from beneath the tank farm move slightly to the west-northwest, but all eventually migrate downridge, being captured by (b) . Results show only slight differences compared to the previous scenario in flow direction with a lesser component of flow to the northwest with Hālawa Shaft off.

The third scenario simulates no groundwater extraction at (b) , Hālawa Shaft, or (b)(3), and explores its effect on groundwater migration. Figure 2-20 shows the simulation results for this scenario, including the potentiometric surface and particle tracking pathlines. Particles from beneath the tank farm travel generally to the west-northwest, eventually discharging to the northwest GHB, traveling toward the springs north of Pearl Harbor. Particles travel beneath Pearl Harbor, but due to the low hydraulic conductivity of the caprock, they eventually discharge to the northwest GHB, then to springs rather than directly into Pearl Harbor.

The fourth scenario simulates no withdrawal from (b) or (b)(3) and 12 mgd withdrawal from Hālawa Shaft. This represents a hypothetical and unlikely scenario in which the Navy ceases pumping while BWS resumes pumping at capacity, and the greatest risk of impact is posed to Hālawa Shaft. Figure 2-21 shows the simulation results for this scenario, including the potentiometric surface and particle tracking pathlines. Particles from beneath the tank farm generally travel to the west-northwest, eventually discharging to the Kalauao Springs, Pearl Harbor, or the northwest GHB. Many particles travel beneath Pearl Harbor, but due to the low hydraulic conductivity of the caprock, they eventually discharge to the northwest GHB or springs rather than Pearl Harbor itself.

The fifth scenario simulates (b mgd withdrawal from (b) and no withdrawals from Hālawa Shaft or (b)(3). This scenario demonstrates the current pumping configuration at the site. Figure 2-22 shows the simulation results for this scenario, including the potentiometric surface and particle tracking pathlines. Particles from beneath the tank farm move slightly to the west-northwest, but all eventually migrate downridge, being captured by (b) .

2.5 Sensitivity Analysis

The impact of uncertainties, errors, and modeling assumptions was evaluated via a sensitivity analysis. A sensitivity analysis was conducted on parameter value bounds, conceptual uncertainties, and boundary stresses, where each sensitivity run was recalibrated with the PEST software. Each sensitivity simulation was evaluated for its impacts on the model calibration, acceptability of the calibrated basalt parameters based on literature values and professional judgment, and the predictive particle tracking results. All sensitivity scenarios were performed on the GWFM without nested grid refinement for flexibility of calibration and because of negligible differences in results prior to implementation of the nested grid. The analysis was performed in accordance with ASTM International Standard Designation D5611-94 (2016a). Each parameter was categorized as Type I, II, III, or IV sensitivity. Definitions for these parameter types are as follows:

- Type I Sensitivity—When variation of an input causes insignificant changes in the calibration residuals as well as the model's conclusions, then that model has a Type I sensitivity to the input. Type I sensitivity is of no concern because regardless of the value of the input, the conclusion will remain essentially the same. Models that use different combinations of Type I parameters and are each acceptably consistent with the available observations may be regarded as equifinal models (Beven 2002; 2019).
- Type II Sensitivity—When variation of an input causes significant changes in the calibration residuals but insignificant changes in the model's conclusions, then that model has a Type II sensitivity to the input. Type II sensitivity is of no concern because regardless of the value of the input, the conclusion will also remain essentially the same.
- Type III Sensitivity—When variation of an input causes significant changes to both the calibration residuals and the model's conclusions, then that model has a Type III sensitivity to the input. Type III sensitivity is of no concern because, even though the model's conclusions change as a result of variation of the input, the parameters used in those simulations cause the model to become uncalibrated. Therefore, the calibration process eliminates those values from being considered realistic.
- Type IV Sensitivity—If, for some value of the input that is being varied, the model's conclusions are changed but the change in calibration residuals is insignificant, then the model has a Type IV sensitivity to that input. Type IV sensitivity can invalidate model results because over the range of that parameter in which the model can be considered calibrated, the conclusions of the model change. A Type IV sensitivity generally requires additional data collection to decrease the range of possible values of the parameter.

Eight sets of simulations were conducted to evaluate sensitivity with varying assumptions of inputs or constraints, then compared to the base model calibration, referred to hereafter as Scenario 0. Each scenario was calibrated in the same manner as the base model with the constraints imposed for each sensitivity scenario and was evaluated using head RMSE for various well groups, gradients along Red Hill ridge, horizontal head differences and vertical head differences. Matches to head, gradients, and head differences were given a relative rank compared to all the sensitivity scenarios, including the base model calibration. Finally, predictive particle tracking was conducted under each of the five pumping configurations ((b) pumping at 4 mgd, Hālawa Shaft pumping at 12 mgd; (b) pumping at mgd, Hālawa Shaft pumping off; (b) (b) Hālawa Shaft pumping at 12 mgd; (b) (b) and Hālawa Shaft off; (b) pumping at (b mgd and Hālawa Shaft off) to assess the capture by (b) and risk to Hālawa Shaft and to guide characterization of each sensitivity type compared to Scenario 0 results. A summary of the changes to each simulation, model calibration, basalt parameters, particle tracking results, and sensitivity type characterization is presented in Table 2-18 and Table 2-19. Documentation of calibration evaluation for each sensitivity scenario is presented in Appendix E. Results for particle tracking are presented on Figure 2-23 through Figure 2-27.

Table 2-18: Summary of Sensitivity Analysis Results – Statistics

Scenario	Change	Hydraulic Properties of Basalt									Statistics							Rank							Sum of Ranks	Relative Rank	Significant Impact on Calibration?
		K_x [a] (ft/d, down-dip)	K_y [b] (ft/d, cross-dip)	Horizontal Anisotropy Ratio	Vertical Anisotropy Ratio	K_z [c] (ft/d, vertical)	Specific Yield (%)	Weathering Factor for Stream Valleys	Weathering Factor for Caprock	Maximum Weathering Depth (ft bgs)	Red Hill Wells Head RMSE (ft)	Transitional Wells Head RMSE (ft)	All Basal Wells Head RMSE (ft)	Red Hill Wells Drawdown RMSE (ft)	Ridge Gradients RMSE (ft)	Horizontal Head Differences RMSE (ft)	Vertical Head Differences RMSE (ft)	Red Hill Wells Head RMSE (ft)	Transitional Wells Head RMSE (ft)	All Basal Wells Head RMSE (ft)	Red Hill Wells Drawdown RMSE (ft)	Ridge Gradients RMSE (ft)	Horizontal Head Differences RMSE (ft)	Vertical Head Differences RMSE (ft)			
0	Base calibration	18,600	1,340	14	50	371	7.4%	6,620	2.65	736	0.25	0.35	0.25	0.17	2.20×10^{-5}	0.23	0.33	3	1	1	1	2	1	5	13	1	N/A
1	K_x fixed at 4,500 ft/d	4,500	738	6	50	90	8.7%	8,510	33	637	0.43	0.65	0.46	0.28	7.36×10^{-5}	0.45	0.39	8	8	8	9	9	8	9	57	9	Yes
2	Horizontal anisotropy fixed at 3:1	19,500	6,501	3	55	355	7.5%	12,500	696	858	0.25	0.39	0.31	0.18	2.57×10^{-5}	0.32	0.30	3	6	4	4	5	5	3	30	5	No
3	Vertical anisotropy fixed at 200:1	47,800	3,850	12	200	239	7.3%	6,000	20.8	879	0.24	0.36	0.27	0.18	2.40×10^{-5}	0.25	0.32	1	3	3	4	4	3	4	20	3	No
4	Eliminated dike flux [d]	17,900	1,490	12	50	358	7.2%	6,200	2.90	759	0.24	0.39	0.25	0.17	2.58×10^{-5}	0.24	0.33	1	5	1	1	6	2	5	19	2	No
5	Northwest flow direction	26,100	1,172	22	50	523	7.7%	1	1	700	0.26	0.35	0.32	0.17	2.11×10^{-5}	0.29	0.36	5	1	5	1	1	4	8	25	4	Yes
6	2-degree dip	16,400	1,170	14	50	329	7.4%	6,280	2.62	799	0.43	0.89	0.47	0.19	6.23×10^{-5}	0.36	0.35	8	9	9	6	8	7	7	54	8	Yes
7	7-degree dip	36,100	705	51	50	722	5.2%	9,040	3.31	900	0.39	0.38	0.39	0.19	2.23×10^{-5}	0.35	0.29	7	4	6	6	3	6	2	32	6	Yes
8	Horizontally Isotropic	6,960	6,960	1	10	696	5.8%	18,700	520	900	0.26	0.40	0.42	0.19	2.78×10^{-5}	0.45	0.28	5	7	7	6	7	8	1	40	7	Yes

Notes:

[a] K_x Hydraulic conductivity in the down-dip direction

[b] K_y Hydraulic conductivity in the cross-dip direction

[c] K_z Hydraulic conductivity in the vertical direction

[d] Assumes all recharge from dike region flows around dikes and into model domain from southeast.

Table 2-19: Summary of Sensitivity Analysis Results – Particle Tracks

Scenario	Change	[redacted] – [redacted] mgd Hālawa Shaft – 12 mgd [redacted] – [redacted] mgd						[redacted] – [redacted] mgd Hālawa Shaft – Off [redacted] – [redacted]						[redacted] – [redacted] mgd Hālawa Shaft – Off [redacted] – [redacted]					[redacted] – Off Hālawa Shaft – 12 mgd [redacted] – Off							[redacted] – [redacted] Hālawa Shaft – Off [redacted] – [redacted]					Results Significantly Affected?	Sensitivity Type
		Particles Captured by [redacted]	Particles Captured by HS	Particles Arriving Springs	Particles Arriving at NW GHB	Particles Arriving at Pearl Harbor	Stagnant Particles	Particles Captured by [redacted]	Particles Arriving at Domain	Particles Arriving Springs	Particles Arriving at NW GHB	Particles Arriving at Pearl Harbor	Stagnant Particles	Particles Captured by [redacted]	Particles Arriving at Springs	Particles Arriving at NW GHB	Particles Arriving at Pearl Harbor	Stagnant Particles	Particles Captured by [redacted]	Particles Captured by HS	Particles Arriving at Springs	Particles Arriving at NW GHB	Particles Arrive at Pearl Harbor	Particles Arriving at Other Wells	Stagnant Particles	Particles Captured by [redacted]	Particles Arriving at Springs	Particles Arriving at NW GHB	Particles Arrive at Pearl Harbor	Stagnant Particles		
0	Base calibration	100%	0.0%	0.0%	0.0%	0.0%	0.0%	100%	0.0%	0.0%	0.0%	0.0%	0.0%	100%	0.0%	0.0%	0.0%	0.0%	18.8%	0.0%	46.9%	6.2%	23.4%	0.0%	4.7%	20.3%	1.6%	76.6%	1.6%	0.0%	N/A	N/A
1	K_x fixed at 4,500 ft/d	100%	0.0%	0.0%	0.0%	0.0%	0.0%	100%	0.0%	0.0%	0.0%	0.0%	0.0%	100%	0.0%	0.0%	0.0%	0.0%	16.7%	0.0%	0.0%	11.7%	70.0%	1.7%	0.0%	21.7%	0.0%	10.0%	66.7%	1.7%	No	II
2	Horizontal anisotropy fixed at 3:1	100%	0.0%	0.0%	0.0%	0.0%	0.0%	100%	0.0%	0.0%	0.0%	0.0%	0.0%	100%	0.0%	0.0%	0.0%	0.0%	86.7%	0.0%	13.3%	0.0%	0.0%	0.0%	0.0%	85.0%	15.0%	0.0%	0.0%	0.0%	No	I
3	Vertical anisotropy fixed at 200:1	100%	0.0%	0.0%	0.0%	0.0%	0.0%	100%	0.0%	0.0%	0.0%	0.0%	0.0%	100%	0.0%	0.0%	0.0%	0.0%	73.3%	0.0%	26.7%	0.0%	0.0%	0.0%	0.0%	71.7%	28.3%	0.0%	0.0%	0.0%	No	I
4	Eliminated dike flux [d]	85%	0.0%	6.7%	0.0%	6.7%	1.7%	88.3%	0.0%	3.3%	1.7%	5.0%	1.7%	88.3%	5.0%	1.7%	5.0%	1.7%	3.3%	1.7%	61.7%	0.0%	31.7%	1.7%	0.0%	6.7%	76.7%	0.0%	15.0%	1.7%	No	I
5	Northwest flow direction	83.4%	0.0%	6.7%	1.7%	8.3%	0.0%	85.0%	18.4%	3.3%	1.7%	8.3%	0.0%	65.0%	26.7%	1.7%	6.7%	0.0%	1.7%	21.7%	20.0%	18.3%	38.3%	0.0%	0.0%	0.0%	21.7%	55.0%	20.0%	3.3%	Yes	III
6	2-degree dip	100%	0.0%	0.0%	0.0%	0.0%	0.0%	100%	0.0%	0.0%	0.0%	0.0%	0.0%	100%	0.0%	0.0%	0.0%	0.0%	0.0%	0.0%	17.2%	1.6%	0.0%	81.2%	0.0%	3.1%	51.6%	43.8%	1.6%	0.0%	Yes	III
7	7-degree dip	100%	0.0%	0.0%	0.0%	0.0%	0.0%	100%	0.0%	0.0%	0.0%	0.0%	0.0%	100%	0.0%	0.0%	0.0%	0.0%	0.0%	7.8%	48.4%	0.0%	0.0%	43.8%	0.0%	10.9%	28.1%	60.9%	0.0%	0.0%	Yes	III
8	Horizontally Isotropic	100%	0.0%	0.0%	0.0%	0.0%	0.0%	100%	0.0%	0.0%	0.0%	0.0%	0.0%	100%	0.0%	0.0%	0.0%	0.0%	86.7%	0.0%	11.7%	0.0%	0.0%	0.0%	1.7%	90.0%	10.0%	0.0%	0.0%	0.0%	No	II

Notes:

[a] K_x Hydraulic conductivity in the down-dip direction

[b] K_y Hydraulic conductivity in the cross-dip direction

[c] K_z Hydraulic conductivity in the vertical direction

[d] Assumes all recharge from dike region flows around dikes and into model domain from southeast

2.5.1 Scenario 1 – K_x fixed at 4,500 ft/d

The purpose of this scenario is to investigate the potential effects of a lower K_x on model results. Scenario 1 assumed that the hydraulic conductivity in the down-dip direction (K_x) is 4,500 ft/d, equivalent to the value used by Oki (2005). The calibrated K_x of the basalt in Scenario 0 was approximately 18,600 ft/d. This parameter was fixed, then the other parameters were adjusted with PEST.

Basalt parameters varied from Scenario 0 with a horizontal anisotropy ratio of 6 and a vertical anisotropy ratio that hit the lower bound of 50. Calibration of Scenario 1 resulted in a significant increase in RMSE of basal aquifer heads from 0.25 to 0.46 ft. Head differences and ridgeline gradients were affected similarly. This scenario was ranked last for calibration quality and is considered to be significantly affected.

Predictive particle tracking runs in all three scenarios with (b) pumping indicated 100% capture at (b), as was the case in Scenario 0. Results from the configurations of (b) and (b)(3) off with Hālawa Shaft at 12 mgd showed some particles passing through (b), but more particles discharging to Pearl Harbor rather than the northwest GHB in Scenario 0. Particle tracking results were not considered significantly affected.

Scenario 1 demonstrated that constraining the K_x to 4,500 ft/d had a negative impact on the model calibration, but no significant changes to particle tracking results. (b) still achieved full capture while pumping. Scenario 1 was categorized as a Type II sensitivity.

2.5.2 Scenario 2 – Horizontal Anisotropy Fixed at 3:1

The purpose of this scenario is to investigate the potential effects of a lower horizontal anisotropy ratio on model results. Scenario 2 assumed that the ratio of K_x to K_y horizontal hydraulic conductivity is 3:1, equivalent to the ratio used by Oki (2005). The calibrated horizontal anisotropy ratio of the basalt in Scenario 0 was approximately 14:1, higher than values used in previous modeling. This ratio was fixed at 3:1, then the model parameters were adjusted with PEST. Resulting basalt hydraulic conductivities were similar to those in Scenario 0, except the K_y which was higher due to the fixed ratio to K_x fixed.

Calibration of Scenario 2 resulted in an increase in RMSE from 0.25 to 0.31 ft. Vertical head differences and ridgeline gradients achieved similar calibration metrics compared to Scenario 0; however, the horizontal head differences were not matched as well with the RMSE increasing from 0.23 ft to 0.32 ft. This scenario was ranked fifth of nine for calibration and is not considered to be significantly affected.

Predictive particle tracking runs in all three scenarios with (b) pumping indicated 100% capture at (b) as was the case in Scenario 0. The pumping configurations with (b) off still resulted in approximately 85% of particles entering (b). The particle tracking software does not allow particles which enter a CLN to re-enter the aquifer; however, groundwater would be flowing through the shaft while the pumps are off, eventually discharging to the northwest GHB, Kalauao Springs, or Pearl Harbor. No particles were captured by Hālawa Shaft. Particle tracking results were not considered significantly affected. Scenario 2 was categorized as a Type I sensitivity.

2.5.3 Scenario 3 – Vertical Anisotropy Fixed at 200:1

The purpose of this scenario was to investigate the potential effects of a higher vertical anisotropy ratio on model results. Scenario 3 assumed that the ratio of down-dip (K_x) to vertical (K_z) hydraulic conductivity is 200:1, lower than the 600:1 ratio used by Oki (2005), but consistent with other reported values (Visher and Mink 1964). The calibrated vertical anisotropy ratio of the basalt in Scenario 0 was 50:1. This ratio was fixed at 200:1, then the model parameters were adjusted with PEST.

Resulting basalt parameters included a K_x of about 47,800 ft/d and a K_y of about 3,850 ft/d, which were significantly higher than Scenario 0. Calibration of Scenario 3 resulted in a relatively small increases in residuals for heads, head differences and ridgeline gradients, but the resulting hydraulic conductivity values were significantly higher than estimated form aquifer testing or from literature values. Changes to the model calibration in this case were considered insignificant. This scenario was ranked third of nine for calibration and is not considered to be significantly affected.

Predictive particle tracking runs in all three scenarios with (b) pumping indicated 100% capture at (b) as was the case in Scenario 0. The pumping configurations with (b) off still resulted in over 70% of particles entering (b). The particle tracking software does not allow particles which enter a CLN to re-enter the aquifer; however, groundwater would be flowing through the shaft while the pumps are off, eventually discharging to the northwest GHB, Kalauao Springs, or Pearl Harbor. No particles were captured by Hālawa Shaft. Particle tracking results were not considered significantly affected. Scenario 3 was categorized as a Type I sensitivity.

2.5.4 Scenario 4 – No Dike Region Flux

The purpose of this scenario was to investigate the impact of no dike region inflow on the model results. Scenario 4 assumed that the interface of the dike region and basalt is a no-flow boundary and that all recharge that occurs in the dike region flows in the direction of anisotropy until discharging into the basalt aquifer before flowing into the GWFM domain from the southeast. This was accomplished by setting the dike region inflow to zero while modifying the boundary flux targets from in Scenario 0 so that the total dike region inflow enters the model through the southeast GHB instead, then the model parameters were adjusted with PEST.

Resulting basalt parameters were similar to those from Scenario 0. Calibration of Scenario 4 caused relatively small increases in residuals for heads, head differences and ridgeline gradients. Changes to the model calibration in this case were considered insignificant. This scenario was ranked second of nine for calibration and is not considered to be significantly affected.

Predictive particle tracking runs in all three pumping configurations with (b) on showed reduced capture, to 85% with (b) on a(b) mgd with Hālawa Shaft on at 12 mgd, and 88.3% with Hālawa Shaft off and (b) on at 4 mgd and (b) mgd, compared to Scenario 0 which showed 100% capture for the three configurations. With (b) off and Hālawa Shaft pumping at 12 mgd, Hālawa Shaft and the other supply wells captured 1.7% particles, compared to 0% in Scenario 0. Particles which were not captured by water supply wells generally discharged to similar locations with some deviation between the northwest GHB, Kalauao

Springs, and Pearl Harbor. Particle tracking results were not considered significantly affected. Scenario 4 was categorized as a Type I sensitivity.

2.5.5 Scenario 5 – Northwest Flow Direction Scenario

The purpose of this scenario was to investigate the potential to create a model that directs the greatest amount of regional flow to the northwest (toward Hālawa Shaft). Scenario 5 represents a scenario where flow direction targets were used to guide flow paths from the tank farm to Hālawa Shaft while calibrating the model parameters with PEST.

Resulting basalt parameters included a K_x value of 26,100 ft/d and a horizontal anisotropy ratio of 22, both higher than Scenario 0. The most significant difference is that parameters for weathering of the basalt were reduced to the point of eliminating the weathering altogether. The residuals for basal aquifer heads, ridgeline gradients, and horizontal head differences were not significantly affected; however, the vertical head differences were. Because weathering was eliminated, the observed downward vertical gradients beneath the stream valleys were not represented. For this reason, the calibration was considered significantly affected.

Predictive particle tracking runs in all three pumping configurations with (b) on showed reduced capture, to 83.4% with (b) on at (mgd with Hālawa Shaft on at 12 mgd, and 85% with Hālawa Shaft off and (b) on at 4 mgd and (b mgd, compared to Scenario 0 which showed 100% capture for the three configurations. With (b) (b) and Hālawa Shaft pumping at 12 mgd, Hālawa Shaft captured 21.6% of particles, compared to 0% in Scenario 0. Particles which were not captured by water supply wells generally discharged to similar locations with some deviation between the northwest GHB, Kalauao Springs, and Pearl Harbor. Particle tracking results were considered significantly affected due to the increase in capture by Hālawa Shaft, although direct flow paths from the tank farm to Hālawa Shaft were not achieved. Scenario 5 was categorized as a Type III sensitivity.

2.5.6 Scenario 6 – 2-Degree Dip of Basalt

The purpose of this scenario was to explore the effects of reducing the dip of the Basalt. Scenario 6 changes the assumption of a 4-degree dip of the basalt used in Scenario 0 to a 2-degree dip. This change required rebuilding the model grid to align layer elevations with a 2-degree dip in basalt layers 5 to 36. The same parameter set was recalibrated with PEST as the other scenarios.

Resulting basalt parameters were very similar to those of Scenario 0 with only minimal differences. The calibration results were significantly worse, however. The RMSE of basal aquifer heads increased from 0.25 ft to 0.47 ft. Increases in residuals for head differences and ridgeline gradients were also observed. This scenario was ranked eighth of nine for calibration and is considered to be significantly affected.

Predictive particle tracking runs in all three scenarios with (b) pumping indicated 100% capture at (b), as was the case in Scenario 0. Results from the configurations of (b) and (b)(3) off with Hālawa Shaft at 12 mgd showed 81.2% of particles discharging to other water supply wells, but none captured by Hālawa Shaft. Particle tracking results were considered significantly affected. Scenario 6 was categorized as a Type III sensitivity.

2.5.7 Scenario 7 – 7-Degree Dip of Basalt

The purpose of this scenario was to explore the effects of increasing the dip of the basalt. Scenario 7 changes the assumption of a 4-degree dip of the basalt used in Scenario 0 to a 7-degree dip. This change required rebuilding the model grid to align layer elevations with a 7-degree dip in basalt layers 5 to 36. To prevent a vertical separation between a model cell and its adjacent down-dip cell, layers that were initially 25 ft thick in Scenario 0 were assigned a 40-ft thickness. The same parameter set was recalibrated with PEST as the other scenarios.

The resulting basalt parameters were significantly different compared to Scenario 0. The K_x value increased from 18,600 ft/d to 36,100 ft/d and the horizontal anisotropy ratio increased from approximately 14 to 51. Both values are larger than values estimated from aquifer testing at the site or from literature. Additionally, the residuals increased significantly for basal aquifer heads from 0.25 ft in Scenario 0 to 0.39 ft. Horizontal head difference residuals also significantly increased, while ridgeline gradients and vertical head difference residuals were similar to Scenario 0. This scenario was ranked sixth of nine for calibration and is considered to be significantly affected.

Predictive particle tracking runs in all three scenarios with (b) pumping indicated 100% capture at (b), as was the case in Scenario 0. Results from the configurations of (b) and (b)(3) off with Hālawa Shaft at 12 mgd showed 43.8% of particles discharging to other water supply wells, and 7.8% captured by Hālawa Shaft. Particle tracking results were considered significantly affected. Scenario 7 was categorized as a Type III sensitivity.

2.5.8 Scenario 8 – Horizontally Isotropic Model

The purpose of this scenario is to investigate the potential effects of a uniform isotropic aquifer, which, although not consistent with the emplacement of lava flows on the island, could potentially increase the risk to Hālawa Shaft. Scenario 8 represents a uniform isotropic aquifer in the horizontal direction with a fixed vertical anisotropy ratio of 10. These two parameters were fixed, then the other parameters were adjusted with PEST.

The resulting basalt parameters were significantly different due to fixing of both the horizontal and vertical anisotropy ratios. In this scenario the calibrated K_x value was 6,960 ft/d compared to 18,600 ft/d in Scenario 0. The residuals increased significantly for basal aquifer heads from 0.25 ft in Scenario 0 to 0.42 ft. Horizontal head difference residuals also significantly increased, while ridgeline gradients and vertical head difference residuals were similar to Scenario 0. This scenario was ranked seventh of nine for calibration and is considered to be significantly affected.

Predictive particle tracking runs in all three scenarios with (b) pumping indicated 100% capture at (b) as was the case in Scenario 0. The pumping configurations with (b) off still resulted in over 85% of particles entering (b). The particle tracking software does not allow particles which enter a CLN to re-enter the aquifer; however, groundwater would be flowing through the shaft while the pumps are off, eventually discharging to the northwest GHB, Kalauao Springs, or Pearl Harbor. No particles were captured by Hālawa Shaft. Particle tracking results were not considered significantly affected. Scenario 8 was categorized as a Type II sensitivity.

2.5.9 Sensitivity Analysis Summary

The sensitivity analysis conducted on the homogenous anisotropic GWFM model was used to evaluate several assumptions and their impacts on both model calibration and particle tracking results. Eight scenarios were analyzed in comparison to the calibrated model described in Section 2.3. Of the eight scenarios, three (Scenarios 2, 3, and 4) were able to maintain an acceptable calibration indicating that changes to assumptions for horizontal and vertical anisotropy, as well as the origin of fluxes between the dike region and the southeast GHB, do not significantly affect the model calibration or predictive outcomes. Two sensitivity scenarios showed reduced capture by (b) . Scenario 4, which was a scenario that maintained adequate calibration, showed a reduction in capture, but still showed greater than 85% capture by (b) . The other scenario that resulted in reduced capture was Scenario 5 with flow direction targets to Hālawa Shaft, which was 83.4% with (b) on at (mgd and Hālawa Shaft on at 12 mgd, 85% with (b) on at (mgd and Hālawa Shaft off, and 65% with (b) on at (b mgd and Hālawa Shaft off. Scenario 5 had similar calibration statistics except for the downward vertical gradients, indicating that the downward gradients below stream valleys are an important feature when evaluating capture at (b) and potential risk to Hālawa Shaft.

3.0 Heterogeneous Basalt Models

Heterogeneity of the basal aquifer plays a critical role in shaping the groundwater flow and contaminant transport dynamics within the hydrogeologic system at the site. Simulation of these effects requires variable properties of the basalt that reflect the complex nature of the cycles of lava flows that formed the basal aquifer. The objective of implementing heterogeneity into the groundwater flow model was to evaluate the effects compared to the homogenized regional GWFM with respect to flow distribution across (b) , compartmentalized drawdowns at various monitoring wells, variations in flow paths and groundwater velocities, and dispersion of contaminants.

A recommended approach was adopted to generate structure-imitating realizations of the basalt aquifer and implement them in a nested grid of the regional GWFM. The sequential indicator simulation software SISIM (Deutsch and Journel 1997) was used to generate a categorical indicator field of massive basalt with relatively low permeability and clinker with very high permeability. Three-dimensional variograms used by SISIM were developed based on site data and publicly available data on Hawaiian geology, and supplemented with results from lava flow simulations using the probabilistic lava flow spread model MrLavaLoba (Vitturi and Tarquini 2018).

Fifty realizations of the MrLavaLoba model were generated to populate the nested grid area of the regional GWFM with variable composition of basalt and clinker. Hydraulic properties of the heterogeneous basalt for each realization were calculated to achieve effective global values consistent with the regional GWFM through the use of a simplified box model of the area. The resulting hydraulic properties were then implemented into a full simulation of the 44-stress period calibration model. Calibration of each model was ranked based on various criteria, then particle tracking was conducted over various pumping scenarios. CF&T modeling using the heterogeneous model was later conducted and is discussed further in Section 5.0.

3.1 Generation of Basalt Realizations

3.1.1 Introduction

The work performed to generate Monte Carlo realizations of the spatial presence of a‘ā clinker was part of an effort to evaluate the potential impact of basalt heterogeneity on groundwater conditions, as described below. Monte Carlo simulations rely on random sampling of input variables based on a probabilistic distribution to obtain model results over a large number of simulations. In this case, the spatial presence of clinker was generated for a series of 50 realizations. Detailed discussion of the sub-types of basalt are documented in the geological CSM addendum (DON 2023a). The a‘ā clinker has a higher permeability by several orders of magnitude compared to massive a‘ā and pāhoehoe. The realizations were generated for the nested grid area within the GWFM domain in the vicinity of the Red Hill Facility and Hālawa Shaft, as shown on Figure 1-1.

Chart 3-1 shows the framework of the overall clinker presence simulation process. The Monte Carlo simulation is primarily based on a geostatistical approach using existing geologic data. Figure 3-1 shows the locations of available boring, shaft, and barrel logs, which are geologic logs developed in the vadose zone during construction of the USTs after blasting the bedrock. While these data provide geostatistical

information at length scale comparable to the spacing of these data, lava flow model simulation was conducted to provide supplemental data to estimate the geostatistical characteristics at larger length scales. The parameter values and implementation of the lava flow model were adopted from published literature or derived from existing data. The analysis of existing data, simulation of the lava flow model, characterization of geostatistical parameters, and generation of Monte Carlo realizations are conceptually discussed below. The details of individual processes in the workflow (Chart 3-1) are presented in individual subsections of this document (section numbers are referenced in Chart 3-1).

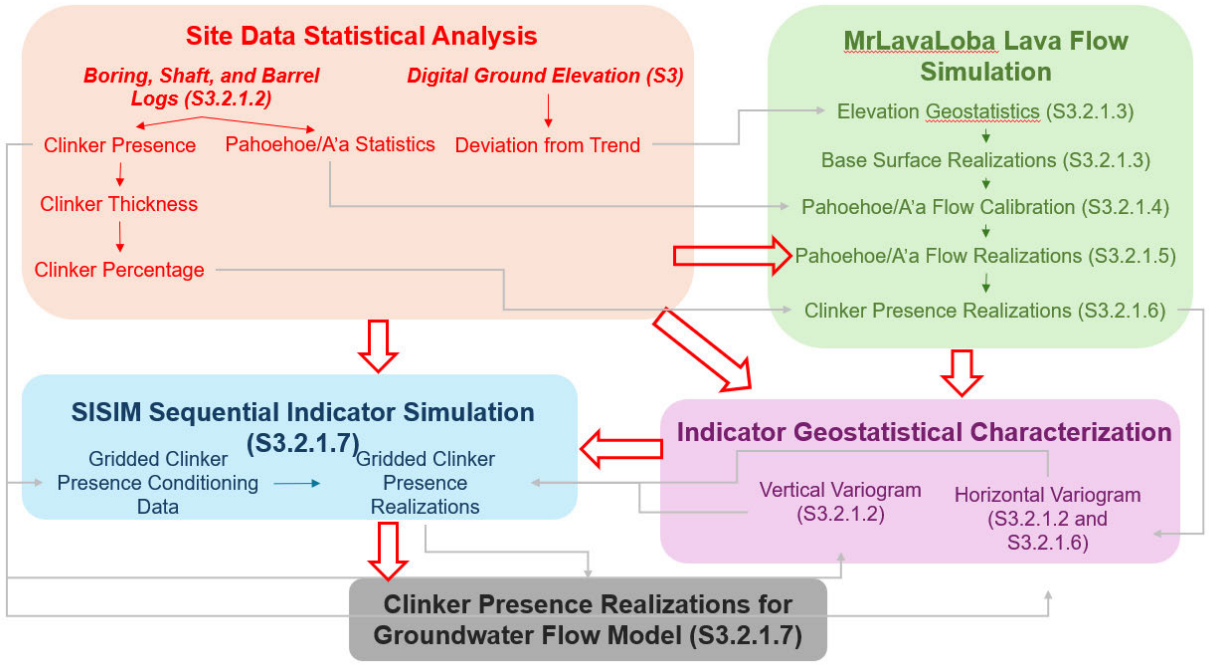

Chart 3-1: Clinker Heterogeneity Simulation Flow Chart (report section number in parenthesis)

3.1.2 Site Data Statistical Analysis

Existing boring, shaft, and barrel logs were used in two ways: 1) to estimate the statistical characteristics of massive a‘ā and pāhoehoe lava flow sequence for use as input to the lava flow model simulation, and 2) to characterize the spatial presence of a‘a clinker for developing a geostatistical model of a‘ā clinker presence. The analysis of these data is described in Section 3.1.5, including the estimation of semi-variograms, the marginal and transition probability of the massive a‘ā and pāhoehoe lava flow types, the statistics of a‘ā clinker thickness, and the percentage of basalt as a‘ā clinker in the top and bottom part of an a‘ā eruption stratum. Secondly, the clinker presence data were used as conditioning data in the Monte Carlo simulation to generate the realization of a‘ā clinker presence, as described in Section 3.1.10.

Existing ground surface elevation data were used to develop a geostatistical representation of the initial and evolving (from subsequent lava flows) ground surface based on the estimated average strike direction and dip angle of the lava strata agreed to in SPM #11 on January 10, 2023. The geostatistical information was used to generate random realizations of the base surface for the Monte Carlo simulation of lava flow

simulation (further discussed below) since the base surface of lava flow at each historical eruption was unknown. The details of base surface generation are presented in Section 3.1.6.

3.1.3 Monte Carlo Lava Flow Model Simulation

There are three general categories of lava flow models (Hyman, Dietterich, and Patrick 2022). The first category is based on stochastic routing (SR) to capture lateral spreading of advancing flows by Monte Carlo modeling of perturbed steepest descent paths, akin to the spreading of a random walk with drift. SR models are computationally fast. The second category of models are cellular automata (CA) models, which commonly use a simple set of rules (often not derived directly from physical laws) to distribute fluid from a central cell to neighboring cells, allowing CA models to develop complex flow fields which mimic real lava flow deposits as settlement processes. The third category comprises the true physics-based models derived from principles of computational fluid dynamics (CFD). These models are slower to run than CA or SR models. They also require more parameters to capture kinematics of lava flow. Some of these parameters are site specific and unknown in the nested grid area.

The computer code MrLavaLoba (Vitturi and Tarquini 2018) was selected for this effort. This code uses CA-like rules to distribute elliptical packets of lava volume in an SR framework. This approach has the benefit of relatively quicker run-time and the ability to succeed on steeper slopes or where lava is not simply filling a basin. It is a probabilistic code for simulation of lava flows and was used for estimating the inundated area and final thickness of the lava deposit. MrLavaLoba relies on the input topography, whose generation over time is difficult to recreate with limited observation data, hence several realizations of possible topographies were created as MrLavaLoba's base digital elevation models (DEMs) to reduce the dependency of a particular initial topography (Section 3.1.6).

Some of the MrLavaLoba parameters were adjusted to match the existing geologic data, such as aʻā and pāhoehoe deposit thicknesses (Section 3.1.7). The generation of MrLavaLoba realizations is presented in Section 3.1.8. It was assumed that aʻā clinker formations are associated with aʻā lava flows and aʻā clinker was formed above and below each massive aʻā core. The spatial extent of aʻā clinker in each realization was estimated based on the statistical information from existing data (Section 3.1.5). The generation of aʻā clinker presence is described in Section 3.1.9.

MrLavaLoba does not incorporate aʻā clinker explicitly. Therefore, the MrLavaLoba simulations were primarily used in a probabilistic framework to generate realizations of lava flows. These realizations were used to generate aʻā clinker spatial distributions to supplement the existing aʻā clinker data for developing a geostatistical model of aʻā clinker presence (Sections 3.1.5 and 3.1.9).

3.1.4 Monte Carlo Simulation of Clinker Presence

Sequential Indicator Simulation (SIS) (Alabert 1987) and Multiple Point Geostatistics (MPG) simulation methods were considered for generating Monte Carlo realizations of spatial clinker presence. Although MPG is capable of simulating complex spatial patterns, the validity of the generated realizations relies heavily on the validity of the training images used. Since geologic data are available only at specific locations and the MrLavaLoba simulation does not condition on existing data, there are no reliable images available for training MPG simulation. Therefore, SIS was selected for this effort (Section 3.1.10). SIS is a

categorical simulation method for structures whose spatial continuity is well described by variograms, which is based on 2-point statistics. It generates realizations of categorical variables, which in this case were the a‘ā clinker and non-a‘ā-clinker materials, while honoring a pre-defined structure of univariate and bivariate statistics and data inputs.

The structure and the observed site data were relayed into the SIS process. In this study, the function SISIM in the code GSLIB (Deutsch and Journel 1997) was used. Existing clinker presence data were used as conditioning data for generating SISIM realizations, i.e., existing clinker presence data are honored in each SISIM realization. The vertical variogram used in SISIM was derived from the existing data. The horizontal variograms in the longitudinal and transverse directions were based on the existing data and MrLavaLoba simulation results. This clinker simulation framework was presented in SPM #28 on August 19, 2023.

3.1.5 Clinker Data Interpretation

Site data used for this project included records from boring logs, shaft logs, and barrel logs. A map of the boring and barrel log locations, the shafts, the GWFM domain and the nested grid domain is provided on Figure 1-1. A summary of the boring log information is shown in Table 3-1. Besides *x*, *y*, and *z* coordinates, the boring logs contained geologic descriptions. Based on interpretation of the geologic information, a‘ā or pāhoehoe flow intervals were assigned. Moreover, the boring logs were evaluated to identify potential sequences of lava eruptions based on material discolorations or indications of material borders. Each member of one lava flow was assigned to a lava flow identifier (ID) unique to the respective boring logs.

The shaft geologic log data and the barrel logs contained *x*, *y*, and *z* coordinates, and soil descriptions. The available information of the shaft and barrel logs is insufficient for interpreting the lava flow type (pāhoehoe or a‘ā) and lava flow sequence (some areas of the barrel logs are simply labelled “rock,” and there did not appear to have been an effort to distinguish individual flows). The boring log, shaft, and barrel log data were converted into binary categorical variables of a‘ā clinker and non-a‘ā-clinker. Locations with weathered and welded a‘ā clinkers were assigned a non-a‘ā-clinker category because their groundwater flow permeability is expected to be significantly lower than highly porous clinker permeability.

The classification of clinker/non-clinker, lava flow type, and flow sequence based on the boring logs, shaft logs, and barrel logs are provided in Appendix F.

Table 3-1: Boring Log Data Summary

Location ID	Easting	Northing	Top Elevation (ft msl)	Bottom Elevation (ft msl)	Top Depth (ft bgs)	Bottom Depth (ft bgs)	Description	Basalt Classification	Thickness	Basalt Flow ID
RHM[redacted]	(b)(9)						Alluvium	-	(b)(9)	—
RHM[redacted]							Saprolite	-		—
RHM[redacted]							Pāhoehoe (Flow 1)	Massive Basalt		1
RHM[redacted]							Massive A‘ā	Massive Basalt		2
RHM[redacted]							Pāhoehoe (Flow 2)	Massive Basalt		3
RHM[redacted]							Pāhoehoe (Flow 3)	Massive Basalt		4
RHM[redacted]							Undifferentiated A‘ā Clinker	Clinker		5
RHM[redacted]							Massive A‘ā	Massive Basalt		
RHM[redacted]							Loose A‘ā Clinker	Clinker		
RHM[redacted]							Loose A‘ā Clinker	Clinker		6
RHM[redacted]							Massive A‘ā	Massive Basalt		
RHM[redacted]							Undifferentiated A‘ā Clinker	Clinker		
RHM[redacted]							Undifferentiated A‘ā Clinker	Clinker		7
RHM[redacted]							Massive A‘ā	Massive Basalt		
RHM[redacted]							Undifferentiated A‘ā Clinker	Clinker		
RHM[redacted]							Massive A‘ā	Massive Basalt		
RHM[redacted]							Alluvium	-		8

The following data were used to estimate the statistical characteristics below for use in the clinker simulations:

- Clinker percentage – Based on the boring log data, the occurrence of loose or unweathered a‘ā clinker was about 10 percent on average. Weathered or welded clinker was not characterized as clinker because of its significantly lower permeability and therefore grouped with massive a‘a and pāhoehoe. Chart 3-2 shows the distribution of the a‘ā clinker percentage by boring log. The spatial clinker percentage distribution is highly variable in the southeastern portion of the model domain, but in the eastern domain, the spatial distribution is less variable. Chart 3-2 also shows a horizontal section of a‘ā clinker/ non-a‘ā-clinker distribution from boring logs around (b) , viewed from south to north. In the (b) water development tunnel, a consistent a‘ā clinker band was detected in the southeast, which is discussed further in Section 3.3 and a few occurrences of a’a clinker are reported in nearby RHM(b) at various depths, but in general, the clinker presence is sparse.
- Lava flow type transition probability – Based on the vertical sequence of the observed lava flow patterns in each boring log, transitional probabilities of a‘ā flows following a‘ā flows, pāhoehoe flows following pāhoehoe flows, a‘ā flows following pāhoehoe flows and vice versa were calculated and are presented in Table 3-2.
- Lava flow thickness – The distributions of lava flow thicknesses were evaluated to calibrate the MrLavaLoba parameters. Chart 3-3 shows the empirical probability density functions of the pāhoehoe and a‘ā flow data from the boring logs. They show that the logged maximum thicknesses were up to 60 ft each and the minimum thicknesses were 0.1 ft (pāhoehoe) and 0.3 ft (a‘ā). The modes (i.e., most frequent occurrences) of the distributions are about 10 ft (pāhoehoe) and 20 ft (a‘ā). In addition, the clinker thicknesses belonging to the tops and bottoms of a‘ā flows logged in the borings were expressed as fractions of total a‘ā flow thicknesses. The histograms of top and bottom clinker fractions are presented in Chart 3-4. Their modes are at about 0.25 (top fraction) and 0.1 (bottom fraction).

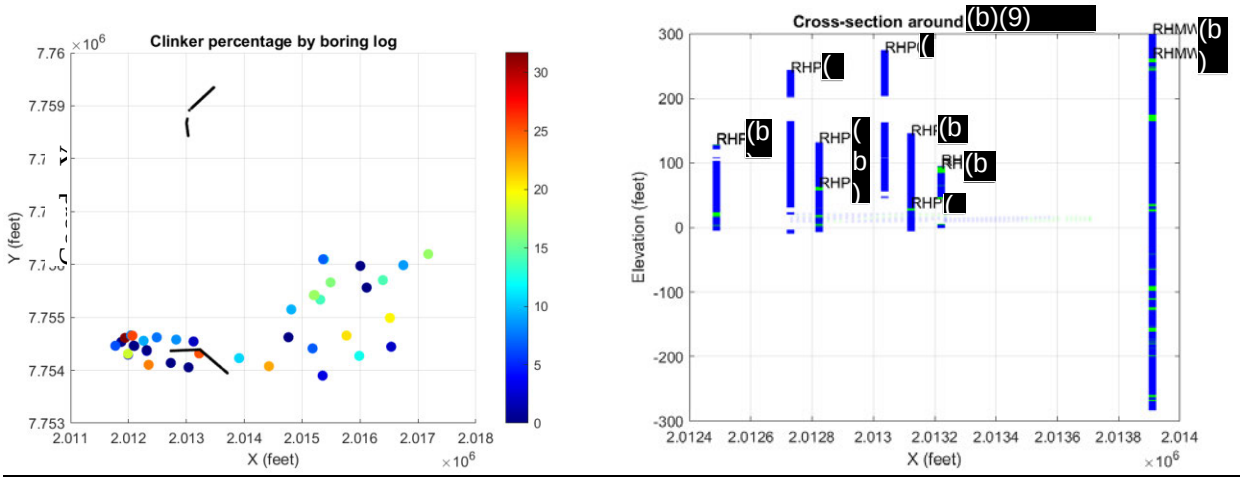

Chart 3-2: Occurrence of Clinker Map (left) and Horizontal Cross Section of Clinker (green) / Non-Clinker (blue) Distribution Around (b)(3)(b)(3) (right)

Table 3-2: Transitional Probabilities of Eruptions by Lava Flow Type

Eruption 2 (down) / based on Eruption 1 (right)	Pāhoehoe	A‘ā (including an a‘ā sequence of massive a‘ā between two a‘ā clinker layers)
Pāhoehoe	0.43	0.324
A‘ā (including an a‘ā sequence of massive a‘ā between two a‘ā clinker layers)	0.57	0.68

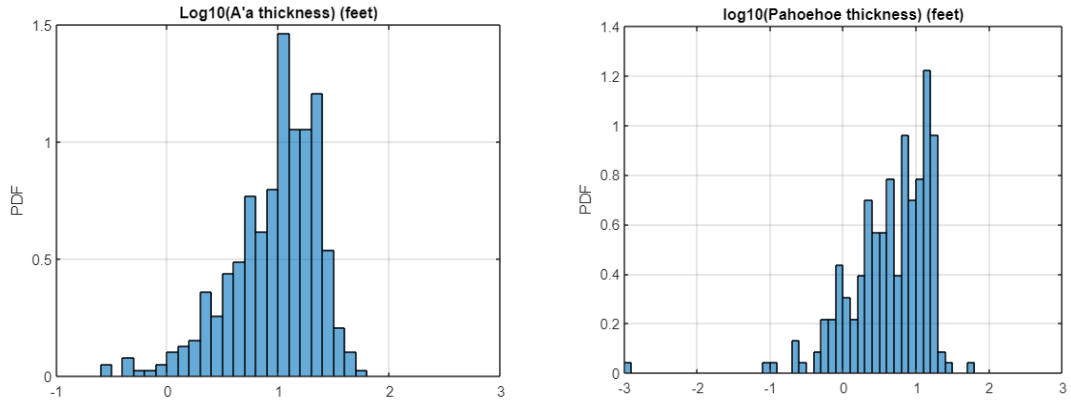

Chart 3-3: Probability Density Functions of A‘ā (left) and Pāhoehoe (right) Flow Thicknesses (log scale base 10, ft)

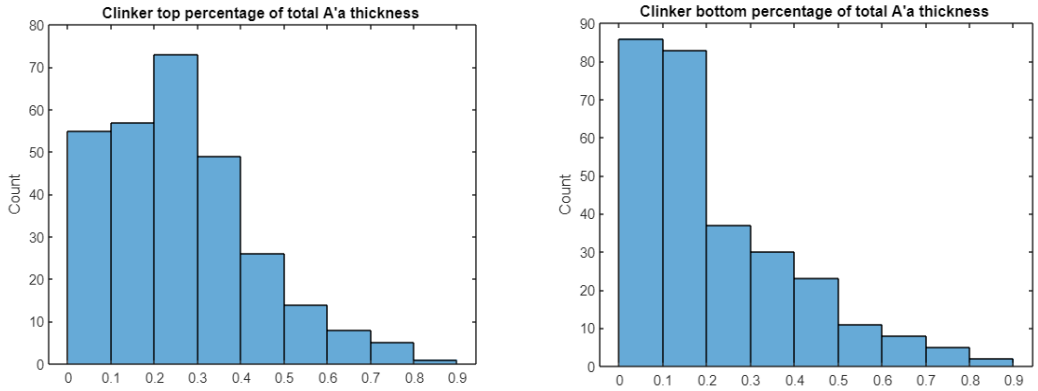

Chart 3-4: Histograms of Top (left) and Bottom (right) Clinker Fraction of Total A‘ā Flow Thickness

Using the available site data, the spatial variability of a‘ā clinker occurrence was analyzed and expressed in variograms. Due to the nature of lava flows down the general dip direction, it was assumed that the variability would not be isotropic, i.e., different in the general dip direction (horizontal) than the strike direction (horizontal) than in the vertical direction. Chart 3-5 presents the semi-variograms in the vertical direction for both boring log and barrel log data. The variograms indicate relatively consistent behavior, showing that the variability does not change significantly over distances greater than about 10 ft. The semi-variograms in the horizontal directions were not reliable due to the sparseness of the data pairs in the general

dip direction and direction perpendicular to the general dip direction (Chart 3-6). Instead, horizontal variograms were computed from the MrLavaLoba results.

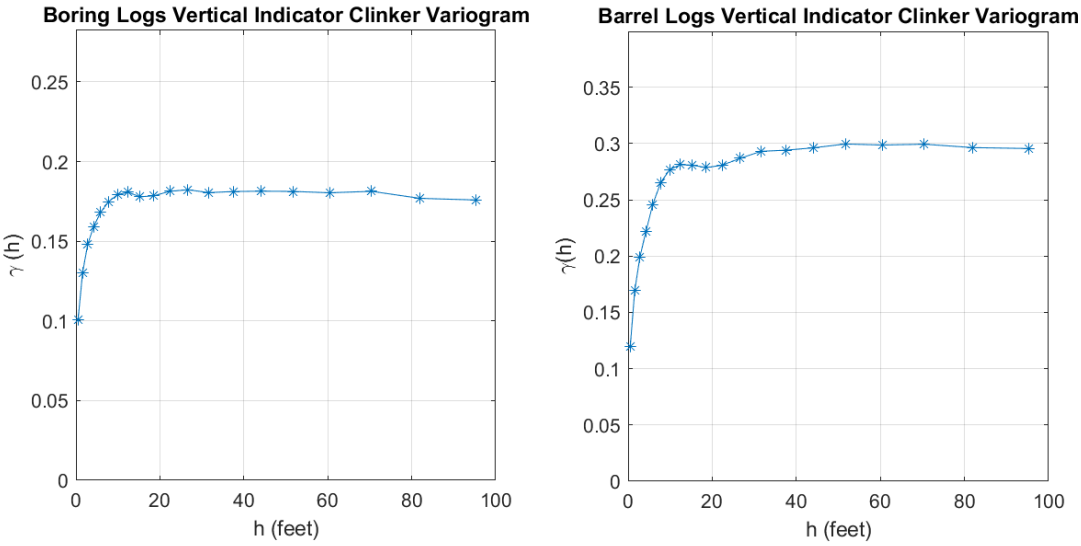

Chart 3-5: Semi-variograms of Clinker Occurrence in Vertical Direction, from Boring Log Data (left)

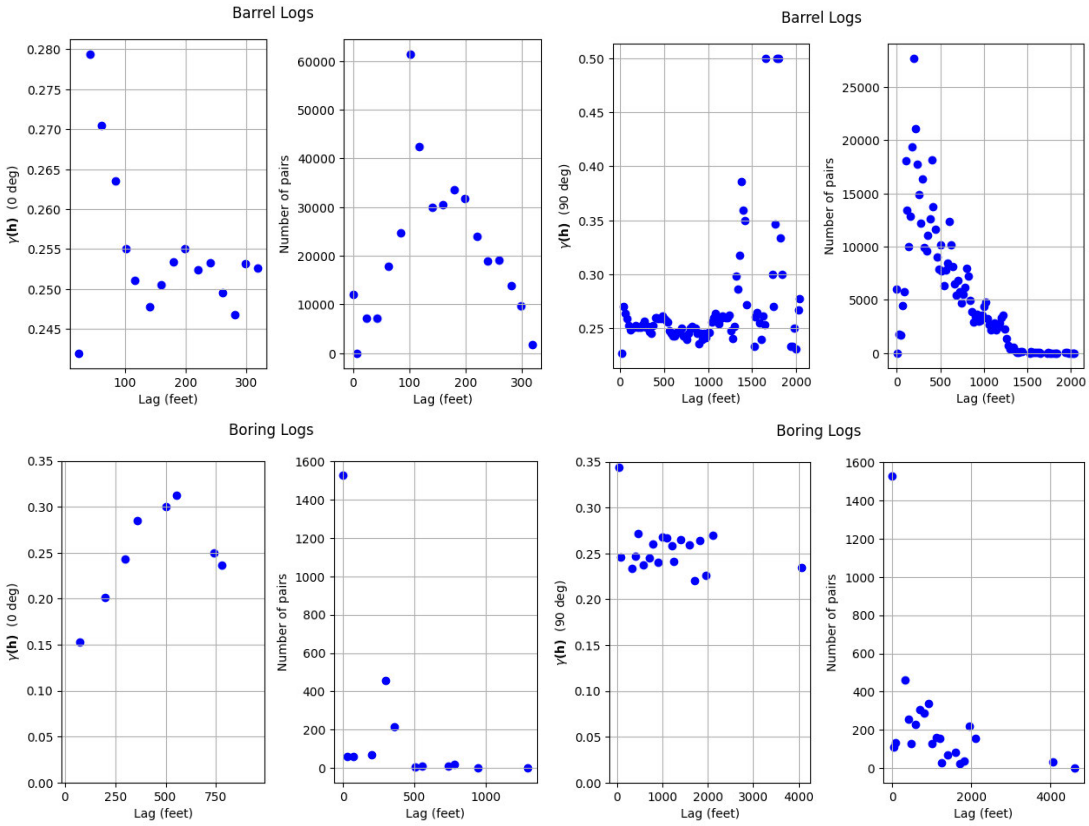

Chart 3-6: Semi-variograms of Clinker Occurrence in Horizontal Directions. General dip direction (left), strike direction (right) from barrel log (top) and boring log data (bottom)

3.1.6 Digital Elevation Model Generation

The lava flows from the MrLavaLoba simulation rely on the base DEM. Since it is impossible to assess the base topographic surface underlying the lava flow structure in the current GWFM domain, several possible DEM realizations were created. The current topography (Chart 3-7) of the GWFM domain was prepared as a rotated mesh with 20-meter (m) × 20-m grid cells with 610 rows and 839 columns, resulting in a 16.78-kilometer (km) (~55,000 ft) × 12.2-km (~40,000 ft) domain. To create DEM realizations, the variability of the current topography, trimmed to the GWFM domain with major ridges and valleys (Chart 3-8) was analyzed. The deviation of the DEM to a base plane oriented in the dip direction of the GWFM and inclined by the dip angle was computed. From this deviation, the variograms in the dip and strike directions were calculated. The resulting semi-variograms are presented in Chart 3-9, indicating maximum variability after 7,000 m (~23,000 ft) in the dip direction and 1,000 m (~3,280 ft) in the strike direction.

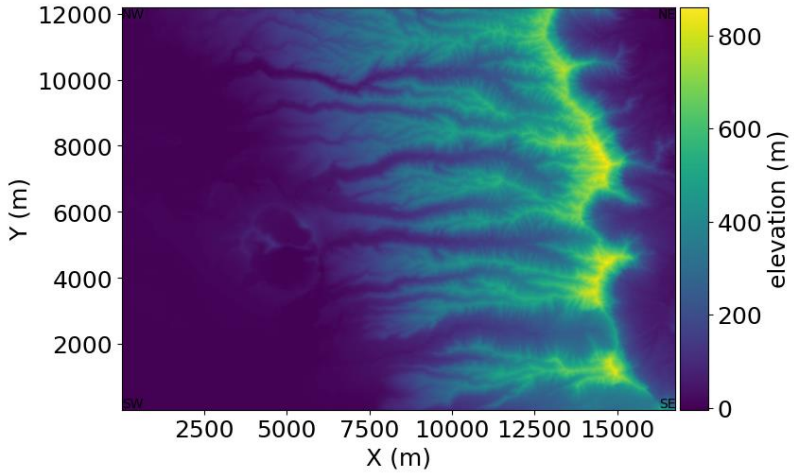

Chart 3-7: Topography in Red Hill GWFM Area

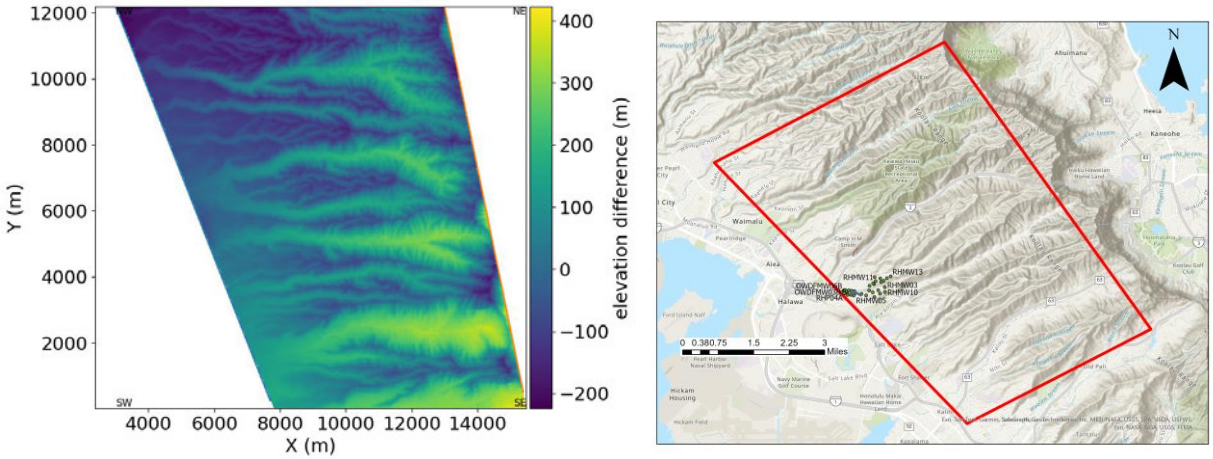

Chart 3-8: Topography Area Used for Variogram Calculation (left) and Approximate Extent of Topography Area on Map (right)

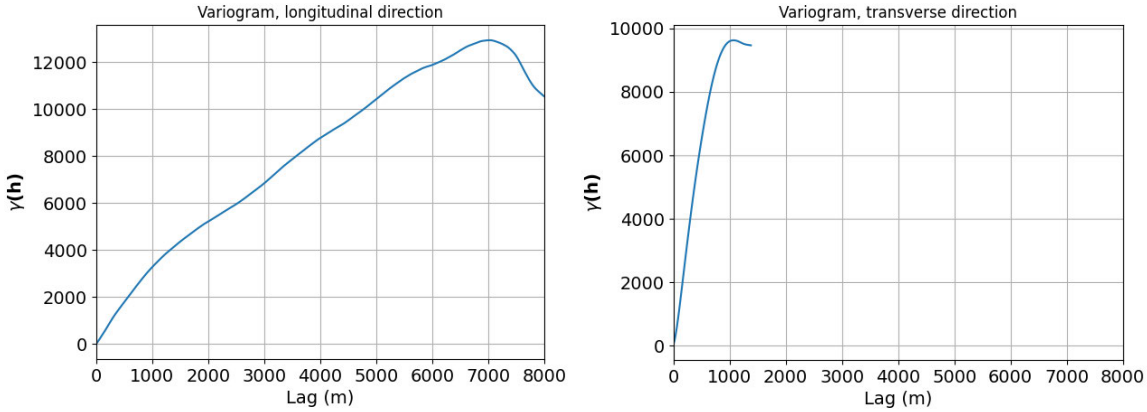

Chart 3-9: Semi-variogram of Topography Elevation Deviation from Longitudinal Base Plane in Dip Direction (left) and Transverse Strike Direction (right). Lag distance is shown on the x-axis with the variogram value shown on the y-axis.

Sequential Gaussian Simulation (SGSIM) (Deutsch and Journel 1997) was used to create DEM realizations with the semi-variogram information. This technique is suitable for Gaussian random fields and applies the definition of conditional probability recursively to draw from conditional univariate distributions instead of multivariate distributions, which decreases computational time. For each sample, the conditional distribution is found by solving kriging equations including all samples. Therefore, the maximum search domain is limited to an ellipse formed by the two correlation lengths. Still, the simulation was computationally intense for a 20-m × 20-m grid. Therefore, the SGSIM was conducted with a 200-m × 200-m grid instead, and the final base plane deviations in 20-m × 20-m resolution were computed from the 200-m × 200-m result through ordinary kriging. Forty DEM realizations were produced. The DEM realizations were calculated by multiplying the simulated, downscaled base plane deviation results with a standard deviation factor and then added to the base plane. The standard deviation of the deviation from the base plane to the actual topography was 121 m. The applied standard deviation factor was reduced by a factor of 5 to avoid deep troughs that could potentially trap the lava flow and produce unreasonable results. One example of a simulated DEM is shown in Chart 3-10.

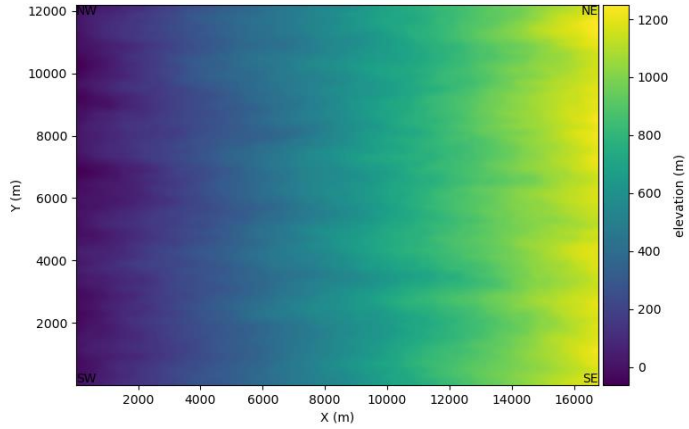

Chart 3-10: Example of Simulated DEM Realization

3.1.7 Lava Flow Parameter Calibration

MrLavaLoba employs various parameters to simulate the lava flow patterns stochastically. Most of the parameters were adopted from examples given by Vitturi & Tarquini (2018), in which a‘ā flow was simulated for a Mount Etna eruption and pāhoehoe flow was simulated for a Kilauea eruption. However, to match the lengths and thicknesses of the prevalent lava flows according to the measured boring log data, the eruption volume, number of lava flows simulated per eruption and the number of lobes simulated were adjusted. Length measurements from a lava flow image published by the Hawaii Volcano Observatory (HVO) were used.[6] The computed MrLavaLoba lava flow lengths did not exceed measured lengths and were of a similar magnitude. In addition, the upper and lower bound of the eruption volume distribution, which is a uniform distribution in log-scale, were adjusted in a calibration run with 500 cumulative eruptions each such that the resulting thickness distribution matched the thickness distribution from boring log data and from the HVO image. A comparison of the MrLavaLoba flow thickness cumulative density function (CDF) distribution to the CDFs of the data is shown for the a‘ā and pāhoehoe flows, respectively, in Chart 3-11. The lava flow eruption volume bounds are 3.5×10^{8} ft^3 and 7.1×10^{8} ft^3 for the a‘ā flows and 8.8×10^{7} ft^3 and 7.1×10^{8} ft^3 for the pāhoehoe flows.

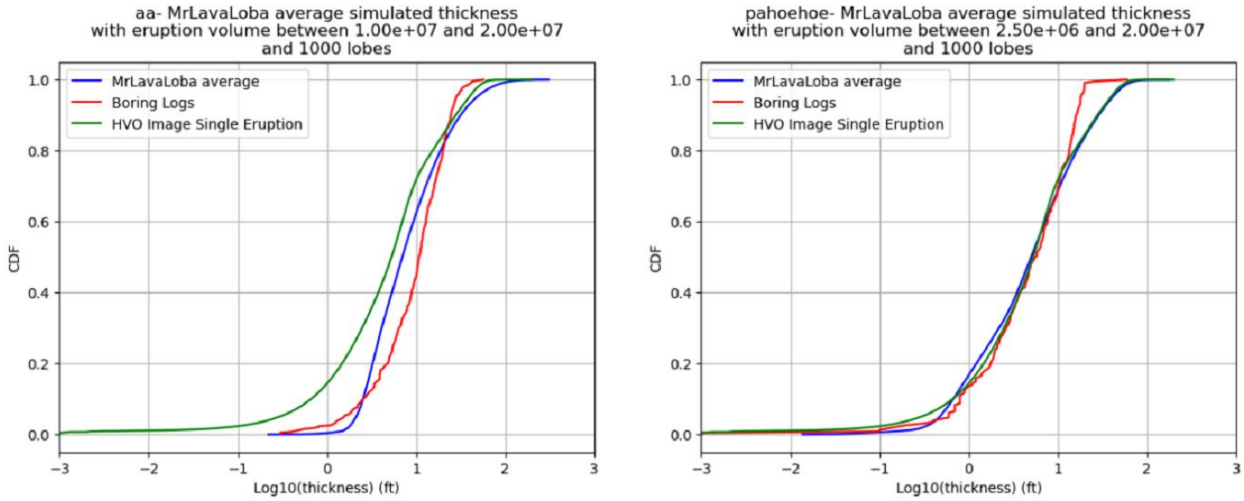

Chart 3-11: CDFs of MrLavaLoba Flow Thicknesses for A‘ā (left) and Pāhoehoe Flows (right)

3.1.8 Lava Flow Simulation

With the parameters calibrated as described in the previous section and based on literature examples, MrLavaLoba was run to simulate possible lava flow patterns in the GWFM domain. One MrLavaLoba run per each of the 40 DEMs as created in Section 3.1.7 was performed. Each run contained a sequence of 1,000 eruptions. For each eruption, a random value from a uniform distribution between 0 and 1 was drawn and

[6] https://www.usgs.gov/node/278888 ; https://www.usgs.gov/maps/december-5-2022-thermal-maps-showing-evolution-mauna-loa-fissure-3-lava-flow ; https://www.usgs.gov/node/278586

based on the transitional probabilities from Table 3-2, a‘ā or pāhoehoe flow parameters were selected The lava eruption location was chosen as follows: the eruption ridge on the true DEM (Chart 3-7) was drawn as a polygon and the standard deviation ($\boldsymbol{\sigma}$) of the distance from polygon points to a linear regression line through the polygon was calculated. An eruption band on a line perpendicular to the main flow direction with a width of 2*$\boldsymbol{\sigma}$ was established on each simulated DEM. Within this band, the eruption could be initiated at any point. The eruptions after an initial eruption were clustered around the previous eruption with a probability of 0.7 along a Gaussian distribution curve with a mean of 0 and standard deviation of $\mathbf{2} * \boldsymbol{\sigma}$. The flow volume for each eruption was selected as uniform distribution in log base 10 scale, with upper and lower bounds as calibrated in Section 3.1.7. Example eruptions using these parameters are shown below. MrLavaLoba saves the individual thickness of each flow and adds the flow thickness to the DEM to use as a new base topography for the next eruption. Therefore, the flow thickness is added up sequentially throughout the 1,000 simulated lava flow eruptions. Chart 3-12 shows examples of a‘ā and pāhoehoe flow results in plan view. Log files were output to track whether the respective eruptions of a simulation were a‘ā or pāhoehoe flows.

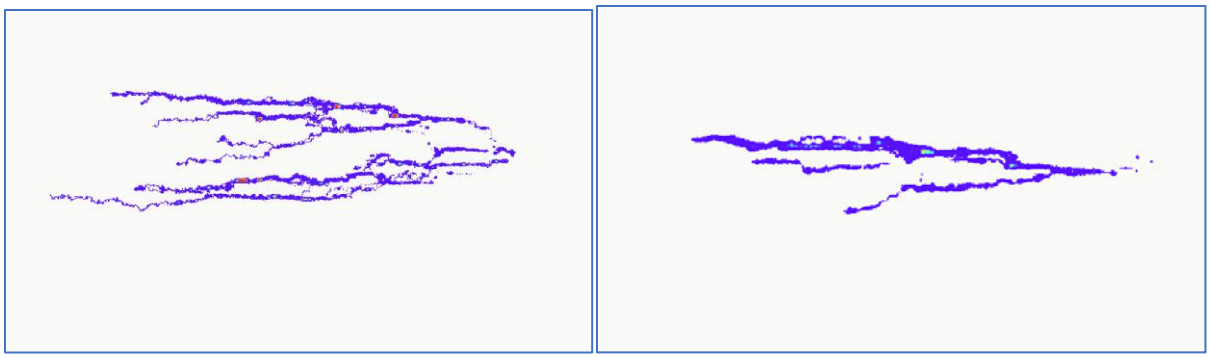

Chart 3-12: Examples of Simulated A‘ā (left) and Pāhoehoe Flows (right)

3.1.9 Horizontal Variogram Calculation

Since MrLavaLoba is not able to honor data during the simulation, the results of MrLavaLoba were used to establish the horizonal correlation structure as input for SISIM. A regular grid indicating the presence of clinker was created for each of the 40 MrLavaLoba results as follows. First, a three-dimensional mesh with same horizontal dimensions as the DEM (610 rows and 839 columns in horizontal directions, sizes of cells are 20 m in both horizontal directions) and 0.5-m-thick cells in vertical dimension was created. Then, the flow thicknesses from each of the 1,000 eruption simulations were added cumulatively, creating a set of 1,000 top elevations. Based on the data evaluation in Section 3.1.5 and Chart 3-4, it was assumed that clinker is present in the top 20% and bottom 20% of the thickness of an a‘ā flow. With this assumption, sets of 1,000 top elevations of bottom clinker portion and 1,000 elevations of bottom of top clinker portions were created. This information was used to check each indicator cell elevation. If an indicator cell overlapped with clinker by more than 50% of the indicator cell thickness, the indicator cell was assigned to be clinker, otherwise it was set to be massive basalt. The indicator grids were then fed into GSLIB’s GAM function to calculate the horizontal variograms in dip and strike directions. The results of the average semi-variograms and their one-standard deviation bounds are shown in Chart 3-13. They show that the variation by using different DEMs is small and that the maximum variation in the strike direction is reached after about 1,000 ft.

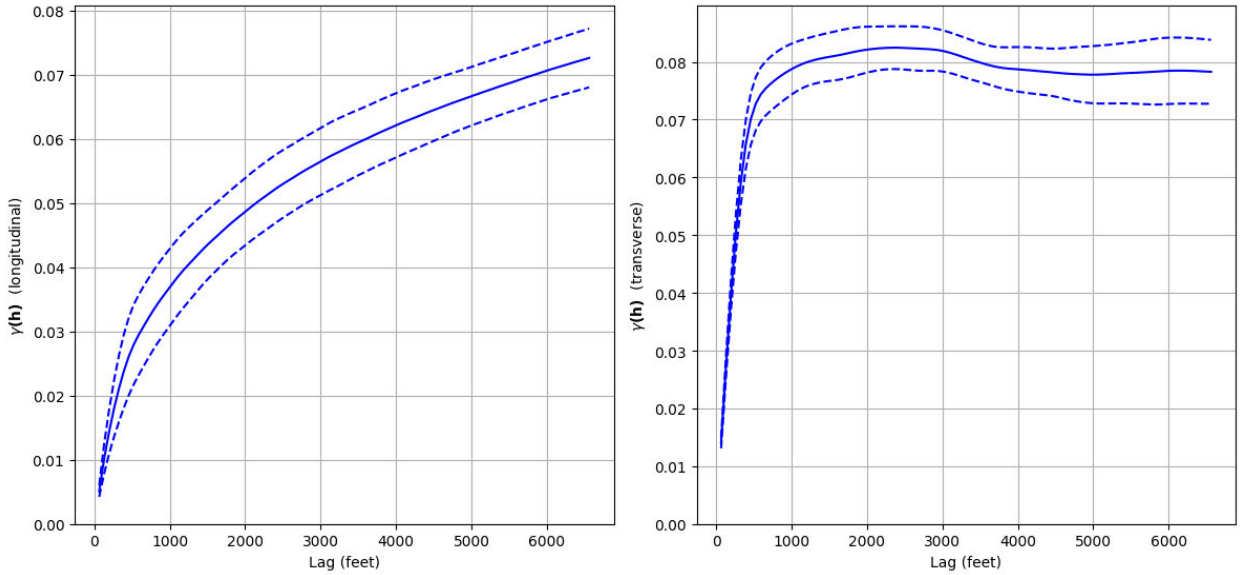

Chart 3-13: Average Semi-variogram (solid line) in Dip Direction (left) and Strike Direction (right). The dashed lines indicate the standard deviation from the average based on the 40 MrLavaLoba simulations.

3.1.10 Clinker Heterogeneity Simulation

Sections 3.1.5 and 3.1.9 described how to establish the spatial correlation structure of the aʻā clinker occurrence with semi-variograms in the dip direction, strike direction and vertical direction of the GWFM domain. This information was used to conduct sequential indicator simulations of aʻā clinker heterogeneity. A three-dimensional regular grid of 240 × 250 cells with a dimension of 25 ft in the horizontal directions, coinciding with the horizontal coordinates of the GWFM, was created. Vertically, the grid cells were set to be 2.5 ft thick, with 520 layers, to cover the vertical extent of the GWFM. The grid was oriented such that the layers were horizontal along the plane dipped by 4 degrees. Based on the data (Section 3.1.5), the global probability of aʻā clinker was set to 10%. The boring log and shaft data were also imported into the SIS mesh. For cells that coincide with multiple data points assigned with either massive basalt / pāhoehoe or aʻā clinker, the average was computed, serving as probability of aʻā clinker for the respective cell. An ordinary kriging option was used. The correlation lengths and search radii were set as 8,000 ft in the dip direction, 1,000 ft in the strike direction and 10 ft in the vertical direction. With these settings, 50 realizations using SIS were created. For the cells that contained boring log data information not equal to 0 or 1 due to data averaging, individual sampling was performed to assign the aʻā clinker value. An example realization of clinker occurrence produced by SISIM is shown in Chart 3-14. As a final step, the realizations were upscaled to the GWFM grid by averaging the clinker assignment of the SISIM cells located within the GWFM cells.

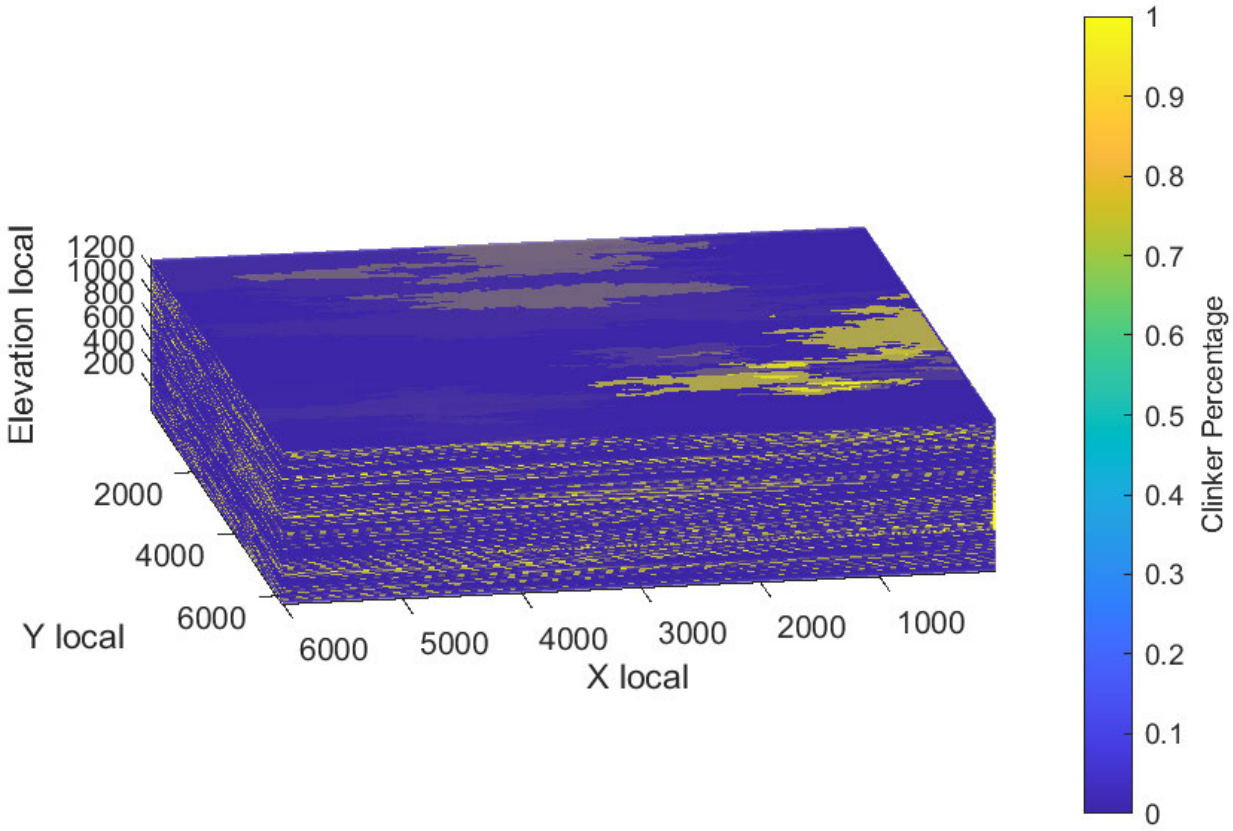

Chart 3-14: Example Realization of Clinker Occurrence. 1 is clinker and 0 is massive basalt.

3.2 Hydraulic Properties

Assignment of the hydraulic properties for heterogeneous basalt based on SISIM outputs upscaled to the regional GWFM's nested grid was conducted to account for plausible behavior of the system based on percentage of clinker in each cell and to maintain flow consistency between the regional and nested grid area. Inconsistency in the effective hydraulic conductivity across the interface between the parent and nested grid would result in non-physical behavior and generate unrealistic hydraulic responses and groundwater flow directions. A simplified box model approach was undertaken to estimate the effective hydraulic conductivity of each realization and adjust the parameter calculations to result in an effective hydraulic conductivity in all three directions (*x, y, z*) equivalent to the values from the calibrated regional GWFM.

A box model was extracted from the regional GWFM encompassing the extent of the nested grid. Layers with thicknesses larger than 25 ft or those where the saprolite layers are incised were excluded resulting in Layers 23 through 32. Three stress periods were introduced, each one with constant head boundaries imposing a fixed 1-ft head drop successively in the *x*, *y*, and *z* directions across the domain. Initially, the model was run with a homogeneous isotropic hydraulic conductivity of 1,000 ft/d to obtain the simulated fluxes during each stress period. Next, calculated heterogeneous hydraulic conductivities were imported into the model, and it was rerun. The simulated fluxes from the heterogeneous model were then compared to the initial fluxes from the uniform model to calculate the effective hydraulic conductivity. Finally, a

PEST simulation was developed to iteratively adjust the input parameters for the hydraulic conductivity calculations, using the calibrated regional model parameters as targets and the calculated effective hydraulic conductivity values as observations. This process was repeated for each realization. An example of the box model for Realization 10 is shown on Figure 3-2.

Calculation of the hydraulic properties was based on the percentage of clinker assigned to each model cell. Variable hydraulic properties included horizontal hydraulic conductivity, horizontal anisotropy ratio, vertical anisotropy ratio, specific yield, and porosity. An example of the percentage of clinker distribution for Realization 10 is presented in Chart 3-15. Note that the first bin of the histogram corresponds to 0% clinker and the bin was widened for visualization purposes.

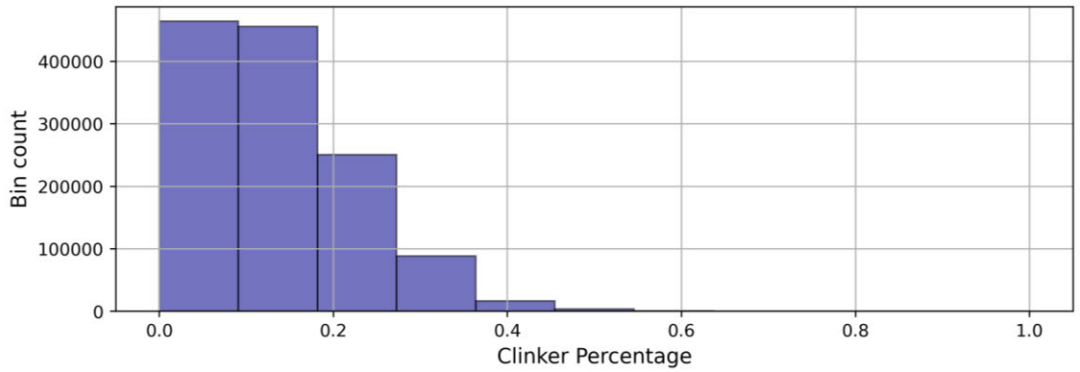

Chart 3-15: Histogram of Clinker Percentage

Horizontal hydraulic conductivity (K_x) in the longitudinal (X) direction, assumed to be down-dip, was calculated as a linear average between hydraulic conductivity values assigned to massive basalt and clinker. No clear site-specific data exist to estimate these values, only the bulk effective properties can be reasonably estimated. Massive basalt, or all non-clinker and weathered clinker, is assumed to be of relatively low hydraulic conductivity, where little flow occurs, whereas the clinker has a very high hydraulic conductivity, and is responsible for the high bulk hydraulic conductivity of the aquifer.

$$K_{cell} = K_{clinker} \times \%_{clinker} + K_{massive} \times \%_{massive}$$

Where:

$\boldsymbol{K_{cell}}$ = Calculated horizontal hydraulic conductivity of the cell (ft/d)

$\boldsymbol{K_{clinker}}$ = Horizontal hydraulic conductivity of clinker (ft/d)

$\%_{\boldsymbol{clinker}}$ = Percentage of clinker (expressed as decimal)

$\boldsymbol{K_{massive}}$ = Horizontal hydraulic conductivity of massive basalt (ft/d)

$\%_{\boldsymbol{massive}}$ = Percentage of massive basalt (expressed as decimal)

An example of the horizontal hydraulic conductivity distribution for Realization 10 is presented in Chart 3-16. The hydraulic conductivity value for clinker in this realization was 249,865 ft/d, and the value for massive basalt was 19 ft/d. Clinker percentages fall mostly in increments of 10% because the SISIM generation used the same 25-ft × 25-ft grid in the horizontal direction and 2.5 ft in the vertical. The majority

of MODFLOW model cells are 25 ft thick; therefore, clinker percentages are calculated based on 10 SISIM cells per MODFLOW model cell. Values in the first bin correspond to massive basalt. In areas of weathered basalt, the reduction factor in hydraulic conductivity for either caprock or beneath streams was applied to the clinker hydraulic conductivity only.

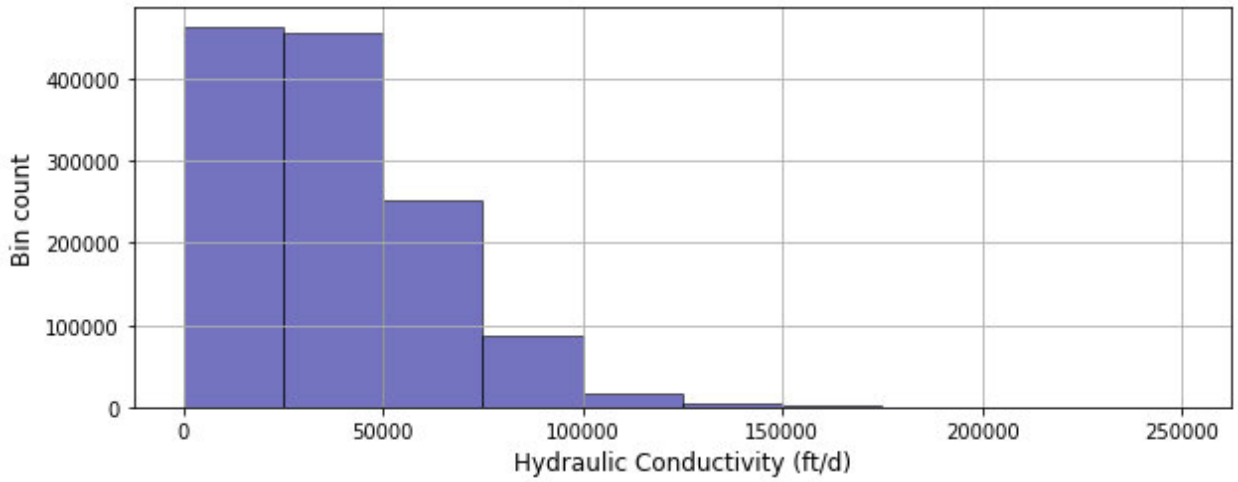

Chart 3-16: Histogram of Hydraulic Conductivity Values

Horizontal anisotropy ratio (K_x/K_y), where K_y is the hydraulic conductivity in the transverse (*y*) cross-dip, was calculated as a linear average between massive basalt and clinker, where the highest value of the anisotropy ratio occurs in massive basalt and clinker alone is assumed to be isotropic in the horizontal direction. The assumption is that as massive basalt becomes more prevalent, it acts as a barrier to flow in portions of the clinker leading to a lower effective hydraulic conductivity in the transverse (*y*) direction. Additionally, vertical cooling fractures in the massive basalt along the direction of lava flow result in higher hydraulic conductivities in the longitudinal direction.

$$K_y\ Ratio = \%_{clinker}\ +\ K_{y-m}Ratio \times\ \%_{massive}$$

Where:

$K_y\ Ratio$ = Calculated horizontal anisotropy ratio of the cell (-)

$\%_{clinker}$ = Percentage of clinker (expressed as decimal)

$K_{y-m}Ratio$ = Horizontal anisotropy ratio of massive basalt (ft/d)

$\%_{massive}$ = Percentage of massive basalt (expressed as decimal)

An example of the horizontal anisotropy distribution for Realization 10 is presented in Chart 3-17. The massive basalt horizontal anisotropy ratio for Realization 10 was 12.2.

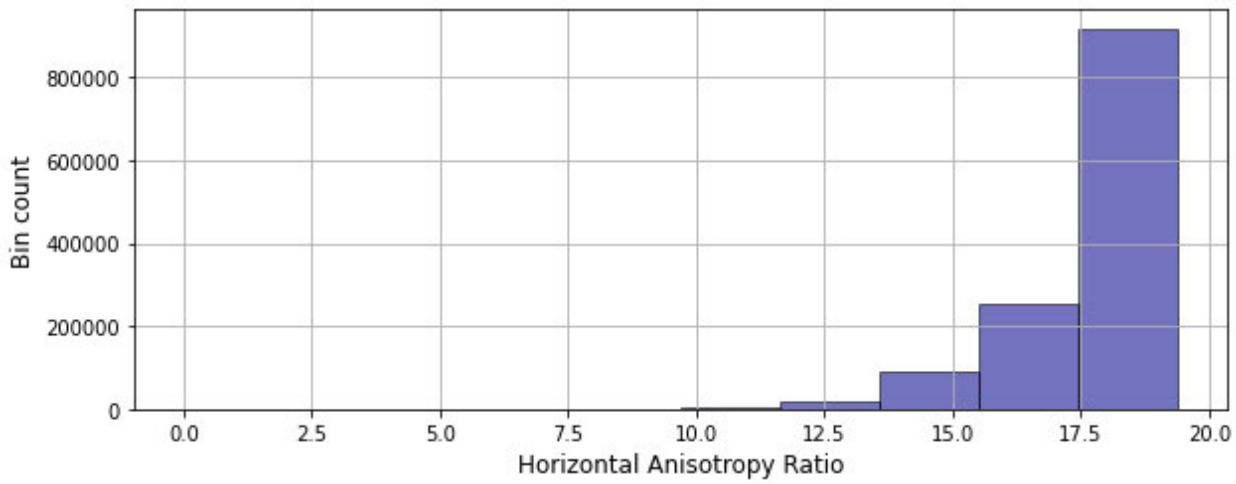

Chart 3-17: Histogram of Horizontal Anisotropy Values

Vertical anisotropy ratio (K_x/K_z), where K_z is the hydraulic conductivity in the vertical (Z), was calculated as a linear average between massive basalt and clinker, where the highest value of the anisotropy ratio occurs in clinker and massive basalt is assumed to be isotropic in the vertical direction. The assumption is that as massive basalt becomes less prevalent, the horizontal hydraulic conductivity increases significantly; however, layers of massive basalt would be limiting flow in in the vertical direction, resulting in a high vertical anisotropy ratio. Although 100% clinker would not be expected to have the highest anisotropy ratio without the presence of some massive basalt, no cells in the model domain are 100% clinker.

$$K_z\ Ratio = K_{z-cl}Ratio\ \times\ \%_{clinker}\ +\ \%_{massie}$$

Where:

$K_z\ Ratio$ = Calculated vertical anisotropy ratio of the cell (-)

$\%_{clinker}$ = Percentage of clinker (expressed as decimal)

$K_{z-cl}Ratio$ = Horizontal anisotropy ratio of massive basalt (ft/d)

$\%_{massive}$ = Percentage of massive basalt (expressed as decimal)

An example of the horizontal anisotropy distribution for Realization 10 is presented in Chart 3-18. The clinker vertical anisotropy ratio for Realization 10 was 46.

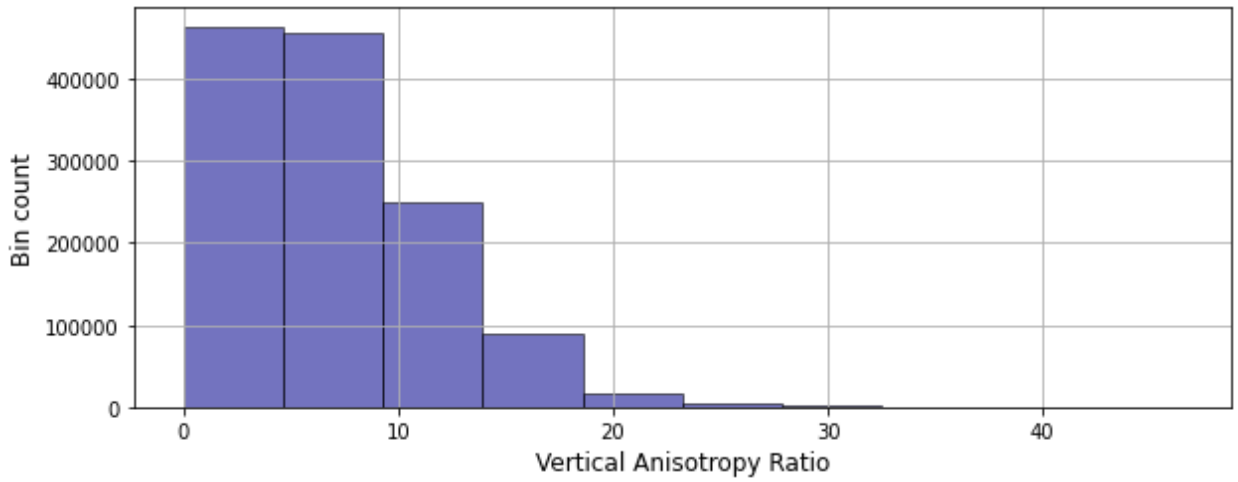

Chart 3-18: Histogram of Vertical Anisotropy Values

Specific yield was calculated as a linear average between values assigned to massive basalt and clinker. No box model estimates were made for specific yield and calibration of the regional GWFM demonstrated specific yield to have a relatively low sensitivity compared to other calibrated parameters. Massive basalt is assumed to be of relatively low specific yield, which was fixed at 5%, whereas the clinker has a very high specific yield, assumed to be 35%.

$$\boldsymbol{S_{y-cell} = S_{y-cl} \times \%_{clinker} + S_{y-m} \times \%_{massive}}$$

Where:

K_{cell} = Calculated horizontal hydraulic conductivity of the cell (ft/d)

$K_{clinker}$ = Horizontal hydraulic conductivity of clinker (ft/d)

$\%_{Clinker}$ = Percentage of clinker (expressed as decimal)

$K_{massive}$ = Horizontal hydraulic conductivity of massive basalt (ft/d)

$\%_{massive}$ = Percentage of massive basalt (expressed as decimal)

An example of the specific yield distribution for Realization 10 is presented in Chart 3-19. The average specific yield in the heterogeneous zone is approximately 8%, consistent with literature values (Oki 2005; Heath 1993). Porosity was estimated to be the specific yield multiplied by 1.375, resulting in an average effective porosity of 11%. Calibration of the GWFM is not sensitive to porosity. This parameter was later adjusted during the history matching phase of contaminant fate and transport modeling and is discussed further in Section 5.3.

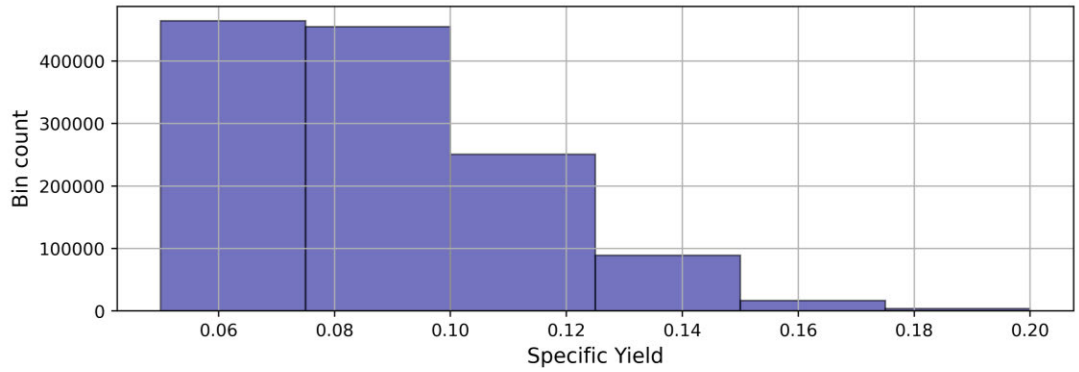

l

Chart 3-19: Histogram of Specific Yield Values

3.3 Comparison of Model Calibration

Resulting parameters distributions for each basalt realization were imported into the 44-stress period calibration model and simulations were conducted with no further adjustment of the parameter values. Model calibration was evaluated in the same manner as the regional model comparing simulated versus observed heads, drawdowns, and hydraulic gradients down Red Hill ridge. Water levels were evaluated in the same groups described in Section 2.3, as well as cumulatively. Additional consideration was given to horizontal head differences in Group 1 wells and vertical head differences in multilevel wells or grouped wells. Regional water budget remained largely unchanged from one realization to another.

Two additional considerations for the heterogeneous models, which were not expected to be replicated with homogeneous parameters, were compartmentalization of drawdowns and the flow distribution along (b) . Compartmentalized drawdowns were plotted in perceived groupings proposed by EPA in Technical Working Group Meeting #39 on May 30, 2021, and are shown on Figure 3-3. Compartmentalization was evaluated in a qualitative manner as contrasted with quantitative metrics used for other evaluation methods.

The flow distribution along (b) was considered an important physical process to be incorporated in the simulation. During construction of the water development tunnel, incoming flow rates and the lithology were recorded along its length (Stearns 1943). The log showed(b) mgd entering the first 500 ft of the tunnel, moving from west to east,(b mgd through the first 700 ft, (b) gd through 1,000 ft, and (b mgd through the full 1,180-ft length of the shaft. The sharp increase in groundwater inflows toward the end of the tunnel correspond to a larger clinker zone present in the final(b)(3) Based on this log, the GWFM was set up with (b) in three segments, from 0 to the angle in the shaft at approximately(b)(3) The three segments were assigned target contributions calculated from the observations of 12%, 29%, and 59%. Simulated percentages of contribution for each segment were compared to these values, Figure 3-4 shows the diagram of (b) from Stearns (1943), along with the segments of (b) considered, and an example of the clinker distribution (in map view) around (b) from Realization 10. An example of the full heterogeneous model setup with Realization 10 is shown on Figure 3-5,

The results from all realizations were compiled presenting the RMSE for each of the eight calibration target categories: flow distribution along (b) , Red Hill well heads, transitional well heads, all basal well heads, Red Hill well drawdowns, hydraulic gradients along and to the northwest of Red Hill ridge, horizontal head

differences in Red Hill wells, and vertical head differences in collocated wells. A comparison of the calibration for each realization as well as the base model with homogeneous parameters is presented in Table 3-3. Rankings were given to each realization based on the RMSE for each category. The sum of ranks was then used to provide a final ranking of the realizations. The table is ordered from best ranking realization to worst. Overall, the variation in RMSE across the realizations was relatively small ranging from 0.23 ft to 0.29 ft for Red Hill wells and 0.23 to 1.16 for all basal aquifer wells. The realizations with large residuals are attributed to larger than observed drawdowns at Hālawa Shaft. The difference in drawdown RMSE was only 0.04 ft, with values ranging from 0.17 to 0.20 ft for Red Hill wells. The RMSE for flow distribution across (b) ranged from 2.5% to 19.8%. The highest RMSE value corresponds to the base model (homogenous anisotropic model), although Realization 34 resulted in a slightly higher RMSE value of 19.9%. The average RMSE across all realizations for the (b) flow distribution was 12.4%. Full documentation of the calibration metrics for each realization are presented in Appendix G.

Table 3-3: Comparison of Realizations

Realization No.	(b) Flow Distribution RMSE (%)	Red Hill Wells Head RMSE (ft)	Transitional Wells Head RMSE (ft)	All Basal Wells Head RMSE (ft)	Red Hill Wells Drawdown RMSE (ft)	Ridge Gradients RMSE (ft)	Horizontal Head Differences RMSE (ft)	Vertical Head Differences RMSE (ft)	(b) Flow Distribution RMSE (%)_Rank	Red Hill Wells Head RMSE (ft)_Rank	Transitional Wells Head RMSE (ft)_Rank	All Basal Wells Head RMSE (ft)_Rank	Red Hill Wells Drawdown RMSE (ft)_Rank	Ridge Gradients RMSE (ft)_Rank	Horizontal Head Differences RMSE (ft)_Rank	Vertical Head Differences RMSE (ft)_Rank	Sum of Ranks	Rank
Realization_47	7.1	0.26	0.34	0.25	0.17	3.6E-05	0.23	0.34	5	13	9	4	1	19	3	3	57	1
Realization_13	4.2	0.24	0.35	0.26	0.17	2.6E-05	0.26	0.34	3	2	13	11	1	10	16	3	59	2
Realization_32	13.8	0.26	0.33	0.25	0.17	3.5E-05	0.23	0.34	30	13	5	4	1	18	3	3	77	3
Base	19.8	0.25	0.35	0.25	0.17	2.2E-05	0.23	0.33	50	8	13	4	1	9	3	1	89	4
Realization_10	14.1	0.27	0.32	0.27	0.17	1.6E-05	0.23	0.34	31	25	3	20	1	3	3	3	89	5
Realization_34	19.9	0.25	0.36	0.25	0.17	2.1E-05	0.23	0.33	51	8	19	4	1	7	3	1	94	6
Realization_8	8.3	0.25	0.40	0.24	0.17	1.8E-05	0.23	0.37	12	8	33	2	1	4	3	31	94	7
Realization_16	12.6	0.27	0.33	0.27	0.17	2.1E-05	0.23	0.35	24	25	5	20	1	8	3	9	95	8
Realization_12	17.0	0.25	0.38	0.25	0.17	1.5E-05	0.23	0.35	45	8	24	4	1	2	3	9	96	9
Realization_20	12.3	0.24	0.37	0.24	0.17	5.9E-05	0.25	0.35	21	2	20	2	1	27	14	9	96	10
Realization_11	12.1	0.28	0.31	0.27	0.17	4.0E-05	0.23	0.34	19	39	1	20	1	20	3	3	106	11
Realization_48	17.9	0.26	0.33	0.27	0.17	2.6E-05	0.24	0.35	47	13	5	20	1	10	12	9	117	12
Realization_26	14.1	0.26	0.35	0.26	0.17	6.2E-05	0.26	0.35	31	13	13	11	1	28	16	9	122	13
Realization_2	17.3	0.26	0.35	0.25	0.18	3.5E-05	0.22	0.35	46	13	13	4	26	17	1	9	129	14
Realization_21	19.6	0.27	0.35	0.27	0.17	1.4E-05	0.24	0.35	48	25	13	20	1	1	12	9	129	15
Realization_1	12.4	0.27	0.33	0.28	0.17	4.8E-05	0.25	0.35	22	25	5	32	1	23	14	9	131	16
Realization_23	9.3	0.27	0.35	0.27	0.17	4.1E-05	0.26	0.36	14	25	13	20	1	21	16	22	132	17
Realization_42	11.5	0.24	0.37	0.29	0.17	5.3E-05	0.29	0.34	18	2	20	36	1	24	30	3	134	18
Realization_45	14.1	0.29	0.31	0.29	0.17	3.1E-05	0.22	0.35	31	47	1	36	1	13	1	9	139	19
Realization_43	2.5	0.28	0.34	0.34	0.17	3.1E-05	0.30	0.35	1	39	9	41	1	14	34	9	148	20
Realization_9	13.7	0.24	0.38	0.38	0.17	1.8E-05	0.36	0.35	28	2	24	44	1	4	43	9	155	21
Realization_30	3.4	0.27	0.37	0.26	0.18	7.8E-05	0.27	0.36	2	25	20	11	26	34	23	22	163	22
Realization_27	13.7	0.23	0.40	0.27	0.17	5.8E-05	0.28	0.37	29	1	33	20	1	26	27	31	168	23
Realization_49	16.1	0.24	0.40	0.25	0.18	3.3E-05	0.26	0.37	41	2	33	4	26	15	16	31	168	24
Realization_29	14.2	0.24	0.41	0.23	0.18	7.2E-05	0.26	0.36	36	2	40	1	26	31	16	22	174	25
Realization_18	15.9	0.29	0.32	0.34	0.17	2.9E-05	0.29	0.35	39	47	3	41	1	12	30	9	182	26
Realization_17	14.4	0.28	0.34	0.33	0.17	1.8E-05	0.29	0.36	37	39	9	40	1	6	30	22	184	27
Realization_4	6.0	0.27	0.40	0.28	0.19	3.4E-05	0.26	0.37	4	25	33	32	38	16	16	31	195	28
Realization_6	14.1	0.27	0.34	0.67	0.17	4.8E-05	0.63	0.35	31	25	9	49	1	22	49	9	195	29
Realization_35	19.6	0.26	0.38	0.26	0.18	6.6E-05	0.27	0.36	49	13	24	11	26	30	23	22	198	30
Realization_40	7.1	0.26	0.40	0.26	0.18	1.1E-04	0.30	0.37	5	13	33	11	26	45	34	31	198	31
Realization_24	11.2	0.27	0.40	0.26	0.18	7.4E-05	0.26	0.38	15	25	33	11	26	33	16	41	200	32
Realization_36	12.1	0.26	0.41	0.26	0.18	8.0E-05	0.28	0.37	19	13	40	11	26	35	27	31	202	33
Realization_38	12.4	0.25	0.38	0.47	0.17	8.2E-05	0.46	0.36	23	8	24	46	1	36	47	22	207	34

Realization No.	(b) Flow Distribution RMSE (%)	Red Hill Wells Head RMSE (ft)	Transitional Wells Head RMSE (ft)	All Basal Wells Head RMSE (ft)	Red Hill Wells Drawdown RMSE (ft)	Ridge Gradients RMSE (ft)	Horizontal Head Differences RMSE (ft)	Vertical Head Differences RMSE (ft)	(b) Flow Distribution RMSE (%)_Rank	Red Hill Wells Head RMSE (ft)_Rank	Transitional Wells Head RMSE (ft)_Rank	All Basal Wells Head RMSE (ft)_Rank	Red Hill Wells Drawdown RMSE (ft)_Rank	Ridge Gradients RMSE (ft)_Rank	Horizontal Head Differences RMSE (ft)_Rank	Vertical Head Differences RMSE (ft)_Rank	Sum of Ranks	Rank
Realization_25	7.4	0.27	0.39	0.28	0.19	5.7E-05	0.27	0.37	8	25	29	32	38	25	23	31	211	35
Realization_28	8.0	0.26	0.43	0.26	0.19	9.5E-05	0.30	0.37	11	13	45	11	38	42	34	31	225	36
Realization_39	7.9	0.27	0.43	0.26	0.19	9.6E-05	0.29	0.38	10	25	45	11	38	43	30	41	243	37
Realization_19	14.1	0.26	0.42	0.28	0.19	7.3E-05	0.28	0.37	31	13	43	32	38	32	27	31	247	38
Realization_31	12.8	0.28	0.39	0.32	0.18	6.5E-05	0.30	0.39	25	39	29	39	26	29	34	46	267	39
Realization_7	13.5	0.28	0.37	0.45	0.18	1.1E-04	0.45	0.36	27	39	20	45	26	46	45	22	270	40
Realization_15	16.2	0.28	0.39	0.27	0.19	8.3E-05	0.27	0.39	43	39	29	20	38	37	23	46	275	41
Realization_44	8.7	0.26	0.41	0.70	0.19	9.3E-05	0.67	0.37	13	13	40	50	38	41	50	31	276	42
Realization_37	11.2	0.27	0.43	0.27	0.20	1.2E-04	0.32	0.38	15	25	45	20	48	48	39	41	281	43
Realization_41	12.8	0.28	0.38	1.16	0.18	1.2E-04	1.14	0.36	25	39	24	51	26	49	51	22	287	44
Realization_3	11.3	0.27	0.45	0.34	0.19	8.3E-05	0.35	0.38	17	25	49	41	38	38	42	41	291	45
Realization_33	7.5	0.29	0.42	0.29	0.19	9.2E-05	0.30	0.39	9	47	43	36	38	40	34	46	293	46
Realization_50	14.9	0.29	0.40	0.27	0.20	1.6E-04	0.37	0.36	38	47	33	20	48	51	44	22	303	47
Realization_5	7.3	0.28	0.49	0.27	0.20	1.3E-04	0.34	0.41	7	39	51	20	48	50	40	51	306	48
Realization_14	16.3	0.27	0.43	0.27	0.20	1.2E-04	0.34	0.39	44	25	45	20	48	47	40	46	315	49
Realization_46	16.1	0.29	0.39	0.47	0.18	1.0E-04	0.45	0.38	41	47	29	46	26	44	45	41	319	50
Realization_22	16.0	0.26	0.46	0.62	0.19	8.6E-05	0.61	0.39	40	13	50	48	38	39	48	46	322	51

Notes:

	RMSE is greater than homogeneous base model.
	RMSE is less than homogeneous base model.

3.4 Particle Tracking Results

Forward particle tracking was conducted with steady-state flow models for each realization under various pumping conditions from the water table beneath the tank farm to estimate the potential flow path of a potential release. Particle tracking considers only advective transport and does not account for dispersion, sorption, and degradation. Particles were simulated using a grid spacing over the tank farm area totaling 64 particles. An example of particle tracking results from Realization 10 for each pumping configuration is shown on Figure 3-6 through Figure 3-10. Particle tracking results from all realizations for each pumping configuration are shown on Figure 3-11 through Figure 3-15. The four scenarios were simulated as follows:

- (b) pumping at (b) gd, Hālawa Shaft pumping at 12 mgd, (b)(3) pumping at (b) mgd (Figure 3-6 and Figure 3-11)
- (b) pumping at (b mgd, Hālawa Shaft off, (b)(3) (b) (Figure 3-7 and Figure 3-12)
- (b) (b) Hālawa Shaft off, (b)(3) (b) (Figure 3-8 and Figure 3-13)
- (b) (b), Hālawa Shaft pumping at 12 mgd, (b)(3) (b) (Figure 3-9 and Figure 3-14)
- (b) pumping at (b mgd, Hālawa Shaft off, (b)(3) (b) (Figure 3-10 and Figure 3-15)

The first scenario represents (b) pumping at (mgd, Hālawa Shaft pumping at 12 mgd, and (b)(3) pumping at (b) mgd. Particles are simulated to originate from the Facility near the water table. From there they move with a small component of flow to the west-northwest before heading predominantly in the southwest direction toward (b) . In many cases, the particles enter through the clinker zone at the eastern end of (b) . Some particles stagnate due to the dipping layer structure or entering into the saprolite. Figure 3-6 shows particle tracking results for Realization 10. Figure 3-11 shows the simulation results for this scenario from all realizations. A summary table of final particle destinations is presented in Table 3-4. In most realizations, upwards of 90% of particles are captured by (b) . Those that did not get captured by (b) were stagnant particles.

Table 3-4: Summary of Particle Destinations for (b) Pumping at (mgd, Hālawa Shaft Pumping at 12 mgd, (b)(3) Pumping at (b) mgd

Realization	Percentage of Particle Destination						
	[redacted]	Springs	Pearl Harbor	Northwest GHB	Other Wells	Hālawa Shaft	Stagnant
Base	100.00%	0.0%	0.0%	0.0%	0.0%	0.0%	0.0%
Realization_1	92.20%	0.0%	0.0%	0.0%	0.0%	0.0%	7.8%
Realization_2	100.00%	0.0%	0.0%	0.0%	0.0%	0.0%	0.0%
Realization_3	96.90%	0.0%	0.0%	0.0%	0.0%	0.0%	3.1%
Realization_4	96.90%	0.0%	0.0%	0.0%	0.0%	0.0%	3.1%
Realization_5	90.60%	0.0%	0.0%	0.0%	0.0%	0.0%	9.4%
Realization_6	95.30%	0.0%	0.0%	0.0%	0.0%	0.0%	4.7%
Realization_7	89.10%	0.0%	0.0%	0.0%	0.0%	0.0%	10.9%
Realization_8	95.30%	0.0%	0.0%	0.0%	0.0%	0.0%	4.7%
Realization_9	100.00%	0.0%	0.0%	0.0%	0.0%	0.0%	0.0%
Realization_10	98.40%	0.0%	0.0%	0.0%	0.0%	0.0%	1.6%
Realization_11	89.10%	0.0%	0.0%	0.0%	0.0%	0.0%	10.9%
Realization_12	96.90%	0.0%	0.0%	0.0%	0.0%	0.0%	3.1%
Realization_13	95.30%	0.0%	0.0%	0.0%	0.0%	0.0%	4.7%
Realization_14	96.90%	0.0%	0.0%	0.0%	0.0%	0.0%	3.1%
Realization_15	96.90%	0.0%	0.0%	0.0%	0.0%	0.0%	3.1%
Realization_16	93.80%	0.0%	0.0%	0.0%	0.0%	0.0%	6.2%
Realization_17	95.30%	0.0%	0.0%	0.0%	0.0%	0.0%	4.7%
Realization_18	96.90%	0.0%	0.0%	0.0%	0.0%	0.0%	3.1%
Realization_19	96.90%	0.0%	0.0%	0.0%	0.0%	0.0%	3.1%
Realization_20	98.40%	0.0%	0.0%	0.0%	0.0%	0.0%	1.6%
Realization_21	96.90%	0.0%	0.0%	0.0%	0.0%	0.0%	3.1%
Realization_22	96.90%	0.0%	0.0%	0.0%	0.0%	0.0%	3.1%
Realization_23	90.60%	0.0%	0.0%	0.0%	0.0%	0.0%	9.4%
Realization_24	93.80%	0.0%	0.0%	0.0%	0.0%	0.0%	6.2%
Realization_25	96.90%	0.0%	0.0%	0.0%	0.0%	0.0%	3.1%
Realization_26	93.80%	0.0%	0.0%	0.0%	0.0%	0.0%	6.2%
Realization_27	93.80%	0.0%	0.0%	0.0%	0.0%	0.0%	6.2%
Realization_28	96.90%	0.0%	0.0%	0.0%	0.0%	0.0%	3.1%
Realization_29	95.30%	0.0%	0.0%	0.0%	0.0%	0.0%	4.7%
Realization_30	95.30%	0.0%	0.0%	0.0%	0.0%	0.0%	4.7%
Realization_31	92.20%	0.0%	0.0%	0.0%	0.0%	0.0%	7.8%
Realization_32	93.80%	0.0%	0.0%	0.0%	0.0%	0.0%	6.2%
Realization_33	82.80%	0.0%	0.0%	0.0%	0.0%	0.0%	17.2%
Realization_34	100.00%	0.0%	0.0%	0.0%	0.0%	0.0%	0.0%
Realization_35	89.10%	0.0%	0.0%	0.0%	0.0%	0.0%	10.9%
Realization_36	93.80%	0.0%	0.0%	0.0%	0.0%	0.0%	6.2%
Realization_37	98.40%	0.0%	0.0%	0.0%	0.0%	0.0%	1.6%

Realization	Percentage of Particle Destination						
	[redacted]	Springs	Pearl Harbor	Northwest GHB	Other Wells	Hālawa Shaft	Stagnant
Realization_38	90.60%	0.0%	0.0%	0.0%	0.0%	0.0%	9.4%
Realization_39	95.30%	0.0%	0.0%	0.0%	0.0%	0.0%	4.7%
Realization_40	95.30%	0.0%	0.0%	0.0%	0.0%	0.0%	4.7%
Realization_41	96.90%	0.0%	0.0%	0.0%	0.0%	0.0%	3.1%
Realization_42	95.30%	0.0%	0.0%	0.0%	0.0%	0.0%	4.7%
Realization_43	92.20%	0.0%	0.0%	0.0%	0.0%	0.0%	7.8%
Realization_44	90.60%	0.0%	0.0%	0.0%	0.0%	0.0%	9.4%
Realization_45	95.30%	0.0%	0.0%	0.0%	0.0%	0.0%	4.7%
Realization_46	95.30%	0.0%	0.0%	0.0%	0.0%	0.0%	4.7%
Realization_47	89.10%	0.0%	0.0%	0.0%	0.0%	0.0%	10.9%
Realization_48	81.20%	0.0%	0.0%	0.0%	0.0%	0.0%	18.8%
Realization_49	100.00%	0.0%	0.0%	0.0%	0.0%	0.0%	0.0%
Realization_50	87.50%	0.0%	0.0%	0.0%	0.0%	0.0%	12.5%

The second scenario simulates [redacted] mgd withdrawal from [redacted], [redacted] from [redacted], and no withdrawals from Hālawa Shaft. This scenario demonstrates the maximum capture of groundwater from beneath the Facility by [redacted] because Hālawa Shaft is not pumping. Particles are simulated to originate from the Facility near the water table. From there they move with a small component of flow to the west-northwest before heading predominantly in the southwest direction toward [redacted]. In many cases, the particles enter through clinker zone at the eastern end of [redacted]. Some particles stagnate due to the dipping layer structure or entering the saprolite. Figure 3-7 shows particle tracking results for Realization 10. Figure 3-12 shows the simulation results for this scenario from all realizations. A summary table of final particle destinations is presented in Table 3-5. In most realizations, upwards of 95% of particles are captured by [redacted]. Those that did not get captured by [redacted] were stagnant particles.

Table 3-5: Summary of Particle Destinations for (b) Pumping at (b) mgd, Hālawa Shaft Off, (b)(3) (b)

Realization	Percentage of Particle Destination						
	[redacted]	Springs	Pearl Harbor	Northwest GHB	Other Wells	Hālawa Shaft	Stagnant
Base	100.00%	0.0%	0.0%	0.0%	0.0%	0.0%	0.0%
Realization_1	96.90%	0.0%	0.0%	0.0%	0.0%	0.0%	3.1%
Realization_2	95.30%	0.0%	0.0%	0.0%	0.0%	0.0%	4.7%
Realization_3	96.90%	0.0%	0.0%	0.0%	0.0%	0.0%	3.1%
Realization_4	98.40%	0.0%	0.0%	0.0%	0.0%	0.0%	1.6%
Realization_5	93.80%	0.0%	0.0%	0.0%	0.0%	0.0%	6.2%
Realization_6	92.20%	0.0%	0.0%	0.0%	0.0%	0.0%	7.8%
Realization_7	93.80%	0.0%	0.0%	0.0%	0.0%	0.0%	6.2%
Realization_8	93.80%	0.0%	0.0%	0.0%	0.0%	0.0%	6.2%
Realization_9	96.90%	0.0%	0.0%	0.0%	0.0%	0.0%	3.1%
Realization_10	95.30%	0.0%	0.0%	0.0%	0.0%	0.0%	4.7%
Realization_11	96.90%	0.0%	0.0%	0.0%	0.0%	0.0%	3.1%
Realization_12	95.30%	0.0%	0.0%	0.0%	0.0%	0.0%	4.7%
Realization_13	90.60%	0.0%	0.0%	0.0%	0.0%	0.0%	9.4%
Realization_14	95.30%	0.0%	0.0%	0.0%	0.0%	0.0%	4.7%
Realization_15	95.30%	0.0%	0.0%	0.0%	0.0%	0.0%	4.7%
Realization_16	98.40%	0.0%	0.0%	0.0%	0.0%	0.0%	1.6%
Realization_17	96.90%	0.0%	0.0%	0.0%	0.0%	0.0%	3.1%
Realization_18	89.10%	0.0%	0.0%	0.0%	0.0%	0.0%	10.9%
Realization_19	92.20%	0.0%	0.0%	0.0%	0.0%	0.0%	7.8%
Realization_20	96.90%	0.0%	0.0%	0.0%	0.0%	0.0%	3.1%
Realization_21	100.00%	0.0%	0.0%	0.0%	0.0%	0.0%	0.0%
Realization_22	95.30%	0.0%	0.0%	0.0%	0.0%	0.0%	4.7%
Realization_23	89.10%	0.0%	0.0%	0.0%	0.0%	0.0%	10.9%
Realization_24	93.80%	0.0%	0.0%	0.0%	0.0%	0.0%	6.2%
Realization_25	95.30%	0.0%	0.0%	0.0%	0.0%	0.0%	4.7%
Realization_26	90.60%	0.0%	0.0%	0.0%	0.0%	0.0%	9.4%
Realization_27	93.80%	0.0%	0.0%	0.0%	0.0%	0.0%	6.2%
Realization_28	95.30%	0.0%	0.0%	0.0%	0.0%	0.0%	4.7%
Realization_29	90.60%	0.0%	0.0%	0.0%	0.0%	0.0%	9.4%
Realization_30	92.20%	0.0%	0.0%	0.0%	0.0%	0.0%	7.8%
Realization_31	95.30%	0.0%	0.0%	0.0%	0.0%	0.0%	4.7%
Realization_32	95.30%	0.0%	0.0%	0.0%	0.0%	0.0%	4.7%
Realization_33	92.20%	0.0%	0.0%	0.0%	0.0%	0.0%	7.8%
Realization_34	100.00%	0.0%	0.0%	0.0%	0.0%	0.0%	0.0%
Realization_35	93.80%	0.0%	0.0%	0.0%	0.0%	0.0%	6.2%
Realization_36	95.30%	0.0%	0.0%	0.0%	0.0%	0.0%	4.7%
Realization_37	92.20%	0.0%	0.0%	0.0%	0.0%	0.0%	7.8%

Realization	Percentage of Particle Destination						
	[redacted]	Springs	Pearl Harbor	Northwest GHB	Other Wells	Hālawa Shaft	Stagnant
Realization_38	89.10%	0.0%	0.0%	0.0%	0.0%	0.0%	10.9%
Realization_39	96.90%	0.0%	0.0%	0.0%	0.0%	0.0%	3.1%
Realization_40	96.90%	0.0%	0.0%	0.0%	0.0%	0.0%	3.1%
Realization_41	96.90%	0.0%	0.0%	0.0%	0.0%	0.0%	3.1%
Realization_42	96.90%	0.0%	0.0%	0.0%	0.0%	0.0%	3.1%
Realization_43	96.90%	0.0%	0.0%	0.0%	0.0%	0.0%	3.1%
Realization_44	95.30%	0.0%	0.0%	0.0%	0.0%	0.0%	4.7%
Realization_45	96.90%	0.0%	0.0%	0.0%	0.0%	0.0%	3.1%
Realization_46	95.30%	0.0%	0.0%	0.0%	0.0%	0.0%	4.7%
Realization_47	93.80%	0.0%	0.0%	0.0%	0.0%	0.0%	6.2%
Realization_48	92.20%	0.0%	0.0%	0.0%	0.0%	0.0%	7.8%
Realization_49	98.40%	0.0%	0.0%	0.0%	0.0%	0.0%	1.6%
Realization_50	89.10%	0.0%	0.0%	0.0%	0.0%	0.0%	10.9%

The third scenario simulates no groundwater extraction at (b) , (b)(3), or Hālawa Shaft. Particles are simulated to originate from the Facility near the water table. Particles from beneath the tank farm travel generally to the west-northwest, eventually discharging mostly to the northwest GHB, with some particles discharging to the Kalauao Springs or Pearl Harbor. Some particles travel beneath Pearl Harbor, but due to the low hydraulic conductivity of the caprock, they eventually discharge to the northwest GHB rather than Pearl Harbor. Figure 3-8 shows particle tracking results for Realization 10. Figure 3-13 shows the simulation results for this scenario from all realizations. A summary table of final particle destinations is presented in Table 3-6. Some particles are listed as ending at (b) despite it being off, because particles are allowed to enter a CLN while off, but mod-PATH3DU does not allow for particles to re-enter the aquifer.

Table 3-6: Summary of Particle Destinations for (b) (b), Hālawa Shaft Off, (b)(3) Pumping (b)

Realization	Percentage of Particle Destination						
	[redacted]	Springs	Pearl Harbor	Northwest GHB	Other Wells	Hālawa Shaft	Stagnant
Base	20.30%	1.6%	1.6%	76.6%	0.0%	0.0%	0.0%
Realization_1	1.60%	15.6%	14.1%	65.6%	0.0%	0.0%	3.1%
Realization_2	6.20%	21.9%	17.2%	51.6%	0.0%	0.0%	3.1%
Realization_3	4.70%	0.0%	1.6%	89.1%	0.0%	0.0%	4.7%
Realization_4	0.00%	9.4%	25.0%	64.1%	0.0%	0.0%	1.6%
Realization_5	3.10%	1.6%	6.2%	84.4%	0.0%	0.0%	4.7%
Realization_6	6.20%	4.7%	21.9%	59.4%	0.0%	0.0%	7.8%
Realization_7	3.10%	26.6%	14.1%	50.0%	0.0%	0.0%	6.2%
Realization_8	6.20%	3.1%	9.4%	68.8%	0.0%	0.0%	12.5%
Realization_9	18.80%	0.0%	6.2%	71.9%	0.0%	0.0%	3.1%
Realization_10	20.30%	0.0%	0.0%	76.6%	0.0%	0.0%	3.1%
Realization_11	6.20%	18.8%	12.5%	57.8%	0.0%	0.0%	4.7%
Realization_12	7.80%	0.0%	0.0%	92.2%	0.0%	0.0%	0.0%
Realization_13	6.20%	1.6%	4.7%	82.8%	0.0%	0.0%	4.7%
Realization_14	4.70%	0.0%	21.9%	64.1%	0.0%	0.0%	9.4%
Realization_15	1.60%	40.6%	9.4%	28.1%	0.0%	0.0%	20.3%
Realization_16	4.70%	25.0%	9.4%	53.1%	0.0%	0.0%	7.8%
Realization_17	1.60%	1.6%	4.7%	92.2%	0.0%	0.0%	0.0%
Realization_18	4.70%	10.9%	10.9%	67.2%	0.0%	0.0%	6.2%
Realization_19	0.00%	4.7%	1.6%	81.2%	0.0%	0.0%	12.5%
Realization_20	4.70%	6.2%	17.2%	67.2%	0.0%	0.0%	4.7%
Realization_21	3.10%	6.2%	31.2%	50.0%	0.0%	0.0%	9.4%
Realization_22	4.70%	1.6%	0.0%	84.4%	0.0%	0.0%	9.4%
Realization_23	6.20%	1.6%	6.2%	82.8%	0.0%	0.0%	3.1%
Realization_24	1.60%	9.4%	3.1%	84.4%	0.0%	0.0%	1.6%
Realization_25	1.60%	0.0%	3.1%	90.6%	0.0%	0.0%	4.7%
Realization_26	3.10%	15.6%	21.9%	54.7%	0.0%	0.0%	4.7%
Realization_27	3.10%	18.8%	23.4%	46.9%	0.0%	0.0%	7.8%
Realization_28	1.60%	20.3%	4.7%	68.8%	0.0%	0.0%	4.7%
Realization_29	3.10%	14.1%	12.5%	65.6%	0.0%	0.0%	4.7%
Realization_30	6.20%	7.8%	6.2%	73.4%	0.0%	0.0%	6.2%
Realization_31	1.60%	10.9%	29.7%	53.1%	0.0%	0.0%	4.7%
Realization_32	4.70%	9.4%	14.1%	67.2%	0.0%	0.0%	4.7%
Realization_33	4.70%	39.1%	28.1%	20.3%	0.0%	0.0%	7.8%
Realization_34	9.40%	0.0%	0.0%	90.6%	0.0%	0.0%	0.0%
Realization_35	4.70%	1.6%	9.4%	76.6%	0.0%	0.0%	7.8%
Realization_36	4.70%	0.0%	37.5%	51.6%	0.0%	0.0%	6.2%
Realization_37	1.60%	28.1%	20.3%	40.6%	0.0%	0.0%	9.4%
Realization_38	1.60%	3.1%	15.6%	76.6%	0.0%	0.0%	3.1%

Realization	Percentage of Particle Destination						
	[redacted]	Springs	Pearl Harbor	Northwest GHB	Other Wells	Hālawa Shaft	Stagnant
Realization_39	1.60%	1.6%	3.1%	89.1%	0.0%	0.0%	4.7%
Realization_40	10.90%	7.8%	32.8%	39.1%	0.0%	0.0%	9.4%
Realization_41	7.80%	3.1%	4.7%	78.1%	0.0%	0.0%	6.2%
Realization_42	6.20%	3.1%	0.0%	84.4%	0.0%	0.0%	6.2%
Realization_43	3.10%	4.7%	15.6%	73.4%	0.0%	0.0%	3.1%
Realization_44	4.70%	0.0%	0.0%	90.6%	0.0%	0.0%	4.7%
Realization_45	3.10%	37.5%	26.6%	29.7%	0.0%	0.0%	3.1%
Realization_46	6.20%	0.0%	9.4%	79.7%	0.0%	0.0%	4.7%
Realization_47	9.40%	0.0%	3.1%	81.2%	0.0%	0.0%	6.2%
Realization_48	0.00%	50.0%	15.6%	26.6%	0.0%	0.0%	7.8%
Realization_49	0.00%	56.2%	9.4%	23.4%	0.0%	0.0%	10.9%
Realization_50	1.60%	0.0%	0.0%	89.1%	0.0%	0.0%	9.4%

The fourth scenario simulates no withdrawal from (b) or (b)(3) and 12 mgd withdrawal from Hālawa Shaft, which represents a hypothetical and unlikely scenario in which the greatest risk is posed to Hālawa Shaft. Particles from beneath the tank farm travel to the west-northwest, slightly more to the west compared to the previous scenario with Hālawa Shaft off. Some particles reach Hālawa shaft in two realizations, while some particles reach other water supply wells to the west in four realizations. Most particle discharge occurred at Kalauao Springs, Pearl Harbor, or the northwest GHB. This was the only pumping scenario where particles reached either Hālawa Shaft or other water supply wells. Two realizations resulted in particles captured at Hālawa Shaft with 4.7% and 6.2% of particles captured. Median travel times of the particles for the realizations were 23 and 25 years, respectively. Four realizations resulted in particles captured by other water supply wells, which ranged from 1.6% to 26.6% of particles. Median travel times in those realizations ranged from 13 to 40 years.

Figure 3-9 shows particle tracking results for Realization 10. Figure 3-14 shows the simulation results for this scenario from all realizations. A summary table of final particle destinations is presented in Table 3-7. Some particles are listed as ending at (b) despite it being off, because particles are allowed to enter a CLN while off, but mod-PATH3DU does not allow for particles to re-enter the aquifer.

Table 3-7: Summary of Particle Destinations for (b) (b), Hālawa Shaft Pumping at 12 mgd, (b)(3) Pumping(b)

Realization	Percentage of Particle Destination						
	[redacted]	Springs	Pearl Harbor	Northwest GHB	Other Wells	Hālawa Shaft	Stagnant
Base	18.80%	46.9%	23.4%	6.2%	0.0%	0.0%	4.7%
Realization_1	4.70%	67.2%	17.2%	4.7%	0.0%	0.0%	6.2%
Realization_2	6.20%	84.4%	3.1%	1.6%	0.0%	0.0%	4.7%
Realization_3	6.20%	28.1%	7.8%	53.1%	0.0%	0.0%	4.7%
Realization_4	3.10%	62.5%	18.8%	6.2%	0.0%	0.0%	9.4%
Realization_5	3.10%	34.4%	43.8%	12.5%	0.0%	0.0%	6.2%
Realization_6	4.70%	51.6%	17.2%	10.9%	0.0%	0.0%	15.6%
Realization_7	3.10%	71.9%	12.5%	4.7%	0.0%	0.0%	7.8%
Realization_8	10.90%	43.8%	25.0%	12.5%	0.0%	0.0%	7.8%
Realization_9	10.90%	0.0%	10.9%	71.9%	0.0%	0.0%	6.2%
Realization_10	18.80%	32.8%	3.1%	42.2%	0.0%	0.0%	3.1%
Realization_11	6.20%	68.8%	14.1%	4.7%	0.0%	0.0%	6.2%
Realization_12	3.10%	0.0%	1.6%	95.3%	0.0%	0.0%	0.0%
Realization_13	6.20%	18.8%	14.1%	51.6%	0.0%	0.0%	9.4%
Realization_14	4.70%	42.2%	21.9%	20.3%	0.0%	0.0%	10.9%
Realization_15	3.10%	82.8%	1.6%	1.6%	4.7%	0.0%	6.2%
Realization_16	3.10%	73.4%	10.9%	7.8%	0.0%	0.0%	4.7%
Realization_17	6.20%	26.6%	25.0%	39.1%	0.0%	0.0%	3.1%
Realization_18	3.10%	79.7%	4.7%	3.1%	0.0%	0.0%	9.4%
Realization_19	3.10%	57.8%	12.5%	17.2%	0.0%	0.0%	9.4%
Realization_20	4.70%	71.9%	14.1%	4.7%	0.0%	0.0%	4.7%
Realization_21	4.70%	31.2%	43.8%	15.6%	0.0%	0.0%	4.7%
Realization_22	1.60%	65.6%	17.2%	7.8%	0.0%	0.0%	7.8%
Realization_23	1.60%	67.2%	15.6%	10.9%	0.0%	0.0%	4.7%
Realization_24	1.60%	42.2%	29.7%	17.2%	0.0%	0.0%	9.4%
Realization_25	3.10%	70.3%	17.2%	0.0%	0.0%	0.0%	9.4%
Realization_26	4.70%	70.3%	10.9%	4.7%	0.0%	0.0%	9.4%
Realization_27	4.70%	56.2%	21.9%	6.2%	0.0%	0.0%	10.9%
Realization_28	0.00%	65.6%	10.9%	15.6%	0.0%	0.0%	7.8%
Realization_29	3.10%	56.2%	14.1%	20.3%	0.0%	0.0%	6.2%
Realization_30	3.10%	68.8%	7.8%	10.9%	0.0%	0.0%	9.4%
Realization_31	1.60%	76.6%	10.9%	3.1%	0.0%	0.0%	7.8%
Realization_32	6.20%	53.1%	20.3%	14.1%	0.0%	0.0%	6.2%
Realization_33	3.10%	75.0%	6.2%	0.0%	0.0%	0.0%	15.6%
Realization_34	9.40%	28.1%	39.1%	20.3%	0.0%	0.0%	3.1%
Realization_35	6.20%	9.4%	32.8%	48.4%	0.0%	0.0%	3.1%
Realization_36	4.70%	0.0%	45.3%	45.3%	0.0%	0.0%	4.7%
Realization_37	4.70%	70.3%	7.8%	4.7%	0.0%	0.0%	12.5%

Realization	Percentage of Particle Destination						
	[redacted]	Springs	Pearl Harbor	Northwest GHB	Other Wells	Hālawa Shaft	Stagnant
Realization_38	1.60%	51.6%	29.7%	15.6%	0.0%	0.0%	1.6%
Realization_39	6.20%	62.5%	12.5%	9.4%	0.0%	0.0%	9.4%
Realization_40	4.70%	42.2%	23.4%	18.8%	0.0%	6.2%	4.7%
Realization_41	3.10%	20.3%	37.5%	34.4%	0.0%	0.0%	4.7%
Realization_42	1.60%	43.8%	6.2%	42.2%	0.0%	0.0%	6.2%
Realization_43	6.20%	34.4%	39.1%	9.4%	4.7%	0.0%	6.2%
Realization_44	1.60%	4.7%	15.6%	78.1%	0.0%	0.0%	0.0%
Realization_45	6.20%	78.1%	7.8%	4.7%	0.0%	0.0%	3.1%
Realization_46	7.80%	20.3%	31.2%	35.9%	0.0%	0.0%	4.7%
Realization_47	4.70%	29.7%	12.5%	48.4%	0.0%	0.0%	4.7%
Realization_48	3.10%	31.2%	25.0%	1.6%	26.6%	4.7%	7.8%
Realization_49	0.00%	82.8%	3.1%	1.6%	1.6%	0.0%	10.9%
Realization_50	4.70%	4.7%	9.4%	70.3%	0.0%	0.0%	10.9%

The fifth scenario simulates (b mgd withdrawal from (b) , (b)(3) from (b)(3), and no withdrawals from Hālawa Shaft. This scenario demonstrates the maximum capture of groundwater from beneath the Facility by (b) because Hālawa Shaft is not pumping. Particles are simulated to originate from the Facility near the water table. From there they move with a small component of flow to the west-northwest before heading predominantly in the southwest direction toward (b) . In many cases, the particles enter through clinker zone at the eastern end of (b) . Some particles stagnate due to the dipping layer structure or entering into the saprolite. Capture at (b) varies from 100% to 50% with an average of 89% captured. Particles which are not captured generally flow under (b) , discharging to the Kalauao Springs, Pearl Harbor, or the northwest GHB. Figure 3-10 shows particle tracking results for Realization 10. Figure 3-15 shows the simulation results for this scenario from all realizations. A summary table of final particle destinations is presented in Table 3-5.

Table 3-8: Summary of Particle Destinations for (b) Pumping at (b) mgd, Hālawa Shaft Off, (b)(3) (b)

Realization	Percentage of Particle Destination						
	[redacted]	Springs	Pearl Harbor	Northwest GHB	Other Wells	Hālawa Shaft	Stagnant
Base	100.00%	0.0%	0.0%	0.0%	0.0%	0.0%	0.0%
Realization_1	78.10%	0.0%	9.4%	12.5%	0.0%	0.0%	0.0%
Realization_2	100.00%	0.0%	0.0%	0.0%	0.0%	0.0%	0.0%
Realization_3	93.80%	0.0%	1.6%	0.0%	0.0%	0.0%	4.7%
Realization_4	95.30%	0.0%	0.0%	0.0%	0.0%	0.0%	4.7%
Realization_5	93.80%	0.0%	0.0%	0.0%	0.0%	0.0%	6.2%
Realization_6	78.10%	0.0%	9.4%	6.2%	0.0%	0.0%	6.2%
Realization_7	89.10%	0.0%	0.0%	1.6%	0.0%	0.0%	9.4%
Realization_8	96.90%	0.0%	0.0%	0.0%	0.0%	0.0%	3.1%
Realization_9	89.10%	0.0%	1.6%	1.6%	0.0%	0.0%	7.8%
Realization_10	98.40%	0.0%	0.0%	0.0%	0.0%	0.0%	1.6%
Realization_11	95.30%	0.0%	0.0%	1.6%	0.0%	0.0%	3.1%
Realization_12	75.00%	0.0%	1.6%	20.3%	0.0%	0.0%	3.1%
Realization_13	89.10%	0.0%	0.0%	0.0%	0.0%	0.0%	10.9%
Realization_14	84.40%	0.0%	4.7%	6.2%	0.0%	0.0%	4.7%
Realization_15	84.40%	0.0%	9.4%	4.7%	0.0%	0.0%	1.6%
Realization_16	98.40%	0.0%	1.6%	0.0%	0.0%	0.0%	0.0%
Realization_17	79.70%	0.0%	1.6%	14.1%	0.0%	0.0%	4.7%
Realization_18	95.30%	0.0%	1.6%	0.0%	0.0%	0.0%	3.1%
Realization_19	68.80%	0.0%	21.9%	1.6%	0.0%	0.0%	7.8%
Realization_20	85.90%	1.6%	4.7%	4.7%	0.0%	0.0%	3.1%
Realization_21	95.30%	0.0%	0.0%	0.0%	0.0%	0.0%	4.7%
Realization_22	100.00%	0.0%	0.0%	0.0%	0.0%	0.0%	0.0%
Realization_23	73.40%	0.0%	1.6%	15.6%	0.0%	0.0%	9.4%
Realization_24	92.20%	0.0%	4.7%	1.6%	0.0%	0.0%	1.6%
Realization_25	93.80%	0.0%	0.0%	0.0%	0.0%	0.0%	6.2%
Realization_26	50.00%	0.0%	14.1%	26.6%	0.0%	0.0%	9.4%
Realization_27	90.60%	0.0%	6.2%	1.6%	0.0%	0.0%	1.6%
Realization_28	100.00%	0.0%	0.0%	0.0%	0.0%	0.0%	0.0%
Realization_29	76.60%	0.0%	9.4%	3.1%	0.0%	0.0%	10.9%
Realization_30	93.80%	0.0%	0.0%	0.0%	0.0%	0.0%	6.2%
Realization_31	96.90%	0.0%	1.6%	0.0%	0.0%	0.0%	1.6%
Realization_32	95.30%	0.0%	0.0%	0.0%	0.0%	0.0%	4.7%
Realization_33	92.20%	0.0%	0.0%	0.0%	0.0%	0.0%	7.8%
Realization_34	100.00%	0.0%	0.0%	0.0%	0.0%	0.0%	0.0%
Realization_35	93.80%	0.0%	0.0%	0.0%	0.0%	0.0%	6.2%
Realization_36	90.60%	0.0%	0.0%	0.0%	0.0%	0.0%	9.4%
Realization_37	92.20%	0.0%	0.0%	1.6%	0.0%	0.0%	6.2%

Realization	Percentage of Particle Destination						
	[redacted]	Springs	Pearl Harbor	Northwest GHB	Other Wells	Hālawa Shaft	Stagnant
Realization_38	90.60%	0.0%	0.0%	0.0%	0.0%	0.0%	9.4%
Realization_39	100.00%	0.0%	0.0%	0.0%	0.0%	0.0%	0.0%
Realization_40	98.40%	0.0%	0.0%	0.0%	0.0%	0.0%	1.6%
Realization_41	84.40%	0.0%	6.2%	7.8%	0.0%	0.0%	1.6%
Realization_42	93.80%	0.0%	0.0%	0.0%	0.0%	0.0%	6.2%
Realization_43	92.20%	0.0%	3.1%	0.0%	0.0%	0.0%	4.7%
Realization_44	89.10%	0.0%	0.0%	4.7%	0.0%	0.0%	6.2%
Realization_45	82.80%	0.0%	12.5%	0.0%	0.0%	0.0%	4.7%
Realization_46	93.80%	0.0%	1.6%	0.0%	0.0%	0.0%	4.7%
Realization_47	92.20%	0.0%	0.0%	0.0%	0.0%	0.0%	7.8%
Realization_48	65.60%	0.0%	12.5%	14.1%	0.0%	0.0%	7.8%
Realization_49	98.40%	0.0%	0.0%	0.0%	0.0%	0.0%	1.6%
Realization_50	84.40%	0.0%	3.1%	3.1%	0.0%	0.0%	9.4%

4.0 Vadose Zone Model

4.1 Introduction and Summary

The VZM used in this model represents summary characteristics that influence groundwater boundary conditions, with the goal of providing input data to the contaminant fate and transport mode. A detailed model of the distribution of light nonaqueous-phase liquid (LNAPL) or dissolved petroleum constituents in the vadose zone has not been developed. Because modeling is usually an iterative process in which new data are analyzed and old data are reassessed, this heuristic model is subject to change as better or more detailed information is collected and analyzed.

The current VZM consists of two parts that quantify the source term, or boundary condition characteristics, for the CF&T model:

- A mass balance model to quantify the potential size and shape of an LNAPL lens on the water table under certain conditions.
- A partitioning module that calculates LNAPL chemical constituent concentrations in groundwater within the LNAPL lens over time.

Because the mass balance model relies on professional judgment for assumptions and model parameters, the mass balance model is called a heuristic model to emphasize that it incorporates elements of professional judgment and was developed for the limited uses described herein. The calculations of heuristic model and partitioning module of the VZM are programmed into a Microsoft Excel spreadsheet, which facilitates the rapid evaluation of many different scenarios and parameter sets.

For a given LNAPL release volume and location, the heuristic model calculates the volume of LNAPL retained in the vadose zone. LNAPL not retained in the vadose zone is assumed to form an LNAPL lens on the water table, where it spreads over an area with a uniform thickness and saturation. The extent of the LNAPL spreading depends on the thickness and saturation values specified by the user. The heuristic model provides input to the chemical partitioning module that calculates the concentration of two LNAPL constituents in groundwater: total petroleum hydrocarbons (TPH) diesel range (TPH-d) and residual oil range (TPH-o) organics. Concentrations of other chemical constituents identified by the user may also be calculated with the partitioning module.

Three historical release scenarios were simulated to constrain the heuristic model predictions based on empirical observations, and twelve hypothetical release scenarios were modeled to estimate the impacts of combinations of three potential release volumes at four potential release locations. Except for the January 2014 historical release, the LNAPL released in all scenarios was assumed to be (b) fuel, which does not typically contain significant soluble TPH-o components. The fuel released in January 2014 was (b)(3) instead of (b). The modeled scenarios, the resulting LNAPL lens sizes, and the initial concentrations of TPH-d in groundwater within the LNAPL lens for each scenario are provided in Table 4-1. The results shown are for the specific set of initial parameters currently used in the model, as shown on Figure 4-1 through Figure 4-6. These results will change based on the sensitivity study and calibration of the CF&T model. Many of the hypothetical release scenarios may no longer be reasonably expected after the defueling of the tanks but are nevertheless retained in this report.v

Issued: 20 June 2024

Table 4-1
Simulated Release Scenarios and Heuristic Model Results

INPUTS					OUTPUTS						
Release Scenario Size	Release Location	Volume of LNAPL released (gal)	Average LNAPL Thickness in Lens (ft)	Average LNAPL Saturation in LNAPL Lens	Volume of LNAPL Retained in VZ[1] (gal)	Volume of LNAPL Reaching WT[2] (gal)	Volumetric NAPL Content at WT[3]	Area of LNAPL Lens (ft^2)	Radius of LNAPL Lens (ft)	TPH-d Conc. in LNAPL Lens[4] (mg/L)	TPH-d Conc. in 25-ft Model Grid Cell[5] (mg/L)
Small	(b)(3)	12,500	2	0.3	680	11,820	0.035	22,000	85	1.69	0.14
Small		12,500	2	0.3	620	11,880	0.031	26,000	90	1.69	0.14
Small		12,500	2	0.3	760	11,740	0.038	21,000	81	1.69	0.14
Small		12,500	2	0.3	830	11,670	0.039	20,000	79	1.69	0.14
Medium		125,000	3	0.4	680	124,320	0.047	120,000	190	2.25	0.27
Medium		125,000	3	0.4	620	124,380	0.041	130,000	210	2.25	0.27
Medium		125,000	3	0.4	760	124,240	0.051	110,000	190	2.25	0.27
Medium		125,000	3	0.4	830	124,170	0.053	110,000	180	2.25	0.27
Large		12,500,000	5	0.5	680	12,499,320	0.059	5,700,000	1,300	2.82	0.56
Large		12,500,000	5	0.5	620	12,499,380	0.052	6,500,000	1,400	2.82	0.56
Large		12,500,000	5	0.5	760	12,499,240	0.063	5,300,000	1,300	2.82	0.56
Large		12,500,000	5	0.5	830	12,499,170	0.066	5,100,000	1,300	2.82	0.56
Jan 2014		27,000	3	0.4	680	26,320	0.047	25,000	89	2.55	0.31
May 2021		100	0.2	0.05	100	0	0.0052	0	0	NA	NA
Nov 2021		5,000	1	0.2	830	4,170	0.026	21,000	82	1.13	0.045

Notes:

1. VZ = vadose zone.
2. WT = water table.
3. Volumetric LNAPL content at WT = the volume of LNAPL per unit total bulk volume within the LNAPL lens in the saturated zone.
4. TPH-d Conc. in LNAPL lens = the dissolved phase TPH-d concentration in groundwater within the LNAPL zone.
5. TPH-d Conc. in 25-ft Model Grid Cell = The groundwater concentration within the LNAPL lens, adjusted for the fact that the LNAPL lens thickness is smaller than the thickness of the 25-ft thick CFT model cell. The LNAPL lens concentrations are multiplied by the ratio of LNAPL lens thickness to CFT model grid thickness to account for this dilution of the boundary condition concentration.

4.2 Model Conceptualization and Key Assumptions

In the heuristic model conceptualization, LNAPL is instantaneously released uniformly over a specified area and migrates downward within the vadose zone. Several structural features, including the strike and dip of underlying rocks as well as rock fractures and void spaces with unknown orientation, numerous layers of clinker, potential presence of lava tubes, and the degree of horizontal to vertical anisotropy, can all cause the path of LNAPL moving through the rock to be unpredictable. In addition, within the vadose zone, some LNAPL can be trapped in fractures, pools, lava tubes, and unconsolidated material. As a result of all these unpredictable effects, transport pathways through the vadose zone are not expressly modeled, and it is simply acknowledged that the LNAPL generally migrates downward and downdip through the vadose zone, which is consistent with what occurred in November 2021. However, the model is flexible in that landing points for the LNAPL on the groundwater table can be adjusted to match any given scenario, and the model can estimate a source term for CF&T modeling of that scenario.

The amount of LNAPL trapped in the vadose zone depends on an assumed vadose zone residual LNAPL saturation specified by the user. Residual LNAPL saturations in vadose zone soils vary widely. Typical residual saturations for middle distillates range from 0.02 for coarse gravel to 0.1 for silt or fine sand (Brost and DeVaull 2000). In lava rock environments such as the Red Hill area, residual saturations are expected to vary much more widely than in unconsolidated soils. For example, residual saturations could approach 1 where LNAPL is retained in the open channels of lava tubes or be less than 0.01 in large-sized clinker. Therefore, for this VZM, the vadose zone LNAPL saturation is not based on an assumption of any specific subsurface geologic architecture or calculations of capillary retention. Instead, the vadose zone LNAPL saturation is simply an estimate of the fraction of the pore space that will retain LNAPL based on professional judgment.

With this LNAPL distribution conceptualization, a much wider range of potential residual saturations can be considered for the VZM and the CF&T model boundary conditions. Although a wide range of residual saturations are possible, initial residual saturations are assumed to be relatively small, which is a conservative assumption that results in more LNAPL reaching the water table, thereby increasing potential groundwater impacts at receptor locations.

Except for its use to determine the volume of LNAPL retained in the vadose zone, the release area at the ground surface does not affect the size of the lens formed by LNAPL on the water table, which depends on the LNAPL lens characteristics specified by the user.

The volume of the released LNAPL that is not retained in the vadose zone reaches the water table where it forms a lens on the groundwater. The LNAPL lens is of uniform thickness and uniform LNAPL saturation. Although an LNAPL lens that forms on the water table will contain different proportions of air, water, and LNAPL, the air phase is ignored in the heuristic model for simplifying purposes, meaning that only LNAPL and water phases are assumed to exist in the LNAPL lens. This assumption allows the saturated form of Darcy's Law to be used in the partitioning module, greatly simplifying the calculations, and resulting in higher aqueous phase concentrations compared to a model in which partitioning into an air phase is considered.

The area of the LNAPL lens is calculated from the volume of LNAPL that reaches the water table, the saturation of LNAPL assumed to exist in the LNAPL lens, and the assumed LNAPL lens thickness. Although the LNAPL saturation and lens thickness will vary across the LNAPL lens area, they are assumed to be uniform in this simple model, so that the specified values represent spatial averages across the lens area. It is assumed that small releases will create relatively thin LNAPL lenses with low LNAPL saturations, while large releases will create thick LNAPL lenses with relatively large LNAPL saturations. Average uniform LNAPL lens saturations and thicknesses are based on professional judgment and are specified by the user. The use of average values for LNAPL lens area, saturation, and thickness eliminates the need to specify or calculate the spatial and temporal variability of these LNAPL lens characteristics. This simplification of LNAPL lens geometry is considered sufficient for the simple mass balance heuristic model described here because the model calculations are based on uniform conditions that are unknowable and so cannot incorporate spatial variability of subsurface characteristics.

The shape of the LNAPL lens on the water table is not specified by the heuristic model. The model simply reports the area of the LNAPL lens. For informational purposes, the model reports a radius of the LNAPL lens based on an assumption of a circular lens shape, but any shape of the LNAPL lens may be assumed for use as a CF&T model boundary condition. By default, the shape of the LNAPL lens is assumed to be a square for the calculation of LNAPL constituent dissolution in the partitioning module to conform to the MODFLOW and CF&T model grids. The square shape is used for convenience so that the constituent dissolution from the LNAPL is more easily calculated because of simplified geometry. Given the unknown true shape of the LNAPL lens that reaches the water table, a square is sufficiently close to a circle.

In the partitioning module of the VZM, LNAPL constituents dissolve into groundwater that flows through the LNAPL lens based on their effective solubilities. As the more soluble LNAPL constituents dissolve, the LNAPL becomes enriched in the less soluble LNAPL constituents, and the individual constituent effective solubilities change with the changing LNAPL composition. The partitioning module tracks both the changes in constituent concentrations in groundwater and LNAPL, and the volume of LNAPL remaining in the LNAPL lens over time. Eventually, all the LNAPL is dissolved, and the constituent concentrations in the lens become zero, although the dissolution of the LNAPL could take a very long time if the LNAPL contains relatively insoluble constituents.

For the VZM partitioning module, dissolution is the only LNAPL depletion mechanism. In reality, volatilization, biodegradation, adsorption, and other natural source-zone depletion (NSZD) processes will also cause LNAPL depletion. Therefore, the heuristic model is conservative in the sense that it overpredicts the persistence of LNAPL constituents in the groundwater source area.

The rate of LNAPL constituent concentration changes and LNAPL depletion depend on the rate of horizontal groundwater flow through the LNAPL lens. The partitioning module also includes a factor to account for the lack of uniform distribution of LNAPL (a sweep efficiency factor), and a factor to account for reductions in water hydraulic conductivity as a function of LNAPL presence. Both these factors are functions of the LNAPL saturation in the LNAPL lens.

Unlike the GWFM and the CF&T model, the vadose zone model is not a standard model coded in a program language to solve the physics of groundwater flow and contaminant transport. Rather, it is a set of

calculations implemented in a spreadsheet that was developed specifically for the Red Hill modeling project. The model input, structure, and output are described in detail below.

4.3 Model Input

VZM input parameters are specified on tabs in the model Excel workbook. The model relies on primary inputs, which are input parameters or specified values entered by the user, and secondary inputs, which are calculated values based on the primary input.

Primary inputs are entered on each spreadsheet tab in the yellow-shaded cells. Blue-shaded cells are lookup values from other spreadsheet tabs that contain primary or secondary inputs. These lookup values may be overwritten by the user.

4.3.1 Main Tab

A screenshot of the Main tab of the VZM spreadsheet is shown on Figure 4-1. On the Main tab, the user specifies the release scenario and the groundwater hydraulic gradient magnitude. Fifteen release scenarios were selected, corresponding to the three historical LNAPL releases and the twelve hypothetical releases listed on the Release Info tab (described in the next section). The groundwater gradient is used by the partitioning module. Several model parameters are calculated based on the selection of the release scenario. The following parameters depend on the selection of the release scenario:

- Average residual saturation of the vadose zone
- Average total porosity of the vadose zone
- Release location
- Release volume
- Release area
- Depth to the water table at the release location
- Thickness of the LNAPL lens
- Total porosity of the saturated zone
- LNAPL saturation in the LNAPL lens
- Hydraulic conductivity of the saturated zone (used in the partitioning module)

The sources of these parameter values are identified in the other tabs from which the values are obtained. The user is not limited to the fifteen release scenarios and may overwrite parameters in the blue-shaded input cells if desired. If the lookup values of these parameters associated with the release scenario are overwritten by the user, the lookup formulas may be restored to the blue cells by clicking the Restore Lookup Formulas button on the Main tab.

4.3.2 Release Info Tab

On the Release Info tab shown on Figure 4-2, the user specifies the type of LNAPL released, the location of the release, the volume of the release, and the area of the release at the ground surface. These values are used in subsequent model calculations. Default average LNAPL lens saturation and LNAPL lens thickness are also shown on this tab based on the volume of release. These parameters can be changed by the user if desired.

4.3.3 Location Info Tab

Key inputs on the Location Info tab include the following:

- Depth to water (DTW) at each release location
- Volume fraction of rock types (a‘ā, pāhoehoe, a‘ā clinker, and saprolite) at each location
- Calculated vadose zone porosity based on the rock types at the location
- Calculated hydraulic conductivity based on the rock types at the location
- Average residual LNAPL volumetric content based on the rock types at the location

The average porosity, hydraulic conductivity, and residual LNAPL volumetric content at each location are weighted averages of these properties for each rock type. The values of these parameters for each rock type are specified on the Hydrogeologic Info tab. A screenshot of the Location Info tab is shown on Figure 4-3.

4.3.4 Hydrogeologic Info Tab

Properties of each rock type used to calculate average rock properties at each location are entered in the Hydrogeologic Info tab. A screenshot of the Hydrogeologic Info tab is shown on Figure 4-4. For each rock type, the user specifies an estimated total porosity, hydraulic conductivity, and residual vadose zone LNAPL saturation (fraction of pore volume occupied by immobile LNAPL). The residual volumetric content (fraction of bulk volume occupied by immobile LNAPL) used in the calculation of the volume of LNAPL retained in the vadose zone is also calculated on this tab for each rock type.

4.3.5 Fuel Info Tab

LNAPL properties are specified on the Fuel Info tab, shown on Figure 4-5. Three fuel types are currently listed: (b) , (b) (b)(9) For each fuel type, an estimated specific gravity and molecular weight are specified. These parameters are used in the partitioning calculations. For each fuel type, the insoluble component of the fuel is indicated, and properties of this insoluble fraction are specified, including specific gravity and molecular weight. The volumetric fraction of the two LNAPL constituents modeled, TPH-d and TPH-o, are also specified for each fuel type, and the properties of these two LNAPL constituents are also included.

4.3.6 Partitioning Tab

The concentrations of soluble LNAPL constituents in groundwater flowing through the LNAPL lens are calculated on the Partitioning tab, shown on Figure 4-6. In the first section on this tab, General Parameters,

the user indicates whether LNAPL presence in the LNAPL lens is assumed to affect relative permeability, and whether the calculated equilibrium concentrations should be diluted because of only partial contact of the groundwater with the LNAPL (sweep efficiency effects). Entering a value of 1 for these flags reduces the concentrations of constituents in the groundwater, causing the LNAPL to persist for a longer time.

In the LNAPL Constituent Parameters and Initial Values section of the Partitioning tab, the user specifies what soluble constituents are present in the LNAPL. The default constituents are TPH-d and TPH-o, although volume fractions of other constituents can also be specified. Each constituent's molecular weight, solubility, and density are obtained from the Chem Props tab. The final constituent, which comprises the more insoluble part of the LNAPL, is obtained from the Chem Props tab. The volume fractions of TPH-d and TPH-o are also obtained from the Fuel Info tab.

The next section of the Partitioning tab contains calculations of input parameters needed for the partitioning calculations. The partitioning calculations are performed below this section at the bottom of the sheet. For each time interval, the concentration of constituents in groundwater in the source zone, the concentrations remaining in the LNAPL, and the remaining LNAPL volume are calculated.

The time increment for the partitioning module can be changed on the main heuristic model tab. If the timestep is too large, the solution may become unstable and the model will not yield accurate calculations or will produce errors in some spreadsheet cells. For LNAPLs that contain mostly insoluble components, longer time increments will not significantly affect the calculated concentrations. For the LNAPL calculations at Red Hill where constituents are mostly TPH-d and TPH-o, a time increment of 5–50 days is suggested. However, this time increment range is not guaranteed to result in model calculation stability, and the user must inspect the model results to evaluate how the time increment affects the results with the specified set of parameters.

4.3.7 Chem Props Tab

Chemical properties including molecular weight, solubility, and density of each constituent are contained in the Chem Props tab. The data in columns 1 through 13 in the Chem Props tab are sourced from the Texas Risk Reduction Program (TRRP) spreadsheets (TCEQ 2023). Users must enter the density in column 14 for constituents that are part of the LNAPL but for which no density is specified. Molecular weights, solubilities, and densities of constituents not included in the TRRP database have been entered starting on row 710 of the Chem Props tab. Additional constituents may be added to the database as needed.

4.4 Model Calculations

Variables used in the VZM calculations are defined in Table 4-2. The example calculations provided for the heuristic mass balance model are for the example input shown on Figure 4-1.

Table 4-2: Definitions of Variables Used in VZM Calculations

Variable	Description	Unit
Heuristic model mass balance calculations:		
A_{lens}	Area of LNAPL lens on water table	square ft (ft^2)
A_{rel}	LNAPL release area at surface	ft^2
b_{lens}	Thickness of LNAPL lens on water table	ft (ft)
DTW	Depth to water table from point of release	ft
n_{sat}	Porosity of saturated zone	cubic ft (ft^3) of pores per ft^3 bulk volume
n_{vad}	Porosity in vadose zone	ft^3 pores per ft^3 total bulk volume
$S_{N,sat}$	LNAPL saturation in the LNAPL lens	ft^3 LNAPL per ft^3 pores
$S_{Nr,vad}$	Residual saturation of LNAPL in vadose zone	ft^3 LNAPL per ft^3 pores
$V_{N,sat}$	Volume of LNAPL reaching water table (saturated zone)	ft^3 LNAPL
$V_{N,vad}$	Volume of LNAPL retained in vadose zone	ft^3 LNAPL
$V_{p,vad}$	Pore volume of affected vadose zone	ft^3
V_{rel}	Volume of LNAPL released	ft^3 LNAPL
V_{vad}	Bulk volume of affected vadose zone	ft^3 pores
$\theta_{N,sat}$	Volumetric content of LNAPL in the LNAPL lens on the water table	ft^3 LNAPL per ft^3 bulk volume
Partitioning model calculations:		
Δt	Time step	days
b	Average thickness of LNAPL lens	meters (m)
f_{sweep}	Sweep efficiency factor	dimensionless
i	Hydraulic gradient	dimensionless (ft/ft)
K	Hydraulic conductivity	m/d
k_{rel}	Water relative permeability	square meters (m^2)
n	Number of constituents in LNAPL	—
N	Moles	moles
N_T	Total moles	moles
q	Specific discharge (Darcy flux)	m/d
Q	Volumetric flow rate of groundwater through LNAPL lens	m^3/d
S	Solubility of pure LNAPL component in water	mg/L
Se	Effective solubility	mg/L
V_N	Volume of LNAPL	cubic meters (m^3)
w	Width of LNAPL lens	m
x	Mole fraction	moles of constituent i/total moles
z	Mass fraction	mass of constituent i/total mass
ω	Molecular weight	grams (g)/mole
ρ	Density of LNAPL constituent	g/cubic centimeter (cm^3)
ρ_N	Density of LNAPL	g/cm^3

Superscripts:
0 initial value (time = 0)
k time step *k*

Subscripts:
i constituent *i*
N LNAPL
p pores
r residual
rel release
vad vadose zone

4.4.1 LNAPL Retained in the Vadose Zone

The volume of LNAPL retained in the vadose zone depends on the volume in which the LNAPL is presumed to be released and the assumed LNAPL residual saturation in the vadose zone. The volume of the vadose zone that incorporates LNAPL is calculated from the DTW and release area at the release location.

First, the volume of LNAPL released (V_{rel}) is converted from gallons (gal) to ft^3:

1) $$V_{rel} = 27{,}000[gal]\frac{0.13368[ft^3]}{[gal]} = 3{,}609[ft^3]$$

The total volume of vadose zone containing LNAPL is:

2) $$V_{vad} = DTW \times A_{rel} = 85[ft]500[ft^2] = 42{,}500[ft^3]$$

where DTW is depth to water and A_{rel} is the area of the release at the ground surface.

The pore volume in the vadose zone is then:

3) $$V_{p,vad} = n_{vad}V_{vad} = 0.1171 \times 42{,}500[ft^3] = 4{,}975[ft_p^3]$$

where $V_{p,vad}$ is the affected pore volume in the vadose zone and n_{vad} is the vadose zone average porosity calculated for the release location.

The volume of LNAPL retained in the vadose zone ($V_{N,vad}$) is the vadose zone pore volume multiplied by the vadose zone LNAPL residual saturation ($S_{Nr,vad}$):

4) $$V_{N,vad} = S_{Nr,vad}V_{p,vad} = 0.0182\frac{ft_N^3}{ft_p^3} \times 4{,}975[ft_p^3] = 91[ft_N^3]$$

In this example calculation, approximately 2.5% of the 27,000 gallons of LNAPL released is retained in the vadose zone, and the remaining 97.5% reaches the water table to form an LNAPL lens.

4.4.2 LNAPL Lens Size on the Water Table

The size of the LNAPL lens depends on the assumed LNAPL thickness and the average LNAPL lens saturation at the water table. First, the volume of LNAPL reaching the water table ($V_{N,sat}$) is calculated from the total release volume and the volume retained in the vadose zone:

5) $$V_{N,sat} = V_{rel} - V_{N,vad} = 3{,}609[ft^3] - 91[ft^3] = 3{,}509[ft^3]$$

The LNAPL volumetric content in saturated zone LNAPL lens ($\theta_{N,sat}$) is the LNAPL saturation multiplied by the specified saturated zone porosity, n_{sat}:

6) $$\theta_{N,sat} = S_{N,sat} n_{sat} = 0.4 \times 0.117 = 0.0468 \left[\frac{ft_N^3}{ft^3}\right]$$

The LNAPL lens area is calculated from the specified LNAPL lens thickness (b_{lens}), the volume of LNAPL in the lens, and the calculated LNAPL volumetric content:

7) $$\boldsymbol{A_{lens} = \frac{V_{N,sat}}{b_{lens}\theta_{N,sat}} = \frac{3{,}509[ft_N^3]}{3[ft]0.0468\frac{ft_N^3}{ft^3}} = 25{,}000[ft^2]}$$

If the LNAPL lens is assumed to be circular, then the radius of the LNAPL lens (r_{lens}) is calculated from the LNAPL lens area:

8) $$\boldsymbol{r_{lens} = \sqrt{\frac{A_{lens}}{\pi}} = \sqrt{\frac{25{,}000[ft^2]}{\pi}} = 89[ft]}$$

4.4.3 Partitioning of LNAPL Constituents into Groundwater

The partitioning module of the VZM calculates the concentrations of LNAPL constituents within the LNAPL lens over time. Groundwater flows through the LNAPL lens and dissolves the LNAPL constituents, reducing the remaining volume of LNAPL and changing its composition as the more soluble compounds dissolve out of the LNAPL. Equilibrium between the water and LNAPL within the lens is assumed, so that the concentration of constituents within the LNAPL lens are equal to the effective solubility of the LNAPL constituents. Effective solubility is the solubility of a pure phase component multiplied by its mole fraction in the LNAPL. Input parameters for the partitioning module are obtained from the other tabs in the heuristic model.

4.4.3.1 INITIAL CALCULATIONS

The partitioning module first calculates the Darcy flux (specific discharge, q) through the LNAPL area using the specified groundwater gradient (i), water relative permeability (k_{rel}), and hydraulic conductivity (K):

9) $$q = K k_{rel} i$$

If the "account for relative permeability" flag is equal to 1 on the Main tab, then the k_{rel} is set equal to the square of the water saturation ($1\text{-}S_{N,sat}$), analogous to the expression for a simplified LNAPL relative

permeability suggested by Charbeneau and Chiang (1995). Otherwise, k_{rel} is equal to 1, indicating that the LNAPL has no effect on the groundwater specific discharge. The volume of water flowing through the LNAPL lens is then calculated by multiplying the specific discharge by the cross-sectional area of the LNAPL lens:

10) $$Q = qwb$$

where w is the LNAPL lens width (assumed equal to the square root of the LNAPL area under the assumption of a square LNAPL lens shape) and b is the specified LNAPL lens thickness. The concentration of each constituent in the groundwater depends on the mole fraction of the constituent in the LNAPL. The mole fraction of each constituent is calculated by dividing the moles of each constituent (N_i^0) by the total moles initially present in the LNAPL (N_T^0):

11) $$x_i^0 = \frac{N_i^0}{N_T^0}$$

The initial effective solubility of the constituent (Se_i^0) is calculated from the mole fraction and pure phase solubility of the constituent, S_i :

12) $$Se_i^0 = x_i^0 S_i$$

The initial LNAPL density is calculated from the density of each LNAPL constituent:

13) $$\rho_N = \sum_{i=1}^{n} x_i \rho_i$$

4.4.3.2 SEQUENTIAL TIME STEP CALCULATIONS

The concentrations of each LNAPL constituent in the groundwater are calculated at each time step based on the current composition of the LNAPL. As water flows through the LNAPL, the water dissolves a fraction of each soluble LNAPL constituent. To account for differential dissolution of the soluble LNAPL component in the model, the composition of the LNAPL is updated at each time step, and the total remaining volume of LNAPL is calculated. In these sequential time step calculations, new values are indicated with a *k+1* superscript, and old values are indicated with a *k* superscript.

First, the number of moles of each constituent (N_i^{k+1}) in the LNAPL lens following loss of the mass dissolved in groundwater is calculated for each time step:

14) $$N_i^{k+1} = N_i^k - \frac{QSe_i^k}{\omega_i}\Delta t$$

where Q is the volumetric flow rate through the LNAPL, ω_i is the molecular weight of the constituent, and Δt is the length of the partitioning module time step. The total number of moles of all constituents remaining in the LNAPL, N_T^{k+1}, is the sum of the moles of each constituent:

15) $$N_T^{k+1} = \sum_{i=1}^{n} N_i^{k+1}$$

The new mole fraction of each constituent (x_i^{k+1}) is then calculated, and the new effective solubility of each constituent (Se_i^{k+1}) is calculated based on the mole fraction and pure phase solubility:

16) $$x_i^{k+1} = \frac{N_i^{k+1}}{N_T^{k+1}}$$

17) $$Se_i^{k+1} = x_i^{k+1} S_i f_{sweep}$$

The f_{sweep} parameter accounts for only partial contact of the groundwater with LNAPL, and is set equal to the LNAPL lens saturation if the "account for sweep efficiency" flag is set to 1 on the Main tab. If the sweep efficiency flag is not set to 1, then f_{sweep} is equal to 1 and the LNAPL presence has no effect on the concentration in equilibrium with LNAPL. Finally, the volume of LNAPL remaining after the loss of each constituent by dissolution in groundwater is calculated based on the molar volumes of each constituent:

18) $$V_N^{k+1} = \sum_{i=1}^{n} \frac{(N_i^{k+1} - N_i^k)\omega_i}{\rho_i}$$

The sequential calculations shown in Equations 14 through 18 above are repeated for each time step to determine the concentration of each constituent in groundwater and the volume of LNAPL remaining over the time desired.

4.4.3.3 PARTITION MODULE CALCULATION VERIFICATION

The calculated dissolved phase concentration histories of the VZM partitioning module were compared to the dissolved phase concentration history calculations of the model published by the 2005 American Geophysical Union (AGU) publication Soil and Groundwater Contamination: Nonaqueous Phase Liquids, AGU Water Resources Monograph 17 (Mayer and Hassanizadeh 2005). As shown on Figure 4-7, the partitioning module of the VZM reproduces the results of the AGU model for the same example set of LNAPL constituents that represent a wide range of chemical properties, indicating that the partitioning model calculations are performed correctly in the VZM spreadsheet.

4.5 Results

The LNAPL lens size and groundwater concentrations calculated with the VZM for the three historical and twelve hypothetical scenarios evaluated are provided in Table 4-1. With the conservative parameters specified for these model runs, very little LNAPL is retained in the vadose zone, and dissolved concentrations diminish very slowly. The maximum lens radius of 1,400 ft calculated for the large release is a function of the relatively large assumed LNAPL lens thickness of 5 ft and the relatively high expected LNAPL lens saturation of 0.5.

In general, the LNAPL lens area and computed lens radius increase with the release size regardless of the release location. For all small release sizes, the computed LNAPL lens radius is approximately 80–90 ft. The LNAPL lens radii ranges for the medium and large releases are approximately 180–210 and 1,300–1,400 ft, respectively. The TPH-d concentrations also increase with release size, which reflects the increase in assumed LNAPL saturation with increasing LNAPL lens thickness. Because the fraction of LNAPL

retained in the vadose zone is small for all release scenarios except for the actual November 2021 release, the depth to water has only a minor effect on the LNAPL lens size.

The area of the LNAPL lens, the TPH-d concentrations in the LNAPL lens, and the LNAPL lens constituent concentrations are used to establish boundary conditions for the CF&T model release scenario simulations. The extent of the LNAPL source in the CF&T model is assumed to be circular, although as discussed previously, a square plume shape is used for partitioning calculations only to simplify the geometry for the partitioning calculations.

At the time of this report, the tanks in the tank farm have been emptied of their petroleum fuels, so a release of even the small release scenario is unlikely. Although the tanks have been defueled, the VZM can be used to assist in estimating the extent of past releases for establishing source extents and strengths from past releases during CF&T modeling.

4.6 Model Limitations

This VZM was developed for the sole purpose of conservatively estimating a source term for the dissolved groundwater CF&T release scenario modeling. The model does not account for the unknown and highly heterogenous subsurface architecture. As a result, the VZM does not depict travel paths or rates through the vadose zone. Rather, the VZM conservatively estimates the amount of LNAPL released at the surface that is retained in the vadose zone and the amount that reaches and spreads on the water table. This conceptual model (Figure 4-8) of instantaneous distribution between the vadose zone and saturated zone is consistent with the rapid downward migration and small horizontal deflection observed after the November 2021 release. While there is value in modeling large releases associated with past releases for purposes of history matching, since defueling was completed in 2024, it is no longer possible for future releases of such volumes. Future releases may be possible from small piping, sumps or voids not known and defueled, and/or residual fuel in the vadose remobilized by precipitation or other water sources.

Because of the extreme complexity of subsurface volcanic environments, many parameters for even the simple VZM described herein are highly uncertain. Specifically, the VZM does not account for the following parameters:

- Strike and dip of rock formations
- Hydraulic conductivity heterogeneity and anisotropy
- Different rates of migration through different types of rock
- Preferential flow pathways created by lava tubes, clinker layers, fractures, low-k zones that act as diversions, and other preferential subsurface heterogeneities
- Flow of water and dissolved LNAPL constituents in the vadose zone
- Long-term changes in drainage of LNAPL from the vadose zone
- Lateral movement of LNAPL in the vadose zone
- Variable residual LNAPL saturation in the vadose zone

- Effects of large precipitation events on LNAPL in the vadose zone
- Variable LNAPL thickness and saturations within the LNAPL lens that forms on the water table
- Capillary retention in the vadose zone and saturated zone
- Variable LNAPL residual saturations caused by imbibement of LNAPL under variable LNAPL head
- Changes in LNAPL physical properties caused by weathering and dissolution of soluble constituents
- Actual shape of the LNAPL lens on the water table
- Transient changes in the groundwater hydraulic gradient
- Specific types of fuel and fuel compositions of potential undocumented historical releases

These substantial limitations should be kept in mind when interpreting the results of the VZM.

5.0 Contaminant Fate and Transport Model

5.1 Introduction

The CF&T model simulates the migration and fate of dissolved chemicals as they move with groundwater (advection) and as they attenuate through certain natural processes such as dispersion. The transport process of diffusion is assumed to be a negligible component of dissolved-phase migration due to relatively high groundwater velocities and large spatial scales, supported by literature values of approximately 1 ft/d (Lau and Mink 2006), and results of the conceptual and groundwater flow models. Diffusion is typically only the dominant process in very low-permeability environments with very low groundwater velocities.

CF&T modeling is based on the groundwater flow patterns simulated in the groundwater flow model, discussed in Sections 2.0 and 3.0. CF&T modeling was conducted in three stages: history matching, predictive simulations, and sensitivity analysis. Simulation of the May 2021 release was selected for the history matching process, which is discussed further in Section 5.2, through which transport parameters were calibrated, including dispersivity and effective porosity. This process was conducted for all 50 heterogeneity realizations, and the parameter values obtained were then used in a series of three predictive scenarios simulating hypothetical future conditions at the site. Finally, a sensitivity analysis was performed to evaluate changes to the parameter values and their impacts on predictive simulation results.

The specific objective of the CF&T model is to provide stakeholders with information that can be used to estimate the risk posed to potable water produced at wells 3-(b)(9) ((b)),(b)(9) (b)(3), BWS municipal water supply wells, 3-2354-00 Hālawa Shaft, Moanalua Wells (3-2153-002, 3-2153-010, 3 2153011, 3-2153-012), and other wells as well as other potential receptors based on changes to conditions at the tank farm. To support this goal, the CF&T model conservatively does not account for any bioattenuation or other petroleum decay mechanisms that are known to occur at Red Hill and other petroleum release sites. Model results were generally compared to both the TPH-d Groundwater Screening Criterion (GWSC) of 400 µg/L from the Consolidated Groundwater Sampling Program (DOH 2024) and 100 µg/L, which is a round number close to the lower limits of most laboratory's reporting levels and the current DOH Environmental Action Level (EAL). Information from these simulations may also help inform decision making about potential site remedy alternatives.

One specific question to be addressed by the model is:

- What are the ranges of concentrations of petroleum fuel constituents likely to be in groundwater at (b) and BWS Hālawa Shaft under a range of potential conditions?

The results of the modeling will be used to inform groundwater monitoring decisions, such as:

- What range and pattern of concentrations detected in the monitoring well network would signal a significant risk to a potential potable water receptor?
- Where might dissolved phase constituents migrate from sources associated with residual LNAPL contamination below the tank farm?
- Where in groundwater might GWSC exceedances be anticipated under various scenarios?

5.2 Forensic Analysis of TPH Data

5.2.1 Special Purpose Meetings on CF&T Modeling and Interpretation of TPH Data for Use in Model Calibration

SPM #27 was held on March 31, 2023, between the Navy and RAs to discuss the CF&T approach. The main topic of the meetings was the selection of appropriate COPCs for which to simulate transport and which data could be used to calibration the CF&T model. The Navy received comments from DOH and EPA on the TPH data use at SPM #31 on January 31, 2024. The RA comments have been considered during the CF&T process, although it was not possible to address all comments and suggestions within the project schedule constraints. Responses to the RA comments and suggestions on the use of TPH data for model calibration are presented in Appendix C. The discussion in this subsection is largely based on the TPH SPM.

5.2.2 General Considerations for CF&T Constituents at Red Hill

A key decision for CF&T simulations performed to assess potential impacts of materials released at the Facility on potable water supplies is the nature of the substance that could cause such impacts. Available information indicates that only petroleum-derived fuels were stored in the tanks composing the Red Hill Bulk Fuel Storage Facility. During the approximately 80 years of Facility operation prior to defueling in 2024, the following fuel types were stored in the tanks at various times:

- (b)(9)
- (b)
- (b)(9)
- (b)(9)
- (b)(9)
- (b)
- (b)(9)
- (b)(9)
- (b)(9)

Although other substances have been used at the Facility, this evaluation addresses only the soluble components of these petroleum fuels that can dissolve into and then migrate in groundwater. The initial task in the CF&T model is to identify these soluble fuel components, and determine which components are potentially useful for calibrating a CF&T model.

In this context, calibration means the adjustment of parameters that govern the transport of dissolved fuel constituents in groundwater until the observed concentrations are best replicated by the simulated concentrations and trends. The set of parameters that result in the best match are then used for subsequent predictive CF&T simulations, and the model is deemed to be calibrated. The parameters that were adjusted during calibration are effective porosity, which governs the average seepage velocity, and dispersivities,

which affect the degree of spreading in and across the direction of flow. The source extent, duration, and strength were also adjusted during calibration.

Calibration of a CF&T model differs from calibration of a GWFM in an important respect. While a GWFM can be calibrated based on unchanging inputs and outputs (steady-state conditions), a CF&T model is inherently transient. As a result, calibration of a CF&T model requires chemical concentration data that is the result of a specific event that introduced the chemicals into the groundwater. Although the exact nature of the event is helpful to know, calibration does not require detailed knowledge of the event, only that the time and duration of the event are known to an acceptable degree of precision, and that the event can be related to the observed concentrations.

In addition to being tied to a specific event, concentration data used for calibration must be sufficient in terms of spatial coverage and the consistency of frequency of measurement. Table 5-1 shows the frequency of analyses and detections of several petroleum compounds associated with fuels among all data collected since 1998. At Red Hill, TPH is detected (defined here as greater than the method detection limit so that laboratory "J-values" count as a detection) as TPH-d and TPH-o much more frequently than other analytes. "J-values" are estimated concentrations above the method detection limit but below the quantitation limit. Table 5-2 shows that TPH is also detected at more locations than other analytes. This relatively high detection frequency and large number of locations where it is detected make TPH a suitable candidate for use in CF&T model calibration, although as explained below, there are disadvantages to using TPH.

Table 5-1: Detection Frequency of Analytes Associated with Petroleum Fuels in Groundwater

COC	Analyses	Detects	J-Values	ND	Det %
TPH as DRO	2,232	283	457	1,492	33%
Lead, Dissolved	2,016	85	526	1,405	30%
TPH as ORO	2,231	205	426	1,600	28%
TPH as DRO SGC	2,642	345	263	2,034	23%
TPH as GRO	177	30	6	141	20%
Chloroform	2,236	166	281	1,789	20%
Naphthalene	4,192	386	152	3,654	13%
1-Methylnaphthalene	3,961	291	141	3,529	11%
TPH as ORO SGC	2,641	44	219	2,378	10%
2-Methylnaphthalene	4,027	271	100	3,656	9%
Acenaphthene	2,816	127	115	2,574	9%
Fluorene	2,815	108	101	2,606	7%
Xylenes (total)	3,890	21	148	3,721	4%
Fluoranthene	2,815	34	83	2,698	4%
Benzo(a)anthracene	2,816	46	70	2,700	4%
Benzo(b)fluoranthene	2,816	42	68	2,706	4%
Pyrene	2,997	56	52	2,889	4%
Phenanthrene	2,816	25	71	2,720	3%
Chrysene	2,815	37	56	2,722	3%
Benzo(a)pyrene	2,815	31	53	2,731	3%
Benzo(ghi)perylene	2,815	32	43	2,740	3%
Indeno(1,2,3-cd)pyrene	2,816	37	37	2,742	3%
Acenaphthylene	2,816	38	32	2,746	2%
Benzo(k)fluoranthene	2,815	27	40	2,748	2%

Table 5-2: Detection of Analytes Associated with Petroleum Fuels in Groundwater by Location

Analyte	Locations	Detects	Det %
TPH as ORO	26	25	96%
TPH as DRO	34	28	82%
Phenanthrene	29	19	66%
1-Methylnaphthalene	29	19	66%
Benzo(b)fluoranthene	34	22	65%
Lead, Dissolved	46	29	63%
TPH as DRO SGC	46	29	63%
Indeno(1,2,3-cd)pyrene	29	18	62%
Benzo(ghi)perylene	29	17	59%
2-Methylnaphthalene	29	15	52%
Chloroform	29	15	52%
Fluorene	29	15	52%
Benzo(a)pyrene	29	13	45%
Acenaphthylene	29	13	45%
Xylenes (total)	29	13	45%
Acenaphthene	29	12	41%
Pyrene	26	10	38%
TPH as GRO	47	18	38%
Chrysene	29	10	34%
Benzo(k)fluoranthene	29	10	34%
Benzo(a)anthracene	47	16	34%
Naphthalene	47	15	32%
TPH as ORO SGC	8	2	25%
Fluoranthene	47	10	21%

Notes: Det % = percent detected, defined as the number of locations where the compound was detected divided by the total number of wells in which the compound was analyzed.

Because TPH is a non-specific analyte, other analytes are generally preferable to TPH for both model calibration and simulations. However, none of the individual compounds listed in Table 5-1 are detected with sufficient frequency, nor are they at enough locations for them to provide a sufficient modeling data set. Therefore, despite its limitations, TPH was chosen as the solute for CF&T simulations.

5.2.3 Characteristics of TPH and TPH Analysis

Although the TPH detections in the monitoring well network at the Facility are relatively more frequent and widespread, than other individual compounds listed in Table 5-1, TPH has certain disadvantages as a constituent for CF&T modeling. TPH is a non-specific analysis. That is, any compound that elutes from a chromatograph in the range of TPH boiling points will be reported as TPH, regardless of the nature or source of the compound. Unlike specific chemical compounds in which there is much less uncertainty about the compound's identity, a detection of TPH does not necessarily mean that the compounds reported as TPH originated in petroleum fuel. Other sources of TPH include, but are not limited to, the following:

- Petroleum carriers for pesticides or herbicides
- Propellants in spray products such as cleaning products, degreasers, sunscreens, lubricants, solvents, mosquito repellant, and paint
- Cosmetic products
- Incidental spillage of gasoline or diesel from commercial equipment (e.g., landscaping)
- Compounds associated with drilling or sampling equipment
- Naturally occurring organic matter (e.g., humic acids or historical weathering of organic material between lava flows)

These other compounds, some of which are petroleum-based but are not exclusive to the petroleum fuels stored at the Facility, can be detected in groundwater samples and reported as TPH. There is no simple way to distinguish these interfering compounds from TPH that originated in the stored fuels. As a result, many TPH detections may not represent compounds transported in groundwater from the Facility, which can confound the interpretation of dissolved phase transport from the tanks. For conservative analyses in this report, all reported TPH was assumed to be petroleum-related.

There are several reasons why interfering compounds that appear in a TPH analysis cannot easily be identified. First, TPH detected in any individual sample may be a mixture of interfering compounds and compounds that originated in the stored fuels. Second, identification of many compounds is difficult because they may not be included in mass spectroscopy libraries for identification. Finally, even if a particular compound is identified in a mass spectrometry library, its molecular fragments used for identification may not be unique. These factors contribute to making the use of TPH for model calibration difficult.

In spite of these difficulties, however, TPH can be used for model calibration under certain circumstances. For use in CF&T simulations, the TPH detected should be detected persistently at elevated concentrations following a release event. For the purposes of model calibration only, background concentrations are approximate average concentrations that were detected in the well in the few months prior to the May 6, 2021 release. A high persistence of detections means that the TPH is less likely to consist of interfering compounds since interfering compounds tend to occur more sporadically than TPH from a well-defined source.

The particular TPH fraction should also be linked to the fuel presumed to be causing the TPH detected in groundwater. At the Facility, two releases of a known petroleum fuel, J (b)(3)(b)(3)(b)(3) occurred. Because the type of fuel released is known, TPH that includes compounds prominent in (b) can be tied to the release. As shown in Chart 5-1, (b) is composed of aromatic and aliphatic compounds with effective carbon numbers of greater than (b)(9) Most of these compounds are aliphatic and are relatively insoluble. However, (b) also contains about 20% by mass of aromatic compounds that are more water-soluble than the aliphatics, so that (b) in groundwater can be detected with a TPH analysis.

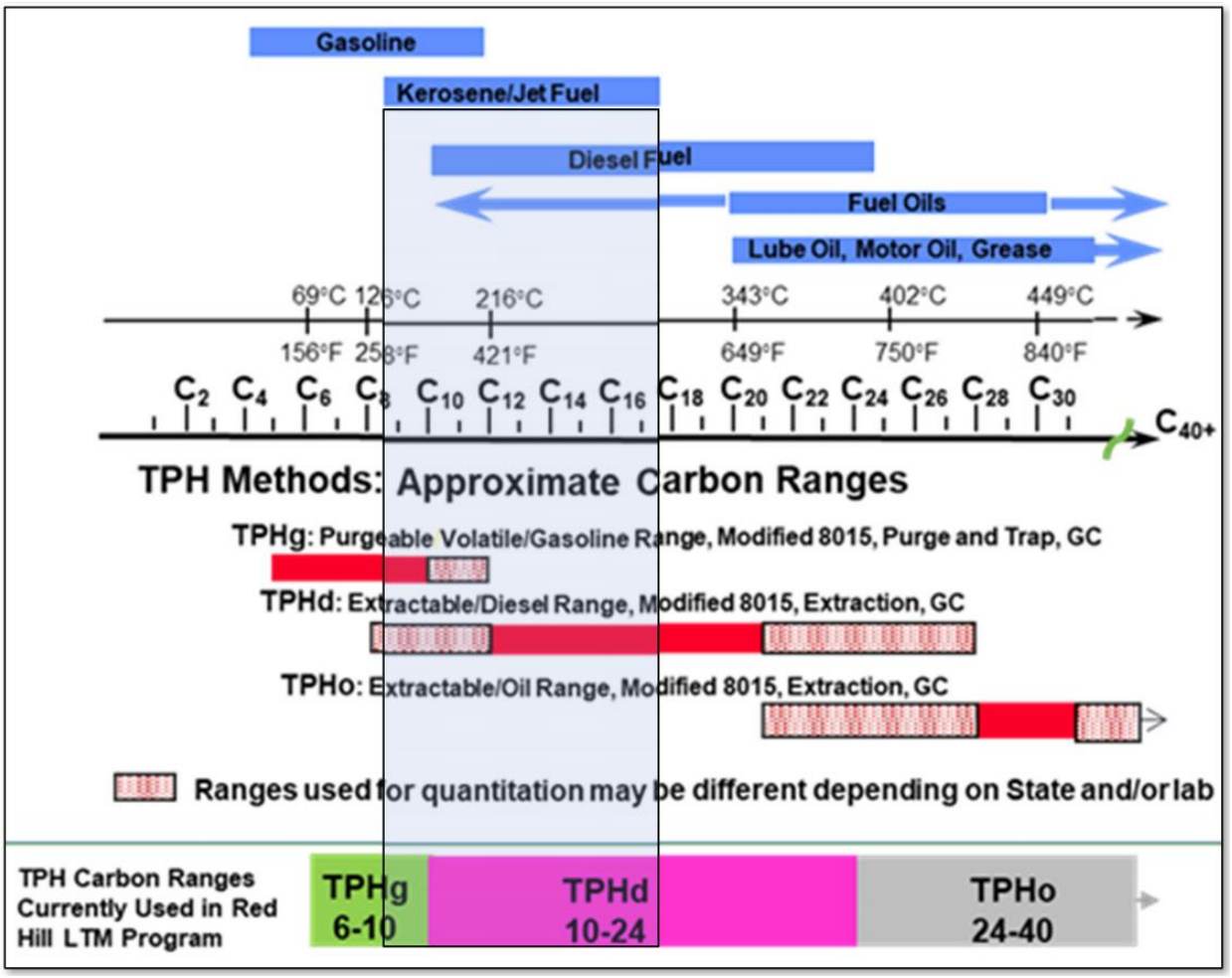

Chart 5-1: TPH Ranges Corresponding to Petroleum Fuel Types and Effective Carbon Numbers

The compounds in (b) elute in the range of both TPH as GRO (TPH-g: TPH as gasoline range organics) and TPH as DRO (TPH-d: TPH as diesel range organics). The TPH-d range includes compounds with effective carbon numbers between C10 and C24, so that the (b) constituents will elute in the early and mid-range of a TPH-d analysis. For this reason, and because TPH-d is detected frequently and at many locations, TPH-d was selected as the best candidate for CF&T simulations. TPH-o was not considered for model calibration because it measures TPH compounds outside the range of jet fuels and is therefore not representative of (b) released in 2021.

5.2.4 Forensic Analysis of TPH-d in Tank Farm Wells RHM(b) , RHM(b) , and RHM(b)

The most frequent and persistent detections of TPH-d occur in the three wells along Red Hill ridge in the tank farm: RHM(b) (and its replacement, RHM(b)), RHM(b) , and RHM(b) . These three wells are located down the spine of Red Hill ridge between the fuel storage tanks and are downhill from the site of the May 2021 (b) release. The TPH-d detections, and detections of other compounds in these three wells, were examined to identify any pattern of TPH-d detections that could be tied to the May 2021 release of (b) .

TPH-d, TPH-o, and other aromatic compounds have been detected in these three wells (especially RHM(b)) for many years prior to the May 2021 release, and concentrations have fluctuated significantly over this period. Following the May 2021 release, the wells were sampled on a weekly basis, providing a more regular and frequent data set from which concentration trends might be more easily discerned. The magnitude of TPH-d concentrations in these wells differs significantly, so as a first step, the TPH-d concentrations in these wells were normalized by dividing each individual concentration by the maximum concentration of TPH-d found over a period from slightly before the May 2021 release through early February 2022. Normalization of the concentrations facilitated comparison of data from different wells by putting the TPH-d detections on the same scale. The raw and normalized TPH-d data for the three tank farm wells is shown in Chart 5-2.

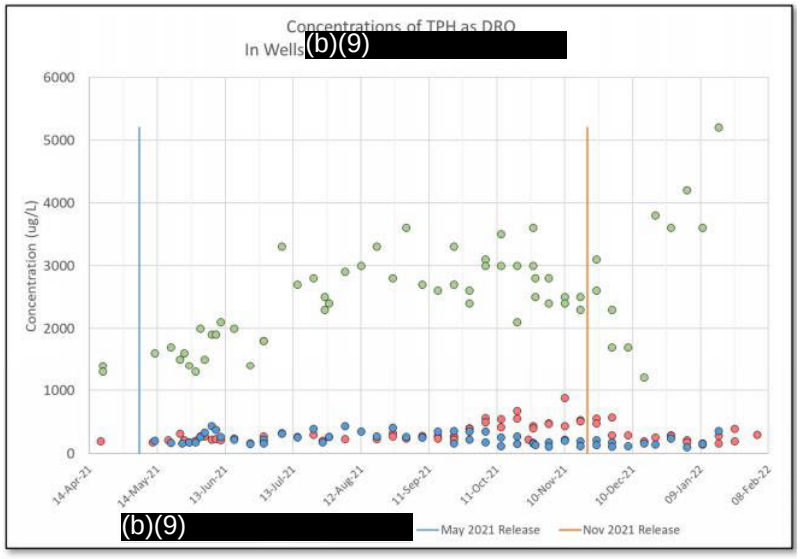

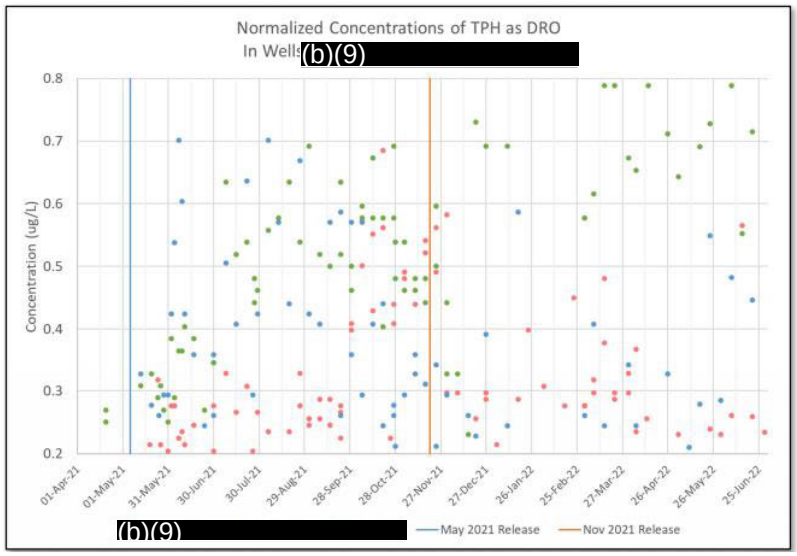

Chart 5-2: Comparison of Raw and Normalized TPH-d in Groundwater from Wells RHM(b) , RHM(b) , and RHM(b)

The large fluctuation of the TPH-d concentrations in the normalized data made identification of trends difficult. These fluctuations were thought to be the result of a number of factors, including changes in hydraulic gradient, infiltration of precipitation to groundwater, temperature, sampling method (bailer or low-flow methods), and laboratory changes, among others. All causes of TPH-d fluctuations were judged to be unlikely by analysis of the TPH-d data except for the effects of sampling method and possibly precipitation. However, no consistent impacts of these two factors could be systematically accounted for in interpreting the TPH-d data, so all the TPH-d data were retained for further examination of concentration trends.

Smoothing can often reveal trends in "noisy" (highly fluctuating) data, so the data were smoothed by calculating a central moving average. Moving averages with the number of data points varying between 5 and 21 were calculated. A moving average with 11 data points was judged to smooth the data sufficiently for trends to be observed while maintaining a relatively faithful representation of the underlying data, so this moving average was selected to identify TPH-d trends in the three tank farm wells.

The smoothed TPH-d data from wells RHM(b) , RHM(b) , and RHM(b) are shown in Chart 5-3. Both the smoothed and raw data are shown in Chart 5-4 for each of the three monitoring wells. The smoothed data revealed three distinct concentration humps that may represent breakthrough curves of TPH-d as it moved near each well in groundwater following the May 2021 release upgradient of RHM(b) . The three humps occur in an order that is consistent with transport of TPH-d in groundwater down Red Hill ridge. Although the timing of the presumed breakthrough curves looks reasonable, there are irregularities in the TPH-d data that are not fully explained or consistent with the hypothesis of migration along or near this potential flow path.

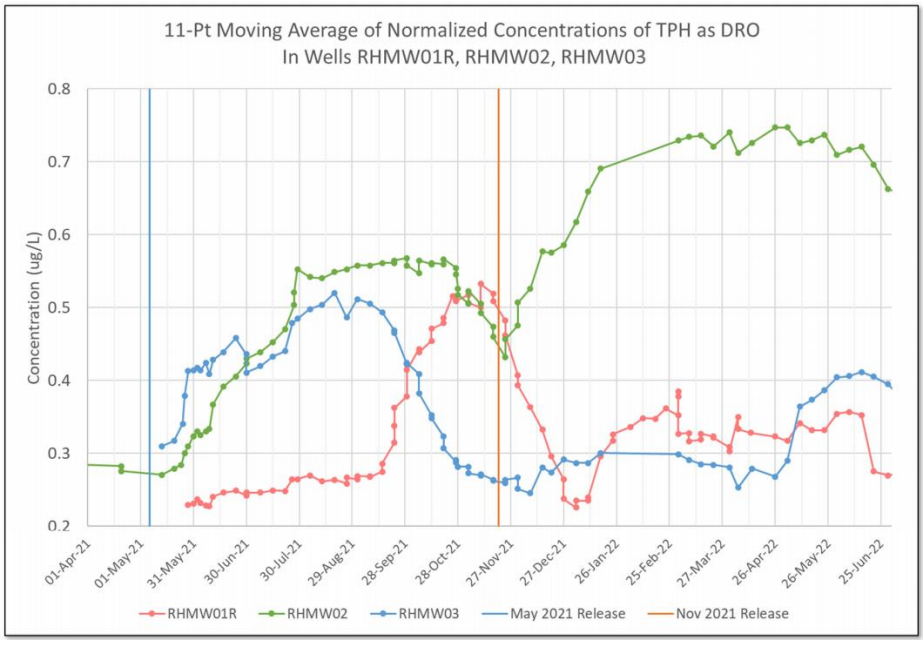

Chart 5-3: Normalized TPH-d Groundwater Concentrations in RHM(b) , RHM(b) , and RHM(b) Smoothed by Calculating an 11-Point Moving Average

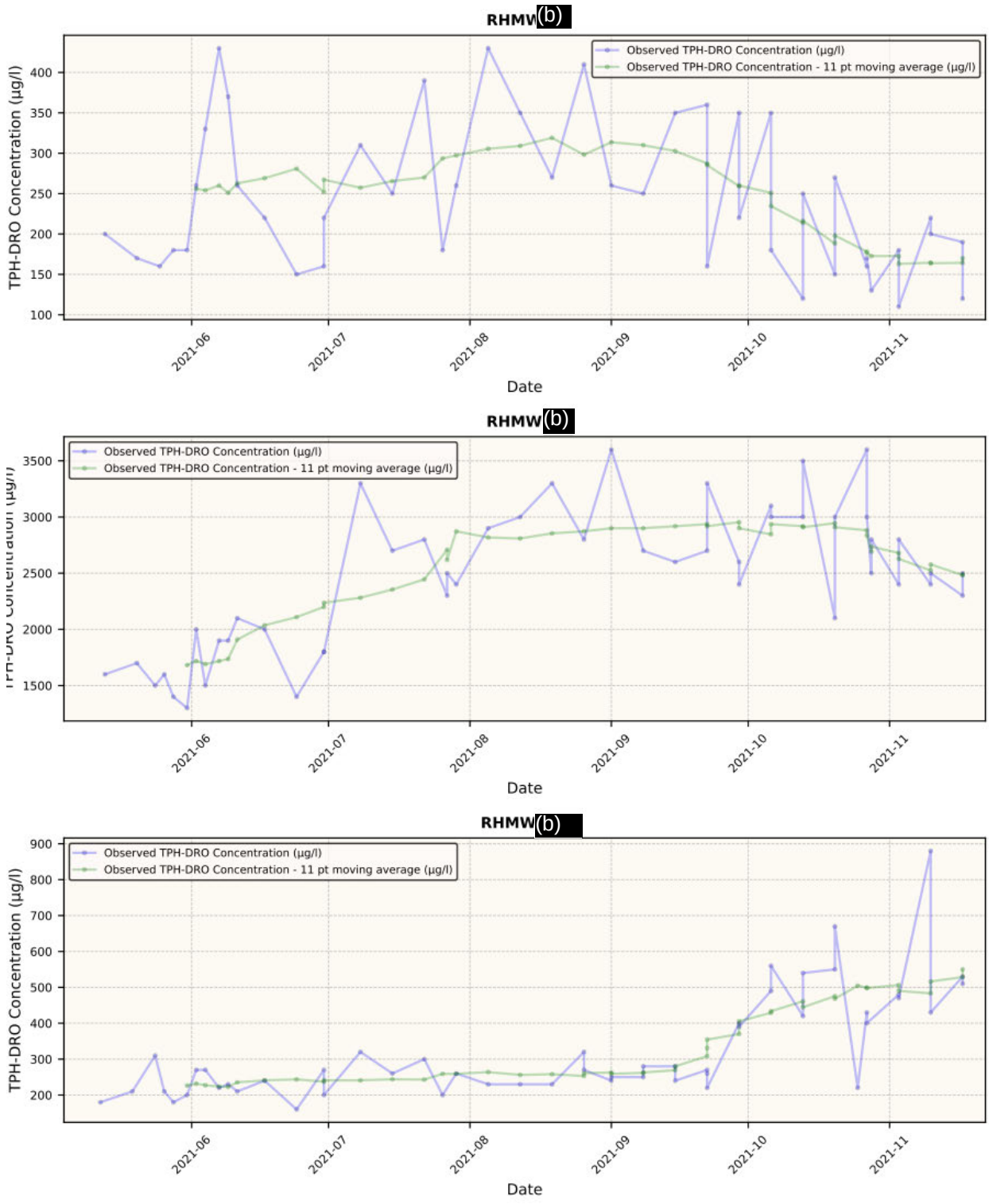

Chart 5-4: TPH-d Concentrations at RHMW(b) , RHMW(b) and RHMW(b)) Following May 2021 Release with 11-Point Moving Average Used for PEST Simulations as Target Data

First, TPH-d arrives at RHM(b) and RHM(b) nearly simultaneously. Because these wells are separated by a substantial distance, the simultaneous arrival of the leading edge of the presumed TPH-d breakthrough curves is anomalous and inconsistent with only dissolved-phase transport in groundwater originating from a point in the aquifer below the release location. Three of the many possible mechanisms to explain the corresponding leading edges of the breakthrough curves seem to be most plausible. One explanation is that vapor transport carried soluble (b) constituents westerly down Red Hill ridge in the vadose zone or in a tunnel, so that it appeared at the water table at many points along the ridge relatively rapidly. A second possible explanation is that (b) constituents were carried to the water table as dissolved constituents in washwater used to clean up the jet fuel spill. A third possible explanation is that the release in the tunnel migrated along different pathlines through the vadose zone and entered the groundwater at various locations near and between wells 2 and 3.

A second irregularity in the TPH-d data is the substantial increase in TPH-d at RHM(b) that follows the November 2021 release in Adit 3 near (b) (without any similar increase in any of the other wells, such as wells 1R, 5, and 8, located between or near well 2 and the (b)). The November release occurred over 1,000 ft west of RHM(b) . Excluding vapor transport, no logical explanation has been identified for why a release near (b) would affect groundwater in an uphill and cross-gradient direction. It is most likely that this second pulse of TPH-d is unrelated to either the May or November 2021 releases and is likely caused by a process other than transport in groundwater from the November release location to RHM(b) . The other process identified as most likely to date is dissolution of LNAPL constituents by infiltrating precipitation. Additionally, TPH-d concentrations are persistently high and variable at RHM(b) , and have varied over the years, presumably related to a nearby LNAPL source. The potential causes of the rise in concentrations at RHM(b) after November 2021 are still being evaluated.

A third irregularity is the magnitude of TPH-d concentrations in the three wells. Peak concentrations of TPH-d in RHM(b) , presumably closest to the original release, are over an order of magnitude lower than concentrations at RHM(b) . Concentrations of TPH-d in RHM(b)), downgradient of RHM(b) , are consistent with what might be expected by groundwater transport from a plume that also migrated through RHM(b) . It is possible that the lower concentrations at RHM(b) are caused by bypassing of infiltrating LNAPL, or a source occurring somewhat cross-gradient from RHM(b) , or washwater migrating to groundwater through preferential flow paths.

In addition to the magnitude of the concentrations at RHM(b) , the composition of the TPH-d at RHM(b) is different than the composition of the TPH-d at the other two downgradient wells. The differences in composition suggest that the pulse of TPH-d at RHM(b) could be caused by a different mechanism related to the May 2021 release, but not from direct transport of the released (b) to the water table. These other mechanisms could include dissolution of residual LNAPL near RHM(b) by washwater or infiltrating (b) , or some other mobilization process yet to be identified.

The timing of the RHM(b) pulse and the differences in composition of TPH-d at this location from the other two wells makes the RHM(b) data much less useful for model calibration. Calibration was therefore focused on simulating the migration of the apparent TPH-d pulse between RHM(b) and RHM(b)) following the May 2021 release.

5.2.5 Forensic Analysis of TPH-d in Perimeter Wells

TPH-d has also been detected in perimeter wells, i.e., other monitoring wells not located within the tank farm. Figure 5-1 compares the history of TPH-d concentrations in the perimeter wells and the tank farm wells between May 2021 and September 2023. Detections of TPH-d in perimeter wells are generally isolated and separated by many non-detects or J-values. Overall, the detections do not show clear patterns associated with the May 2021 or November 2021 releases.

This does not mean the detections in perimeter wells were not related to fuel, only that they are not of the type that can be used for calibration. These detections may be related to historical releases from the fuel storage tanks, but they are not sufficiently persistent for use in calibrating the CF&T model. They can potentially be considered in establishing outer limits of transport from the tank farm area, if these occurrences are the result of groundwater transport from the tank farm.

A possible exception is the TPH-d data from RHM(b) . This is the first well downgradient of RHM(b)) (based on the results of flow model particle tracks for most scenarios) and would be the perimeter well most likely to show impacts from groundwater transport after a tank farm release. TPH-d concentrations in RHM(b) are elevated in December 2021 over three to four sampling events, depending on how the data are interpreted. TPH-o was also elevated in RHM(b) during this period.

The timing of the TPH-d detections in RHM(b) is consistent with groundwater transport past RHM(b)) from the tank farm following the May 2021 release. However, the detections are too intermittent and sparse to be definitively attributed to a specific tank farm release and was therefore not used for model calibration. Further analysis of the TPH-d history at RHM(b) may indicate that this data can be used to refine model calibration and possibly to assess the rate of TPH-d biodegradation.

5.3 History Matching

5.3.1 Approach

Simulation of the May 2021 release was selected as the event to be simulated for CF&T history matching and model calibration. On May 6, 2021, a pipeline carrying (b) near Red Hill Tanks 18 and 20 was damaged during a fuel transfer procedure. Fuel was released to the tunnel floor, and attempts were made to recover the fuel. Some fuel was also released to the subsurface environment, likely through soil vapor monitoring points. It was later determined that fuel not recovered was pumped from a fire suppression retention system into a fire suppression recovery drain line. That fuel remained contained and undetected in the drain line until that drain line was damaged in Adit 3 on November 20, 2021.

The relatively small volume of (b) that was released to the subsurface from the lower access tunnel in May 2021 was described by the Navy as incalculable but less than 100 gallons. It is suspected that post-release washing of the tunnel may have solubilized residual LNAPL in the unsaturated zone, sending a temporary slug to the water table, from where it then migrated.

Uncertainty remains as to the specific mechanisms of fuel transport to the basal aquifer from this release; therefore, two separate sets of simulations were conducted with differing conceptual models of the breakthrough curves. The first set of simulations assumed that washwater travelling down-dip dissolved

residual contamination and caused near simultaneous effects on RHM(b) and RHM(b) . This conceptual model is referred to as the one-source model. In the second conceptual model, the breakthrough curve at RHM(b) is assumed to be related to the May 2021 release, but the breakthrough at RHM(b) is more related to existing residual contamination at RHM(b) . This conceptual model is referred to as the two-source model. The two-source model is also conceptually consistent with how rapid vapor transport through the tunnel may have contributed to dissolved-phase concentrations in groundwater.

The source zones for each of the two conceptual models, defined as constant concentration TPH-d source zones, are shown on Figure 5-2 and Figure 5-3. The constant TPH-d concentration sources are established in the uppermost saturated layer in each plan view location. The one-source conceptual model uses two zones with differing concentrations accounting for the higher concentrations at RHM(b) likely related to higher levels of residual contamination in the area that may have been solubilized in washwater. Both conceptual models use two different concentrations: one assigned to reach number 100, near RHM(b) , and the other assigned to reach number 200, near RHM(b) , as shown on Figure 5-2 and Figure 5-3.

The simulations were set up with a single steady-state flow stress period, with (b) pumping at 4.3 mgd for all 50 realizations of the heterogeneous model. Pumping rates for all other supply wells were derived from DLNR-supplied data for that time period. Prior to the simulated release, a 1,000-day transport stress period was run to establish background conditions, then the simulation of the May 2021 release was run from May 6 for a total duration of 200 days. Over those 200 days, five stress periods were implemented to account for increases and decreases in source concentration corresponding to observed general trends in TPH-d concentrations. After this period, the November 2021 release near (b) occurred, as well as several significant precipitation events, obscuring TPH-d data for comparison. The stress period setup and source concentrations are presented in Table 5-3.

Table 5-3: History Matching Model Stress Period Setup

Stress Period	Period Length (days)	RHM(b) Source Concentration	RHM(b) Source Concentration
1	1,000	Background	Background
2	30	Maximum	Background + 0.15*Maximum
3	60	Maximum	Background + 0.5*Maximum
4	40	Maximum	Maximum
5	40	Background + 0.67*Maximum	Maximum
6	30	Background + 0.1*Maximum	Background + 0.67*Maximum

Notes:
Background – input source concentration prior to the release, which replicates background concentrations.
Maximum – the maximum input source concentration that replicates the peak of the nearby breakthrough curve.

Several parameters were adjusted to match measured TPH-d data, including background and maximum source concentration, longitudinal dispersivity, transverse dispersivity, and effective porosity. Vertical dispersivity was held at 1/100 of longitudinal dispersivity. Effective porosity was calibrated as a multiplier

on specific yield, which varied spatially according to a heterogeneous matrix of clinker percentages in each realization, discussed in Section 3.0. Degradation of TPH-d was insignificant at the time scale of the calibration simulations as the TPH-d data set includes petroleum and polar breakdown products, as discussed in Section 5.2. Parameters were modified in an automated fashion using the PEST software described in Section 2.3. Prior information was used to regularize parameters and maintain reasonable values during the calibration process, meaning an increasingly large penalty is applied to the total objective function as estimated value deviated farther from the preferred value. Parameter inputs for the PEST simulations are shown in Table 5-4.

Table 5-4: PEST Input Parameters for History Matching

Parameter	Initial Value	Minimum Value	Maximum Value	Preferred Value
Longitudinal Dispersivity (ft)	45	2	200	45
Transverse Dispersivity (ft)	15	1	100	1/4 of Longitudinal Dispersivity
Vertical Dispersivity (ft)	0.45	Fixed to 1/100 Longitudinal Dispersivity		—
Porosity Multiplier (-)	1.375	1	2	1.375
RHM(b) Source (Background; µg/L)	4,500	150	25,000	—
RHM(b) Source (Maximum; µg/L)	3,500	150	25,000	—
RHM(b) Source (Background; µg/L)	800	150	25,000	—
RHM(b) Source (Maximum; µg/L)	8,000	150	25,000	—

Notes:
µg/L micrograms per liter

Target data for the PEST simulations included 11-point central moving averages of TPH-d concentrations measured at RHM(b) , RHM(b) , and RHM(b)). Measurements at RHM(b)) received the highest weight of 5 per observation target because it represents the most important well for saturated zone transport whereas RHM(b) and RHM(b) represent source area conditions. Weights on RHM(b) and RHM(b) were assigned to be 1 and 1.5, respectively. An additional consideration in the weighting was the magnitude of measurements because matching lower concentrations, such as at RHM(b)), was the most important, and greater variance is expected and acceptable at the higher concentrations observed in RHM(b) . Data used for calibration are presented in Chart 5-4.

5.3.2 Results

Parameter estimation with PEST was conducted for each realization, as well as the base homogeneous model, for both the one- and two-source conceptual models. Results for the one- and two-source models,

including estimated parameter values, weighted RMSE, and ranking, are presented in Table 5-5 and Table 5-6. While some realizations calibrated well, others resulted in poor matches to the target data and parameter values that reached the bounds set in Table 5-4. Figure 5-4 and Figure 5-5 show the simulated plumes on the date of May 13, 2024 (103 days after release) for the one- and two-source models, respectively.

Table 5-5: History Matching Results for One-Source Conceptual Model

Realization	Weighted RMSE (µg/L)	Longitudinal Dispersivity (ft)	Transverse Dispersivity (ft)	Vertical Dispersivity (ft)	Porosity Multiplier (-)	Initial RHM[redacted] Source (µg/L)	Initial RHM[redacted] Source (µg/L)	Maximum RHM[redacted] Source (µg/L)	Maximum RHM[redacted] Source (µg/L)	Rank
Realization_41	176.8	56	17.1	0.6	1.3	254	2945.2	596.7	6568.5	1
Realization_13	183.6	85.9	33.3	0.9	1.3	281.9	3029.8	570.2	6799.1	2
Realization_16	184.8	40.3	9.6	0.4	1.6	212.9	3053.4	587.3	7010	3
Base	186.4	74.6	25.3	0.7	1.2	315.3	2909.4	517.7	6360.4	4
Realization_31	202.4	45.8	22.5	0.5	1	3816.5	13420.6	18958.7	20492.5	5
Realization_45	209.1	107.3	39.1	1.1	1.2	294	3199.9	499.4	6963.6	6
Realization_15	212.1	73.2	35.8	0.7	1.8	150	20814.6	3580.2	25000	7
Realization_49	221.7	53.3	20.9	0.5	1.1	466.4	2586	496.7	5273.1	8
Realization_40	226.5	106.6	92.4	1.1	1.1	310.7	2566.7	406.1	5620.4	9
Realization_12	231.6	132.9	56.1	1.3	1.2	331.6	3085.4	405.5	6521.2	10
Realization_17	236.6	37	11.8	0.4	1.5	150	7041.2	655.7	15490.2	11
Realization_1	244	108.9	79.1	1.1	1.1	369	12273.6	441.5	25000	12
Realization_10	251.7	127.5	56.6	1.3	1.2	232.2	3476.9	361.5	7178.5	13
Realization_24	261.1	33.5	16.5	0.3	1	10306.6	6925	25000	13753.1	14
Realization_28	264.2	119.1	32.1	1.2	1	334.9	10648.6	471.9	18793.1	15
Realization_7	271.6	167.2	96.6	1.7	1.6	150	4326.7	315.8	11363	16
Realization_42	279.6	159.9	32.9	1.6	1.1	353.8	9800.8	470.6	17429.4	17
Realization_27	285.9	114.4	59.4	1.1	1.2	469.3	6868.4	460.5	14085	18
Realization_32	294.3	105.5	100	1.1	1.7	150	9353.9	1264.5	17915.6	19
Realization_33	307.9	90.9	19.7	0.9	1.1	725.6	3154.3	422.4	5996.9	20
Realization_46	315.2	141.2	80.6	1.4	1.1	591	6619	418.7	11549.9	21
Realization_21	320.7	128.9	96.4	1.3	1.1	474	2825.6	408.7	5398	22
Realization_2	376.9	196.8	27	2	1.1	1122	4502.6	1818.8	7686.5	23
Realization_30	380.1	143.4	94.4	1.4	1.1	588.2	3768.9	384.5	6565.5	24
Realization_34	403.7	66.6	19.7	0.7	1.4	1953.2	4169.1	150	6678.5	25
Realization_38	426.1	141.6	100	1.4	1.2	653.8	4409.8	455.1	7660.7	26
Realization_47	440.3	67	21.8	0.7	1.5	1279.9	3668.5	593.6	6466.4	27
Realization_44	452.8	63.3	87.1	0.6	2	150	5958.1	352.2	25000	28
Realization_14	462	200	100	2	1.2	617.5	3653.5	403.7	5225.8	29

Realization	Weighted RMSE (µg/L)	Longitudinal Dispersivity (ft)	Transverse Dispersivity (ft)	Vertical Dispersivity (ft)	Porosity Multiplier (-)	Initial RHM[redacted] Source (µg/L)	Initial RHM[redacted] Source (µg/L)	Maximum RHM[redacted] Source (µg/L)	Maximum RHM[redacted] Source (µg/L)	Rank
Realization_6	476.7	83.8	29.6	0.8	1.6	1273	4095.7	227.4	6257.2	30
Realization_11	502.3	200	100	2	1.3	739.4	2956.1	442.9	5379.7	31
Realization_22	521.3	98.8	86.8	1	2	892.8	25000	254.4	25000	32
Realization_29	533.2	81.2	100	0.8	1.6	827.1	25000	349.5	25000	33
Realization_36	593.1	14.1	7.1	0.1	2	2533.3	25000	150	1407.5	34
Realization_39	633.1	189	100	1.9	1.9	1502	3691.9	150	5301.4	35
Realization_9	655.3	92.3	46.2	0.9	2	2621.1	4189.3	150	5675.4	36
Realization_50	668.3	200	100	2	1.7	1737.8	25000	234.4	25000	37
Realization_37	668.6	200	100	2	1.6	1561	3117.3	150	4044.9	38
Realization_18	778.1	200	100	2	1.8	1518.4	3676.8	190.7	5360.7	39
Realization_43	795.4	200	35.2	2	1.3	150	25000	1204.1	25000	40
Realization_20	894.6	200	37.1	2	1.2	150	24152.9	1265.9	25000	41
Realization_23	904.6	200	100	2	1	6240.6	25000	150	25000	42
Realization_35	921.2	176.9	97.8	1.8	1.4	1683.1	15057.6	150	24229.8	43
Realization_48	941.7	200	37.3	2	1.9	2106.1	25000	211.3	25000	44
Realization_19	1002.3	200	100	2	1.8	1753.6	25000	150	25000	45
Realization_8	1033.1	152.9	100	1.5	1.5	659.5	25000	460.9	25000	46
Realization_3	1089.8	200	79.6	2	2	2784.2	25000	150	25000	47
Realization_5	1136.8	200	40.7	2	2	2360.3	25000	300.1	25000	48
Realization_25	1139	200	67	2	2	1589.1	25000	395.4	25000	49
Realization_4	1213.2	200	25.1	2	2	2847.1	25000	150	25000	50
Realization_26	1326.8	200	67	2	2	2785.9	25000	150	25000	51

Table 5-6: History Matching Results for Two-Source Conceptual Model

Realization	RMSE (µg/L)	Longitudinal Dispersivity	Transverse Dispersivity	Vertical Dispersivity	Porosity Multiplier	Initial RHM[redacted] Source	Initial RHM[redacted] Source	Maximum RHM[redacted] Source	Maximum RHM[redacted] Source	Rank
Realization_15	177.6	106.2	66.6	1.1	1.5	294.9	9782.7	20645.5	25000	1
Realization_28	190.9	104.9	28.3	1	1	816.4	8958.4	1447	19084.9	2
Base	192	74.3	26.6	0.7	1.3	928.8	2518	1153.6	6209.3	3
Realization_40	197	91.7	55	0.9	1.2	806.2	2046	913.8	5243.9	4
Realization_27	200.3	104.1	40.6	1	1.4	828.5	5940.9	1242.6	15006.2	5
Realization_41	201.6	60	20.1	0.6	1.5	639	2527.6	1200.4	6401.3	6
Realization_13	204.7	83.2	32.6	0.8	1.5	821.7	2680.7	1615.9	6672.7	7
Realization_17	206.4	30.4	8.1	0.3	1.5	345.6	8192.4	1532.2	18020.6	8
Realization_42	217.3	144.6	38.2	1.4	1.1	947.6	7533.5	1020.8	15931.2	9
Realization_16	221	40.2	10.1	0.4	1.8	170.6	2809.9	861.9	6767.7	10
Realization_1	226.5	111.6	79.8	1.1	1.2	2241.4	10291.8	1348.9	25000	11
Realization_49	234.3	52.3	20.9	0.5	1.2	1387.8	2377.4	1164.5	5220.6	12
Realization_21	244.1	106.2	60.6	1.1	1.3	1124.8	2404.9	664.5	5521.2	13
Realization_45	245.5	111.4	41.6	1.1	1.3	721.2	2874.1	1063.4	6756.8	14
Realization_10	248.3	111.8	48	1.1	1.4	549.2	2998	583.6	6972.7	15
Realization_46	254.2	143.5	78.3	1.4	1.1	1451.4	5257	703.6	11399.7	16
Realization_12	254.4	132.8	53.4	1.3	1.3	926.8	2744.6	686.7	6357	17
Realization_33	307.2	108.6	26.2	1.1	1.1	2550.7	2732.7	514.5	5666.7	18
Realization_7	313.5	146.6	100	1.5	2	150	3409.8	1395.9	11898.9	19
Realization_32	331.3	76.6	100	0.8	1.7	150	7145.4	19619.3	14658.2	20
Realization_30	365	135.5	83.7	1.4	1.3	2452.8	3234.5	463.1	6329.1	21
Realization_38	371	126.9	100	1.3	1.4	3083.3	3492.2	243	7551.2	22
Realization_34	375.3	127.1	42.2	1.3	1.1	2549.7	4436	150	6595	23
Realization_31	394.3	139.3	70.1	1.4	1.1	25000	13480.1	25000	21462.5	24
Realization_6	413.6	114.2	46.9	1.1	1.4	1795.5	3383	177.5	6129.1	25
Realization_50	424.9	186.6	55.6	1.9	1.2	150	25000	2736	25000	26
Realization_47	444	67.1	26.2	0.7	1.7	7903.2	3347.1	150	6400.1	27
Realization_24	451.9	110.5	94.6	1.1	1.2	25000	4420.9	25000	10319.2	28
Realization_2	455	200	27.2	2	1.1	9307.1	5527.3	150	8215.2	29

Realization	RMSE (µg/L)	Longitudinal Dispersivity	Transverse Dispersivity	Vertical Dispersivity	Porosity Multiplier	Initial RHM[redacted] Source	Initial RHM[redacted] Source	Maximum RHM[redacted] Source	Maximum RHM[redacted] Source	Rank
Realization_22	468.1	151.2	39.1	1.5	1.9	2448.4	25000	548.1	25000	30
Realization_14	481.2	200	100	2	1.2	2257.8	3938	1500.4	5016.1	31
Realization_39	490.7	200	100	2	1.4	2965	3503.2	150	5593.8	32
Realization_11	528.9	200	100	2	1.6	3179.4	3180.6	150	5183.3	33
Realization_29	545.1	43.8	50.2	0.4	1.3	755.4	24045.2	1772.5	25000	34
Realization_9	650.1	86.7	100	0.9	1.5	7959.4	4262.8	150	5814.7	35
Realization_37	682.1	200	100	2	1.3	2273.7	3477.8	150	3904	36
Realization_36	688.9	13.4	4.3	0.1	1.6	2344.6	24086	453.6	25000	37
Realization_18	718.8	200	100	2	1.6	4499.6	3256.4	150	5168.9	38
Realization_44	775.3	68.7	64.5	0.7	2	416.9	7047.2	1521.3	16705.8	39
Realization_43	800.5	200	47.8	2	1.4	532.3	8767.8	2973.7	25000	40
Realization_48	864.7	200	100	2	1.9	3840.5	25000	426.7	25000	41
Realization_20	908.9	200	25.8	2	1.4	4202.8	7802.5	1200.9	25000	42
Realization_35	942.8	165.1	100	1.7	1.2	4012.4	15125	150	22828.8	43
Realization_8	1006.3	146	100	1.5	1.4	1297.2	22481.9	399.6	25000	44
Realization_23	1018	200	100	2	1	19058.3	25000	150	25000	45
Realization_3	1041.2	200	100	2	1.3	7103.4	25000	150	25000	46
Realization_25	1044.6	200	84.6	2	1.4	2054.9	25000	895.2	25000	47
Realization_19	1061.8	200	100	2	1.5	4181.5	25000	150	25000	48
Realization_5	1094.1	200	44.5	2	1.2	2705	14648.4	1455.3	25000	49
Realization_26	1181.8	200	100	2	1.5	5832.7	25000	150	25000	50
Realization_4	1232.4	200	36.1	2	1.8	5664.4	25000	150	25000	51

In assessing the results, a weighted RMSE calibration threshold value of 250 µg/L was imposed for a realization to be considered reasonably well-calibrated, based on qualitative review of time series plots for simulated and observed concentrations. Time series plots for all realizations are presented in Appendix H. Both conceptual models behaved similarly in calibration. The one-source conceptual model resulted in 12 reasonably well-calibrated realizations, including the base model, while the two-source model resulted in 18 realizations, including the base model. Realizations that were below the specified weighted RMSE threshold are presented in Table 5-7, along with their overall rank among the 50 realizations and base model for both conceptual models.

Table 5-7: Realizations Below Calibration Threshold

Realization	One- Source	One-Source Overall Rank	Two-Source	Two-Source Overall Rank
Realization_41	x	1	x	10
Realization_13	x	3	x	12
Realization_16	x	4	x	17
Base (Homogeneous)	x	5	x	7
Realization_31	x	11	—	—
Realization_45	x	14	x	26
Realization_15	x	15	x	2
Realization_49	x	18	x	22
Realization_40	x	19.5	x	8
Realization_12	x	21	x	30
Realization_17	x	23	x	13
Realization_1	x	24	x	19
Realization_28	—	—	x	6
Realization_27	—	—	x	9
Realization_42	—	—	x	16
Realization_21	—	—	x	25
Realization_10	—	—	x	27
Realization_46	—	—	x	29

Calibrated parameters between the two conceptual models were mostly consistent. A summary of average final parameter values for both conceptual models is presented in Table 5-8. Dispersivity in general is a parameter used to account for unsimulated spatial and temporal variability within the flow system, particularly small-scale variations in velocity. In cases where uncertainty exists in the orientation of a plume axis, as is the case at the Facility, dispersion may help account for deviations of simulated flow paths from actual flow paths. Realizations that calibrated with lower dispersivity demonstrated flow paths similar to the apparent migration path from RHM(b) to RHM(b) and had the best matches to the data. Realizations with poorer matches to the target data typically calibrated with higher dispersivity values, particularly in the transverse direction, smearing the simulated plume across the distance between simulated and apparent flow paths. The ratio of longitudinal to transverse dispersivity ranged from approximately 2.1

to 2.3. Although this ratio may be lower than typical values in an anisotropic system such as this, it may be another indication of differences between simulated and apparent flow paths.

Table 5-8: Average Calibrated Model Parameter Values

Conceptual Model	Calibration Result	Longitudinal Dispersivity (ft)	Transverse Dispersivity (ft)	Longitudinal to Transverse Dispersivity Ratio	Vertical Dispersivity (ft)	Effective Porosity Multiplier
One-Source	Below Threshold	77	37	2.1	0.8	1.3
One-Source	All	131	60	2.2	1.3	1.5
Two-Source	Below Threshold	95	42	2.3	1.0	1.0
Two-Source	All	134	62	2.1	1.3	1.4

5.4 Predictive Simulations

5.4.1 Approach

Predictive simulations were conducted to leverage the calibrated groundwater flow and contaminant transport models to assess potential future conditions and impacts on nearby environmental receptors (e.g. water supply wells) based on conditions after defueling. This approach focuses on using existing information regarding historical contamination to evaluate and bound anticipated future conditions, as well as exploring monitoring conditions that would signal future impacts on receptors. Large hypothetical releases were not simulated as in the BAM study because the tank farm has since been defueled and the risk of new large-volume releases to the environment is no longer present.

The current risk concern is associated with residual contamination or LNAPL that may be present in the unsaturated zone and near the water table beneath the tank farm. Historical releases have likely occurred over many decades, and three have occurred in recent years at known locations, including a release in 2014 from (b)(3), the May 2021 release from the lower access tunnel of the tank farm, and the November 2021 release in Adit 3 near (b) . TPH-d concentrations at RHM(b) after the May 2021 release have since decreased to below the detection limit. TPH-d concentrations at RHM(b) have returned to their historical ranges. The most recent documented fuel release (November 2021) occurred above (b) where LNAPL was observed within the shaft itself. Since that release, water has been pumped from (b) at a rate of approximately (b) mgd on a consistent basis, and samples of water from the shaft and surrounding "P wells" have been below detection limits. Pumping was reduced to an average of approximately (b mgd starting on April 29, 2024.

Two different scenarios for future conditions were simulated:

- Scenario 1 employed a constant concentration hypothesized source zone around (b)(3) with a fixed concentration of 4,250 µg/L. This source concentration results in TPH-d concentrations at

RHM(b) that are consistent with recent measurements of approximately 1,200 µg/L. An example simulation result is shown on Figure 5-6.

- Scenario 2 employed hypothesized constant concentration TPH-d sources both around (b)(3) and the May 2021 release location. Concentrations at each location were assigned to approximate the maximum historical TPH-d values at RHM(b) (5,200 µg/L) and RHM(b) (613 µg/L), which correspond to TPH-d source concentrations of 15,000 µg/L and 2,700 µg/L, respectively. An example simulation result is shown on Figure 5-7.

Both scenarios conservatively assume that the simulated source will not deplete over time. Each simulation was run for 100,000 days to reach steady state conditions. In addition, no degradation was assumed for the purpose of obtaining conservative estimates of steady-state concentrations. Individualized porosity and dispersivity values obtained during calibration history matching were applied to each heterogenous realization. The two source scenarios were run under the same five pumping conditions as were used for particle tracking. This resulted in 10 total scenarios and 17 calibrated realizations plus the homogeneous model, totaling 170 simulations. The following five pumping scenarios were used:

- (b) pumping at (b) mgd — Hālawa Shaft pumping at 12 mgd — (b)(3) pumping at (b) mgd
- (b) pumping at (b) mgd — Hālawa Shaft off — (b)(3) (b)
- (b) (b) — Hālawa Shaft off — (b)(3) (b)
- (b) (b) — Hālawa Shaft pumping at 12 mgd — (b)(3) (b)
- (b) pumping at (b) mgd — Hālawa Shaft off — (b)(3) (b)

5.4.2 Results

Results from the two source scenarios and five pumping configurations were analyzed by: 1) evaluating final TPH-d concentrations at each of the monitoring and water supply wells within the model domain; and 2) compiling the maximum concentration at each plan view model cell location. Simulation results were compared both to the total petroleum hydrocarbon – diesel range organics (TPH-d) Groundwater Screening Criterion (GWSC) of 400 micrograms per liter (µg/L) from the Consolidated Groundwater Sampling Program (DOH 2024) and to 100 µg/L, which is a round number close to the lower limits of most laboratory reporting levels and the current EAL. (Future modeling will also compare results to the specific EALs at that time.) Results were then compiled into maps showing the maximum concentrations at each location in a color flood and the percentage of realizations with GWSC exceedance contours. Only the 17 heterogeneous models that met the calibration threshold in either of the conceptual model simulations were included in the results maps. Examples of the final simulated plumes for Realization 10 under the pumping configuration with (b) pumping at (b) gd and Hālawa Shaft pumping at 12 mgd are shown on Figure 5-6 and Figure 5-7.

5.4.2.1 SCENARIO 1

Scenario 1 evaluates TPH-d concentrations under a representation of current groundwater source conditions, assuming that the most significant remaining source is residual contamination around (b)(3) with a fixed concentration of 4,250 µg/L. Figure 5-8 through Figure 5-11 show the maximum TPH-d

concentration in plan-view along with contours of the percentage of realizations with GWSC exceedances for each of the five pumping scenarios in Scenario 1.

Results for simulated TPH-d concentrations at monitoring wells and water supply wells are shown in Table 5-9. Results are discussed in comparison to the approximate detection limit of 100 µg/L and TPH-d GWSC of 400 µg/L. The rows are sorted by greatest percentage of realizations with GWSC exceedance in the (b) pumping at (b mgd, Hālawa Shaft off configuration.

Table 5-9: Simulated TPH-d Concentrations at Monitoring Wells and Water Supply Wells in Scenario 1

Well_Name	Type	[redacted] ([redacted]mgd, Hālawa Shaft 12 mgd			[redacted] ([redacted] mgd, Hālawa Shaft Off			[redacted] [redacted](b) Hālawa Shaft Off			[redacted] [redacted](b) Hālawa Shaft 12 mgd			[redacted] [redacted] mgd, Hālawa Shaft[redacted](b)		
		Avg. Conc. (µg/L)	Max. Conc. (µg/L)	% GWSC Exceed-ance	Avg. Conc. (µg/L)	Max. Conc. (µg/L)	% GWSC Exceed-ance	Avg. Conc. (µg/L)	Max. Conc. (µg/L)	% GWSC Exceed-ance	Avg. Conc. (µg/L)	Max. Conc. (µg/L)	% GWSC Exceed-ance	Avg. Conc. (µg/L)	Max. Conc. (µg/L)	% GWSC Exceed ance
RHM[redacted]	MW	1,541	2,657	100%	1,565	2,682	100%	1,308	2,285	94%	1,279	2,290	88%	1,495	2,547	100%
RH[redacted]	MW	17	65	0%	17	95	0%	6	20	0%	5	19	0%	137	907	12%
RHM[redacted]	MW	254	750	6%	271	783	12%	128	367	0%	118	349	0%	220	669	6%
RHM[redacted]	MW	267	755	12%	284	786	18%	135	389	0%	124	362	0%	231	681	6%
OWDFM[redacted]	MW	5	49	0%	6	45	0%	3	19	0%	3	18	0%	14	104	0%
OWDFM[redacted]	MW	5	48	0%	6	51	0%	3	16	0%	3	16	0%	15	124	0%
OWDFM[redacted]	MW	4	46	0%	6	46	0%	3	17	0%	3	17	0%	11	75	0%
OWDFM[redacted]	MW	7	59	0%	8	62	0%	6	26	0%	5	25	0%	26	188	0%
OWDFM[redacted]	MW	2	20	0%	2	19	0%	1	4	0%	1	4	0%	3	24	0%
OWDFM[redacted]	MW	4	44	0%	5	41	0%	4	19	0%	4	19	0%	12	88	0%
OWDFM[redacted]	MW	3	37	0%	4	32	0%	4	19	0%	4	20	0%	10	72	0%
OWDFM [redacted]	MW	3	29	0%	4	43	0%	1	6	0%	1	6	0%	8	82	0%
RHM[redacted]	MW	0	0	0%	0	0	0%	0	1	0%	0	1	0%	0	0	0%
RHM[redacted]	MW	0	0	0%	0	0	0%	0	0	0%	0	0	0%	0	0	0%
RHM[redacted]	MW	90	297	0%	94	310	0%	49	158	0%	45	148	0%	82	267	0%
RHM[redacted]	MW	0	0	0%	0	0	0%	11	123	0%	12	130	0%	0	0	0%
RHM[redacted]	MW	46	233	0%	45	235	0%	29	157	0%	29	139	0%	42	177	0%
RHM[redacted]	MW	1	6	0%	1	7	0%	0	3	0%	0	2	0%	1	4	0%
RHM[redacted]	MW	0	0	0%	0	0	0%	0	0	0%	0	0	0%	0	0	0%
RHM[redacted]1	MW	0	0	0%	0	0	0%	4	36	0%	5	38	0%	0	0	0%
RHM[redacted]2	MW	0	0	0%	0	0	0%	7	55	0%	8	61	0%	0	0	0%
RHM[redacted]	MW	0	0	0%	0	0	0%	6	42	0%	9	45	0%	0	0	0%
RHM[redacted]	MW	0	0	0%	0	0	0%	4	21	0%	6	25	0%	0	0	0%
RHM[redacted]	MW	0	0	0%	0	0	0%	0	3	0%	1	7	0%	0	0	0%
RHMW[redacted](b)	MW	0	0	0%	0	0	0%	1	15	0%	2	15	0%	0	0	0%
RHM[redacted]	MW	0	0	0%	0	0	0%	0	0	0%	0	0	0%	0	0	0%
RHM[redacted]	MW	0	0	0%	0	0	0%	0	0	0%	0	0	0%	0	0	0%

Well_Name	Type	[redacted] (b) gd, Hālawa Shaft 12 mgd			[redacted] (mgd, Hālawa Shaft Off			[redacted] (b) Hālawa Shaft Off			[redacted](b) Hālawa Shaft 12 mgd			[redacted] [redacted] mgd, Hālawa Shaft off		
		Avg. Conc. (µg/L)	Max. Conc. (µg/L)	% GWSC Exceed-ance	Avg. Conc. (µg/L)	Max. Conc. (µg/L)	% GWSC Exceed-ance	Avg. Conc. (µg/L)	Max. Conc. (µg/L)	% GWSC Exceed-ance	Avg. Conc. (µg/L)	Max. Conc. (µg/L)	% GWSC Exceed-ance	Avg. Conc. (µg/L)	Max. Conc. (µg/L)	% GWSC Exceed ance
RHM[redacted](b)(9)	MW	0	0	0%	0	0	0%	0	0	0%	0	0	0%	0	0	0%
RHM[redacted]	MW	0	0	0%	0	0	0%	0	0	0%	0	0	0%	0	0	0%
RHM[redacted]	MW	0	0	0%	0	0	0%	0	0	0%	0	0	0%	0	0	0%
RHM[redacted]	MW	0	0	0%	0	0	0%	8	60	0%	12	68	0%	0	0	0%
RHM[redacted]	MW	0	0	0%	0	0	0%	30	107	0%	52	319	0%	0	2	0%
RHM[redacted]	MW	1	5	0%	1	4	0%	34	151	0%	48	229	0%	2	20	0%
RHM[redacted]	MW	0	1	0%	0	1	0%	30	136	0%	33	142	0%	0	1	0%
RHM[redacted]	MW	42	145	0%	40	144	0%	159	735	6%	152	634	6%	59	166	0%
RHM[redacted]	MW	72	201	0%	69	200	0%	179	750	6%	169	626	6%	96	226	0%
RHM[redacted]	MW	88	220	0%	87	221	0%	20	79	0%	20	84	0%	86	208	0%
RHM[redacted]	MW	69	181	0%	70	183	0%	9	47	0%	9	51	0%	59	153	0%
RHM[redacted]	MW	0	0	0%	0	0	0%	7	76	0%	9	76	0%	0	0	0%
RHM[redacted]	MW	0	0	0%	0	0	0%	0	4	0%	0	6	0%	0	0	0%
RHM[redacted]	MW	0	1	0%	0	1	0%	0	1	0%	0	1	0%	0	1	0%
RHM[redacted]	MW	0	0	0%	0	0	0%	9	109	0%	10	117	0%	0	0	0%
RHP[redacted](b	MW	6	48	0%	8	66	0%	6	18	0%	5	18	0%	29	214	0%
RH[redacted]	MW	3	31	0%	4	26	0%	1	6	0%	1	7	0%	10	67	0%
RH[redacted]	MW	5	50	0%	6	44	0%	4	18	0%	4	18	0%	15	103	0%
RHP[redacted]	MW	9	98	0%	7	89	0%	45	159	0%	42	154	0%	33	137	0%
RHP[redacted])	MW	3	32	0%	1	14	0%	53	159	0%	49	153	0%	26	130	0%
RH([redacted]	MW	6	57	0%	8	51	0%	5	24	0%	5	23	0%	31	163	0%
RH[redacted]	MW	0	1	0%	0	0	0%	3	8	0%	3	8	0%	1	6	0%
[redacted]	MW	0	1	0%	0	0	0%	3	8	0%	3	8	0%	1	4	0%
[redacted]	MW	0	1	0%	0	0	0%	5	11	0%	5	12	0%	2	7	0%
(b)(9)[redacted]	MW	0	0	0%	0	0	0%	0	0	0%	0	0	0%	0	0	0%
(b)(9)[redacted]	MW	0	0	0%	0	0	0%	0	0	0%	0	0	0%	0	0	0%
(b)(9)[redacted]	MW	0	0	0%	0	0	0%	4	9	0%	4	10	0%	1	5	0%
(b)(9)[redacted]	MW	0	0	0%	0	0	0%	0	0	0%	0	0	0%	0	0	0%

Well_Name	Type	[redacted] (mgd, Hālawa Shaft 12 mgd			[redacted] (b)mgd, Hālawa Shaft Off			[redacted] (b) Hālawa Shaft Off			[redacted] (b) Hālawa Shaft 12 mgd			[redacted] mgd, Hālawa Shaft off		
		Avg. Conc. (µg/L)	Max. Conc. (µg/L)	% GWSC Exceed-ance	Avg. Conc. (µg/L)	Max. Conc. (µg/L)	% GWSC Exceed-ance	Avg. Conc. (µg/L)	Max. Conc. (µg/L)	% GWSC Exceed-ance	Avg. Conc. (µg/L)	Max. Conc. (µg/L)	% GWSC Exceed-ance	Avg. Conc. (µg/L)	Max. Conc. (µg/L)	% GWSC Exceed ance
(b)(9) [redacted]	MW	0	0	0%	0	0	0%	0	0	0%	0	0	0%	0	0	0%
(b)(9) [redacted]	MW	0	0	0%	0	0	0%	0	0	0%	0	0	0%	0	0	0%
(b)(9) [redacted]	MW	0	0	0%	0	0	0%	0	0	0%	0	0	0%	0	0	0%
(b)(9) [redacted]	MW	0	0	0%	0	0	0%	0	0	0%	0	0	0%	0	0	0%
(b)(9) [redacted]	MW	0	0	0%	0	0	0%	0	0	0%	0	0	0%	0	0	0%
(b)(9) [redacted]	WS	22	152	0%	19	132	0%	2	10	0%	2	10	0%	172	1,610	12%
(b)(9) [redacted]	WS	0	0	0%	0	0	0%	0	0	0%	0	0	0%	0	0	0%
Halawa_Shaft	WS	0	0	0%	0	0	0%	5	13	0%	6	14	0%	1	4	0%
Kalihi_Shaft	WS	0	0	0%	0	0	0%	0	0	0%	0	0	0%	0	0	0%
(b)(9) [redacted]	WS	0	0	0%	0	0	0%	0	0	0%	0	0	0%	0	0	0%
Moanalua	WS	0	0	0%	0	0	0%	0	0	0%	0	0	0%	0	0	0%
Moanalua_1	WS	0	0	0%	0	0	0%	2	6	0%	3	6	0%	1	2	0%
Honolulu_ International_ Country_Club	WS	0	0	0%	0	0	0%	0	1	0%	0	1	0%	0	0	0%
Halawa_2	WS	0	0	0%	0	0	0%	2	4	0%	2	5	0%	1	2	0%
Aiea_Gulch_1	WS	0	0	0%	0	0	0%	0	0	0%	0	0	0%	0	0	0%
Aiea_1	WS	0	1	0%	0	1	0%	11	26	0%	11	26	0%	4	14	0%
Kalauao_P1	WS	0	1	0%	0	1	0%	3	11	0%	4	12	0%	1	6	0%
WG_Minami_2007	WS	0	1	0%	0	1	0%	5	15	0%	6	16	0%	2	9	0%
Pearl_C_C_Golf	WS	0	0	0%	0	0	0%	1	2	0%	1	2	0%	0	1	0%
Kaonohi_I-2	WS	0	1	0%	0	1	0%	10	22	0%	10	22	0%	3	13	0%
Kaamilo_1	WS	0	0	0%	0	0	0%	1	2	0%	1	2	0%	0	1	0%
Waimalu_II-1	WS	0	0	0%	0	0	0%	1	2	0%	1	2	0%	0	1	0%
Kaonohi_II-3	WS	0	2	0%	0	1	0%	10	35	0%	11	35	0%	4	21	0%
Lau_Farm	WS	0	1	0%	0	1	0%	10	24	0%	11	25	0%	3	15	0%
Waimalu-002	WS	12	71	0%	17	52	0%	0	0	0%	0	0	0%	1	6	0%
Waimalu-003	WS	0	0	0%	0	0	0%	0	0	0%	0	1	0%	0	0	0%

Notes:
Avg. average MW monitoring well

Conc.	concentration	WS	water supply well
Max.	maximum		

Scenario 1 results for the specific pumping configurations are summarized below.

(b) Pumping at (mgd, Hālawa Shaft Pumping at 12 mgd, (b)(3) Pumping at(b) mgd

- RHM(b) was the only well where the average predicted TPH-d concentration across all calibrated realizations exceeded the 400 µg/L GWSC.
- Three monitoring wells had average TPH-d concentrations over 100 µg/L across all calibrated realization.
- Three monitoring wells had maximum TPH-d concentrations over the 400 µg/L GWSC in any calibrated realization.
- Nine monitoring wells had maximum TPH-d concentrations over 100 µg/L in any calibrated realization.
- Only RHM(b) had more than 50% of calibrated realizations with an GWSC exceedance. Two additional wells resulted in GWSC exceedances, but the percentages were 12% or less.
- Maximum simulated concentration in (b) (RHMW(b)(9)) was 152 µg/L in any calibrated realization.
- No concentrations over 100 µg/L were predicted for any other water supply wells in any calibrated realization.
- Average simulated concentrations across all calibrated realizations (Figure 5-8) dissipate to below 100 µg/L at the eastern end of (b) .
- GWSC exceedances (Figure 5-8) are localized to the immediate area around the source at (b)(3), extending approximately 0.4 mile to the southwest of the source.

(b) Pumping at (mgd, Hālawa Shaft Off, (b)(3)(b)

- RHM(b) was the only well where the average predicted TPH-d concentration across all calibrated realizations exceeded the 400 µg/L GWSC.
- Three monitoring wells had average TPH-d concentrations over 100 µg/L across all calibrated realization.
- Three monitoring wells had maximum TPH-d concentrations over the 400 µg/L GWSC in any calibrated realization.
- Nine monitoring wells had maximum TPH-d concentrations over 100 µg/L in any calibrated realization.
- Only RHM(b) had more than 50% of calibrated realizations with an GWSC exceedance. Two additional wells resulted in GWSC exceedances, but the percentages were 18% or less.
- Maximum simulated concentration in (b) (RHMW(b)(9)) was 132 µg/L in any calibrated realization.
- No concentrations over 100 µg/L were predicted for any other water supply wells in any calibrated realization.

- Average simulated concentrations across all calibrated realizations (Figure 5-9) dissipate to below 100 µg/L at the eastern end of (b) .
- GWSC exceedances (Figure 5-9) are localized to the immediate area around the source at (b)(3), extending approximately 0.4 mile to the southwest of the source.

(b) (b), Hālawa Shaft Off, (b)(3) (b)

- RHM(b) was the only well where the average predicted TPH-d concentrations across all calibrated realizations exceeded the 400 µg/L GWSC.
- Five monitoring wells had average TPH-d concentrations over 100 µg/L across all calibrated realization.
- Three monitoring wells had maximum TPH-d concentrations over the 400 µg/L GWSC in any calibrated realization.
- Fourteen monitoring wells had maximum TPH-d concentrations over 100 µg/L in any calibrated realization.
- Only RHM(b) had over 50% of calibrated realizations with an GWSC exceedance. Two additional wells resulted in GWSC exceedances, but the percentages were 10% or less.
- Simulated concentrations in (b) did not exceed 100 µg/L in any calibrated realization.
- No concentrations over 100 µg/L were predicted for any water supply wells in any calibrated realization.
- Average simulated concentrations across all calibrated realizations (Figure 5-10) dissipate to below 100 µg/L at the western end of (b) .
- GWSC exceedances (Figure 5-10) are localized to the immediate area around the source at (b)(3), extending approximately 0.4 mile to the southwest of the source.

(b) (b) Hālawa Shaft Pumping at 12 mgd, (b)(3) (b)

- RHM(b) was the only well where the average predicted TPH-d concentration across all calibrated realizations exceeded the 400 µg/L GWSC.
- Five monitoring wells had average TPH-d concentrations over 100 µg/L across all calibrated realization.
- Three monitoring wells had maximum TPH-d concentrations over the 400 µg/L GWSC in any calibrated realization.
- Fourteen monitoring wells had maximum TPH-d concentrations over 100 µg/L in any calibrated realization.
- Only RHM(b) had an GWSC exceedance in over 50% of calibrated realizations.
- Simulated concentrations in (b) did not exceed 100 µg/L in any calibrated realization.
- No concentrations over 100 µg/L were predicted for any water supply wells in any calibrated realization.

- Average simulated concentrations across all calibrated realizations (Figure 5-11) dissipate to below 100 µg/L at the western end of (b) .
- GWSC exceedances (Figure 5-11) are localized to the immediate area around the source at (b)(3), extending through the eastern end of (b) .

(b) Pumping at (b mgd, Hālawa Shaft Off, (b)(3) (b)

- RHM(b) was the only well where the average predicted TPH-d concentration across all calibrated realizations exceeded the 400 µg/L GWSC.
- Four monitoring wells had average TPH-d concentrations over 100 µg/L across all calibrated realization.
- Four monitoring wells had maximum TPH-d concentrations over the 400 µg/L GWSC in any calibrated realization.
- Nineteen monitoring wells had maximum TPH-d concentrations over 100 µg/L in any calibrated realization.
- Only RHM(b) had more than 50% of calibrated realizations with an GWSC exceedance. Three additional monitoring wells resulted in GWSC exceedances, but the percentages were 12% or less.
- Simulated concentrations in (b) (RHMW(b)(9)) exceeded the 400 µg/L GWSC in 12% of calibrated realizations with a maximum concentration of 1,610 µg/L.
- No concentrations over 100 µg/L were predicted for any other water supply wells in any calibrated realization.
- Average simulated concentrations across all calibrated realizations (Figure 5-12) dissipated to below 100 µg/L at the eastern end of (b) .
- GWSC exceedances (Figure 5-12) are localized to the immediate area around the source at (b)(3), extending through the eastern end of (b) .

5.4.2.2 SCENARIO 2

Scenario 2 evaluates TPH-d concentrations under the conditions that represent the maximum historical values at RHM(b) (5,200 µg/L) and RHM(b) (613 µg/L), which correspond to source concentrations of 15,000 µg/L and 2,700 µg/L, respectively. These source concentrations are held constant during the simulation. Figure 5-13 through Figure 5-17 show the maximum TPH-d concentration in plan view along with contours of the percentage of realizations with GWSC exceedances for each of the five pumping scenarios in Scenario 2. Results for simulated TPH-d concentrations at monitoring wells and water supply wells are shown in Table 5-10 The rows are sorted by greatest percentage of realizations with GWSC exceedance in (b) pumping at (mgd, Hālawa Shaft pumping at 12 mgd configuration.

Table 5-10: Simulated TPH-d Concentrations at Monitoring Wells and Water Supply Wells in Scenario 2

Well_Name	Type	[redacted] (mgd, Hālawa Shaft 12 mgd			[redacted] (b) mgd, Hālawa Shaft Off			[redacted] (b) Hālawa Shaft Off			[redacted] (b), Hālawa Shaft 12 mgd			[redacted] mgd, Hālawa Shaft Off		
		Avg. Conc. (µg/L)	Max. Conc. (µg/L)	% GWSC Exceed-ance	Avg. Conc. (µg/L)	Max. Conc. (µg/L)	% GWSC Exceed-ance	Avg. Conc. (µg/L)	Max. Conc. (µg/L)	% GWSC Exceed-ance	Avg. Conc. (µg/L)	Max. Conc. (µg/L)	% GWSC Exceed-ance	Avg. Conc. (µg/L)	Max. Conc. (µg/L)	% GWSC Exceed ance
RHM[redacted]	MW	5,492	9,429	100%	5,581	9,526	100%	4,639	8,075	100%	4,535	8,090	100%	5,317	9,011	100%
RHM[redacted]	MW	992	2,758	76%	1,057	2,871	88%	498	1,426	53%	457	1,393	41%	857	2,488	76%
RHM[redacted]	MW	564	1,000	76%	590	1,072	76%	329	828	35%	313	821	35%	491	861	76%
RHM[redacted]	MW	947	2,740	76%	1,011	2,858	82%	473	1,376	53%	433	1,344	41%	815	2,443	71%
RHM[redacted]-(b)(9)	MW	308	790	29%	295	782	29%	681	2,661	71%	645	2,213	71%	408	886	47%
RHM[redacted]-(b)[redacted]	MW	362	844	35%	356	845	29%	75	296	0%	75	314	0%	353	798	47%
RHM[redacted]	MW	346	1,109	35%	364	1,160	35%	183	589	18%	169	572	18%	314	999	29%
RHM[redacted]-(b)(9)	MW	190	591	12%	180	584	12%	622	2,612	71%	594	2,242	71%	274	675	24%
RH[redacted]	MW	81	284	0%	77	381	0%	22	75	0%	20	71	0%	558	3,613	24%
RHM[redacted]	MW	186	871	18%	183	877	18%	110	563	12%	109	496	12%	167	675	18%
RHM[redacted]-(b)(9)	MW	285	694	24%	285	701	24%	34	178	0%	35	190	0%	242	585	18%
RHP[redacted]	MW	27	225	0%	31	207	0%	21	93	0%	19	89	0%	126	633	18%
OWDFM[redacted]	MW	30	231	0%	34	249	0%	23	100	0%	21	95	0%	108	750	12%
RHP[redacted]	MW	40	384	0%	30	349	0%	176	599	12%	164	576	12%	146	535	12%
OWDFM[redacted]	MW	20	193	0%	25	183	0%	13	72	0%	12	70	0%	55	416	6%
OWDFM[redacted]A	MW	20	189	0%	25	206	0%	11	61	0%	11	63	0%	60	496	6%
RHP(b)	MW	27	190	0%	32	266	0%	22	71	0%	21	69	0%	117	852	6%
RH[redacted]	MW	22	197	0%	26	178	0%	17	70	0%	16	68	0%	61	410	6%
RHP[redacted]	MW	16	129	0%	8	57	0%	207	595	12%	192	572	12%	118	509	6%
OWDFM[redacted]A	MW	17	181	0%	23	186	0%	12	66	0%	12	66	0%	43	297	0%
OWDFM[redacted]A	MW	7	78	0%	10	78	0%	4	15	0%	4	15	0%	14	95	0%
OWDFM[redacted]A	MW	18	173	0%	21	166	0%	16	71	0%	15	72	0%	51	350	0%
OWDFM[redacted]A	MW	15	144	0%	17	131	0%	14	71	0%	14	77	0%	42	287	0%
OWDFM[redacted]A	MW	12	116	0%	18	174	0%	4	22	0%	5	21	0%	32	328	0%

Well_Name	Type	[redacted] (mgd, Hālawa Shaft 12 mgd			[redacted] (mgd, Hālawa Shaft Off			[redacted](b) Hālawa Shaft Off			[redacted] (b), Hālawa Shaft 12 mgd			[redacted] mgd, Hālawa Shaft Off		
		Avg. Conc. (µg/L)	Max. Conc. (µg/L)	% GWSC Exceed-ance	Avg. Conc. (µg/L)	Max. Conc. (µg/L)	% GWSC Exceed-ance	Avg. Conc. (µg/L)	Max. Conc. (µg/L)	% GWSC Exceed-ance	Avg. Conc. (µg/L)	Max. Conc. (µg/L)	% GWSC Exceed-ance	Avg. Conc. (µg/L)	Max. Conc. (µg/L)	% GWSC Exceed ance
(b)(9)	MW	0	0	0%	0	0	0%	0	0	0%	0	0	0%	0	0	0%
	MW	4	56	0%	3	51	0%	105	458	6%	145	480	6%	6	77	0%
	MW	4	24	0%	5	27	0%	1	14	0%	1	12	0%	3	21	0%
	MW	1	15	0%	1	16	0%	1	9	0%	1	9	0%	1	13	0%
	MW	0	0	0%	0	0	0%	27	170	0%	33	181	0%	0	2	0%
	MW	0	2	0%	0	1	0%	53	212	0%	67	233	0%	1	9	0%
	MW	1	6	0%	0	4	0%	48	151	0%	64	165	0%	3	12	0%
	MW	1	8	0%	1	5	0%	30	89	0%	42	138	0%	3	17	0%
	MW	0	3	0%	0	1	0%	4	18	0%	6	31	0%	1	4	0%
	MW	0	1	0%	0	1	0%	11	55	0%	16	74	0%	0	2	0%
	MW	0	0	0%	0	0	0%	0	0	0%	0	0	0%	0	0	0%
	MW	0	0	0%	0	0	0%	0	0	0%	0	0	0%	0	0	0%
	MW	0	0	0%	0	0	0%	0	0	0%	0	0	0%	0	0	0%
	MW	0	0	0%	0	0	0%	0	0	0%	0	0	0%	0	0	0%
	MW	0	0	0%	0	0	0%	0	0	0%	0	0	0%	0	0	0%
	MW	0	1	0%	0	0	0%	57	220	0%	74	309	0%	1	9	0%
	MW	2	10	0%	1	5	0%	173	442	12%	255	1,144	18%	12	87	0%
	MW	17	67	0%	12	47	0%	187	600	18%	241	821	18%	40	146	0%
	MW	4	37	0%	3	34	0%	140	551	6%	147	564	6%	7	56	0%

Well_Name	Type	(b) mgd, Hālawa Shaft 12 mgd			(mgd, Hālawa Shaft Off			(b) Hālawa Shaft Off			(b) Hālawa Shaft 12 mgd			mgd, Hālawa Shaft Off		
		Avg. Conc. (µg/L)	Max. Conc. (µg/L)	% GWSC Exceed-ance	Avg. Conc. (µg/L)	Max. Conc. (µg/L)	% GWSC Exceed-ance	Avg. Conc. (µg/L)	Max. Conc. (µg/L)	% GWSC Exceed-ance	Avg. Conc. (µg/L)	Max. Conc. (µg/L)	% GWSC Exceed-ance	Avg. Conc. (µg/L)	Max. Conc. (µg/L)	% GWSC Exceed ance
RHM	MW	0	0	0%	0	0	0%	49	307	0%	60	304	0%	1	5	0%
RHM	MW	0	0	0%	0	0	0%	1	17	0%	6	72	0%	0	0	0%
RHM	MW	2	8	0%	2	9	0%	1	3	0%	1	3	0%	1	5	0%
RHM	MW	11	131	0%	10	121	0%	112	491	6%	132	550	12%	18	156	0%
RH	MW	14	122	0%	15	103	0%	6	29	0%	6	26	0%	40	267	0%
RH	MW	1	2	0%	0	1	0%	14	33	0%	13	33	0%	6	23	0%
	MW	0	2	0%	0	1	0%	14	37	0%	14	34	0%	5	16	0%
(b)(3)	MW	1	3	0%	0	2	0%	19	48	0%	19	47	0%	8	29	0%
	MW	0	0	0%	0	0	0%	0	0	0%	0	0	0%	0	0	0%
	MW	0	0	0%	0	0	0%	0	0	0%	0	0	0%	0	0	0%
	MW	1	2	0%	0	1	0%	15	41	0%	17	43	0%	5	18	0%
	MW	0	0	0%	0	0	0%	0	0	0%	0	0	0%	0	0	0%
	MW	0	0	0%	0	0	0%	0	0	0%	0	0	0%	0	0	0%
	MW	0	0	0%	0	0	0%	0	0	0%	0	0	0%	0	0	0%
	MW	0	0	0%	0	0	0%	0	0	0%	0	0	0%	0	0	0%
	MW	0	0	0%	0	0	0%	0	0	0%	0	0	0%	0	0	0%
	MW	0	0	0%	0	0	0%	0	0	0%	0	0	0%	0	0	0%
	WS	147	1,517	6%	90	530	12%	8	40	0%	7	38	0%	736	6,428	35%
	WS	0	0	0%	0	0	0%	0	0	0%	0	0	0%	0	0	0%
Halawa_Shaft	WS	0	2	0%	0	1	0%	22	65	0%	24	70	0%	5	25	0%
Kalihi_Shaft	WS	0	0	0%	0	0	0%	0	0	0%	0	0	0%	0	0	0%
(b)(3)	WS	0	0	0%	0	0	0%	0	0	0%	0	0	0%	0	0	0%
Moanalua	WS	0	0	0%	0	0	0%	0	0	0%	0	0	0%	0	0	0%
Moanalua_1	WS	0	1	0%	0	0	0%	10	27	0%	13	31	0%	3	11	0%
Honolulu_ International_ Country_Club	WS	0	0	0%	0	0	0%	2	4	0%	2	5	0%	0	1	0%
Halawa_2	WS	0	1	0%	0	0	0%	8	21	0%	9	22	0%	2	9	0%

Well_Name	Type	[redacted](b)mgd, Hālawa Shaft 12 mgd			[redacted](b)mgd, Hālawa Shaft Off			[redacted](b) Hālawa Shaft Off			[redacted](b), Hālawa Shaft 12 mgd			[redacted] mgd, [redacted] Off		
		Avg. Conc. (µg/L)	Max. Conc. (µg/L)	% GWSC Exceed-ance	Avg. Conc. (µg/L)	Max. Conc. (µg/L)	% GWSC Exceed-ance	Avg. Conc. (µg/L)	Max. Conc. (µg/L)	% GWSC Exceed-ance	Avg. Conc. (µg/L)	Max. Conc. (µg/L)	% GWSC Exceed-ance	Avg. Conc. (µg/L)	Max. Conc. (µg/L)	% GWSC Exceed ance
Aiea_Gulch_1	WS	0	0	0%	0	0	0%	0	1	0%	0	1	0%	0	0	0%
Aiea_1	WS	2	7	0%	1	4	0%	45	123	0%	48	124	0%	16	57	0%
Kalauao_P1	WS	1	3	0%	0	2	0%	15	42	0%	16	46	0%	5	26	0%
WG_Minami_2 007	WS	1	4	0%	1	3	0%	22	58	0%	24	63	0%	8	35	0%
Pearl_C_C_Gol f	WS	0	0	0%	0	0	0%	3	8	0%	4	9	0%	1	3	0%
Kaonohi_I-2	WS	2	6	0%	1	4	0%	40	103	0%	43	104	0%	15	51	0%
Kaamilo_1	WS	0	0	0%	0	0	0%	3	8	0%	4	9	0%	1	5	0%
Waimalu_II-1	WS	0	0	0%	0	0	0%	3	8	0%	4	8	0%	1	4	0%
Kaonohi_II-3	WS	2	9	0%	1	6	0%	45	140	0%	46	144	0%	17	84	0%
Lau_Farm	WS	2	6	0%	1	3	0%	42	100	0%	45	103	0%	16	59	0%
Waimalu-002	WS	49	275	0%	70	201	0%	0	0	0%	0	0	0%	2	22	0%
Waimalu-003	WS	0	0	0%	0	0	0%	0	0	0%	0	3	0%	0	0	0%

MW monitoring well
WS water supply well

Scenario 2 results for the specific pumping configurations are summarized below.

(b) Pumping at (mgd, Hālawa Shaft Pumping at 12 mgd

- Average TPH-d concentrations in four monitoring wells in any calibrated realizations exceeded the 400 µg/L GWSC.
- Ten monitoring wells had average TPH-d concentrations over 100 µg/L across all calibrated realizations.
- Twenty-five monitoring wells had maximum TPH-d concentrations of over 100 µg/L in any calibrated realizations.
- Ten monitoring wells had maximum concentrations over 400 µg/L in any calibrated realization.
- At four monitoring wells, over 50% of realizations had GWSC exceedances. Six additional wells exhibited in GWSC exceedances, but the percentages were 35% or less.
- Simulated concentrations in (b) (RHMW(b)(9)) averaged 147 µg/L, with a maximum of 1,517 µg/L. The GWSC was exceeded in 6% of realizations.
- No concentrations over the 400 µg/L GWSC were predicted for any other water supply wells in any realization.
- Average simulated concentrations across all calibrated realizations (Figure 5-13) dissipate to below 100 µg/L at (b) .
- GWSC exceedances Figure 5-13) are localized to the area under the tank farm, extending 0.1 mile southwest of (b) and slightly to the northwest, beneath the valley fill.

(b) Pumping at (mgd, Hālawa Shaft Off

- Average TPH-d concentrations in four monitoring wells across all calibrated realizations exceeded the 400 µg/L GWSC.
- Average TPH-d concentrations in ten monitoring wells across all calibrated realizations exceeded in 100 µg/L.
- Ten monitoring wells had maximum concentrations over 400 µg/L in any calibrated realization.
- Twenty-four monitoring wells had maximum TPH-d concentrations of over 100 µg/L across all realizations.
- At four monitoring wells, over 50% of realizations had GWSC exceedances. Six additional wells exhibited GWSC exceedances, but the percentages were 35% or less.
- Simulated concentrations in (b) (RHMW(b)(9)) averaged 90 µg/L, with a maximum of 530 µg/L. The GWSC was not exceeded in any realization.
- No concentrations over the 400 µg/L GWSC were predicted for any water supply wells in any realization.
- Average simulated concentrations across all calibrated realizations (Figure 5-14) dissipate to below 100 µg/L at (b) .

- GWSC exceedances (Figure 5-14) are localized to the area under the tank farm, extending 0.1 mile to the southwest of (b) and slightly to the northwest, extending beneath the valley fill.

(b) (b) Hālawa Shaft Off

- Average TPH-d concentrations in five monitoring wells across all calibrated realizations exceeded the 400 µg/L GWSC.
- Average TPH-d concentrations in fifteen monitoring wells across all calibrated realizations exceeded 100 µg/L.
- Fifteen monitoring wells had maximum concentrations over 400 µg/L in any calibrated realization.
- Twenty-three monitoring wells had maximum TPH-d concentrations of over 200 µg/L across all realizations.
- At five monitoring wells, the percentage of realizations with an GWSC exceedance was over 50%. Ten additional wells exhibited GWSC exceedances, but the percentages were 35% or less.
- Simulated concentrations in (b) averaged 8 µg/L, with a maximum of 40 µg/L. The GWSC was not exceeded in any realization.
- No concentrations over the 400 µg/L GWSC were predicted for any other water supply wells in any realization.
- Average simulated concentrations across all calibrated realizations (Figure 5-15) dissipate to below 100 µg/L approximately 0.2 mile to the southwest and 0.3 mile to the north of (b), extending beneath the valley fill.
- GWSC exceedances (Figure 5-15) are located to the west of the source areas extending approximately 0.2 mile to the southwest and 0.3 mile to the north of (b), beneath the valley fill.

(b) (b), Hālawa Shaft Pumping at 12 mgd

- Average TPH-d concentrations in five monitoring wells across all calibrated realizations exceeded the 400 µg/L GWSC.
- Average TPH-d concentrations in fifteen monitoring well across all calibrated realizations exceeded 100 µg/L.
- Fifteen monitoring wells had maximum concentrations over 400 µg/L across all realizations.
- Twenty-three monitoring wells had maximum TPH-d concentrations of over 100 µg/L across all realizations.
- At three monitoring wells, the percentage of realizations with an GWSC exceedance was over 50%. Twelve additional wells exhibited GWSC exceedances, but the percentages were 42% or less.
- Simulated concentrations in (b) (RHMW(b)(9)) averaged 7 µg/L, with a maximum of 38 µg/L. The 400 µg/L GWSC was not exceeded in any realization.
- No concentrations over the 400 µg/L GWSC were predicted for any water supply wells in any realization.

- Average simulated concentrations across all calibrated realizations (Figure 5-16) dissipate to below 100 µg/L approximately 0.2 mile to the southwest and 0.3 mile to the north of (b) , extending beneath the valley fill.
- GWSC exceedances (Figure 5-16) are located to the west of the source areas extending approximately 0.2 mile to the southwest and 0.3 mile to the north of (b) , beneath the valley fill.

(b) Pumping at (b mgd, Hālawa Shaft Off

- Average TPH-d concentrations in six monitoring wells across all calibrated realizations exceeded the 400 µg/L GWSC.
- Average TPH-d concentrations in sixteen monitoring wells across all calibrated realizations exceeded in 100 µg/L.
- Nineteen monitoring wells had maximum concentrations over 400 µg/L in any calibrated realization.
- Twenty-six monitoring wells had maximum TPH-d concentrations of over 100 µg/L across all realizations.
- At four monitoring wells, over 50% of realizations had GWSC exceedances. Sixteen additional wells exhibited GWSC exceedances, with percentages ranging from 47% to 6%.
- Simulated concentrations in (b) (RHMW(b)(9)) averaged 736 µg/L, with a maximum of 6,428 µg/L.
- No concentrations over the 400 µg/L GWSC were predicted for any other water supply wells in any realization.
- Average simulated concentrations across all calibrated realizations (Figure 5-17) dissipated to below 100 µg/L approximately 0.4 mile to the southwest and 0.3 mile to the north of (b) , extending beneath the valley fill.
- GWSC exceedances (Figure 5-17) are located to the west of the source areas extending approximately 0.4 mile to the southwest and 0.3 mile to the north of (b) , beneath the valley fill.
- The apparent increases in TPH-d concentrations under this scenario are due to a greater proportion of groundwater flow to (b) originating from under the tank farm with less dilution from other areas.

5.4.3 Evaluation of Hālawa Shaft

A key consideration in this study is the potential exposure of Hālawa Shaft to dissolved-phase constituents related to residual contamination at the tank farm. In the sensitivity analysis of the groundwater flow model, discussed in Section 2.5, several attempts were made to evaluate situations where groundwater would migrate from the tank farm to Hālawa Shaft, particularly Sensitivity Scenario 5 where flow direction targets were used to guide groundwater flow toward Hālawa Shaft to the northwest. While capture of particles by (b) was reduced to 55% in the lowest case, direct flow paths from the tank farm to Hālawa Shaft were not achieved. With (b) pumping, no particles were captured by Hālawa Shaft. With (b) off, the highest percentage of capture by Hālawa Shaft was 21.6%. This is from regional model Sensitivity Model 5 with

flow direction targets to Hālawa Shaft, and 6.2% from Realization 40, both under the pumping configuration with (b) off and Hālawa Shaft pumping at 12 mgd.

Table 5-11 shows TPH-d concentrations at Hālawa Shaft by percentage of groundwater beneath the tank farm captured based on mass originating from the source zones in the predictive simulations for the base homogeneous-anisotropic model with (b) pumping at (mgd and Hālawa Shaft pumping 12 mgd at described in Section 5.4. For example, if 6.2% of the groundwater from the tank farm were captured by Hālawa Shaft, for Scenario 1 (based on the mass discharge rate for the source zone in Scenario 1), the TPH-d concentration at Hālawa Shaft would be 0.9 µg/L. The calculations assume Hālawa Shaft is pumping at 8 mgd and that there is no attenuation along the groundwater flow path (e.g., bioattenuation, degradation, or dispersion). Although the model runs were conducted with Hālawa Shaft pumping 12 mgd, 8 mgd was used for these calculations because the lower dilution capacity would result in higher concentrations and a more conservative result. The mass fluxes from the source were calculated from model simulations for the base case in each scenario with (b) pumping at (b mgd and Hālawa Shaft pumping at 12 mgd.

Table 5-11: Calculated TPH-d Concentrations at Hālawa Shaft Pumping at 8 mgd, by Percentage of Tank Farm Groundwater Captured by Hālawa Shaft

Source Term	TPH-d Mass Flux from Source (kg/d)	Simulated TPH-d Concentration (µg/l) in Hālawa Shaft by Percent of Tank Farm Groundwater Captured		
		6.2%	21.6%	100%
Scenario 1	0.42	0.9	3.0	13.8
Scenario 2	1.62	3.3	11.5	53.4

Notes:
kg/d kilograms per day

In addition to the simulation results indicating the highest percentages of capture (6.2% and 21.6%), a third calculation was performed, assuming 100% of the contaminant mass discharge from sources at the tank farm is captured by Hālawa Shaft. While this is not supported by any simulation result, it represents an upper-bound impact at Hālawa Shaft, assuming all dissolved mass leaving the tank farm reaches Hālawa Shaft without attenuation. The calculations represent conservative assumptions, yet still lead to TPH-d concentrations significantly below the 400 µg/L GWSC, with the highest concentration estimated to be 53 µg/L. These calculations indicate that the risk to Hālawa Shaft from residual petroleum at Red Hill is very low.

5.5 Travel Times to (b)(3)(b)(3)

Travel times to (b)(3)(b)(3) were evaluated from the tank farm based on the porosity values calibrated in the history matching process. Particle track travel times were calculated from the particle tracking simulations discussed in Section 2.4, where 64 particles were released spaced evenly in a 250-ft × 250-ft grid over the footprint of the tank farm. Table 5-12 shows the average (mean), minimum, maximum, and median travel times for each realization where acceptable calibration was achieved for CF&T, under the pumping configuration with (b) on at (mgd, Hālawa Shaft on at 12 mgd, and (b)(3) on at (b) mgd. Only particles that were captured by (b) were included in the calculations. Table 5-12 also presents the

percentage of the particles included. The average travel time for all calibrated realizations ranged from 225 to 819 days, with an average of 562 days compared to 547 days in the base homogeneous-anisotropic model. The minimum travel time for all calibrated realizations ranged from 86 to 260 days, with an average of 142 days compared to 203 days in the base homogeneous-anisotropic model. The maximum travel time for all calibrated realizations ranged from 784 to 12,491 days, with an average of 4,026 days compared to 1,200 days in the base homogeneous-anisotropic model. The median travel time for all calibrated realizations ranged from 205 to 625 days, with an average of 384 days compared to 508 days in the base homogeneous-anisotropic model.

Table 5-12: Summary of Particle Track Travel Times

Realization	Percent Capture by (b)	Travel Time to (b) (days)			
		Average	Minimum	Maximum	Median
Base	100%	547	203	1200	508
Realization_1	92%	715	260	3399	550
Realization_10	98%	782	135	8675	375
Realization_12	97%	453	89	1733	362
Realization_13	95%	426	110	1785	329
Realization_15	97%	696	112	3603	403
Realization_16	94%	225	105	784	205
Realization_17	95%	760	159	2930	516
Realization_21	97%	272	86	867	255
Realization_27	94%	433	139	1848	302
Realization_28	97%	725	260	2165	625
Realization_31	92%	581	107	7667	312
Realization_40	95%	819	212	12491	449
Realization_41	97%	484	121	5566	270
Realization_42	95%	485	174	2937	417
Realization_45	95%	595	119	3296	450
Realization_46	95%	463	99	3422	294
Realization_49	100%	649	133	5271	415
	Average	562	142	4026	384
	Minimum	225	86	784	205
	Maximum	819	260	12,491	625
	Median	581	121	3296	375

The shortest travel times are generally associated with the particles starting at the southwestern end of the tank farm closest to (b) , whereas the particles with the longest travel times are generally those that started in massive basalt and moved slowly through the basalt until reaching a clinker zone where groundwater

velocities are significantly higher. Average and median travel times for the realizations show a distribution of travel times which includes both faster and slower arrivals at (b) , with the distribution skewed toward faster travel times. Although the particles tracks do not show a significant horizontal spread on the scale of Figure 3-6, greater variability in the vertical direction resulted in longer flow paths, as shown on Figure 5-18; however preferential flow through clinker zones create faster pathways for groundwater to flow. A histogram of median travel times to (b) for calibrated realizations is presented in Chart 5-5.

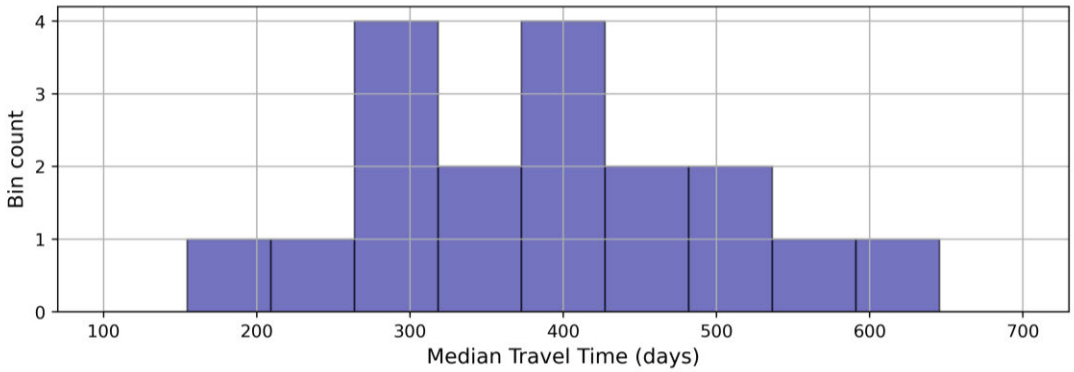

Chart 5-5: Histogram of Median Travel Times to (b) for Calibrated Realizations

5.6 Sensitivity Analysis

A sensitivity analysis was conducted to assess the variability in results from the predictive simulations based on modifications to the transport parameters, including effective porosity and dispersivity. Two sets of simulations were conducted with increases and decreases of 50% in the input porosity values:

- Model runs with 50% decreased porosity are referred to as Sensitivity Run S1.
- Model runs with 50% increased porosity are referred to as Sensitivity Run S2.

Two additional sets of simulations were conducted with the dispersivity values set to low and high values:

The high dispersivity values used were 200 ft in the longitudinal direction, 50 ft in the transverse direction, and 2 ft in the vertical direction.

- Model runs with decreased dispersivity are referred to as Sensitivity Run S3. The low dispersivity values used were 30 ft in the longitudinal direction, 8 ft in the transverse direction, and 0.3 ft in the vertical direction.
- Model runs with increased dispersivity are referred to as Sensitivity Run S4. The high dispersivity values used were 200 ft in the longitudinal direction, 50 ft in the transverse direction, and 2 ft in the vertical direction.

Table 5-13 shows results from the sensitivity analysis comparing sensitivity model runs to the calibrated model results at monitoring and water supply wells.

Findings from changing the porosity and dispersivity parameters presented in Section 5.5 are summarized below:

- Increasing or decreasing porosity had a minimal effect on the model simulated TPH-d concentrations at monitoring wells and water supply wells.
- Decreasing dispersivity slightly increased simulated TPH-d concentrations at monitoring and water supply wells in Scenarios 1 and 2 compared to the calibrated model runs.
  - Maximum simulated TPH-d concentrations increased exceeding the GWSC for between zero and six monitoring wells.
  - In one instance, a GWSC exceedance was simulated at a water supply well other than (b) .
  - Simulated concentrations at (b) increased, exceeding the GWSC in zero to four realizations.
- Increasing dispersivity generally decreased simulated TPH-d concentrations at monitoring and water supply wells.

Table 5-13: Sensitivity Analysis Results

Sensitivity	Predictive Scenario	Pumping Configuration	MW Average Exceedance of 100 µg/L	Difference	MW Average Exceedance of 400 µg/L	Difference	MW Max Exceedance of 100 µg/L	Difference	MW Max Exceedance of 400 µg/L	Difference	MW with >50% GWSC Exceedance	Difference	MW with >0% GWSC Exceedance	Difference	Realizations with [redacted] >100 µg/L	Difference	Realizations with [redacted] >400 µg/L	Difference	Additional Water Supply Wells with GWSC Exceedance	Difference
S1	Scenario1	(b)(3)	4	0	1	0	18	0	4	0	1	0	4	0	6	0	2	0	0	0
S1	Scenario1		3	0	1	0	9	0	3	0	1	0	3	0	1	0	0	0	0	0
S1	Scenario1		3	0	1	0	9	0	3	0	1	0	3	0	1	0	0	0	0	0
S1	Scenario1		5	0	1	0	14	0	3	0	1	0	3	0	0	0	0	0	0	0
S1	Scenario1		5	0	1	0	14	0	3	0	1	0	3	0	0	0	0	0	0	0
S2	Scenario1		4	0	1	0	18	0	4	0	1	0	4	0	6	0	2	0	0	0
S2	Scenario1		3	0	1	0	9	0	3	0	1	0	3	0	1	0	0	0	0	0
S2	Scenario1		3	0	1	0	9	0	3	0	1	0	3	0	1	0	0	0	0	0
S2	Scenario1		5	0	1	0	14	0	3	0	1	0	3	0	0	0	0	0	0	0
S2	Scenario1		5	0	1	0	14	0	3	0	1	0	3	0	0	0	0	0	0	0
S3	Scenario1		7	3	2	1	18	0	5	1	1	0	5	1	10	4	6	4	0	0
S3	Scenario1		9	6	1	0	13	4	4	1	1	0	4	1	3	2	2	2	0	0
S3	Scenario1		8	5	1	0	13	4	4	1	1	0	4	1	3	2	1	1	0	0
S3	Scenario1		7	2	1	0	15	1	3	0	1	0	3	0	0	0	0	0	0	0
S3	Scenario1		7	2	1	0	14	0	3	0	1	0	3	0	0	0	0	0	0	0
S4	Scenario1		4	0	1	0	10	-8	4	0	1	0	4	0	4	-2	1	-1	0	0
S4	Scenario1		4	1	1	0	9	0	3	0	1	0	3	0	0	-1	0	0	0	0
S4	Scenario1		4	1	1	0	9	0	3	0	1	0	3	0	0	-1	0	0	0	0
S4	Scenario1		6	1	1	0	14	0	3	0	1	0	3	0	0	0	0	0	0	0
S4	Scenario1		5	0	1	0	13	-1	3	0	1	0	3	0	0	0	0	0	0	0
S1	Scenario2		16	0	6	0	26	0	19	0	4	0	19	0	9	1	6	0	0	0
S1	Scenario2		10	0	4	0	24	0	10	0	4	0	10	0	4	0	2	0	0	0
S1	Scenario2		10	0	4	0	25	0	10	0	4	0	10	0	5	0	1	0	0	0
S1	Scenario2		15	0	5	0	23	0	15	0	3	0	15	0	0	0	0	0	0	0
S1	Scenario2		15	0	5	0	22	-1	15	0	5	0	15	0	0	0	0	0	0	0
S2	Scenario2		16	0	6	0	26	0	19	0	4	0	19	0	9	1	6	0	0	0
S2	Scenario2		10	0	4	0	24	0	10	0	4	0	10	0	4	0	2	0	0	0
S2	Scenario2		10	0	4	0	25	0	10	0	4	0	10	0	5	0	1	0	0	0
S2	Scenario2		15	0	5	0	23	0	15	0	3	0	15	0	0	0	0	0	0	0
S2	Scenario2		15	0	5	0	23	0	15	0	5	0	15	0	0	0	0	0	0	0
S3	Scenario2		21	5	8	2	28	2	20	1	6	2	20	1	12	4	10	4	0	0
S3	Scenario2		15	5	10	6	27	3	16	6	5	1	16	6	8	4	3	1	0	0
S3	Scenario2		15	5	9	5	28	3	16	6	5	1	16	6	12	7	4	3	1	1
S3	Scenario2		21	6	8	3	31	8	18	3	5	2	18	3	0	0	0	0	0	0
S3	Scenario2		21	6	8	3	28	5	17	2	5	0	17	2	0	0	0	0	0	0
S4	Scenario2		12	-4	5	-1	18	-8	12	-7	4	0	12	-7	5	-3	4	-2	0	0
S4	Scenario2		11	1	5	1	13	-11	11	1	4	0	11	1	2	-2	1	-1	0	0
S4	Scenario2		11	1	5	1	16	-9	11	1	4	0	11	1	2	-3	0	-1	0	0
S4	Scenario2		13	-2	6	1	25	2	15	0	3	0	15	0	0	0	0	0	0	0
S4	Scenario2		12	-3	5	0	23	0	15	0	3	-2	15	0	0	0	0	0	0	0

Notes:

Indicates an increase compared to Base Case.
Indicates a decrease compared to Base Case.

6.0 Summary and Conclusions

The modeling study documented in this report is intended to be responsive to the RA concerns outlined in their March 2022 GWFM disapproval letter while improving the understanding of the direction and rate of groundwater flow within the aquifers around the Facility. The CF&T modeling is intended to support long-term site management and risk evaluation. Key issues identified in the RA letter are addressed, including regional water budget calculations to inform model boundary conditions, revised model gridding and layering, use of temperature and chloride to inform source water contributions to (b) and Hālawa Shaft, a revised model calibration approach that focused on matching water levels and gradients, and implementation of lava flow structure-imitating heterogeneous basalt. The models also provide a framework where concepts can continue to be tested as new information becomes available.

This report represents improvements on previous models, but as with any model, will likely require revision as new data become available. Improvements over previous models, including the BAM and FOS-related models, include the following:

- Improved water budget calculations
- Further constraining of calibration parameters
- Incorporation of FOS data for model calibration
- Improved calibration of GHB conditions
- Additional methods to evaluate model calibration, including comparisons of horizontal head differences, vertical head differences, and the flow distribution along (b)
- Implementation of structure-imitating basalt in 50 realizations
- Revised CF&T target history matching data
- Predictive simulations focused on long-term management under post-defueling conditions

The GWFM and CF&T models documented in this report used the MODFLOW-USG Transport code (Panday 2022; Panday et al. 2013) to discretize the model domain into 36 layers, including two layers representing caprock/valley fill, two layers representing saprolite, and 32 layers representing basalt. Model grid cells are aligned with the agreed-upon general regional dip azimuth of 246 degrees in plan view, and the basalt layers dip at 4 degrees, pinching out where intersected by valley fill, caprock, tuff, or saprolite. Revised boundary conditions were derived through regional water budget calculations that estimate an anticipated range of inflows and outflows through each model boundary. The GWFM was parameterized using uniform (homogenous anisotropic) hydraulic properties for the various hydrogeologic units, though the caprock was divided into alluvium and marine sediments and into shallow and deep zones.

The regional GWFM was calibrated using the PEST software (Doherty 2015), adjusting model parameter inputs to minimize the differences between simulated and observed water levels, drawdown, and fluxes. Evaluation of the model calibration was performed using multiple criteria, including standard statistics comparing observed and simulated heads, drawdowns, scatter plots of heads, gradients down Red Hill ridge, horizontal head differences, vertical head differences, comparison to observed flow distribution along (b),

comparisons to water level and drawdown hydrographs, comparisons to conceptual water budget estimates, and comparisons to chloride concentrations and temperature of water from (b) and Hālawa Shaft using unit concentration source simulations. After model calibration was complete, forward particle tracking from the water table beneath the tank farm was conducted to estimate groundwater flow patterns under five pumping configurations:

1. (b) pumping at (b) mgd, Hālawa Shaft pumping at 12 mgd, and (b)(3) pumping at (b) mgd
2. (b) pumping at (b) mgd, Hālawa Shaft off, and (b)(3) (b)
3. (b) (b) Hālawa Shaft pumping at 12 mgd, and (b)(3) (b)
4. (b) (b) Hālawa Shaft off, and (b)(3) (b)
5. (b) pumping at (b) mgd, Hālawa Shaft off, and (b)(3) (b)

A sensitivity analysis was conducted using the calibrated model as a base scenario to evaluate relative changes to model calibration and changes to particle tracking results under each scenario. Eight sensitivity scenarios were evaluated, each with different input assumptions or constraints. Each sensitivity scenario was recalibrated with PEST under the prescribed conditions, and forward particle tracks were run for each of the five pumping configurations.

Based on suggestions from the RAs, an approach was adopted to generate structure-imitating realizations of the basalt aquifer and implement each realization within a nested grid of the regional model. The sequential indicator simulation software SISIM (Deutsch and Journel 1997) was used to generate a categorical indicator field of massive basalt with relatively low permeability and clinker with very high permeability. Three-dimensional variograms used by SISIM were developed based on site data and supplemented with results from lava flow simulations using the probabilistic lava flow spread model MrLavaLoba (Vitturi and Tarquini 2018). Fifty realizations were generated and upscaled to the nested grid in the regional GWFM by transferring the percentage of clinker present in each model cell. Hydraulic properties of the heterogeneous basalt were calculated using a box model to ensure that the bulk groundwater fluxes through the heterogeneous region were consistent with the calibrated regional model. Each realization was then carried through the simulation of the full calibration data set, forward particle tracking from the tank farm, and CF&T history matching.

The VZM is unchanged from the BAM. The VZM does not attempt to model the distribution of petroleum constituents in the vadose zone. Instead, it consists of a series of calculations to estimate the retention of LNAPL in the vadose zone, the mass of LNAPL reaching the water table, and the size of the LNAPL lens on the water table in order to conduct CF&T modeling. A transient partitioning module of the VZM calculates the concentration of constituents that dissolve out of the LNAPL into the groundwater. The VZM can be used to establish source boundary conditions for the CF&T model.

A forensic analysis was performed on TPH data collected at the site, resulting in the conclusion that the most useful data indicative of saturated zone transport was that of TPH-d collected in the weeks and months after the May 2021 release. Therefore, TPH-d was selected as the constituent for CF&T modeling. While uncertainty exists in the explanation of the simultaneous TPH-d concentration increases at RHM(b) and

RHM(b) , the apparent TPH-d breakthrough curves between RHM(b) and RHM(b)) were considered most representative of saturated zone transport and were considered the most reliable for purposes of transport parameter calibration. If these apparent breakthroughs are not due to the May 2021 release, then these assumptions would be conservative with regards to contaminant transport risk.

The CF&T modeling was developed through a history matching process. Predictive simulations were performed for long-term site management, and a sensitivity analysis determined how key parameters affected the distribution of TPH-d concentrations. All 50 realizations and the base model were calibrated by adjusting transport parameters and did not include degradation or retardation. Of the 50 realizations, 17 and the base model were considered to have been adequately calibrated. Those 18 models were carried forward through predictive simulations.

Predictive simulations were conducted to assess potential future conditions and impacts on nearby environmental receptors (e.g., water supply wells). Two different source scenarios for future conditions were simulated. Source Scenario 1 employs a constant TPH-d concentration source zone around (b)(3) that approximates the most recent concentrations (as of May 2024) measured at RHM(b) of approximately 1,200 µg/L. Source Scenario 2 employs constant TPH-d concentration sources both around (b)(3) and the May 2021 release location. TPH-d concentrations for each were assigned to approximate the maximum historical values at RHM(b) (5,200 µg/L) and RHM(b) (613 µg/L). A sensitivity analysis was conducted on the predictive simulations by increasing and decreasing porosity and dispersivity to evaluate impacts to the model's conclusions.

Significant conclusions from the GWFM include the following:

- The 50 heterogeneity realizations resulted in a RMSE of simulated-to-observed water levels that ranged from 0.23 to 1.16 ft. These compare to the homogeneous model which had an RMSE of 0.25 ft.
- The GWFMs were considered well calibrated to the various calibration metrics such that predictive scenarios could be considered and the model could be used for CF&T modeling.
- Conceptual transport simulations using unit source concentration sources were performed to assess the contributions of water at (b) and Hālawa Shaft attributable to each water source, including recharge, inflow from the dike region, inflow from the southeast GHB, and inflow from the freshwater/saltwater interface. The freshwater/saltwater interface was included in these simulations as a constant head boundary. Assumptions were made for the chloride concentration and temperature at each source. Estimates of the chloride concentration and temperature at each shaft compared favorably to observed values.
  - The unit source simulations showed that a relatively small percentage of water drawn from the saltwater (approximately 1%) can significantly increase the concentration of chloride in the water supply shafts, while temperature is much less sensitive to flow contributions from the freshwater/saltwater interface.
  - Although the observed chloride concentrations were not matched as closely as temperature, the pattern of higher chlorides but lower temperature at Hālawa Shaft compared to (b) was

replicated. The implication is that higher pumping rates in Hālawa Shaft pull more water from depths near the freshwater-saltwater interface compared to (b), despite being farther from the interface, while at the same time pulling most of its water from the colder uphill regions.

- Forward particle tracking simulations were conducted to evaluate potential flow paths from beneath the Facility under a variety of stresses from (b) and Hālawa Shaft. Particle tracking does not account for contaminant transport processes such as dispersion, sorption, and degradation.
  - Forward particle tracks from the tank farm with (b) pumping at (b) mgd and Hālawa Shaft pumping at 12 mgd as well as with (b) pumping at (b) mgd and Hālawa Shaft off resulted in nearly all particles being captured by (b). In cases where particles escaped capture, they bypassed (b) either slightly to the northwest or underneath.
  - Forward particle tracks from the tank farm with (b) pumping at (b) mgd with Hālawa Shaft and (b)(3) off indicated more variable capture when heterogeneity was considered. The homogeneous-anisotropic base model simulated 100% capture. In contrast, the capture across all heterogeneous realizations ranged from 50% to 100% with an average of 89.4%.
  - Forward particle tracks from the tank farm with (b) off and Hālawa Shaft off resulted in the particles discharging mostly at the northwest GHB, which represents groundwater flowing out of the model domain to the northwest toward the springs to the north of Pearl Harbor, with some particles discharging to Kalauao Springs or Pearl Harbor.
  - Forward particle tracks from the tank farm with (b) off and Hālawa Shaft on at 12 mgd resulted in the particles discharging mostly at Kalauao Springs, Pearl Harbor and the northwest GHB. In two of the realizations, some particles discharged at Hālawa Shaft; however, those were 6.2% and 4.7% of particles. Median travel times in those realizations ranged from 23 to 25 years. Four realizations resulted in particles captured by other water supply wells, which ranged from 1.6% to 26.6% of particles. Median travel times in those realizations ranged from 13 to 40 years.
- A sensitivity analysis of the regional GWFM was conducted for eight scenarios without implementing heterogeneous basalt. Of those eight scenarios, three were able to maintain an acceptable calibration. None of the particle tracking results deviated significantly from the base calibration case.
  - The most significant deviation from the base case was that in Scenario 4, where with no dike region flux, the capture at (b) was reduced to approximately 85% for all pumping configurations in which (b) was pumped.
- One additional model, Scenario 5, which utilized flow direction targets toward Hālawa Shaft, and where the calibration was no longer acceptable, demonstrated slightly lower capture of particles by (b), down to 83% with (b) pumping at (b) mgd and 62% with (b) pumping at (b) mgd. The key parameter that controlled this outcome was the weathering of the basalt, which was effectively removed by the automated calibration attempts, indicating that the downward vertical gradients beneath the stream valleys greatly affect the potential for groundwater to flow to the northwest of the tank farm.

Significant conclusions from the CF&T modeling include the following:

- Significant uncertainties exist in the nature of TPH-d sources and the history matching process for CF&T.
- Forensic analysis yielded few data that could be both tied to an individual release and indicative of saturated zone transport.
- The May 2021 (b) release yielded the best data for use in history matching of the CF&T model.
  - Only 100 gallons of fuel were reported to have not been recovered after the release, which would not likely have been expected to arrive at the water table or at the very least be detected by the monitoring well network sampling and analysis.
  - Data from the May 2021 release show apparent breakthrough of TPH-d at RHM(b) , RHM(b) , and RHM(b) .
  - Concentrations increased between RHM(b) and RHM(b) and arrived simultaneously. Potential causes for this simultaneous arrival of TPH-d were:
    - groundwater flow paths that miss RHM(b) but intersect RHM(b) ;
    - unsaturated zone transport with washwater;
    - vapor transport through the tunnel; and/or
    - separate sources between RHM(b) and RHM(b) related to either washwater, precipitation, or rising water levels during the same time period as the release.
- History matching was performed using two conceptual models:
  - One with a singular elongated source from the release point to RHM(b) , representing the release and washwater reaching the water table along the entire source
  - One with two sources, indicative of two separate sources causing the release

  Both conceptual models result in the emphasis on saturated zone transport between RHM(b) and RHM(b) .
- Transport parameters, including source concentrations, porosity, and dispersivity, were calibrated to match measured TPH-d concentrations for each of the 50 realizations and the base homogeneous model.
- A threshold was established for acceptable matching of the measured TPH-d concentrations. The one-source conceptual model resulted in 12 acceptable calibrated realizations including the base homogeneous-anisotropic model and the two-source conceptual model resulted in 82 acceptable calibrated realizations including the base homogeneous-anisotropic model
- Both conceptual models performed similarly in history matching with average porosities of 11% and 8%, longitudinal dispersivity of 77 ft and 95 ft, transverse dispersivity of 37 ft and 42 ft, and vertical dispersivity of 0.77 ft and 0.95 ft.

- Calibrated transport parameters were carried forward to predictive simulations under two source scenarios:
  - Scenario 1 approximates the most recent TPH-d concentrations measured at RHM(b) of approximately 1,200 µg/L.
  - Scenario 2 approximates the maximum historical TPH-d values at RHM(b) (5,200 µg/L) and RHM(b) (613 µg/L).
- Nearly all realizations predicted some TPH-d GWSC exceedances at monitoring wells near the source zones.
- In Scenario 1, 12% of realizations showed TPH-d GWSC exceedances at (b) when (b) was pumping at (b mgd, but no exceedances were simulated when (b) was pumping at 4 mgd.
- In Scenario 2, 6% of realizations had TPH-d GWSC exceedances at (b) with (b) pumping at (mgd and Hālawa Shaft on a 12 mgd, 12% of realizations had exceedances at (b) with (b) pumping at (mgd and Hālawa Shaft off, and 35% of realizations had exceedances at (b) with (b) pumping at (b mgd.
- Hālawa Shaft did not register TPH-d in excess of the 400 µg/L GWSC or the 100 µg/L approximate laboratory reporting level in any realization..
  - Additional calculations demonstrated that even if all groundwater at the water table from the tank farm flowed directly toward Hālawa Shaft, transporting TPH-d without attenuation, there is not enough TPH-d mass released from the simulated source zones to register simulated concentrations above approximately 53 µg/L at Hālawa Shaft.
- A sensitivity analysis was conducted on the predictive simulations by modifying porosity and dispersivity.
  - Modification of porosity values had minimal impact on the model results.
  - Increasing dispersivity values was associated with slight increases in simulated concentrations and some additional TPH-d GWSC exceedances at monitoring and water supply wells; however, the increase did not significantly change the conclusion of the predictive simulation results.
  - Decreasing porosity generally decreased simulated TPH-d concentrations at monitoring and water supply wells.
- The mechanism and nature of the mismatch in heads in transitional (Group 3) wells in not well understood.
- The effect of the deep highly weathered basalt at NM(b) has not been fully explored as this well was under construction at the time of this reporting.
- Although 50 heterogeneous basalt realizations were developed, this clearly represents only a tiny fraction of the possibility distributions of basalt types and associated hydraulic properties.

7.0 Model Limitations

Groundwater models are necessarily simplified mathematical representations of complex natural systems. Because of this fact, there are limits to the accuracy with which groundwater systems can be simulated, especially in highly heterogenous environments such as those present at this site. These limitations must be recognized when using models and interpreting model results.

There are many sources of error and uncertainty in models. Model error commonly stems from practical limitations of grid spacing, time discretization, parameter structure, insufficient calibration data, and the effects of processes not simulated by the model. These factors, along with unavoidable error in observations, result in uncertainty in model predictions.

Specific sources of uncertainty for the Red Hill Facility GWFM and CF&T model include grid spacing and parameter structure. The 25-ft × 25-ft grid spacing of the regional flow model is an improvement on prior models but still limits the ability to simulate conditions on smaller spatial scales. The model layering may also impose some uncertainty on predictions as the model predicts groundwater heads averaged over vertical distances. Additionally, the layer structure of this model assumes an average dip azimuth and dip magnitude of the basalt over the entire model domain, which dictates the layer structure. Actual dip azimuth and magnitude are quite variable in horizontal and vertical space and cannot be accurately estimated in all locations through field investigations. Hydraulic conductivities are known to vary over orders of magnitude in even relatively homogeneous systems. The basal aquifer beneath the facility is known to be highly heterogeneous with widely varying hydraulic properties of sub-units within the basalt that includes highly transmissible flow paths such as fractures, a‘ā clinker, clinker bridges, and lava tubes, and low-transmissive massive a‘ā and pāhoehoe and highly weathered and saprolitic zones. For the regional GWFM, the simplifying assumption of equivalent porous media was made, implying that the aquifer behaves as a homogenous system of porous media rather than dual porosity with fracture flow and porous media flow. While this assumption can generally be valid at larger scales, using a uniform hydraulic conductivity does not capture local variations in groundwater flow.

Stochastic renderings of the basalt were developed to help understand the heterogeneity and their impact on outcomes but will primarily serve to understand small-scale heterogeneity and their impacts on groundwater flow behavior. The generations of the basalt rely on interpretations of field data and the underlying assumptions of MrLavaLoba to generate the massive basalt and clinker distribution. Additional assumptions were required to upscale the basalt realizations to the numerical model grid, as well as to estimate the hydraulic properties of the basalt based on the percentage of clinker. No site-specific studies were available to characterize the behavior and hydraulic properties of the basalt sub-types; therefore, the calculation of the hydraulic properties relies on the bulk behavior and consistency with the calibrated homogeneous anisotropic parameters from the regional GWFM.

The approach used to generate the heterogeneous basalt realizations, which has not been applied prior to this study, introduces several specific limitations and uncertainties. First, the novel methodology lacks validation against established techniques. Furthermore, interpreting the outcomes of these novel realizations requires a cautious approach, as overconfidence in the new method's capabilities without sufficient cross-validation can lead to incorrect conclusions and implications for decision making. The

overall purpose of the realizations is to explore the implications of structure imitating heterogeneity within the hydrogeological system and not to accurately predict contaminant concentrations at every discrete location within the domain. As new data and information become available about the behavior of the system with regard to both groundwater flow and solute transport, model results should be checked, and updates made as necessary.

Specification of model boundary conditions can have significant impacts on model calibration and predictive results. Boundary condition setup for the GWFM and the overall model water budget were guided by conceptual water budget calculations. Conceptual water budget calculations rely on several assumptions, including average recharge estimated by the USGS, water supply well pumping rates reported by Hawai‘i DLNR, calculations of flux through the caprock, and estimates of spring discharge. The most significant source of uncertainty may be the recharge estimates that were made for average conditions. Recent precipitation trends that deviate from average conditions will alter the water budget. The GWFM does not consider individual storm events, which cause periodic rises in groundwater levels anywhere throughout the domain. The overall water budget cannot be accurately measured in the field, thus estimates of the water budget must be used, considering the uncertainties and broader implications, rather than seeking exact matches in model calibration.

Substantial data are available for the Facility and area around it to support model inputs and constrain the calibration. These data include geologic logs, downhole geophysical logs, surface geophysics, synoptic and periodic groundwater levels, and calculated hydraulic conductivities. All this information constrains the model input parameter values during the calibration process, thus increasing the accuracy of the calibrated model. Less information is available outside the Facility area. Model error and uncertainty are not uniformly distributed. The model fit to observations is best where abundant data are available. Simulated conditions are more uncertain where data are sparse, such as unpopulated upland areas. The GWFM matches the data as well as practicable given the constraints of the grid, boundary conditions, and parameterization.

Several monitoring wells that exhibited water levels slightly above the water table in the basal aquifer were characterized as transitional wells. Generally, these are shallow wells located in the vicinity of saprolite and interpreted confining unit beneath South Hālawa Stream, though some are located further under Red Hill ridge. The cause of the elevated water levels is interpreted to be the gradual transition from saprolite to weathered basalt to unweathered basalt. In model construction, the simplifying assumption was made to have a sharp transition between the confining unit and unweathered basalt of the basal aquifer. This assumption makes simulating the slightly elevated heads in those wells problematic because heads will be significantly elevated in the confining unit and quickly equilibrated to the basal aquifer head within a single 25-ft model cell. Because the implication of elevated heads is that the permeability of the aquifer material is lower, groundwater flow through these areas is likely to be lower than through the higher permeability portions of the aquifer, down-weighting these wells and focusing on calibration to the basal aquifer itself was considered appropriate.

Calibration through PEST helps to quantify parameter values relative to an adequate calibration, and the sensitivity analysis helps to understand relative importance of inputs, but neither process is intended to predict hydraulic properties at any given location. In GWFMs, a common uncertainty is associated with non-unique solutions of recharge and hydraulic conductivity. That is, the same model calibration may be

achieved with many combinations of hydraulic conductivity and recharge. For this GWFM, recharge remained fixed. Non-uniqueness of solutions remains an issue, as many combinations of other aquifer parameters may lead to similar model calibration results. The sensitivity analysis conducted for the GWFM is intended to demonstrate how various parameter and boundary condition changes and constraints may affect model predictions, and it highlights the parameters and assumptions most impactful on these results. While this does not eliminate uncertainty or non-uniqueness completely, it does reduce them by demonstrating how various input assumptions affect model behavior and how that behavior translates to the interpretation of results.

The numerical results of the flow model have an associated but un-quantified uncertainty. The GWFM provides sensitivity analyses designed to provide insight into model outcomes for a range of model inputs. Understanding model limitations and uncertainty is a dynamic process, employing an adaptive approach focused on reducing model error and uncertainty as new calibration data are collected and used to refine the model. Even with the limitations described above, the GWFM is a useful tool to meet current needs and provides the basis for future improvements consistent with AOC objectives, if necessary.

The VZM is a heuristic model with calculations based largely on input parameters estimated through professional judgment. The lack of detailed knowledge of the subsurface geology and distribution of petroleum constituents limits the VZM use to exploration of the effects of input parameters on LNAPL distribution and fate in the subsurface for use in the CF&T modeling. Preferential pathways, including drain pipes, drain line backfill, lava tubes, open boreholes, and other natural and manmade pathways, can cause unpredictable and significant pathways for constituent migration. Flow through these potential preferential pathways is not simulated by the VZM. The presence of unknown preferential pathways can cause large differences in constituent distributions from those that are simulated by the model.

The CF&T modeling work is intended to provide insights into the potential migration of fuel from residual contamination from fuel at the Facility after defueling. While these insights can be useful for future decision making and long-term site management, certain limitations must be recognized when using models and interpreting results. Many assumptions are made to support this modeling project. Each assumption comes with inherent uncertainty. There are many sources of error and uncertainty in models. Model error commonly stems from practical limitations of grid spacing, time discretization, parameter structure, insufficient calibration data, and the effects of processes not simulated by the model. These factors, along with unavoidable error in observations, result in uncertainty in model predictions.

The GWFM is a simplified representation of reality with the assumption of uniform basal aquifer parameters including orientation of anisotropy. While reasonable calibration was achieved fitting simulated groundwater levels to observed levels, complex small-scale geological heterogeneities and preferential flow paths will have impacts on contaminant transport as a scale that cannot be modeled, both in space and time.

MODFLOW is designed to simulate the flow of water and dissolved constituents through porous media. However, it is not a multiphase flow model, and is therefore not equipped to handle the complexities associated with multiple fluid phases, such as liquids and gases, interacting within the subsurface. Consequently, this study did not include the transport of LNAPL or vapor transport of fuel constituents. These processes involve the movement and interaction of different fluid phases, requiring a more

sophisticated modeling approach that accounts for phase behavior, interphase mass transfer, and the distinct physical and chemical properties of each phase. Simplifying assumptions were made in the VZM to guide setup of boundary conditions for contaminant transport without explicitly simulating three-dimensional multiphase flow.

History matching and calibration of the CF&T models carry inherent uncertainties from the outset, including compounding errors in the GWFM and interpretations of TPH data at the site. Of the three documented releases, the December 2013 release at (b)(3) and November 2021 release show only very localized and short-term impacts. The May 2021 release appears to show TPH-d breakthrough curves at three wells, RHM(b) , RHM(b) , and RHM(b) , suggesting that residual contamination from the vadose zone may have been solubilized during cleaning of the tunnel following that event. Nearly simultaneous elevated observations and GWSC exceedances of TPH-d occur at RHM(b) and RHM(b) . These occurrences were attempted to be modeled through two different conceptual models as they cannot be replicated through model simulations and may not be related to the same source local to the May 2021 release and may in fact be unrelated to the release and associated with historical contamination. The primary focus of the history matching was on the simulation of saturated zone transport of TPH-d between RHM(b) and RHM(b) . Significant uncertainty is also associated with the TPH-d data, including source identification, because significant fuel was present in the system prior to the three recent releases modeled in this effort. The variability in the compounds that can be measured by the analytical methods associated with TPH-d add significant uncertainty associated with fate and transport characteristics. In addition, external changes likely influenced the data consistency, including changes in laboratory, sampling methods, background aqueous-phase contamination, and mobilization of residual contamination through precipitation events and fluctuations in the water table.

Calibration of transport parameters such as effective porosity and dispersivity can lead to a high degree of non-uniqueness, particularly in cases such as this where a limited number of monitoring wells show systematic responses. Often, the result of such calibration is high dispersivity values that can conceal uncertainties and errors in the input assumptions. The basal aquifer at the site contains significant heterogeneity, leading to local variability in groundwater velocity. While heterogeneity of the basal aquifer has been incorporated, no singular realization can be correct and each realization is subject to upscaling to the model grid, which is larger than field-scale heterogeneity. Dispersivity is used as a parameter to represent these local variations in groundwater velocities, but also can be used to account for uncertainty. In the CF&T model, the predictions of TPH concentration carry uncertainty, and the values predicted should be interpreted as such. Simulated TPH concentrations are more indicative of qualitative likelihoods of TPH impacts to water supplies. For example, the simulations of different release scenarios might be interpreted as indicating a high, moderate, or low probability of an impact at a location. However, the possibilities of unknown preferential flow paths mean that TPH detections at water supply locations could occur even if the simulation results suggest that the likelihood of an impact is low.

Models documented in this study do not include any form of degradation of TPH over time. In reality, biodegradation of TPH occurs both aerobically and anaerobically, reducing the duration and strength of LNAPL sources and substantially reducing concentrations in the saturated zone with distance from the source. The assumption of no degradation is intended to provide conservative estimates of potential TPH

migration. While this assumption may not be significant on the short time scale and distances, associated with CF&T model calibration, the substantial degradation of TPH in the oxygen-rich groundwater would cause TPH groundwater plumes to be substantially smaller than those simulated with the CF&T model.

8.0 Path Forward

This modeling study has been completed based on field data available as of the specified data cut-off dates and is subject to approval by the RAs. The University of Hawai‘i is currently conducting and preparing to conduct several field studies, including surface and off-shore geophysics, in-well testing, sampling and laboratory testing, hydraulic gradient calculations, and tracer testing, to help evaluate groundwater flow directions and rates in the area of the tank farm. Their study will also include geophysical and groundwater modeling. Additionally, new monitoring wells continue to be installed; and water levels and analytical data will continue to be collected. It is anticipated that the University of Hawai‘i work will be completed in 2026. Once the data from this study have been made available, the modeling documented in this report will be updated to incorporate these new data and RA comments after final submittal.

9.0 References

Alabert, F. G. 1987. "Stochastic Imaging of Spatial Distributions Using Hard and Soft Information." Master's thesis, Stanford University.

ASTM International (ASTM). 2016a. *Standard Guide for Conducting a Sensitivity Analysis for a Groundwater Flow Model Application*. D5611-94(2016). West Conshohocken, PA.

———. 2016b. *Standard Guide for Defining Boundary Conditions in Groundwater Flow Modeling*. D5609 − 16. West Conshohocken, PA.

———. 2017. *Application of a Numerical Groundwater Flow Model to a Site-Specific Problem*. D5447−17. West Conshohocken, PA.

———. 2018. *Standard Guide for Calibrating a Groundwater Flow Model Application*. D5981/D5981M - 18. West Conshohocken, PA.

Belcher, W. R., P. E. Elliot, and A. L. Geldon. 2001. *Hydraulic-Property Estimates for Use With a Transient Ground-Water Flow Model of the Death Valley Regional Ground-Water Flow System, Nevada and California*. Water-Resources Investigations Report 01-4120. U.S. Geological Survey.

Beven, K. 2002. "Towards a Coherent Philosophy for Modelling the Environment." *Proc. R. Soc. Lond. A* 458:2465–84.

———. 2019. "Towards a Methodology for Testing Models as Hypotheses in the Inexact Sciences." *Proc. R. Soc. A* 475. https://doi.org/10.1098/rspa.2018.0862.

Brost, E. J., and G. E. DeVaull. 2000. *Non-Aqueous Phase Liquid (NAPL) Mobility Limits in Soil*. Soil & Groundwater Research Bulletin, No. 9. Washington, DC: American Petroleum Institute. June.

C Tech, C Tech Development Corporation. 2022. *Earth Volumetric Studio (EVS) Version 2022.10.2*.

Charbeneau, R. J., and C. Y. Chiang. 1995. "Estimation of Free-Hydrocarbon Recovery from Dual-Pump Systems." *Ground Water* 33 (4): 627–34.

Cooperative Institute for Research in Environmental Sciences (CIRES) at the University of Colorado, Boulder. 2014. *Continuously Updated Digital Elevation Model (CUDEM) - 1/9 Arc-Second Resolution Bathymetric-Topographic Tiles: Hawaii.* NOAA National Centers for Environmental Information. Retrieved 12 15, 2022, from Https://Doi.Org/10.25921/Ds9v-Ky35.

Deutsch, C. V., and A. G. Journel. 1997. *GSLIB Geostatistical Software Library and User's Guide*. 2nd Ed. New York: Oxford University Press.

Department of Defense, United States (DoD). 2022. *Defueling Plan, Red Hill Bulk Fuel Storage Facility, Oahu, Hawaii*. Prepared by Secretary of the Navy (SECNAV), in Coordination with Director, Defense Logistics Agency (DLA), on Behalf of DoD. June 30, 2022.

Department of Health, State of Hawaii (DOH). 2024. *Revised Consolidated Groundwater Sampling Plan*. Enclosure 1 to April 22, 2024 Letter from: K. S. Ho, DOH Deputy Director for Environmental Health; to: Rear Admiral S. Barnett, Commander, Navy Region Hawaii; SUBJECT: Disapproval of Navy's Consolidated Groundwater Sampling Program in Support of Request to Reduce (b)(3)(b)(3) Flow.

Doherty, J. 2015. *PEST: Model-Independent Parameter Estimation and Uncertainty Analysis*. Brisbane, Australia: Watermark Numerical Computing. http://pesthomepage.org/.

Domenico, P. A., and M. D. Mifflin. 1965. "Water from Low-Permeability Sediments and Land Subsidence." *Water Resources Research* 1 (4): 563–76.

Department of the Navy (DON). 2014. *Interim Update, Red Hill Bulk Fuel Storage Facility Final Groundwater Protection Plan, Pearl Harbor, Hawaii. (January 2008)*. Pearl Harbor, HI: Naval Facilities Engineering Command, Pacific. August.

———. 2018. *Groundwater Protection and Evaluation Considerations for the Red Hill Bulk Fuel Storage Facility, Joint Base Pearl Harbor-Hickam, Oʻahu, Hawaiʻi; July 27, 2018, Revision 00*. Prepared by AECOM Technical Services, Inc., Honolulu, HI. Prepared for Defense Logistics Agency Energy, Fort Belvoir, VA, under Naval Facilities Engineering Command, Hawaii, JBPHH HI.

———. 2019. *Conceptual Site Model, Investigation and Remediation of Releases and Groundwater Protection and Evaluation, Red Hill Bulk Fuel Storage Facility, Joint Base Pearl Harbor-Hickam, Oʻahu, Hawaiʻi; June 30, 2019, Revision 01*. Prepared by AECOM Technical Services, Inc., Honolulu, HI. Prepared for Defense Logistics Agency Energy, Fort Belvoir, VA, under Naval Facilities Engineering Command, Hawaii, JBPHH HI.

———. 2020. *Groundwater Flow Model Report, Red Hill Bulk Fuel Storage Facility, Joint Base Pearl Harbor-Hickam, Oʻahu, Hawaiʻi; March 25, 2020, Revision 00*. Prepared by AECOM Technical Services, Inc., Honolulu, HI. Prepared for Defense Logistics Agency Energy, Fort Belvoir, VA, under Naval Facilities Engineering Command, Hawaii, JBPHH HI.

———. 2021. *Final Site Assessment Work Plan Red Hill Oily Waste Disposal Facility Joint Base Pearl Harbor-Hickam Oahu HI*. Prepared by AECOM Technical Services, Inc. JBPHH HI: Naval Facilities Engineering Systems Command, Hawaii. February.

———. 2022a. *Draft Work Plan Groundwater Flow and Velocity Evaluation Red Hill Bulk Fuel Storage Facility Joint Base Pearl Harbor-Hickam Oʻahu HI*. Prepared by AECOM Technical Services, Inc. Honolulu, HI: Prepared for Defense Logistics Agency Energy, Fort Belvoir, VA, under Naval Facilities Engineering Systems Command, Hawaii. October.

———. 2022b. (b)(3)(b)(3) *Flow Optimization, Work Plan, Red Hill Bulk Fuel Storage Facility, JBPHH, Oʻahu, Hawaiʻi*. Prepared for NAVFAC Hawaii by AECOM Technical Services Inc. October 26.

———. 2022c. *Summary of Groundwater Transducer Study, Oily Waste Disposal Facility, Joint Base Pearl Harbor-Hickam, O'ahu, Hawai'i*. July 28. JBPHH HI: Naval Facilities Engineering Command, Hawaii.

———. 2023a. *Conceptual Site Model Appendix E Addendum: Geological Modeling Framework Technical Memorandum, Red Hill Bulk Fuel Storage Facility, JBPHH, O'ahu, Hawai'i*. Prepared for NAVFAC Hawaii by AECOM Technical Services Inc.

———. 2023b. *Contaminant Fate and Transport Model Technical Memorandum, Red Hill Bulk Fuel Storage Facility. JBPHH, O'ahu, Hawai'i*. Prepared for NAVFAC Hawaii by AECOM Technical Services Inc. June 26.

———. 2023c. *Final Report of Findings,* (b)(3)(b)(3) *Flow Optimization Study, September 19, 2023*. Prepared for NAVFAC Hawaii by AECOM Technical Services Inc. Naval Facilities Engineering Systems Command, Hawaii. September.

———. 2023d. *Groundwater Flow Model Technical Memorandum, Red Hill Bulk Fuel Storage Facility. JBPHH, O'ahu, Hawai'i*. Prepared for NAVFAC Hawaii by AECOM Technical Services Inc. May 17.

———. 2023e. *Vadose Zone Model Technical Memorandum, Red Hill Bulk Fuel Storage Facility. JBPHH, O'ahu, Hawai'i*. Prepared for NAVFAC Hawaii by AECOM Technical Services Inc. May 17.

Engott, J. A., A. G. Johnson, M. Bassiouni, S. K. Izuka, and K. Rotzoll. 2017. *Spatially Distributed Groundwater Recharge for 2010 Land Cover Estimated Using a Water-Budget Model for the Island of O'ahu, Hawai'i (Version 2.0, December 2017)*. Scientific Investigations Report 2015–5010. Revised December 2017. Prepared in cooperation with the State of Hawai'i Commission on Water Resource Management and the City and County of Honolulu Board of Water Supply. U.S. Geological Survey.

Environmental Protection Agency, United States (EPA). 2008. *A Systematic Approach for Evaluation of Capture Zones at Pump and Treat Systems - Final Project Report*. EPA 600/R-08/003. Office of Research and Development: National Risk Management Research Laboratory | Ground Water and Ecosystems Restoration Division. January.

Environmental Protection Agency, United States, Region 9; and Department of Health, State of Hawaii (EPA Region 9 and DOH). 2015. *Administrative Order on Consent In the Matter of Red Hill Bulk Fuel Storage Facility, EPA Docket No: RCRA 7003-R9-2015-01; DOH Docket No: 15-UST-EA-01*. September.

Eyre, P. R., C. Ewart, and P. J. Shade. 1986. *Hydrology of the Leeward Aquifers, Southeast Oahu, Hawaii: Regional Analysis of the Southern Oahu Ground-Water Flow System*. Water-Resources Investigations Report 85-4270. U.S. Geological Survey.

Freeze, R. A., and J. A. Cherry. 1979. *Groundwater*. Englewood Cliffs, NJ: Prentice Hall.

Hantush, M. S., and R. G. Thomas. 1966. "A Method for Analyzing a Drawdown Test in Anisotropic Aquifers." *Water Resources Research* 2 (2): 281–85. https://doi.org/10.1029/WR002i002p00281.

Heath, R. C. 1993. *Basic Ground-Water Hydrology*. U.S. Geological Survey Water-Supply Paper 2220. Revised 2004. Reston, VA: U.S. Geological Survey.

Hunt Jr., C. D. 1996. *Geohydrology of the Island of Oahu, Hawaii*. Professional Paper 1412-B. Regional Aquifer-System Analysis—Oahu, Hawaii. U.S. Geological Survey.

———. 2004. *Ground-Water Quality and Its Relation to Land Use on Oahu, Hawaii, 2000–01*. Water-Resources Investigations Report 03-4305. National Water-Quality Assessment Program. U.S. Geological Survey.

Hyman, D. M. R., H. R. Dietterich, and M. R Patrick. 2022. "Toward Next-Generation Lava Flow Forecasting: Development of a Fast, Physics-Based Lava Propagation Model." *Journal of Geophysical Research: Solid Earth* 127. https://doi.org/doi.org/10.1029/2022JB024998.

Interagency Drinking Water System Team (IDWST). 2022. (b)(3)(b)(3) *Recovery and Monitoring Plan (RHSRMP), JBPHH, O'ahu, Hawai'i*. Navy, Army, State of Hawaii Department of Health, and United States Environmental Protection Agency. January.

Lahoud, R. G., D. H. Lobmeyer, and M S. Whitfield. 1984. *Geohydrology of Volcanic Tuff Penetrated by Test Well UE-25b#1, Yucca Mountain, Nye County, Nevada*. Prepared in Cooperation with U.S. Department of Energy.\. U.S. Geological Survey.

Mayer, A., and S. M. Hassanizadeh. 2005. *Soil and Groundwater Contamination: Nonaqueous Phase Liquids – Principles and Observations*. AGU Water Resources Monograph 17. Washington, DC: American Geophysical Union.

Miller, M. E. 1987. *Hydrogeologic Characteristics of Central Oahu Subsoil and Saprolite: Implications for Solute Trans Port*. M.S. Thesis, University of Hawaii at Manoa, 231 p.

Mitchell, J. N., and D. S. Oki. 2018. *Groundwater-Level, Groundwater-Temperature, and Barometric-Pressure Data, July 2017 to February 2018, Hālawa Area, O'ahu, Hawai'i*. USGS Open-File Report 2018–1147. Prepared in Cooperation with the U.S. Navy. Reston, VA: U.S. Geological Survey.

Morris, D. A., and A. I. Johnson. 1967. *Summary of Hydrologic and Physical Properties of Rock and Soil Materials as Analyzed by the Hydrologic Laboratory of the U.S. Geological Survey*. U.S. Geological Survey Water-Supply Paper 1839-D. U.S. Geological Survey.

Mutch, Jr., R. D. 2005. "A Distance-Drawdown Aquifer Test Method for Aquifers with Areal Anisotropy." *Ground Water* 43 (6): 935–38. https://doi.org/10.1111/j.1745-6584.2005.00105.x.

Niswonger, R. G., S. Panday, and M. Ibaraki. 2011. *MODFLOW-NWT, A Newton Formulation for MODFLOW-2005*. U.S. Geological Survey Techniques and Methods 6–A37.

Oki, D. S. 1998. *Geohydrology of the Central Oahu, Hawaii, Ground-Water Flow System and Numerical Simulation of the Effects of Additional Pumping*. Water-Resources Investigations Report 97–4276. Prepared in Cooperation with the Honolulu Board of Water Supply. U.S. Geological Survey.

———. 2005. *Numerical Simulation of the Effects of Low-Permeability Valley-Fill Barriers and the Redistribution of Ground-Water Withdrawals in the Pearl Harbor Area, Oahu, Hawaii*. Scientific Investigations Report 2005-5253. U.S. Geological Survey.

Oki, D. S., W. R. Souza, E. I. Bolke, and G. R. Bauer. 1996. *Numerical Analysis of Ground-Water Flow and Salinity in the Ewa Area, Oahu, Hawaii*. Open-File Report 96-442. Prepared in Cooperation with the State of Hawaii Commission on Water Resource Management. U.S. Geological Survey.

Panday, S. 2022. *USG-Transport Version 1.10.0: The Block-Centered Transport Process for MODFLOW-USG*. GSI Environmental. http://www.gsi-net.com/en/software/free-software/USG-Transport.html.

Panday, S., C. D. Langevin, R. G. Niswonger, M. Ibaraki, and J. D. Hughes. 2013. *MODFLOW–USG Version 1: An Unstructured Grid Version of MODFLOW for Simulating Groundwater Flow and Tightly Coupled Processes Using a Control Volume Finite-Difference Formulation*. U.S. Geological Survey Techniques and Methods, Book 6, Chap. A45. https://dx.doi.org/10.5066/F7R20ZFJ.

Rotzoll, K. 2012. *Numerical Simulation of Flow in Deep Open Boreholes in a Coastal Freshwater Lens, Pearl Harbor Aquifer, O‘ahu, Hawai‘i*. Scientific Investigations Report 2012-5009. Prepared in Cooperation with the Honolulu Board of Water Supply. Reston, VA: U.S. Geological Survey.

Rotzoll, K., and A. I. El-Kadi. 2007. *Numerical Ground-Water Flow Simulation for Red Hill Fuel Storage Facilities, NAVFAC Pacific, Oahu, Hawaii*. Prepared for The Environmental Company (TEC). Appendix L in: Department of the Navy (2007), *Red Hill Bulk Fuel Storage Facility Final Technical Report, Pearl Harbor, Hawaii*; Naval Facilities Engineering Command, Pacific. Honolulu, HI: University of Hawaii, Water Resources Research Center. August.

Rumbaugh, J., and D. Rumbaugh. 2020. *Groundwater Vistas Version 8*. Environmental Simulations, Inc.

Sherrod, D. R., J. M. Sinton, S. E. Watkins, and K. M. Brunt. 2007. “Geologic Map of the State of Hawai‘i, Sheet 3—Island of O‘ahu.” Open-File Report 2007-1089.

Souza, W. R., and C. I. Voss. 1987. “Analysis of an Anisotropic Coastal Aquifer System Using Variable-Density Flow and Solute Transport Simulation.” *Journal of Hydrology* 92 (1–2): 17–41.

S.S. Papadopulos & Associates, Inc. (SSPA). 2022. *Mod-PATH3DU: A Ground-Water Path and Travel-Time Simulator*. Bethesda, MD.

Stearns, H. T. 1943. *Print of Log of* (b)(3)(b)(3) *Water Development Tunnel*. Letter from: H. T. Stearns, USGS Senior Geologist, to: O. E. Meizner, Geologist in Charge, USGS Division of Ground Water. Provided as Attachment to Stearns April 12, 1941 Report: A Maui-Type Well for the U. S. Navy at Red Hill, Oahu.

Texas Commission on Environmental Quality (TCEQ). 2023. *Current PCL Tables*. March. Accessed April 14, 2023. https://www.tceq.texas.gov/ remediation/trrp/trrppcls.html.

Todd, David Keith. 1980. *Groundwater Hydrology, Second Edition*.

United States Geological Survey (USGS). 2017. *Final Synoptic Water Level Study Work Plan, Hālawa Area, Oʻahu, Hawaiʻi*. Honolulu, HI: Pacific Islands Water Science Center. August 10.

———. 2022a. *December 23, 2021, Red Hill Synoptic Groundwater-Level Survey, Hālawa Area, Oʻahu, Hawaiʻi*. Open-File Report 2022–1018. By Rylen K. Nakama, Jackson N. Mitchell, and Delwyn S. Oki. Prepared in Cooperation with the U.S. Navy. doi.org/10.3133/ofr20221018.

———. 2022b. *January 18, 2022, Red Hill Synoptic Groundwater-Level Survey, Hālawa Area, Oʻahu, Hawaiʻi*. Open-File Report 2022–1048. By Rylen K. Nakama, Jackson N. Mitchell, and Delwyn S. Oki. Prepared in Cooperation with the U.S. Navy. doi.org/10.3133/ofr20221048.

Visher, F. N., and J. F. Mink. 1964. *Ground-Water Resources in Southern Oahu, Hawaii*. Geological Survey Water Supply Paper 1778. Prepared in Cooperation with the State of Hawaii, Department of Land and Natural Resources, Division of Water and Land Development. U.S. Geological Survey.

Vitturi, M. D. M., and S. Tarquini. 2018. "MrLavaLoba: A New Probabilistic Model for the Simulation of Lava Flows as a Settling Process." *Journal of Volcanology and Geothermal Research* 349:323–34.

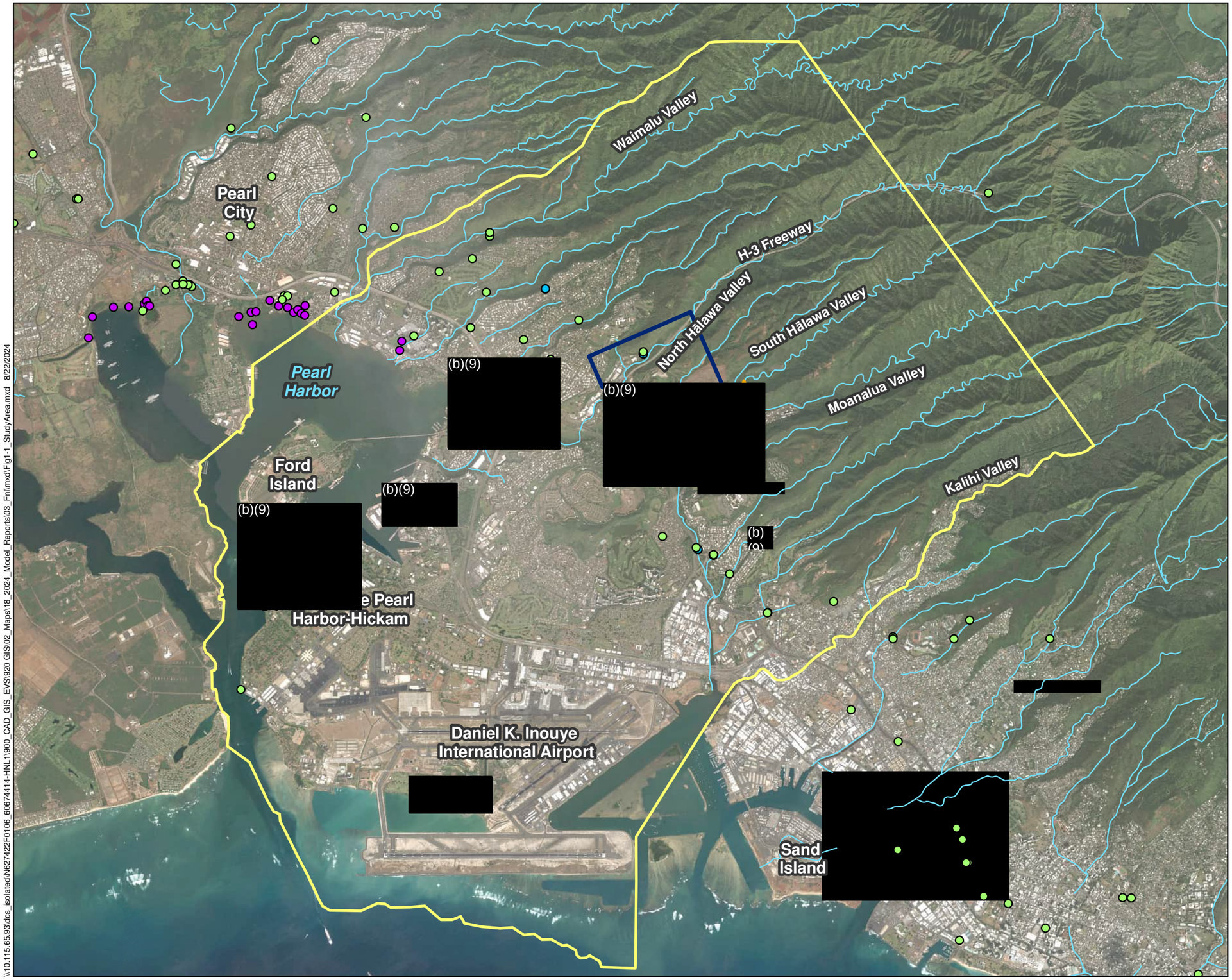

Location Map

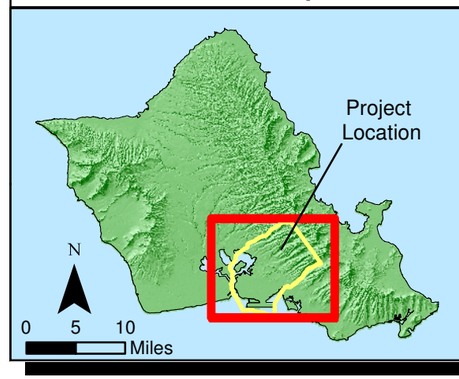

Legend

- Supply Well / Shaft
- Monitoring Well
- Spring
- Stream
- Red Hill Facility Boundary and Fuel Storage Tanks
- Groundwater Flow Model Domain
- Nested Grid

Notes

1. Map projection: NAD 1983 Hawaii State Plane Zone 3 feet.
2. Base Map: DigitalGlobe, Inc. (DG) and NRCS. Publication_Date: 2015
3. Spring locations provided by USGS.
4. Water supply well locations provided by DLNR.

N

0 5,000 10,000 15,000 Feet

Figure 1-1
Groundwater Flow Model Domain and Study Area
GWFM, VZM, CF&T Model Report
Red Hill Bulk Fuel Storage Facility
JBPHH, O'ahu, HI

\\10.115.65.93\dcs_isolated\N627422F0106_60674414-HNL1\900_CAD_GIS_EVS\920 GIS\02_Maps\18_2024_Model_Reports\03_Fnl\mxd\Fig1-1_StudyArea.mxd 8/22/2024

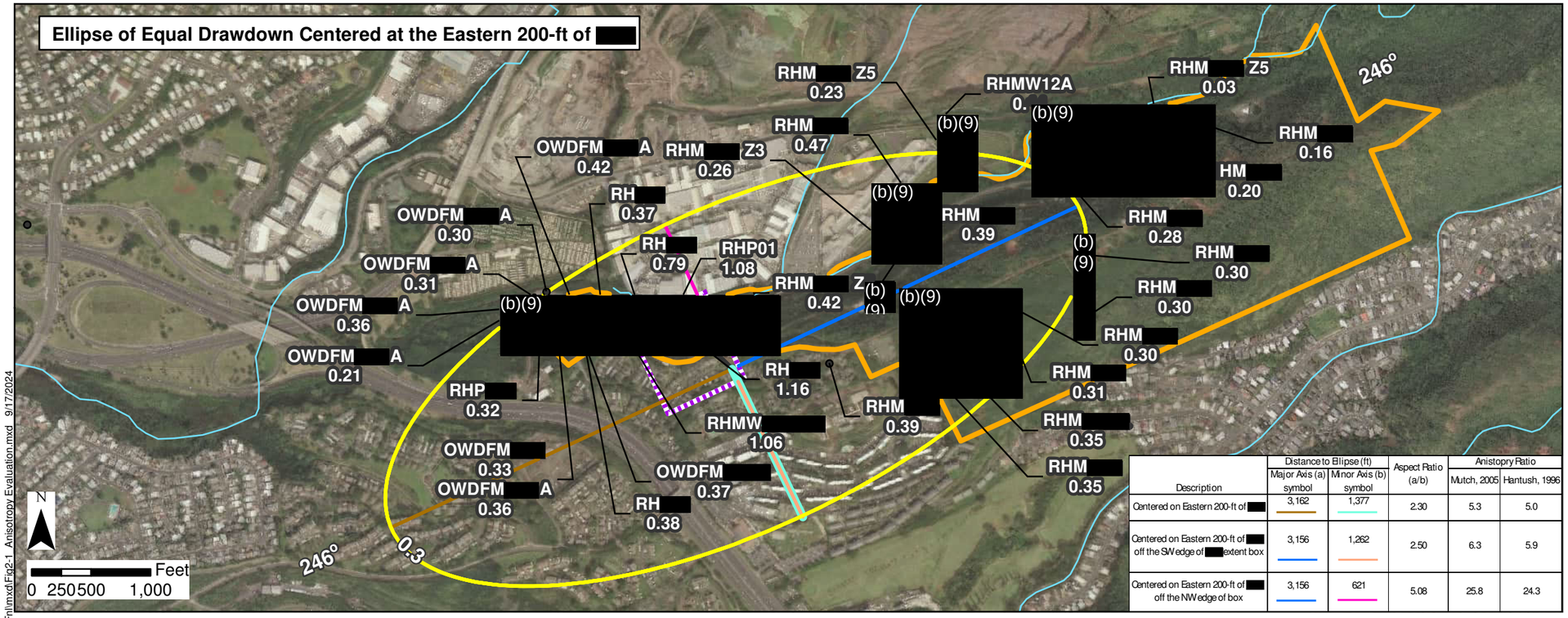

Description	Distance to Ellipse (ft) Major Axis (a) symbol	Distance to Ellipse (ft) Minor Axis (b) symbol	Aspect Ratio (a/b)	Anistopry Ratio Mutch, 2005	Anistopry Ratio Hantush, 1996
Centered on Eastern 200-ft of [redacted]	3,162	1,377	2.30	5.3	5.0
Centered on Eastern 200-ft of [redacted] off the SW edge of [redacted] extent box	3,156	1,262	2.50	6.3	5.9
Centered on Eastern 200-ft of [redacted] off the NW edge of box	3,156	621	5.08	25.8	24.3

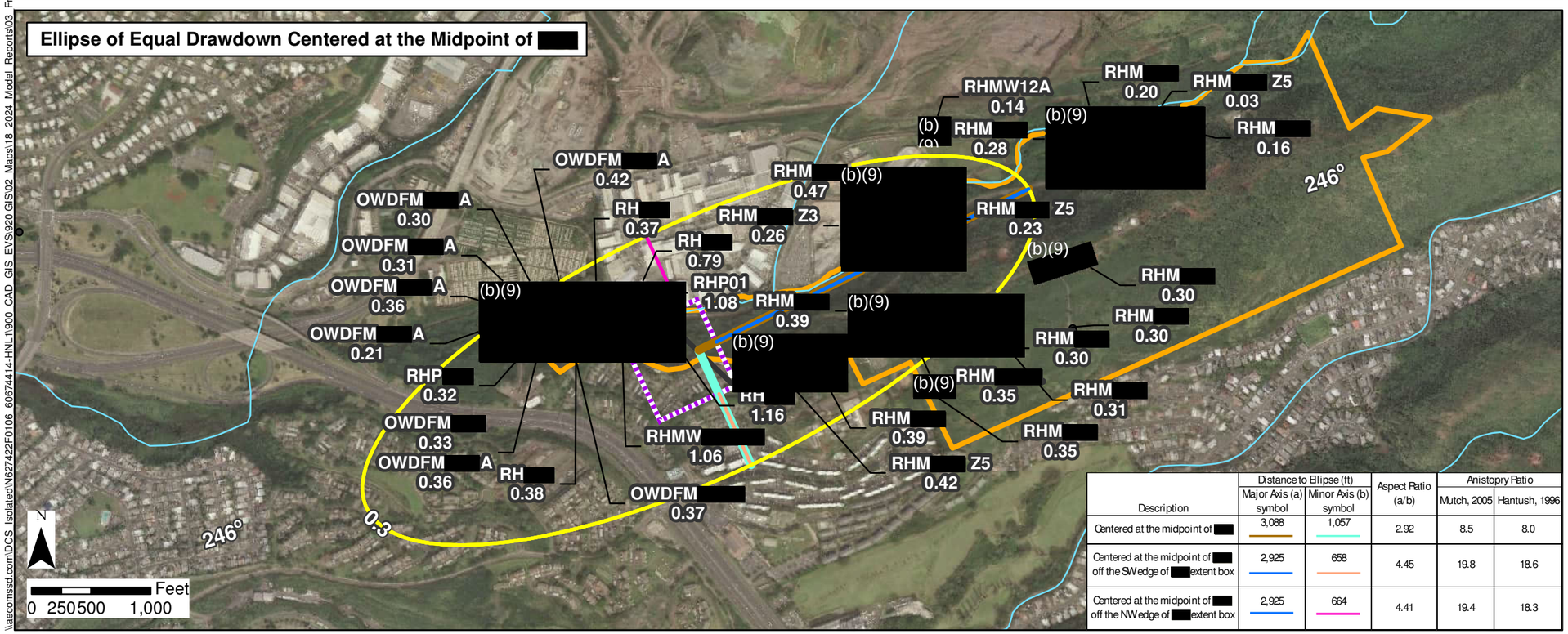

Description	Distance to Ellipse (ft) Major Axis (a) symbol	Distance to Ellipse (ft) Minor Axis (b) symbol	Aspect Ratio (a/b)	Anistopry Ratio Mutch, 2005	Anistopry Ratio Hantush, 1996
Centered at the midpoint of [redacted]	3,088	1,057	2.92	8.5	8.0
Centered at the midpoint of [redacted] off the SW edge of [redacted] extent box	2,925	658	4.45	19.8	18.6
Centered at the midpoint of [redacted] off the NW edge of [redacted] extent box	2,925	664	4.41	19.4	18.3

Location Map

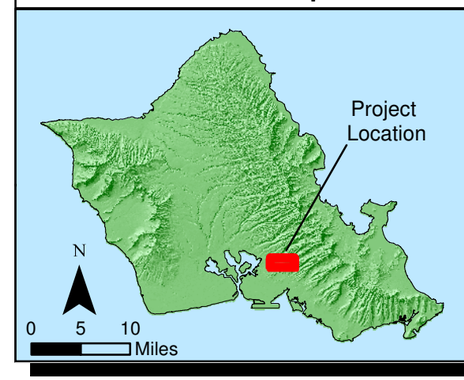

Legend

Major Axis **Minor Axis**

- Ellipse of Equal Drawdown (0.3ft)
- Monitoring Well Location
- [redacted] Extent
- Water Development Tunnel / Infiltration Gallery
- Stream
- Red Hill Facility Boundary

Notes

1. Map projection: NAD 1983 Hawaii State Plane Z3 ft
2. Base Map: Service Layer Credits: Source: Esri, Maxar, GeoEye, Earthstar Geographics, CNES/Airbus DS, USDA, USGS, AeroGRID, IGN, and the GIS User Community
3. Coordinates: NAD 1983 Hawaii State Plane Z3 ft

Figure 2-1
Anisotropy Evaluation Drawdown with Pumping at 4.3 MGD after 18 Days
GWFM, VZM, & CF&T Model Report
Red Hill Bulk Fuel Storage Facility
JBPHH, O'ahu HI

\\aecomssd.com\DCS_Isolated\N627422F0106_60674414-HNL1\900_CAD_GIS_EVS\920_GIS\02_Maps\18_2024_Model_Reports\03_Fri\mxd\Fig2-1_Anisotropy_Evaluation.mxd 9/17/2024

B (Northwest)

Bend in Section

(Southeast) (North)

South Hālawa Valley

B' (South)

Elevation, feet MSL

550 500 450 400 350 300 250 200 150 100 50 0 -50 -100 -150 -200 -250 -300

Hālawa Quarry Excavation

South Hālawa Stream

(b)(9)

RHMW

RHMW

(b)(9)

(b)(9)

RHMW

RHMW

(b)(9)

RHM

Tank 1

Tank 2

RHMW01R

GW [redacted].0 ft. msl
(Dames and Moore,10/1991)

GW 99.84 ft. msl
(1/4/2018)

GW 18.14 ft. msl
(RHM[redacted] 08/23/2024)

3,400 3,600 3,800 4,000 4,200 4,400 4,600 4,800 5,000 5,200 5,400 5,600 5,800 6,000 6,200 6,400 6,600 6,800 7,000

0 300 600 900

SCALE FEET

Horizontal Scale: 1" = 300', Vertical Scale: 1" = 150'

Note: Vertical exaggeration = 1H : 2V (approximate)

Key Plan

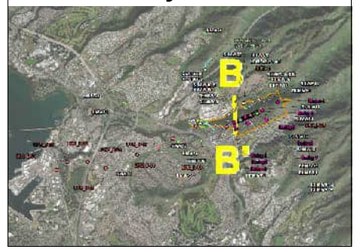

Legend

Lithology from Cores

- Alluvium
- Saprolite
- Tuff
- Welded A'a Clinker
- Highly Weathered Massive A'a
- Highly Weathered Pahoehoe
- Moderately Weathered Massive A'a
- Moderately Weathered Pahoehoe
- Slightly Weathered Massive A'a
- Slightly Weathered Pahoehoe
- Unweathered Massive A'a
- Unweathered Pahoehoe
- Loose A'a Clinker
- Weathered Basalt

General Geology for Cross Section

- Alluvium
- Undifferentiated Weathered Basalt
- Saprolite
- Undifferentiated Clinker
- Basal Grounwater (approximate)
- Approximate Contact

Figure 2-2
Cross Section B-B' (View Looking East)
GWFM, VZN, & CF&T Model Report
Red Hill Bulk Storage Facility
JBPHH, O'ahu, Hawai'i

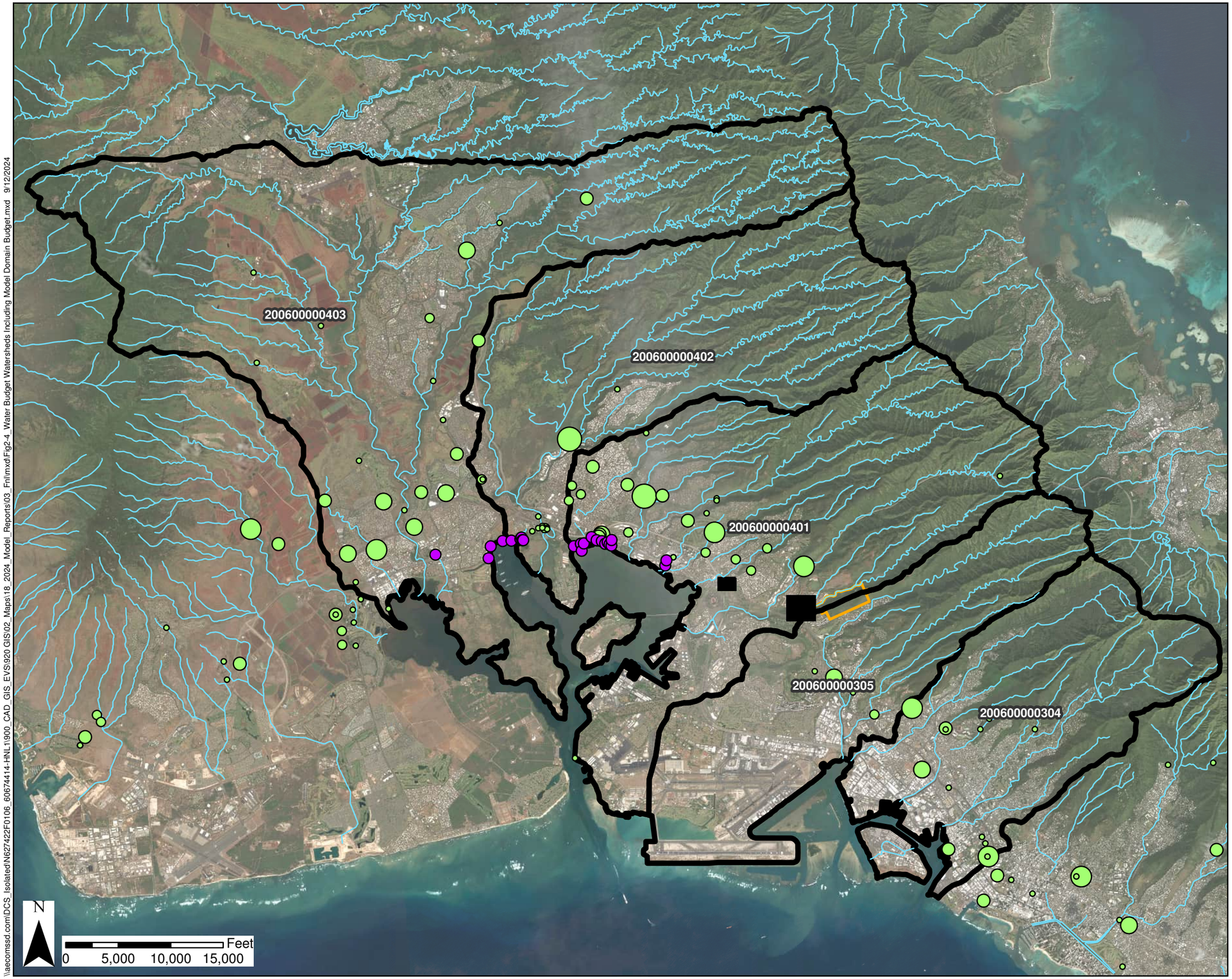

Location Map

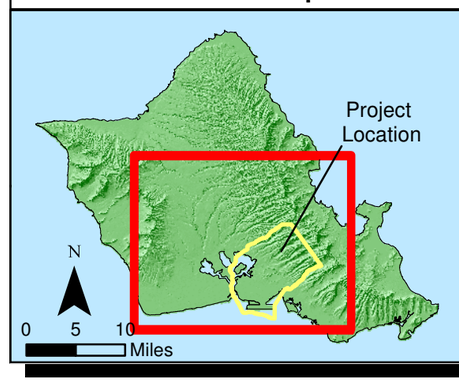

Legend

- Spring

Water Supply Well / Shaft (MGD)

- 0.0 - 0.5
- 0.5 - 1.0
- 1.0 - 2.0
- 2.0 - 5.0
- 5.0 - 10.0
- 10.0 - 15.0
- Stream
- HUC-12 Watershed Boundary
- Red Hill Facility Boundary and Fuel Storage Tanks
- 200600000305 USGS 12 Digit Hydrologic Unit Code

Notes

1. Map projection: NAD 1983 Hawaii State Plane Zone 3 feet.
2. Base Map: DigitalGlobe, Inc. (DG) and NRCS. Publication_Date: 2015
3. HUC-12 = 12 Digit Hydrologic Unit Code.
4. Spring locations provided by USGS.
5. Water supply well locations provided by DLNR.
6. Weather station location provided by State of Hawaii.

Figure 2-3
Water Budget Watersheds Analysis Area
GWFM, VZM, CF&T Model Report
Red Hill Bulk Fuel Storage Facility
JBPHH, O'ahu, HI

\\aecomnssd.com\DCS_Isolated\N\627422F0106_60674414-HNL1\900_CAD_GIS_EVS\920 GIS\02_Maps\18_2024_Model_Reports\03_Fnl\mxd\Fig2-4_Water Budget Watersheds including Model Domain Budget.mxd 9/12/2024

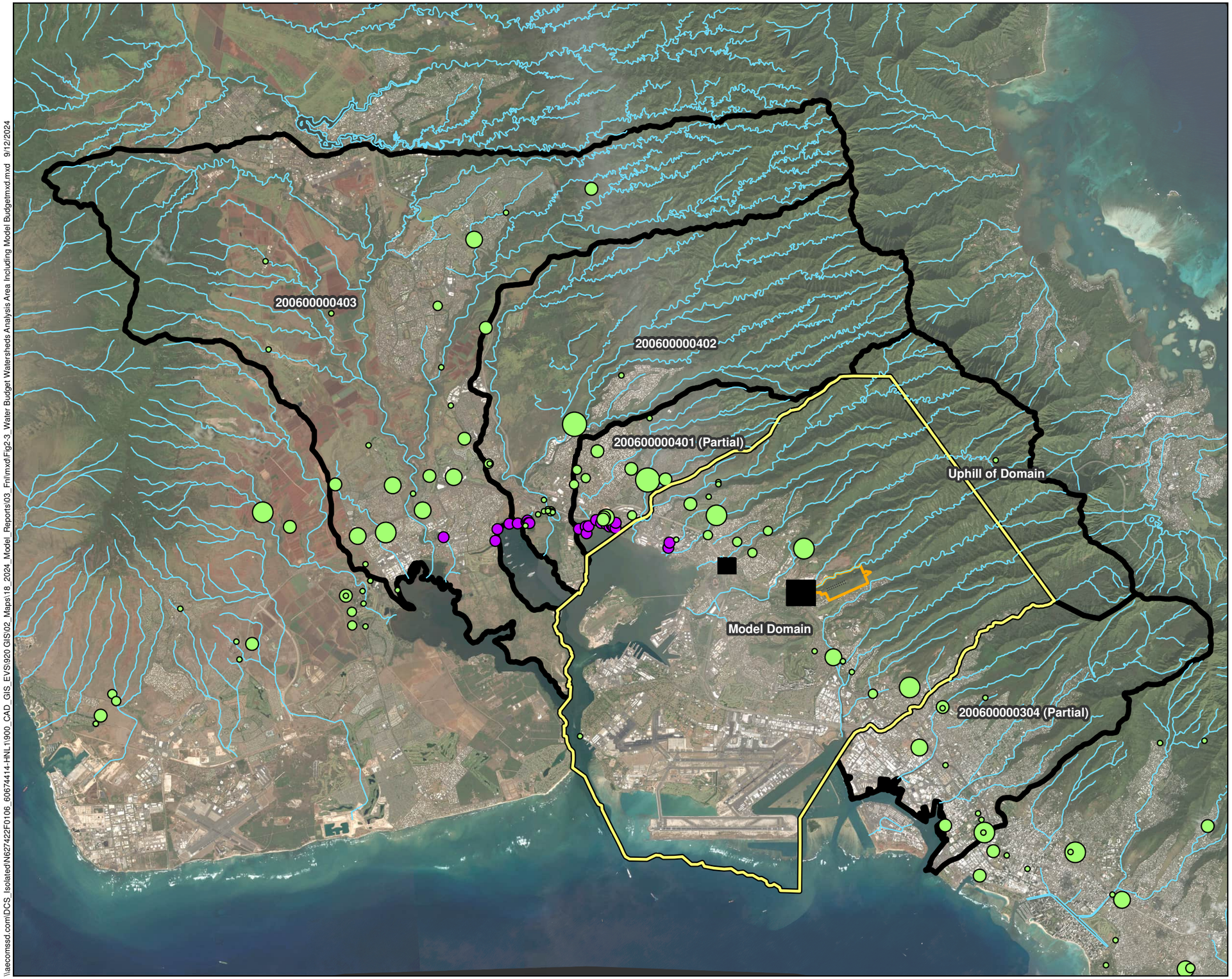

Location Map

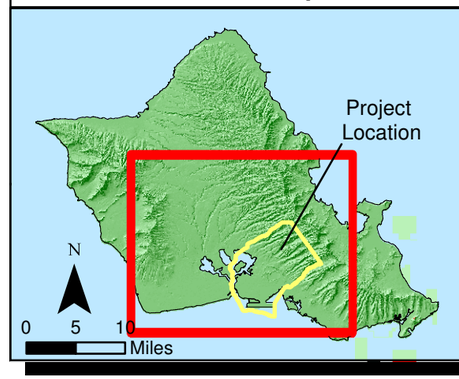

Legend

- Spring
- **Water Supply Well / Shaft (MGD)**
  - 0.0 - 0.5
  - 0.5 - 1.0
  - 1.0 - 2.0
  - 2.0 - 5.0
  - 5.0 - 10.0
  - 10.0 - 15.0
- Stream
- Boundaries used for Model Domain Water Budget Calculations
- Red Hill Facility Boundary and Fuel Storage Tanks
- Groundwater Flow Model Domain

Notes

1. Map projection: NAD 1983 Hawaii State Plane Zone 3 feet.
2. Base Map: DigitalGlobe, Inc. (DG) and NRCS. Publication_Date: 2015
3. Spring locations provided by USGS.
4. Water supply well locations provided by DLNR.

N

0 5,000 10,000 15,000 Feet

Figure 2-4
Water Budget Watersheds Including Model Domain Budget
GWFM, VZM, CF&T Model Report
Red Hill Bulk Fuel Storage Facility
JBPHH, O'ahu, HI

\\aecomssd.com\DCS_Isolated\N627422F0106_60674414-HNL11\900_CAD_GIS_EVS\920 GIS\02_Maps\18_2024_Model_Reports\03_Fnl\mxd\Fig2-3_Water Budget Watersheds Analysis Area Including Model Budgetmxd.mxd 9/12/2024

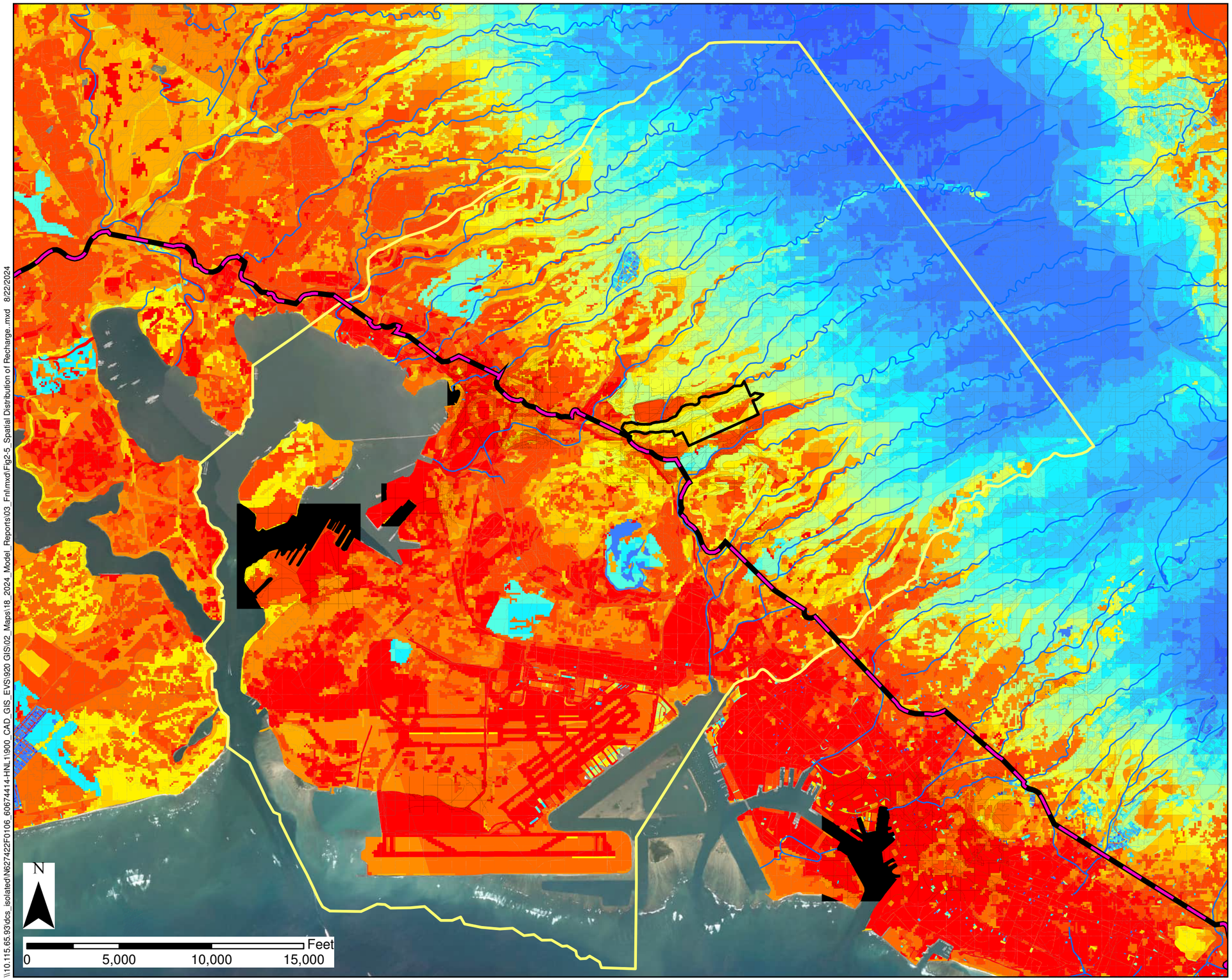

Location Map

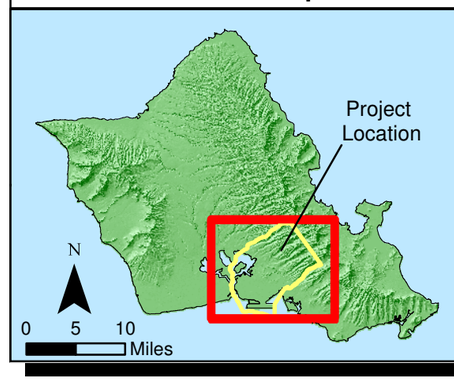

Legend

Average Recharge (inches per year)

0.0 - 1.0	18.2 - 21.5
1.1 - 2.8	21.6 - 25.9
2.9 - 4.8	26.0 - 31.2
4.9 - 6.4	31.3 - 38.6
6.5 - 8.1	38.7 - 48.2
8.2 - 9.7	48.3 - 59.4
9.8 - 11.3	59.5 - 75.3
11.4 - 13.2	75.4 - 101.0
13.3 - 15.4	101.1 - 143.1
15.5 - 18.1	143.2 - 245.9

Caprock Extent

Groundwater Flow Model Domain

Red Hill Facility Boundary

Stream

Notes

1. Map projection: NAD 1983 Hawaii State Plane Zone 3 feet.
2. Base Map: DigitalGlobe, Inc. (DG) and NRCS. Publication_Date: 2015
3. Average Recharge conditions from 1978 to 2007 (Engott et al., 2017).

\\10.115.65.93\dcs_isolated\N627422F0106_60674414-HNL11900_CAD_GIS_EVS\920 GIS\02_Maps\18_2024_Model_Reports\03_Fnl\mxd\Fig2-5_Spatial Distribution of Recharge..mxd 8/22/2024

Figure 2-5
Spatial Distribution of Recharge
GWFM, VZM, CF&T Model Report
Red Hill Bulk Fuel Storage Facility
JBPHH, O'ahu, HI

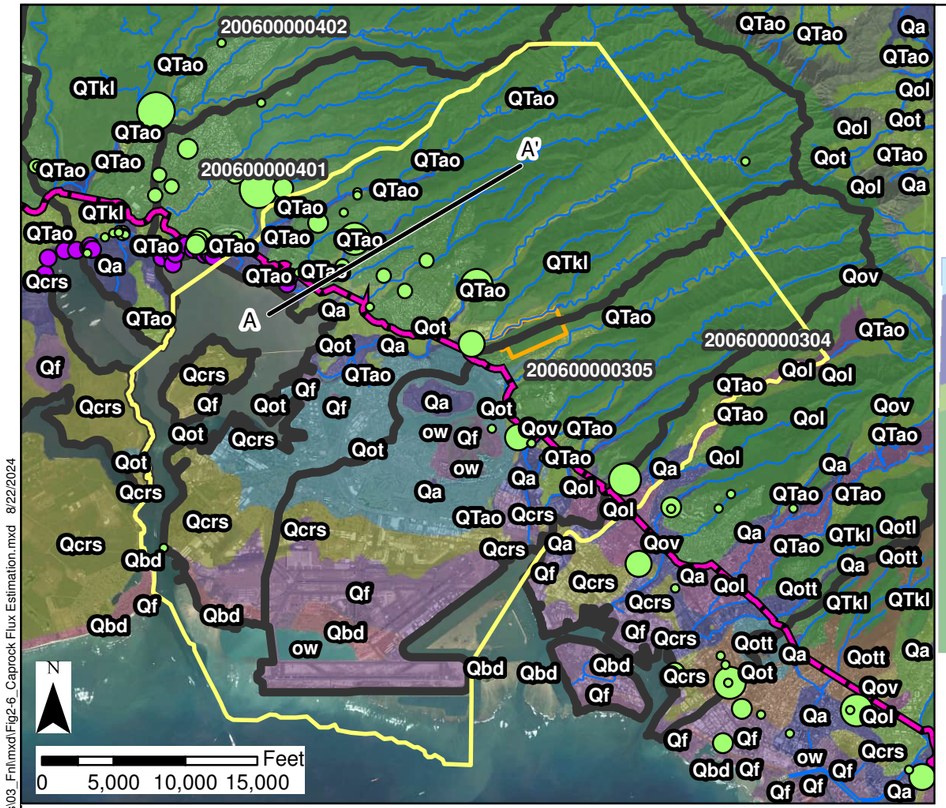

Cross Section

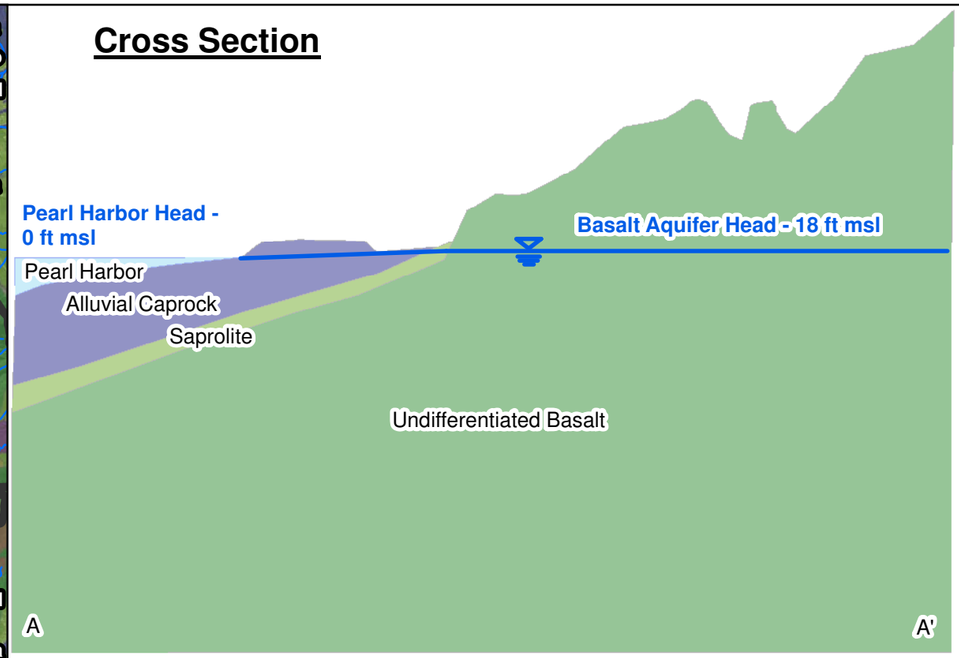

Simplistic Cross Section

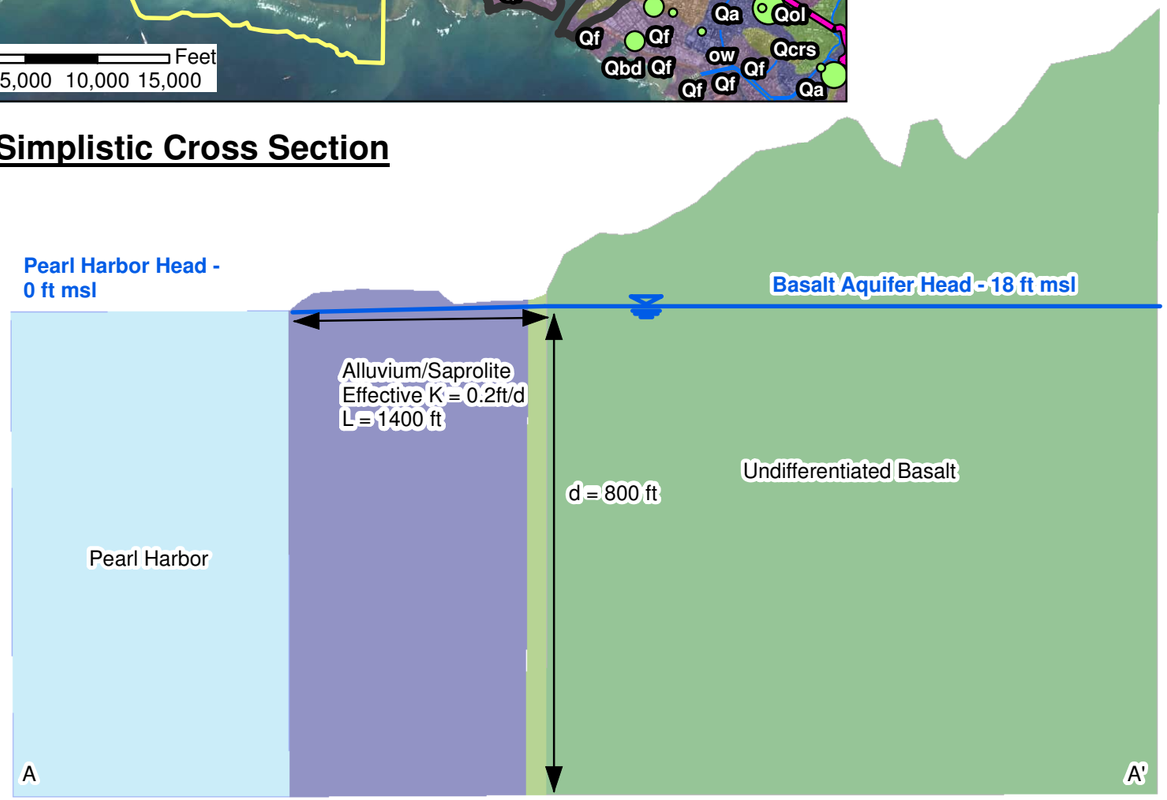

Location Map

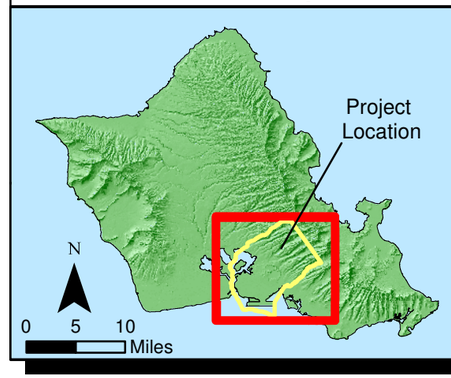

Legend

- Spring
- Water Supply Well / Shaft (MGD)
  - 0.0 - 0.5
  - 0.5 - 1.0
  - 1.0 - 2.0
  - 2.0 - 5.0
  - 5.0 - 10.0
  - 10.0 - 15.0
- Caprock Extent
- HUC-12 Watershed Boundary
- Stream
- Red Hill Facility Boundary and Fuel Storage Tanks
- Groundwater Flow Model Domain
- 200600000305 USGS 12 Digit Hydrologic Unit Code

Geological Units

- QTao, Older alluvium, Sand and gravel
- QTkl, Koolau Basalt, Lava flows
- Qa, Alluvium, Sand and gravel
- Qbd, Beach deposits, Beach deposits
- Qcrs, Lagoon and reef deposits, Limestone and mudstone
- Qf, Fill, Manmade fill
- Qol, Honolulu Volcanics, Lava flows
- Qot, Honolulu Volcanics, Tuff
- Qotl, Honolulu Volcanics, Lava flows
- Qott, Honolulu Volcanics, Vent deposits
- Qov, Honolulu Volcanics, Vent deposits
- ow, Open water, Open water

Notes

1. Map projection: NAD 1983 Hawaii State Plane Zone 3 feet.
2. Base Map: DigitalGlobe, Inc. (DG) and NRCS. Publication_Date: 2015
3. Geologic map from Sherrod et al 2007.
4. Spring locations provided by USGS.
5. Water supply well locations provided by DLNR.
6. HUC-12 = USGS Hydrologic Unit.
7. Caprock is present from the coast to the "caprock extent" ("makai of the caprock extent").
8. Cross sections are not to scale

Figure 2-6
Caprock Flux Estimation
GWFM, VZM, & CF&T Model Report
Red Hill Bulk Fuel Storage Facility
JBPHH, O'ahu, HI

\\10.115.65.93\dcs_isolated\N627422F0106_60674414-HNL1\900_CAD_GIS_EVS\920 GIS\02_Maps\18_2024_Model_Reports\03_Fnl\mxd\Fig2-6_Caprock Flux Estimation.mxd 8/22/2024

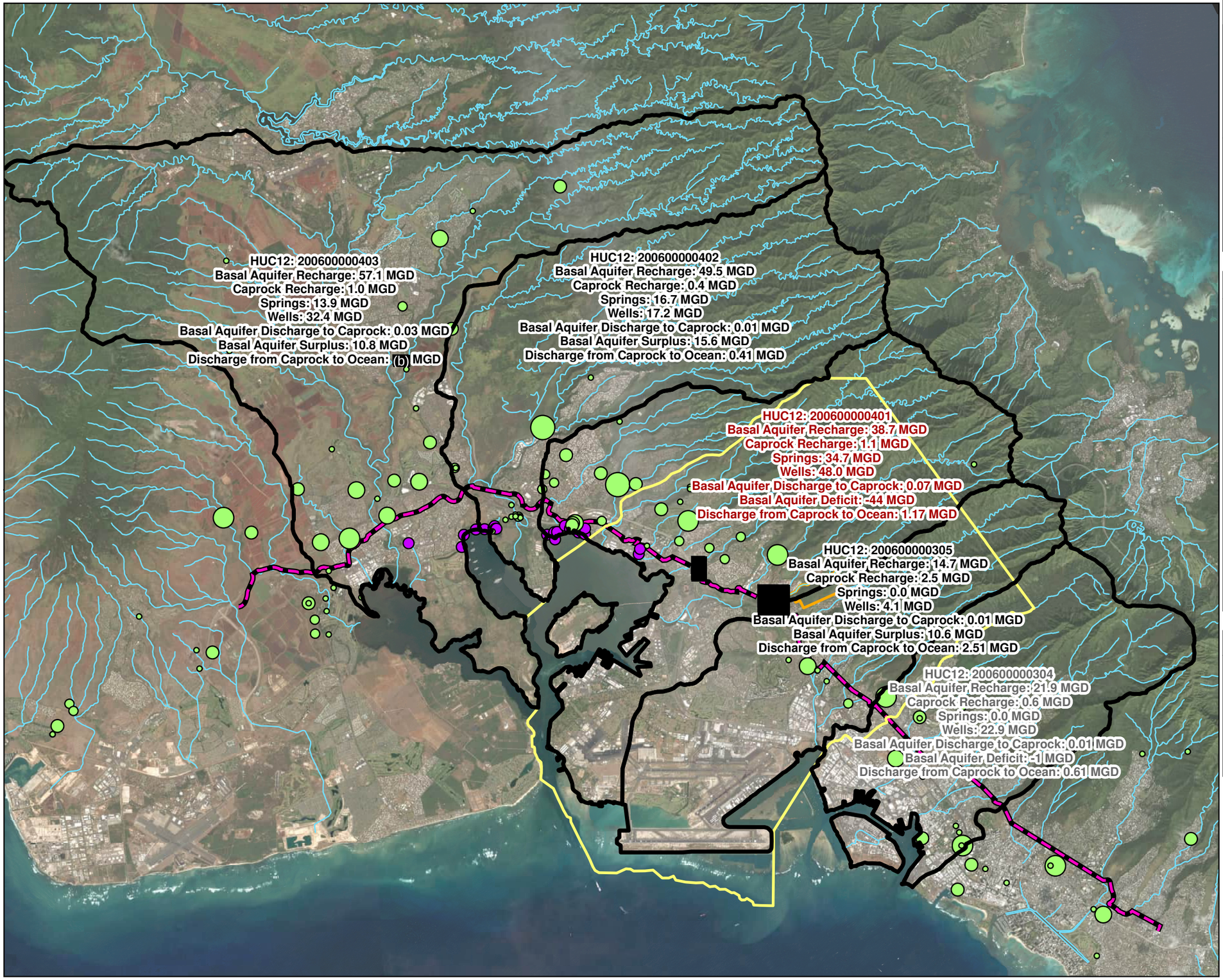

Location Map

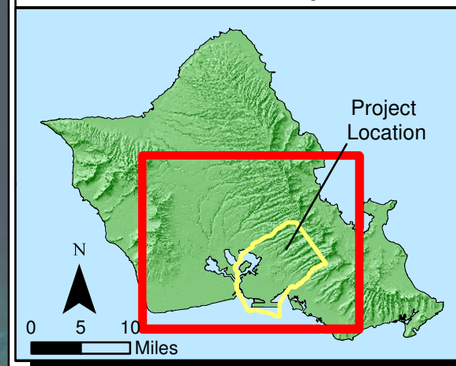

Legend

- Spring

Water Supply Well / Shaft (MGD)

- 0.0 - 0.5
- 0.5 - 1.0
- 1.0 - 2.0
- 2.0 - 5.0
- 5.0 - 10.0
- 10.0 - 15.0
- HUC12 Watershed Boundary
- Groundwater Flow Model Domain
- Caprock Line
- Stream
- Red Hill Facility Boundary and Fuel Storage Tanks

Notes

1. Map projection: NAD 1983 Hawaii State Plane Zone 3 feet.
2. Base Map: DigitalGlobe, Inc. (DG) and NRCS. Publication_Date: 2015
3. Spring locations provided by USGS.
4. Water supply well locations provided by DLNR.
5. HUC-12 = USGS Hydrologic Unit.

N

0 5,000 10,000 15,000 Feet

Figure 2-7
Water Budget for Watersheds in the Model Domain HUC12 Watersheds
GWFM, VZM, & CF&T Model Report
Red Hill Bulk Fuel Storage Facility
JBPHH, O'ahu, HI

\\10.115.65.93\dcs_isolated\N627422F0106_60674414-HNL\1900_CAD_GIS_EVS\920 GIS\02_Maps\18_2024_Model_Reports\03_Fnl\mxd\Fig2-7_Water Budget for Watersheds in the Model Domain HUC12 Watersheds.mxd 8/22/2024

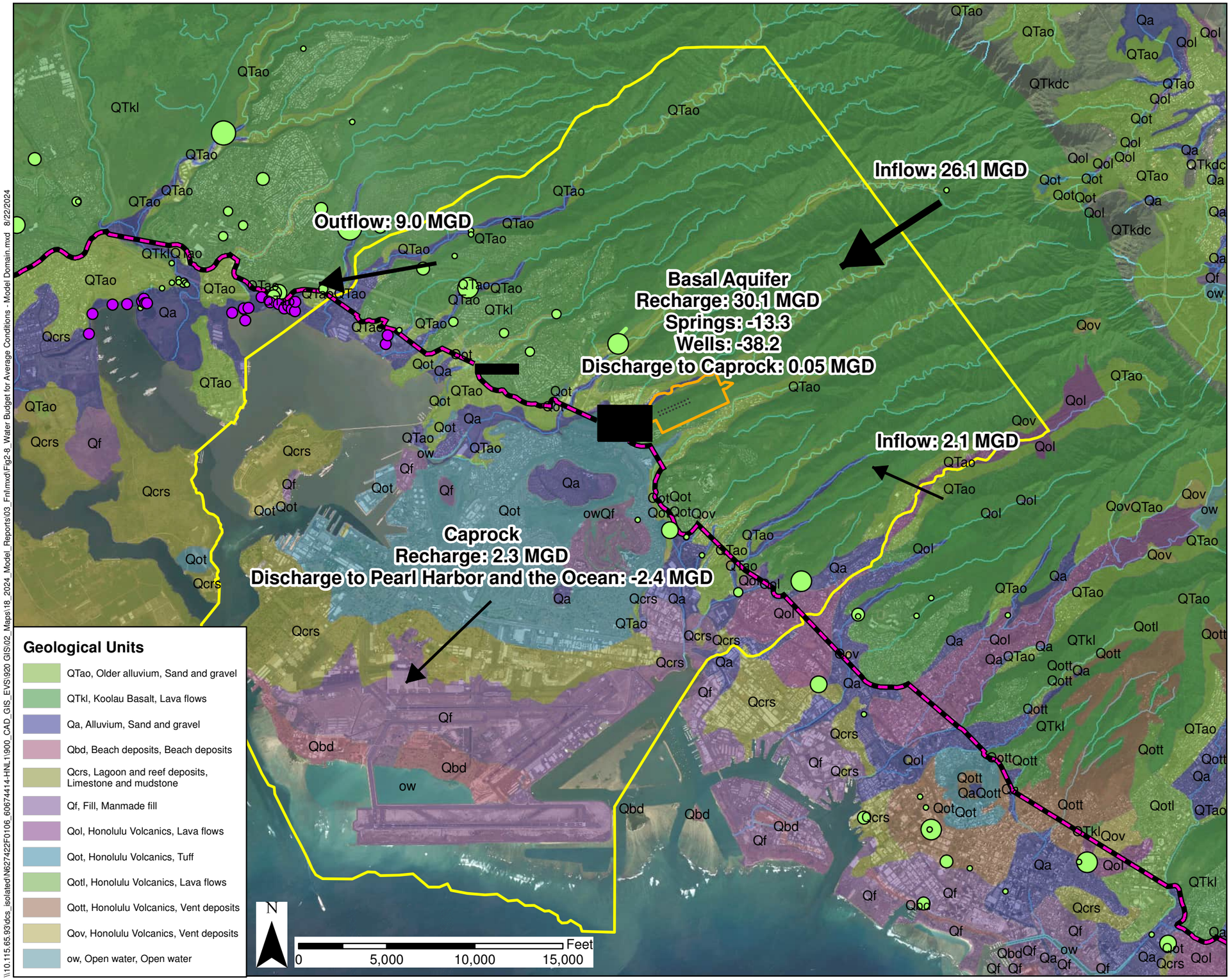

Geological Units

- QTao, Older alluvium, Sand and gravel
- QTkl, Koolau Basalt, Lava flows
- Qa, Alluvium, Sand and gravel
- Qbd, Beach deposits, Beach deposits
- Qcrs, Lagoon and reef deposits, Limestone and mudstone
- Qf, Fill, Manmade fill
- Qol, Honolulu Volcanics, Lava flows
- Qot, Honolulu Volcanics, Tuff
- Qotl, Honolulu Volcanics, Lava flows
- Qott, Honolulu Volcanics, Vent deposits
- Qov, Honolulu Volcanics, Vent deposits
- ow, Open water, Open water

Location Map

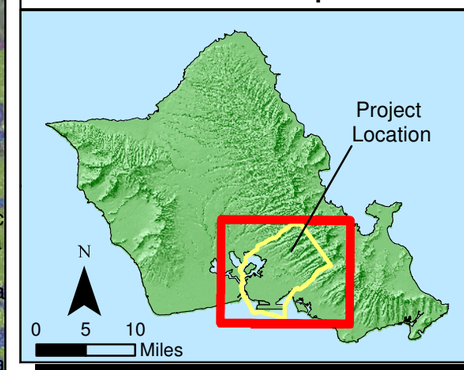

Legend

- Spring (Icon indicates location only, and not magnitude of flow)

Water Supply Well / Shaft (MGD)

- 0.0 - 0.5
- 0.5 - 1.0
- 1.0 - 2.0
- 2.0 - 5.0
- 5.0 - 10.0
- 10.0 - 15.0
- Caprock Line
- Stream
- Red Hill Facility Boundary and Fuel Storage Tanks
- Groundwater Flow Model Domain

Notes

1. Map projection: NAD 1983 Hawaii State Plane Zone 3 feet.
2. Base Map: DigitalGlobe, Inc. (DG) and NRCS. Publication_Date: 2015
3. Geologic map from Sherrod et al 2007.
4. Spring locations provided by USGS.
5. Water supply well locations provided by DLNR.
6. Water Levels from USGS Synoptic Survey, December 2021.
7. Spring flows estimated based on correlations to water level at Well 2256-10 (Oki, 1998).

Figure 2-8
Water Budget for Average Conditions - Model Domain
GWFM, VZM, & CF&T Model Report
Red Hill Bulk Fuel Storage Facility
JBPHH, O'ahu, HI

\\10.115.65.93\dcs_isilated\N627422F0106_60674414-HNL\1900_CAD_GIS_EVS\920 GIS\02_Maps\18_2024_Model_Reports\03_Fnl\mxd\Fig2-8_Water Budget for Average Conditions - Model Domain.mxd 8/22/2024

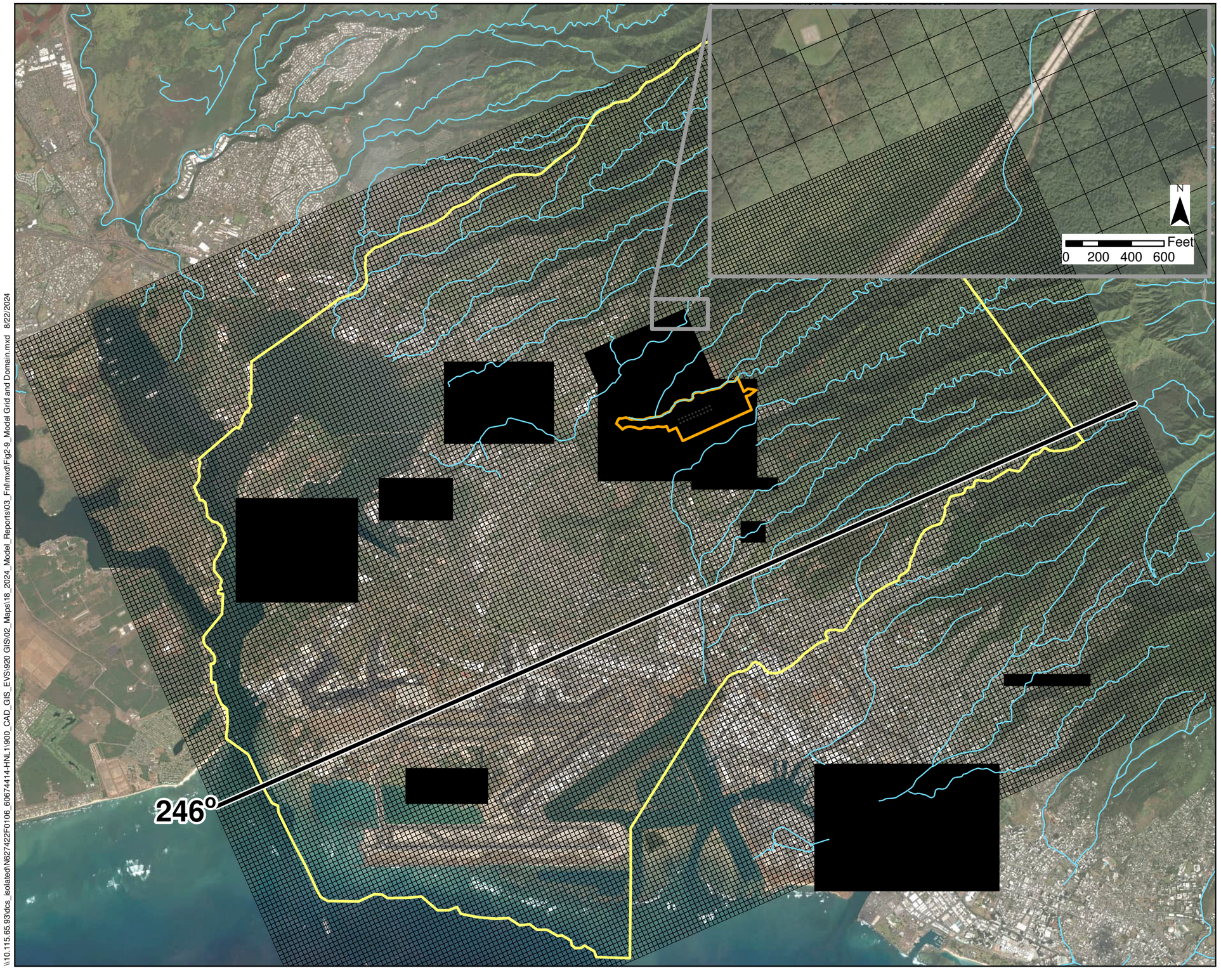

Location Map

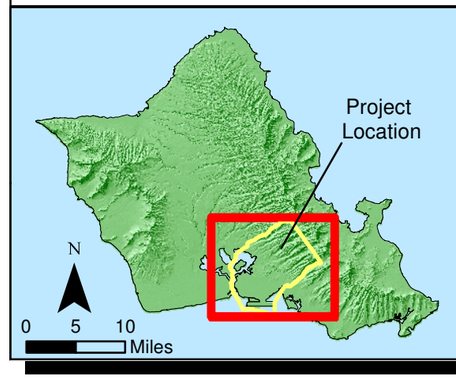

Legend

- Model Grid Cell (250 x 250 ft); Nested Grid Cell (25 x 25 ft)
- Stream
- Red Hill Facility Boundary and Fuel Storage Tanks
- Groundwater Flow Model Domain

Notes

1. Map projection: NAD 1983 Hawaii State Plane Zone 3 feet.
2. Base Map: DigitalGlobe, Inc. (DG) and NRCS. Publication_Date: 2015

N

0 5,000 10,000 15,000 Feet

Figure 2-9
Model Grid and Domain
GWFM, VZM, & CF&T Model Report
Red Hill Bulk Fuel Storage Facility
JBPHH, O'ahu, HI

\\10.115.65.93\dcs_isolated\N627422F0106_60674414-HNL11900_CAD_GIS_EVS\920 GIS\02_Maps\18_2024_Model_Reports\03_Fnl\mxd\Fig2-9_Model Grid and Domain.mxd 8/22/2024

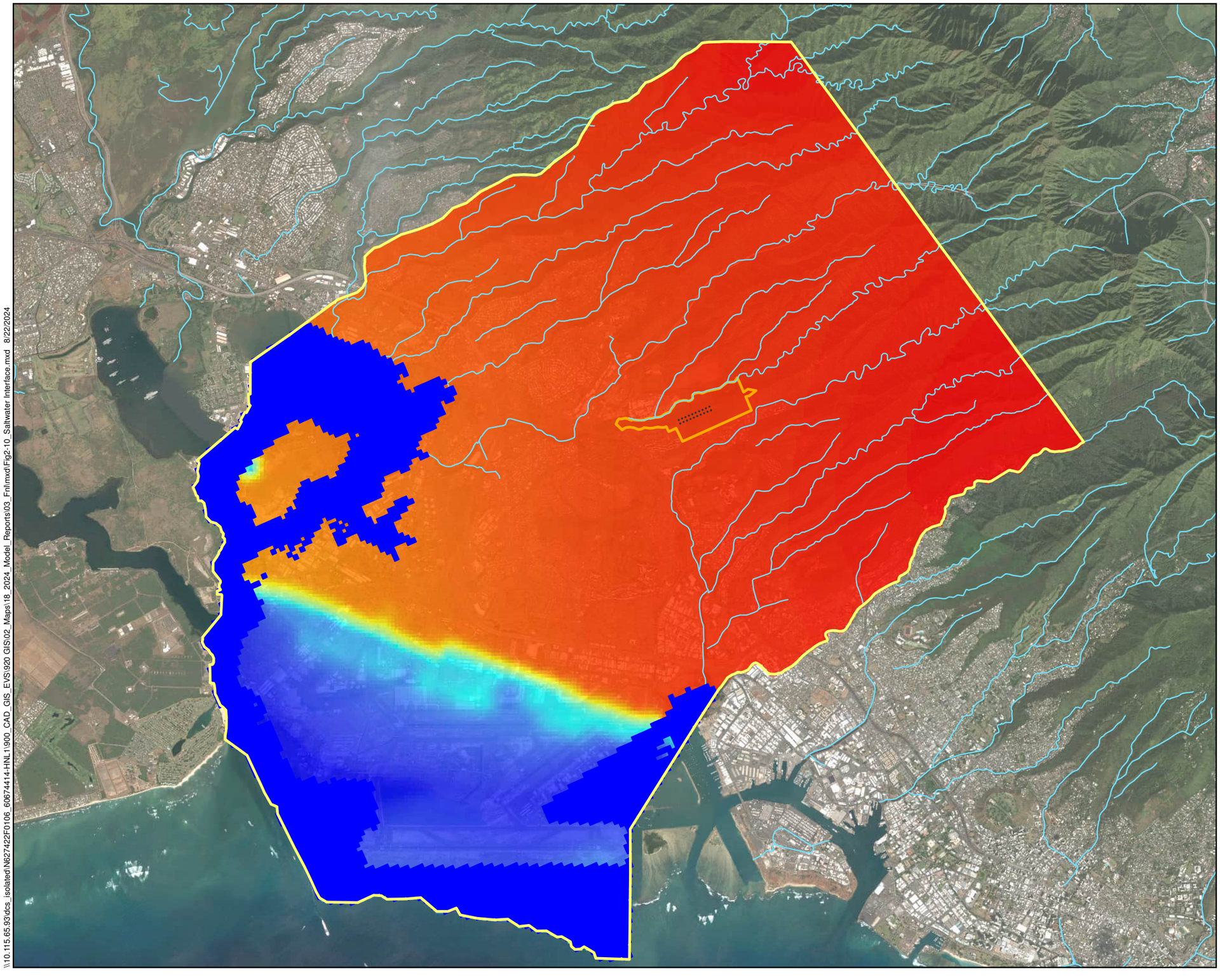

Location Map

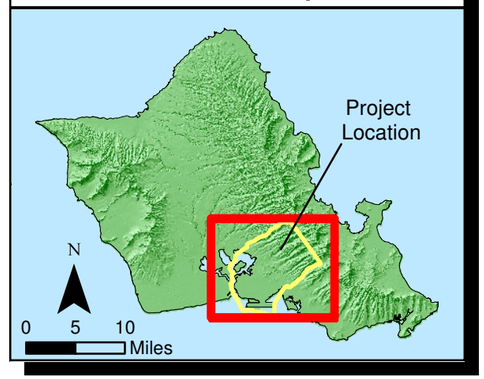

Legend

Saltwater Interface (Model Bottom) (ft msl)

High: -2.1679

Low: -895.781

Pacific Ocean / Pearl Harbor

Stream

Red Hill Facility Boundary and Fuel Storage Tanks

Groundwater Flow Model Domain

Notes

1. Map projection: NAD 1983 Hawaii State Plane Zone 3 feet.
2. Base Map: DigitalGlobe, Inc. (DG) and NRCS. Publication_Date: 2015

N

0 5,000 10,000 15,000 Feet

Figure 2-10
Freshwater/Saltwater Interface (Model Bottom)
GWFM, VZM, & CF&T Model Report
Red Hill Bulk Fuel Storage Facility
JBPHH, O'ahu, HI

\\10.115.65.93\dcs_isolated\N627422F0106_60674414-HNL\1900_CAD_GIS_EVS\920 GIS\02_Maps\18_2024_Model_Reports\03_Fnl\mxd\Fig2-10_Saltwater Interface.mxd 8/22/2024

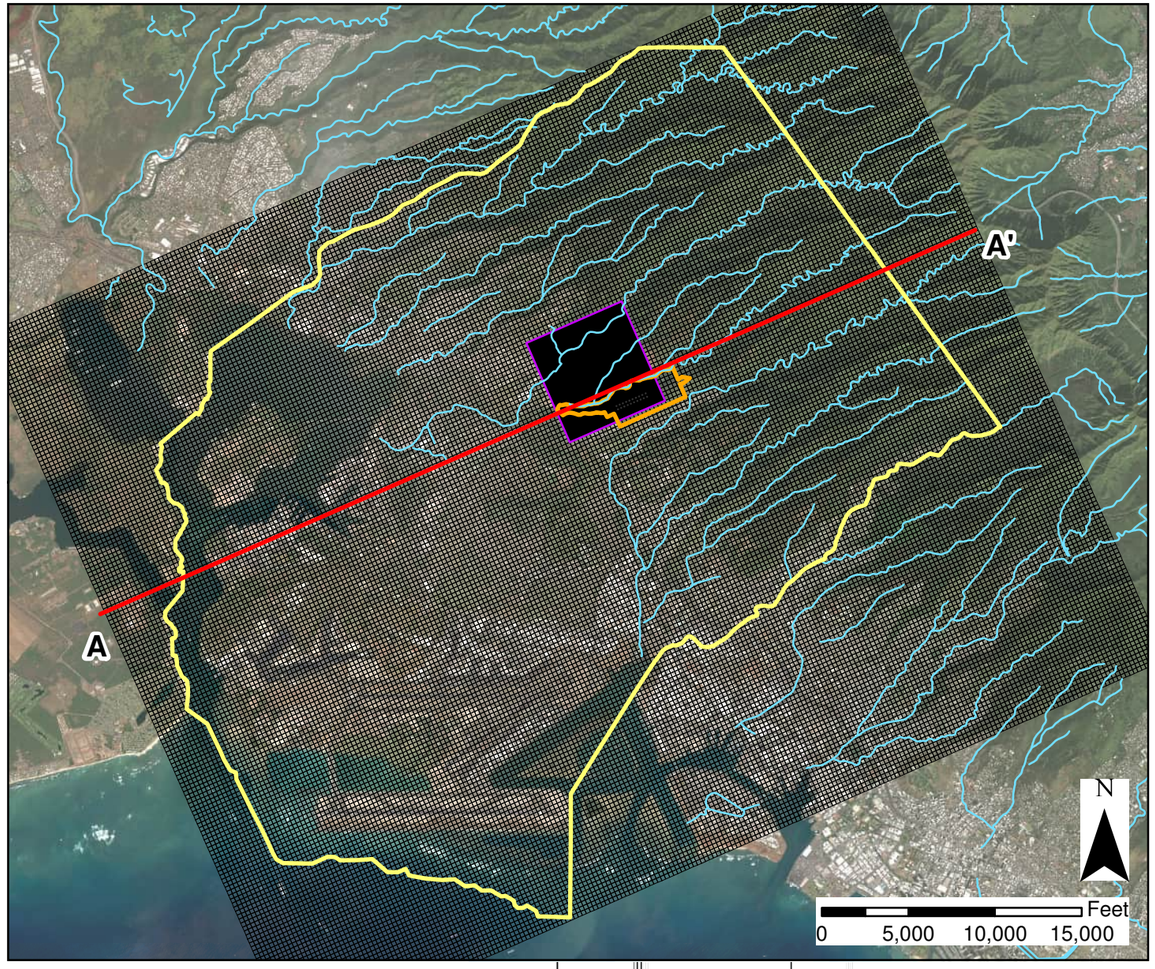

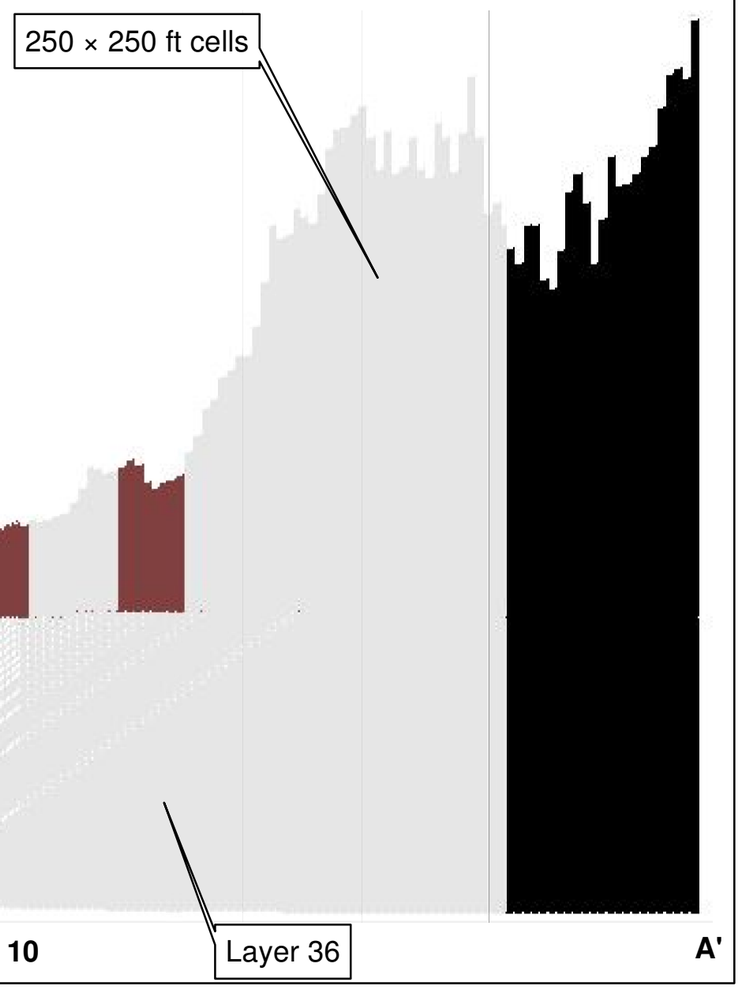

Location Map

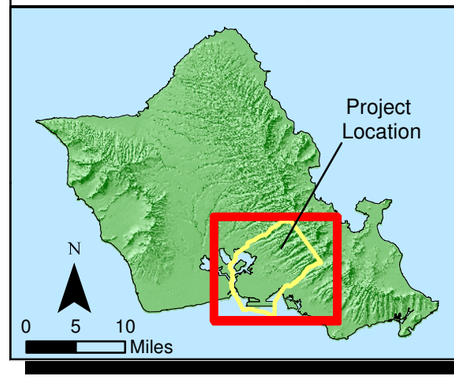

Legend

Hydrogeologic Unit Parameterization for Layer 1

- Basalt
- Saprolite
- Caprock - Alluvium/ Valley Fill
- Confining Unit
- Caprock - Marine Sediments
- Caprock - Deep Marine Sediments
- Tuff
- No Flow (outside model domain)

- Nested Grid
- Model Grid Cell
- Groundwater Flow Model Domain
- Stream
- Red Hill Facility Boundary and Fuel Storage Tanks

Notes

1. Map projection: NAD 1983 Hawaii State Plane Zone 3 feet.
2. Base Map: DigitalGlobe, Inc. (DG) and NRCS. Publication_Date: 2015

Figure 2-11
Cross Section of Model Grid
GWFM, VZM, & C&FT Model Report
Red Hill Bulk Fuel Storage Facility
JBPHH, O'ahu, HI

\\10.115.65.93\dcs_isolated\N627422F0106_60674414-HNL1\900_CAD_GIS_EVS\920 GIS\02_Maps\18_2024_Model_Reports\03_Fnl\mxd\Fig2-11_Cross Section of Model Grid.mxd 8/22/2024

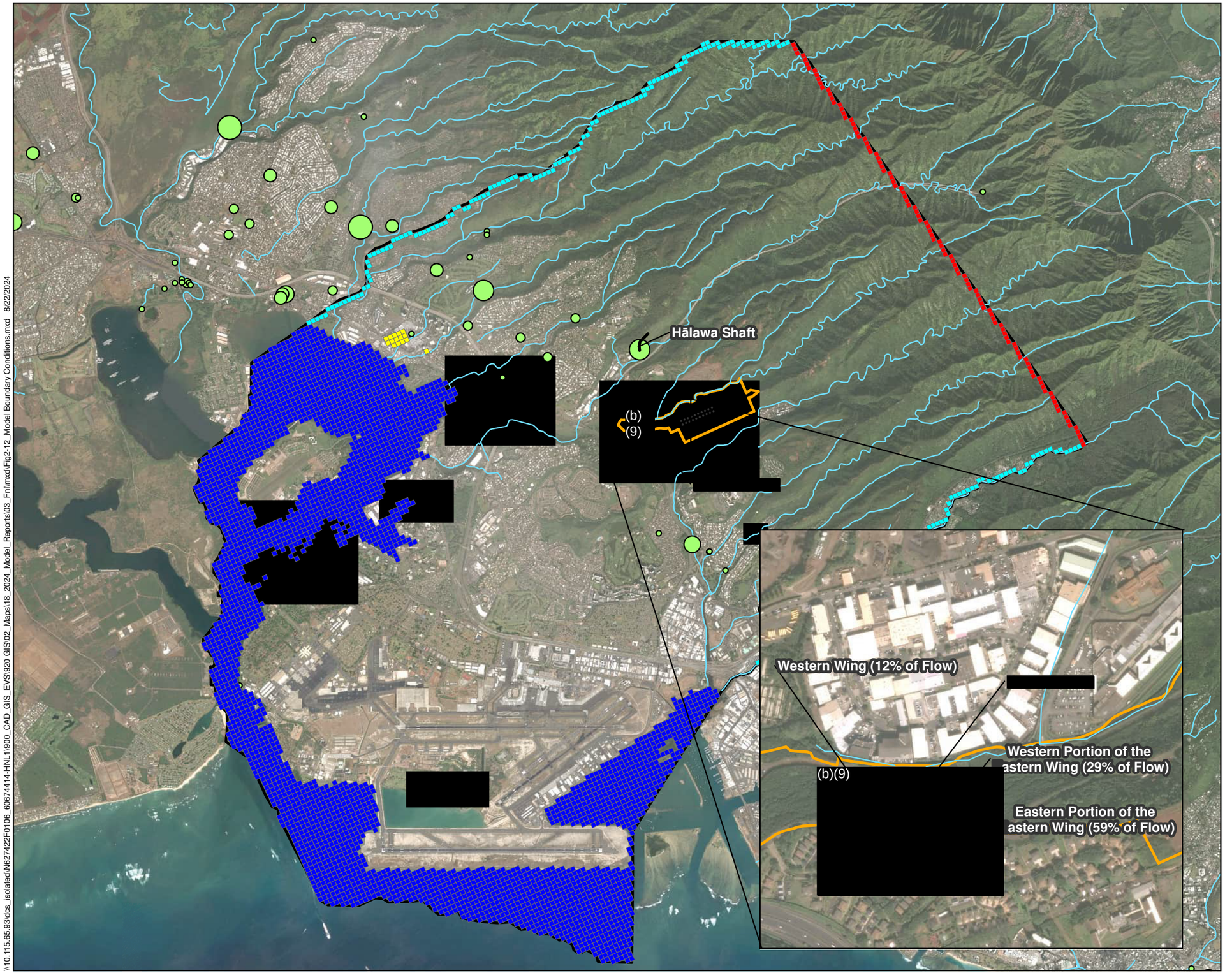

Location Map

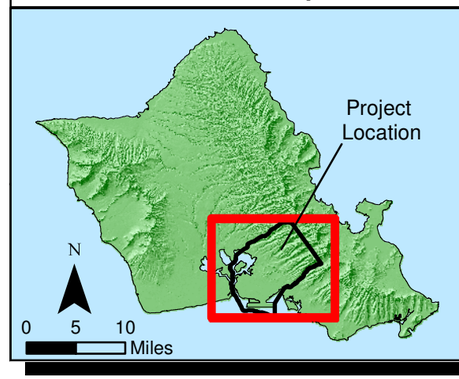

Legend

Water Supply Well / Shaft (MGD)

- 0.0 - 0.5
- 0.5 - 1.0
- 1.0 - 2.0
- 2.0 - 5.0
- 5.0 - 10.0
- 10.0 - 15.0
- Constant Heads (Layer 1 only)
- Drains
- Specified Flux
- General Head Bounadry
- Connected Linear Network Polyline
- Stream
- Red Hill Facility Boundary and Fuel Storage Tanks
- Groundwater Flow Model Domain

Notes

1. Map projection: NAD 1983 Hawaii State Plane Zone 3 feet.
2. Base Map: DigitalGlobe, Inc. (DG) and NRCS. Publication_Date: 2015

N

0 5,000 10,000 15,000 Feet

Figure 2-12
Model Boundary Conditions
GWFM, VZM, & CF&T Model Report
Red Hill Bulk Fuel Storage Facility
JBPHH, O'ahu, HI

\\10.115.65.93\dcs_isolated\N627422F0106_60674414-HNL\1900_CAD_GIS_EVS\920 GIS\02_Maps\18_2024_Model_Reports\03_Fnl\mxd\Fig2-12_Model Boundary Conditions.mxd 8/22/2024

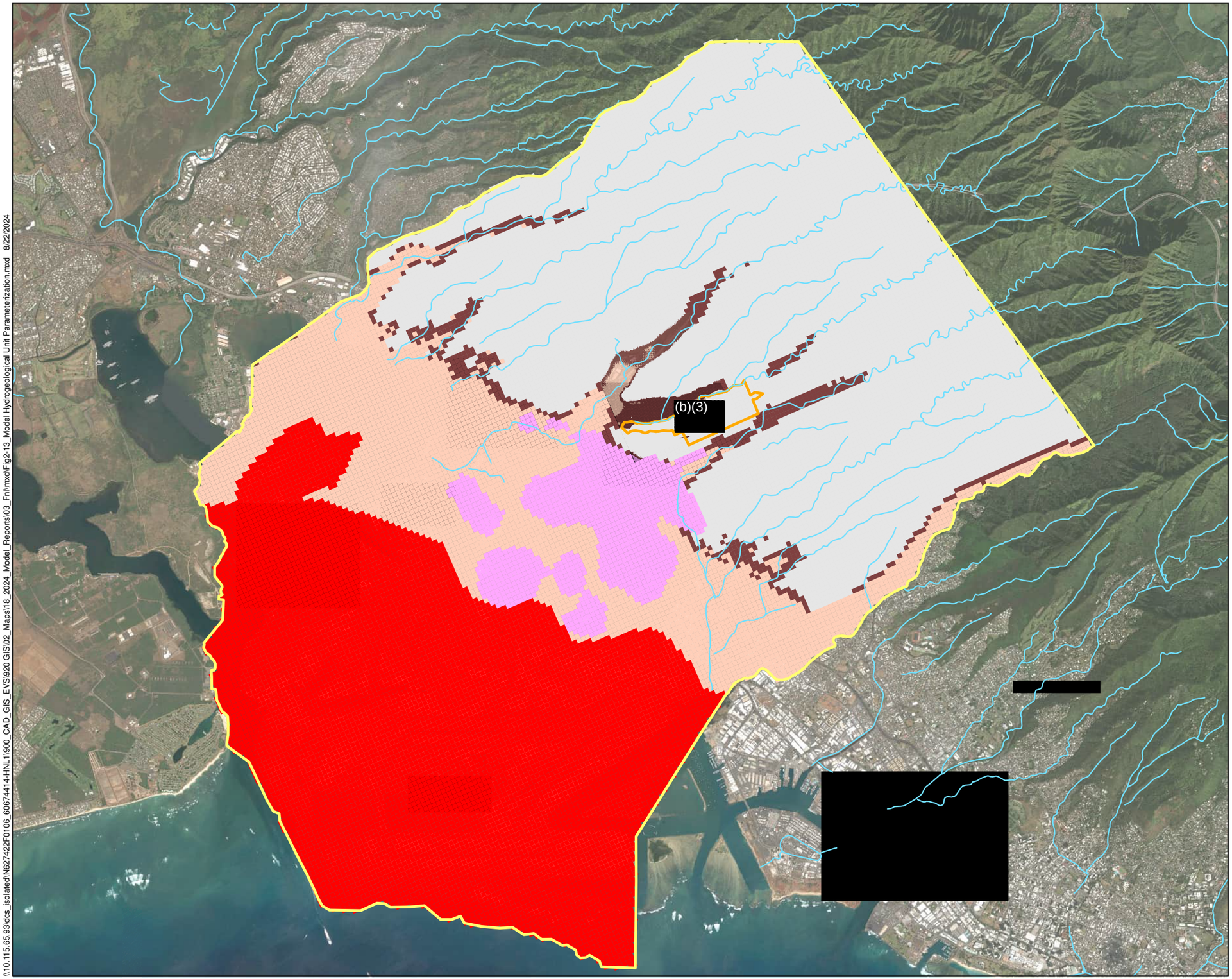

Location Map

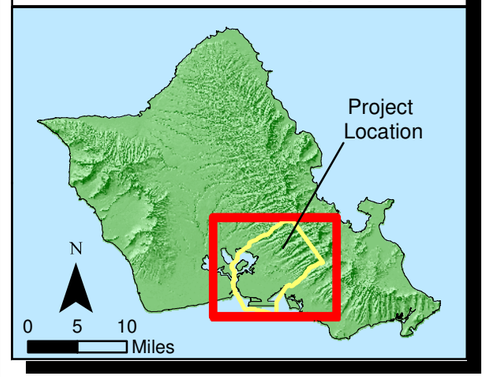

Legend

Hydrogeologic Unit Parameterization for Layer 1

- Basalt
- Saprolite
- Caprock - Alluvium / Valley Fill
- Caprock - Marine Sediments
- Tuff
- Groundwater Flow Model Domain
- Stream
- Red Hill Facility Boundary and Fuel Storage Tanks

Notes

1. Map projection: NAD 1983 Hawaii State Plane Zone 3 feet.
2. Base Map: DigitalGlobe, Inc. (DG) and NRCS. Publication_Date: 2015

N

0 5,000 10,000 15,000 Feet

Figure 2-13
Model Hydrogeological Unit Parameterization
GWFM, VZM, & CF&T Model Report
Red Hill Bulk Fuel Storage Facility
JBPHH, Oʻahu, HI

\\10.115.65.93\dcs_isolated\N627422F0106_60674414-HNL1\900_CAD_GIS_EVS\920 GIS\02_Maps\18_2024_Model_Reports\03_Fnl\mxd\Fig2-13_Model Hydrogeological Unit Parameterization.mxd 8/22/2024

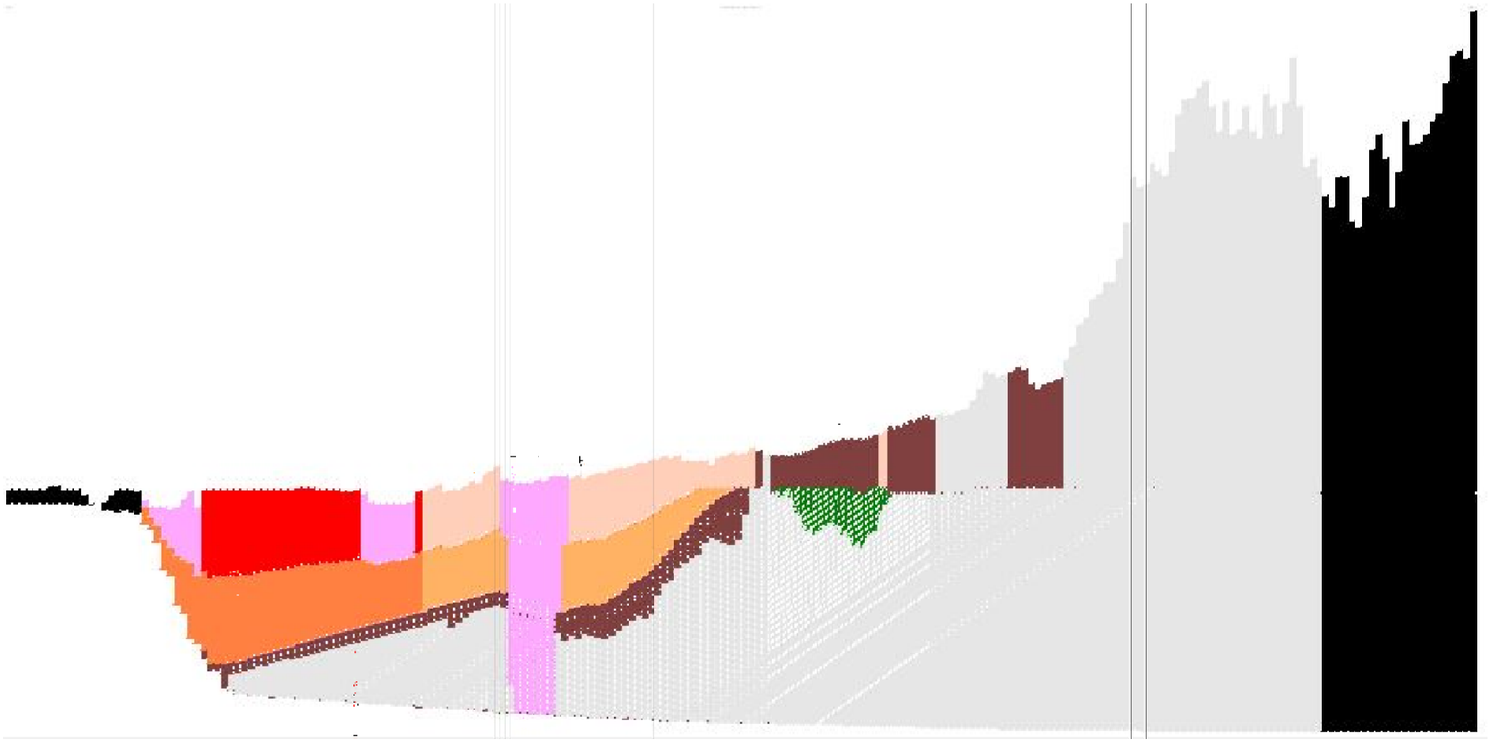

Vertical exaggeration = 10

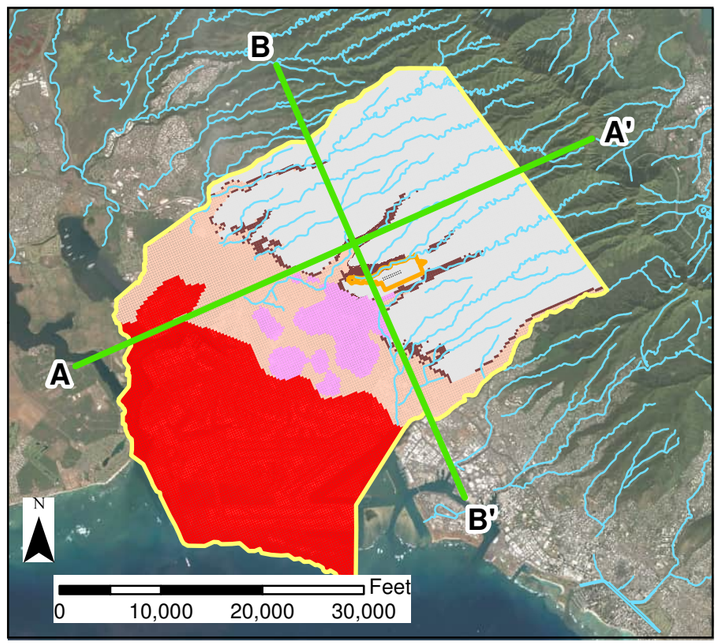

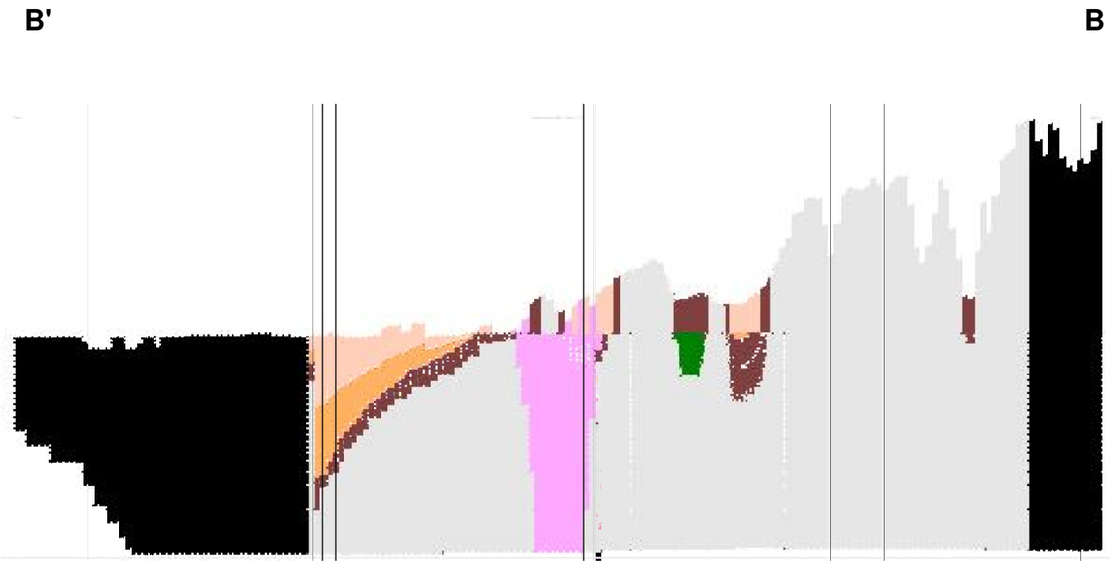

Vertical exaggeration = 10

Location Map

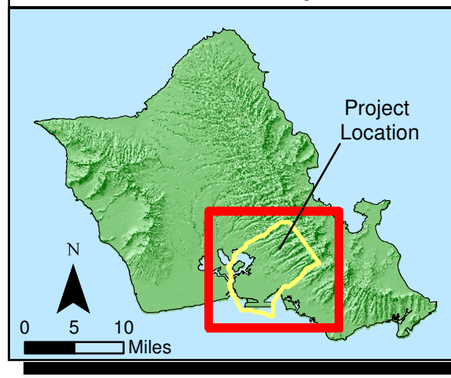

Legend

Hydrogeologic Unit Parameterization for Layer 1

- Basalt
- Saprolite
- Caprock - Alluvium/ Valley Fill
- Confining Unit
- Caprock - Marine Sediments
- Caprock - Deep Marine Sediments
- Tuff
- No Flow
- Stream
- Red Hill Facility Boundary and Fuel Storage Tanks
- Groundwater Flow Model Domain

Notes

1. Map projection: NAD 1983 Hawaii State Plane Zone 3 feet.
2. Base Map: DigitalGlobe, Inc. (DG) and NRCS. Publication_Date: 2015

Figure 2-14
Model Hydrogeological Unit Parameterization Cross Sections
GWFM, VZM, & CF&T Model Report
Red Hill Bulk Fuel Storage Facility
JBPHH, O'ahu, HI

\\10.115.65.93\dcs_isolated\N627422F0106_60674414-HNL1\900_CAD_GIS_EVS\920 GIS\02_Maps\18_2024_Model_Reports\03_Fnl\mxd\Fig2-14_Model Hydrogeological Unit X Section.mxd 8/22/2024

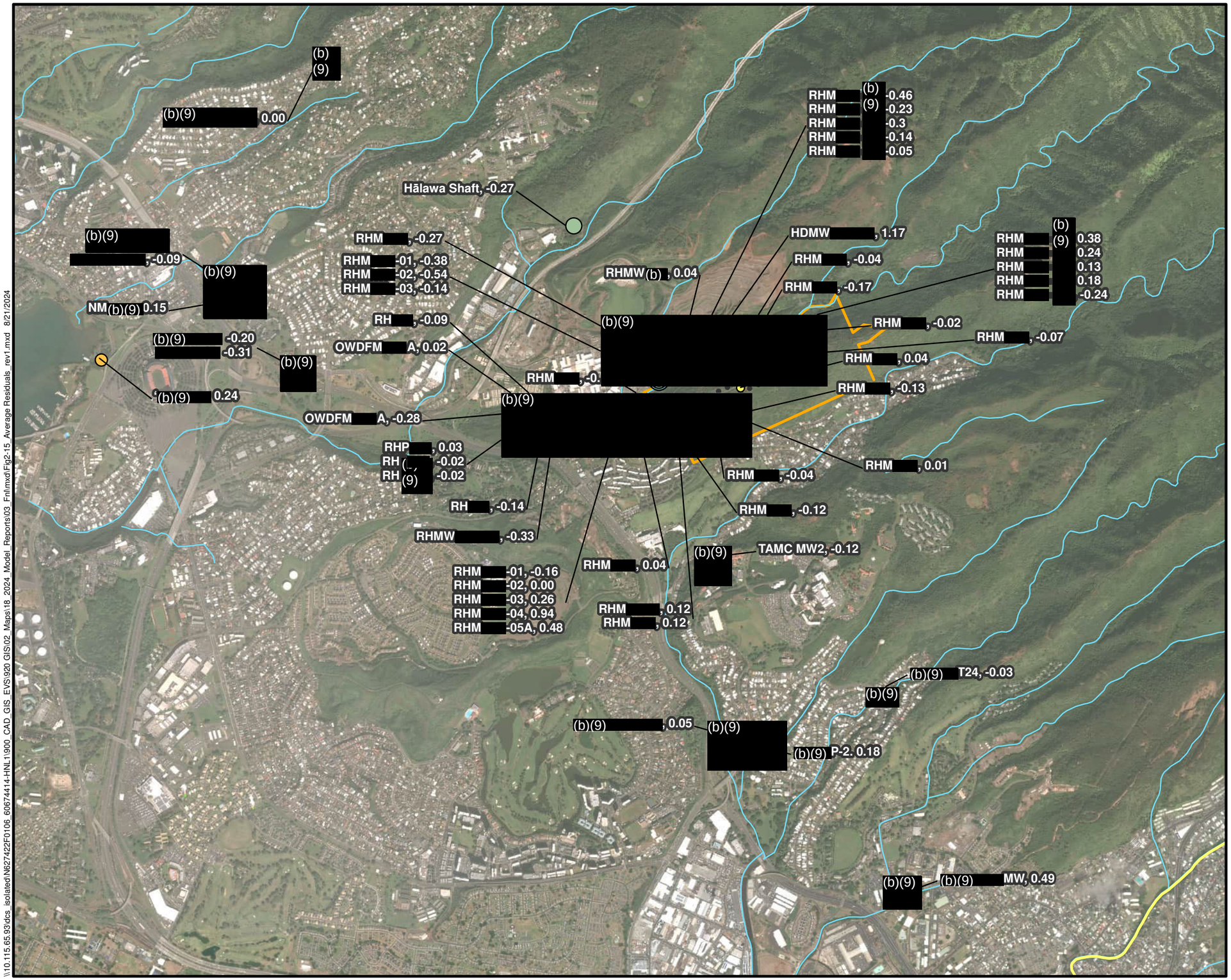

Location Map

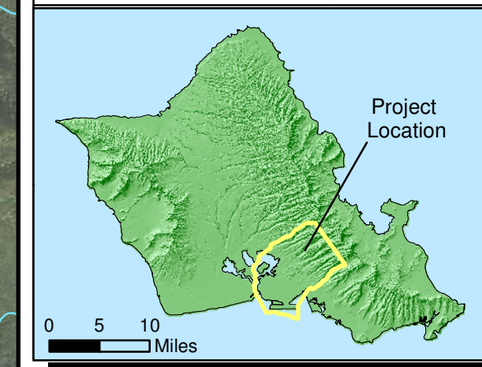

Legend

Average Residual (feet)

- > -0.8 to 0.6
- > -0.6 to -0.4
- > -0.4 to -0.2
- > -0.2 to 0
- > 0 to 0.2
- > 0.2 to 0.4
- > 0.4 to 0.6
- > 0.6 to 0.8
- > 0.8 to 1.0

MW-53,-3.63 Well, Average Residual (feet)

Groundwater Flow Model Domain

Stream

Red Hill Facility Boundary and Fuel Storage Tanks

Notes

1. Map projection: NAD 1983 Hawaii State Plane Zone 3 feet.
2. Base Map: DigitalGlobe, Inc. (DG) and NRCS. Publication_Date: 2015
3. Residual = Observed Minus Simulated Head. Positive residuals indicate simulated heads are less than observed heads. Negative residuals indicate simulated heads are greater than observed heads.

N

0 1,000 2,000 3,000 Feet

Figure 2-15
Average Residuals for Basal Aquifer Wells
GWFM, VZM, & CF&T Model Report
Red Hill Bulk Fuel Storage Facility
JBPHH, O'ahu, HI

\\10.115.65.93\dcs_isolated\N627422F0106_60674414-HNL1900_CAD_GIS_EVS\920 GIS\02_Maps\18_2024_Model_Reports\03_Fnl\mxd\Fig2-15_Average Residuals_rev1.mxd 8/21/2024

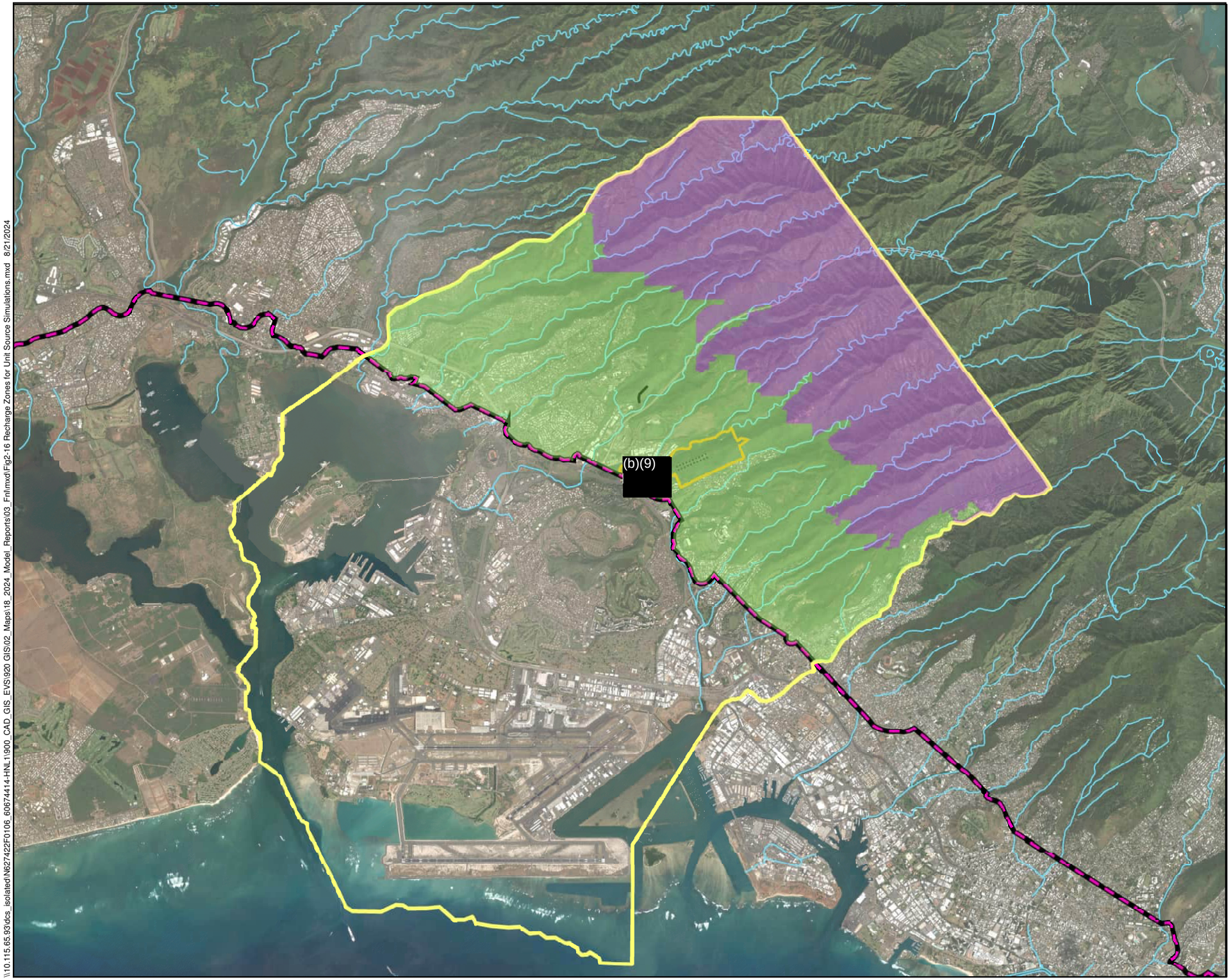

Location Map

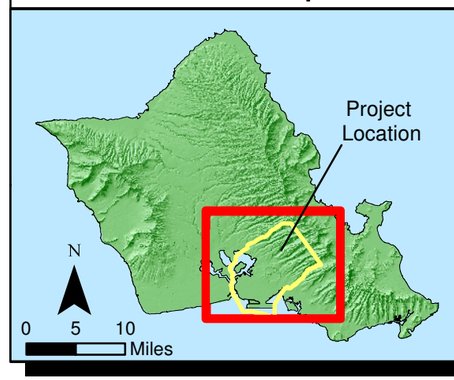

Legend

Percentage of Contribution from Saltwater Interface

- North Recharge Zone
- South Recharge Zone
- Groundwater Flow Model Domain
- Caprock Line
- Water Development Tunnel / Infiltration Gallery
- Red Hill Facility Boundary and Fuel Storage Tanks
- Stream

Notes

1. Map projection: NAD 1983 Hawaii State Plane Zone 3 feet.
2. Base Map: DigitalGlobe, Inc. (DG) and NRCS. Publication_Date: 2015

N

0 5,000 10,000 15,000 Feet

Figure 2-16
Recharge Zones for Unit Source Simulations
GWFM, VZM, & CF&T Model Report
Red Hill Bulk Fuel Storage Facility
JBPHH, O'ahu, HI

\\10.115.65.93\dcs_isolated\N627422F0106_60674414-HNL\900_CAD_GIS_EVS\920 GIS\02_Maps\18_2024_Model_Reports\03_Fnl\mxd\Fig2-16 Recharge Zones for Unit Source Simulations.mxd 8/21/2024

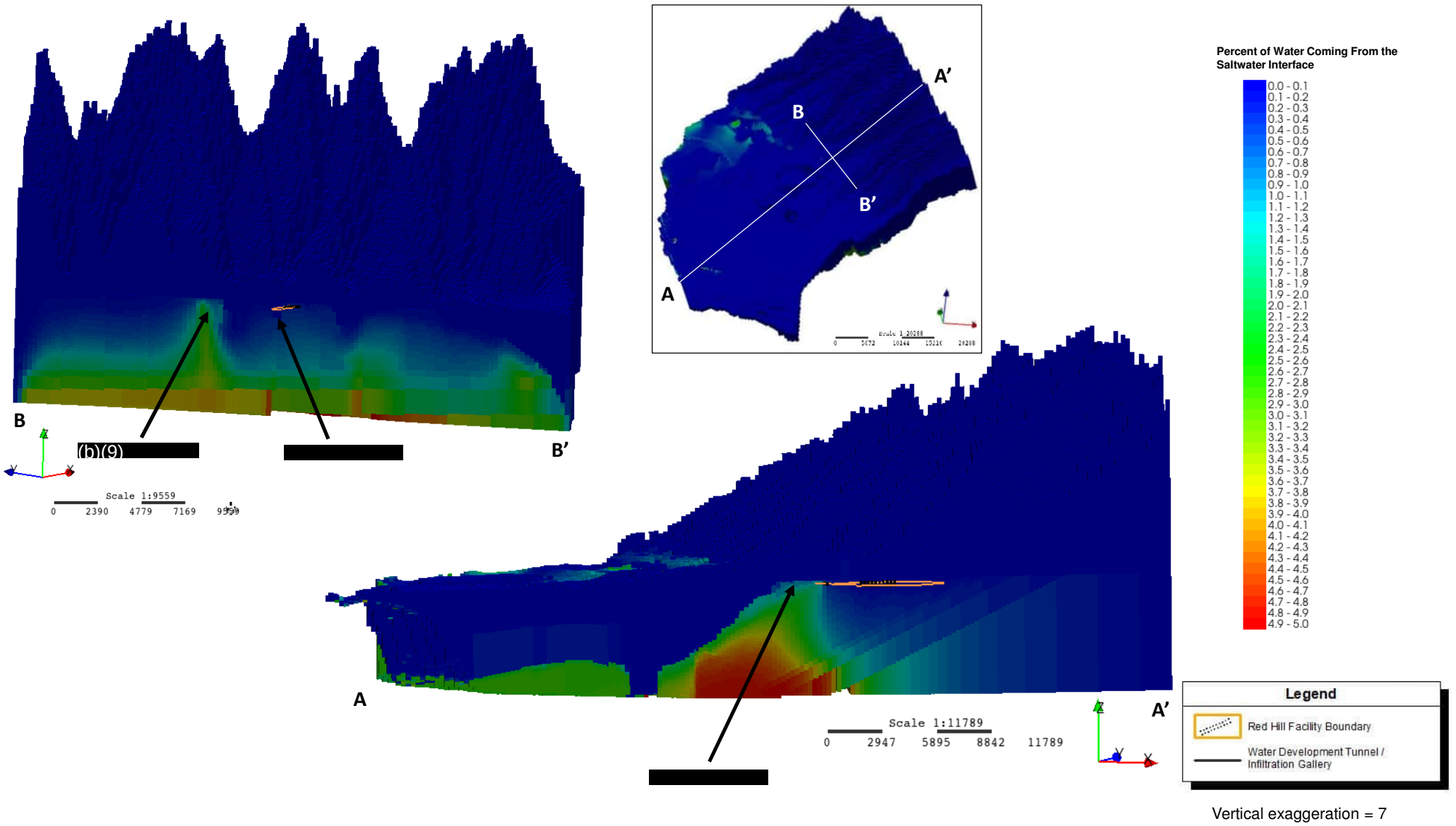

Figure 2-17
Simulation of Upconing from the Saltwater Interface
GWFM, VZM, & CF&T Model Report
Red Hill Bulk Fuel Storage Facility
JBPHH, Oʻahu, Hawaiʻi

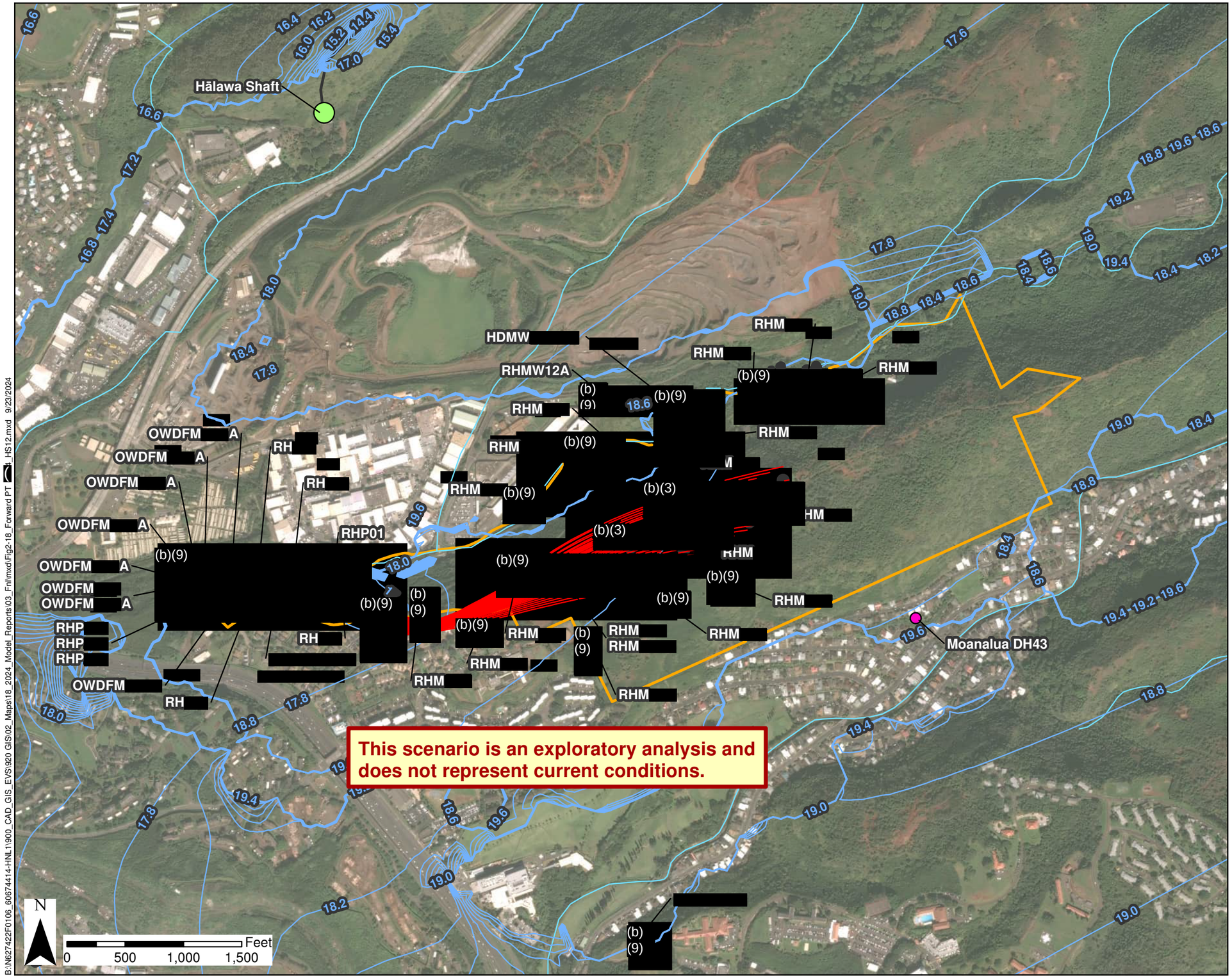

Location Map

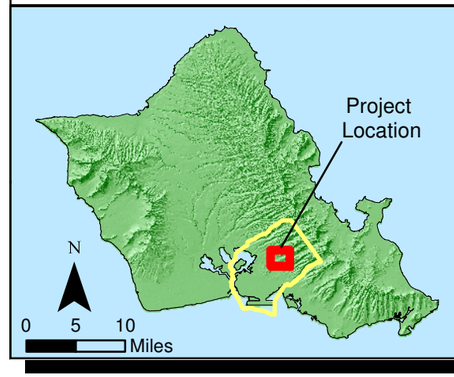

Legend

Water Supply Well / Shaft (MGD)

- 0.0 - 0.5
- 0.5 - 1.0
- 1.0 - 2.0
- 2.0 - 5.0
- 5.0 - 10.0
- 10.0 - 15.0

- Basal Aquifer Wells
- Forward Particle Track
- Potentiometric Surface (ft msl)
- Water Development Tunnel / Infiltration Gallery
- Stream
- Red Hill Facility Boundary and Fuel Storage Tanks
- Groundwater Flow Model Domain

Notes

1. Map projection: NAD 1983 Hawaii State Plane Zone 3 feet.
2. Base Map: DigitalGlobe, Inc. (DG) and NRCS. Publication_Date: 2015
3. Spring locations provided by USGS.
4. Water supply well locations provided by DLNR.

Figure 2-18
Forward Particle Tracking from Tank Farm - [redacted] Pumping at [redacted] mgd, Hālawa Shaft Pumping at 12 mgd, (b)(3) [redacted] umping at (b) [redacted] mgd
GWFM, VZM, & CF&T Model Report
Red Hill Bulk Fuel Storage Facility
JBPHH, O'ahu, HI

B:\N627422F0106_60674414-HNL1\900_CAD_GIS_EVS\920 GIS\02_Maps\18_2024_Model_Reports\03_Fnl\mxd\Fig2-18_Forward PT_HS12.mxd 9/23/2024

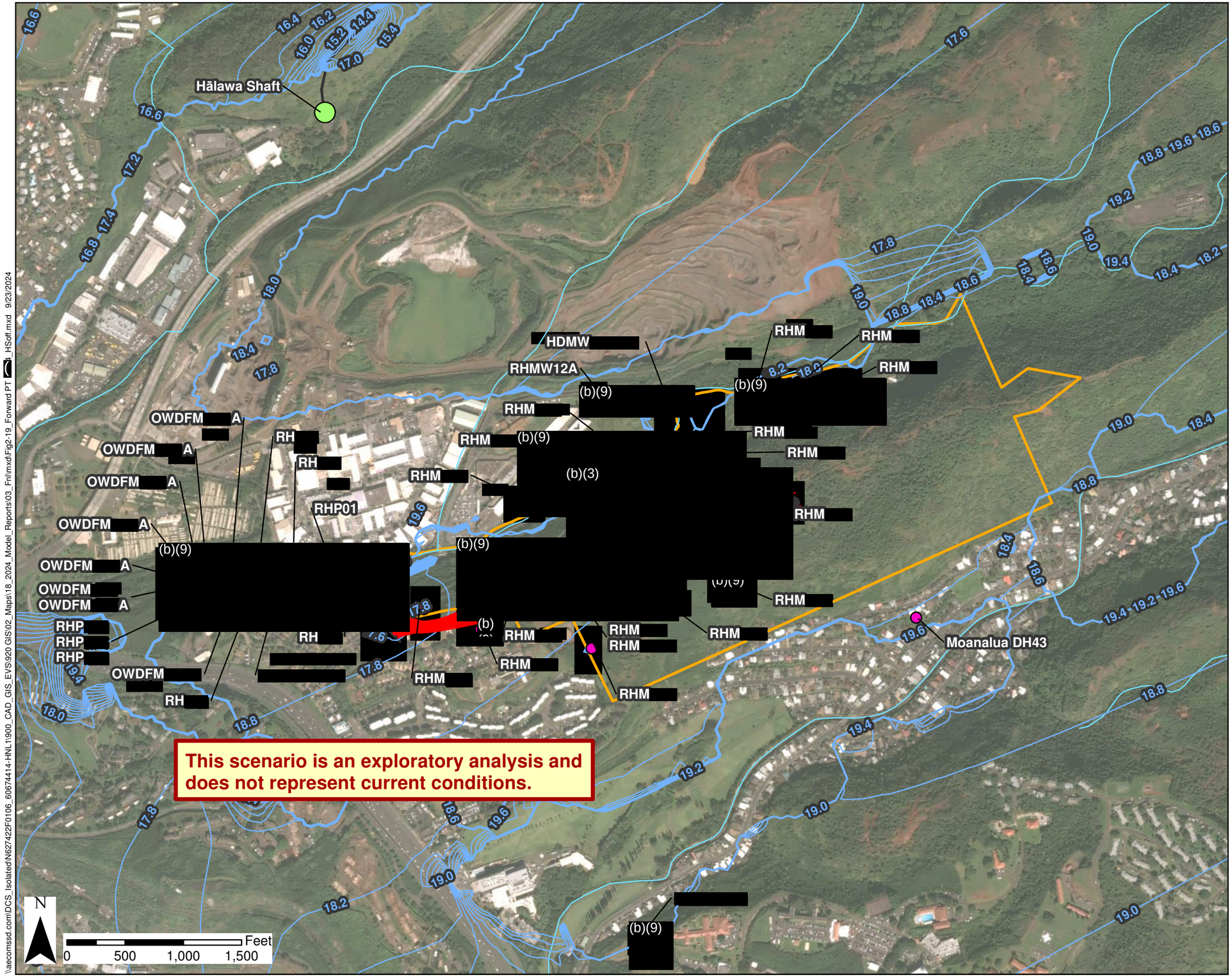

Location Map

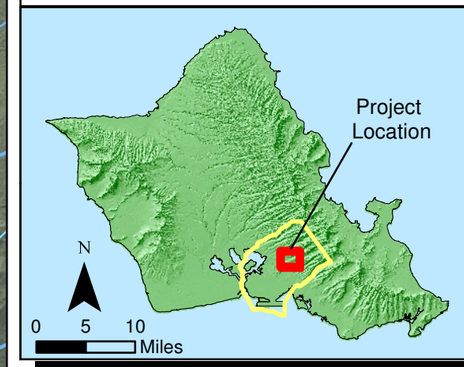

Legend

Water Supply Well / Shaft (MGD)

- 0.0 - 0.5
- 0.5 - 1.0
- 1.0 - 2.0
- 2.0 - 5.0
- 5.0 - 10.0
- 10.0 - 15.0
- Basal Aquifer Wells
- Forward Particle Tack
- Potentiometric Surface (ft msl)
- Water Development Tunnel / Infiltration Gallery
- Stream
- Red Hill Facility Boundary and Fuel Storage Tanks
- Groundwater Flow Model Domain

Notes

1. Map projection: NAD 1983 Hawaii State Plane Zone 3 feet.
2. Base Map: DigitalGlobe, Inc. (DG) and NRCS. Publication_Date: 2015
3. Spring locations provided by USGS.
4. Water supply well locations provided by DLNR.

Figure 2-19
Forward Particle Tracking from Tank Farm-[redacted] Pumping at [redacted] mgd, Hālawa Shaft Off, [redacted] Pumping [redacted]
GWFM, VZM, & CF&T Model Report
Red Hill Bulk Fuel Storage Facility
JBPHH, Oʻahu, HI

\\aecomssd.com\DCS_Isolated\N627422F0106_60674414-HNL1\900_CAD_GIS_EVS\920 GIS\02_Maps\18_2024_Model_Reports\03_Fnl\mxd\Fig2-19_Forward PT [redacted]_HSoff.mxd 9/23/2024

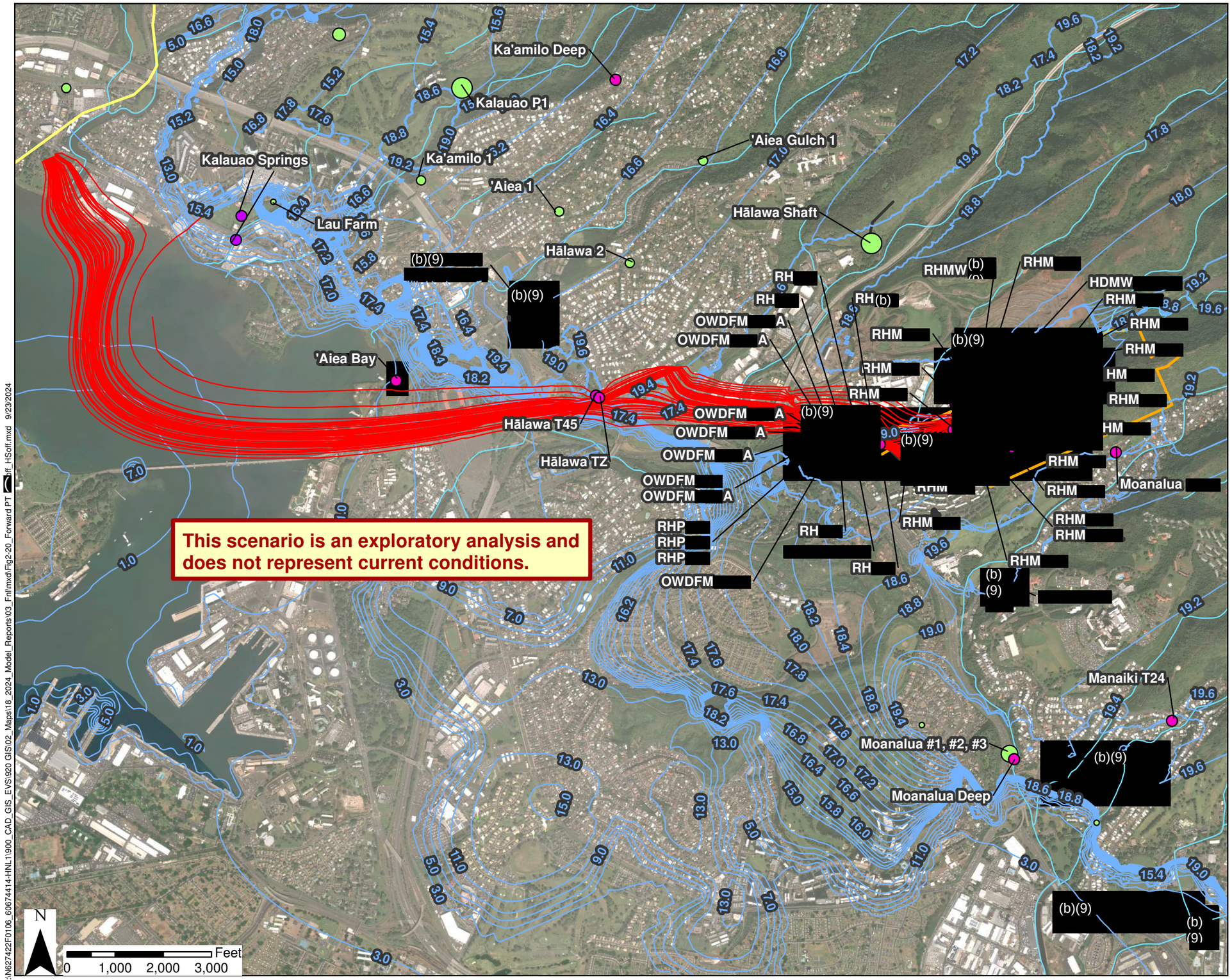

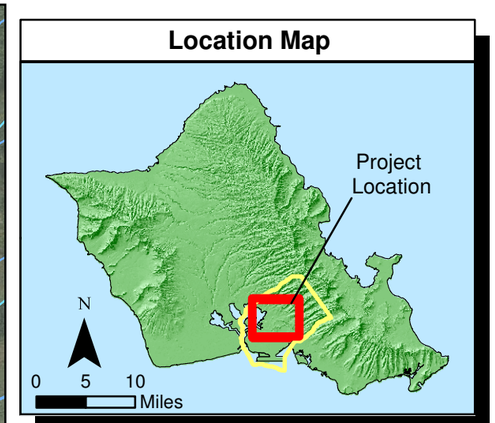

Legend

Water Supply Well / Shaft (MGD)

- 0.0 - 0.5
- 0.5 - 1.0
- 1.0 - 2.0
- 2.0 - 5.0
- 5.0 - 10.0
- 10.0 - 15.0

- Basal Aquifer Well
- Spring
- Forward Particle Track
- Potentiometric Surface (ft msl)
- Water Development Tunnel / Infiltration Gallery
- Stream
- Red Hill Facility Boundary and Fuel Storage Tanks
- Groundwater Flow Model Domain

Notes

1. Map projection: NAD 1983 Hawaii State Plane Zone 3 feet.
2. Base Map: DigitalGlobe, Inc. (DG) and NRCS. Publication_Date: 2015
3. Spring locations provided by USGS.
4. Water supply well locations provided by DLNR.

Figure 2-20
Forward Particle Tracking from Tank Farm-[redacted], Hālawa Shaft Off, N[redacted] Pumping [redacted]
GWFM, VZM, & CF&T Model Report
Red Hill Bulk Fuel Storage Facility
JBPHH, O'ahu, HI

B:\N627422F0106_60674414-HNL11900_CAD_GIS_EVS\920 GIS\02_Maps\18_2024_Model_Reports\03_Fnl\mxd\Fig2-20_Forward PT_Off_HSoff.mxd 9/23/2024

Ka'amilo Deep
Kalauao P1
'Aiea Gulch 1
Kalauao Springs
Ka'amilo 1
'Aiea 1
Lau Farm
Hālawa Shaft
Hālawa 2
(b)(9)
RH
RHP
RHMW1
RHM
HDMW
OWDFM
Hālawa T45
Hālawa TZ
Moanalua
Manaiki T24
Moanalua #1, #2, #3
Moanalua Deep

This scenario is an exploratory analysis and does not represent current conditions.

N
0 1,000 2,000 3,000 Feet

B:\N627422F0106_60674414-HNL\1900_CAD_GIS_EVS\920 GIS\02_Maps\18_2024_Model_Reports\03_Fnl\mxd\Fig2-21_Forward PT (b)(3) 9bff_HSoff.mxd 9/5/2024

Location Map

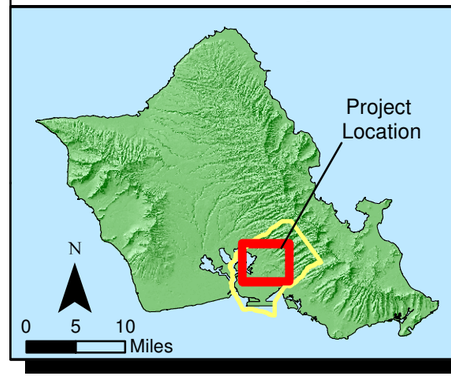

Legend

Water Supply Well / Shaft (MGD)

- 0.0 - 0.5
- 0.5 - 1.0
- 1.0 - 2.0
- 2.0 - 5.0
- 5.0 - 10.0
- 10.0 - 15.0
- Basal Aquifer Wells
- Spring
- Forward Particle Track
- Potentiometric Surface (ft msl)
- Water Development Tunnel / Infiltration Gallery
- Stream
- Red Hill Facility Boundary and Fuel Storage Tanks
- Groundwater Flow Model Domain

Notes

1. Map projection: NAD 1983 Hawaii State Plane Zone 3 feet.
2. Base Map: DigitalGlobe, Inc. (DG) and NRCS. Publication_Date: 2015
3. Spring locations provided by USGS.
4. Water supply well locations provided by DLNR.

Figure 2-21
Forward Particle Tracking from Tank Farm-[redacted], Hālawa Shaft 12 mgd, (b)(3) [redacted]f.
GWFM, VZM, & CF&T Model Report
Red Hill Bulk Fuel Storage Facility
JBPHH, O'ahu, HI

This scenario is an exploratory analysis and does not represent current conditions.

Ka'amilo Deep
Kalauao P1
'Aiea Gulch 1
Kalauao Springs
Ka'amilo 1
'Aiea 1
Lau Farm
Hālawa Shaft
Hālawa 2
(b)(9)
'Aiea Bay
Hālawa T45
Hālawa TZ
RH
RHMW12A
RHM
HDMW
RHP01
OWDFM A
RHP
Moanalua
Manaiki T24
Moanalua #1, #2, #3
Moanalua Deep
N
Feet
0 1,000 2,000 3,000

Location Map

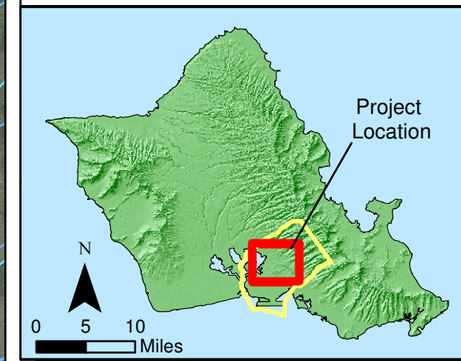

Legend

Water Supply Well / Shaft (MGD)

- 0.0 - 0.5
- 0.5 - 1.0
- 1.0 - 2.0
- 2.0 - 5.0
- 5.0 - 10.0
- 10.0 - 15.0
- Basal Aquifer Wells
- Spring
- Forward Particle Track
- Potentiometric Surface (ft msl)
- Water Development Tunnel / Infiltration Gallery
- Stream
- Red Hill Facility Boundary and Fuel Storage Tanks
- Groundwater Flow Model Domain

Notes

1. Map projection: NAD 1983 Hawaii State Plane Zone 3 feet.
2. Base Map: DigitalGlobe, Inc. (DG) and NRCS. Publication_Date: 2015
3. Spring locations provided by USGS.
4. Water supply well locations provided by DLNR.

Figure 2-22
Forward Particle Tracking from Tank Farm- [redacted] mgd, Hālawa Shaft Off, (b)(3)
GWFM, VZM, & CF&T Model Report
Red Hill Bulk Fuel Storage Facility
JBPHH, O'ahu, HI

B:\N627422F0106_60674414-HNL1\900_CAD_GIS_EVS\920 GIS\02_Maps\18_2024_Model_Reports\03_Fnl\mxd\Fig2-22_Forward PT_HSoff.mxd 9/5/2024

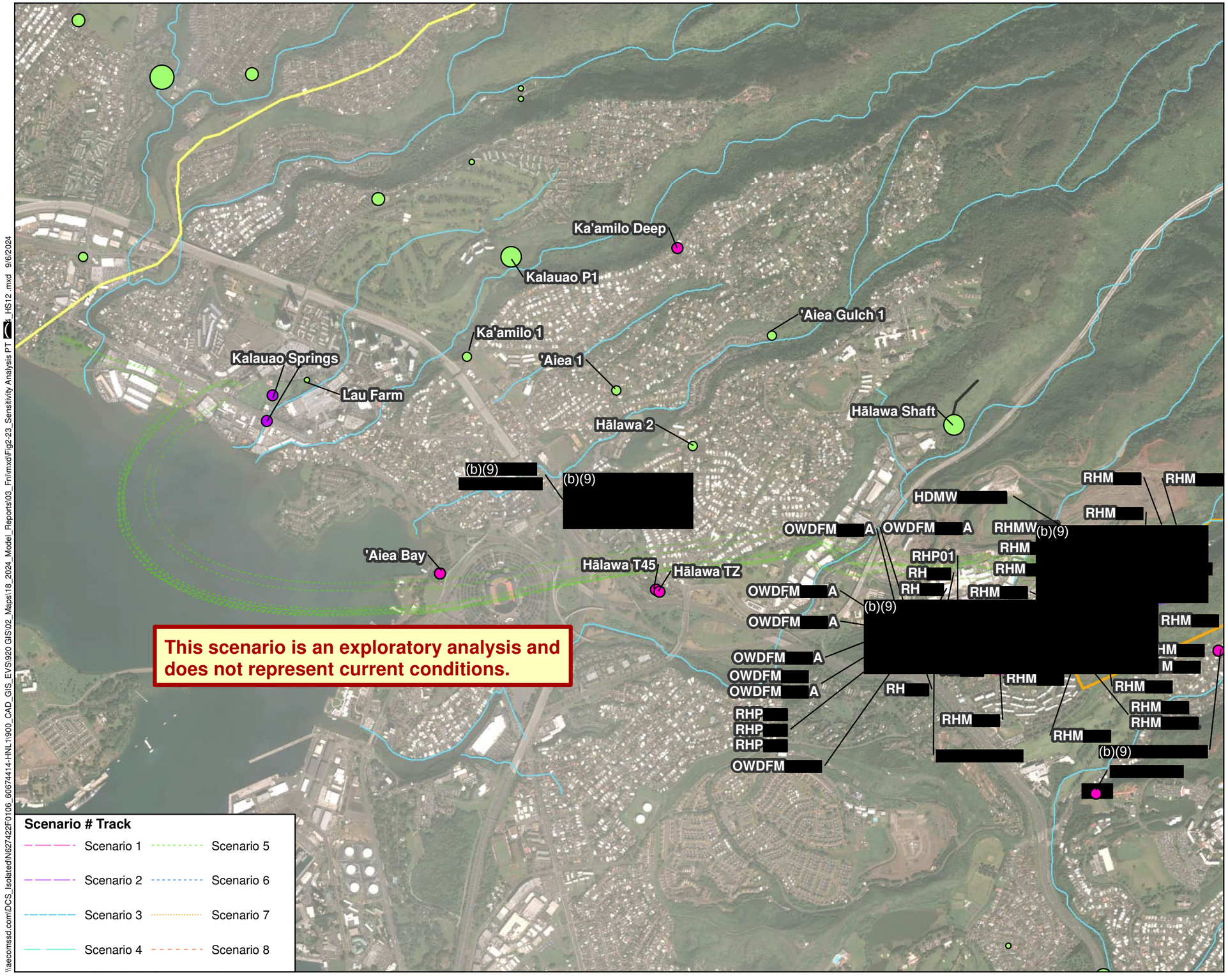

Location Map

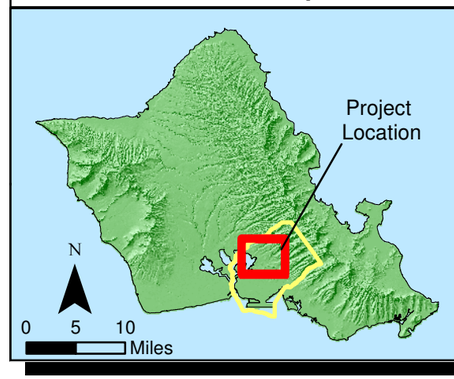

Legend

Water Supply Well / Shaft (MGD)

- 0.0 - 0.5
- 0.5 - 1.0
- 1.0 - 2.0
- 2.0 - 5.0
- 5.0 - 10.0
- 10.0 - 15.0
- Basal Aquifer Well
- Spring
- Groundwater Flow Model Domain
- Water Development Tunnel / Infiltration Gallery
- Stream
- Red Hill Facility Boundary

Notes

1. Map projection: NAD 1983 Hawaii State Plane Zone 3 feet.
2. Base Map: DigitalGlobe, Inc. (DG) and NRCS. Publication_Date: 2015
3. Spring locations provided by USGS.
4. Water supply well locations provided by DLNR.

N

0 1,000 2,000 3,000 Feet

Figure 2-23
Sensitivity Analysis Particle Tracking - [redacted] Pumping at [redacted] mgd, Hālawa Shaft Pumping at 12 mgd, (b)(3) [redacted]
GWFM, VZM, & CF&T Model Report
Red Hill Bulk Fuel Storage Facility
JBPHH, O'ahu, HI

\\aecomssd.com\DCS_Isolated\N627422F0106_60674414-HNL1\900_CAD_GIS_EVS\920 GIS\02_Maps\18_2024_Model_Reports\03_Fnl\mxd\Fig2-23_Sensitivity Analysis PT (b)(3)_HS12.mxd 9/6/2024

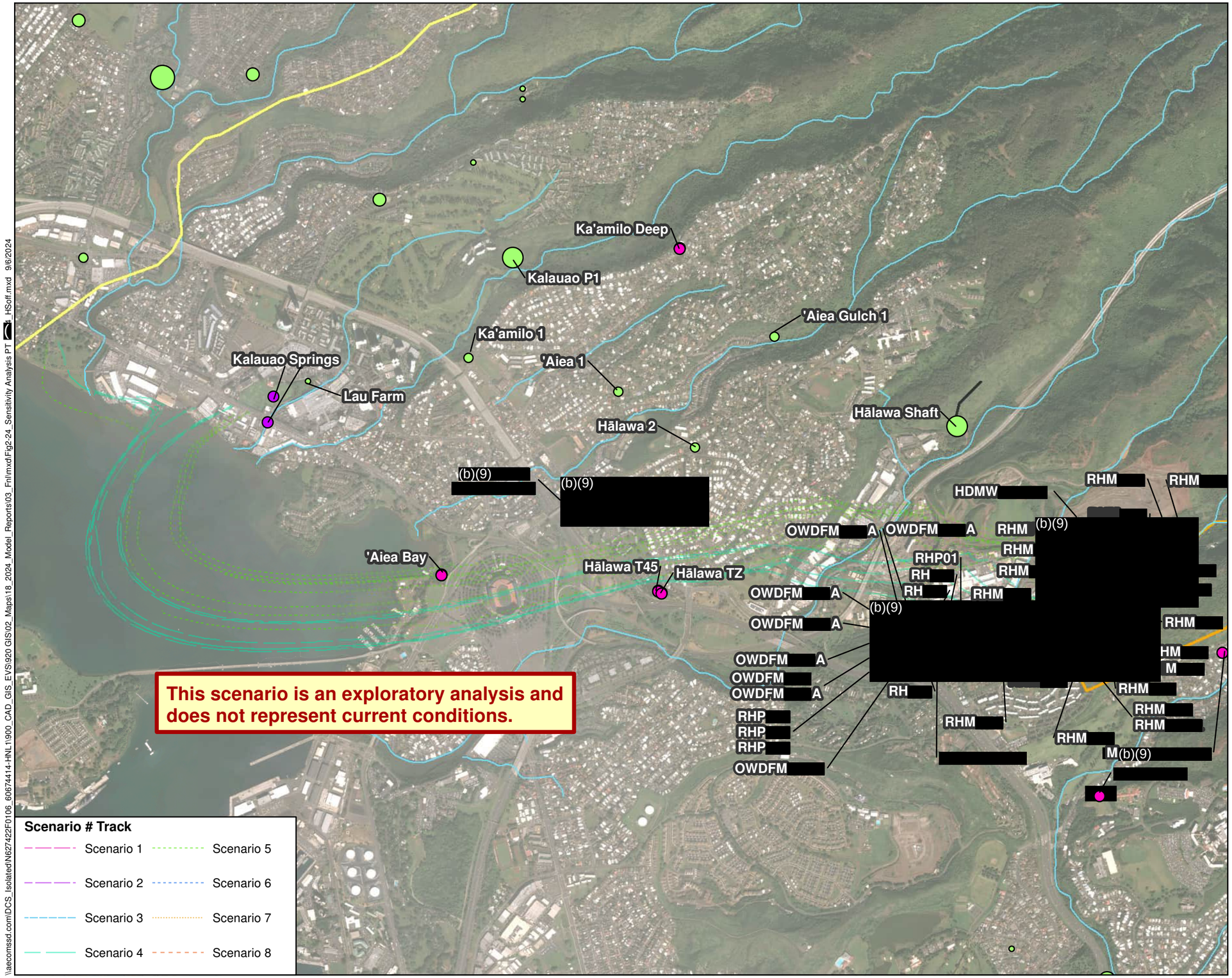

Location Map

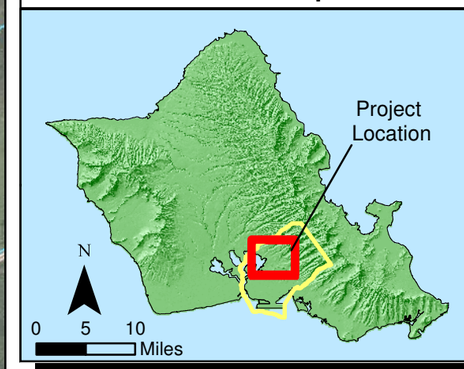

Legend

Water Supply Well / Shaft (MGD)

- 0.0 - 0.5
- 0.5 - 1.0
- 1.0 - 2.0
- 2.0 - 5.0
- 5.0 - 10.0
- 10.0 - 15.0
- Basal Aquifer Well
- Spring
- Water Development Tunnel / Infiltration Gallery
- Groundwater Flow Model Domain
- Stream
- Red Hill Facility Boundary and Fuel Storage Tanks

Notes

1. Map projection: NAD [redacted]3 Hawaii State Plane Zone 3 feet.
2. Base Map: DigitalGlobe, Inc. (DG) and NRCS. Publication_Date: 2015
3. Spring locations provided by USGS.
4. Water supply well locations provided by DLNR.

N

0 1,000 2,000 3,000 Feet

Figure 2-24
Sensitivity Analysis Particle Tracking - [redacted] Pumping at (b) mgd, Hālawa Shaft Pumping Off, (b)(3) [redacted]
GWFM, VZM, & CF&T Model Report
Red Hill Bulk Fuel Storage Facility
JBPHH, O'ahu, HI

\\aecomssd.com\DCS_Isolated\N\627422F0106_60674414-HNL1900_CAD_GIS_EVS\920 GIS\02_Maps\18_2024_Model_Reports\03_Fnl\mxd\Fig2-24_Sensitivity Analysis PT_HSoff.mxd 9/6/2024

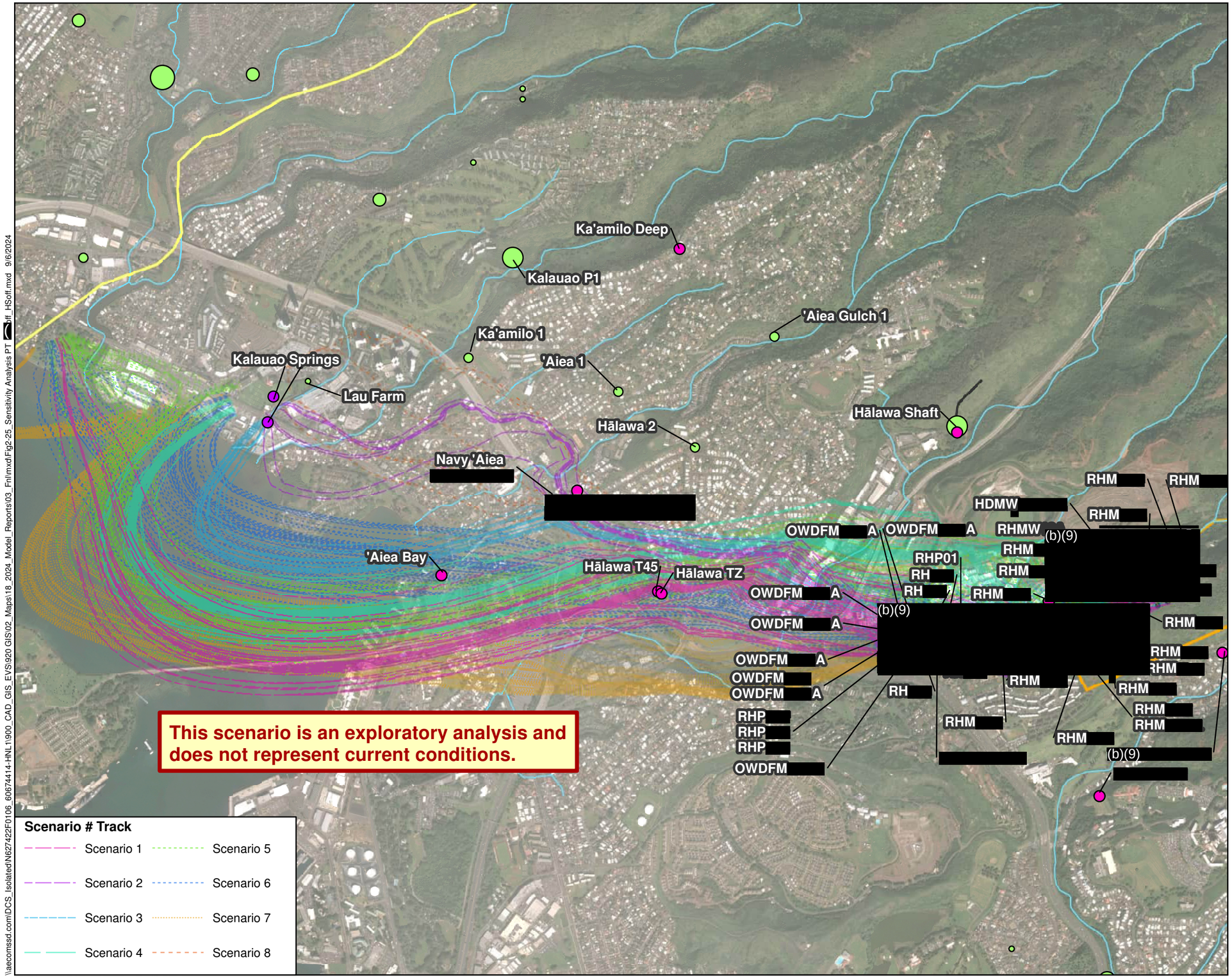

Location Map

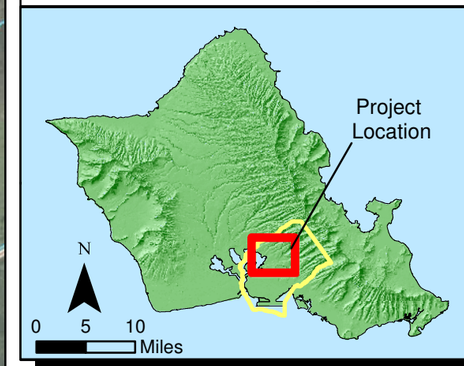

Legend

Water Supply Well / Shaft (MGD)

- 0.0 - 0.5
- 0.5 - 1.0
- 1.0 - 2.0
- 2.0 - 5.0
- 5.0 - 10.0
- 10.0 - 15.0
- Basal Aquifer Well
- Spring
- Groundwater Flow Model Domain
- Water Development Tunnel / Infiltration Gallery
- Stream
- Red Hill Facility Boundary and Fuel Storage Tanks

Notes

1. Map projection: NAD 1983 Hawaii State Plane Zone 3 feet.
2. Base Map: DigitalGlobe, Inc. (DG) and NRCS. Publication_Date: 2015
3. Spring locations provided by USGS.
4. Water supply well locations provided by DLNR.

N

0 1,000 2,000 3,000 Feet

Figure 2-25
Sensitivity Analysis Particle Tracking - [redacted] Pumping(b)
Hālawa Shaft Pumping Off,
(b)(3) [redacted]
GWFM, VZM, & CF&T Model Report
Red Hill Bulk Fuel Storage Facility
JBPHH, O'ahu, HI

\\aecomssd.com\DCS_Isolated\N627422F0106_60674414-HNL11900_CAD_GIS_EVS\920 GIS\02_Maps\18_2024_Model_Reports\03_Fnl\mxd\Fig2-25_Sensitivity Analysis PT (b)(3)ff_HSoff.mxd 9/6/2024

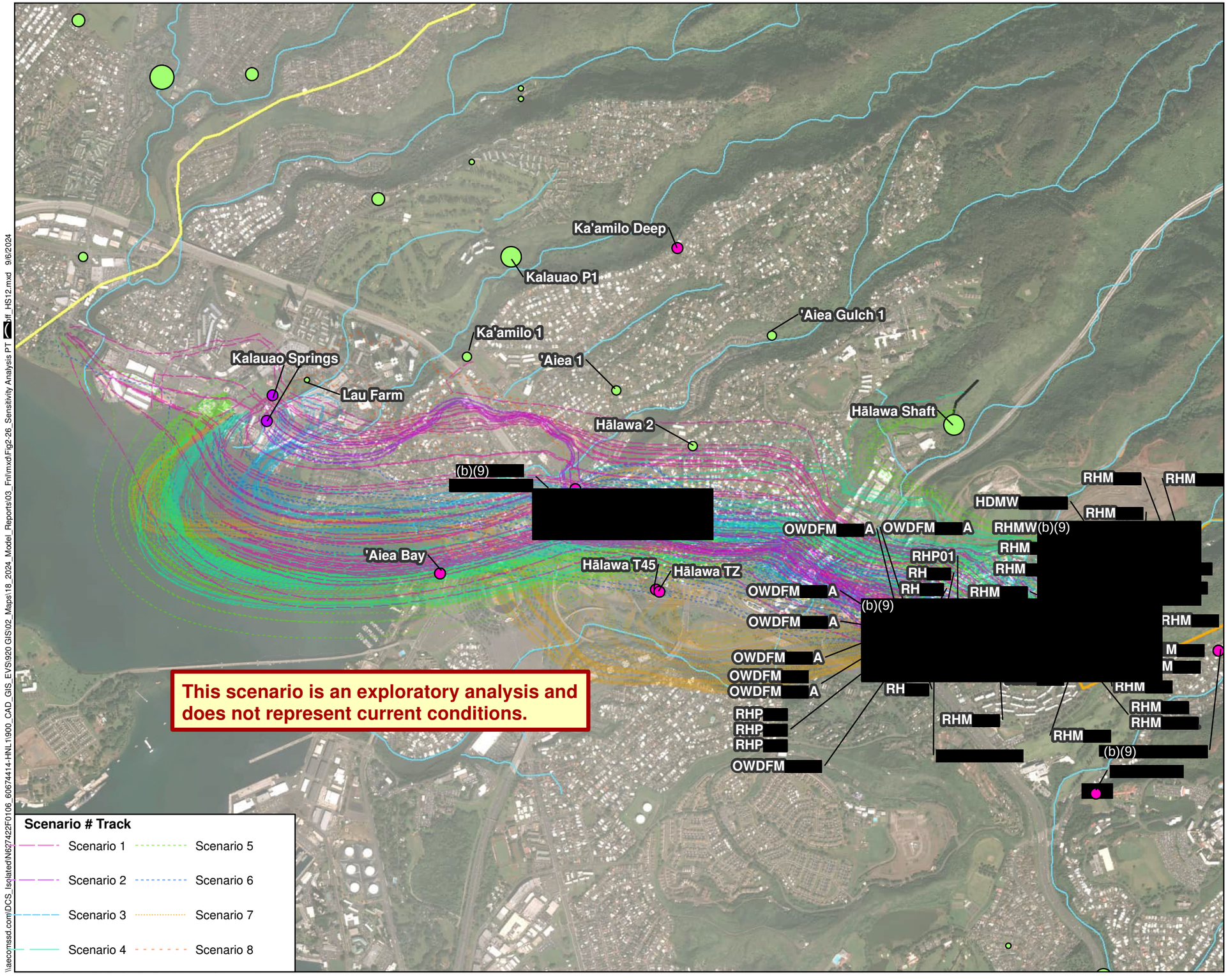

Location Map

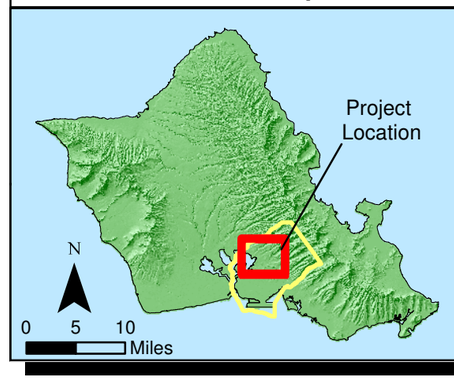

Legend

Water Supply Well / Shaft (MGD)

- 0.0 - 0.5
- 0.5 - 1.0
- 1.0 - 2.0
- 2.0 - 5.0
- 5.0 - 10.0
- 10.0 - 15.0
- Basal Aquifer Well
- Spring
- Water Development Tunnel / Infiltration Gallery
- Groundwater Flow Model Domain
- Stream
- Red Hill Facility Boundary and Fuel Storage Tanks

Notes

1. Map projection: NAD 1983 Hawaii State Plane Zone 3 feet.
2. Base Map: DigitalGlobe, Inc. (DG) and NRCS. Publication_Date: 2015
3. Spring locations provided by USGS.
4. Water supply well locations provided by DLNR.

N

0 1,000 2,000 3,000 Feet

Figure 2-26
Sensitivity Analysis Particle Tracking - [redacted] Pumping (b)
Hālawa Shaft Pumping at 12 mgd, (b)(3)
GWFM, VZM, & CF&T Model Report
Red Hill Bulk Fuel Storage Facility
JBPHH, O'ahu, HI

\\aecomssd.com\DCS_Isolated\N627422F0106_60674414-HNL1\900_CAD_GIS_EVS\920 GIS\02_Maps\18_2024_Model_Reports\03_Fnl\mxd\Fig2-26_Sensitivity Analysis PT (b)(3)_HS12.mxd 9/6/2024

Kalauao P1
Ka'amilo Deep
Ka'amilo 1
'Aiea Gulch 1
Kalauao Springs
'Aiea 1
Lau Farm
Hālawa 2
Hālawa Shaft
(b)(9)
'Aiea Bay
Hālawa T45
Hālawa TZ
OWDFM A
RHP01
RH
RHM
HDMW
RHMW
RHP
OWDFM
(b)(9)

This scenario is an exploratory analysis and does not represent current conditions.

Scenario # Track

- Scenario 1
- Scenario 2
- Scenario 3
- Scenario 4
- Scenario 5
- Scenario 6
- Scenario 7
- Scenario 8

Location Map

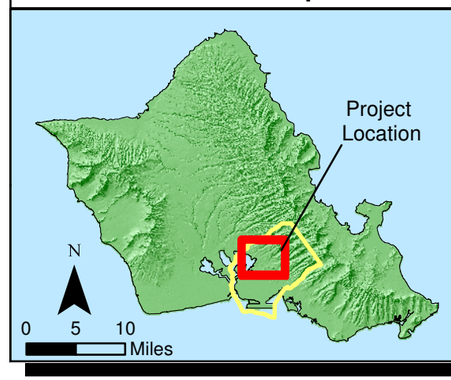

Legend

Water Supply Well / Shaft (MGD)

- 0.0 - 0.5
- 0.5 - 1.0
- 1.0 - 2.0
- 2.0 - 5.0
- 5.0 - 10.0
- 10.0 - 15.0
- Basal Aquifer Well
- Spring
- Water Development Tunnel / Infiltration Gallery
- Groundwater Flow Model Domain
- Stream
- Red Hill Facility Boundary and Fuel Storage Tanks

Notes

1. Map projection: NAD [redacted]3 Hawaii State Plane Zone 3 feet.
2. Base Map: DigitalGlobe, Inc. (DG) and NRCS. Publication_Date: 2015
3. Spring locations provided by USGS.
4. Water supply well locations provided by DLNR.

N

0 1,000 2,000 3,000 Feet

Figure 2-27
Sensitivity Analysis Paticle Tracking - [redacted] Pumping [redacted] mgd, Hālawa Shaft Pumping Off, (b)(3) [redacted]
GWFM, VZM, & CF&T Model Report
Red Hill Bulk Fuel Storage Facility
JBPHH, O'ahu, HI

\\aecomssd.com\DCS_Isolated\N627422F0106_60674414-HNL\1900_CAD_GIS_EVS\920 GIS\02_Maps\18_2024_Model_Reports\03_Fnl\mxd\Fig2-27_Sensitivity Analysis PT [redacted] HSoll.mxd 9/6/2024

Location Map

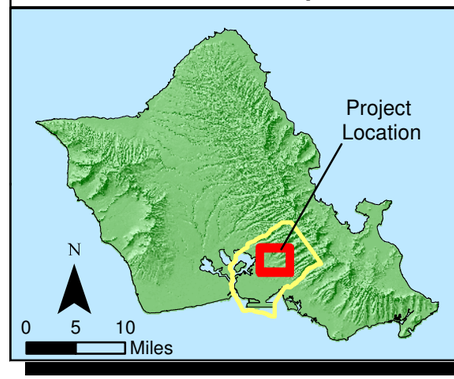

Legend

- Boring
- Water Development Tunnel / Infiltration Gallery
- Nested Grid
- Stream
- Red Hill Facility Boundary and Barrel Logs
- Groundwater Flow Model Domain

Notes

1. Map projection: NAD 1983 Hawaii State Plane Zone 3 feet.
2. Base Map: DigitalGlobe, Inc. (DG) and NRCS. Publication_Date: 2015
3. Spring locations provided by USGS.
4. Water supply well locations provided by DLNR.

N

0 1,000 2,000 3,000 Feet

Figure 3-1
Available Geology Data for Use in Developing Basalt Realizations
GWFM, VZM, & CF&T Model Report
Red Hill Bulk Fuel Storage Facility
JBPHH, O'ahu, HI

\\10.115.65.93\dcs_isolated\N627422F0106_60674414-HNL1\900_CAD_GIS_EVS\920 GIS\02_Maps\18_2024_Model_Reports\03_Fnl\mxd\Fig3-1_Geology_Data_for_Basalt_Realizations.mxd 8/29/2024

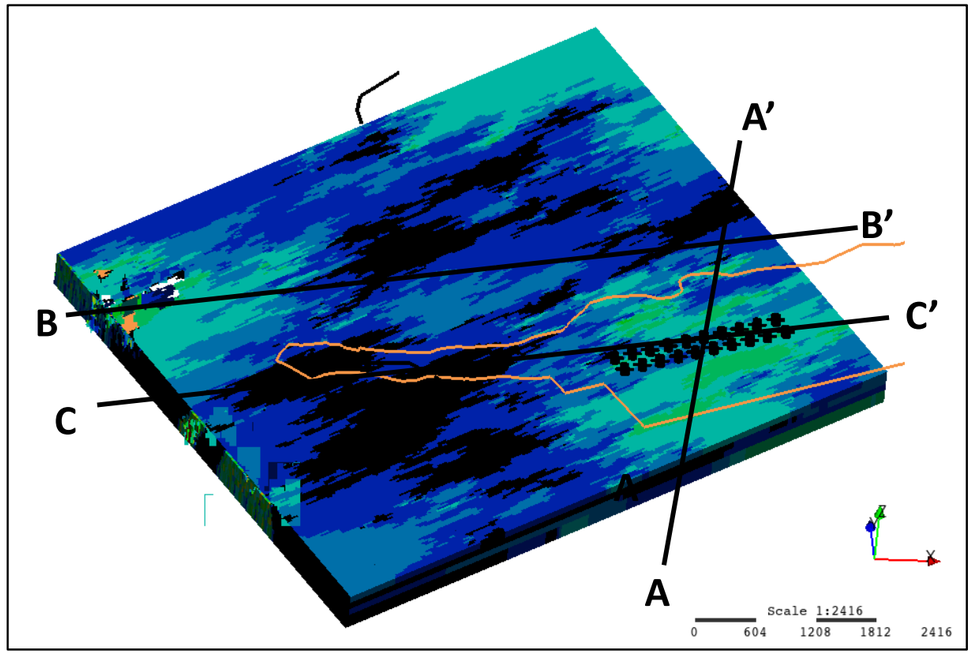

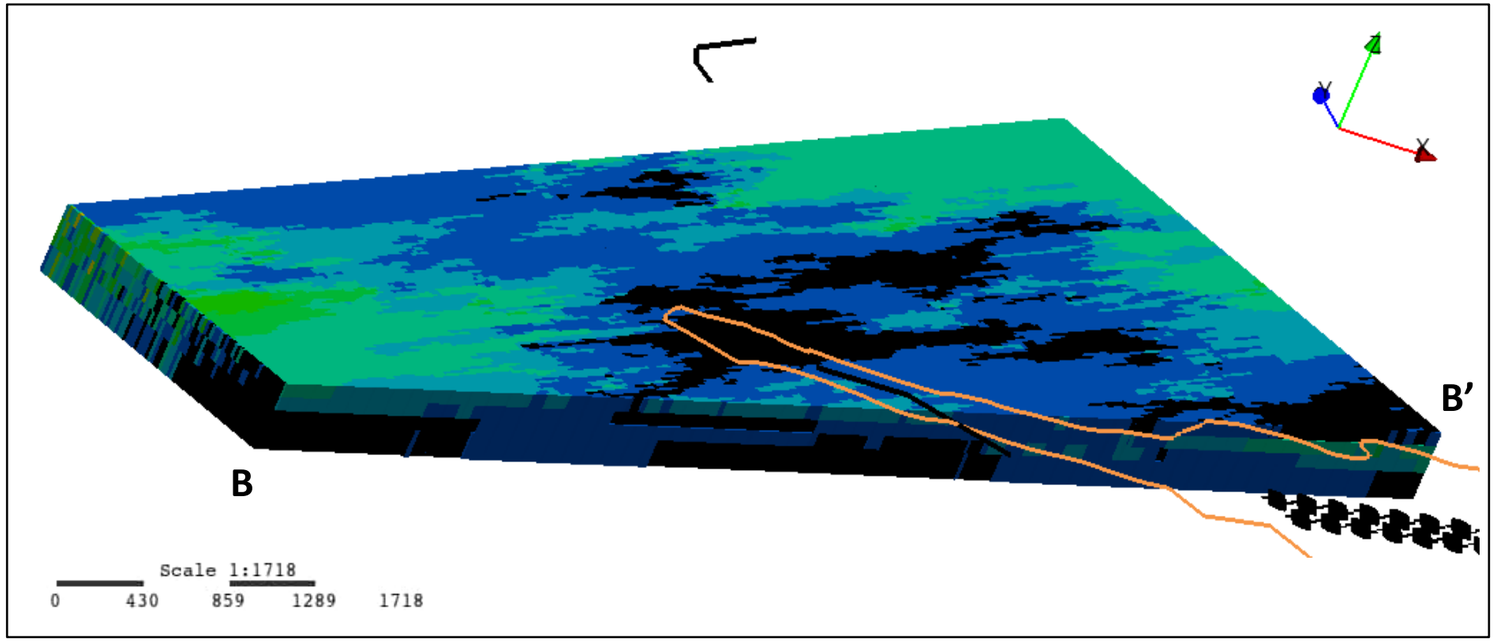

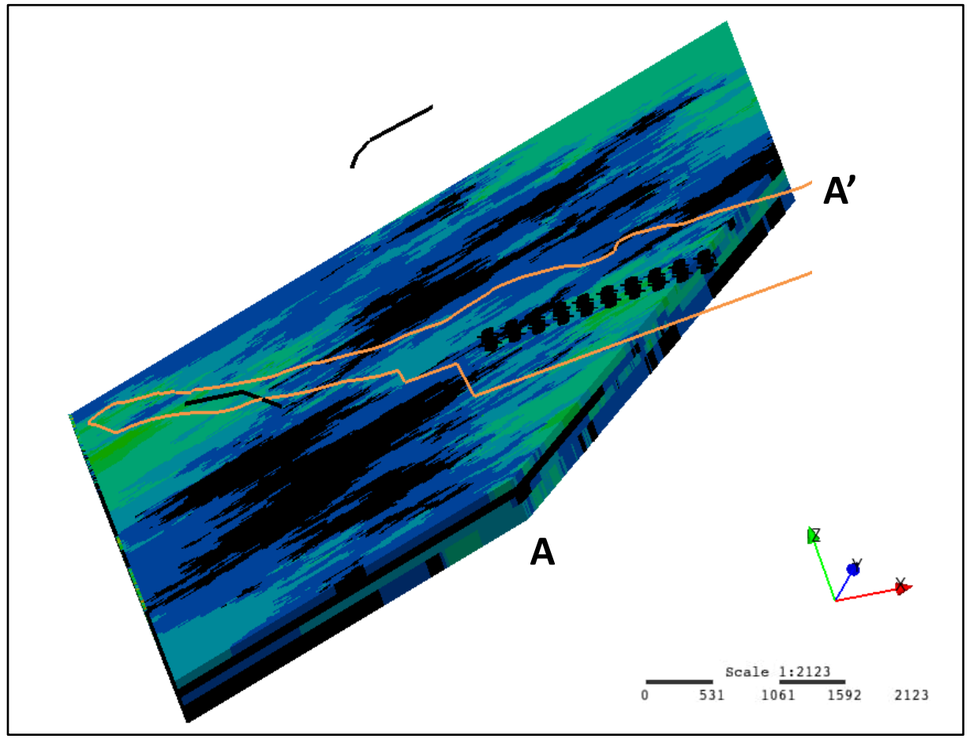

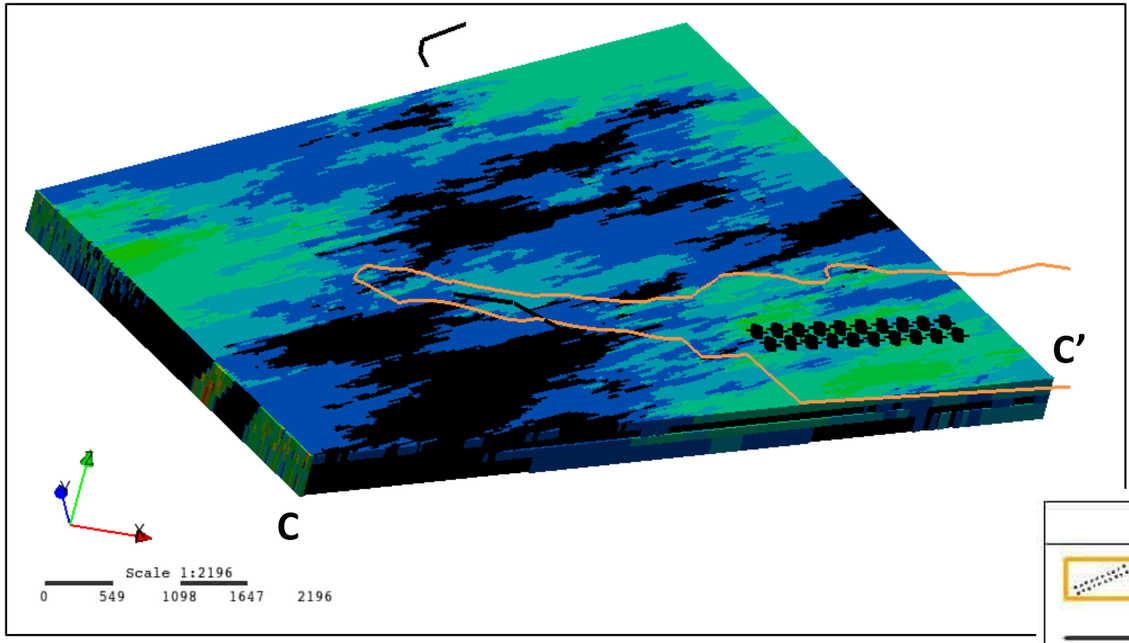

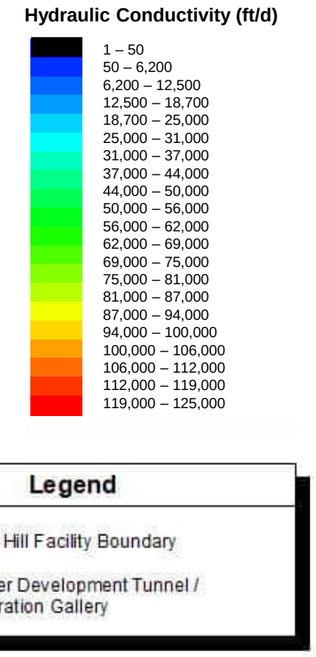

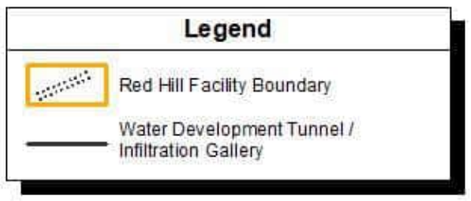

Vertical exaggeration = 3

Figure 3-2
Box Model Example – Realization 10
GWFM, VZM, & CF&T Model Report
Red Hill Bulk Fuel Storage Facility
JBPHH, O'ahu, Hawai'i

Plot from EPAs 5/7/2021 Presentation, pg. 10
2017/2018 Synoptic Survey
[redacted] pumping at [redacted] MGD

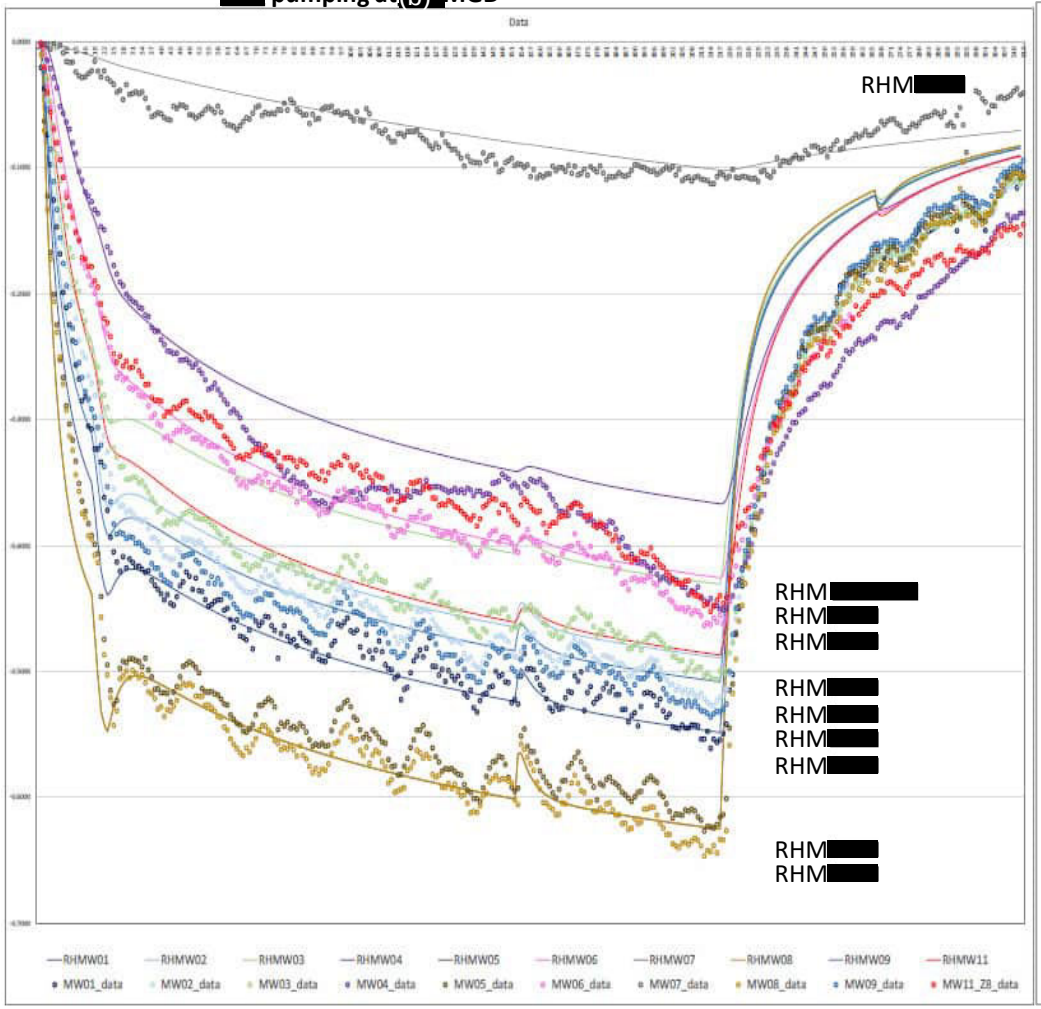

Recent Drawdown Data – January 2022
[redacted] pumping at ~[redacted] MGD

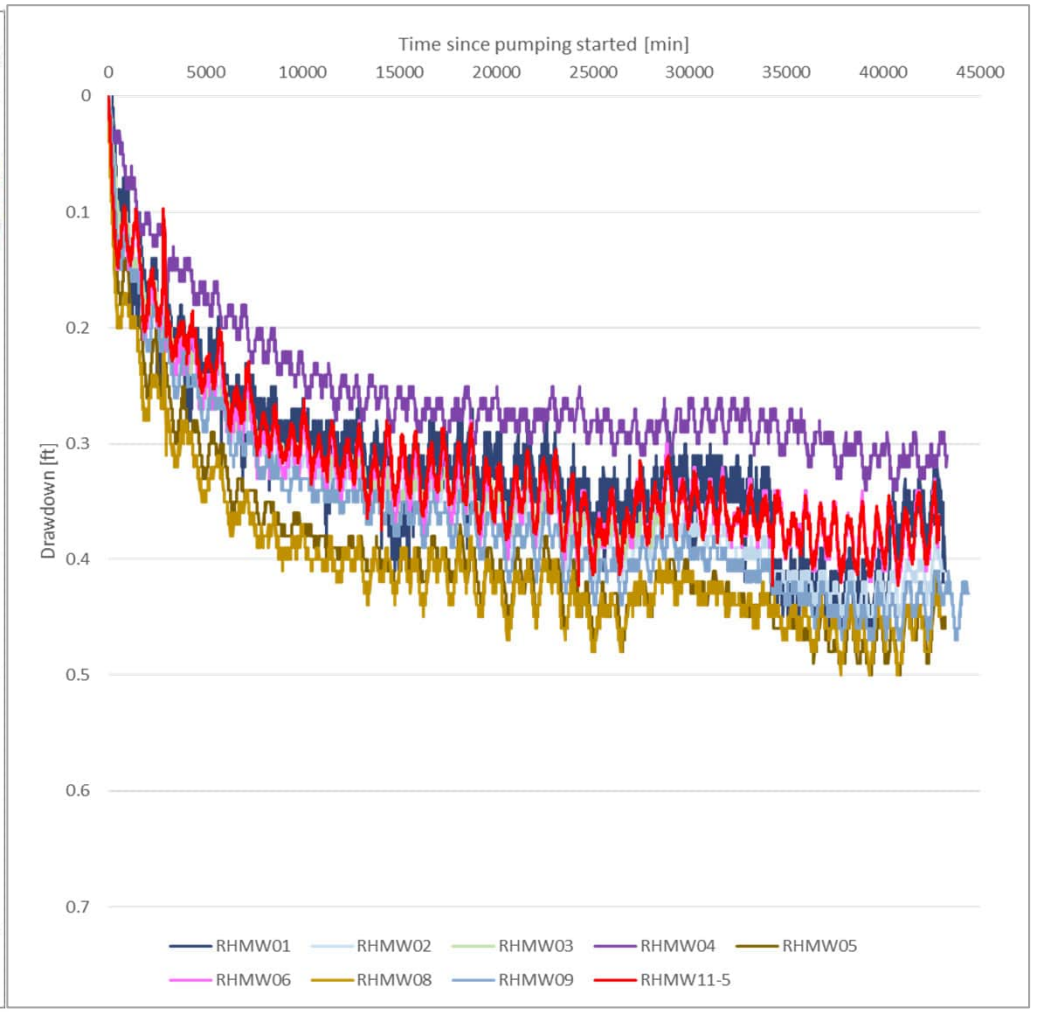

Figure 3-3
Compartmentalization Groups
GWFM, VZM, & CF&T Model Report
Red Hill Bulk Fuel Storage Facility
JBPHH, O‘ahu, Hawai‘i

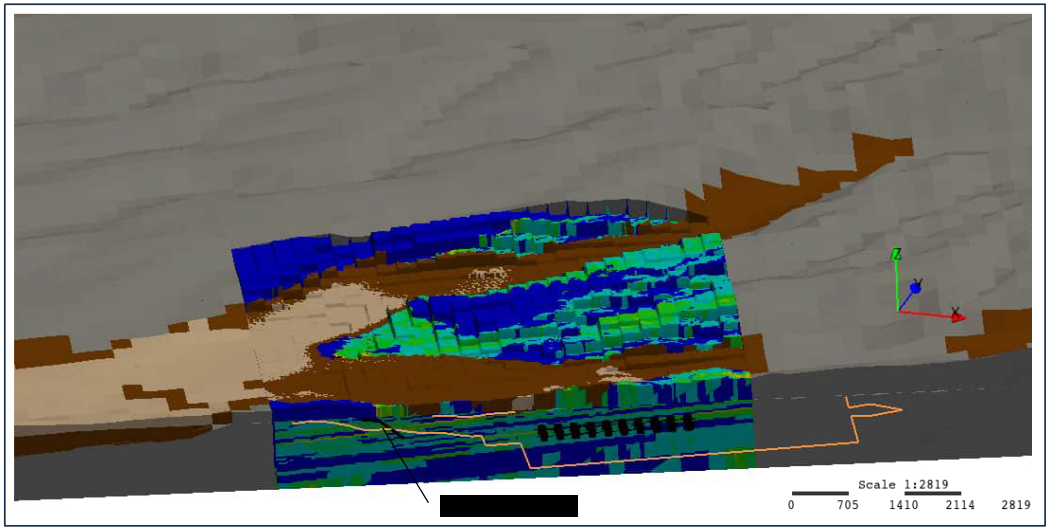

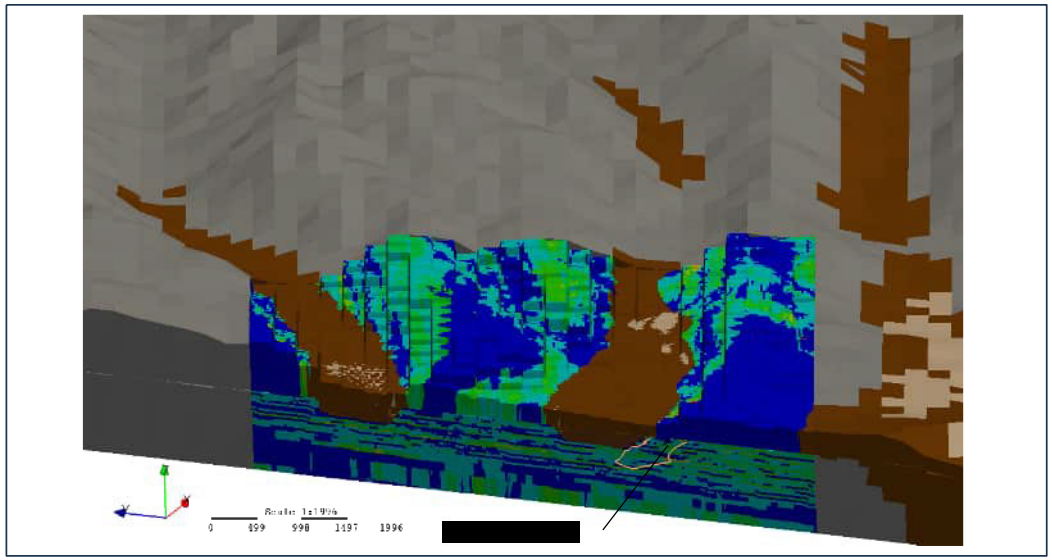

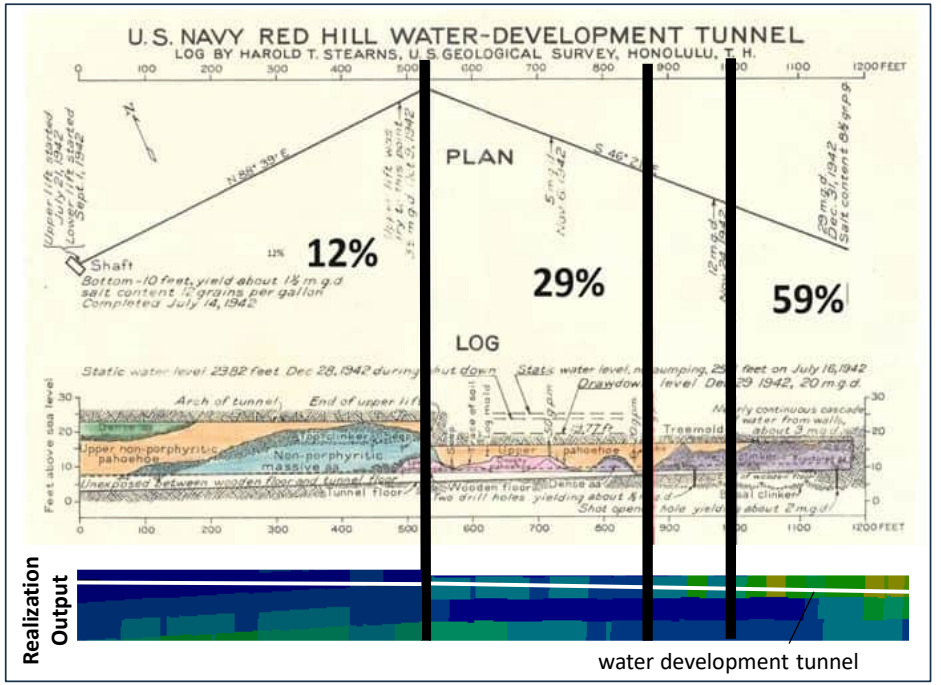

Alluvium
Saprolite
Homogeneous Basalt
Heterogeneous Basalt – Percentage of Clinker
0%
5% to 10%
10% to 15%
15% to 20%
20% to 25%
25% to 30%
30% to 35%
35% to 40%
40% to 45%
45% to 50%
50% to 55%
55% to 60%
60% to 65%
65% to 70%
70% to 75%
75% to 80%
80% to 85%
85% to 90%
90% to 95%
100%

Legend
Red Hill Facility Boundary and Fuel Storage Tanks
Water Development Tunnel / Infiltration Gallery

Figure 3-4
[redacted] Flow Distribution
GWFM, VZM, & CF&T Model Report
Red Hill Bulk Fuel Storage Facility
JBPHH, O'ahu, Hawai'i

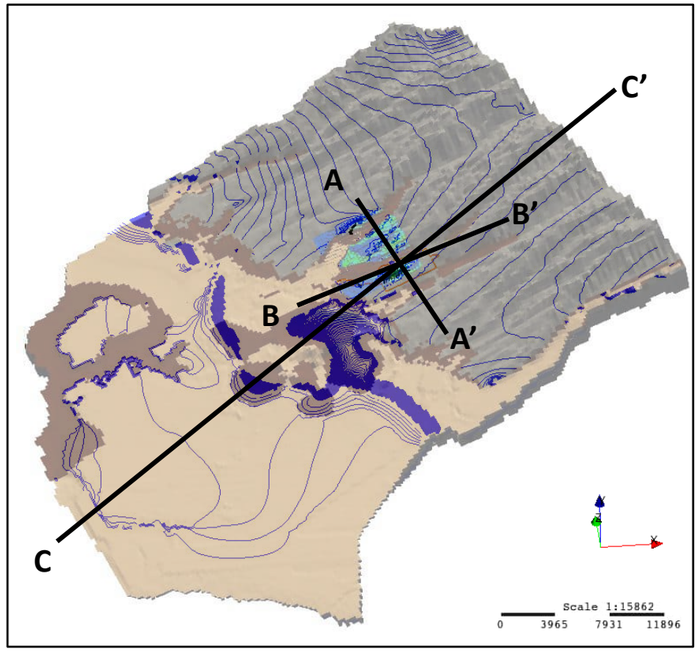

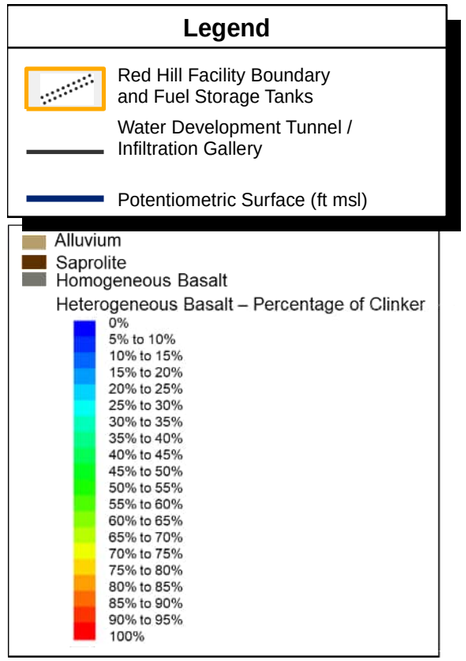

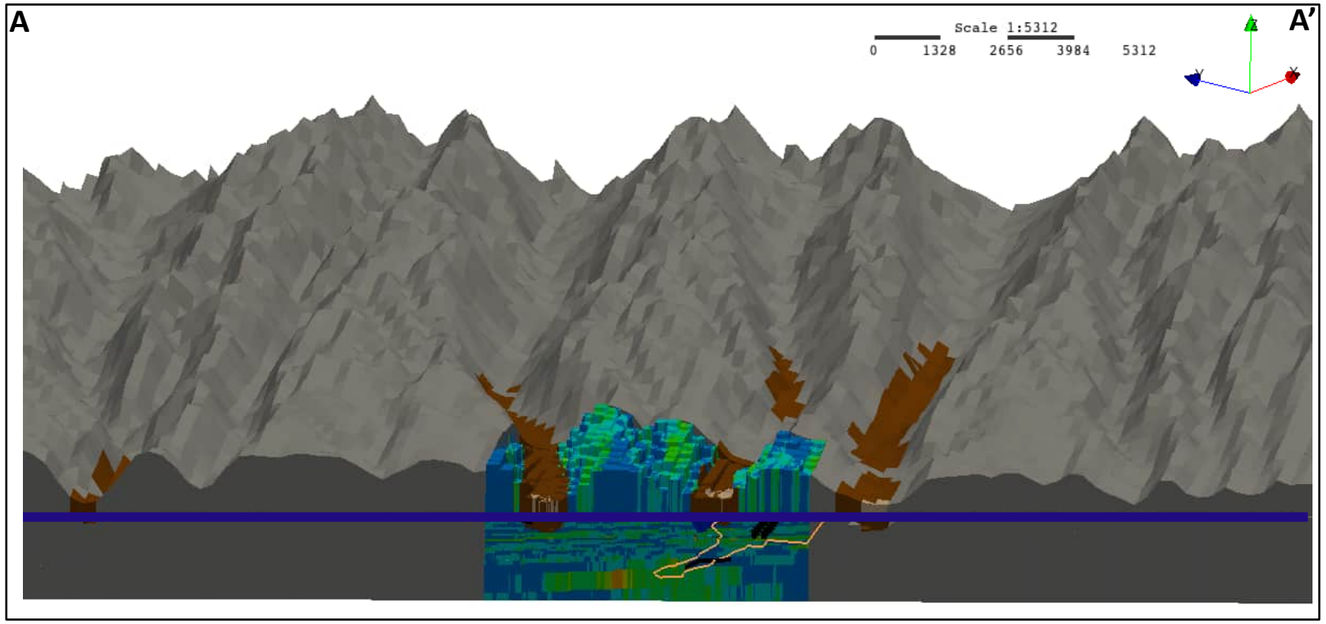

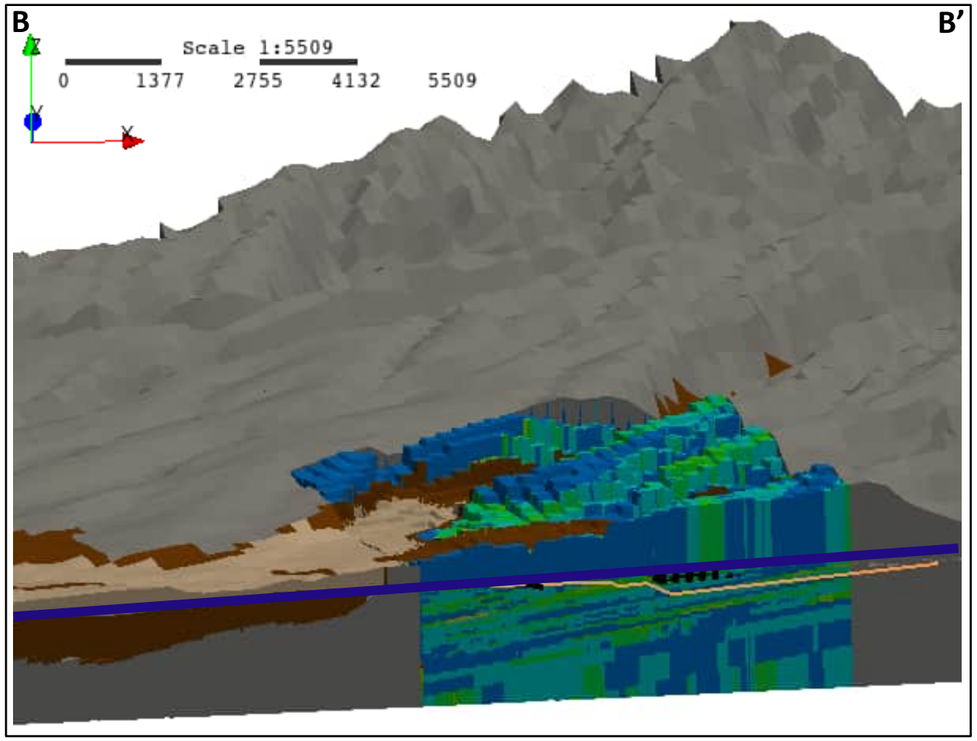

Vertical exaggeration = 2

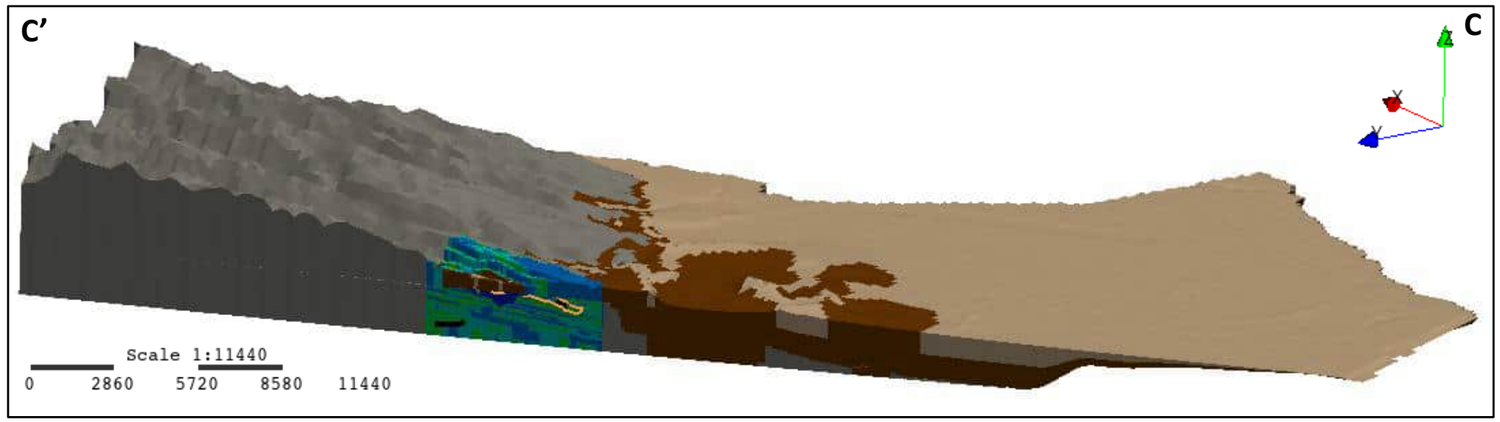

Figure 3-5
Regional Model with Example Realization 10
GWFM, VZM, & CF&T Model Report
Red Hill Bulk Fuel Storage Facility
JBPHH, O‘ahu, Hawai‘i

This scenario is an exploratory analysis and does not represent current conditions.

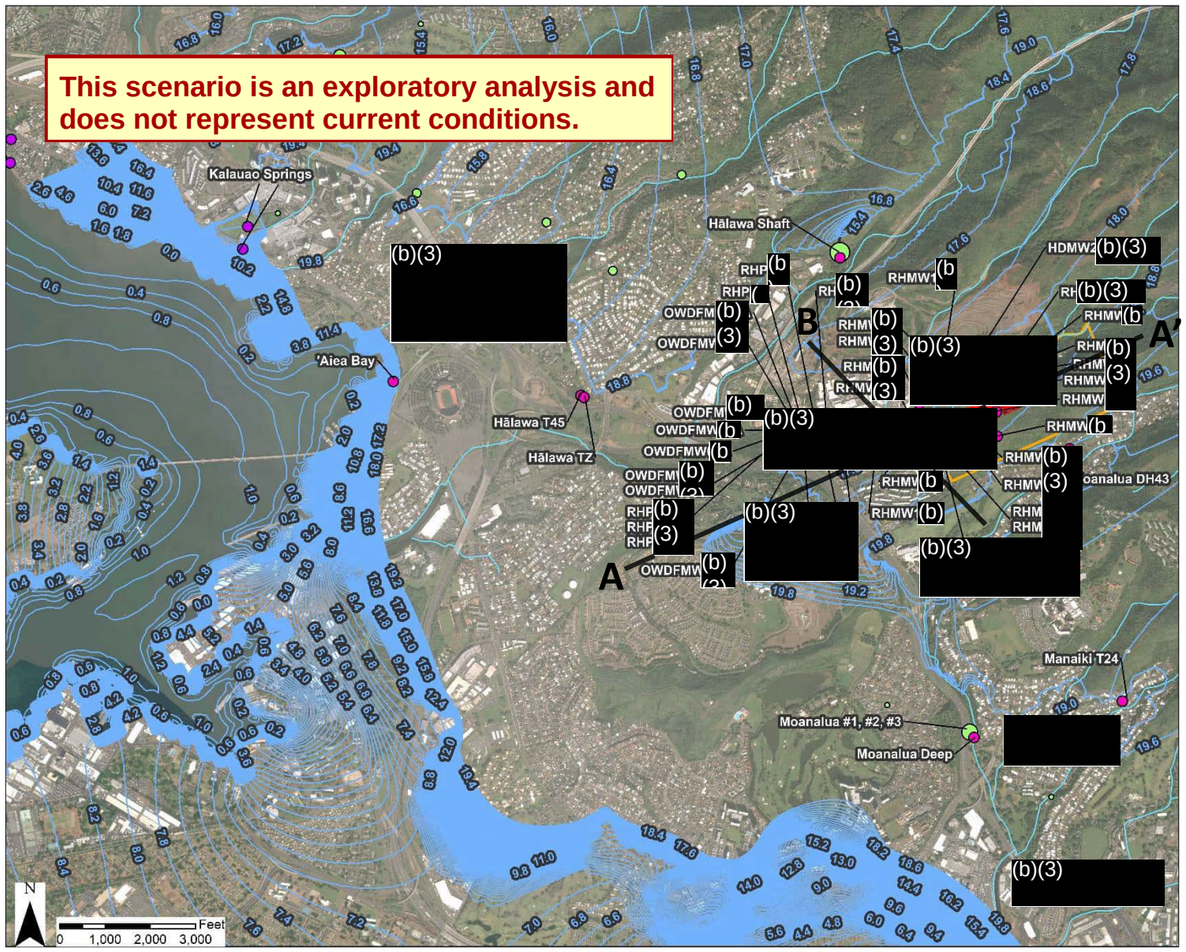

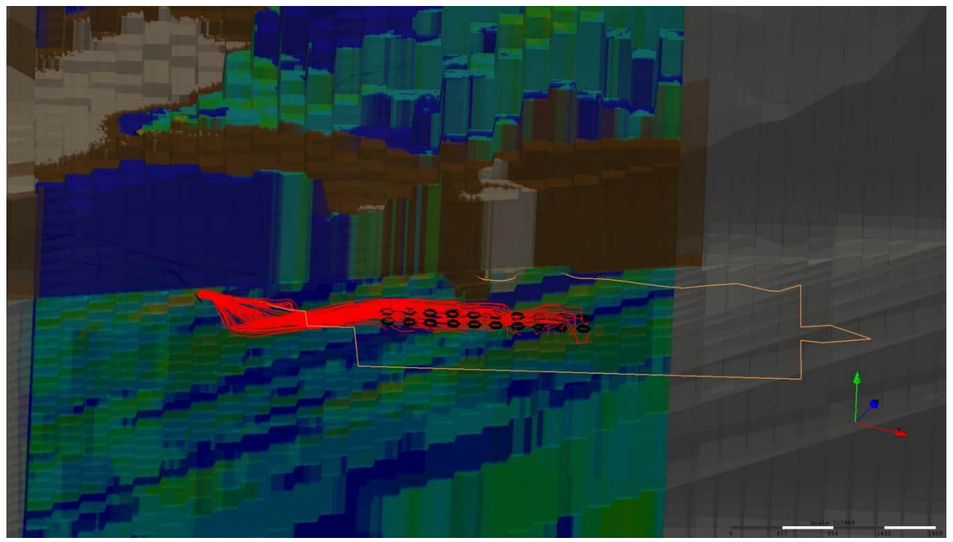

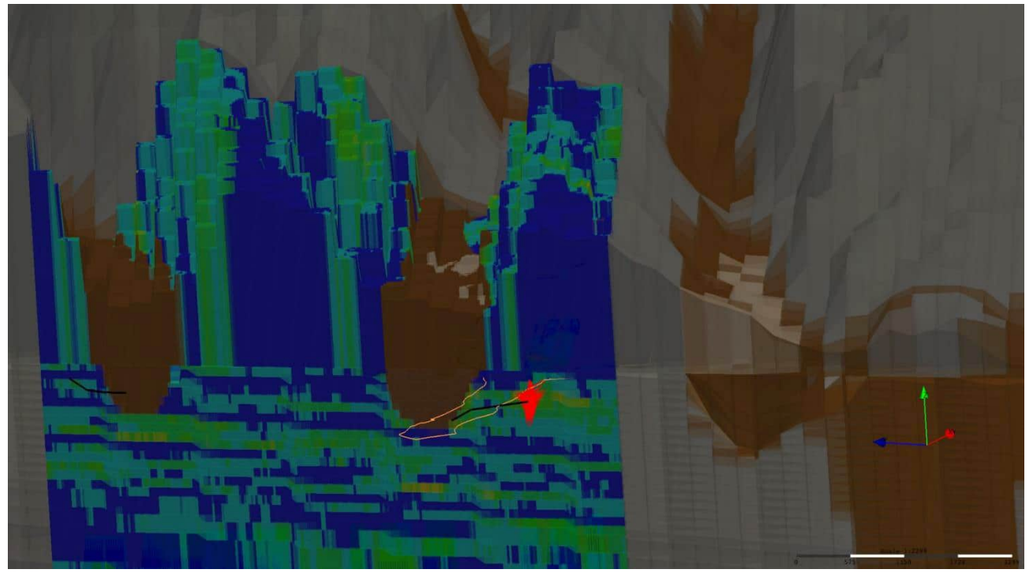

Alluvium
Saprolite
Homogeneous Basalt
Heterogeneous Basalt – Percentage of Clinker
- 0%
- 5% to 10%
- 10% to 15%
- 15% to 20%
- 20% to 25%
- 25% to 30%
- 30% to 35%
- 35% to 40%
- 40% to 45%
- 45% to 50%
- 50% to 55%
- 55% to 60%
- 60% to 65%
- 65% to 70%
- 70% to 75%
- 75% to 80%
- 80% to 85%
- 85% to 90%
- 90% to 95%
- 100%

Legend

Water Supply Well / Shaft (MGD)
- 0.0 - 0.5
- 0.5 - 1.0
- 1.0 - 2.0
- 2.0 - 5.0
- 5.0 - 10.0
- 10.0 - 15.0

Basal Aquifer Well
Spring
Forward Particle Track
Potentiometric Surface (ft msl)
Water Development Tunnel / Infiltration Gallery
Stream
Red Hill Facility Boundary and Fuel Storage Tanks

Figure 3-6
Particle Tracking Results
Example – Realization 10
(b)(3)(b)(3) Pumping at (b) mgd, Hālawa Shaft Pumping at 12 mgd, (b)(3) (b)(3) (b)(3) Pumping at mgd
GWFM, VZM, & CF&T Model Report
Red Hill Bulk Fuel Storage Facility
JBPHH, O'ahu, Hawai'i

*Note that vertical exaggeration is 4

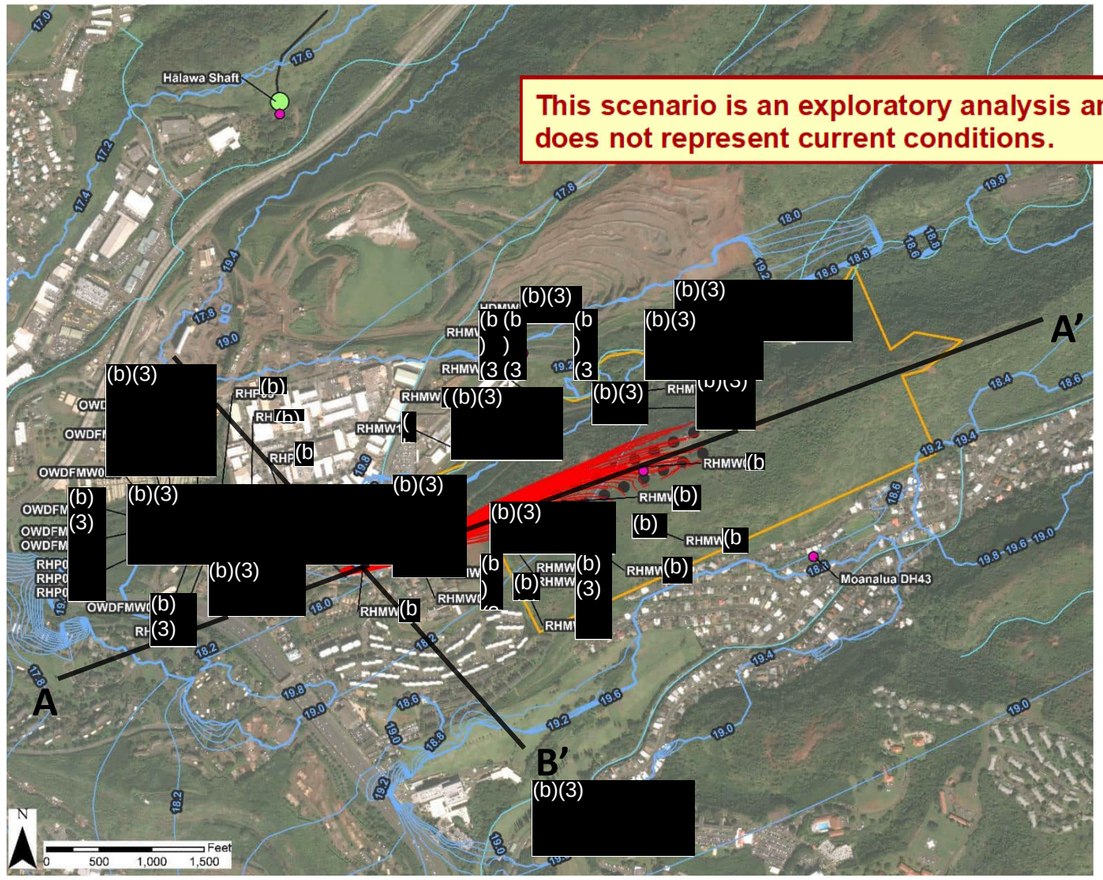

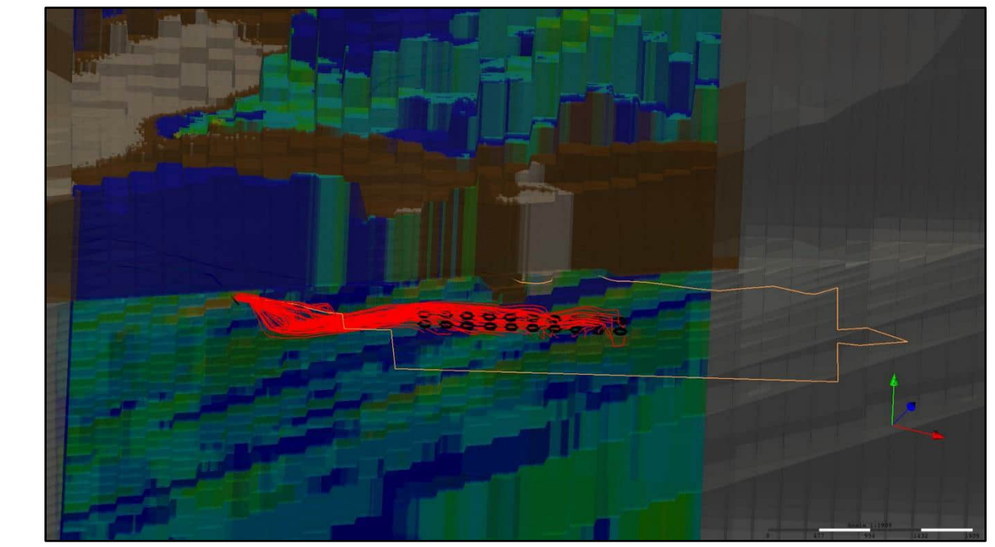

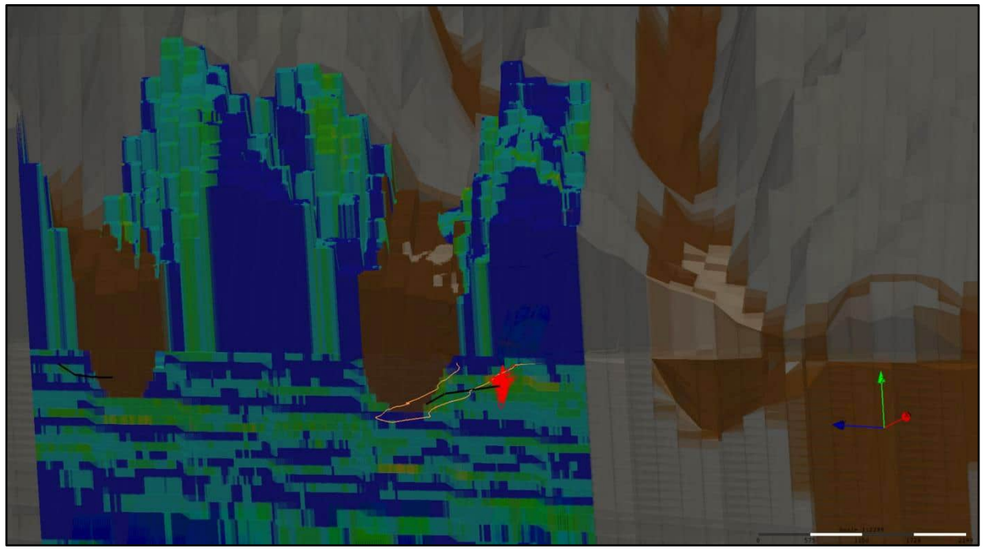

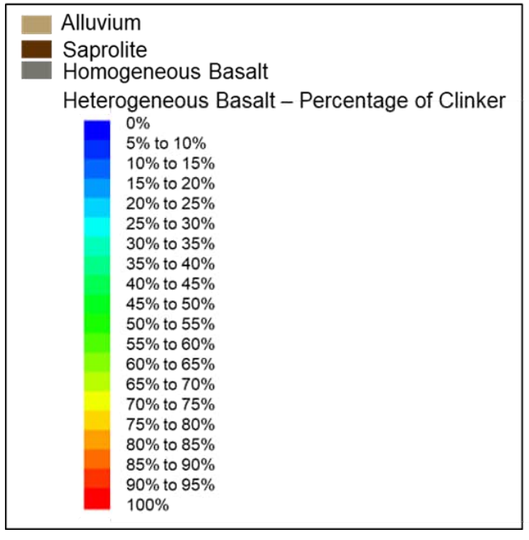

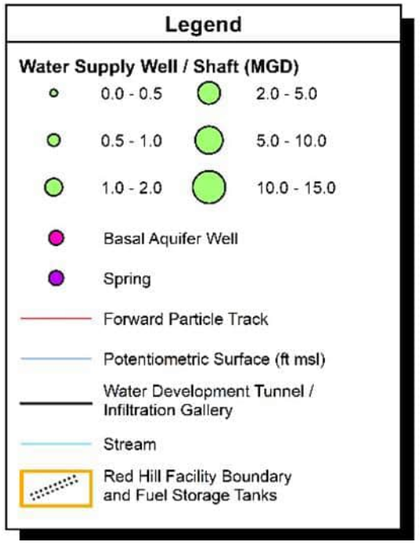

*Note that vertical exaggeration is 4

Figure 3-7
Particle Tracking Results
Example – Realization 10
(b)(3)(b)(3) Pumping at (b) mgd, Hālawa Shaft Off, (b)(3) Pumping (b)
GWFM, VZM, & CF&T Model Report
Red Hill Bulk Fuel Storage Facility
JBPHH, Oʻahu, Hawaiʻi

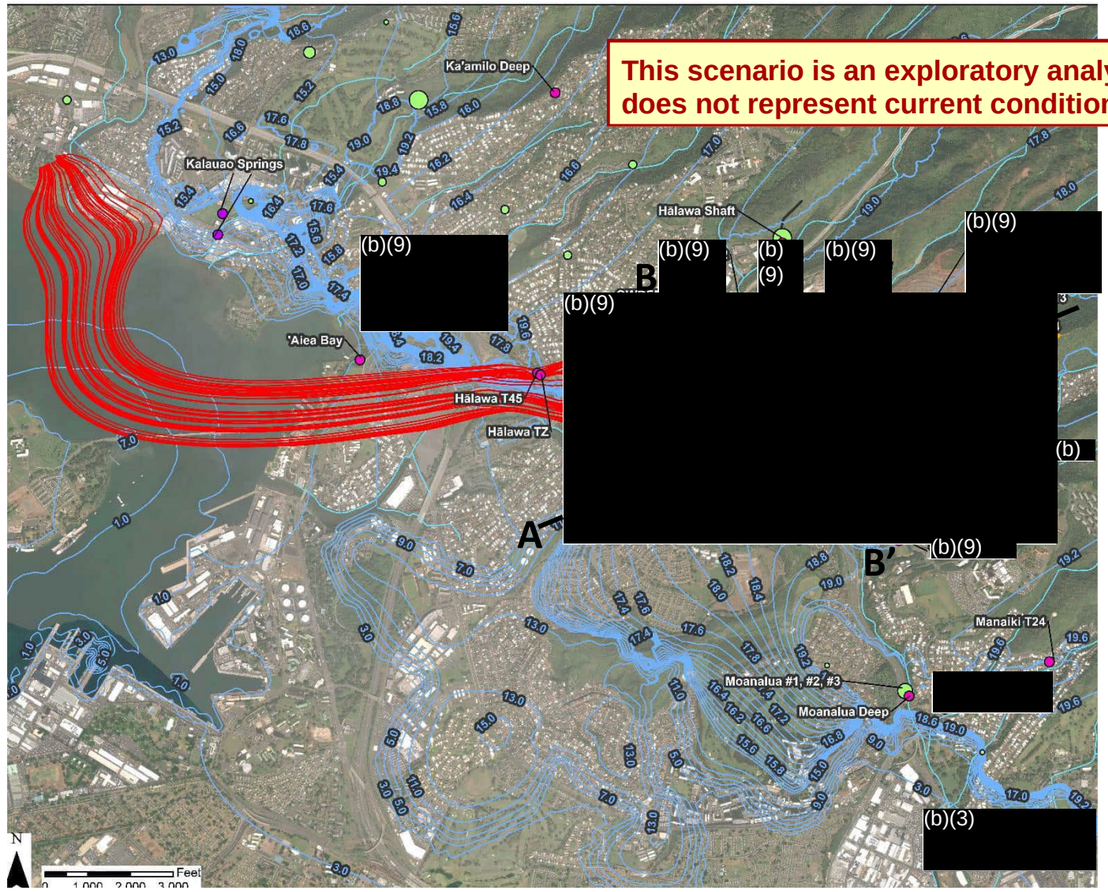

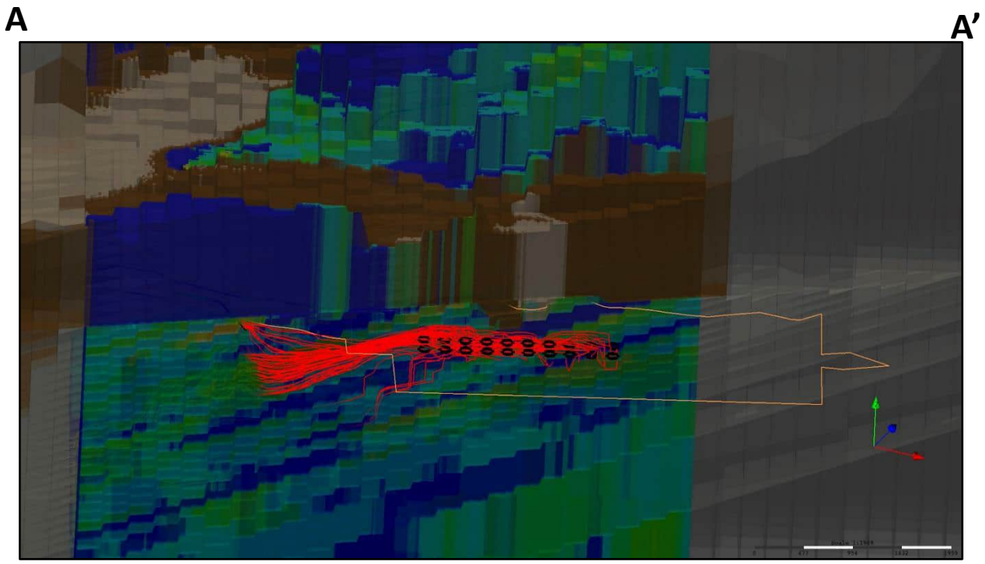

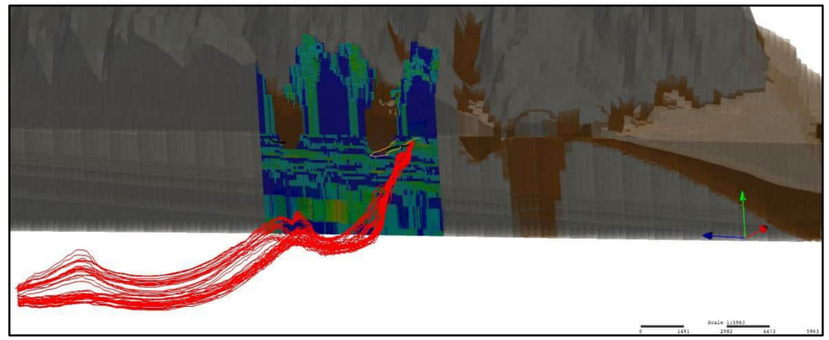

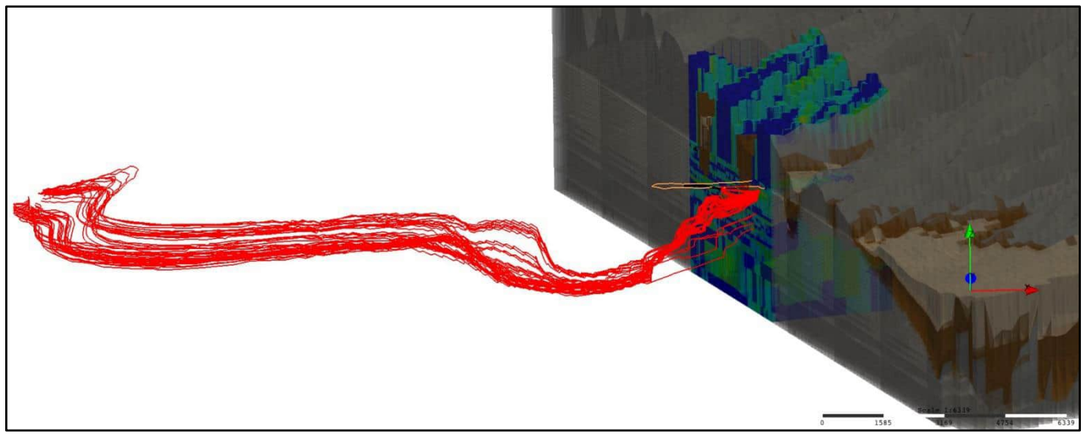

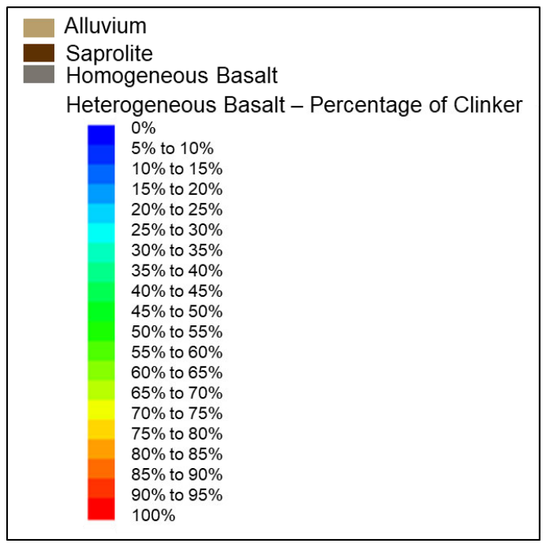

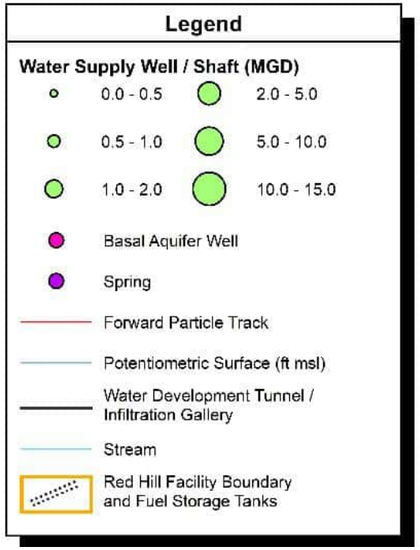

Figure 3-8
Particle Tracking Results
Example – Realization 10
(b)(3)(b)(3) Pumping(b)(9) Hālawa Shaft Pumping Off, (b)(3) (b)(3) Pumping at (b)
GWFM, VZM, & CF&T Model Report
Red Hill Bulk Fuel Storage Facility
JBPHH, O'ahu, Hawai'i

*Note that vertical exaggeration is 4

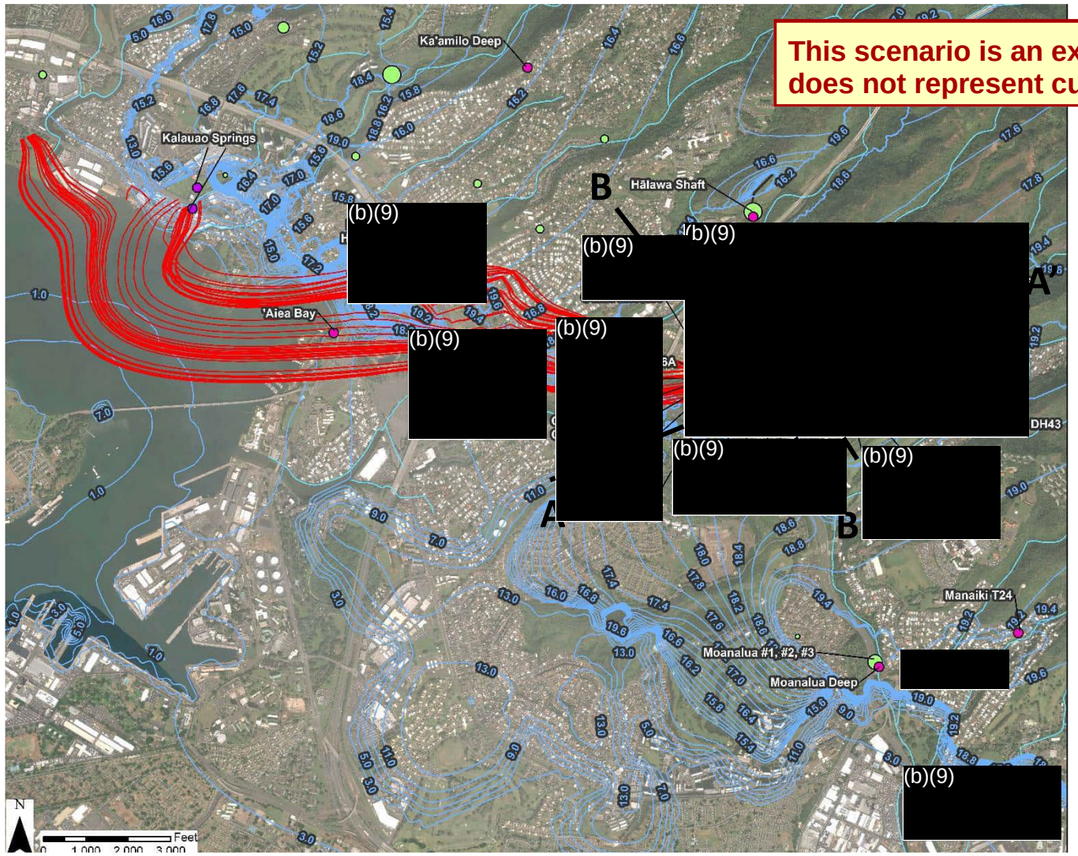

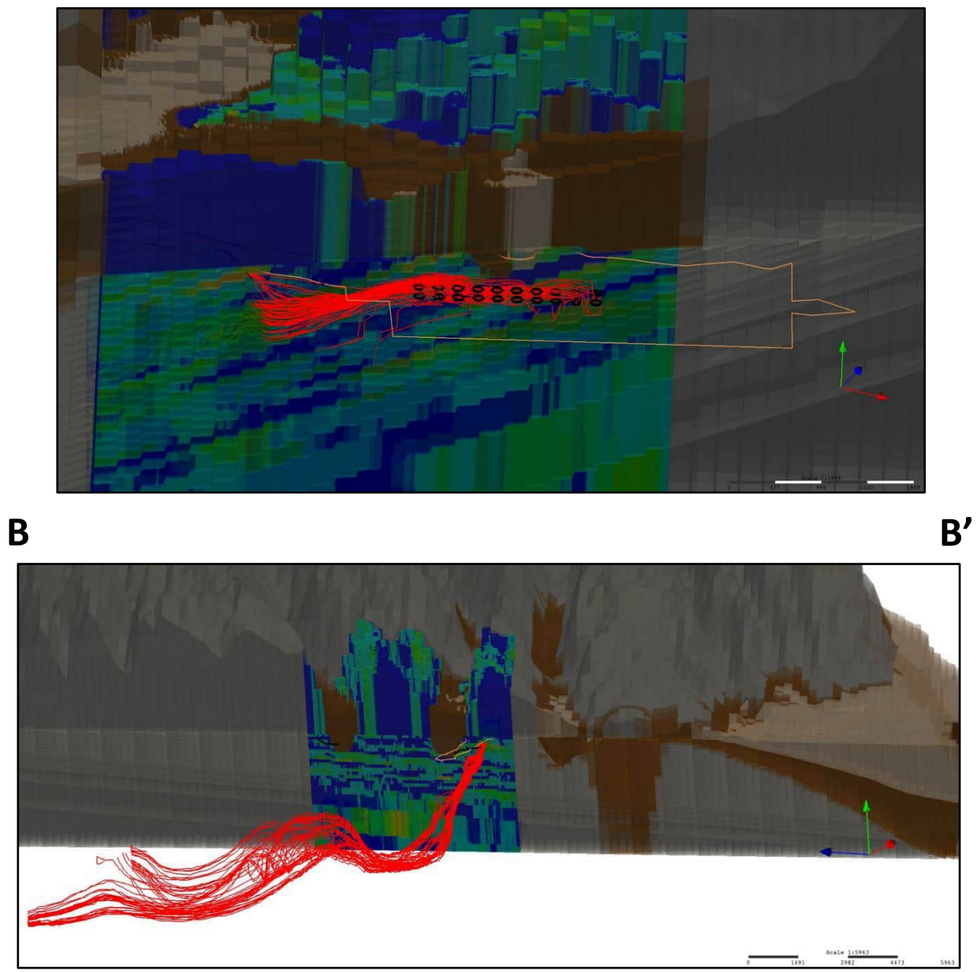

Figure 3-9
Particle Tracking Results
Example – Realization 10
(b)(3)(b)(3) Pumping (b) Hālawa Shaft Pumping at 12 mgd, (b)(3) (b)(3) Pumping (b)
GWFM, VZM, & CF&T Model Report
Red Hill Bulk Fuel Storage Facility
JBPHH, O'ahu, Hawai'i

*Note that vertical exaggeration is 4

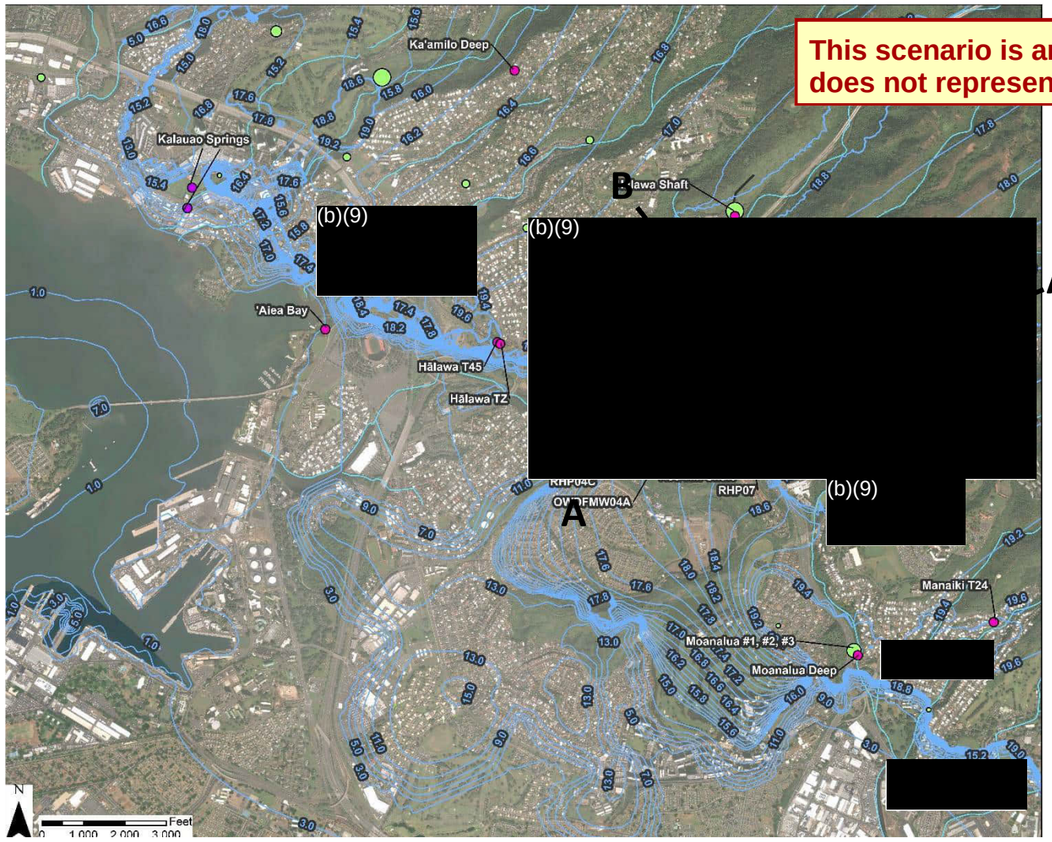

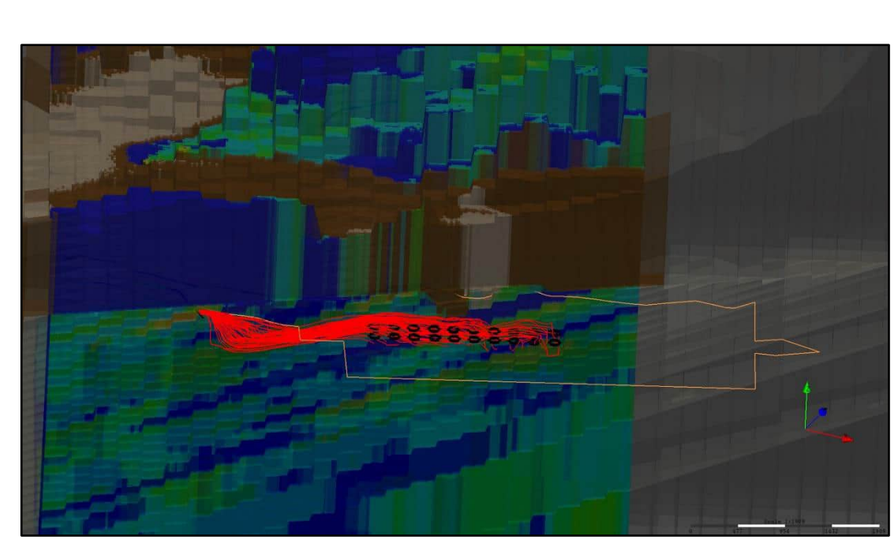

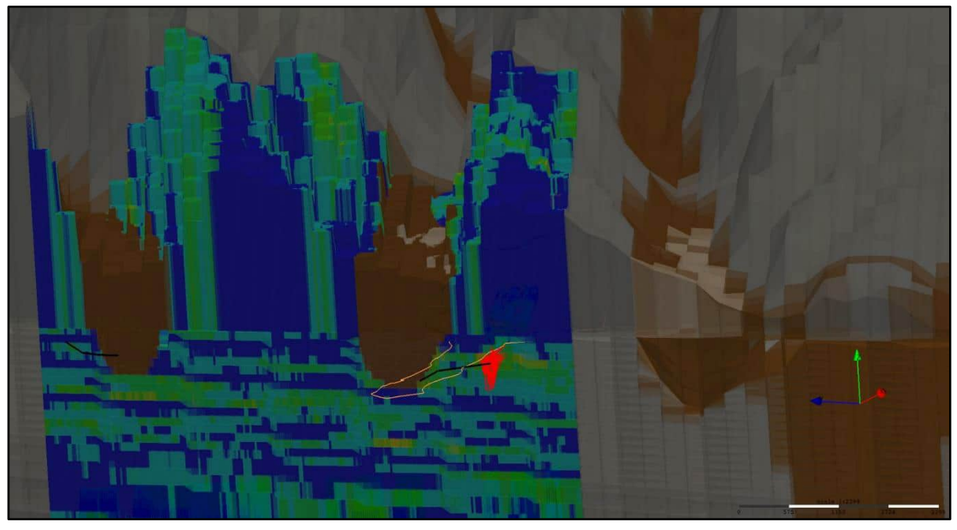

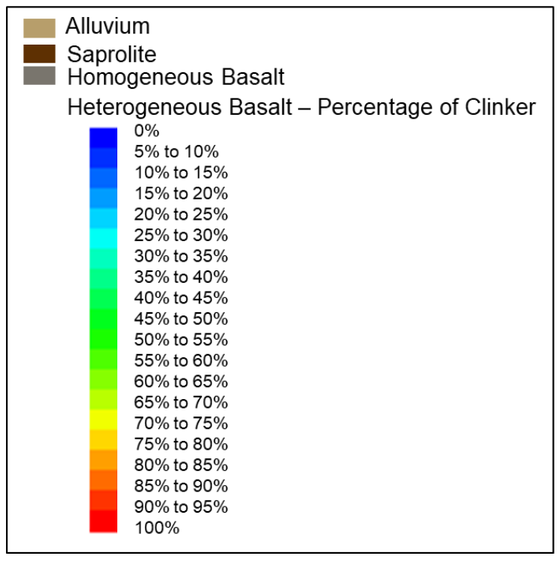

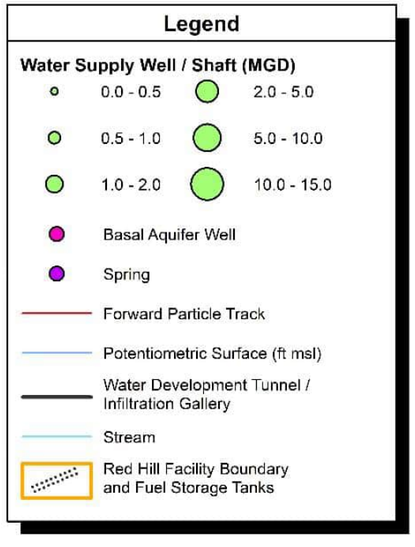

Figure 3-10
Particle Tracking Results
Example – Realization 10
(b)(3)(b)(3) Pumping at (b) mgd, Hālawa Shaft Pumping (b)(9) (b)(3) (b)(3) Pumping (b)
GWFM, VZM, & CF&T Model Report
Red Hill Bulk Fuel Storage Facility
JBPHH, Oʻahu, Hawaiʻi

*Note that vertical exaggeration is 4

Ka'amilo Deep
Kalauao P1
'Aiea Gulch 1
Ka'amilo 1
'Aiea 1
Kalauao Springs
Lau Farm
Hālawa Shaft
Hālawa 2
(b)(9)
'Aiea Bay
Hālawa T45
Hālawa TZ
OWDFM A
RH
RHM
HDMW
RHP
Moanalua DH 43

This scenario is an exploratory analysis and does not represent current conditions.

Rank #

0 1 2 3 4 5 6 7 8 9 10 11 12 13 14 15 16 17 18 19 20 21 22 23 24 25 26 27 28 29 30 31 32 33 34 35 36 37 38 39 40 41 42 43 44 45 46 47 48 49 50 51 52 53 54 55 56 57 58 59 60 61 62 63

Location Map

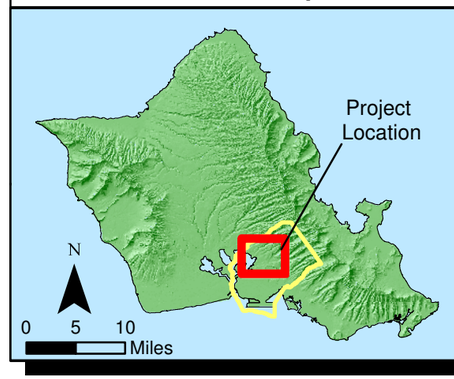

Legend

Water Supply Well / Shaft (MGD)

- 0.0 - 0.5
- 0.5 - 1.0
- 1.0 - 2.0
- 2.0 - 5.0
- 5.0 - 10.0
- 10.0 - 15.0
- Basal Aquifer Well
- Spring
- Water Development Tunnel / Infiltration Gallery
- Groundwater Flow Model Domain
- Stream
- Red Hill Facility Boundary and Fuel Storage Tanks

Notes

1. Map projection: NAD 1983 Hawaii State Plane Zone 3 feet.
2. Base Map: DigitalGlobe, Inc. (DG) and NRCS. Publication_Date: 2015
3. Spring locations provided by USGS.
4. Water supply well locations provided by DLNR.

N

0 1,000 2,000 3,000 Feet

Figure 3-11
Particle Tracking Results for All Realizations - [redacted] Pumping at 4 mgd, Hālawa Shaft Pumping at 12 mgd, (b)(3) [redacted] t(b) [redacted] mgd
GWFM, VZM, & CF&T Model Report
Red Hill Bulk Fuel Storage Facility
JBPHH, O'ahu, HI

B:\N6274422F0106_60674414-HNL11900_CAD_GIS_EVS\920 GIS\02_Maps\18_2024_Model_Reports\03_Fnl\mxd\Fig3-11_Particle Tracking Results for All Realizations_HS12.mxd 9/23/2024

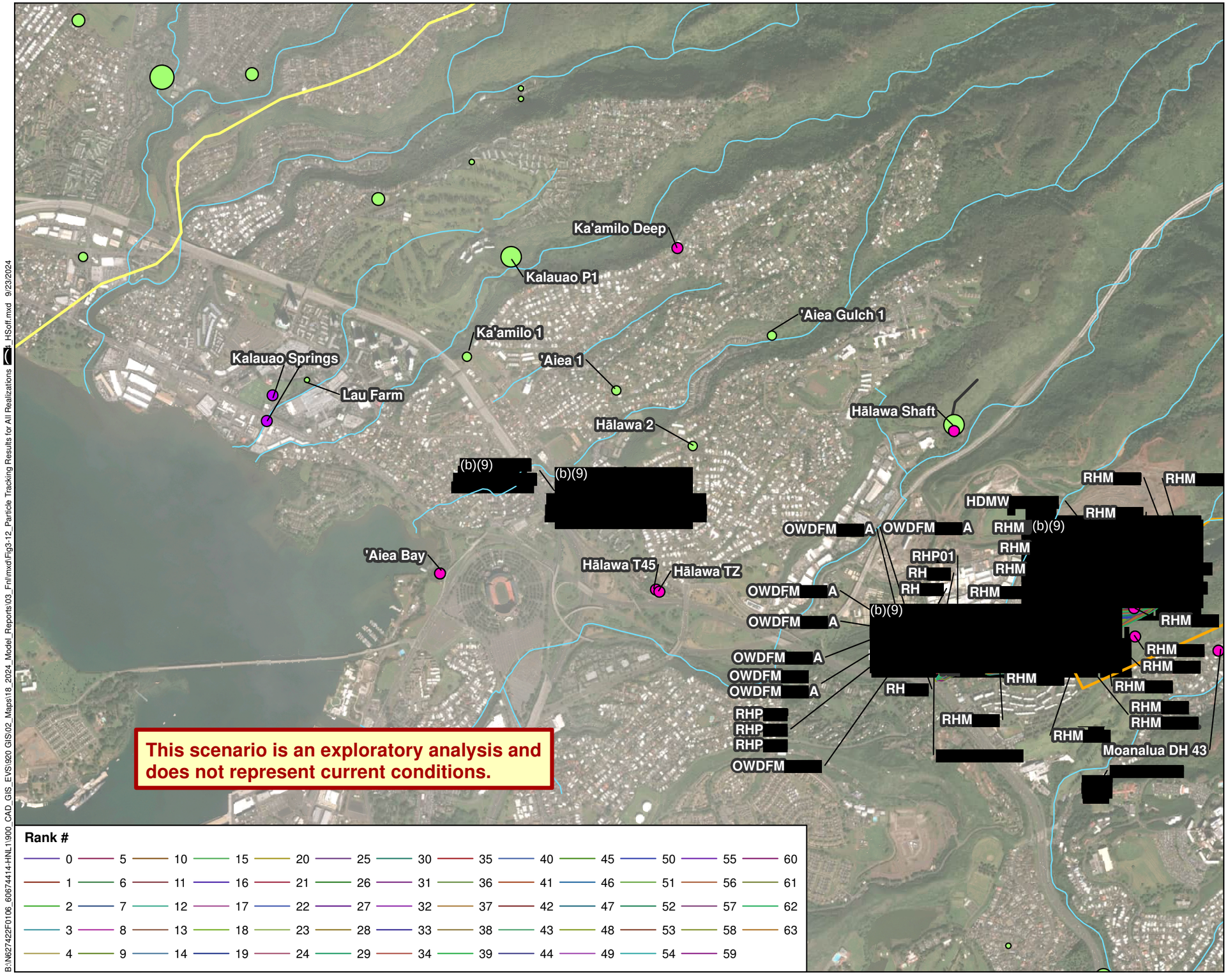

Location Map

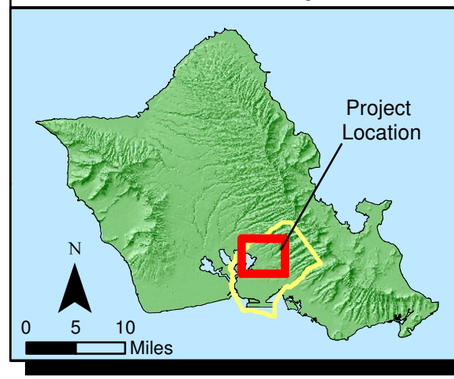

Legend

Water Supply Well / Shaft (MGD)

- 0.0 - 0.5
- 0.5 - 1.0
- 1.0 - 2.0
- 2.0 - 5.0
- 5.0 - 10.0
- 10.0 - 15.0
- Basal Aquifer Well
- Spring
- Water Development Tunnel / Infiltration Gallery
- Groundwater Flow Model Domain
- Stream
- Red Hill Facility Boundary and Fuel Storage Tanks

Notes

1. Map projection: NAD 1983 Hawaii State Plane Zone 3 feet.
2. Base Map: DigitalGlobe, Inc. (DG) and NRCS. Publication_Date: 2015
3. Spring locations provided by USGS.
4. Water supply well locations provided by DLNR.

N

0 1,000 2,000 3,000 Feet

Figure 3-12
Particle Tracking Results for All Realizations
[redacted] Pumping at [redacted] mgd, Hālawa Shaft Off, (b)(3) [redacted]
GWFM, VZM, & CF&T Model Report
Red Hill Bulk Fuel Storage Facility
JBPHH, O'ahu, HI

B:\N6274422F0106_60674414-HNL\1900_CAD_GIS_EVS\920 GIS\02_Maps\18_2024_Model_Reports\03_Fnl\mxd\Fig3-12_Particle Tracking Results for All Realizations_HSoff.mxd 9/23/2024

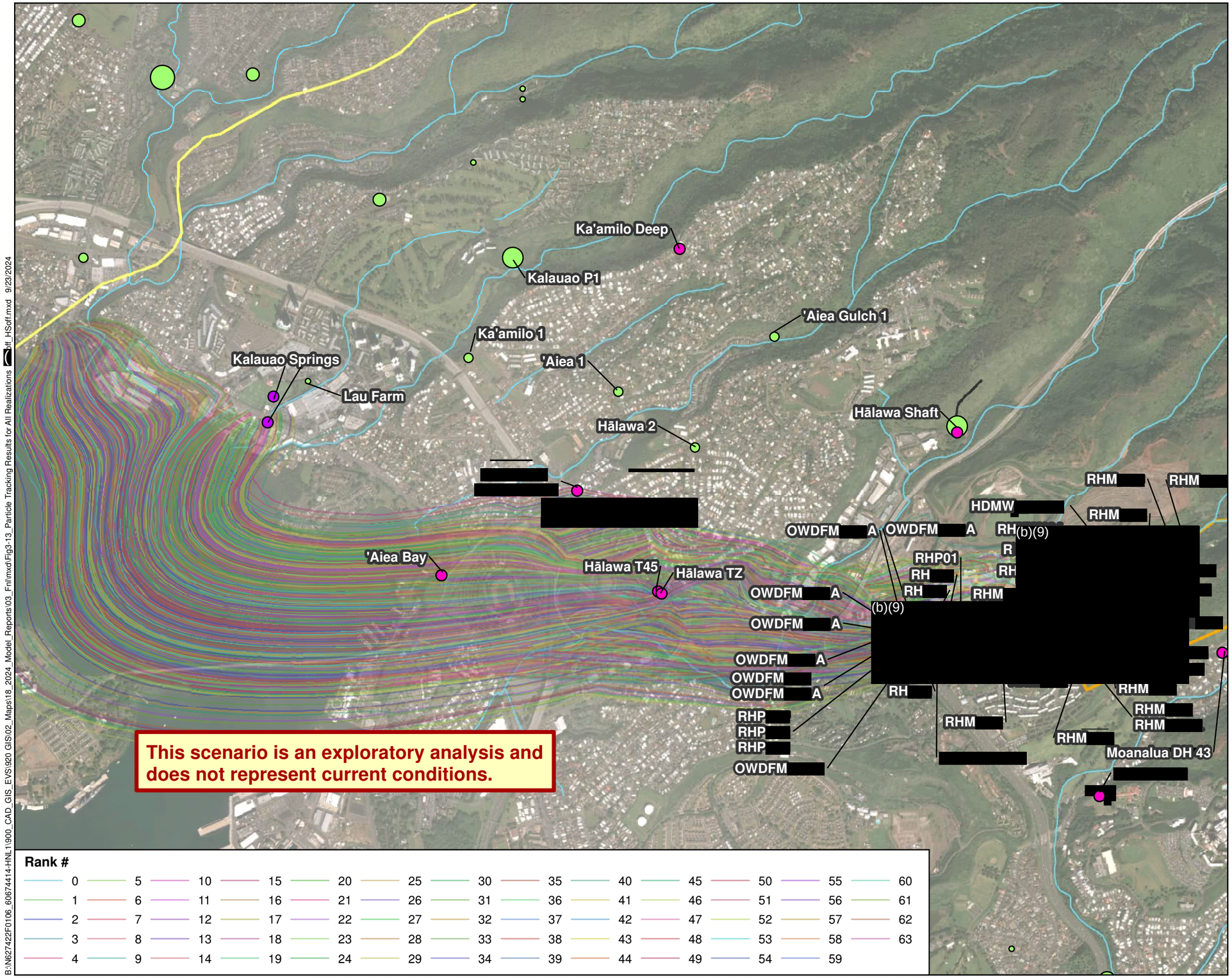

B:\N627422F0106_60674414-HNL1\900_CAD_GIS_EVS\920 GIS\02_Maps\18_2024_Model_Reports\03_Fnl\mxd\Fig3-13_Particle Tracking Results for All Realizations_Pumping_(b)(3)_HSoff_HSoff.mxd 9/23/2024

Location Map

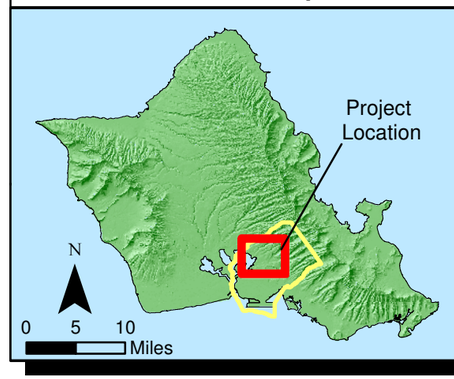

Legend

Water Supply Well / Shaft (MGD)

- 0.0 - 0.5
- 0.5 - 1.0
- 1.0 - 2.0
- 2.0 - 5.0
- 5.0 - 10.0
- 10.0 - 15.0
- Basal Aquifer Well
- Spring
- Water Development Tunnel / Infiltration Gallery
- Groundwater Flow Model Domain
- Stream
- Red Hill Facility Boundary and Fuel Storage Tanks

Notes

1. Map projection: NAD 1983 Hawaii State Plane Zone 3 feet.
2. Base Map: DigitalGlobe, Inc. (DG) and NRCS. Publication_Date: 2015
3. Spring locations provided by USGS.
4. Water supply well locations provided by DLNR.

N

0 1,000 2,000 3,000 Feet

Figure 3-13
Particle Tracking Results for All Realizations - [redacted] Pumping (b) Hālawa Shaft Pumping Off, (b)(3) [redacted]
GWFM, VZM, & CF&T Model Report
Red Hill Bulk Fuel Storage Facility
JBPHH, Oʻahu, HI

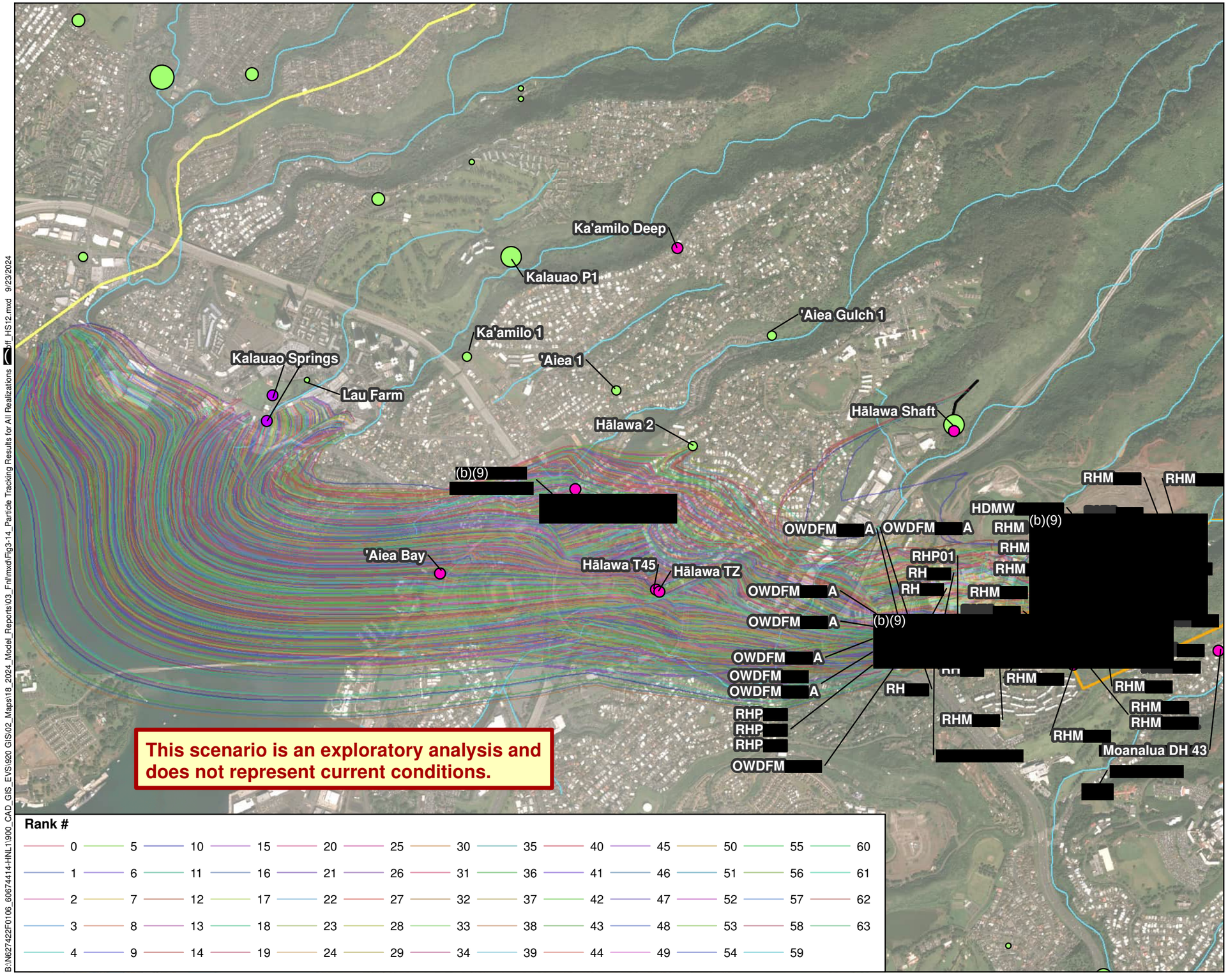

B:\N627422F0106_606744\14-HNL1\900_CAD_GIS_EVS\920 GIS\02_Maps\18_2024_Model_Reports\03_Fnl\mxd\Fig3-14_Particle Tracking Results for All Realizations_(b)(3)_HS12.mxd 9/23/2024

Location Map

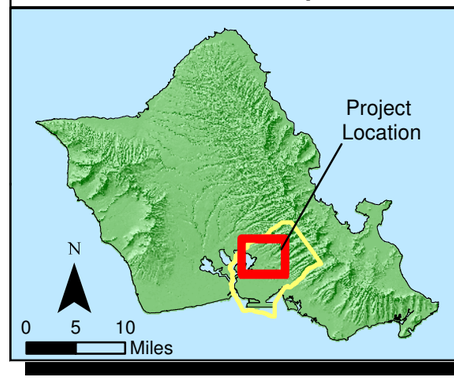

Legend

Water Supply Well / Shaft (MGD)

- 0.0 - 0.5
- 0.5 - 1.0
- 1.0 - 2.0
- 2.0 - 5.0
- 5.0 - 10.0
- 10.0 - 15.0
- Basal Aquifer Well
- Spring
- Water Development Tunnel / Infiltration Gallery
- Groundwater Flow Model Domain
- Stream
- Red Hill Facility Boundary and Fuel Storage Tanks

Notes

1. Map projection: NAD 1983 Hawaii State Plane Zone 3 feet.
2. Base Map: DigitalGlobe, Inc. (DG) and NRCS. Publication_Date: 2015
3. Spring locations provided by USGS.
4. Water supply well locations provided by DLNR.

N

0 1,000 2,000 3,000 Feet

Figure 3-14
Particle Tracking Results for All Realizations - [redacted] Pumping (b)(3), Hālawa Shaft Pumping 12, (b)(3) [redacted]
GWFM, VZM, & CF&T Model Report
Red Hill Bulk Fuel Storage Facility
JBPHH, O'ahu, HI

Ka'amilo Deep
Kalauao P1
'Aiea Gulch 1
Ka'amilo 1
Kalauao Springs
'Aiea 1
Lau Farm
Hālawa Shaft
Hālawa 2
(b)(9)
(b)(9)
'Aiea Bay
Hālawa T45
Hālawa TZ
OWDFM (b)(9) A
OWDFM (b)(9) A
RHM
RHM
HDMW (b)(9)
RHM
RHM
RHP01
RH
RH
RHM
(b)(9)
OWDFM (b)(9) A
OWDFM (b)(9) A
OWDFM (b)(9)
OWDFM (b)(9) A
OWDFM (b)(9)
OWDFM (b)(9) A
RHP (b)(9)
RHP (b)(9)
RHP (b)(9)
OWDFM (b)(9)
RH
RHM
RHM
RHM
RHM
RHM
RHM
RHM
Moanalua DH 43
(b)(9)

This scenario is an exploratory analysis and does not represent current conditions.

Rank #

0	5	10	15	20	25	30	35	40	45	50	55	60		
1	6	11	16	21	26	31	36	41	46	51	56	61		
2	7	12	17	22	27	32	37	42	47	52	57	62		
3	8	13	18	23	28	33	38	43	48	53	58	63		
4	9	14	19	24	29	34	39	44	49	54	59			

B:\N627422F0106_606744\4-HNL\1\900_CAD_GIS_EVS\920 GIS\02_Maps\18_2024_Model_Reports\03_Fnl\mxd\Fig3-15_Particle Tracking Results for All Realizations - (b)(3) HSoff.mxd 9/5/2024

Location Map

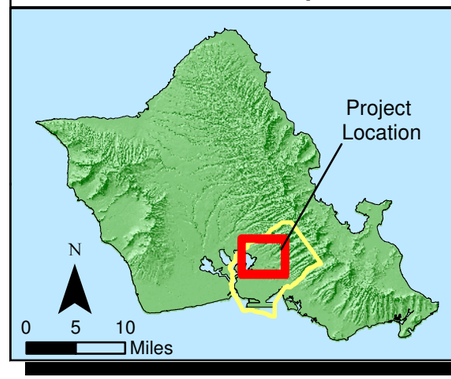

Legend

Water Supply Well / Shaft (MGD)

- 0.0 - 0.5
- 0.5 - 1.0
- 1.0 - 2.0
- 2.0 - 5.0
- 5.0 - 10.0
- 10.0 - 15.0
- Basal Aquifer Well (Group 1 and 2)
- Spring
- Water Development Tunnel / Infiltration Gallery
- Groundwater Flow Model Domain
- Stream
- Red Hill Facility Boundary and Fuel Storage Tanks

Notes

1. Map projection: NAD (b)(3) Hawaii State Plane Zone 3 feet.
2. Base Map: DigitalGlobe, Inc. (DG) and NRCS. Publication_Date: 2015
3. Spring locations provided by USGS.
4. Water supply well locations provided by DLNR.

N

0 1,000 2,000 3,000 Feet

Figure 3-15
Particle Tracking Results forAll Realizations - (b)(3) Pumping (b)(3) mgd, Hālawa Shaft Pumping Off, (b)(3)
GWFM, VZM, & CF&T Model Report
Red Hill Bulk Fuel Storage Facility
JBPHH, O'ahu, HI

Figure 4-1
Main Tab of the Heuristic Model

INPUT			
PARAMETER	**Symbol**	**Value**	**Units**
Vadose Zone Properties			
Avg residual LNAPL sauration in vadose zone	Snr_vad	0.0182	fraction
Avg porosity, total, vadose zone	n_vad	0.1171	fraction
Saturated Zone Properties			
Hydraulic gradient	i	0.000013	
Hydraulic conductivity		12170.00	ft/d
Porosity, total, saturated zone	n_sat	0.117	
LNAPL Properties			
LNAPL type		(b)(9)	
LNAPL density		0.775	g/cm^3
Molecular weight of LNAPL		180	g/mol
Release Details			
Release Scenario		Jan 2014	
Release Location		(b)(9)	
Volume of LNAPL released		27000	gal
Area of release	A_rel	500	ft^2
Depth to water table	DTW	85	ft bgs
Thickness of LNAPL lens	b_lens	3	ft
LNAPL saturation in LNAPL lens on water table	Sn_sat	0.4	
Model Options and Numerical Control			
Solution scheme timestep for partitioning calculations		7.3	days
Account for relative permeability in partitioning?		1	Flag
Account for sweep efficiency in partitioning?		1	Flag
UNIT CONVERSION			
ft3 per gallon	ft3_gal	0.133681	ft^3/gal
m3 per gallon	m3_gal	0.0037854	m^3/gal
m per foot	m_ft	0.3048	m/ft
CALCULATIONS			
Volume of LNAPL released	V_rel	3,600	ft^3
Bulk volume of affeced vadose zone	V_vad	43,000	ft^3
Pore volume of affected vadose zone	Vp_vad	5,000	ft^3
Volume of LNAPL retained in VZ	Vn_vad	91	ft^3
Volume of LNAPL reaching WT	Vn_sat	3,500	ft^3
Volumetric NAPL content at WT	theta_N_wt	0.047	
Area of LNAPL lens	A_lens	25,000	ft^2
Radius of LNAPL lens	**rad_lens**	**89.**	**ft**

Figure 4-2
Release Info Tab of the Heuristic Model

Release ID	Real/Hypothetical	Fuel	Location	Volume (gal)	Area (ft^2)	Average LNAPL Lens Saturation	LNAPL Lens Thickness
Jan 2014	Real	(b)(9)	(b)(9)	27,000	500	0.4	3
May 2021	Real		(b)(9)	100	500	0.05	0.2
Nov 2021	Real		(b) / Adit 3	5,000	500	0.2	1
Small	Hypothetical		(b) / Adit 3	12,500	500	0.3	2
Medium	Hypothetical		(b) / Adit 3	125,000	500	0.4	3
Large	Hypothetical		(b) / Adit 3	12,500,000	500	0.5	5

Notes:

The Navy states that the small volume of (b)(6) released to the environment on May 6, 2021 was incalculable. For purposes of model calculations, a volume of 100 gallons is used as representative of a very small volume release.

Large release assumes release of 100% of single tank volume

Medium release assumes release of 1% of single tank volume

Small release assumes release of 0.1% of single tank volume

Figure 4-3
Location Info Tab of the Heuristic Model

Location	Depth to water table (ft below tunnel floo	% A'a	% Pahoehoe	% Clinker	% Saprolite	Porosity	Hydraulic Conductivity (ft/d)	Avg VZ Residual LNAPL Saturation
(b)(9) [redacted]	85	35.3%	52.9%	11.8%	0.0%	0.12	12170.00	0.0182
	100	20.0%	70.0%	10.0%	0.0%	0.10	10317.50	0.0160
	80	50.0%	37.5%	12.5%	0.0%	0.13	13961.13	0.0200
	80	62.5%	25.0%	12.5%	0.0%	0.13	15490.00	0.0213
Notes:								
Lithology information provided by AECOM (b)(9) [redacted] in 19 January 2023 email correspondence								

Figure 4-4
Hydrogeologic Info Tab of the Heuristic Model

	A'a	Pahoehoe	Clinker	Saprolite	
Total Porosity	0.09	0.05	0.5	0.3	
Hydraulic Conductivity (ft/d)	20205	7974	6947	0.5	
Residual LNAPL Sat in VZ	0.02	0.01	0.05	0.15	
Residual LNAPL Vol Content in VZ	0.0018	0.0005	0.025	0.045	
Notes:					
Hydraulic conductivity values are derived from an average of various aquifer tests from synoptic studies conducted at the site					
A'a, pahoehoe, and clinker porosity source:		USGS (Hunt, 1996)		Ishizaki and others (1967)	
Hydraulic gradient is 0.000013 (from measured data presented by HDOH in 10 May 2021 SME meeting)					
Pahoehoe literature value for porosity and A'a, pahoehoe, clinker values for K for undifferentiated basalt					
Literature values for hydraulic conductivity (not utilized here):				USGS (Hunt	Mink (1980)
Saprolite is a highly variable and non-specific medium; the hydraulic conductivity utilized here for saprolite is an educated estimate based on professional judgment.					

Figure 4-5
Fuel Info Tab of the Heuristic Model

Fuel	Specific Gravity	Molecular Weight (g/mol)	Non-TPH LNAPL Constituents	Volumetric fraction of soluble TPH-d components	Volumetric fraction of soluble TPH-o component
(b)(9)	0.79	185	(b)(3)	0.16	0
	0.78	180		0.18	0
	0.87	200		0.352	0.088
Notes:					
(b)(3)					
				https://www.ncbi.nlm.nih.gov	
				https://www.docs.citgo.com/msds_pi/13176.pdf	

Figure 4-6
Partitioning Tab of the Heuristic Model

Parameter	Symbol	Value	Units	Comments				INPUT CELLS / TABS		
General Parameters:								FROM HEURISTIC MODEL		
Hydraulic conductivity	K_sat	4721.352	m/d	Unit conversion.				LOOKUP CELLS		
Hydraulic gradient	i	0.000013								
Width of LNAPL lens	w	217	m	Assume a square shape.						
Average thickness of LNAPL lens	b	1.52	m	Unit conversion.						
Length of LNAPL lens	L	217	m	Assume a square shape.						
Solution scheme time step	dt	7	d							
LNAPL volume in lens	V_N	4728.621363	m^3	Unit conversion.						
Porosity of saturated zone	por	0.13	fraction							
Account for relative permeability?	RFLAG	1		1 = Yes, 0 = No. Multipies Q_gw by k_rel in calc of mols.						
Account for sweep eff?	SWPFLAG	1		1 = Yes, 0 = No. Multiplies Se by Sn in calculation of Conc.						
LNAPL Constituent Parameters and Initial Values:										
Constituent	**MW g/mol**	**Solubility (mg/L)**	**Vol Fract yi**	**Vol (m^3)**	**Density (g/cm^3)**	**Initial mols**	**Initial Mol Fract**	**Initial Mass Fract**	**Initial Mass (kg)**	**Difference Mass/Vol Fract**
TPH-d soluble components (C10-C24)	130	25	0.16	756.579418	0.780	4.54E+06	0.225	0.158	5.90E+05	1%
TPH-o soluble components (C24-C40)	240	0.0066	0	0	0.870	0.00E+00	0.000	0.000	0.00E+00	NA
(b)(3)	201.04	0	0.84	3972.04195	0.790	1.56E+07	0.775	0.842	3.14E+06	0%
			1.000	4728.62136		2.01E+07	1.000	1.000	3.73E+06	
Calculated Quantities:										
Specific discharge	q	6.14E-02	m/d							
Seepage velocity	v	4.68E-01	m/d	5.60E+02	ft/yr					
LNAPL lens cross-sectional area	Ax_lens	3.31E+02	m^2							
Volumetric flow rate through LNAPL	Q_gw	2.03E+01	m^3/d							
Average LNAPL molecular weight	MW_LNAPL	1.85E+02	g/mol							
Total initial moles	N_T^0	2.01E+07	mol							
LNAPL density	den_N	7.88E-01	g/cm^3							
Initial LNAPL mass	M_N	3.73E+06	kg							
Release media volume	V_T	7.21E+04	m^3							
Release media pore volume	V_P	9.46E+03	m^3							
Initial LNAPL saturation	S_Ni	5.00E-01	fraction							
Initial LNAPL content	theta_N	6.56E-02	fraction							
Initial water content	theta_w	6.56E-02	fraction	-						
Initial water relative permeability	k_rel	2.50E-01	fraction							

Figure 4-7
VZM Partitioning Module Output Compared to
the AGU Model of Mayer and Hassanizadeh (2005)

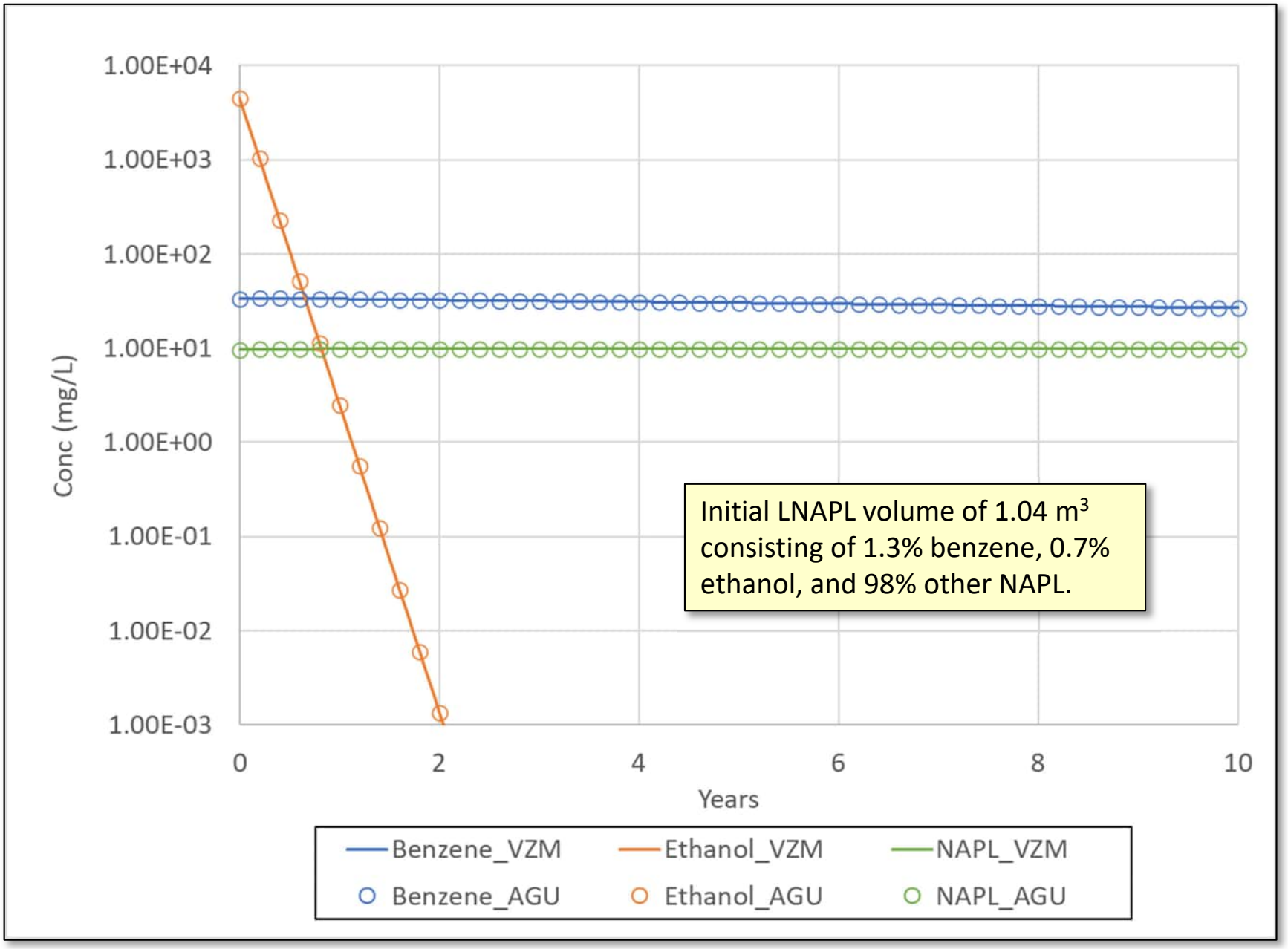

Figure 4-8
VZM Conceptual Model

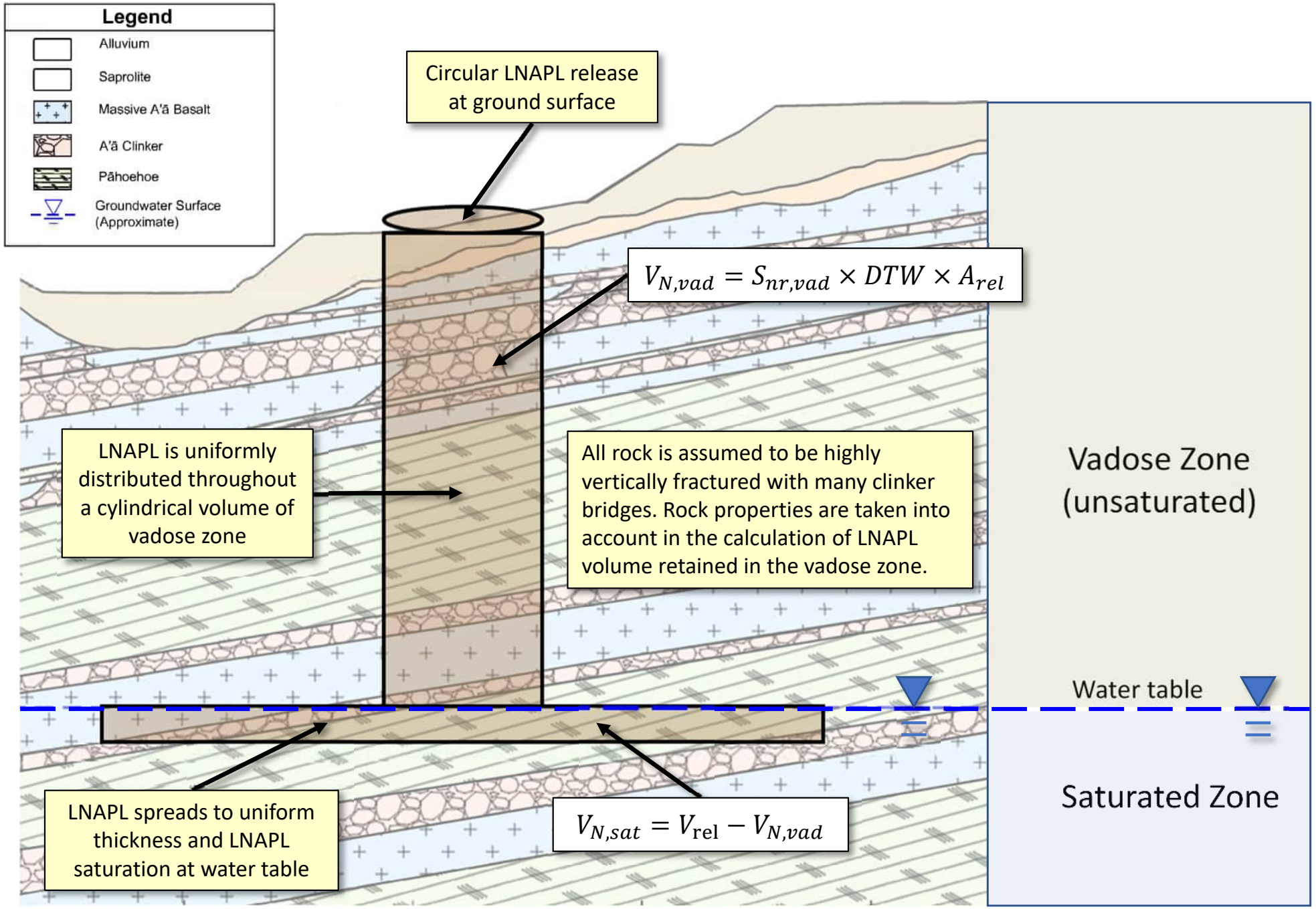

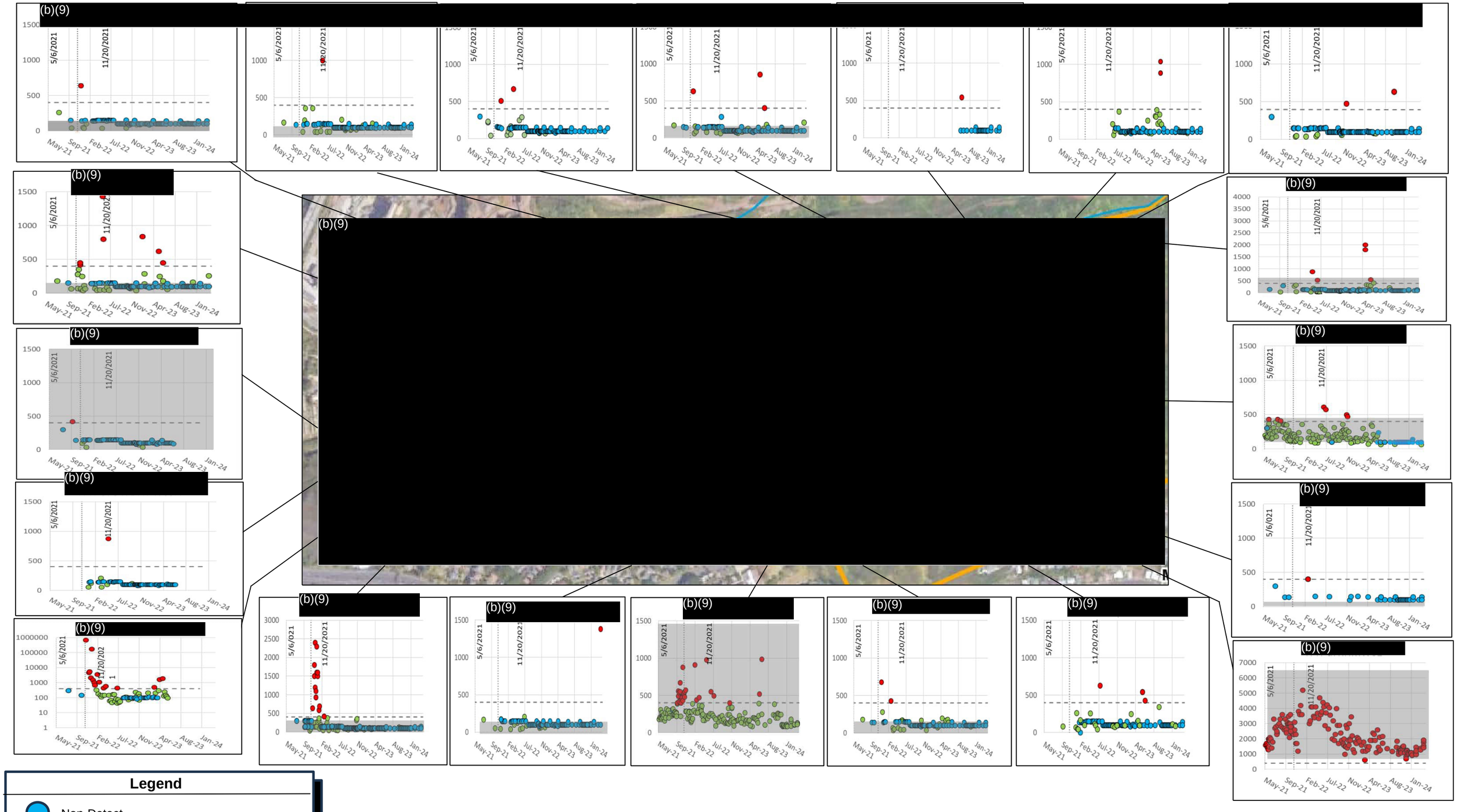

Figure 5-1
Sampling Locations with TPH-d Exceedances
GWFM, VZM, & CF&T Model Report
Red Hill Bulk Fuel Storage Facility
JBPHH, O‘ahu, Hawai‘i

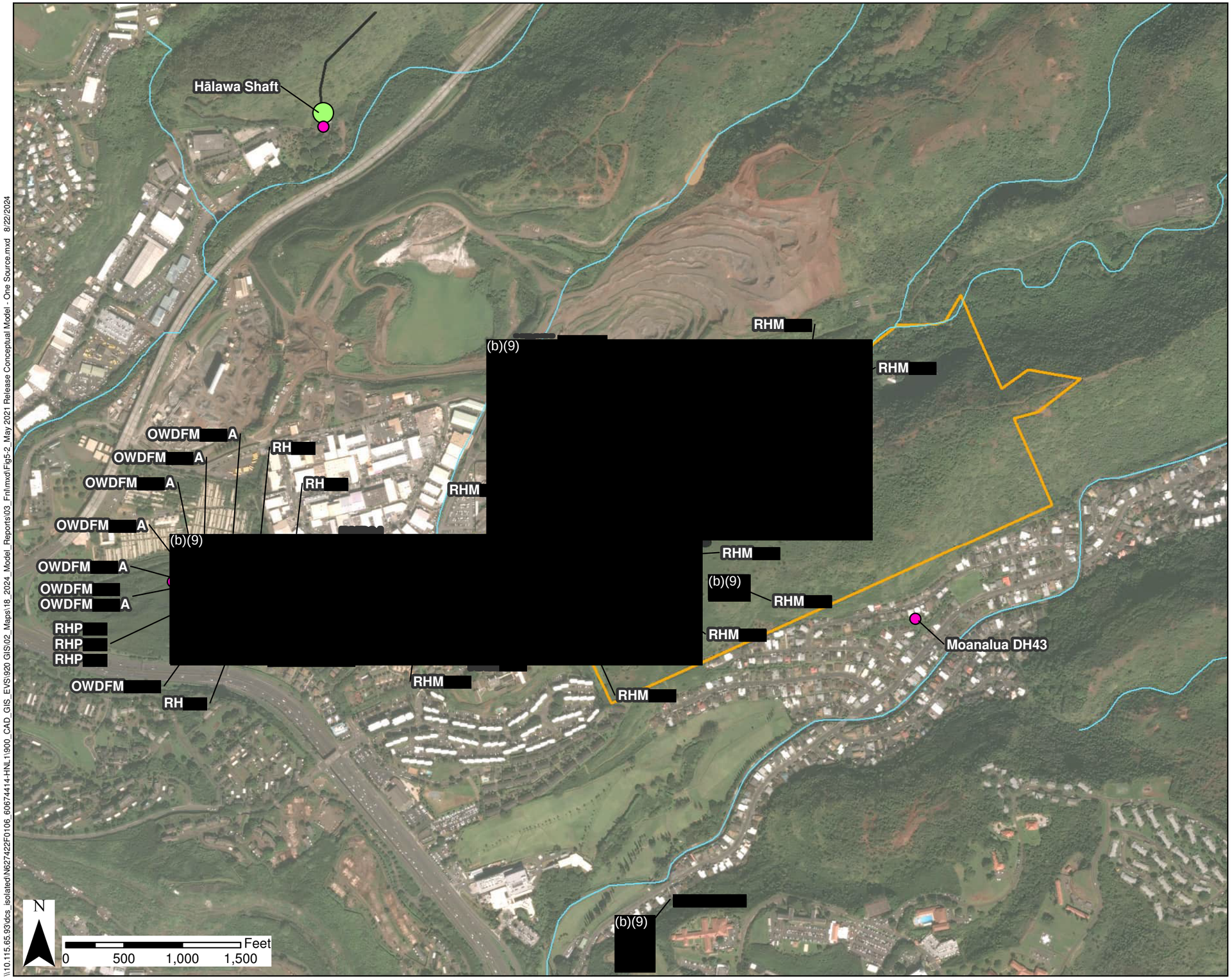

Location Map

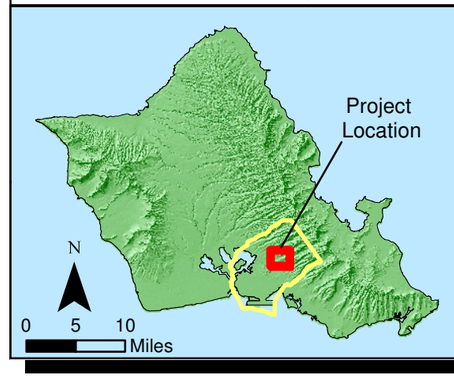

Legend

Water Supply Well / Shaft (MGD)

- 0.0 - 0.5
- 0.5 - 1.0
- 1.0 - 2.0
- 2.0 - 5.0
- 5.0 - 10.0
- 10.0 - 15.0

One Source - Reach:

- 100
- 200
- Basal Aquifer Well
- Water Development Tunnel / Infiltration Gallery
- Stream
- Red Hill Facility Boundary and Fuel Storage Tanks
- Groundwater Flow Model Domain

Notes

1. Map projection: NAD 1983 Hawaii State Plane Zone 3 feet.
2. Base Map: DigitalGlobe, Inc. (DG) and NRCS. Publication_Date: 2015
3. Spring locations provided by USGS.
4. Water supply well locations provided by DLNR.

Figure 5-2
May 2021 Release Conceptual Model - One Source
GWFM, VZM, & CF&T Model Report
Red Hill Bulk Fuel Storage Facility
JBPHH, O'ahu, HI

\\10.115.65.93\dcs_isolated\N627422F0106_60674414-HNL\1900_CAD_GIS_EVS\920 GIS\02_Maps\18_2024_Model_Reports\03_Fnl\mxd\Fig5-2_May 2021 Release Conceptual Model - One Source.mxd 8/22/2024

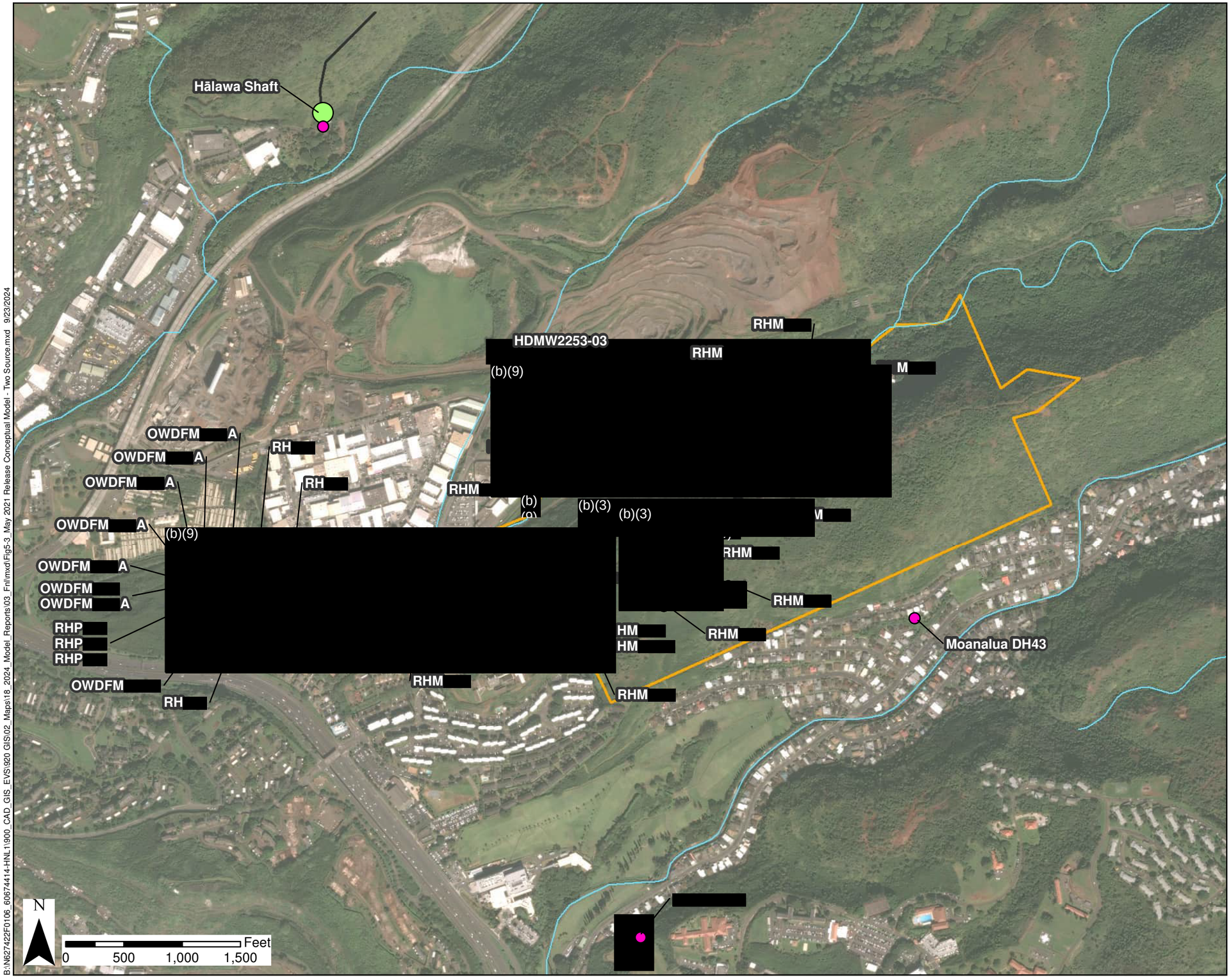

Location Map

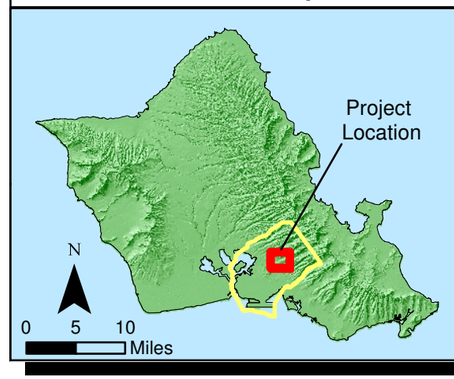

Legend

Water Supply Well / Shaft (MGD)

- 0.0 - 0.5
- 0.5 - 1.0
- 1.0 - 2.0
- 2.0 - 5.0
- 5.0 - 10.0
- 10.0 - 15.0

Two Sources - Reach:

- 100
- 200
- Basal Aquifer Well
- Water Development Tunnel / Infiltration Gallery
- Stream
- Red Hill Facility Boundary and Fuel Storage Tanks
- Groundwater Flow Model Domain

Notes

1. Map projection: NAD 1983 Hawaii State Plane Zone 3 feet.
2. Base Map: DigitalGlobe, Inc. (DG) and NRCS. Publication_Date: 2015
3. Spring locations provided by USGS.
4. Water supply well locations provided by DLNR.

B:\N627422F0106_60674414-HNL1\900_CAD_GIS_EVS\920 GIS\02_Maps\18_2024_Model_Reports\03_Fnl\mxd\Fig5-3_May 2021 Release Conceptual Model - Two Source.mxd 9/23/2024

Figure 5-3
May 2021 Release Conceptual Model - Two Sources
GWFM, VZM, & CF&T Model Report
Red Hill Bulk Fuel Storage Facility
JBPHH, O'ahu, HI

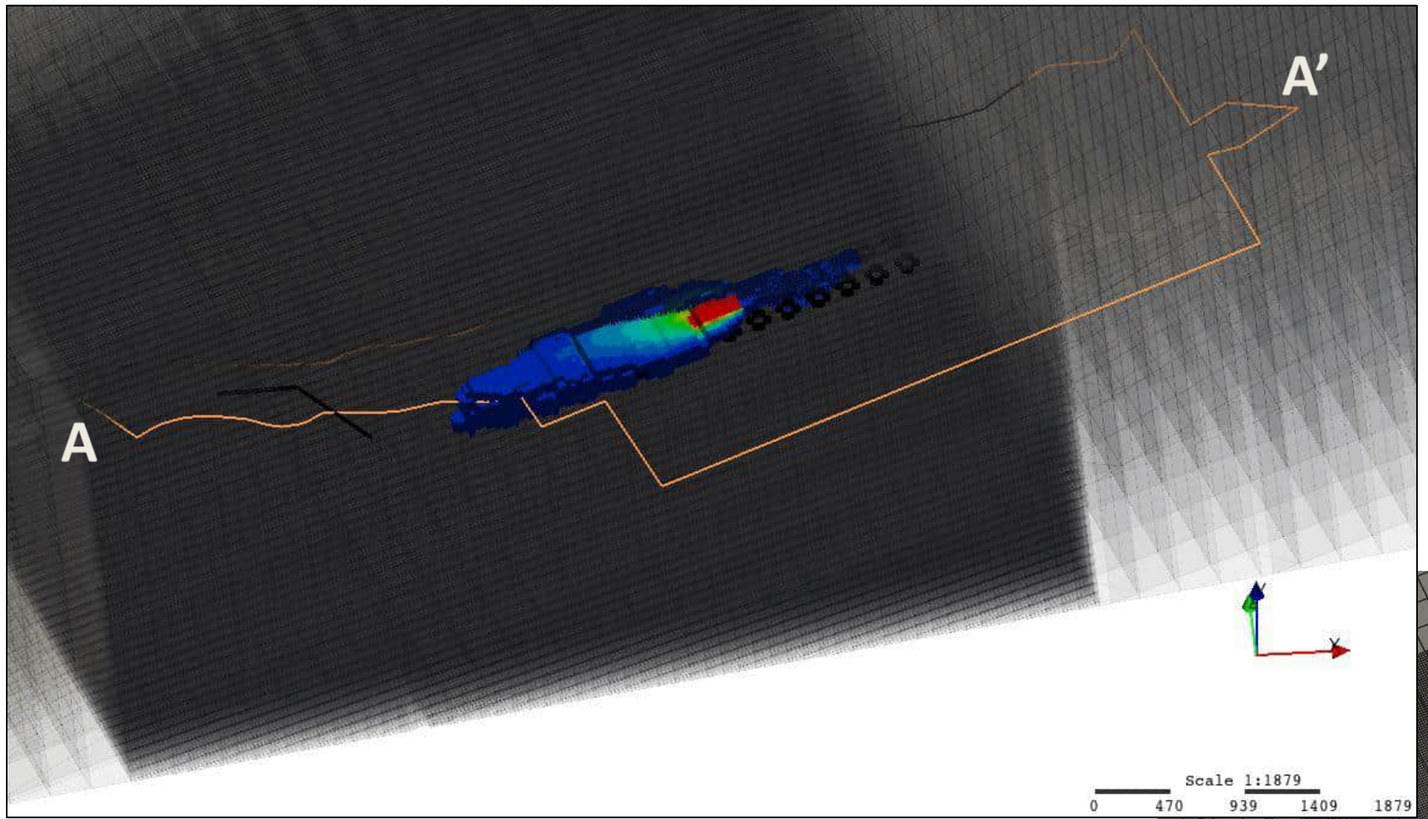

Vertical exaggeration = 4
TPH-d GWSC = 400 µg/L

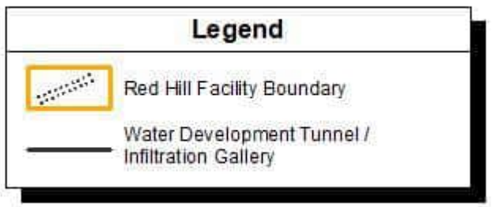

This scenario is an exploratory analysis and does not represent current conditions

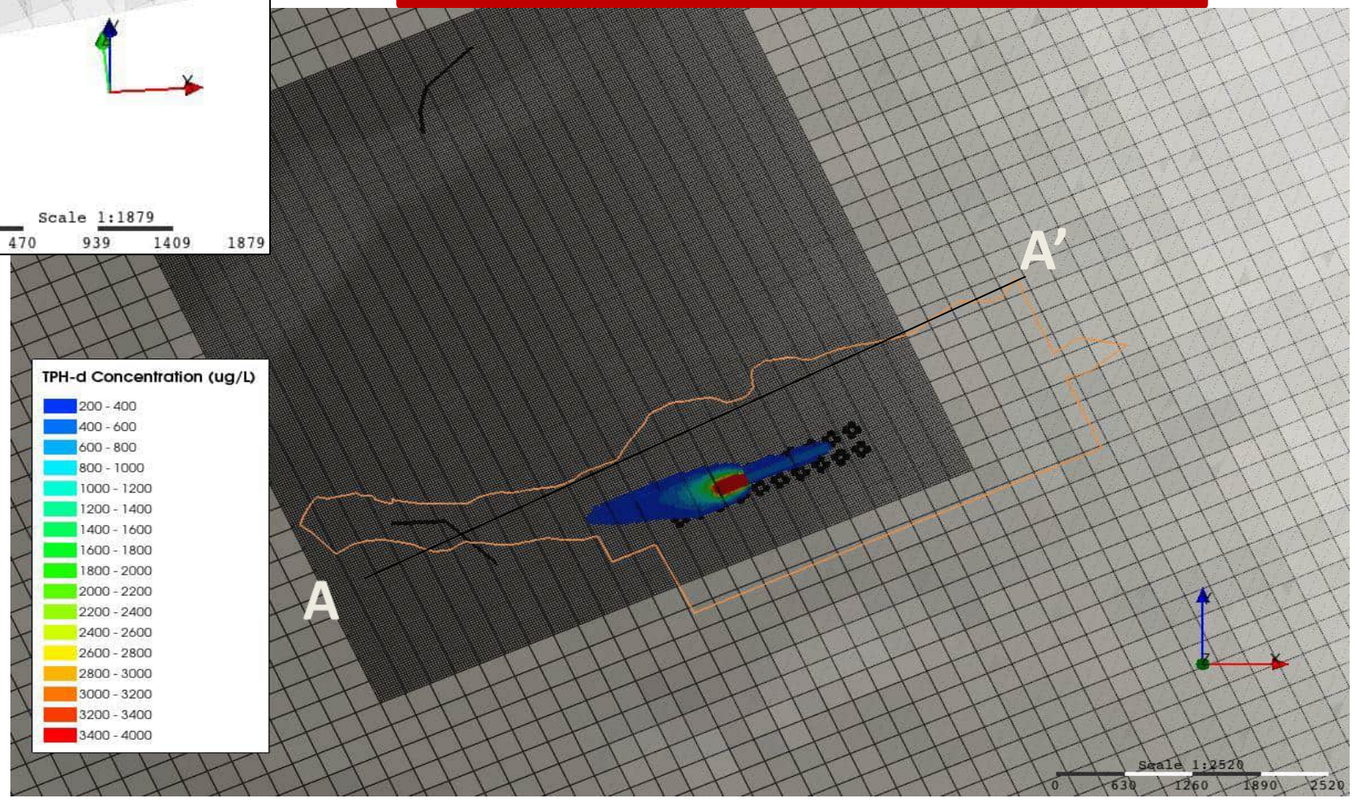

Figure 5-4
May 2021 Release Results for Example Realization - One Source
GWFM, VZM, & CF&T Model Report
Red Hill Bulk Fuel Storage Facility
JBPHH, O‘ahu, Hawai‘i

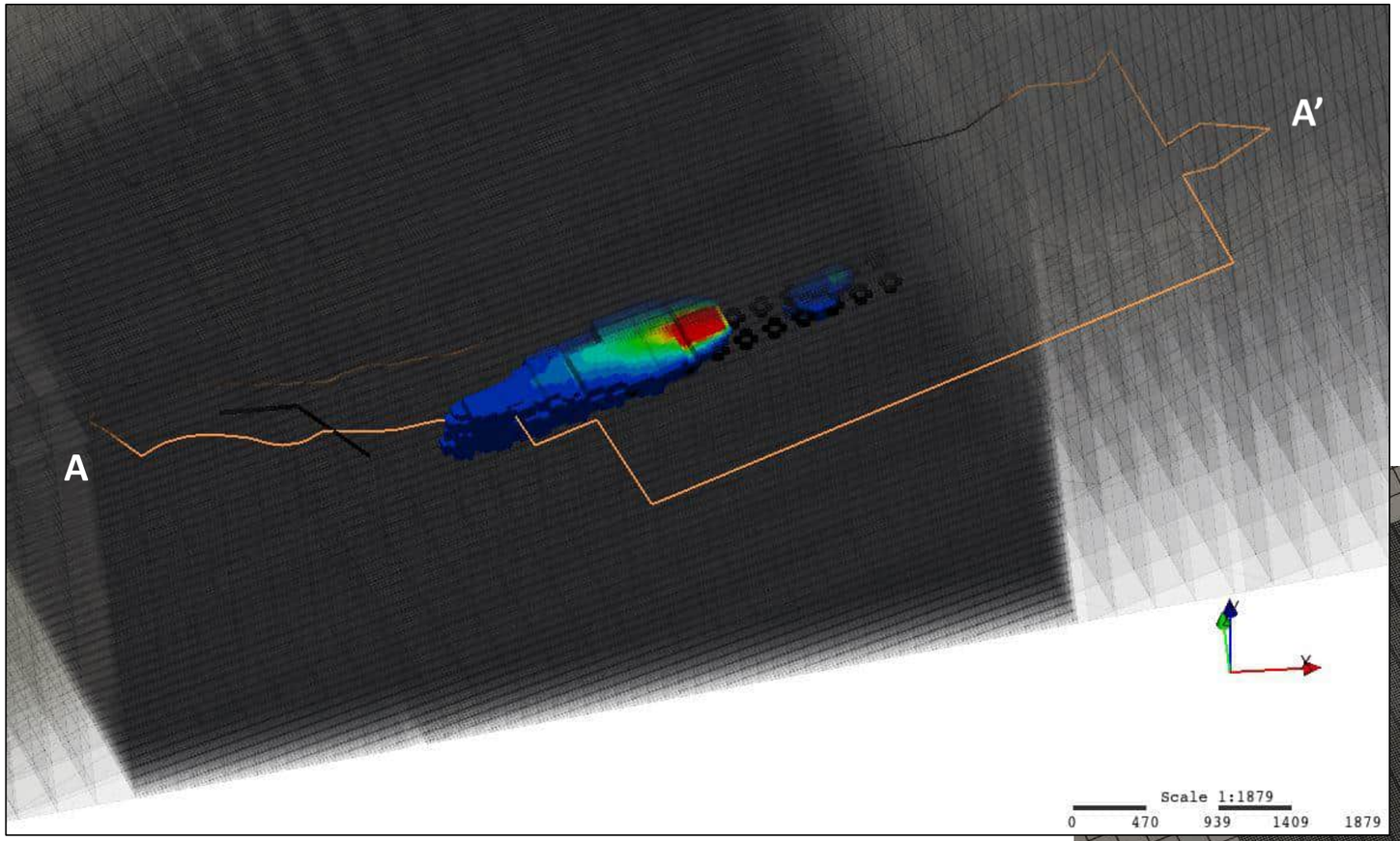

Vertical exaggeration = 4
TPH-d GWSC = 400 µg/L

Legend

Red Hill Facility Boundary

Water Development Tunnel / Infiltration Gallery

This scenario is an exploratory analysis and does not represent current conditions

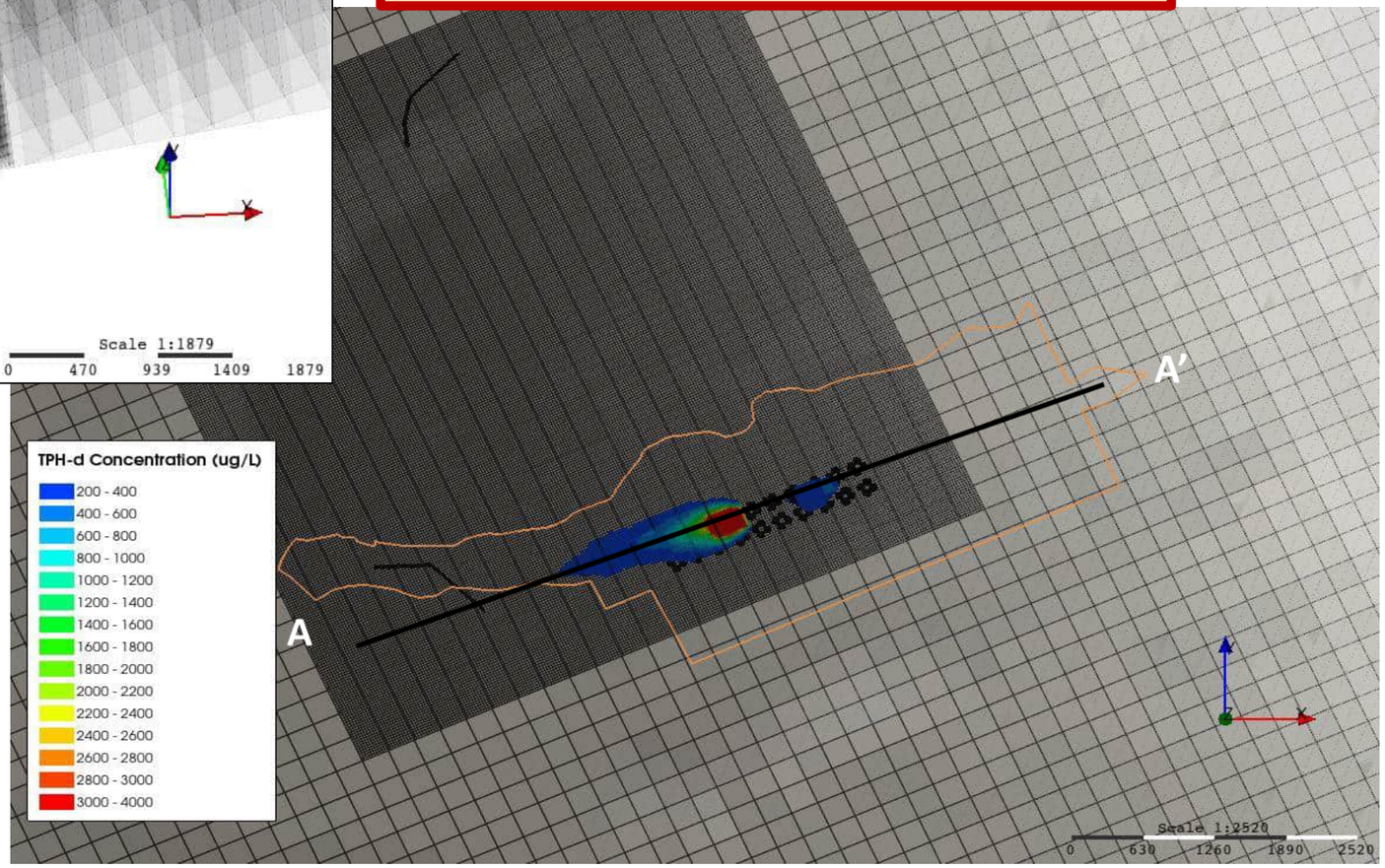

Figure 5-5
May 2021 Release Results for Example Realization - Two Sources
GWFM, VZM, & CF&T Model Report
Red Hill Bulk Fuel Storage Facility
JBPHH, O‘ahu, Hawai‘i

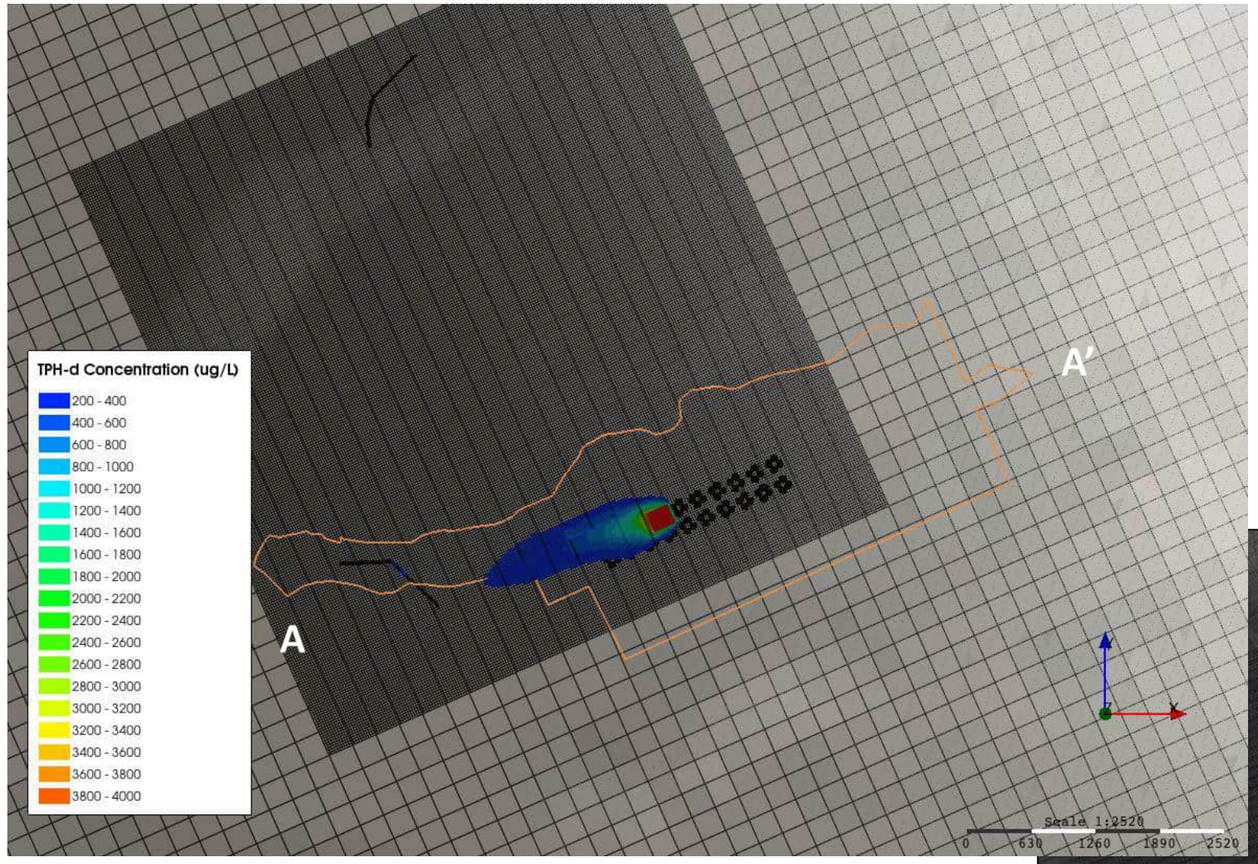

Vertical exaggeration = 4
TPH-d GWSC = 400 µg/L

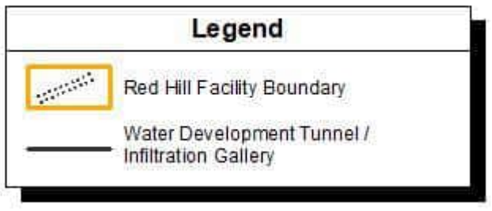

This scenario is an exploratory analysis and does not represent current conditions

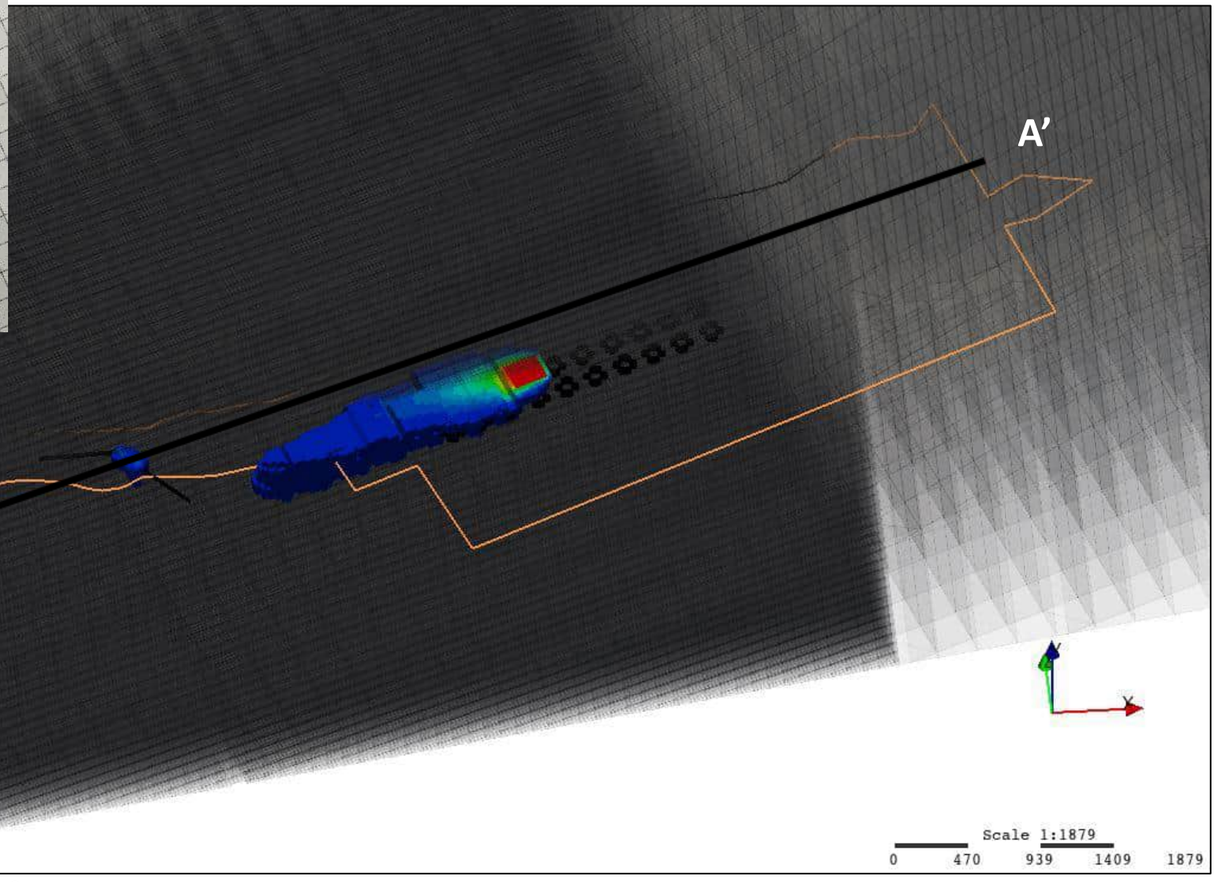

Figure 5-6
Predictive Simulation Results – Scenario 1 (example realization)
GWFM, VZM, & CF&T Model Report
Red Hill Bulk Fuel Storage Facility
JBPHH, O‘ahu, Hawai‘i

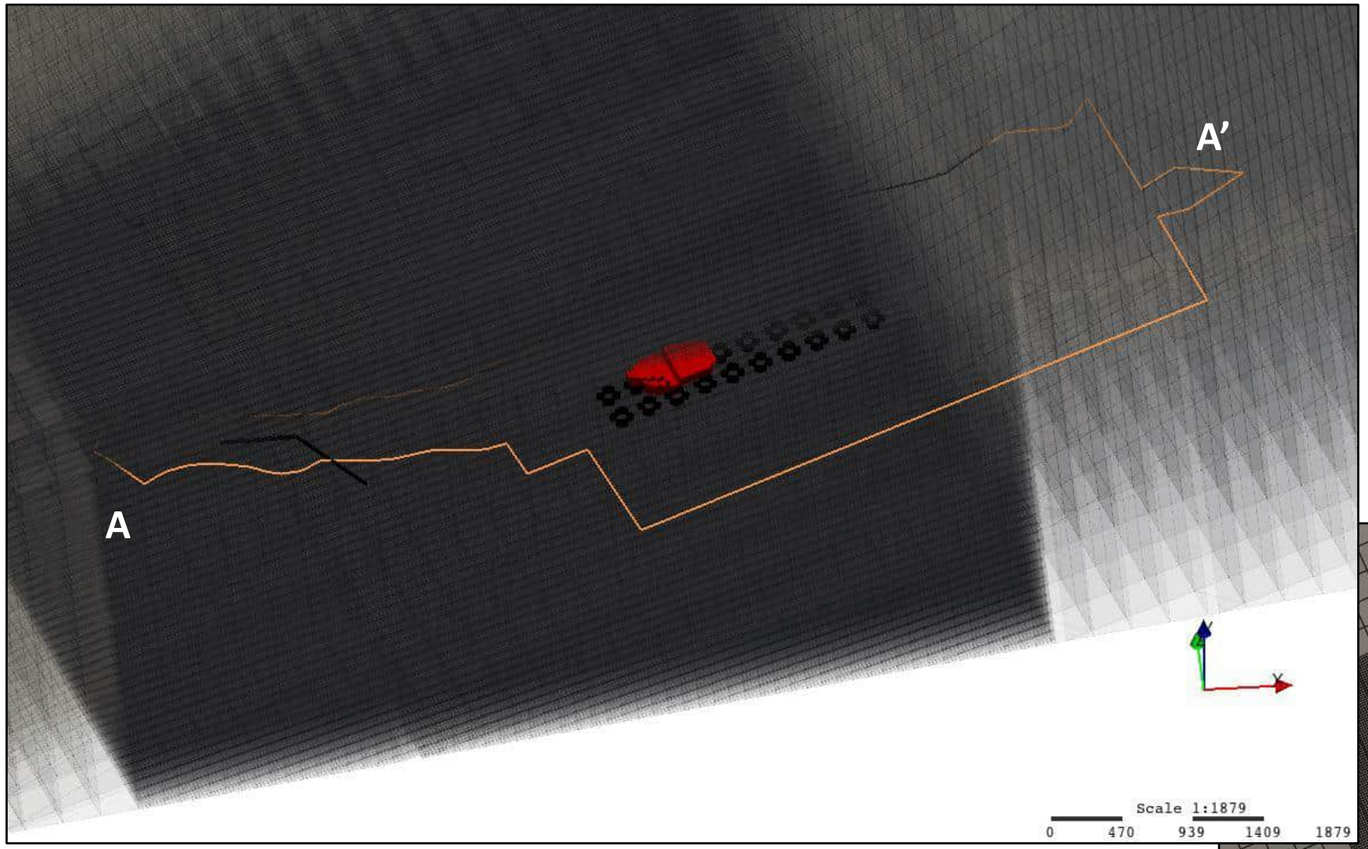

This scenario is an exploratory analysis and does not represent current conditions

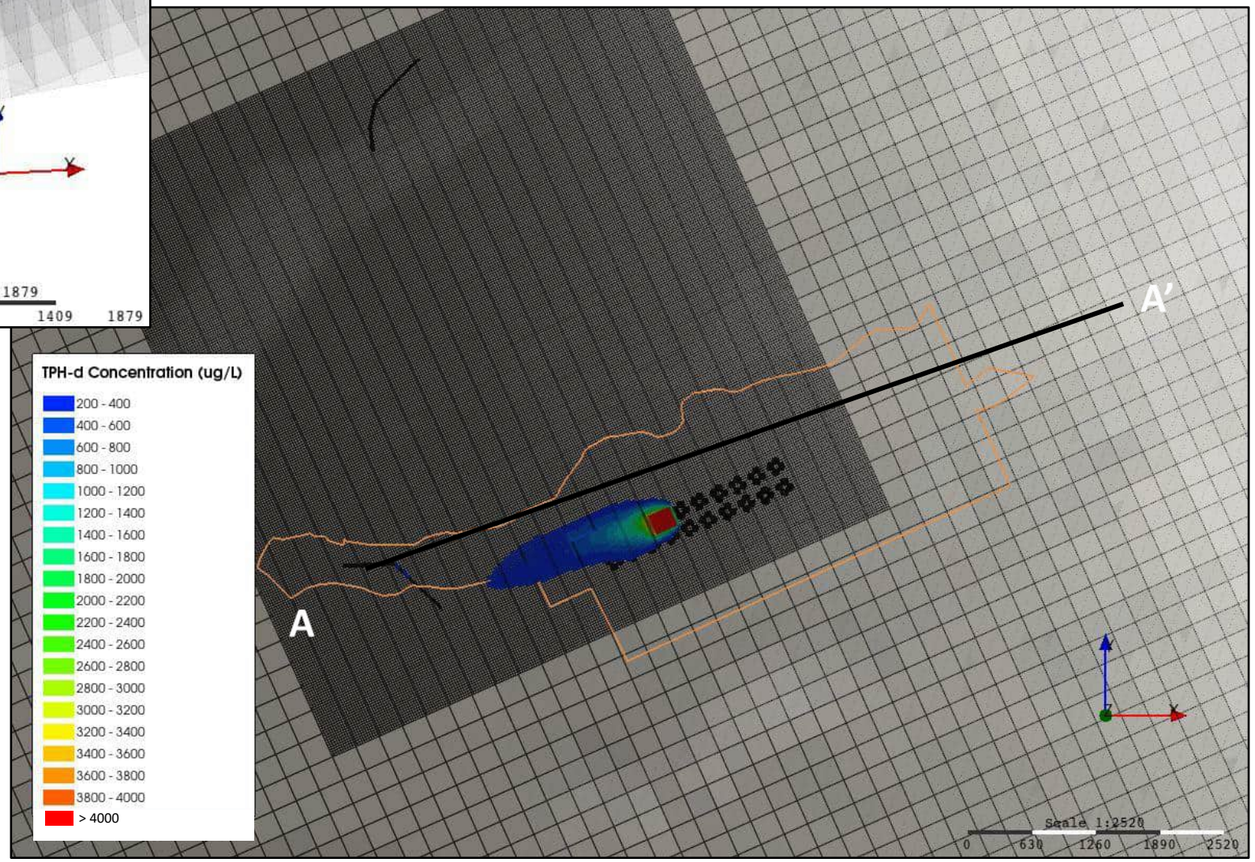

Vertical exaggeration = 4
TPH-d GWSC = 400 µg/L

Legend

Red Hill Facility Boundary

Water Development Tunnel / Infiltration Gallery

Figure 5-7
Predictive Simulation Results – Scenario 2 (example realization)
GWFM, VZM, & CF&T Model Report
Red Hill Bulk Fuel Storage Facility
JBPHH, Oʻahu, Hawaiʻi

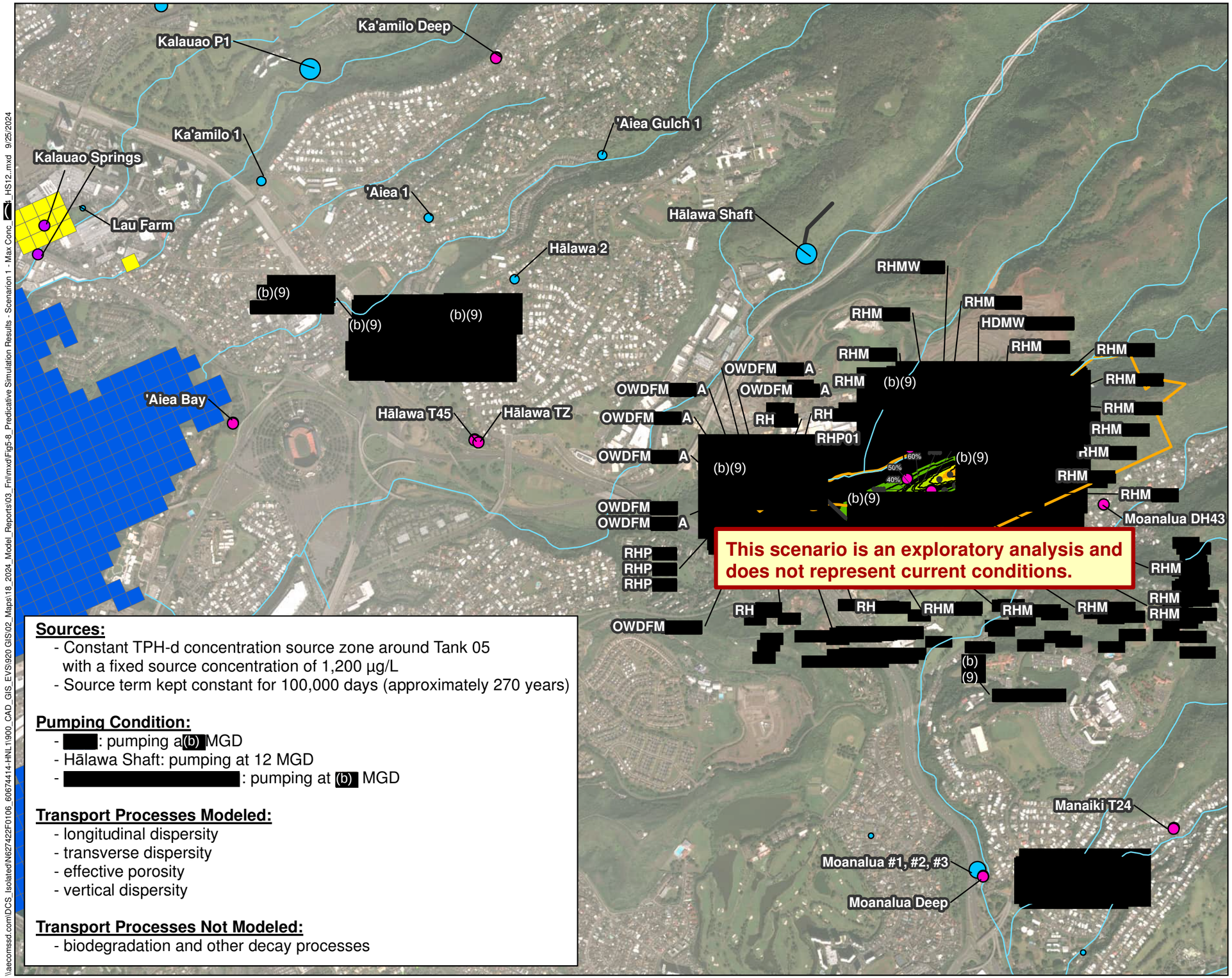

Sources:

- Constant TPH-d concentration source zone around Tank 05 with a fixed source concentration of 1,200 µg/L
- Source term kept constant for 100,000 days (approximately 270 years)

Pumping Condition:

- [redacted]: pumping at (b) MGD
- Hālawa Shaft: pumping at 12 MGD
- [redacted]: pumping at (b) MGD

Transport Processes Modeled:

- longitudinal dispersity
- transverse dispersity
- effective porosity
- vertical dispersity

Transport Processes Not Modeled:

- biodegradation and other decay processes

Legend

Water Supply Well / Shaft (MGD)

- 0.0 - 0.5
- 0.5 - 1.0
- 1.0 - 2.0
- 2.0 - 5.0
- 5.0 - 10.0
- 10.0 - 15.0

Boundary Conditions

- Constant Heads (Layer 1 only)
- Drains

Average Calibration TPH-d Results (µg/L)

- 100 to < 200
- 200 to < 400
- 400 to < 600
- 600 to < 800
- 800 to < 1,000
- 1,000 to < 2,000
- 2,000 to < 3,000
- 3,000 to < 4,000
- > 4,000

- 10% — Percentage of Realizations with GWSC Exceedance
- Basal Aquifer Well
- Spring
- Water Development Tunnel / Infiltration Gallery
- Stream
- Red Hill Facility Boundary

Notes

1. Map projection: NAD 1983 Hawaii State Plane Zone 3 feet.
2. Base Map: DigitalGlobe, Inc. (DG) and NRCS. Publication_Date: 2015
3. Spring locations provided by USGS.
4. Water supply well locations provided by DLNR.
5. GWSC for TPH-d = 400 µg/L

N

0 1,000 2,000 3,000 Feet

Figure 5-8
Predictive Simulation Results - Scenario 1 - Average Simulated TPH-d Concentration Across All Calibrated Realizations
[redacted] Pumping at (b) mgd, Hālawa Shaft Pumping at 12 mgd, (b)(3) [redacted] mgd
GWFM, VZM, & CF&T Model Report
Red Hill Bulk Fuel Storage Facility
JBPHH, O'ahu, HI

\\aecomssd.com\DCS_Isolated\N627422F0106_60674414-HNL11900_CAD_GIS_EVS\920 GIS\02_Maps\18_2024_Model_Report\03_Fnl\mxd\Fig5-8_Predicative Simulation Results - Scenarion 1 - Max Conc_HS12..mxd 9/25/2024

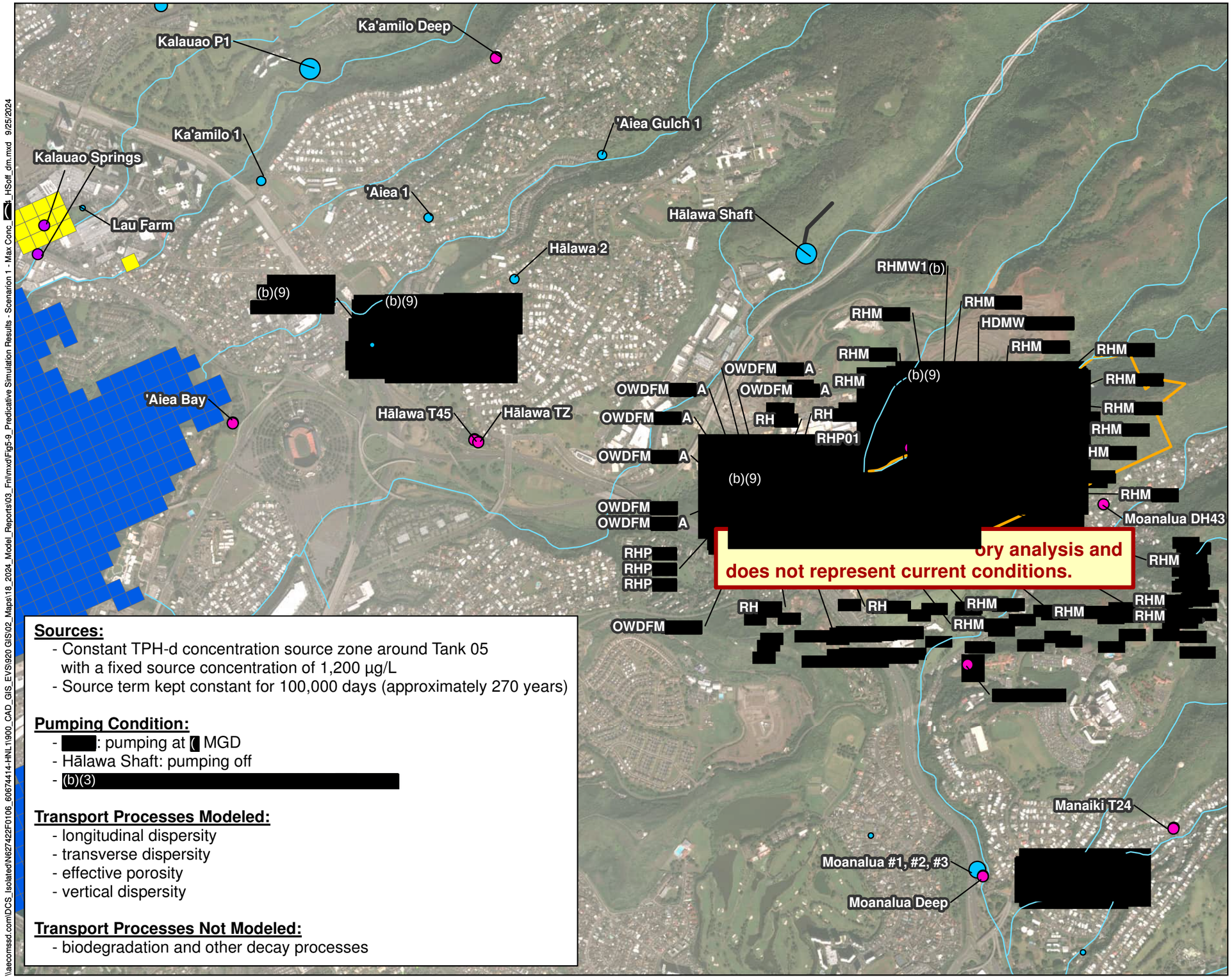

\\aecomssd.com\DCS_Isolated\N627422F0106_60674414-HNL1\900_CAD_GIS_EVS\920 GIS\02_Maps\18_2024_Model_Reports\03_Fnl\mxd\Fig5-9_Predicative Simulation Results - Scenarion 1 - Max Conc_HSoff_dm.mxd 9/25/2024

Sources:
- Constant TPH-d concentration source zone around Tank 05 with a fixed source concentration of 1,200 µg/L
- Source term kept constant for 100,000 days (approximately 270 years)

Pumping Condition:
- [redacted]: pumping at [redacted] MGD
- Hālawa Shaft: pumping off
- (b)(3) [redacted]

Transport Processes Modeled:
- longitudinal dispersity
- transverse dispersity
- effective porosity
- vertical dispersity

Transport Processes Not Modeled:
- biodegradation and other decay processes

Legend

Water Supply Well / Shaft (MGD)

0.0 - 0.5	2.0 - 5.0
0.5 - 1.0	5.0 - 10.0
1.0 - 2.0	10.0 - 15.0

Boundary Conditions
- Constant Heads (Layer 1 only)
- Drains

Average Calibration TPH-d Results (µg/L)

100 to < 200	800 to < 1,000
200 to < 400	1,000 to < 2,000
400 to < 600	2,000 to < 3,000
600 to < 800	3,000 to < 4,000
	> 4,000

- 16% — Percentage of Realizations with GWSC Exceedances
- Basal Aquifer Well
- Spring
- Water Development Tunnel / Infiltration Gallery
- Stream
- Red Hill Facility Boundary

Notes

1. Map projection: NAD 1983 Hawaii State Plane Zone 3 feet.
2. Base Map: DigitalGlobe, Inc. (DG) and NRCS. Publication_Date: 2015
3. Spring locations provided by USGS.
4. Water supply well locations provided by DLNR.
5. GWSC for TPH-d = 400 µg/L

Figure 5-9
Predictive Simulation Results - Scenario 1 - Maximum Simulated TPH-d Concentration Across All Calibrated Realizations
[redacted] Pumping at (b) mgd, Hālawa Shaft Pumping at Off, (b)(3) [redacted]
GWFM, VZM, & CF&T Model Report
Red Hill Bulk Fuel Storage Facility
JBPHH, O'ahu, HI

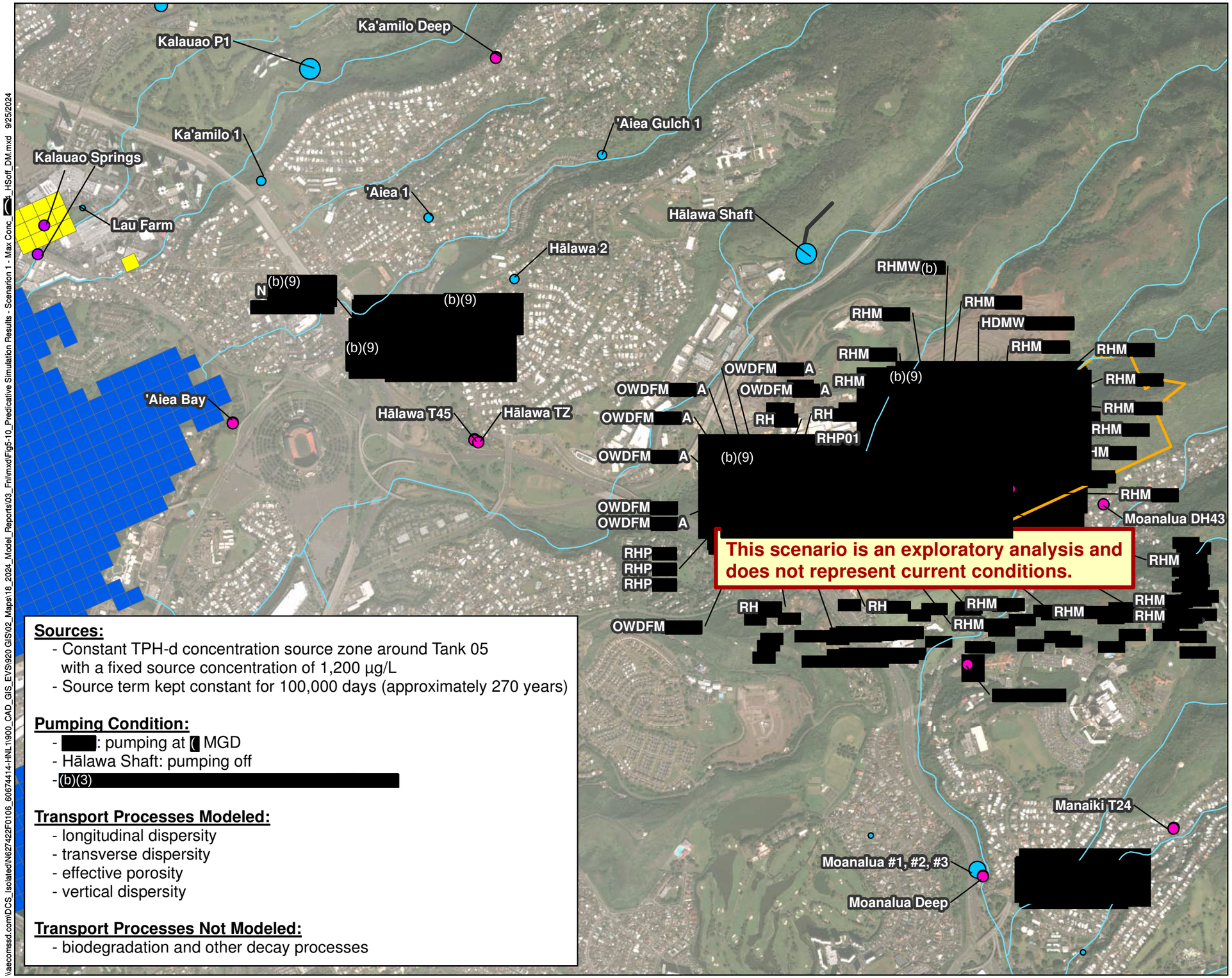

Sources:
- Constant TPH-d concentration source zone around Tank 05 with a fixed source concentration of 1,200 µg/L
- Source term kept constant for 100,000 days (approximately 270 years)

Pumping Condition:
- [redacted]: pumping at [redacted] MGD
- Hālawa Shaft: pumping off
- (b)(3) [redacted]

Transport Processes Modeled:
- longitudinal dispersity
- transverse dispersity
- effective porosity
- vertical dispersity

Transport Processes Not Modeled:
- biodegradation and other decay processes

Legend

Water Supply Well / Shaft (MGD)

0.0 - 0.5	2.0 - 5.0
0.5 - 1.0	5.0 - 10.0
1.0 - 2.0	10.0 - 15.0

Boundary Conditions
- Constant Heads (Layer 1 only)
- Drains

Average Calibration TPH-d Results (µg/L)

100 to < 200	800 to < 1,000
200 to < 400	1,000 to < 2,000
400 to < 600	2,000 to < 3,000
600 to < 800	3,000 to < 4,000
	> 4,000

- 10% Percentage of Realizations with GWSC Exceedance
- Basal Aquifer Well
- Spring
- Water Development Tunnel / Infiltration Gallery
- Stream
- Red Hill Facility Boundary

Notes

1. Map projection: NAD 1983 Hawaii State Plane Zone 3 feet.
2. Base Map: DigitalGlobe, Inc. (DG) and NRCS. Publication_Date: 2015
3. Spring locations provided by USGS.
4. Water supply well locations provided by DLNR.
5. GWSC for TPH-d = 400 µg/L

N

0 1,000 2,000 3,000 Feet

Figure 5-10
Predictive Simulation Results - Scenario 1 - Maximum Simulated TPH-d Concentration Across All Calibrated Realizations
[redacted] Pumping at (b)
Hālawa Shaft Pumping at Off,
(b)(3) [redacted]
GWFM, VZM, & CF&T Model Report
Red Hill Bulk Fuel Storage Facility
JBPHH, O'ahu, HI

\\aecomnssd.com\DCS_Isolated\N627422F0106_60674414-HNL1\900_CAD_GIS_EVS\920 GIS\02_Maps\18_2024_Model_Reports\03_Fnl\mxd\Fig5-10_Predicative Simulation Results - Scenarion 1 - Max Conc_(b)(3)_HSoff_DM.mxd 9/25/2024

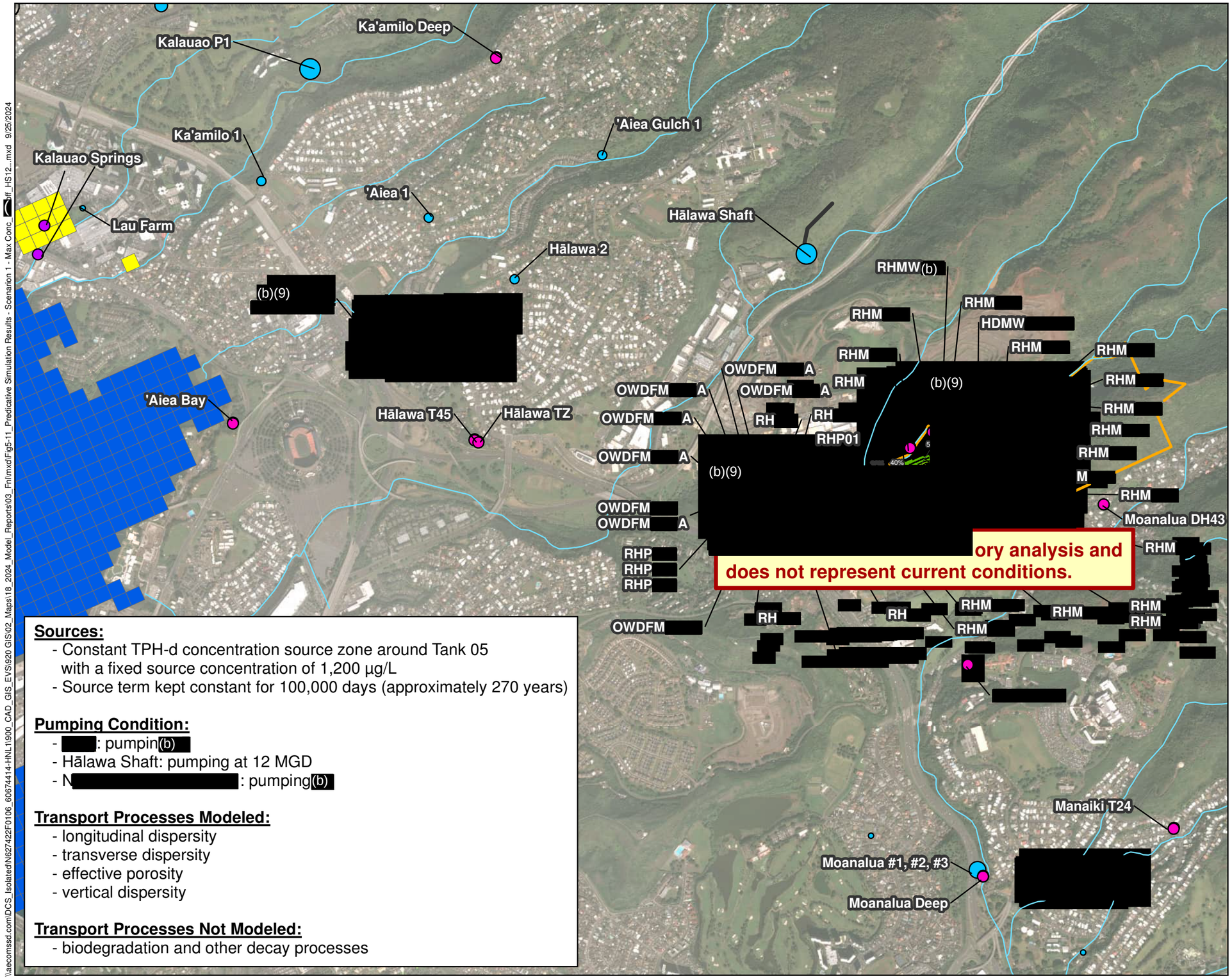

Legend

Water Supply Well / Shaft (MGD)

- 0.0 - 0.5
- 0.5 - 1.0
- 1.0 - 2.0
- 2.0 - 5.0
- 5.0 - 10.0
- 10.0 - 15.0

Boundary Conditions

- Constant Heads (Layer 1 only)
- Drains

Average Calibration TPH-d Results (µg/L)

- 100 to < 200
- 200 to < 400
- 400 to < 600
- 600 to < 800
- 800 to < 1,000
- 1,000 to < 2,000
- 2,000 to < 3,000
- 3,000 to < 4,000
- > 4,000

- 10% — Percentage of Realizations with GWSC Exceedances
- Basal Aquifer Well
- Spring
- Water Development Tunnel / Infiltration Gallery
- Stream
- Red Hill Facility Boundary

Notes

1. Map projection: NAD 1983 Hawaii State Plane Zone 3 feet.
2. Base Map: DigitalGlobe, Inc. (DG) and NRCS. Publication_Date: 2015
3. Spring locations provided by USGS.
4. Water supply well locations provided by DLNR.
5. GWSC for TPH-d = 400 µg/L

N

0 1,000 2,000 3,000 Feet

Figure 5-11
Predictive Simulation Results - Scenario 1 - Average Simulated TPH-d Concentration Across All Calibrated Realizations
[redacted] Pumping (b)
Hālawa Shaft Pumping at 12 mgd,
[redacted] Pumping (b)
GWFM, VZM, & CF&T Model Report
Red Hill Bulk Fuel Storage Facility
JBPHH, O'ahu, HI

\\aecomssd.com\DCS_Isolated\N627422F0106_606744\14-HNL1\900_CAD_GIS_EVS\920 GIS\02_Maps\18_2024_Model_Reports\03_Fnl\mxd\Fig5-11_Predicative Simulation Results - Scenarion 1 - Max Conc_Aff_HS12...mxd 9/25/2024

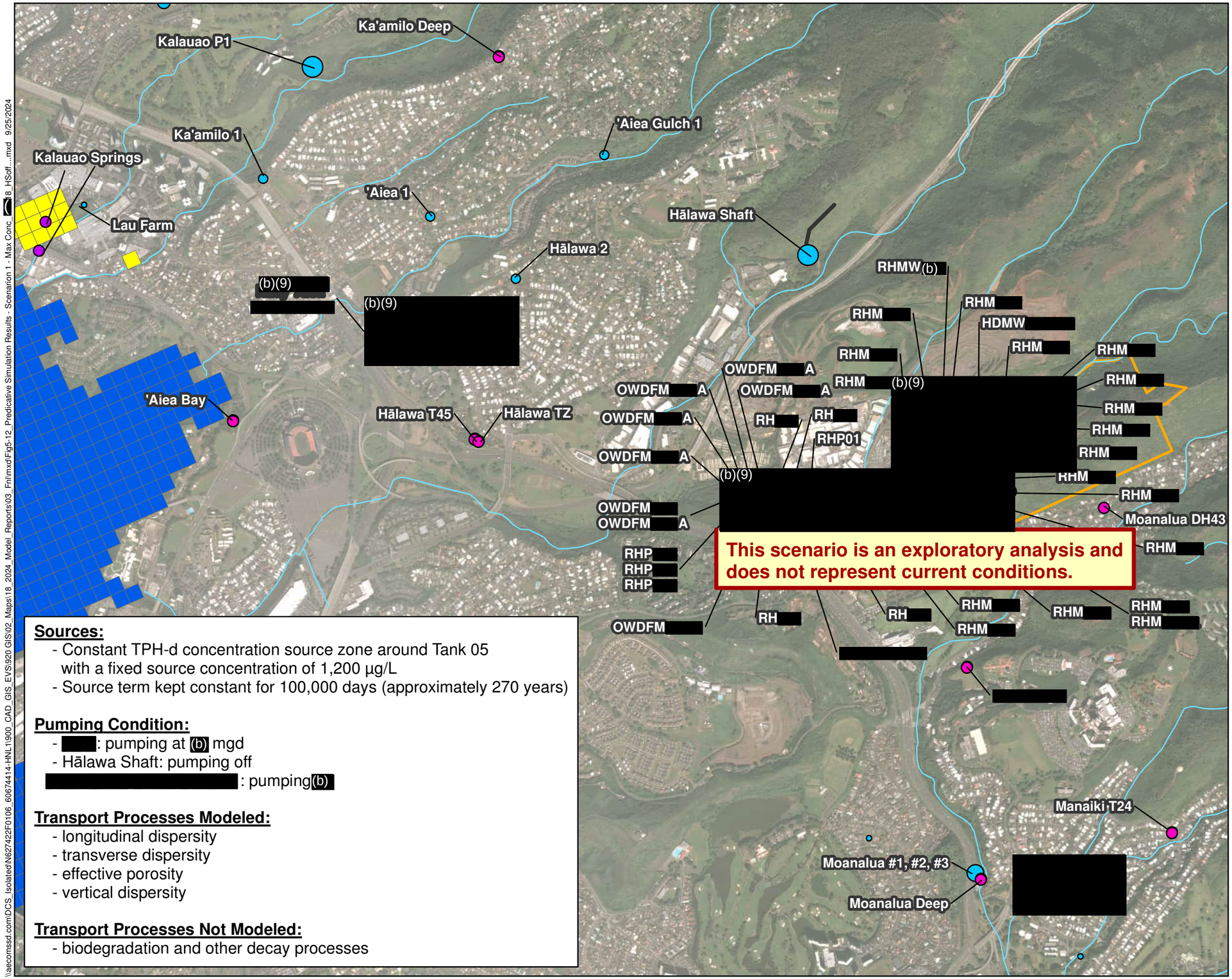

Sources:

- Constant TPH-d concentration source zone around Tank 05 with a fixed source concentration of 1,200 µg/L
- Source term kept constant for 100,000 days (approximately 270 years)

Pumping Condition:

- [redacted]: pumping at (b) mgd
- Hālawa Shaft: pumping off
- [redacted]: pumping (b)

Transport Processes Modeled:

- longitudinal dispersity
- transverse dispersity
- effective porosity
- vertical dispersity

Transport Processes Not Modeled:

- biodegradation and other decay processes

Legend

Water Supply Well / Shaft (MGD)

- 0.0 - 0.5
- 0.5 - 1.0
- 1.0 - 2.0
- 2.0 - 5.0
- 5.0 - 10.0
- 10.0 - 15.0

Boundary Conditions

- Constant Heads (Layer 1 only)
- Drains

Average Calibration TPH-d Results (µg/L)

- 100 to < 200
- 200 to < 400
- 400 to < 600
- 600 to < 800
- 800 to < 1,000
- 1,000 to < 2,000
- 2,000 to < 3,000
- 3,000 to < 4,000
- > 4,000

- 10% — Percentage of Realizations with GWSC Exceedances
- Basal Aquifer Well
- Spring
- Water Development Tunnel / Infiltration Gallery
- Stream
- Red Hill Facility Boundary

Notes

1. Map projection: NAD 1983 Hawaii State Plane Zone 3 feet.
2. Base Map: DigitalGlobe, Inc. (DG) and NRCS. Publication_Date: 2015
3. Spring locations provided by USGS.
4. Water supply well locations provided by DLNR.
5. GWSC for TPH-d = 400 µg/L

N

0 1,000 2,000 3,000 Feet

Figure 5-12
Predictive Simulation Results - Scenario 1 - Average Simulated TPH-d Concentration Across All Calibrated Realizations
[redacted] Pumping at [redacted] mgd, Hālawa Shaft Pumping off, [redacted] Pumping (b)
GWFM, VZM, & CF&T Model Report
Red Hill Bulk Fuel Storage Facility
JBPHH, O'ahu, HI

\\aecomssd.com\DCS_Isolated\N627422F0106_60674414-HNL11900_CAD_GIS_EVS\920 GIS\02_Maps\18_2024_Model_Report\03_Fnl\mxd\Fig5-12_Predicative Simulation Results - Scenarion 1 - Max Conc_8_HSoff....mxd 9/25/2024

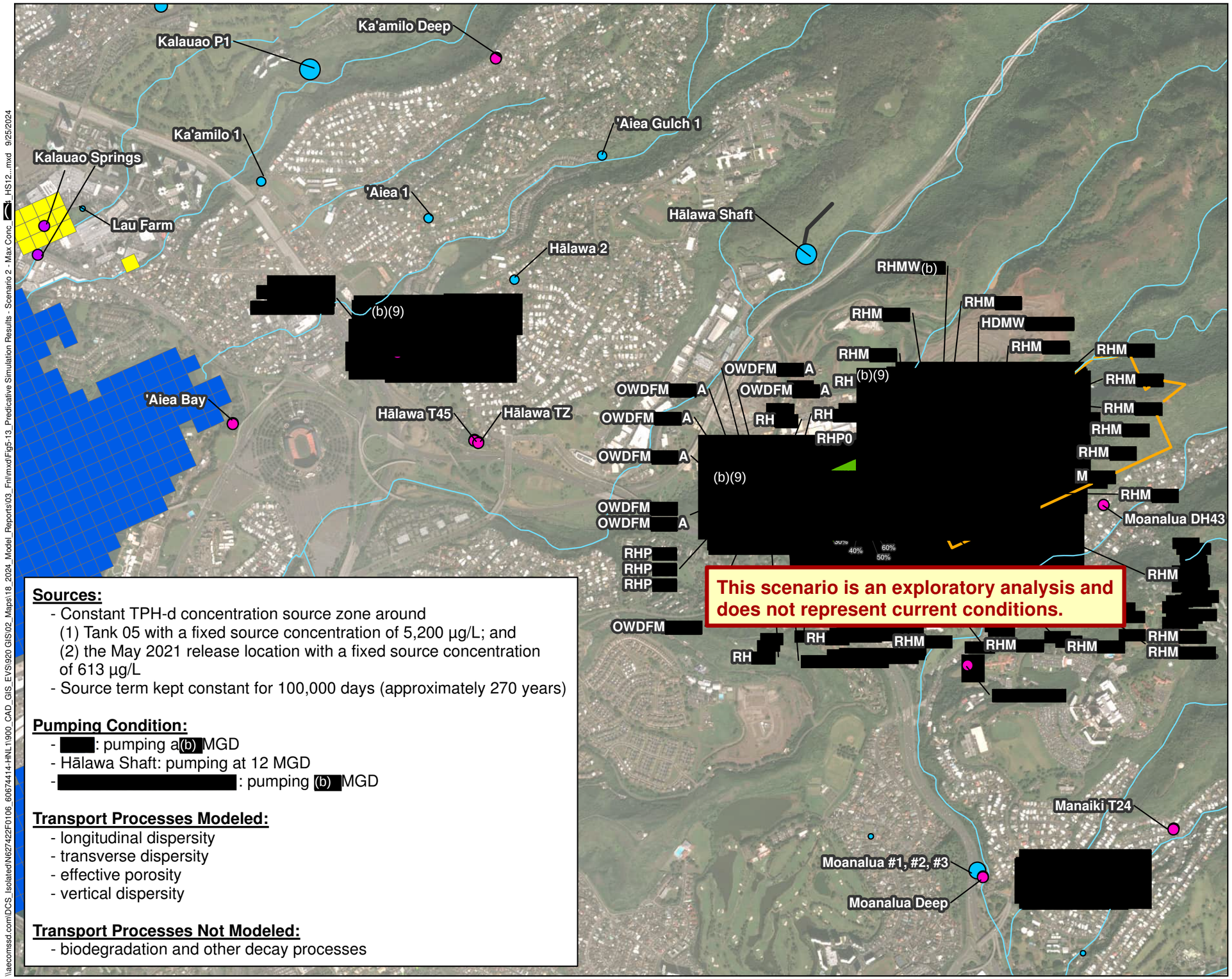

Sources:

- Constant TPH-d concentration source zone around
  (1) Tank 05 with a fixed source concentration of 5,200 µg/L; and
  (2) the May 2021 release location with a fixed source concentration of 613 µg/L
- Source term kept constant for 100,000 days (approximately 270 years)

Pumping Condition:

- [redacted]: pumping a(b) MGD
- Hālawa Shaft: pumping at 12 MGD
- [redacted]: pumping (b) MGD

Transport Processes Modeled:

- longitudinal dispersity
- transverse dispersity
- effective porosity
- vertical dispersity

Transport Processes Not Modeled:

- biodegradation and other decay processes

Legend

Water Supply Well / Shaft (MGD)

- 0.0 - 0.5
- 0.5 - 1.0
- 1.0 - 2.0
- 2.0 - 5.0
- 5.0 - 10.0
- 10.0 - 15.0

Boundary Conditions

- Constant Heads (Layer 1 only)
- Drains

Average Calibration TPH-d Results (µg/L)

- 100 to < 200
- 200 to < 400
- 400 to < 600
- 600 to < 800
- 800 to < 1,000
- 1,000 to < 2,000
- 2,000 to < 3,000
- 3,000 to < 4,000
- > 4,000

- Percentage of Realizations with GWSC Exceedances
- Basal Aquifer Well
- Spring
- Water Development Tunnel / Infiltration Gallery
- Stream
- Red Hill Facility Boundary

Notes

1. Map projection: NAD 1983 Hawaii State Plane Zone 3 feet.
2. Base Map: DigitalGlobe, Inc. (DG) and NRCS. Publication_Date: 2015
3. Spring locations provided by USGS.
4. Water supply well locations provided by DLNR.
5. GWSC for TPH-d = 400 µg/L

N

0 1,000 2,000 3,000 Feet

Figure 5-13
Predictive Simulation Results - Scenario 2 - Average Simulated TPH-d Concentration Across All Calibrated Realizations
[redacted] Pumping at (b) mgd, Hālawa Shaft Pumping at 12 mgd, [redacted] Pumping at (b) mgd
GWFM, VZM, & CF&T Model Report
Red Hill Bulk Fuel Storage Facility
JBPHH, O'ahu, HI

\\aecomssd.com\DCS_Isolated\N627422F0106_60674414-HNL11900_CAD_GIS_EVS\920 GIS\02_Maps\18_2024_Model_Report\03_Fnl\mxd\Fig5-13_Predicative Simulation Results - Scenario 2 - Max Conc_HS12...mxd 9/25/2024

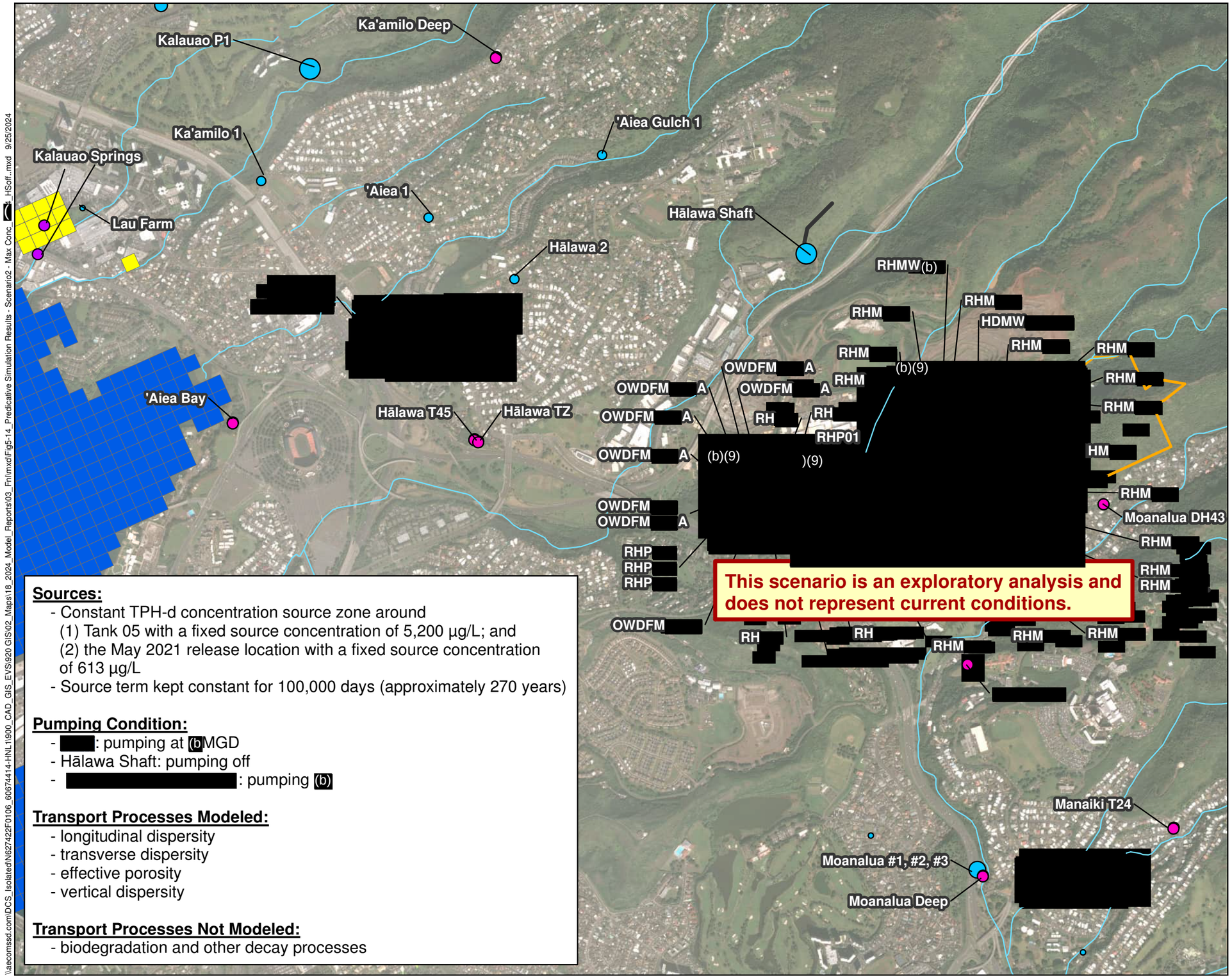

Sources:

- Constant TPH-d concentration source zone around
  (1) Tank 05 with a fixed source concentration of 5,200 µg/L; and
  (2) the May 2021 release location with a fixed source concentration of 613 µg/L
- Source term kept constant for 100,000 days (approximately 270 years)

Pumping Condition:

- [redacted]: pumping at (b) MGD
- Hālawa Shaft: pumping off
- [redacted]: pumping (b)

Transport Processes Modeled:

- longitudinal dispersity
- transverse dispersity
- effective porosity
- vertical dispersity

Transport Processes Not Modeled:

- biodegradation and other decay processes

Legend

Water Supply Well / Shaft (MGD)

- 0.0 - 0.5
- 0.5 - 1.0
- 1.0 - 2.0
- 2.0 - 5.0
- 5.0 - 10.0
- 10.0 - 15.0

Boundary Conditions

- Constant Heads (Layer 1 only)
- Drains

Average Calibration TPH-d Results (µg/L)

- 100 to < 200
- 200 to < 400
- 400 to < 600
- 600 to < 800
- 800 to < 1,000
- 1,000 to < 2,000
- 2,000 to < 3,000
- 3,000 to < 4,000
- > 4,000

- 16% — Percentage of Realizations with GWSC Exceedances
- Basal Aquifer Well
- Spring
- Water Development Tunnel / Infiltration Gallery
- Stream
- Red Hill Facility Boundary

Notes

1. Map projection: NAD 1983 Hawaii State Plane Zone 3 feet.
2. Base Map: DigitalGlobe, Inc. (DG) and NRCS. Publication_Date: 2015
3. Spring locations provided by USGS.
4. Water supply well locations provided by DLNR.
5. GWSC for TPH-d = 400 µg/L

N

0 1,000 2,000 3,000 Feet

Figure 5-14
Predictive Simulation Results - Scenario 2 - Average Simulated TPH-d Concentration Across All Calibrated Realizations
[redacted] Pumping at (b) mgd, Hālawa Shaft Pumping Off, [redacted] f.
GWFM, VZM, & CF&T Model Report
Red Hill Bulk Fuel Storage Facility
JBPHH, O'ahu, HI

\\aecomnssd.com\DCS_Isolated\N627422F0106_60674414-HNL1\900_CAD_GIS_EVS\920 GIS\02_Maps\18_2024_Model_Reports\03_Fnl\mxd\Fig5-14_Predicative Simulation Results - Scenario2 - Max Conc_1_HSoff..mxd 9/25/2024

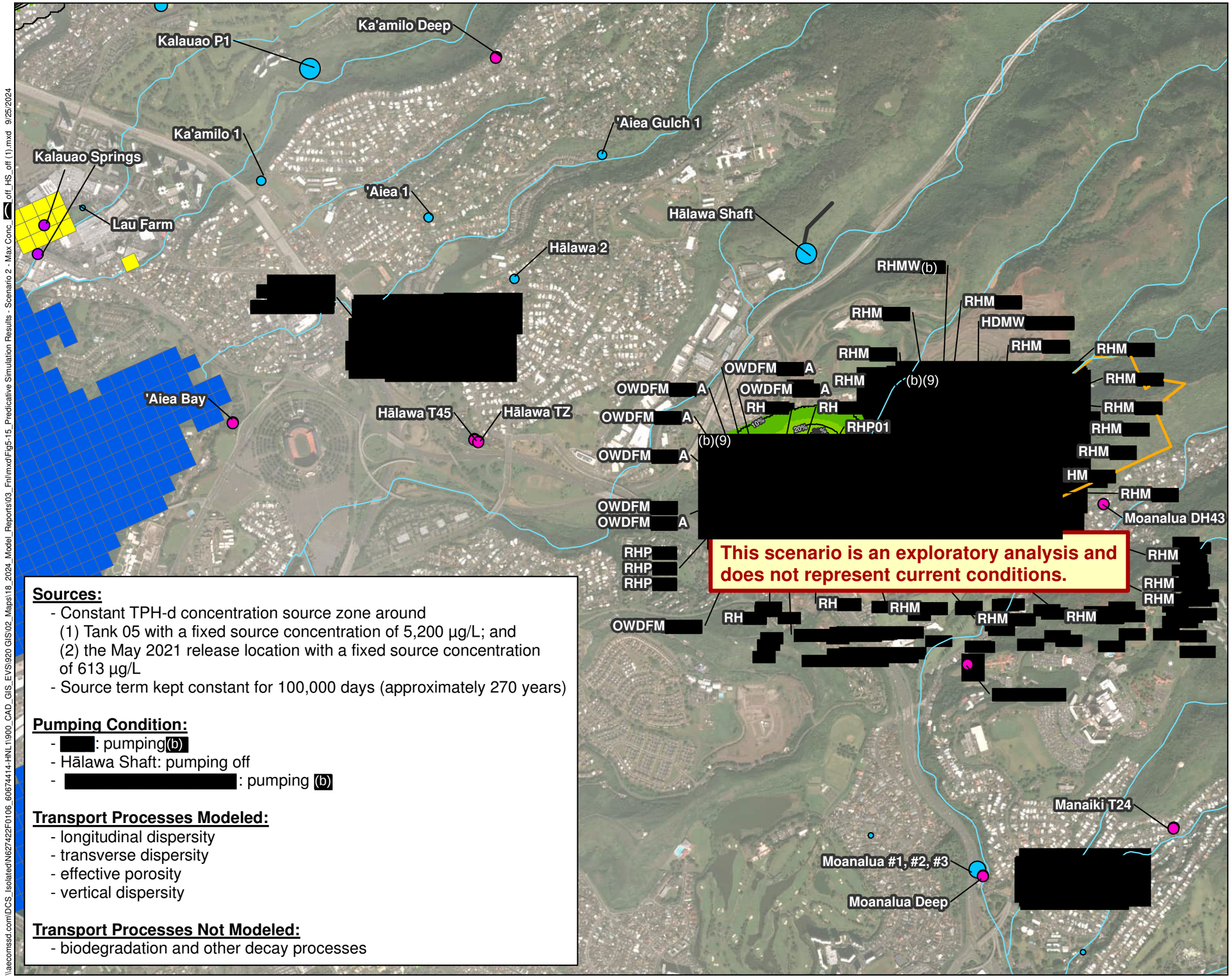

Sources:

- Constant TPH-d concentration source zone around
  (1) Tank 05 with a fixed source concentration of 5,200 µg/L; and
  (2) the May 2021 release location with a fixed source concentration of 613 µg/L
- Source term kept constant for 100,000 days (approximately 270 years)

Pumping Condition:

- [redacted]: pumping(b)
- Hālawa Shaft: pumping off
- [redacted]: pumping (b)

Transport Processes Modeled:

- longitudinal dispersity
- transverse dispersity
- effective porosity
- vertical dispersity

Transport Processes Not Modeled:

- biodegradation and other decay processes

Legend

Water Supply Well / Shaft (MGD)

- 0.0 - 0.5
- 0.5 - 1.0
- 1.0 - 2.0
- 2.0 - 5.0
- 5.0 - 10.0
- 10.0 - 15.0

Boundary Conditions

- Constant Heads (Layer 1 only)
- Drains

Average Calibration TPH-d Results (µg/L)

- 100 to < 200
- 200 to < 400
- 400 to < 600
- 600 to < 800
- 800 to < 1,000
- 1,000 to < 2,000
- 2,000 to < 3,000
- 3,000 to < 4,000
- > 4,000

- 10% — Percentage of Realizations with GWSC Exceedances
- Basal Aquifer Well
- Spring
- Water Development Tunnel / Infiltration Gallery
- Stream
- Red Hill Facility Boundary

Notes

1. Map projection: NAD 1983 Hawaii State Plane Zone 3 feet.
2. Base Map: DigitalGlobe, Inc. (DG) and NRCS. Publication_Date: 2015
3. Spring locations provided by USGS.
4. Water supply well locations provided by DLNR.
5. GWSC for TPH-d = 400 µg/L

N

0 1,000 2,000 3,000 Feet

Figure 5-15
Predictive Simulation Results - Scenario 2 - Average Simulated TPH-d Concentration Across All Calibrated Realizations
[redacted] Pumpin(b)[redacted], Hālawa Shaft Pumping Off, (b)(3) [redacted]
GWFM, VZM, & CF&T Model Report
Red Hill Bulk Fuel Storage Facility
JBPHH, O'ahu, HI

\\aecomnssd.com\DCS_Isolated\N627422F0106_60674414-HNL1\900_CAD_GIS_EVS\920 GIS\02_Maps\18_2024_Model_Reports\03_Fnl\mxd\Fig5-15_Predicative Simulation Results - Scenario 2 - Max Conc_off_HS_off (1).mxd 9/25/2024

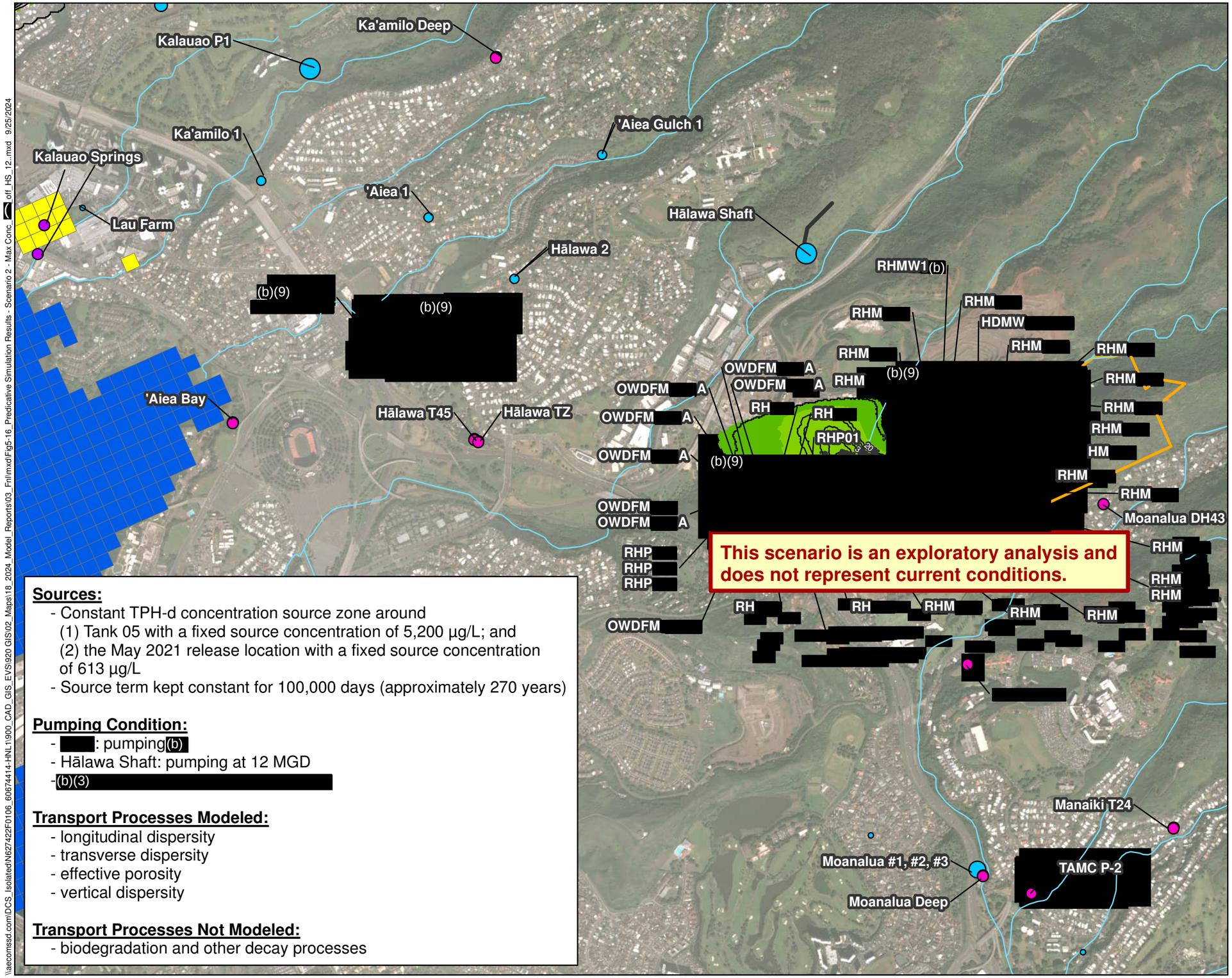

This scenario is an exploratory analysis and does not represent current conditions.

Sources:

- Constant TPH-d concentration source zone around
  (1) Tank 05 with a fixed source concentration of 5,200 µg/L; and
  (2) the May 2021 release location with a fixed source concentration of 613 µg/L
- Source term kept constant for 100,000 days (approximately 270 years)

Pumping Condition:

- [redacted]: pumping(b)
- Hālawa Shaft: pumping at 12 MGD
- (b)(3) [redacted]

Transport Processes Modeled:

- longitudinal dispersity
- transverse dispersity
- effective porosity
- vertical dispersity

Transport Processes Not Modeled:

- biodegradation and other decay processes

Legend

Water Supply Well / Shaft (MGD)

- 0.0 - 0.5
- 0.5 - 1.0
- 1.0 - 2.0
- 2.0 - 5.0
- 5.0 - 10.0
- 10.0 - 15.0

Boundary Conditions

- Constant Heads (Layer 1 only)
- Drains

Average Calibration TPH-d Results (µg/L)

- 100 to < 200
- 200 to < 400
- 400 to < 600
- 600 to < 800
- 800 to < 1,000
- 1,000 to < 2,000
- 2,000 to < 3,000
- 3,000 to < 4,000
- > 4,000

- 10% Percentage of Realizations with GWSC Exceedances
- Basal Aquifer Well
- Spring
- Water Development Tunnel / Infiltration Gallery
- Stream
- Red Hill Facility Boundary

Notes

1. Map projection: NAD 1983 Hawaii State Plane Zone 3 feet.
2. Base Map: DigitalGlobe, Inc. (DG) and NRCS. Publication_Date: 2015
3. Spring locations provided by USGS.
4. Water supply well locations provided by DLNR.
5. GWSC for TPH-d = 400 µg/L

N

0 1,000 2,000 3,000 Feet

Figure 5-16
Predictive Simulation Results - Scenario 2 - Average Simulated TPH-d Concentration Across All Calibrated Realizations
[redacted] Pumping(b)[redacted]
Hālawa Shaft Pumping at 12 mgd,
(b)(3) [redacted]
GWFM, VZM, & CF&T Model Report
Red Hill Bulk Fuel Storage Facility
JBPHH, O'ahu, HI

\\aecomssd.com\DCS_Isolated\N627422F0106_60674414-HNL1\900_CAD_GIS_EVS\920 GIS\02_Maps\18_2024_Model_Reports\03_Fnl\mxd\Fig5-16_Predicative Simulation Results - Scenario 2 - Max Conc_off_HS_12..mxd 9/25/2024

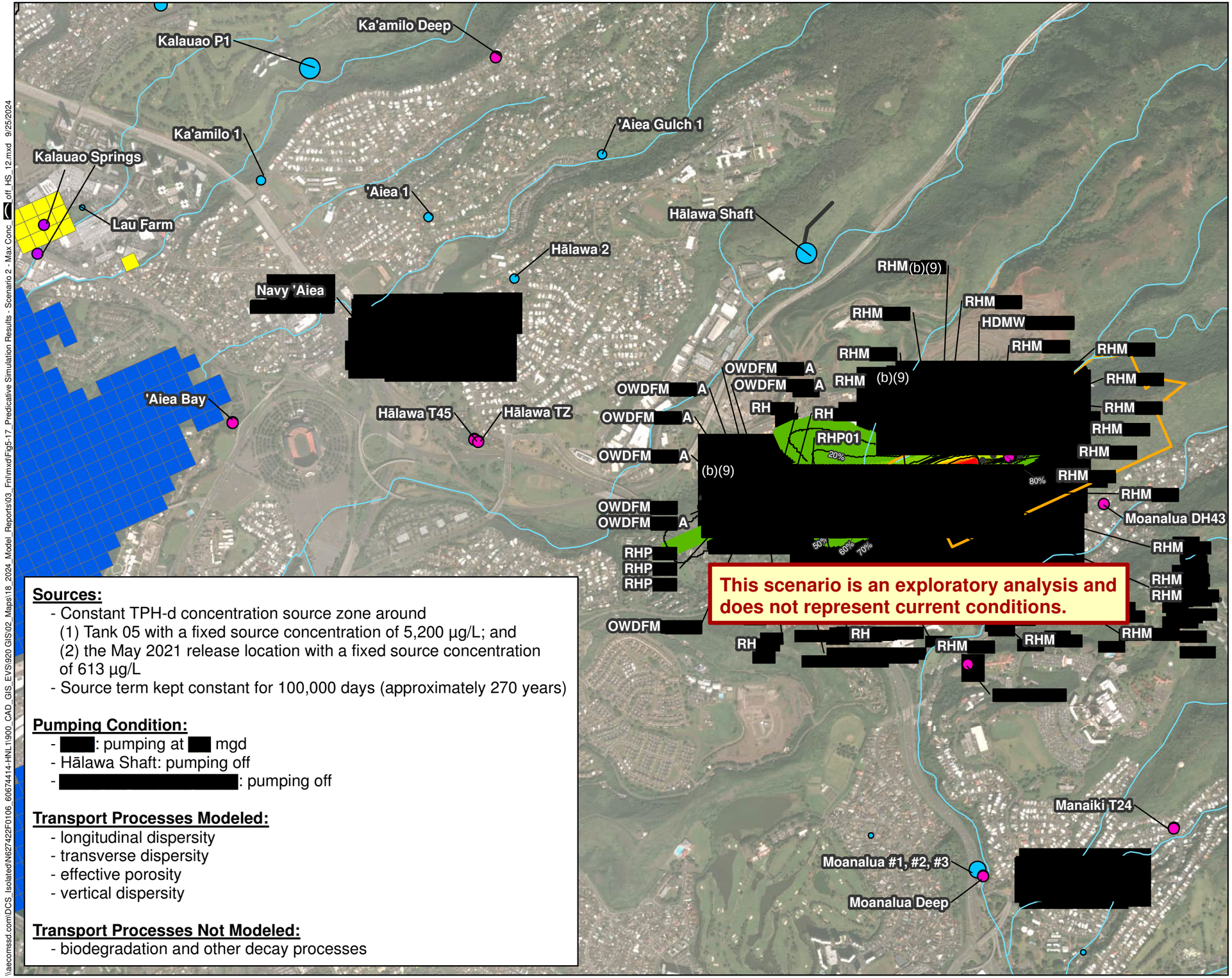

This scenario is an exploratory analysis and does not represent current conditions.

Sources:

- Constant TPH-d concentration source zone around
  (1) Tank 05 with a fixed source concentration of 5,200 µg/L; and
  (2) the May 2021 release location with a fixed source concentration of 613 µg/L
- Source term kept constant for 100,000 days (approximately 270 years)

Pumping Condition:

- [redacted]: pumping at [redacted] mgd
- Hālawa Shaft: pumping off
- [redacted]: pumping off

Transport Processes Modeled:

- longitudinal dispersity
- transverse dispersity
- effective porosity
- vertical dispersity

Transport Processes Not Modeled:

- biodegradation and other decay processes

Legend

Water Supply Well / Shaft (MGD)

- 0.0 - 0.5
- 0.5 - 1.0
- 1.0 - 2.0
- 2.0 - 5.0
- 5.0 - 10.0
- 10.0 - 15.0

Boundary Conditions

- Constant Heads (Layer 1 only)
- Drains

Average Calibration TPH-d Results (µg/L)

- 100 to < 200
- 200 to < 400
- 400 to < 600
- 600 to < 800
- 800 to < 1,000
- 1,000 to < 2,000
- 2,000 to < 3,000
- 3,000 to < 4,000
- > 4,000

- 10% — Percentage of Realizations with GWSC Exceedances
- Basal Aquifer Well
- Spring
- Water Development Tunnel / Infiltration Gallery
- Stream
- Red Hill Facility Boundary

Notes

1. Map projection: NAD 1983 Hawaii State Plane Zone 3 feet.
2. Base Map: DigitalGlobe, Inc. (DG) and NRCS. Publication_Date: 2015
3. Spring locations provided by USGS.
4. Water supply well locations provided by DLNR.
5. GWSC for TPH-d = 400 µg/L

N

0 1,000 2,000 3,000 Feet

Figure 5-17
Predictive Simulation Results - Scenario 2 - Average Simulated TPH-d Concentration Across All Calibrated Realizations
[redacted] Pumping at [redacted] mgd, Hālawa Shaft Pumping Off, [redacted]
GWFM, VZM, & CF&T Model Report
Red Hill Bulk Fuel Storage Facility
JBPHH, Oʻahu, HI

\\aecomssd.com\DCS_Isolated\N627422F0106_60674414-HNL1\900_CAD_GIS_EVS\920 GIS\02_Maps\18_2024_Model_Reports\03_Fnl\mxd\Fig5-17_Predicative Simulation Results - Scenario 2 - Max Conc_ off_HS_12.mxd 9/25/2024

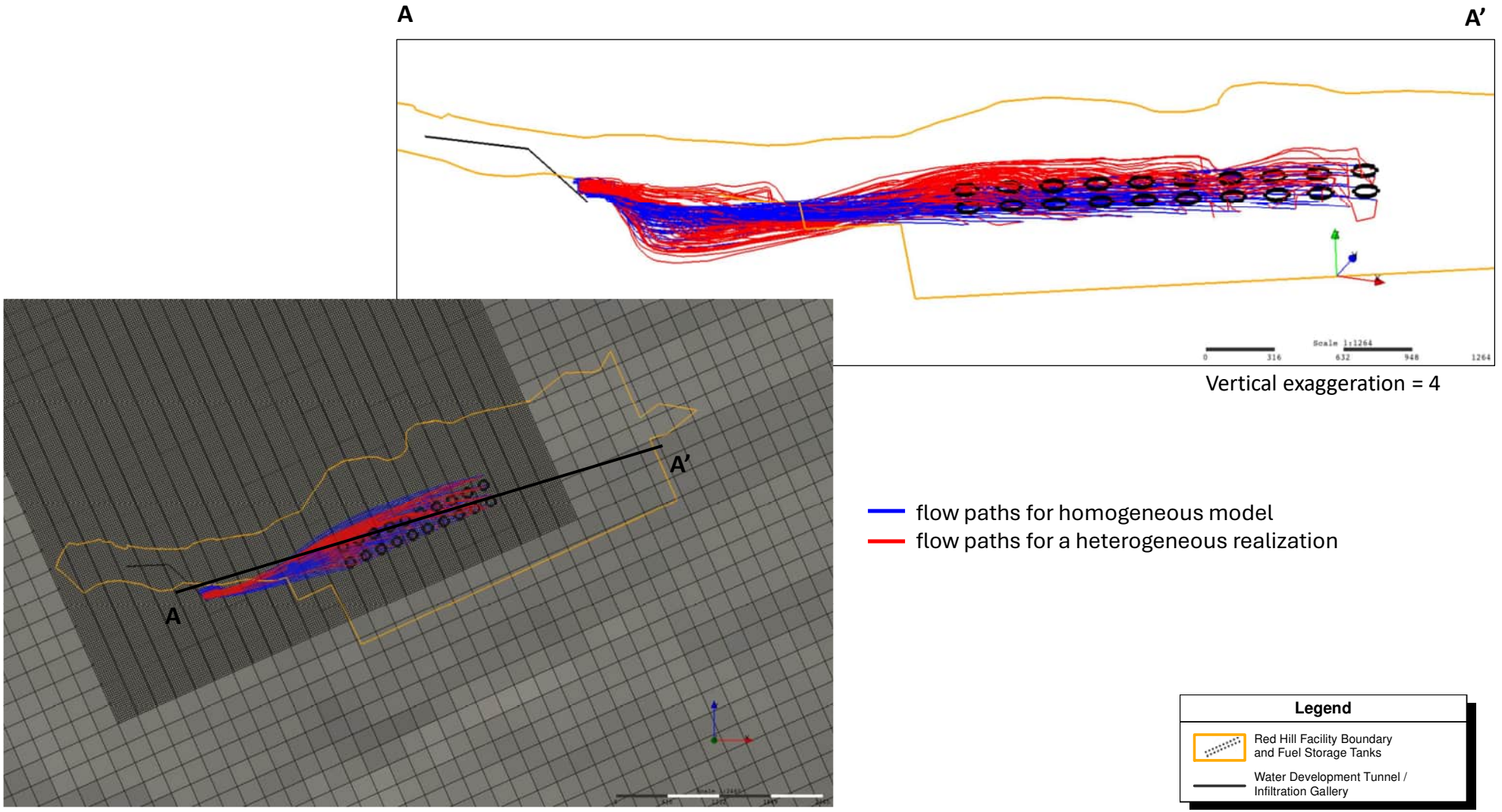

Figure 5-18
Homogeneous vs Heterogeneous Particle Tracking Results
GWFM, VZM, & CF&T Model Report
Red Hill Bulk Fuel Storage Facility
JBPHH, O'ahu, Hawai'i

Appendix A: Navy Groundwater Modeling Meetings and Calls with Regulators and SMEs Since Submittal of March 2020 GWFM Report

Meeting Date	Meeting Topic
2020-05-15	Technical Working Group (TWG) Mtg #27 Model Report Feedback from EPA and DOH
2020-10-22	EPA-DOH Water Level Discussion
2021-04-28	TWG Mtg #38 Matt Becker Initial Call
2021-05-10	TWG Mtg #39 Groundwater Flow Model (GWFM) Regulatory Agency (RA) Comments
2021-06-03	TWG Mtg #40 GWFM RA Comment Follow Up
2021-07-08	TWG Mtg #41 DOH Geology Presentation
2021-07-16	TWG Mtg #42 Navy Presents In-Well Testing Approach
2021-07-27	TWG Mtg #43 In-Well Testing Objectives Refinement
2021-08-03	TWG Mtg #44 In-Well Objectives Refinement with Dr. Matt Becker
2021-08-26	TWG Mtg #45 In-Well Testing-Work Plan Comments
2021-10-18/19	Groundwater Modeling Working Group Mtg 16
2022-02-04	In-Well Test Path Forward with Dr. Becker
2022-05-04	Groundwater Model Check In-EPA-DOH
2022-05-09	Groundwater Model-Questions-Objectives-EPA-DOH
2022-05-26	Geological Conceptual Site Model (CSM) Kickoff
2022-09-14	Special Purpose Meeting (SPM) #03 Confining Units
2022-09-21	SPM #5 Stochastic Basalt Subtype Generation using a Geologic Fabric Exploration Tool
2022-09-28	SPM #6 MODFLOW Model Setup
2022-10-25	SPM #8 In-Well Testing Work Plan
2022-12-07	SPM #9 Geologic Fabric Explorer (GFE) Technical Support Session
2022-12-14	SPM #10 Geologic Modeling Framework Conceptual Site Model
2023-01-10	SPM #11 Strike & Dip
2023-01-13	SPM #13 Geologic Fabric Explorer (FE) Meeting 2
2023-02-01	SPM #15 Tracer Study Work Plan
2023-02-14	SPM #16 Modeling Schedule Update
2023-02-15	SPM #17 Dr. Becker's Comments on the Navy's In-Well Testing Work Plan
2023-03-01	SPM #18 Dr. Becker’s Comments on the Navy’s In-Well Testing Work Plan, Continued
2023-3-03	Flow Optimization-University of Hawai‘i Transducer Study
2023-03-15	SPM #20 Modeling = RA SME Perspective and Questions

Meeting Date	Meeting Topic
2023-03-29	**Small Group Vadose Zone Model (VZM) Meeting**
2023-04-05	**SPM #21 Approach to Vadose Zone Modeling**
2023-05-17	**SPM #25 RA Comments on the Groundwater Flow Model**
2023-05-31	**SPM #27 Contaminant Fate and Transport Modeling Approach**
2023-08-19	**SPM #28 Representation of Basalt Heterogeneity**
2023-08-30	**SPM #29 Flow Optimization Study**
2024-01-31	**SPM #31 TPH Contaminant Fate and Transport Modeling Issues**

Appendix B: Summary of 2022 Regulator GWFM Comments and Approach

Theme #	Theme	RA Comment #	Approach to Address RA Comment(s)	Addressed in Best Available Model
1	**Basalt Representation**	**12**	• Address via multiple renderings of basalt fabric using multipoint training images (local-scale basalt modeling using the Geologic Fabric Explorer [GFE]).	✓
2	**Boundary Conditions**	**28, 35, 52, 53, 54, 55, 60, 64, 65, 66, 70, 79**	• Perform regional water balance calculations to estimate model water budget, boundary inflows/outflows. • Test various concepts and assess range of potential outcomes via sensitivity analysis. • Provide more detailed justification of boundary condition assignments.	✓

Theme #	Theme	RA Comment #	Approach to Address RA Comment(s)	Addressed in Best Available Model
3	**Data and Calibration**	**2, 3, 5, 6, 9, 10, 13, 17, 21, 25, 27, 29, 31, 36, 39, 43, 44, 45, 46, 56, 57, 61, 67, 68, 69, 72, 73, 74, 75, 76, 77, 78**	• Primary focus on quasi-steady heads/gradients, secondary focus on transient drawdown matching. • Model boundaries (particularly lateral boundaries) to better match regional groundwater gradients and supported by water balance calculations. • Replace previous multi-model approach with one model structure with multiple basalt fabric realizations. • Provide clear road map defining a successful flow model calibration. Ensure results are reproducible in review. • Geologic realizations may help explain observed compartmentalization of water level responses.	✓
4	**Documentation and Communications**	**58, 80, 81, 82, 83**	• Frequent and transparent engagement with RAs and SMEs.	✓
5	**Field Investigation**	**18, 19, 20, 23, 32, 33**	• In-well testing program (and potentially a tracer test) has been proposed.	**UH to perform tracer study. USGS and Navy/UH conducting in-well testing. Results to be incorporated when available.**
6	**Geochemical Proxies**	**8, 38, 47, 48**	• Evaluate chloride / temperature data. • Apply as additional lines of evidence for water balance calculations. • Use various strategies to apply mixing model calculations to model results.	✓

Theme #	Theme	RA Comment #	Approach to Address RA Comment(s)	Addressed in Best Available Model
7	**Hydrostratigraphy**	**1, 15, 22, 40, 62, 71**	• Revisit large-scale stratigraphic structures and incorporate new data. • EVS model updated with new borings and other data. • GFE with multiple point statistics and training images used to represent basalt heterogeneity.	✓
8	**Model Layering**	**11, 59, 63**	• Geologically independent gridding approach will be used with layers dipping with basalt.	✓
9	**Parameter Ranges**	**7, 14, 26, 30, 34, 37, 49, 50, 51**	• Will document anticipated / acceptable parameter ranges.	✓
10	**Transient Modeling**	**4, 16, 24**	• Capture zones simulated based on transient model calibration. Specific transient capture scenarios can be simulated.	✓

The RAs' May 17, 2022 Disapproval Letter of the June 2000 Groundwater Flow Model Report is attached.

UNITED STATES ENVIRONMENTAL PROTECTION AGENCY
REGION IX

STATE OF HAWAII
DEPARTMENT OF HEALT(b)
P. O. BOX 3378
(b)(6)
(b)(6)

The U.S. Environmental Protection Agency ("USEPA") and Hawaii Department of Health ("DOH"), collectively the "Regulatory Agencies", have reviewed the *Groundwater Flow Model Report* ("GWFMR") dated March 25, 2020 submitted by the U.S. Department of Navy ("Navy") and Defense Logistics Agency ("DLA") to satisfy the requirements of Section 7.1 of the 2015 Administrative Order on Consent Statement of Work ("AOC SOW") for the Red Hill Bulk Fuel Storage Facility ("Facility") located in O'ahu, Hawai'i.

The Regulatory Agencies disapprove the GWFMR and its associated numerical models. The many deficiencies in the Navy's models have been discussed in detail throughout the modeling process and most recently in our May 2021 critique provided to the Navy and their consultants, followed by a summary critique by our subject matter experts given to the Groundwater Flow Modeling Working Group on October 18 & 19, 2021. These deficiencies are extensive and relate to foundational assumptions in the Navy's GWFMR that render the results unreliable for Agency decision-making regarding aquifer protection, as well as unreliable as an underlying basis to evaluate contaminant fate and transport (CF&T). A list of the deficiencies in the GWFMR is enclosed. We are providing the Navy and DLA an opportunity to cure the deficiencies identified and resubmit the GWFMR.

The Navy and DLA shall hold a meeting within 30 days of receipt of this letter with USEPA and DOH to discuss next steps as to which models should be carried forward and what model modifications should be incorporated. Next steps may include establishing specific technical groundwater flow model objectives and regular meetings with the Regulatory Agencies and other

stakeholders to discuss modeling assumptions and approaches. Within 60 days of receipt of this letter, the Navy and DLA shall submit in writing the next steps with an associated timeline. Once the groundwater flow models have been refined, but no later than 90 days of receipt of this letter, the Navy and DLA shall revise and re-submit the GWFMR. The Navy and DLA shall summarize all changes made and relevant model run results in an addendum to the revised GWFMR.

If you have any questions, please contact us.

(b)(6)

[redacted]

Enclosures:
1. Attachment A Joint Agency Deficiencies on the Groundwater Flow Model Report for the Red Hill Bulk Fuel Storage Facility, dated March 25, 2020, delivered March 17, 2022
2. Attachment B – HDOH SME Deficiencies Identified, Red Hill Groundwater Flow Model Report, dated December 3, 2020, delivered to Navy March 17, 2022
3. Attachment C EPA SME Deficiencies Identified, Red Hill Groundwater Flow Model Report, dated November 10th, 2021
4. Attachment D - DOH Review: Navy Groundwater Flow Models & Related Issues with the Navy CSM for the Red Hill Facility, dated October 19, 2021

UNITED STATES ENVIRONMENTAL PROTECTION AGENCY
REGION IX

(b)(6) [redacted]

STATE OF HAWAII
DEPARTMENT OF HEALTH

(b)(6) [redacted]

March 17, 2022

Attachment A: Joint Agency Deficiencies on the Groundwater Flow Model Report, Red Hill Bulk Fuel Storage Facility, dated March 25, 2020

Background

The primary objectives of the of the Groundwater Flow Model Report (GWFMR) is to refine the existing groundwater flow model and improve the understanding of the direction and rate of groundwater flow within the aquifers around the Facility, in order to evaluate risk to groundwater resources that may be posed by the Facility.

The Navy and DLA have expended considerable effort to further knowledge and understanding of the complex subsurface around the Facility since 2015, however, the resulting models in the GWFMR do not reflect site specific data and associated heterogeneity with sufficient accuracy to provide confidence in model predictions. During 2017, the Navy reviewed the previous groundwater model as reported in the Red Hill Bulk Fuel Storage Facility Final Technical Report (Rotzoll and El-Kadi [2007] as published in Navy [2007]). Based on discussions with Groundwater Flow Model Working Group (GWFMWG) members, development of an interim groundwater flow model commenced with the 2007 model, with refined and expanded lateral boundaries and other hydrogeologic data. However, the geologic detail associated with past and recent data collection, some of which was included in the Navy's 2019 Conceptual Site Model (CSM), was not incorporated into the 2020 Groundwater Flow Models (GWFMs) at an adequate degree of detail. For instance, CSM Figures 5-2 through 5-11 show interpretive geologic renderings of the heterogeneous subsurface geologic system; the GWFMs are geologically implausible as compared with this subsurface data.

In 2018, the interim flow model was developed, in part, to evaluate hydrogeologic system behavior and help identify data needs. In late 2018, in response to feedback from Regulatory Agency subject matter experts (SMEs) including an August 2018 "Top Ten Comments" summary regarding the CSM, interim model calibration, and representation in the interim model of the basalt dip and strike, saprolite, caprock, tuffs, and sediments –the Navy conducted several

additional simulations using the interim flow model. Considering the complex and imperfectly known hydrogeologic setting and sparse data set, model development followed a multi-model approach to evaluate the potential importance of various features of the CSM on local flow patterns and enable the testing of alternative scenarios. Building on the interim flow modeling effort, the Navy presented several groundwater models in the 2020 GWFMR that incorporate various parameters and depict alternate potential groundwater flow patterns throughout the area of interest (AOI) encompassing Red Hill Bulk Storage Facility, (b)(3)(b)(3) ((b)), and (b)(3)(b)(3) (HS).

Despite the expansion of the modeling efforts, the Navy's 2020 GWFMs exhibit many of the same limitations as did the 2018 interim models, and consequently do not provide the improvements sought. None of the models reflect site specific data and associated heterogeneity with sufficient accuracy to provide confidence in model predictions. Consequently, the GWFMR and the accompanying models that it describes require substantial improvement. Thus, the Regulatory Agencies' disapproval of the GWFMR.

Summary of Deficiencies

Some key concerns regarding the Navy models are summarized below and detailed in the attached Regulatory Agency SME technical memoranda. Any one of the deficiencies below would be sufficient grounds for disapproval, but taken as a whole, demonstrate the significant degree of model unreliability. While some of the deficiencies detailed in the attached SME memoranda stem from review of the Navy's 2020 GWFMR, the general themes were previously communicated to the Navy and its technical team during Technical Working Group (TWG) meetings, GWFMWG meetings, as well as in letters such as those dated October 29, 2018 (for the GWFM) and March 30, 2020 (for the CSM[1]). The DOH Safe Drinking Water Branch also detailed concerns on both documents in the *Assessment of Groundwater Flow Paths in the Moanalua, Red Hill and Halawa Regions, Revision 2* (July 11, 2019):

1. The hydrostratigraphic units, as represented in the GWFMs, are implausible and do not reflect the detail or characteristics of the system that will control Contaminant Fate and Transport (CF&T) and ultimately, risks posed by the Red Hill Bulk Fuel Storage Facility to the aquifer system.

2. Calibration and validation efforts over-emphasize drawdown and recovery matches at the expense of actual groundwater elevations. Consequently, while some of the Navy models demonstrate reasonable correspondence with drawdown and recovery data, they do not adequately represent groundwater elevations. Matching elevations is critical to ensuring the modeling represents water budgets and hydrogeologic behaviors to an adequate degree of certainty.

3. Further to (2), the GWFMR and GWFMs fail basic validation procedures, meaning they fail the testing intended to provide confidence in the modeling construction and results. The GWFMR uses non-standard techniques in the validation testing, and validation

[1] **Department of Health 3/30/20 Response to *Conceptual Site Model, Investigation and Remediation of Releases and Groundwater Protection and Evaluation, Red Hill Bulk Fuel Storage Facility, Joint Base Pearl Harbor-Hickam, Oahu, Hawaii***

charts misleadingly show a goodness of fit to measured groundwater elevations that cannot be replicated in the actual model results. The Navy's modelers admitted that their validation charts are in fact a superposition of transient modeled aquifer drawdown/recovery responses onto measured elevation data

4. The GWFMs are run in steady-state mode. As the Regulatory Agencies have pointed out on numerous occasions to the Navy and its modeling team, the conditions of interest are transient. Contaminant migration is transient, groundwater capture is transient, and other aspects of potential risk are transient. The Regulatory Agencies cannot accept steady-state modeling outputs for decision-making, although we recognize it can have value as a conditioning procedural step in the model construction and calibration processes.

5. Measured groundwater responses to pumping at (b), which show differences between monitoring wells suggestive of hydraulic compartmentalization, are not represented in the Navy models. This is likely due to the absence of sufficient geologic heterogeneity and the unrealistic representations of the geologic system in the Navy models.

6. The Navy models do not adequately reflect local-area hydraulic gradient directions and magnitudes, tending to substantially over-estimate gradients along Red Hill Ridge as well as not reflect local gradients toward Moanalua Valley. These results imply a probability of hydraulic capture by pumping (b) that is inconsistent with actual observational data. The Navy GWFMs are non-conservative in this regard.

7. The Navy models use, with insufficient technical justification, parameter ranges and other inputs that are often outside the bounds of published Hawai'ian literature, including values used in the previous (Navy [2007]) groundwater model.

8. Likely flow paths, capture zones, and general flow patterns, that are simulated by the Navy models do not correspond with flow patterns that are implied by groundwater geochemistry. For example: chloride concentrations at several Red Hill monitoring wells are substantially higher than can be accounted for via the predominantly upslope source water that is simulated by most of the Navy models.

In summary, the current Navy models have not advanced the understanding of groundwater flow and dissolved constituent migration patterns within the AOI sufficiently to support risk management decisions. Similarly, the Navy models do not provide a basis, at present, for CF&T evaluations that are inherently more complex than groundwater flow. Calibration results for the collective set of Navy models implies that widely differing conditions cannot be distinguished from one another as more or less representative of actual conditions, and substantial uncertainties remain regarding overall groundwater flow directions across the AOI. Consequently, it is the Regulatory Agencies' position that capture zone predictions for (b) – one basis for the Investigation and Remediation of Releases (IRR) recommendations, tying to the Navy's conclusions about their ability to respond to releases and protect drinking water resources – are not reliable.

Next Steps

A premise of the Navy's multi-model approach was to explore a range of hydrogeologic conditions to improve understanding of groundwater flow and the underlying hydrogeologic

system. At the present time no single model incorporates all features, events, or processes, that are likely to be important to accurately simulate groundwater conditions in the AOI. Given this, the Regulatory Agencies require a consolidation of CSM features into a smaller number of locally behavioral groundwater flow models with the intent that the consolidated model(s) will demonstrate sufficiently improved correspondence with field data. If successful, then the models can be carried into the next phase of modeling-based analyses to support CF&T modeling. In addition, to better improve on the reliability of modeling efforts, further site-specific investigation and characterization, such as in-well testing and inter-well tracer studies, should proceed. Modeling and site-specific investigation activities can occur concurrently so that remedial mitigation measures can be developed and implemented in a timely manner.

Therefore, based on the Regulatory Agency comments and observations to date, the Navy will implement the following improvements, and consolidation of, the Navy models as detailed in the attachments:

- Refocus near-term modeling efforts, including calibration and verification, within the AOI and in particular the Red Hill Ridge area.
- Revise model layering to improve the representation of valley fill and saprolite incision within, rather than deformation of, basalts.
- Revise representation of the (un-weathered) basalt aquifer to improve realism and reflect the general character of documented subsurface heterogeneity. This includes, but is not limited to, geostatistical evaluations of the distributions of key hydrostratigraphic units and incorporation into the models within the AOI as demonstrated by (b)(6)
- After completing the foregoing:
    - Consolidate models to identify a smaller set of models representing the most probable conditions within the AOI and document the hydrogeologic distinctions between them.
    - Justify through technical analysis any deviations from more commonly used and accepted parameter values, inputs, and assumptions.
    - Refine the representation of geology to better reflect subsurface heterogeneity which may affect flow.
    - Re-evaluate the (transient) capture zone analysis using the updated, consolidated, models.
    - Provide standard transient model validation evaluation, with no changes to boundary or other hydrogeologic conditions and using aquifer heads as the criteria for goodness of representation. Map view plots of modeled versus measured flow fields should also be produced as part of the validation procedures.
- Work concurrently:

- Seek regulatory concurrence approval on short term, in-well testing program to gather additional data about inter-well connectivities and local water conditions, using recent USGS transducer study results and other lines of evidence.
- Work closely with 3rd party subject matter expert (b)(6) to design a tracer study to collect data to be used to assess GWFM flow predictions and match with natural tracer data studies conducted by DOH.
- Final verification of Regulatory Agency prioritized well locations, permitting and installation of the new wells

Further details regarding the technical recommendations above, together with additional review comments, are included in Attachments B, C and D. Re-submittal of the flow models and accompanying report for approval will require revising the model assumptions to address Regulatory Agency concerns.

HAWAII DEPARTMENT OF HEALTH TECHNICAL REVIEW

Groundwater Flow Model Report, Red Hill Bulk Fuel Storage Facility – Joint Base Pearl Harbor-Hickam, Oahu, Hawaii, Dated December 3, 2020 Revision 01

Delivered to Navy March 17, 2022

Executive Summary

The Hawaii DOH subject matter experts (SMEs) have reviewed the *Groundwater Flow Model Report, Red Hill Bulk Fuel Storage Facility – Joint Base Pearl Harbor-Hickam* (GWFM Report, March 25, 2020). This report and modeling work are a deliverable required under Task 7 of the Administrative Order on Consent – Statement of Work (AOC-SOW, 2014). Its purpose is to refine the existing groundwater flow model (Rotzoll and El-Kadi, 2007) and improve the understanding of the direction and rate of groundwater flow within the aquifers around the Facility. Underlying this purpose is the requirement for an improved understanding of the hydrogeology that controls groundwater flow. The improved models are intended to serve as a primary basis for subsequent contaminant fate and transport (CF&T) modeling and associated evaluations of current and potential future risks that may arise from fuel releases at the Site. Finally, those risk evaluations will provide guidance on response and remediation strategies for potential future releases at the Site and inform subsequent changes to the Groundwater Protection Plan.

The groundwater flow models (GWFMs), are well constructed and have the potential for representing the regional scale conditions at the Site and surrounding area. However, Site-area data directly indicate that the GWFMs fail to represent critical aspects of the system at a local scale around Red Hill, as detailed further below. Site-area data indicate a high degree of complexity in the aquifer system behavior and it is this local scale that is most relevant to CF&T and risk evaluations. In our review of the GWFM Report, we have identified multiple deficiencies that render the model(s) unreliable for increasing our understanding of the direction and rate of groundwater flow within the aquifers around the Site and for related decision-making. Similarly, these deficiencies make groundwater capture and plume containment conclusions in the GWFM report equally unreliable. DOH's overarching concern is the lack of verifiable metrics to ensure that the model replicates the hydrogeologic dynamics with sufficient certainty to support response mitigation planning. The most significant of the model deficiencies are the following:

- The GWFMs do not adequately reflect local area Red Hill groundwater gradients, elevations and individual well responses to pumping stresses. Further, the models indicate flow paths and rates that are inconsistent with background groundwater solutes, such as chloride, that are natural groundwater tracers.
- The GWFMs do not adequately utilize the available geologic and hydrogeologic data to interpret hydrostratigraphic conditions at and near the water table which is the interval most relevant to CF&T and risk concerns. Relevant information in the CSM and other Navy technical materials has not been used to refine that portion of the hydrogeologic model which, in turn, should feed into the numerical model framework.
- The deficiencies above and other associated issues make the groundwater capture conclusions by pumping Red Hill Shaft at 4.65 million gallons per day unreliable. The Navy GWFM Report uses particle tracking to develop Red Hill Shaft capture zones that the Navy concludes in other AOC documents (e.g. Tank Upgrade Alternatives and Release Detection Decision Document) to

demonstrate that a release from the USTs will be directed to the Red Hill Shaft under normal pumping conditions. These particle tracks are driven, in part, by the modeled hydraulic gradients that we find are not adequately reflective of site monitoring data. As described briefly below and in detail in the body of these comments, the disparity between the measured and modeled groundwater gradients beneath the USTs, and between the USTs and the Red Hill Shaft cast significant doubt that the simulated capture zone actually represents the flow field to the Red Hill Shaft, and, more critically, places doubt on the utility of pumping the Red Hill Shaft as a release response measure.

- Beyond the unreliability of the modeled groundwater capture zones are the implications drawn from the steady-state method of analysis. Future potential fuel releases will migrate most rapidly during their initial release period and so any associated risks to the groundwater system will be time-dependent (transient). All mitigation measures under consideration (inclusive of groundwater capture) will need to address the time-dependent considerations of plume release and transport and how those vary with release scenarios and the hydrogeologic conditions in and around the Site. Steady-state approximations are inappropriate for this level of groundwater protection considerations.
- The suite of models in the GWFM report represent a multi-model approach, which is typically used to resolve uncertainty or define the sensitivity of hydrogeologic assumptions that control the behavior of the aquifer system. In turn, that should lead to interpretations about the most likely suite of conditions that define and represent the aquifer system; i.e., an improved base model(s). The GWFM report does not lead to an updated set of interpretations that eliminates non-viable assumptions and validates those most likely present. That resulting base model (or limited set of models) should be a substantial improvement relative to the past modeling work that was the starting point of this effort. This improvement has not been achieved.
- The GWFMs use certain parameters and distributions that are not supported by site or area data, nor past modeling efforts. For instance, low porosity values are assumed (relative to past modeling), but no technical justification is provided. That results in groundwater flow that is likely too rapid and transient capture by pumping that is too large. This example assumption would also result in unrealistic estimates of contaminant degradation rates. These examples are non-conservative and are not useful to decision-making unless definitively shown to be more reflective of actual conditions than in past modeling work.
- The GWFMs do not appear to weight the area nearest the Site as the most significant from a calibration standpoint, in spite of having the highest data density and quality of any other areas in the model domain. As noted in the attached memo, the GWFMs do not adequately represent conditions in the local area of key regulatory interest and the remainder of the model domain is not particularly relevant in light of this deficiency.
- The GWFMs use a variable range of boundary conditions that, at present, are not verifiable and cannot be validated, and whose effects have not been adequately tested over a plausible range of values and, hence, the model results can't be considered unique or definitive. These amount to hypotheses without the associated technical evaluations to determine which (if any) is most likely representative.
- Based on our review of the Navy's draft numerical models, the verification model runs exhibit the same general issues as the precursor models. They do not adequately represent groundwater

elevations or gradients, which implies fundamental issues with the underlying conceptualization and parameter distribution framework. Although the Navy's validation models appear to match transient stresses (pumping and recovery), as did the precursor model (2007), groundwater elevations are equally critical to understanding the hydrogeologic behavior.

- The GWFM report claims to have selected conservative parameters and approaches. We do not find that to be accurate in many cases. But more important with regard to the AOC objective noted above, the models should refine hydrogeologic parameters and distributions that are most likely representative of the system to further our understanding of its characteristics to serve as a basis for future contaminant fate and transport (CF&T) and risk evaluations. The modeling does not achieve that goal.

Because of the uncertainties in the validity of the GWFMs local-area structure and parameterization, the DOH cannot reliably depend on the resulting flow rates, trajectories and capture zones generated by the models. Fundamentally, the models have not advanced our understanding of the aquifer system as compared to prior modeling work (e.g. Oki, 2005; and Rotzoll and El-Kadi, 2007) and the work does not meet the objective of the AOC.

The overarching deficiency that DOH recognizes is that the suite of models described in that document lack verifiability of the simulated groundwater flow trajectories and rates resulting in simulated drinking water source capture zones that are unreliable. DOH requires that the Navy provide a field verification plan to confirm or refute the representativeness of the simulated groundwater flow trajectories as indicated by modeled particle tracks. There are many field tests that can be employed to test the GWFM results. We have recommended a limited suite of field-scale testing to expand the local-area understanding of the aquifer system behavior including: i) a statistically robust suite of borehole measurements of flow rates and directions in the vicinity of the Facility; ii) borehole dye dilution-rate measurements; and iii) a controlled pump test of Red Hill Shaft (b)(3) mgd with transducers placed in all available local area monitoring wells, coupled with local-scale multi-well dye tracers, to provide clear evidence of the rate and trajectory of flow beneath the Facility and its capture by Red Hill pumping. The Navy can choose to follow these recommendations or propose other tests to evaluate the representativeness of the GWFM results. The tests the Navy proposes shall confirm or refute key aspects of the GWFMs output including flow rates, directions, and the ability of the Red Hill Shaft to capture groundwater and possibly contaminants around the Site at the modeled pumping rate o(b)(6) mgd.

Introduction

The *Groundwater Flow Model Report, Red Hill Bulk Fuel Storage Facility – Joint Base Pearl Harbor-Hickam* (GWFM Report) is a deliverable required under Task 7 of the Administrative Order on Consent – Statement of Work (AOC-SOW). The purpose of the AOC-SOW Section 7 is to "Monitor and characterize the flow of groundwater around the Facility". The groundwater model is a key deliverable for accomplishing this task. Task 7.1 – Groundwater Flow Model Report - states "The purpose of this deliverable is to refine the existing groundwater flow model and improve the understanding of the direction and rate of groundwater flow within the aquifers around the Facility." The effort dedicated to the groundwater flow model (GWFM) has gone well beyond "refining" the existing model. But, in so doing, have yielded modelled flow rates and trajectories that conflict with many of the most critical field-measured groundwater parameters around the facility and, hence are not credible without further validation beyond the model. Further, because the Navy will rely on the GWFM to justify the Tank Upgrade Alternatives decision proposing that pumping Red Hill Shaft will be able to capture, or otherwise contain, any fuel release within the confines of the Facility (Department of the Navy, 2019a), **it is imperative that the modeled groundwater flow trajectories and velocities are defensible and can be validated by field measurements.**

The AOC-SOW mandate is that the model will provide a more refined understanding of the groundwater system. In turn, that refinement will allow us to ask pertinent area/tank-specific questions about what might happen under a range of plausible release conditions from individual in-service tanks and how receptors might be impacted. As the model currently stands, there is a substantial disconnect between the modeled relative groundwater elevations within the Facility monitoring wells and currently available field data; this results in an array of interpretational conflicts and uncertainties, described below, such that the model more likely obscures, rather than informs, actual risk conditions which we believe will lead to poorly informed decisions.

General Review Comments

The models are well constructed. The engineers and geologists doing the modeling are among the best in the field. However, due to the complexity of the site, a critical weakness of the model is the absence of verifiability of many of the model inputs. To be informative for predicting contaminant migration and release response planning, the results must be shown to be consistent with actual groundwater flow trajectories. However, the model results show a number of conflicts with field measurements (e.g. water levels, water table gradients, concentrations of natural tracers, etc.) and, to date, there has been no independent assessment of groundwater flow trajectories against which the model can be tested.

The primary concerns that the Hawaii Department of Health (DOH) has with the GWFM are summarized below.

1. The model suffers from an over reliance on automated parameter selection and calibration-driven model zonation of hydraulic parameters. Greater attention should be paid to valuable field data collected that indicate groundwater flow trajectories other than those simulated. Examples are provided below and include: local gradients within the Facility monitoring wells that are inconsistent with the modeled groundwater flow trajectories; the diverse range of groundwater chemistry concentrations indicating a poorly mixed system with sluggish flow in the upper part of the aquifer; and the absence of a verified hydraulic barrier between the upper part of the Facility and the Halawa Shaft.

2. The modeling approach relies on boundary condition assumptions that can't be independently validated. Whereas there is a broad range of possible hydrologic conditions at the model boundaries, only a small fraction of those possible have been tested. There is currently no methodology available to determine the prevailing hydrologic conditions at the model boundaries and, because boundary conditions can't be verified with confidence, the model results can't be considered unique or definitive.
3. Insufficient attention is given to, arguably, the most important measured field data available: the relative groundwater elevations within the Red Hill Groundwater Monitoring Network. The Navy contends that relative water level elevations in closely-spaced wells are unreliable for determining groundwater flow trajectories. The Navy places greater emphasis on the groundwater elevation across the Moanalua/Halawa region, hypothesizing that the greater well spacing and differences in groundwater elevation provide a much more reliable water table map for flow trajectory analysis. This is counter-intuitive since a great deal of effort and expense has been applied to minimizing measurement errors within the Facility monitoring wells. Conversely, the observations wells in the Moanalua and Halawa regions used for model calibration are <u>not</u> tied to the same elevation reference point used for the Facility monitoring wells and no true vertical depth corrections have been applied. Hence, the level of confidence in the relative groundwater elevations between the Facility monitoring wells and the outlying observation wells is much less than that within the Facility monitoring network.
4. The hydraulic parameters used in the calibrated model diverge significantly from those used by experienced and respected hydrogeologists in previous South Oahu modeling efforts. Specifically, the values used for the vertical hydraulic conductivity of the basalt, the horizontal anisotropy of the basalt, and the basalt porosity in the Navy model differ, in some cases, by more than a factor of ten from those used previously in peer reviewed and published studies.
5. Qualitatively, the simulated GWFM trajectories fail to account for the distribution of chloride concentrations in the Facility monitoring wells. Chloride is a natural groundwater tracer and can be a more diagnostic indicator of groundwater flow trajectory than water levels if the chloride source zones and distribution are understood. The modeled particle tracks, which represent the simulated groundwater flow trajectories, conflict with the distribution of the elevated chloride concentrations in many of the Facility monitoring wells.

<u>Specific Comments</u>

<u>Modeling Approach and Complexity</u>

This evaluation considers the technical aspects of the GWFM as well as the philosophy behind the modeling approach. In 2011, Dr. Clifford Voss as Executive Editor of the Hydrogeology Journal wrote two essays on groundwater modeling (Voss, 2011 a and b). The Navy quotes from Voss (2011b) to provide independent support for their modeling approach. However, the quote from Voss (2011b) is incomplete and the entire paragraph from Voss (2011b) is provided below for greater context. The omitted phrases are underlined.

> <u>"In the view of this writer</u>, the best way to go forward with practical management is to rise above groundwater models as final products, and instead, empower hydrologists to provide advice by using groundwater models in simple ways that are intended to elucidate

understanding. Pursuit of complexity in groundwater models intended for practical management is a diversion from the real work at hand."

Voss recommended against over-reliance on automated parameterization of groundwater models and arbitrarily assigning hydraulic parameter values for calibration point-matching as was done in Models 53, 54, and 55. Below are two paragraphs excerpted from Voss (2011a)

> "Whether warranted or not, whether useful or not, parameter estimation has become a major part of model creation and this evolution has been fueled by the recent wide availability of automatic estimation software. In some sense, this wide availability has promulgated greater fallacious use of groundwater models. Automatic estimation software is truly a wonderful convenience when used properly, but it is no more than a convenience—and it should not be the primary objective of a modeling analysis to use it.
>
> An error in zonation, assumed model structure, or in some value assumed for input parameters, will cause automatic fitting to generate errors in other parameter values. These erroneous values may be organized in a realistic-appearing spatial trend that some modelers naively accept as reality. How can reality of a trend or newly discovered model parameter zone be determined without further targeted collection of field data?"

The emphasis on automated parameterization/calibration should be replaced with a comprehensive review of the conceptual site model to better constrain scenarios for the various model runs. For example, Model 59 tests the model response to lateral inflow into the southeast boundary. It appears that the 10 million gallons per day (mgd) value was chosen arbitrarily and distributed uniformly along the southeast model boundary. An inflow of 10 mgd equates to the entire recharge from the adjoining Kalihi Aquifer. Is the Navy hypothesizing that there is no groundwater flow from the Kalihi Aquifer to the ocean? Further, any realistic assessment of inter-aquifer flow would be biased toward inland portions of the aquifer since the depth of valley fill and saprolite in the coastal plain is known to be much deeper than the bottom of the freshwater lens. This is one of several examples in which too little geologic thought and justification has been invested into the various model scenarios. A multi-model approach is typically used to test valid hydrogeologic hypotheses to tease out unexpected details and ask, "does this make more sense relative to the hydrogeologic system and behavior and how can it be demonstrated via the available data?" That, then, should lead to the most likely set of conditions that explain the system and agree with all available data. This does not seem to have happened in the current modeling effort and no specific model seems to rise above the rest.

The Representation of the Hydrogeology of the Shallow Aquifer Zone is Inadequate

The GWFMs do not adequately utilize the available geologic and hydrogeologic data to interpret hydrostratigraphic conditions at and near the water table. This interval is the most relevant to risk concerns and the follow-on contaminant fate and transport model because it is where released contaminants will first encounter the groundwater, whether from recharge dissolving hydrocarbons during transport through the vadose zone or from a non-aqueous phase contaminant plume resulting from a release. In the latter case, that plume will serve as primary, continuing source of the dissolved phase contaminants of concern. However, information relevant to conditions in the shallow water table, that were developed for the CSM and other Navy technical materials, has not been used to refine that portion of the hydrogeologic model which should be used to constrain the numerical model framework.

For example, the Navy's GWFMs depend on a high permeability layer in the shallow aquifer, that can move large amounts of water down the Red Hill Ridge resulting in rapid transit times from beneath the USTs to Red Hill Shaft. A review of boring logs for the monitoring wells within the Facility show no evidence of a spatially expansive clinker zone that lies at or just below the water table. Further, the dip azimuth stated by the Navy would preclude a preferential highly permeable path along the water table since the reported dips of the lava flows vary from 3 to 11 degrees (Department of the Navy. 2019b; Sections 5.1.2 and 5.1.3) and are much steeper than the dip of top of the water table. Rather than developing models that rely on a high hydraulic conductivity zone that extends from beneath the tanks to the [redacted], the models should portray the much more likely scenario that require the groundwater flow in the shallow aquifer to move through or around lava flows that intersect and dive beneath the water table on the hypothesized path from the USTs to the Red Hill Shaft. To capture the importance of the shallow aquifer zone for contaminant trasport, the conceptual model of groundwater flow requires revision to reflect field measured conditions and that revised model should be reflected in the structural controls on groundwater flow in the GWFMs.

Fuel Transport and Potential Hydraulic Capture

Fuel transport following a release is driven by the gradients created by that release and their interaction with the hydraulic properties of the subsurface setting. Many of these geologic aspects parallel those used in groundwater modeling, but with significantly more complexity. In hard-rock settings, fuel transport can be further complicated by inter-connected pathways within the matrix that are likely to be present, but that cannot be easily characterized at relevant scales. The DOH SME's collective experience, coupled with literature studies, indicates that fuel releases will move rapidly and in directions that may differ from the prevailing geologic fabric of the subsurface materials. The DOH has observed at multiple on-Island sites that free product pathways may not be identifiable at common scales of sampling. This is further accentuated by the geographic sparsity of data points at the Red Hill Facility due to access limitations.

Fuel transport is more complex and heterogeneous than contaminant fate and transport in the dissolved-phase. The distance and directions of the dissolved-phase impacts depend on groundwater flow, dispersion, and other attenuative processes that will generally limit that migration distance relative to the fuel generating those impacts. The fuel transport, however, can be very rapid and heterogeneous. At present, the potential rates, directions and character of fuel transport through the vadose zone, to the water table and outward is undefined by any study or characterization work with which the DOH has concurred.

Before any fuel release mitigation measures can be considered by the agencies, the ranges of behavior of fuel releases must be defined and agreed upon by the agencies. Any mitigation action, such as the suggested hydraulic capture by pumping Red Hill Shaft, must first be put into context with that transient fuel migration behavior. For instance, if fuel transport is more rapid and or/distant than the short-term (transient) ability of pumping to capture that release, the mitigation measure will be ineffective at protecting distal receptors. The timing and dimensions of any mitigation measure must be placed in specific context with the rates, directions, and magnitude of potential releases from the Site. No final mitigation measures, inclusive of the proposed groundwater pumping and implied containment, will be considered by the agencies absent this linkage between fuel migration potentials and the associated transient effectiveness of any proposed measures.

Lastly, while some interim mitigation measures may be appropriate as first-steps in the protection of the area groundwater aquifers, all mitigation measures must be demonstrated through field-validation. The EPA Superfund program requires that all remediation measures must be demonstrated to be operating "properly and successfully" as a pre-condition to deed transfer (EPA, 2019). The DOH believes a similar level of validation is required for the Site to protect this sole-source groundwater resource. As noted by the EPA:

The phrase "operating properly and successfully" involves two separate concepts. A remedial action is operating "properly" if it is operating as designed. That same system is operating "successfully" if its operation will achieve the cleanup levels or performance goals delineated in the decision document. Additionally, in order to be successful," that remedy must be protective of human health and the environment.

As noted, the DOH has significant doubts that the remedy basis provided by the Navy's GWFMs is reliable for decision-making, even if specifically applied only to groundwater flow and capture. Field demonstration is a relatively simple and straightforward endeavor to validate the concept and its design parameters, the modeled capture pumping rate o(b)(6) being key among those. Demonstration of groundwater capture as modeled is the first step, followed by demonstration that LNAPL migration will not escape that transient capture zone.

The Relative Groundwater Elevations in the Facility Monitoring Wells do not Support the Modeled Groundwater Flow Trajectories.

Development of an accurate understanding of the groundwater flow trajectory beneath the underground storage tanks (USTs), along with any pathways to the Red Hill Shaft, are critical to any risk assessment and contaminant plume containment plan. In the absence of physical tests such as a tracer test or borehole flow vector survey, the relative water level differences in the wells beneath the USTs and in the hypothesized migration path to the Red Hill Shaft Infiltration Gallery are the prime metrics for an evaluation of groundwater flow trajectories. These differences provide the hydraulic potential to move groundwater, and dissolved contaminants, from areas of higher hydraulic head to areas of lower hydraulic head. However, the Navy has characterized the small differences in groundwater elevations across the Facility monitoring wells as unreliable and chose instead to use the drawdown response in the individual wells as the primary calibration parameter. The key questions for evaluating the groundwater flow model becomes: are the relative elevations between wells across the Facility monitoring wells so unreliable as to be dismissed; and should the priority for groundwater flow path analysis be placed on the relative differences in groundwater elevations between the Facility monitoring wells and the outlying observation wells in the Moanalua, and Halawa/Aiea area? It is DOH's position that the relative groundwater elevations within the Facility monitoring well network are most important for groundwater flow path analysis as it relates to risk assessment and plume capture evaluation.

The regulatory agencies have expressed concern about the Navy's failure to meaningfully address the local gradients within the Facility monitoring well network multiple times in last two years including in an agency letter to Navy in 2018 (EPA/DOH, 2018a), a presentation to the Red Hill Groundwater Modeling Working Group (EPA/DOH, 2018b), and a DOH report on probable groundwater paths in the Red Hill region (DOH, 2019). The weaknesses in the Navy's interpretation of the relative groundwater elevations and implied gradients are still present in the current GWFM Report and are an unacceptable deficiency that precludes DOH's reliance on any conclusions drawn from the models.

A review of Model 54 results offers informative insights into the models' deficiencies. Model 54 is an alternate parameter model developed to determine whether greater flexibility in the assignment of hydraulic conductivity to the basalt aquifer could capture localized variations in the observed water levels. Model 54 was selected because the overall calibration of this model was very good and similar to the other models presented in the GWFM report. Model 54 closely replicates the elevations across the model domain, but within the Facility monitoring wells, the model results are <u>not representative</u> of the observed groundwater elevation gradient changes that occur in response to changing pumping stress at the Red Hill Shaft.

Figure 1a and 1b show the observed groundwater elevations compared to those simulated by Model 54. The observed groundwater elevation values for Stress Period 1 (SP1, Red Hill Shaft pumping at an average rate) and Stress Period 3 (SP3, Red Hill Shaft not pumping) were taken from Figures 3.1-2 and 3.1-3 of the GWFM report respectively. The simulated groundwater elevation values were computed by subtracting the Model #54 residual mean error in Figure 5.4-5 from the target hydraulic heads in Figures 3.1-2 (SP1) and 3.1-3 (SP3). Figures 1a and 1b reflect the Navy's priority of calibrating the model to match the measured groundwater elevations across the model domain from the Moanalua Ridge to Aiea. This agreement between modeled and measured groundwater elevations is indicated by the high coefficient of correlation with data points falling along the 1:1 observed versus simulated line shown by the green dashes. However, as described below, the model performs poorly when simulating the response of the Facility monitoring wells to changes in pumping stresses at the Red Hill Shaft.

The Navy emphasizes that under normal pumping conditions at the Red Hill Shaft, the model indicates capture of water from beneath the USTs (Page 5-34, Lines 17 and 18). Using this conclusion, the Navy proposes pumping the Red Hill Shaft as means of capturing any fugitive contamination that may be released from the Facility. DOH used data from the GWFM Report to evaluate the Navy's hypothesis. For capture to occur, a hydraulic gradient needs to exist along a line from the USTs to the Red Hill Shaft, a line that includes wells RHM[redacted], RHM[redacted], RHM[redacted], and RHM[redacted]. Figure 2 shows the measured and modeled groundwater elevations for the wells along the centerline of the Red Hill Ridge (a) and along the northwest boundary of the Facility (b). The groundwater elevations for SP1 (Red Hill Shaft pumping) are shown in dark grey while the groundwater elevations for SP3 (Red Hill Shaft off) are shown in violet. The measured groundwater elevations are shown as diamonds whereas the modeled groundwater elevations are shown as squares. Best fit lines are shown for measured (solid lines) and modeled (dashed lines).

The key observation for Figure 2(a) is that the measured response to changes in pumping stresses in the groundwater elevations is markedly different from that modeled. The slope of the best fit line for the **measured** groundwater elevations is **the same** for the **Red Hill Shaft off (SP3)** and the **Red Hill Shaft pumping (SP1)** showing no increase in the hydraulic gradient between a non-pumping and pumping condition. By contrast, the best fit lines for the **<u>modeled gradients</u>** for **both SP1 and SP3 show**: **a much greater slope than that for the measured groundwater elevations**; and**, a much steeper slope** for the Red Hill Shaft pumping stress period (SP1) than for the Red Hill Shaft off (SP3). The modeled groundwater elevations show the gradient that is necessary to move groundwater down Red Hill Ridge along the flow trajectory indicated by the particle tracks. Because there is **no change in the slope** of the best fit line for the **measured water levels between the Red Hill Shaft pumping and non-pumping conditions**, we conclude, contrary to the modeling results, that **the groundwater beneath the USTs and along the path to the Red Hill Shaft is not significantly mobilized by normal pumping of the Shaft.** We

further conclude that the modeled particle tracks are not representative of actual groundwater flow trajectories during pumping and non-pumping conditions of Red Hill Shaft.

Figure 2(b) performs the same evaluation for the wells along the northwest boundary of the Facility (RHM[redacted], RHM[redacted], RHM[redacted], and RHM[redacted]). **There is a definitive response in the measured gradients observed** in the northwest wells between Red Hill Shaft pumping (SP1) and not pumping (SP3). The **critical observation for these wells is the apparent reversal in the observed gradient from downslope when the Red Hill Shaft is pumping to upslope when the Red Hill Shaft is off**. By contrast, the **modeled groundwater elevations show the gradient going downslope under both pumping and non-pumping conditions,** and show no reversal, but only a steepening of that gradient, when the Red Hill Shaft is on.

The divergence in the measured and modeled responses to changes in pumping conditions at the Red Hill Shaft cast serious doubt on the ability of the model to predict a capture zone for the Red Hill Shaft. Hence, these models, as presented, can't provide a reliable groundwater flow field for the contaminant fate and transport models. **These discrepancies indicate the modeled groundwater flow trajectories beneath the USTs are neither valid nor sufficiently reliable to guide response and remediation strategies or for use in assessing risk associated with future releases.**

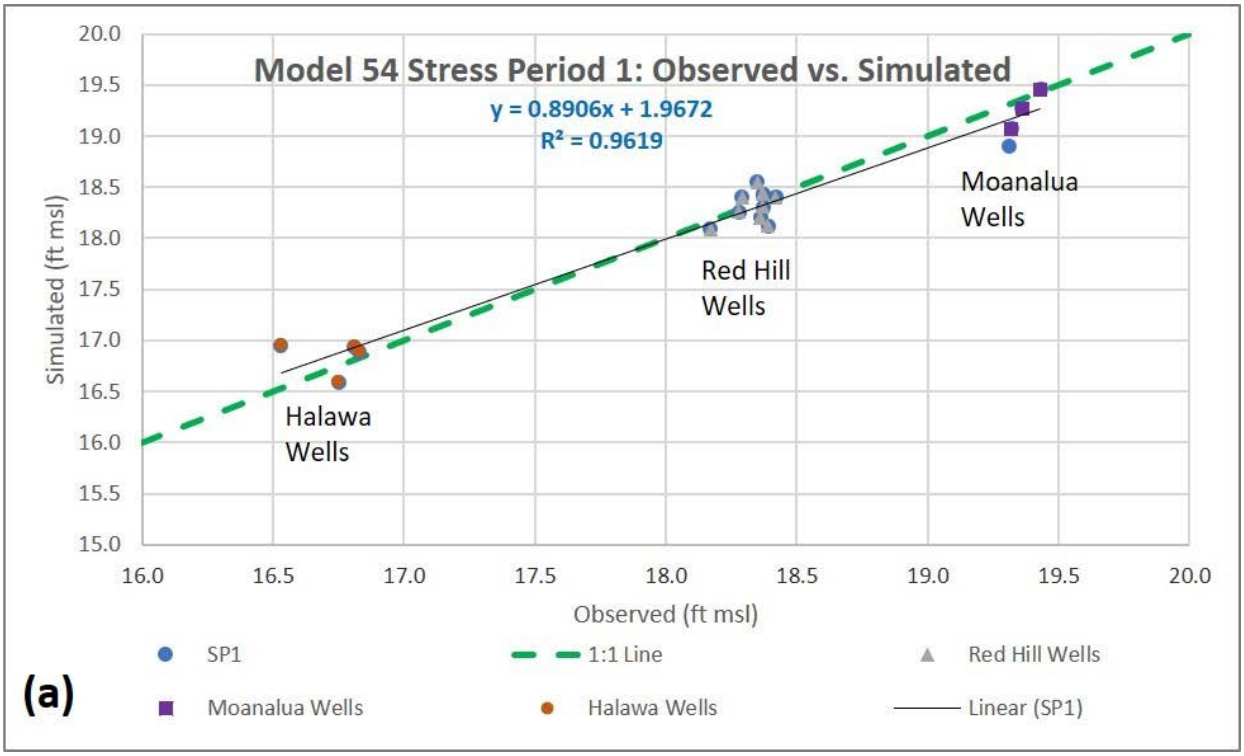

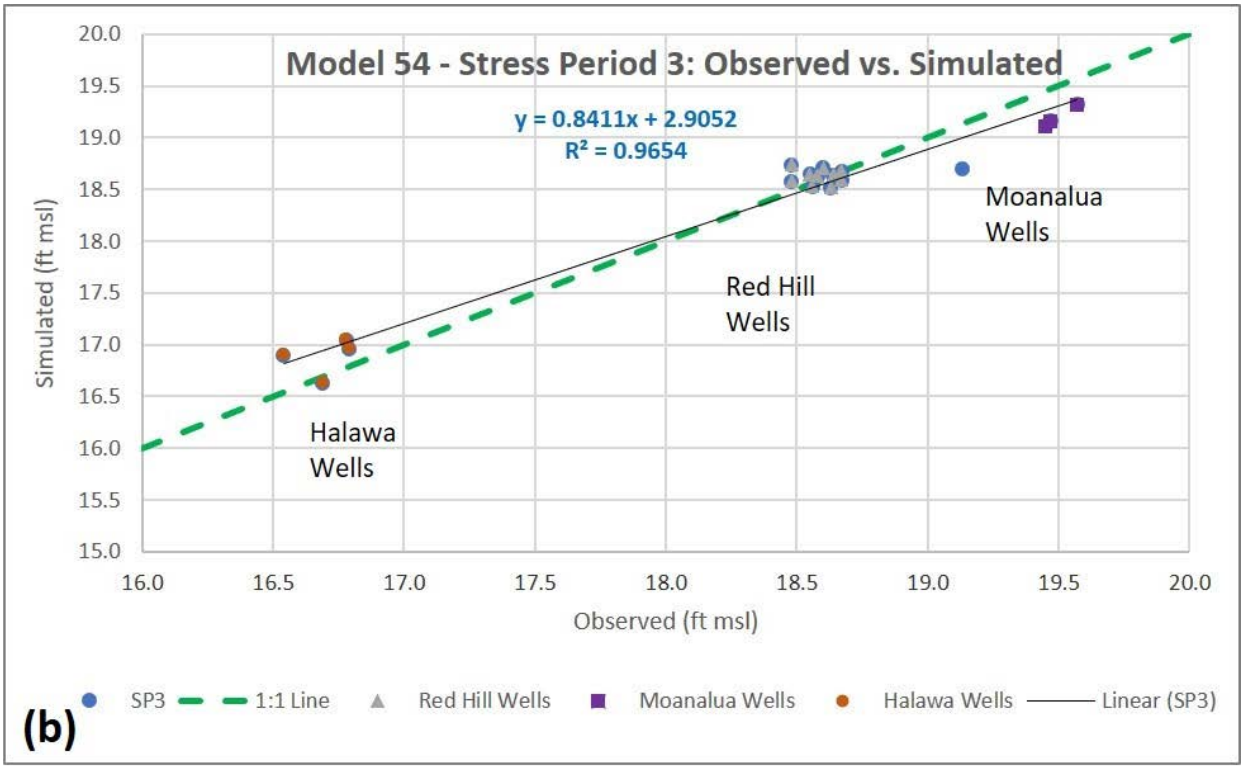

Figure 1. A comparison of the observed and modeled water levels across the model domain for Stress Period 1 (a) and Stress Period 3 (b) as simulated by Model #54.

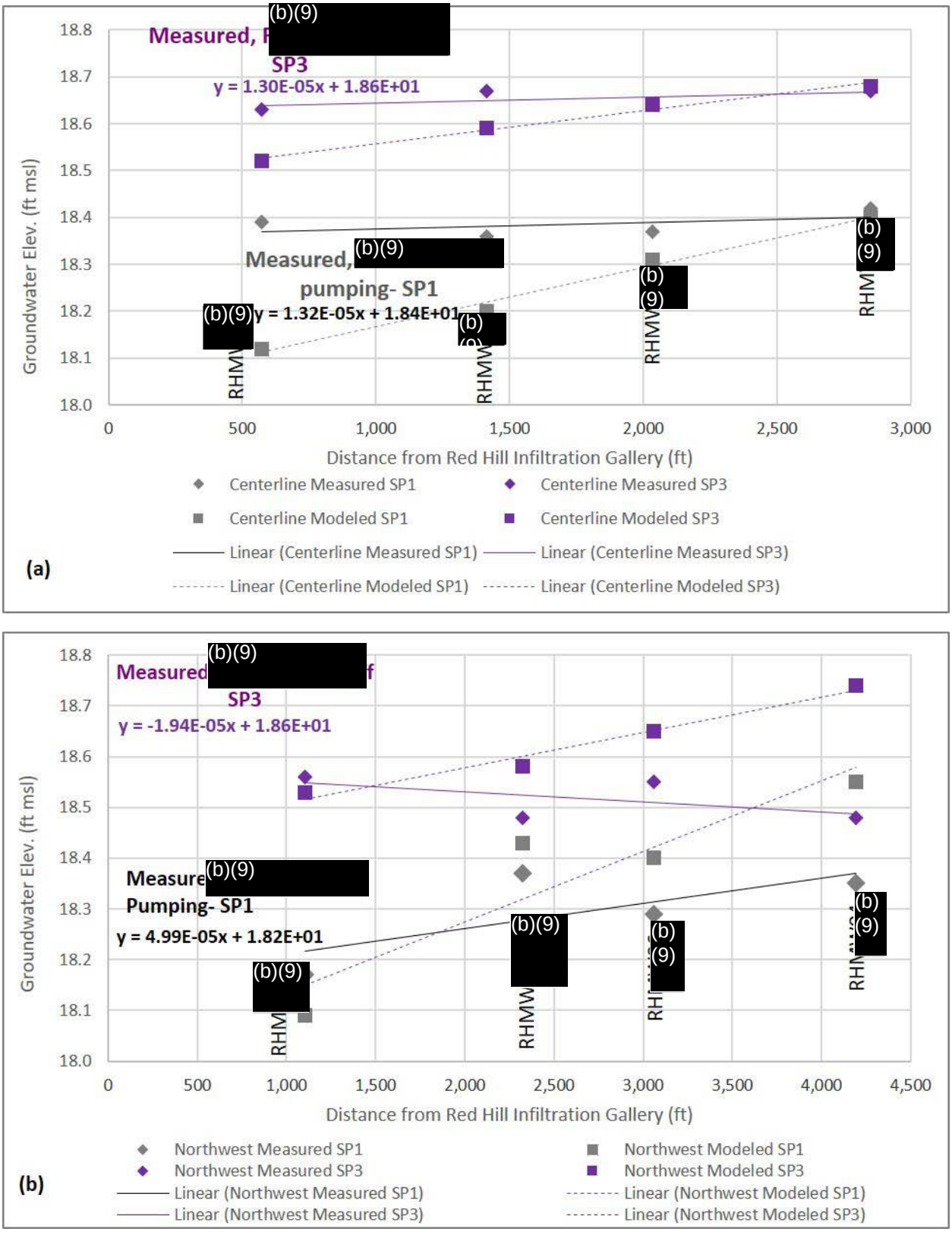

Figure 2. Groundwater elevation measured, modeled, and best fit lines for the wells along the centerline of the Red Hill Ridge (a) and along northwest side of the Red Hill Ridge (b)

Whereas the Navy has claimed that these gradients should be disregarded, no rigorous analysis is provided to support that position. The rationale given for disregarding local gradients is that the "datum or borehole alignment inaccuracies and the low precision of the gyroscopic corrections" (Page 3-2 lines 33 to 34) render the water level measurements unreliable. A review of the gyroscopic directional survey data sheets (Wellbore Navigation, Inc., 2017) show the resolution of the gyroscopic corrections for true vertical depth is 0.01 ft. A review of the top of casing leveling survey (Department of the Navy, 2018) shows that mean misclosure was 3.9×10^{-7} ft per ft of survey loop length. The greatest misclosure (Leveling Loop 4 from RHM[redacted] to RHM[redacted]) was -0.002 ft over a loop distance of 2,372 ft or 5.6×10^{-7} ft per ft of loop length. The apparent uncertainty in the relative top of casing elevations is extremely small relative to the differences in groundwater elevations within the Red Hill Groundwater Monitoring Network. For example, the apparent gradient from RHM[redacted] to RHM[redacted], about 2,300 ft, is 1.3×10^{-5}, about 20 times larger than the uncertainty in the top of casing elevations.

The simple conclusion is that the modeled gradient going down the axis of the Red Hill Ridge accurately shows what is required to move groundwater in this direction (under the modeled hydraulic conductivity conditions described in the model) to meet the demands of the Red Hill Shaft pumpage and the assumed mauka-to-makai groundwater flow. The fact that the **measured gradient** going down the axis of the Red Hill Ridge **is nearly an order of magnitude lower** shows that the underlying assumptions of the model are incorrect. Further, the fact that the **measured** gradient going down the axis of the Red Hill Ridge changes minimally between pumping and non-pumping conditions shows that pumping the Red Hill Shaft can't be depended upon to contain any fugitive contamination from the Facility. The groundwater gradient in the wells along the northwest and southeast side of the Red Hill Ridge do show a response when the Red Hill Shaft transitions from a normal pumping condition to no pumping. This suggests that rather than capturing water from beneath the USTs, the water flowing to the Red Hill Shaft is drawn more from the periphery of the Red Hill Ridge rather than from beneath the tanks. Therefore, the proposed strategy of pumping Red Hill Shaft to capture a future release is uncertain/unlikely and will be an ineffective strategy for contaminant management.

Evaluation of Modeled Groundwater Flow Paths using Chloride Distribution

DOH has suggested on numerous occasions (e.g. DOH, 2018b; DOH, 2020; and the Technical Working Group No. 24 Webinar on March 5, 2020) that the distribution of chloride in the groundwater beneath the Facility can be informative when evaluating the groundwater flow trajectories simulated by the GWFM. It appears that the Navy may have given this approach some consideration because, on Page 1-4, Lines 6-8 of the GWFM Report, the Navy indicates a chloride calibration was done at select wells. However, no further mention is made of the simulation of chloride concentrations or what the results were.

DOH has completed a conceptual assessment to demonstrate that it is difficult to reconcile the measured groundwater chloride concentrations with the simulated groundwater flow trajectories as indicated by the particle tracks. According to Visher and Mink (1964) the sources of chloride to south Oahu's groundwater are rainfall, deposition of sea spray, and chloride from the saline water beneath the basal lens. A simple box model, shown in Figure 3(a) and 3(b), will suffice for this demonstration with representative chloride concentrations applied to the box model boundaries based on literature or measured values. The groundwater chloride concentration in the recharge zones upslope is very low at about 16 mg/L (Visher and Mink, 1964). The particle tracks displayed in GWFM Report and the water

budget (Table 3-4) show that 40 percent of the groundwater comes from the northeast boundary, which should have a chloride concentration of about 16 mg/L. The freshwater lens is very thick at that northeast boundary and, hence, no mixing with deeper brackish water would be expected. Water recharging along the groundwater flow path to the Facility will have higher chloride concentrations than that in the upslope recharge zones: the chloride concentration in rainfall increases closer to the coast, as does evapotranspiration, and therefore, the chloride concentration in the infiltrating water will be greater than that of local rainfall. Visher and Mink (1964) state that the chloride concentration in Honolulu coastal rainfall varied from 3.0 to 29 mg/L for an average value of 16 mg/L. Average chloride concentration in the upland areas in the Kipapa drainage basin was 6.5 mg/L making 11 mg/L a representative rainfall concentration. Assuming that chloride is a conservative species, the chloride concentration of the recharging water can be approximated by:

[Cl]recharge = 11 mg/L * Recharge/(Rainfall-runoff)

The spatial distribution of rainfall, runoff, and recharge can be taken from the USGS recharge coverage for Oahu (Engott et al., 2017). This simple approximation returns a chloride concentration for recharge directly into the subsurface of the Facility of about 45 mg/L. However, if the GWFM is correct, the groundwater chloride concentration beneath the facility would be dominated by upslope recharge and would be much less than 45 mg/L. Figure 3a uses identical color schemes to show the chloride concentrations in the Moanalua and Halawa area wells, within the Facility monitoring wells, and false color shading showing a hypothetical chloride distribution within the Facility based on the GWFM "mauka to makai" particle tracks. The hypothetical chloride distribution assumes the groundwater flowing into the northeast boundary of the model has a chloride concentration of 30 mg/L and reflects the increase in chloride concentration due to increased evapotranspiration as elevation decreases. Within the box model the chloride concentrations continue to rise due to increasing evapotranspiration and the general trend of increasing chloride concentrations in the Moanalua/Halawa Region wells going down slope (refer to Figure 3(a)). The regional chloride values are from the 2004 USGS National Water Quality Assurance study (Hunt, 2004) and in samples collected for the UH geothermal resources study that were provided to the Navy in November of 2017 (Lautze et al., 2017). The high chloride concentration at the southwest part of the facility assumes some chloride is brought up from depth and from zones nearer the coast due to the large pumping rates of the Halawa Shaft and the Red Hill Shaft. This is indicated by the relatively high chloride concentration of 152 mg/L at the Halawa Shaft. In summary, the false color shading approximates the chloride concentrations that would be expected in groundwater beneath the Facility wells if the Model 52 particle tracks are representative of the actual groundwater flow trajectories. Differences in color shading between the background and the color shading representing measured chloride values in the monitoring wells show significant conflicts between the modeled and measured chloride values implied by the GWFM flow trajectories.

Figure 3(b) focuses on the Facility and shows the particle tracks simulated by Model 52. As with nearly all the GWFM simulations, the flow trajectory is only slightly oblique from going down the axis of the Red Hill Ridge. Most of the path lines don't pass beneath any developed area or known source of chloride prior to reaching the Facility boundaries. This suggests that chloride concentration within the Facility should be closer to that of the recharge areas than to the downslope production wells. Compared to the hypothetical chloride distribution, wells RHM[redacted], RHM[redacted], RHM[redacted], RHM[redacted], RHM[redacted], and (b)(3) [redacted] stand out as having chloride concentrations significantly greater than those implied by the GWFM. The chloride concentrations in wells RHM[redacted], RHM[redacted], and (b)(6) [redacted] are

an order magnitude or more than what would be expected given the large simulated flux of upslope recharge water down the axis of the Red Hill Ridge. The cause of these elevated chloride anomalies is currently unknown, but clearly conflict with the simulated groundwater flow trajectories.

The key point of this analysis is to show that the modeled groundwater flow field and the measured groundwater chloride within the facility wells can't be reconciled unless a source of chloride can be identified that falls within the modeled zone of contribution to the Red Hill Shaft. If the footprint of the particle tracks shown in Figure 3(b) indicates the zone of contribution to the Red Hill Shaft, there must be a source of significantly elevated chlorides within that zone of contribution. Figure 4(b) also shows the location of elevated chloride hypothesized by the Navy. Both the Halawa Quarry and the area "north of South Halawa Valley" (CSM Page 6-31, Line 44 and 6-32, Line 1) are well outside of the simulated zone of contribution for flow down the Red Hill Ridge.

DOH recognizes that the GWFM and its particle tracks are not the same as a contaminant transport model. However, particle tracks do show the simulated groundwater flow field from areas of recharge to the point of capture by the Red Hill Shaft, essentially identifying that part of the aquifer that the model indicates contributes water to beneath the USTs and to the Red Hill Shaft. Nowhere within that flow field is there a source of chlorides that could account for the great disparity between measured and expected groundwater chloride concentrations in the monitoring wells. The GWFM is intended to provide the groundwater flow field for the follow-on contaminant fate and transport model. If the GWFM can't account for the measured chloride distribution, the contaminant fate and transport model will not be reliable for simulating the migration of fuel-related contaminants or for planning release response measures.

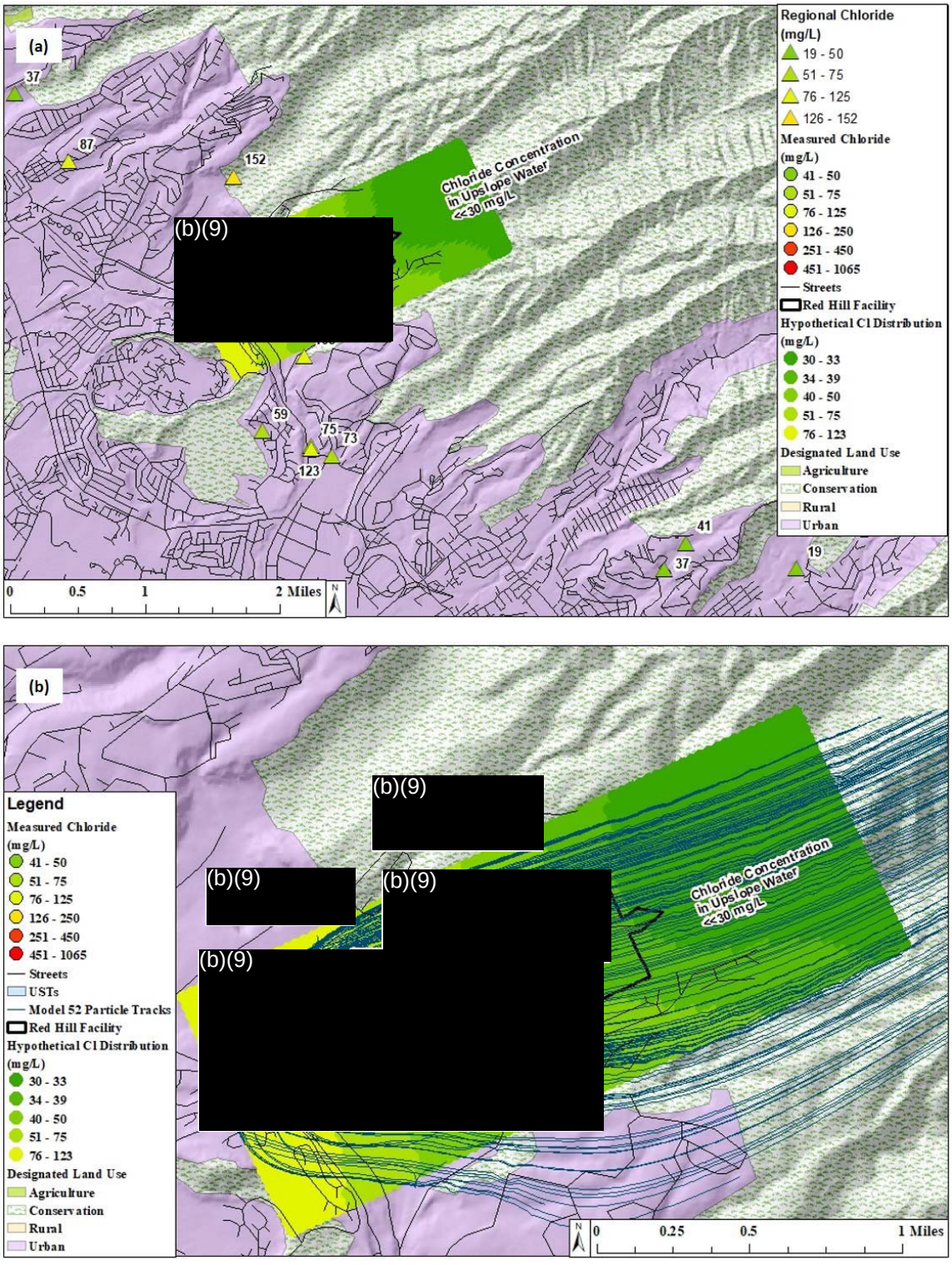

Figure 3. (a) regional chloride concentration in Moanalua/Halawa Area Wells and a hypothetical distribution of chloride in the groundwater beneath the Facility based on regional chloride concentrations. (b) Particle tracks from Model 52, and the Navy's proposed chloride source areas are added

Deficiencies of the Multi-Model Approach

The DOH agreed in concept with the use of a multi-model approach in the Navy's groundwater flow modeling efforts first discussed in July 2019. As discussed in several technical working group meetings since that time, the DOH's expectation was that this approach would systematically test plausible and defensible hydrogeologic conditions to arrive at the most likely set of conditions that represent the hydrogeologic system (i.e., the "best" model or models). The model suite presented in the Navy's GWFM report does not drive toward any definitive conclusions about the nature and behavior of the groundwater system. In the language of the AOC, it does not *"improve the understanding of the direction and rate of groundwater flow within the aquifers around the Facility."* (Site AOC, 2015). To achieve that goal, the multi-model approach needs to test and support or eliminate various assumptions in order to arrive at defensible conclusions about the nature of the hydrogeologic system that controls the direction and rate of groundwater flow around the Facility.

The conclusions section of the GWFM report (section 5.10) does not provide any significant interpretations regarding the actual in situ conditions. Rather it discusses observations of modeled outcomes and differences in that modeled behavior; those are closer to findings, not the conclusions anticipated under the AOC and groundwater modeling extensions. A number of divergent models were tested using non-traditional parameter values; all calibrated equally well; and, hence, provided little insight into which of the approaches best represent the processes occurring in the groundwater system below the tanks. Further, that the quite different models all yielded the same results using the divergent parameters suggest that the results are more reflective of the parameters selected than they are of the different models tested. A discussion of the parameters follows in the next section.

A Comparison of the Red Hill Groundwater Flow Model Hydraulic Parameters with Those Used by Other Modelers

Model parameters vary among past individual modeling efforts that simulate groundwater in the Red Hill region. Reasons for the differences in parameter values include differences in modeling codes; varying hydrogeologic assumptions; the extent of field data that are available at the time the model was developed; and the preferences of the different modelers. However, the parameters used by the various modeling efforts should fall within a reasonable range of each other and, if they don't, the reasons for the differences should be explained. Table 1 compares the USGS model of the Pearl Harbor Aquifer (Oki, 2005), the 2007 Navy model of Red Hill (Rotzoll and El-Kadi, 2007), the Board of Water Supply model of the Honolulu Aquifer (Honolulu Board of Water Supply, 2005), with the current Navy groundwater flow model for Red Hill.

This comparison of hydraulic parameters, such as the basalt horizontal hydraulic conductivity values, shows that the GWFM falls well within the range used by other modelers. However, the values the Navy chose to use for other hydraulic parameters, as highlighted in Table 1, are much different from those used in prior efforts. These parameters include vertical hydraulic conductivity, horizontal anisotropy, and porosity. The vertical hydraulic conductivity values used by the Navy are much higher than those used by Oki (2005), and Rotzoll and El-Kadi (2007). Conceptually, the effect of using a high value for vertical hydraulic conductivity is to reduce the influence that the alluvial/saprolite wedge exerts over cross-valley groundwater flow. A high vertical hydraulic conductivity will increase the ease with which the groundwater can move downward through the basalt layers and flow deeper into the aquifer, bypassing the poorly permeable alluvial/saprolite wedge. The effect of the valleys' alluvial/saprolite

wedges is further reduced by modeling layers 4 through 9 as continuous, and passing beneath the alluvial/saprolite wedge, rather than a more conceptually correct approach of having the basalt layers terminate at the contact between the basalt and alluvial/saprolite wedge and resume at the contact on the opposing side of the wedge.

Table 1. Comparison of Model Parameters Used by Various Modelers to Simulate Groundwater Flow in South Oahu

Geology	Parameter	Units	Oki, 2005	Rotzoll & El-Kadi, 2007	Honolulu Board of Water Supply, 2005	Mdl 51a	Mdl 51b	Mdl 51d	Mdl 51e Zone 3
Basalt	Kh	ft/d	4500	4428	1500	2828	5316	8280	2152
	Kv	ft/d	7.5	7.4	150	200	66.3	54.9	1355
	K_L:K_T	(ft/d)/(ft/d)	3	3	1	3	10	17	
	Porosity	ft^3/ft^3	0.04	0.05	0.3	0.01	0.01	0.01	0.01
Caprock Limestone	Kh	ft/d	2500	na	50	5000	5000	5000	5000
	Kv	ft/d	25	na	50	9.45	11.87	11.9	10
	Porosity	ft^3/ft^3	0.2	na	0.4	0.073	0.095	0.095	0.07
Caprock Sediments	Kh	ft/d	0.6	115	1	20	20	20	20
	Kv	ft/d	0.6	115	1	20	0.1	0.1	20
	Porosity	ft^3/ft^3	0.1	0.1	0.4	0.03	0.022	0.022	0.03
Valley Fill	Kh	ft/d	0.058	0.066	10	1	1	1	1
	Kv	ft/d	0.058	0.066	10	0.001	0.001	0.001	0.001
	Porosity	ft^3/ft^3	0.1	0.15	0.4	0.02	0.02	0.02	0.02

Abbreviations:

Kh – horizontal hydraulic conductivity
Kv – vertical hydraulic conductivity
K_L:K_T – horizontal anisotropy ratio
ft – feet
ft^3 – cubic feet

This page is intentionally left blank

Horizontal anisotropy is another important hydraulic parameter where there is a significant difference between some of the values used in the Navy GWFM and that used by other modelers. The base horizontal anisotropy of 3:1 agrees well with values used by other modelers. However, the Navy's GWFM calibrates more closely to measured heads when horizontal anisotropies of 10:1 and 17:1 (the limit imposed during the PEST runs) were used. Other modelers found better model calibration with anisotropies of 3:1 (Oki, 2005; and Rotzoll and El-Kadi, 2007) and 1:1 (Honolulu Board of Water Supply, 2005). While it can't be determined definitively what the most appropriate horizontal anisotropy values are, the model that uses the most extreme values should include a concise physical explanation to justify that the more extreme values are in fact real and not just an artifact of the automated parameterization that produces the very high horizontal anisotropy.

The aquifer porosity selected for the Navy's GWFM is much lower than that used by any other comparable model. The USGS uses aquifer porosity in their density dependent flow models to reach agreement between the measured and modeled profile of the freshwater/saltwater transition zone (e.g. Gingerich, 2008) giving their selection of porosity a physical basis. The simulated aquifer porosity will affect the calibrated value for other hydraulic parameters such as hydraulic conductivity when simulating aquifer drawdown in response to changes in pumping stresses. A lower porosity will increase the aquifer drawdown when pumping is increased. Since the simulated drawdown in response to changes in pumping stresses was a calibration parameter, the selection of an inappropriate porosity will have a compounding effect as the values for other hydraulic parameters will need to be adjusted for the model output to match the measured drawdowns.

The Navy contends that using a low porosity is conservative from a risk evaluation perspective (Page 5-9, Lines 18 through 25). A non-conservative effect of the low porosity value is an artificial increase in the plume attenuation rate due to the erroneously high groundwater flow velocity. If the contaminant fate and transport model is calibrated with an erroneously high groundwater flow velocity, an unrealistically high contaminant attenuation rate will also be simulated. DOH assumes that GWFM results will be used in a manner like that presented in Section 3.5 of the conceptual site model report (Department of the Navy, 2019b). As described in the DOH conceptual site model review comments (DOH, 2020), the plume attenuation rates using the modeled groundwater velocities resulted in high attenuation coefficients that were inconsistent with the anoxic conditions between RHM[redacted] and RHM[redacted].

The groundwater velocities stated in the GWFM Report are much higher than any previously reported velocities. Based on travel times listed in Table 5-6, the groundwater particle velocity from the USTs to the (b)(6) varied from a low 16 ft/d to a high of 110 ft/d with an average for the model runs of 51 ft/d. These velocities are much higher than generally accepted values for Oahu groundwater. For example, Lau and Mink (2006) state the average groundwater velocity in Hawaii is on the order of 1 ft/d. Whereas the geometry of the alluvial/saprolite wedges may increase the groundwater flow velocity by constraining the seepage face to between these barriers, a groundwater velocity of more than 50 ft/d is not supported by any evidence independent of the model and is inherently non-conservative.

The only direct measurement of Hawaii groundwater transport velocity on the scale of the distances present within the Facility is the Lahaina groundwater tracer study (Glenn et al., 2013). While there are distinct differences between wastewater injection in West Maui and the movement of groundwater beneath the USTs, there are also clear similarities. The wastewater injection rate is comparable to the (b)(6) long term pumping rate, with both at about 4 million gallons per day. The travel distances

are also similar, about 3,000 ft. The average groundwater flow velocity measured by the Lahaina groundwater tracer study was about 10 ft/d. Modeled groundwater velocities that are several times that value must be viewed with a significant amount of skepticism and require additional explanation. DOH contends that unrealistically high groundwater velocities are non-conservative and non-informative since erroneously high contaminant natural attenuation rates will be estimated.

Boundary conditions

Boundary conditions set hydrologic conditions at the perimeter of a numerical model because simulating an entire hydrologic system is not always reasonable. As described on pages 226 and 227 of National Academy Press (1990):

> "Groundwater and associated contaminants can also enter or leave the region across boundaries. The boundary conditions imposed on a model's solution can have an important impact on the predicted flow and transport behavior. Parameters included in the boundary conditions (such as specified heads, concentrations, and fluxes) can sometimes be inferred from field observations. They are more often simply postulated."

While there is physical logic for the boundary conditions used in the GWFM, the important details of how these boundary conditions influence groundwater flow within the model domain are largely postulated. The variability seen between the model run results are much less than would be expected given the significant changes to the values and distribution of hydraulic parameters and features within the model domain. This suggests that the boundary conditions are driving the model results.

The model's upper boundary condition has the best scientific basis. This boundary condition represents recharge and should not be varied. The next best supported boundary condition is the bottom boundary that is the mid-point of the freshwater/saltwater transition as simulated by Oki (2005). All other boundary conditions are subject to a great deal of uncertainty.

Figure 4 shows southeast Oahu, the GWFM domain and boundaries, and water levels measured in each of the aquifer systems in southeast Oahu.

Northeast Boundary Discussion

The northeast boundary is the assumed contact between the flank lavas and marginal dike zone. There is a great deal of uncertainty about where this contact occurs and the relationship between the groundwater flow in the marginal dike zone and flank lavas. The Navy assumes that groundwater recharged upslope of the northeast boundary flows into the model. While this assumption is reasonable, whether this condition exists is currently unknown/unproven. Dikes within rift zones generally align with the axis of the rift zone (Walker, [redacted]7), which is perpendicular to the assumed groundwater flow direction. This divergence in the directions of maximum hydraulic conductivity between the dike system and the flow basalts could impart a large anisotropy to the movement of groundwater from the dike system into the basal groundwater system. Further, adding all upslope recharge to the bottom layer of the model is questionable.

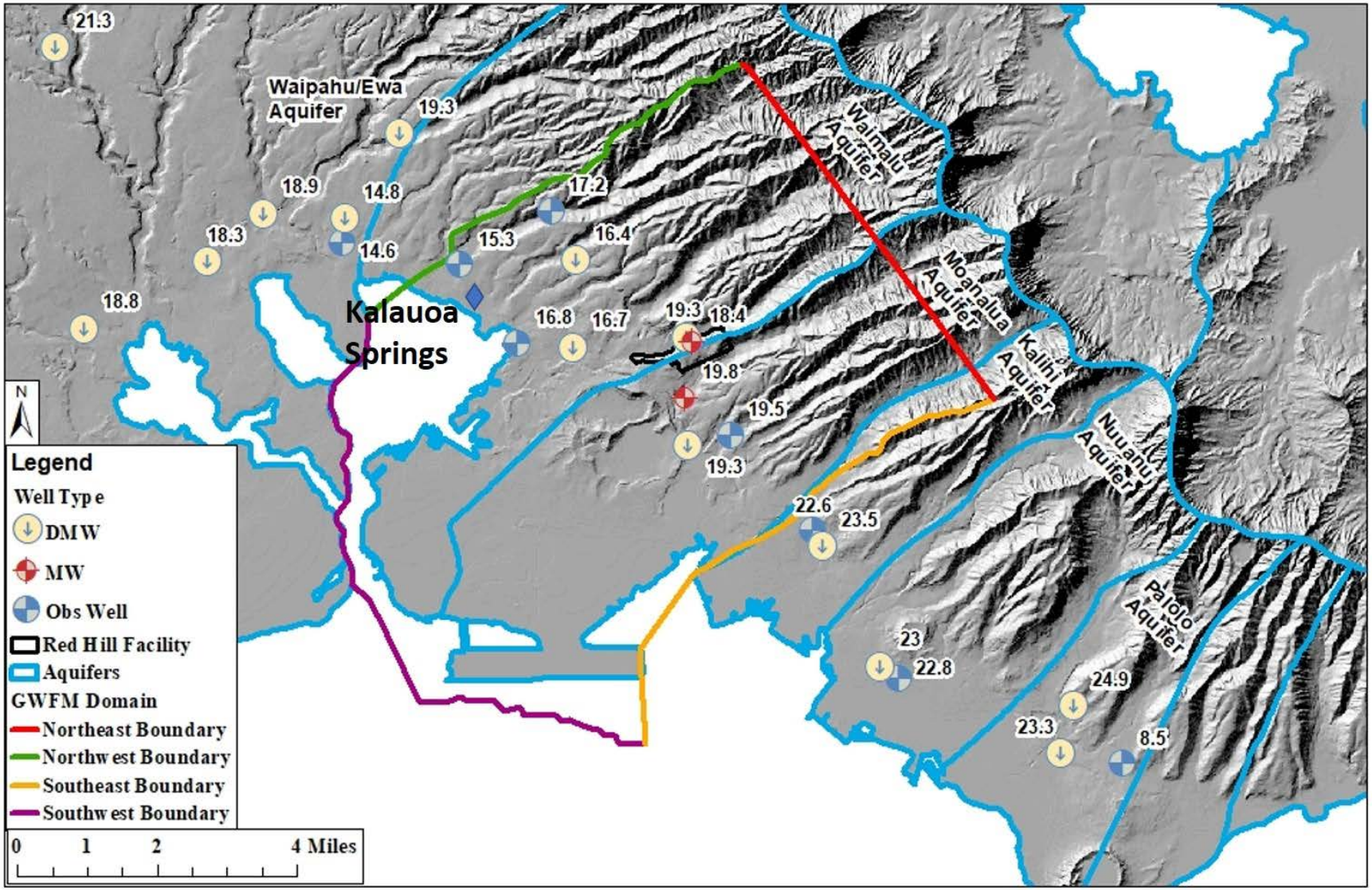

Figure 4. Southeast Oahu showing average 2017 to 2018 groundwater elevations and the model domain.
DMW – Deep monitoring well; MW – Red Hill Monitoring Well; Obs Well – HBWS water level observation well

This page is intentionally left blank

Southeast Boundary Discussion

The southeast boundary assumes no flow from Kalihi Valley into the model domain for all model runs except Model 59 that simulated 10 mgd inflow at this boundary. As with the northwest boundary, assuming little to no flow across this boundary is reasonable, but the actual flow relationship beneath and around the alluvial and saprolite wedge is not known. As Figure 4 shows, the groundwater elevation on the Kalihi (east) side of Kalihi Valley is about 2 feet higher than on the Moanalua side (Honolulu Board of Water Supply, 2018). The geometry of the alluvium and saprolite wedge in Kalihi Valley is unknown. It is also not known how far upslope from the coast the valley fill and saprolite act as an effective barrier to cross aquifer flow. Investigations in Halawa Valley indicate that the depth of the alluvial/saprolite wedge decreases rapidly as the topography transitions from the coastal plain to upslope valleys. If this is true in Kalihi Valley, differences in groundwater elevations would result in groundwater flux into the model domain. Model 59 was run to test the effect of inflow across the southeast boundary and the Navy's assessment was that model results were very similar to Model 51a. That is, any water from the Red Hill area that would be captured by the Halawa Shaft, would pass down the Red Hill Ridge on its way to Pearl Harbor. However, if other boundary conditions are simultaneously changed, the model results could be altered dramatically. As will be discussed later in this review, it is likely that testing boundary conditions individually will not adequately evaluate groundwater flow trajectories within the vicinity of the Facility.

Southwest Boundary Discussion

The southwest boundary is a general head boundary meant to represent groundwater flow from the terrestrial model domain to Pearl Harbor and the Pacific Ocean. A general head boundary assumes a hydraulic head at some distance from the physical model boundary with a bulk hydraulic conductance parameter value being assigned to represent the distance and permeability of the intervening aquifer material. As with the previous boundary conditions, the assumptions made by the Navy are reasonable but not verifiable. How accurately this important boundary represents actual hydrologic conditions is difficult to verify. The is no definitive way to determine if groundwater flow from the beneath the Red Hill Ridge flows to Pearl Harbor or to Kalauao Springs as many of the model runs indicate, or takes another pathway. The implications for groundwater flow beneath the Facility are quite different depending on which of the terminal flow possibilities is most correct.

Northwest Boundary Discussion

The northwest boundary assumes no flow across Waimalu Valley either into or out of the model. As with the other boundary conditions used, this assumption is reasonable based on the groundwater flow trajectory illustrations that dominate USGS publications such as Hunt (1996) and Oki (2005). But again, the conditions at the northwest boundary are unknown. The alluvium/saprolite wedge barrier in Waimalu Valley, located near the northwest boundary, is likely not an effective barrier resulting in groundwater flow across this boundary. For example, the large amount of discharge from the Pearl Harbor and Kalauao Springs will undoubtedly result in some groundwater flow across this boundary into the model domain.

Boundary Conditions Concluding Remarks

In summary, all the model boundary conditions are reasonable, but reasonable does not equate to accurate or even correct. Regardless, the hydrologic conditions at the model's lateral boundaries are currently unknown and therefore not verifiable. In the interim modeling phase, and to a limited extent in the final model phase, the Navy has attempted to test various boundary conditions. However, this was done in the same manner that sensitivity analysis is typically done: change is made to a single parameter (or boundary condition) and the model response is evaluated. In the case of Red Hill, it is likely that multiple boundary conditions must be changed simultaneously for the model to best represent actual conditions. This combination of boundary condition changes will likely have a compounding effect on the model output. The uncertainty about the boundary conditions is so great that it is not possible to adequately test their full range in a model, yet it is the boundary conditions that exert a large influence on modeled groundwater flow trajectory. What is needed to gain confidence in the groundwater flow model and to identify specific areas for revision are field tests that have been asked for by DOH that include, but are not limited to: a borehole flow vector survey and a tracer test of water flow velocities and vectors beneath the Facility.

Model Verification Simulations

Model verification runs are done to validate that models calibrated to the primary data sets adequately reflect groundwater conditions for a different time period. In the GWFM report, the verification simulations appear to adequately reflect the measured groundwater elevations over the period from January 10, 2018 to February 10, 2018. This is a period when there were distinct changes in pumping regimes at the Red Hill and Halawa Shafts. The DOH concurs that this is a suitable verification test period.

However, in the draft numerical models provided, the DOH SME team is unable to duplicate the results that are presented in the Navy GWFM report. This was discussed in one or more working meetings. It appears to the DOH reviewers that the GWFM drawdown results were superimposed on measured groundwater elevation data, as opposed to the modeled groundwater elevations. The DOH is unable to replicate the model verification results presented by the Navy in the GWFM report.

In our execution of the Navy's draft numerical groundwater flow models, there is substantial variance between the measured groundwater elevations versus those modeled. Groundwater elevations are much more important than drawdown/recovery because they reflect aspects of the total water budget and system behavior. Figure 5 shows the head variance between various verification model runs and the actual heads from the synoptic water level data. Except for Model 56 the simulated hydraulic head is significantly higher than the measured head hydraulic head. Transient drawdown/recovery is relatively easy to match by modeling, groundwater elevations are typically more difficult to match, but are more important. Unless the draft models were updated relative to those the agencies received, the verification simulations are unacceptable. Rather than showing strong concurrence with measured data, they are highly in error. If these observations are the result of model changes not available to the DOH, then we request those model updates so that we can again compare the verification simulation against measured groundwater elevations. If the models have not been updated in any substantial manner, then the verification runs directly demonstrate that full suite of GWFMs are demonstrably flawed.

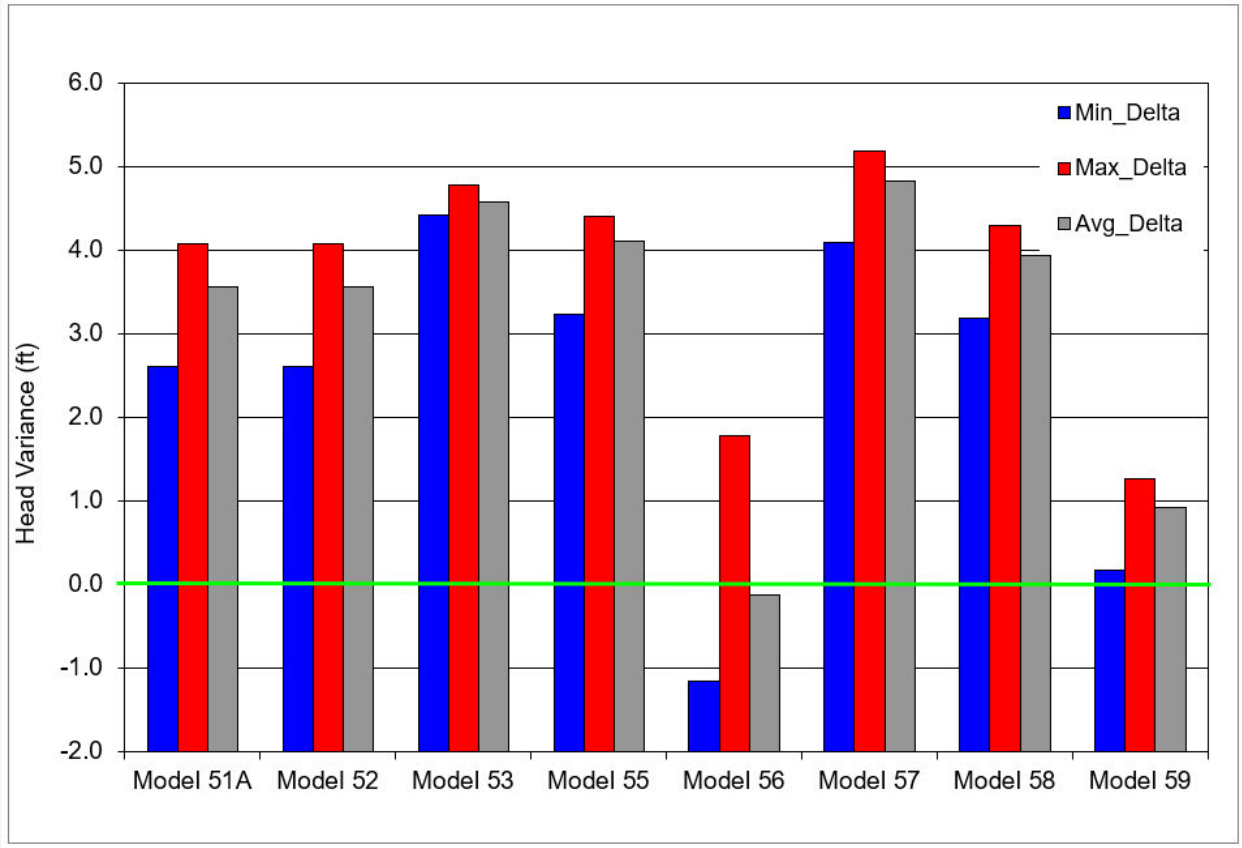

Figure 5. Modeled Groundwater Elevations Compared to Actual Synoptic Data Verification Model Variances to Measured Red Hill Area Well

Risk Conservatism

The word "conservative" is used frequently throughout the GWFM report. But rarely is there a distinct technical framing for that conservatism, or, as the degradation rate example discussed above shows, a model result may be conservative from one perspective, it can also be equally non-conservative from a different perspective. The GWFMs have elements that are conservative in some ways and non-conservative in others. But the core issue is that none of these models drives us toward a more refined understanding of the system characteristics and flow behavior. For these reasons, DOH does not find this suite of models to be adequately consistent with the area data to meet the primary AOC objective of refining our understanding of the aquifer system and its related parametric characteristics.

Further, results that the Navy labels as conservative may be an artifact of model weaknesses. An example is the degree of simulated hydraulic connectivity between the Facility and the Halawa Shaft (Page 5-33, Lines 13 through 17) the Navy concludes that because the modeled response in the Facility monitoring wells to changes in pumping stresses at the Halawa Shaft is greater than that observed, the model conservatively overestimates the connectivity between the Facility and the Halawa Shaft. However, this apparent overestimation of connectivity is almost certainly due to the high vertical hydraulic conductivity value used for the basalt and that the basalt layers are continuous from the Red Hill Ridge to the Halawa side of Halawa Valley. This overestimation of hydraulic conductivity is non-conservative since the hydraulic factors responsible for the increased response allow groundwater to

flow more easily under the saprolite wedge where LNAPL floating on the water table would be blocked by the saprolite and valley fill. What is not adequately tested is the possibility that, while using values of vertical hydraulic conductivity more similar to those used in prior models, groundwater from beneath the upper part of the Facility flows around the upper toe of the saprolite toward the Halawa Shaft, a potential pathway for LNAPL.

Concluding Statements

In response to this evaluation of the GWFM the Navy will correctly point out that multiple model runs have been done to test the potential boundary conditions and hydraulic parameter values. However, in nearly all of these runs a single parameter or boundary change was tested. It is highly probable that simultaneous changes to multiple aquifer parameters and boundary conditions will be needed to properly represent the groundwater flow trajectories in the vicinity of the Facility. For example, modification to the flux from the southeast boundary (Model 59), a more extensive coverage for the Honolulu Volcanics (Model 56), a more representative geometry for the alluvial/saprolite wedge; all combined with a more realistic vertical hydraulic conductivity, and basalt layers terminating at the contact with the alluvial/saprolite wedge would likely produce a much different outcome than the individual sensitivity runs. The problem is that the possible combinations are endless and, without a definitive method of testing the model, there is no way of knowing if the models can provide useful guidance in the development of release response plans or for developing a realistic risk assessment of the threat that future releases may pose to Oahu's drinking water supplies.

The key weakness of the GWFMs is the lack of verifiability. The Moanalua/Red Hill/Halawa region is complex, likely more complex than the Navy currently realizes. This complexity leads to simplifying assumptions about critical model components such as the hydrologic conditions at the model boundaries. Boundary conditions exert great influence on the model results and the similarity between the numerous model runs suggests that it is the boundary conditions, rather than the conceptualization within the model that are driving simulated groundwater flow trajectories. Because the boundary conditions can't be verified, yet appear to constrain the model results, it is difficult to have confidence in the model results. Further, in many cases cited in these comments, the modeled groundwater flow trajectories don't comport with the measured data within the Facility monitoring wells. Because one of the goals of the GWFM is to have a tool that can be used for risk assessment and release response planning, the simulated groundwater flow trajectories beneath the USTs need some form of independent verification. Currently the most likely groundwater flow trajectories beneath the USTs and elsewhere in the Facility are unknown due to the disagreement between the modeled and measured relative water levels and that both the relative water levels and natural groundwater tracers present a confusing picture. Verifiability will only come from an interactive process of physical tests and model modification based on the results of the physical tests. For example, a borehole flow vector survey that has been recommended by DOH could be done in the Facility monitoring wells. The flow vector survey results could be evaluated for correlation with measured groundwater gradients, groundwater chemistry gradients, and the modeled groundwater flow trajectories. Then modifications made to the model to bring the simulated groundwater flow trajectories in alignment with what the physical evidence indicates is most probable. DOH understands that there is no guarantee that the borehole flow vector survey will produce definitive results. However, based on success in evaluating groundwater flow trajectories at the Waimanalo Gulch Landfill, the probability of success justifies the modest investment for this approach. Ultimately, a well-designed and executed tracer test is needed to provide

verifiability of groundwater flow trajectories. While a tracer test is a complex undertaking, the Lahaina Tracer Test demonstrated that this approach combined with evaluation of natural groundwater tracers is very effective at removing the ambiguity of groundwater flow trajectories. Dyes like Fluorescein are measurable at very trace concentrations and have been shown to be stable in contaminated groundwater for a period of years (United States Air Force, 2001 and 2007; and Glenn et al., 2013). Due to the dye stability in the aquifer and the very low detection limit, a properly designed tracer test can be done without risk of fouling a drinking water source.

Our review of the GWFM, as detailed above, finds that the modeling approach used by the Navy has sufficiently serious deficiencies that the DOH cannot accept the simulated flow rates and trajectories without further field verification. We believe that reliance on the model results for assessment of contaminant fate and transport, or for guidance for planning response and remediation actions in the event of future releases would be so uncertain that the threat to public drinking water supplies is currently not determined. DOH arrived at this conclusion due to model weakness that include, but are not limited to:

1. A modeling approach that favors an emphasis on automated hydraulic parameter estimation and statistical/analytical methods, but with insufficient attention to hydrogeologic principles that govern groundwater flow in the subsurface;
2. Model boundary conditions that are likely constraining the simulated groundwater flow trajectories to a narrow range;
3. Simulated groundwater gradients and elevation responses to changes in pumping stress that do not agree with field measurements in the Facility monitoring wells;
4. Use of critical hydraulic parameter values that differ significantly from those used for Hawaii's geology by other experienced and respected groundwater modelers with inadequate-to-no scientifically-based rationale offered to justify these large differences;
5. The simulated groundwater flow trajectories as indicated by the particle tracks are inconsistent with the observed diverse groundwater chemistry observed in the Facility monitoring wells; and
6. The groundwater flow models form a non-conservative foundation for the follow-on contaminant flow and transport models in that unrealistically high natural attenuation rates will be estimated and the risk that releases from the Facility pose to the Navy's and the Honolulu Board of Water Supply's drinking water sources will be underestimated.

Lack of model verifiability is the overarching factor that prevents DOH from accepting the GWFM. DOH has suggested field studies that if they verify model predictions can be instrumental in DOH approving the GWFM. These or other mutually agreed upon field studies are critical for resolving the uncertainties that are needed to develop an understanding of the groundwater flow dynamics beneath the USTs and in vicinity of the Facility. This understanding is essential to guide informed decision making about the degree of risk posed by the fuel storage at the Facility, and the response actions that would be required in the event of a release.

References

Department of the Navy. 2018. Well elevation Survey Report, Red Hill Bulk Fuel Storage Facility – Joint Base Pearl Harbor-Hickam, Oahu, Hawaii. Naval Facilities Engineering Command, NAVAC Hawaii. January 5, 2018

Department of the Navy. 2019a. Red Hill Bulk Fuel Storage Facility Administrative Order on Consent Tank Upgrade Alternatives and Release Detection Decision Document. Naval Facilities Engineering Command, NAVAC Hawaii. September 2019

Department of the Navy. 2019b. Conceptual Site Model, Investigation and Remediation of Releases and Groundwater Protection and Evaluation, Red Hill Bulk Fuel Storage Facility – Joint Base Pearl Harbor-Hickam, Oahu, Hawaii. Naval Facilities Engineering Command, NAVAC Hawaii. June 30, 2019

DOH. 2019. Hawaii Department of Health Evaluation of Groundwater Flow Paths in the Moanalua, Red Hill, and Halawa Regions. Prepared by Whittier, Robert B.; Thomas, Donald M.; and Beckett, G.D. July 2019

DOH. 2020. Hawaii Department of Health Technical Review – Conceptual Site Model, Investigation and Remediation of Releases and groundwater Protection and Evaluation, Red Hill Bud Fuel Storage Facility, Joint base Pearl Harbor-Hickam, Oahu, Hawaii, dated June 30 2019 Revision 01. March 30, 2020

Engott, J.A., Johnson, A.G., Bassiouni, Maoya, Izuka, S.K., and Rotzoll, Kolja, 2017, Spatially distributed groundwater recharge for 2010 land cover estimated using a water-budget model for the Island of O‘ahu, Hawai‘i (ver. 2.0, December 2017): U.S. Geological Survey Scientific Investigations Report 2015–5010, 49 p., https://doi.org/10.3133/sir20155010.

EPA/DOH. 2018a. Agency letter to Mr. Mark Manfredi, Red Hill Regional Program Director, Naval Facilities Hawaii: Re: Comments on Ongoing Work to Satisfy the Red Hill Bulk Fuel Storage Facility (“Facility”) Administrative Order on Consent (“AOC”) Statement of Work requirements 7.1.3 (Groundwater Flow Model Report) and 7.2.3 (Contaminant Fate and Transport Report). Dated February 23, 2018

EPA/DOH. 2018b. Agency presentation to the Red Hill Groundwater Modeling Working Group Number 13, August 16, 2018

Gingerich, S.B., 2008, Ground-water availability in the Wailuku area, Maui, Hawai‘i: U.S. Geological Survey Scientific Investigations Report 2008–5236, 95 p.

Glenn, C.R., Whittier, R.B., Dailer, M.L., Dulaiova, H., El-Kadi, A.I., Fackrell, J., Kelly, J.L., Waters, C.A., and J. Sevadjian, 2013. Lahaina Groundwater Tracer Study – Lahaina, Maui, Hawaii, Final Report, prepared for the State of Hawaii Department of Health, the U.S. Environmental Protection Agency, and the U.S. Army Engineer Research and Development Center

Honolulu Board of Water Supply. 2005. Final Report – Development of a Groundwater Management Model – Honolulu Area of the Southern Oahu Groundwater System. Prepared by Todd Engineers and ETIC Engineering. October 2005

Honolulu Board of Water Supply. 2018. Water level and deep monitoring well conductivity, temperature, and depth profile data for the wells in the Honolulu and Pearl Harbor Aquifers provided to the Hawaii Department of Health to support the Oahu Groundwater Flow Path Investigation. Data delivered December 2018

Hunt, C.D. 1996. Geohydrology of the Island of Oahu, Hawaii – U.S. Geological Survey Professional Paper 1412-B. https://pubs.er.usgs.gov/publication/pp1412B

Hunt, C.D. 2004. Ground-Water Quality and its relation to Land Use on Oahu, Hawaii, 2000-01 – Water Resources Investigations Report 03-3405. https://pubs.usgs.gov/wri/wri034305/

Lau, L.S. and Mink, J.F. 2006. Hydrology of the Hawaiian Islands. University of Hawaii Press. Honolulu Hawaii. Page 129

Lautze, N; Thomas, D; and Whittier, R. 2017. Hawaii Play Fairway compilation of Oahu geochemical data. Provided to the Navy on November 2017.

National Academy Press. 1990. Groundwater Models – Scientific and Regulatory Applications. Committee on Ground Water Modeling Assessment. Water Science and Technology Board, Commission on Physical Sciences, Mathematics, and Resources, National Research Council.

Oki, D.S., 2005, Numerical Simulation of the Effects of Low-Permeability Valley-Fill Barriers and the Redistribution of Ground-Water Withdrawals in the Pearl Harbor Area, Oahu, Hawaii: U.S. Geological Survey Scientific Investigations Report 2005-5253, 111 p.

Rotzoll, K., and El-Kadi, A.I. 2007. Numerical Ground-Water Flow Simulation for Red Hill Fuel Storage Facilities, NAVFAC Pacific, Oahu, Hawaii. Prepared for TEC Inc. by University of Hawaii, Water Resources Research Center. August 2007

United States Air Force. 2001. Final-Remedial Investigation for Waikakalaua and Kipapa Fuel Storage Annexes at Hickam Petroleum, Oils, and Lubricants (POL) Pipeline and Facilities, Oahu, Hawaii – Volume I, Contract No. F41624-95-D-8002, Delivery Order 0004 2001. Prepared by TEC, Inc.

United States Air Force. 2007. Final – Waikakalaua Fuel Storage Annex Comprehensive Remedial Investigation Report OU-1 and OU-2 Hickam Pol Facilities, Oahu, Hawaii. Prepared by TEC, Inc. July 2007

Visher, F.N. and Mink, J.F. 1964. Ground-Water Resources in Southern Oahu, Hawaii – U.S. Geologic Survey Water-Supply Paper 1778. https://pubs.usgs.gov/wsp/1778/report.pdf

Voss, C.I. 2011a. Editor's message: Groundwater modeling fantasies-Part 1, adrift in the details. Hydrogeology Journal. 19. [redacted]1-[redacted]4

Voss, C.I. 2011b. Editor's message: Groundwater modeling fantasies-part 2, down to earth. Hydrogeology Journal. 19. 1455-1458

Walker, G.P.L. [redacted]7. Chapter 41 - The Dike Complex of Koolau Volcano, Oahu: Internal Structure of a Hawai'ian Rift Zone. In Volcanism in Hawaii, Volume 2. U.S. Geological Survey Professional Paper 1350. Pages 961-993.

WellBore Navigation, Inc. 2017. Gyroscopic Directional Survey by Minimum Curvature for Valley Well Drilling. November 2017

November 10th, 2021

(b)(6)
[redacted]

Re: Comments on the Report "Groundwater Flow Model Report, Red Hill Bulk Fuel Storage Facility", March 25, 2020 (Revision 00) and Accompanying Draft Model Files

Dear (b)(6) [redacted],

S.S. Papadopulos & Associates, Inc. (SSP&A) has completed a detailed review of Revision 00 of the report "*Groundwater Flow Model Report, Red Hill Bulk Fuel Storage Facility*" (GWFMR) prepared by AECOM Technical Services, Inc. (AECOM) on behalf of the Naval Facilities Engineering Command (NAVFAC) Defense Logistics Agency (DLA). SSP&A also reviewed draft versions of the various groundwater flow models that are described in the GWFMR and the Conceptual Site Model (CSM). This letter summarizes the review of both the GWFMR and the draft model files, presents conclusions and provides recommendations.

At times during the completion of this review, SSP&A participated in phone calls and netmeetings together with representatives of, and subject matter experts (SMEs) contracted by, the United States Environmental Protection Agency (EPA), Department of Health for the State of Hawaii (DOH) (collectively, the Agencies), and the United States Department of the Navy (Navy). During these calls, there was opportunity to ask questions and to obtain some clarifications regarding the contents of the groundwater model files, and portions of the GWFMR.

Comprehensive review of a large modeling report that describes multiple alternative models of a complex setting can result in innumerable observations and comments. This letter does not provide an exhaustive set of comments, instead provides sufficient comments in each technical area to illustrate concerns and guide appropriate actions. This letter commences with a high-level summary of the review and major conclusions; an overview of modeling objectives as outlined in the 2015 Administrative Order on Consent (AOC); and an overview of the multi-model approach. Following these overviews, more detailed comments are provided referring to contents of the GWFMR, the draft model files, or both.

Review Summary and Conclusions

The Navy has employed substantial expertise and expended substantial effort in the development of several groundwater flow models that depict, in various ways, aspects of the complex subsurface at and around Red Hill Bulk Storage Facility (RHBSF). In part because the complex hydrogeologic setting is not uniquely characterized, the Navy appropriately adopted a multi-model project approach. The Navy then endeavored to incorporate within some of the models some of the features or processes recommended for consideration and inclusion by Agency subject matter experts (SMEs) in meetings conducted during 2018 and 2019. The GWFMR documents most aspects of the multi-model development process and provides a fairly thorough description of the multiple models that were produced. Together with the extensive field characterization that took place simultaneously with model development, knowledge

about subsurface conditions in the vicinity of the RHBSF has advanced considerably since the execution of the AOC.

It is important to be clear that, at this stage in the development process, no single model incorporates all features, events, and processes (FEPs) that may be important for the reliable simulation of conditions in, around, and beyond RHBSF. Although this is expected from a multi-model development process, there remain important aspects of subsurface conditions and patterns exhibited by monitoring well data in proximity to RHBSF, Red Hill Shaft ([redacted]), and in the direction of [redacted] (HS) – referred to as the primary area of interest (AOI) – that are not accurately reproduced by any of the models in their present form. Furthermore, several lessons learned from the development of the multiple models – some of which are documented in the GWFMR, some of which have been communicated via in-person and virtual meetings – require further analysis, discussion, and integration before a smaller set of plausible or "behavioral" flow models can be developed as a reliable basis for fate-and-transport (F&T) modeling.

Of the models produced by the Navy, Model 51e may represent the single most plausible representation of the Navy's conceptual site model (CSM), for the reasons outlined below:

- The model structure represents a reasonable effort to include the main FEPs.
- The geometry of the simulated HS capture zone appears to be more in alignment with the CSM and with previous modeling such as that conducted by Rotzoll (2007).
- The model presents one of the closer reproductions of low-valued hydraulic gradients that are evident in the measured data in and around RHBSF, although the simulated gradients remain substantially higher than measured values in many cases.

Model 51e does not, however, incorporate all FEPs that are reasonably supported by SME knowledge or that are incorporated within and appear "behavioral" in other models. For example: Model 51e does not include a realistic representation of basalt heterogeneity or plausible features of the volcanic tuffs downgradient of RHBSF, which are included to some extent in other models. Where Model 51e does include parameter zones in the basalt – enabling the calibration process to estimate hydraulic conductivity values beneath saprolite – values for basalt vertical and horizontal conductivity underlying saprolite were estimated at more than order of magnitude less than surrounding basalts, which may reflect the presence of saprolite penetrating un-weathered basalt. As noted elsewhere in this letter, the approach used to develop the model layers may prevent the saprolite from impeding flow within the basalts, an important feature of the CSM. Many of the models may therefore amplify the propensity and rates of water and dissolved contaminant migration beneath saprolite toward HS, which may in turn exaggerate the risk posed by releases at RHBSF to this potential receptor via this migration pathway. The combination of empirical data and groundwater modeling also has not provided great insight into groundwater flow and dissolved constituent migration patterns local to RHBSF, such that the extent of hydraulic containment that is developed by [redacted] remains poorly understood. Further work is needed in this area because estimation of the extent of hydraulic containment developed by [redacted] is an important aspect of the assessment of risk posed to water supplies.

Consequently, further work is needed to obtain model outputs that correspondence more closely with observed conditions, particularly within the AOI. That work would be most efficiently undertaken following a period of model integration and consolidation. Thus, although the combination of field characterization, data analysis, and groundwater modeling, completed by the Navy has furthered knowledge within the AOI, the ensemble of models described in the GWFMR requires further

improvement, consolidation, and review, before providing a reliable basis for F&T modeling and risk evaluation. Areas of emphasis for additional work are outlined in this letter.

Administrative Order on Consent (AOC) and Objectives of Groundwater Flow Modeling

Context for this review is provided by written agreements between the EPA, DOH, Navy and DLA (the Parties). The GWFMR was prepared in accordance with the 2015 AOC signed between the Parties. The primary objectives of the AOC and Statement of Work (SOW) therein are to "*take steps to ensure that the groundwater resource in the vicinity of the Facility is protected and to ensure that the Facility is operated and maintained in an environmentally protective manner*", including "*developing a better understanding of the hydrogeology of the area surrounding the Facility, and conducting an assessment of the risk to the groundwater resources that may be posed by the Facility*". The GWFMR is a deliverable under AOC SOW Section 7 "*Groundwater Protection and Evaluation*" which in turn supports Section 8 "*Risk/Vulnerability Assessment*" and Section 6 "*Investigation and Remediation of Releases*". The purpose of the GWFMR is described under Section 7.1 "*Groundwater Flow Model Report*" as "*to refine the existing groundwater flow model and improve the understanding of the direction and rate of groundwater flow within the aquifers around the Facility*." Groundwater flow modeling is also intended to support the development of a contaminant fate-and-transport model (CFTMR) (AOC SOW Section 7.2), and design of the groundwater monitoring network (AOC SOW Section 7.3). Specific components of the work detailed under the AOC SOW that relate to modeling are as follows:

> *(4) Navy and DLA will further develop models to better understand groundwater flow in the areas around the Facility and evaluate the fate and transport of contaminants in the subsurface around the Facility. As set forth below, based on the modeling effort, as approved by the Regulatory Agencies, Navy and DLA will develop and improve the existing groundwater monitoring network to the extent determined necessary.*
>
> *(5) Navy and DLA will develop a risk/vulnerability assessment, subject to approval by the Regulatory Agencies, in an effort to further understand the potential for and potential impacts of fuel releases from the Facility and to inform the Parties in development of subsequent BAPT decisions.*

Use of a Multi-Model Approach

Complex aquifer settings such as that encountered beneath RHBSF present many challenges to the development of groundwater models. Perhaps foremost among these at Red Hill is the role of basalt aquifer heterogeneity and compartmentalization, which presents difficulties for empirically interpreting water level and quality data laterally and vertically or developing models that correspond with those data. Field measurements alone are often insufficient to discriminate between potentially plausible alternate conceptual models (ACMs) of the subsurface, and calibration will often demonstrate unsatisfying correspondence and also not provide a single best model. In light of this, initial modeling efforts should not be anticipated to provide the "right answer" but to provide useful results that present defensible water budgets, incorporate primary FEPs, and reasonably re-produce field data such that they can be used to test hypotheses and provide a basis for F&T analysis.

In such settings, it is advisable in the early stages of model development not to attempt to produce a single model, but rather to consider a set of plausible models and then distinguish between those models

that are in some sense behavioral and those that are not (Beven and Binley, 2014). This was in essence the approach used by the Navy. Although Beven and Binley (2014) distinguish models based primarily on fit ("*models that provide good fits to any observables available [behavioral models] and those that do not [non-behavioral models]*"), identifying the relative plausibility and value for decision making of different models also relies upon the knowledge and judgment of SMEs. For example, conceptual errors or simplifications in models can introduce bias that can be amplified by seeking "too good" a calibration fit (White et al., 2014). As a result, a model that provides a good fit to data but is missing one or more critical FEPs should not necessarily be considered more reliable or behavioral – and as such, weighted more heavily in subsequent applications – than a model that includes all known FEPs but provides a poorer fit. This is particularly true when the calibration objective function includes multiple components, as is the case of the Navy models. Given the current stage of model development, this review considers the representation of key FEPs in addition, and at times in preference, to calibration fit.

Primary Comments with Recommendations

Overall, through the various model incarnations, attempts have been made to incorporate the major FEPs that have been discussed by the Parties and their SMEs. This includes representation of the effect of basalt flow structure on anisotropy; the incorporation of downgradient volcanic deposits and cinder cones; and other FEPs. Although aspects of these FEPs are not known with a high degree of certainty or accuracy, reasonable efforts were nonetheless made to incorporate some of them. Exceptions to this statement are described in the comments below. The subjects of these comments are fundamental to flow model development and application, as one basis as use for F&T analysis and risk evaluation.

<u>Representation of Subsurface Heterogeneity</u>

There is abundant evidence for strong contrasts in the hydraulic properties of the basalt aquifer material, ranging from relatively non-conductive dense pahoehoe interiors, through to rough a'a and coarse clinkers. The basalt host rock is also intercepted by vertical and (less commonly) lateral fractures, together with lava tubes that follow the general dip and fabric of the lava flows (**Figure C-1**). The Navy groundwater models represent the subsurface using an equivalent porous media (EPM) approach. In doing so, the cumulative average effect of these heterogeneities, together with the prevailing basalt dip and strike, is represented using directional anisotropy of aquifer properties simulated in all models (with contracting values between models, and some zonation) plus, for some models, the use of the pilot point method (LaVenue and deMarsily, 2001; Doherty, 2003). The EPM assumption is very likely applicable at some scale for flow and dissolved-phase transport modeling purposes at the site; however, that scale has not been determined or demonstrated at this time. In addition, while the overall approach is fairly common practice for regional-scale flow modeling and water-resource analysis purposes, it has limitations at the scale of RHBSF for purposes of evaluating the hydraulic containment of [redacted] and contaminant F&T, two examples of which are provided below.

Example 1: predicting transport directions and rates. It is expected, based on the structure of the basalts, that regions of connected transmissive materials – clinker, for example – would be oriented in the direction of dip of the host lava flows. At the typical scale of clinker and a'a flows in this region, this would be expected to produce a fabric similar to that depicted in **Figure C-2**. The geometry of such a fabric can be visualized schematically and described qualitatively but cannot be represented deterministically. Work completed by the Navy consultants included a Monte-Carlo simulation of potential preferential pathways in the vicinity of RHBSF as described in the CSM Section 5.1.4:

"A total of 10,000 Monte Carlo simulations of random pathlines were generated …. 3,635 pathlines passed through the tank farm area. None of the pathlines through the tank farm area also passed through the Red Hill Shaft area. Therefore, the results indicated that it is unlikely that a preferential pathway exists between the tank farm area and Red Hill Shaft area in relation to historical lava flows."

Figure D-1 from the CSM (included here as **Figure C-3**) illustrates 20 of these 10,000 Monte Carlo paths. The pattern of stochastic pathways is generally consistent with expectations based upon SME knowledge and with the concept depicted in **Figure C-2**. However, it appears from this analysis that preferential transport pathways may not pass through substantial portions of the groundwater monitoring network nor be detectable at [redacted] (at least, when it is not pumping). As previously noted by the EPA/DOH in comments provided on the CSM (April 22, 2019):

"For the Red Hill groundwater system, dissolved-phase fuel impacts are not expected to travel further than approximately 200-ft from the LNAPL source mass …. however dissolved phase impacts have been detected further than 200 feet from the tank farm, thus atypical transport conditions, such as fast-track transport features (open voids, lava tubes), may also contribute to the detections observed at [redacted]."

The presence of unknown preferential migration pathways presents difficulties for interpreting historical groundwater sample results; for using the groundwater model without such features as the basis for F&T modeling or to support monitoring network design; and for incorporating the presence and effects of such features in the groundwater flow and F&T models.

Example 2: predicting hydraulic containment (capture zones) particularly at smaller or transient rates. The presence of an aquifer fabric like that depicted in **Figure C-2** presents difficulties in the deterministic interpretation of hydraulic containment (capture). In such a system, groundwater flow compartmentalization can be as significant laterally (such as between adjacent clinker zones) as it is vertically; and this can mean that the water recovered by pumped wells is more vertically derived than would be anticipated using a homogeneous-anisotropic assumption and approach. This possibility is supported by the easternmost extents of the boring log of the Red Hill tunnel (**Figure C-4**). Although the effects of compartmentalization may appear to homogenize at very large pumping rates, at lower pumping rates the effects of compartmentalization can be pronounced and can lead to misinterpretation of the source of water to pumped wells.

Recommendation(s): evaluate and implement alternate methods to represent subsurface heterogeneity. The subsurface in the vicinity of RHBSF is neither homogeneous such as represented in several of the models, nor does it demonstrate radially symmetric heterogeneity such as generally produced using the pilot point method. Alternative, structure-imitating, methods for representing subsurface heterogeneity in basalt settings should be considered that, while not deterministic, provide more realistic parameter fields and can be calibrate. Examples include multiple-indicator and multi-point (geo-)statistical methods that can be conditioned on local stratigraphic data such as that recorded in the barrel logs; and methods derived from sequence-stratigraphy to stack and accumulate lava sequences.

Model Layering

The groundwater models were developed using an approach that, broadly speaking, follows the topography and more importantly follows the bounding geometry of the major formations or hydro-stratigraphic units (HSUs). When combined with the use of lateral layer "pinch-outs" and appropriate elevation adjustments, this approach leads to certain layers being in most places dedicated to specific hydro-stratigraphic units (HSUs). This approach is commonly used to provide numerical stability in simulations, particularly in settings with heterogeneous HSUs. However, the approach can have unintended consequences for the simulation of groundwater flow patterns in the presence of abrupt lateral transitions between HSUs. Two examples are provided to illustrate this.

Example 1: as detailed in the GWFMR Section 4.2:

> "*Layers 2 and 3 discretize the saprolite that lies largely underneath the valleys and portions of the caprock. These model layers are absent where saprolite is absent.*" and "*Layers 4 through 9 discretize the basalt aquifer.*"

As a result, Layer 4 represents basalts adjacent to and beneath the saprolite. This is accomplished by deforming (lowering) the top and bottom elevations of the layers representing basalt in the areas where saprolite is present. At RHBSF, however, this may allow for the simulation of flow within numerically contiguous basalt units beneath saprolites that are actually discontinuous (so that flow is inhibited) in the field. The saprolites formed by the weathering of basalts in such a manner that the saprolite cuts vertically downward into the stratified and sinuous basalt flows (**Figure C-5**, left panel). As a result, lateral movement in the field within otherwise contiguous basalt flow zones can be laterally impeded. However, in the groundwater models this impedance appears to be reduced by deforming layers beneath the saprolite rather than bisecting it (**Figure C-5**, right panel). Some impedance remains, however, rather than being controlled primarily by lateral conductivity contrasts between basalt and saprolite (and secondarily the basalt vertical conductivity), the simulated flow distribution it is controlled by a combination of (local) bulk transmissivity reduction (and secondarily the basalt vertical conductivity). Support for this includes the apparent relative insensitivity of simulated pathlines in many areas to the depth and conductivity of the saprolites. Different, more plausible, results would likely be obtained by constructing the model using more uniform layers aligned with the dip and using parameter value contrasts to represent changes in material type and HSU (**Figure C-6**).

Example 2: basalt layers "pinch-out" approaching Pearl Harbor, requiring groundwater discharge to be vertically upward through the overlying anisotropic basalts: consequently, there is essentially no horizontal discharge to Pearl Harbor from the basalts. As noted above, the method used to define the model layers may diminish the effect of horizontal anisotropy and indeed lateral transitions between HSUs. Taken together, the impediment of groundwater movement and discharge towards Pearl harbor due to pinching of layers, combined with the method used to define model layers, transition between HSUs, and describe the vertical extent of saprolites (noted above), the model structure may increase the propensity for simulated groundwater to flow from RHBSF beneath the saprolites to the west-northwest (i.e., toward HS and shoreline springs located in that direction) (**Figure C-7**, **Figure C-8**). Partly as a result, there is relatively little difference in particle paths between most models parameterized with different anisotropies. This restriction of discharge toward Pearl Harbor may also contribute to the necessity (documented in the GWFMR and the subject of additional comments below) that changes in simulated

groundwater pumping appear to require near-equivalent volumetric changes in recharge input to the groundwater models, which should not be necessary in a properly designed model.

> ***Recommendation(s)***: consider and evaluate alternate methods to represent lateral and vertical transitions between hydro-stratigraphic units (HSUs), and the heterogeneity within layers and within HSUs. This includes re-evaluating the method used to develop the top and bottom elevations of the model layers and their correspondence with the HSUs; and, the methods used to parameterize the HSUs within and between model layers.

Recharge

The representation and relative spatial distribution of dominantly precipitation-derived recharge at the water table is based on analyses completed previously by the United States Geological Survey (USGS). As presented in the GWFMR Section 3.6:

> "*The recharge distribution is similar for these different weather conditions, and therefore it is appropriate to uniformly scale the recharge values up or down depending on the weather. The highest recharge occurs in upland areas with lowest recharge toward the coast. This is the case within the model domain as well as to the NW and SE of the model domain. These recharge maps were developed considering several factors including land use, rainfall, irrigation, and evapotranspiration and are the most detailed representations available for areally distributed recharge across the site. Their accuracy at a local level could be questioned, but the trend is appropriate in that most recharge occurs in higher elevations, with less toward the coast*."

This approach is commonly used for parsimony in the estimation of infiltration patterns and rates at the base of the soil horizon, sometimes referred to as "deep percolation". However, the total net contribution of precipitation-derived recharge to the groundwater system remains uncertain. In addition, issues can arise if (a) the model does not incorporate appropriate routes and mechanisms to discharge the deep percolation; and (b) if complex surface conditions or strong contrasts in subsurface conditions are not accounted for when presuming that deep percolation becomes net groundwater recharge. For example, in hydrogeologic settings where there are substantial slopes, the soil infiltration capacity is limited, or where there are strong conductivity contrasts between the soil horizon and underlying aquifer, infiltration that is presumed to reach the water table and form recharge can be locally rejected, resulting in actual patterns and rates of aquifer recharge that differ substantially from apparent surface infiltration patterns and rates. Three examples are provided to illustrate these concerns and possible consequences of the recharge simulation approach currently used in the Navy models.

Example 1: As noted above, it appears it was necessary to adjust recharge during calibration to scale approximately with groundwater pumping rates that are simulated in different stress periods. This is a concern because it suggests that the sources and sinks of water to the model, as provided via the boundaries, recharge, and in transient simulations storage change, are not properly meeting pumping demands. This also appears to contradict previous correspondence which indicated that recharge would be fixed between stress periods. For example, as presented in Navy comments on the letter prepared October 19th, 2019 by SSP&A as presented in the Navy response to the EPA/DOH extension letter of January 28th, 2020:

"3a) The Navy team determined during preliminary calibration efforts that when recharge was used as a calibration parameter, the Parameter Estimation (PEST) software frequently assigned recharge rate multiplier values that did not match the conceptual model. The conceptual model anticipated mild differences in calibrated recharge rates to accommodate the two sets of synoptic head targets. In practice, PEST tended to make large changes to recharge rates (and therefore to the regional water budget) of 20 percent or more, which suggested that the field data did not constrain the recharge rates sufficiently to permit their use as calibration parameters. The team concluded that achieving a mild improvement in calibration to synoptic heads did not warrant the unrealistic changes to the regional water budget. The final set of models (models 51 through 59) did not use recharge rate as a calibration parameter."

This is also evidenced in flow simulations used for particle tracking in which [redacted] pumping rates were increased by 2.51 million gallons per day (MGPD) from the calibrated model which leads to simulated heads across RHBSF falling to or below historical minimum levels. For simulated heads to be more comparable to historical levels, recharge would likely have to be increased by about (b)(3) [redacted]. A water budget analysis of the models suggests that the simulated aquifer system is heavily pumped, with about 70% of the water that enters the system via recharge and boundary inflows extracted by wells and shafts. [redacted] pumping alone accounts for the withdrawal of about one quarter of system inflows (at a pumping rate of 12 MGPD) compared to total inflow of about 46.7 to 52 MGPD (excluding the 10 MGPD entering via the SE boundary in some model variants).

Example 2: Recharge patterns and relative rates are based primarily on land use and cover, rather than the underlying bedrock geologic texture. It is not clear whether and how account is made for surface run-off or the possible presence of perched or low-receiving-capacity materials that may reduce the net recharge received by the basalts. It might perhaps be expected that net recharge entering the basalts at RHBSF may be greater than net recharge entering the basalts in areas beneath the valley fill and saprolites because of the very different thicknesses and character of the intervening materials. Model 57 explored recharge uncertainty under reduced (dry though not quite drought recharge conditions); however, the inference from this simulation was undermined by the re-estimation of recharge rates, and there is no corresponding evaluation of [redacted] containment during wet periods.

Example 3: Apparent differences in specific capacity at [redacted] year-to-year suggest that the zone of containment by [redacted] may change substantially under wet and dry conditions (it appears the [redacted] specific capacity was higher in 2015 than observed in 2006 and 2017). This observation suggests that the sources of water to [redacted] change substantially under different conditions, and consequently that during wet periods, contamination may migrate off-site due to the combination of preferential pathways (see above) and reduced extent of containment by [redacted].

***Recommendation(s)**:* The necessity of adjusting recharge by stress period may highlight underlying issues with the representation of water sources in the model, or with the use of steady-state simulations for certain analyses, or both. Either a more comprehensive rainfall-runoff-recharge calculation approach may be needed, or some ability may be needed in the calibration to adjust recharge based upon the bedrock (receiving aquifer) geologic material type. An additional scenario should also be considered to assess containment during "wet" periods during which there is greater inflow from aerial recharge, from the dyke region, and potentially from the Moanalua valley.

Lateral Boundary Conditions

Each of the models exhibits different boundary inflows than the previously published regional groundwater model (Rotzoll, 2007: "Rotzoll's model"). While strict adherence to previous estimates is not expected or required, and differences would be anticipated from a multi-model analysis, further explanation is needed to support values that were obtained and used in the Navy models. Two examples are provided to illustrate this.

Example 1: In Rotzoll's Model, the flow into the model domain along the location of the southeastern boundary was estimated to be about 2.0 MGPD. The Navy models exhibit flows that were either essentially zero or ranged up to 9.0 to 10.7 MGPD. The higher range of values – roughly 10 MGPD – appears unlikely given that the total recharge estimated for the adjacent aquifer is only about 12 MGPD. In addition, it appears from Rotzoll's Model that the influx estimated from the upslope dyke area is about 50% greater (roughly 30 MGPD) than is assumed in the Navy models, and that the inflow is conceptually interpreted as occurring higher up in the geologic sequence than in the Navy models. Although the Navy and Regulator SMEs have discussed the possibility of substantial groundwater flow from the Moanalua Valley direction through the AOI, further justification is needed to lend support to this possibility.

Example 2: Previous modeling together with groundwater elevation mapping and water budget analyses suggest there may be a non-trivial inflow of water from the northwest area from the Schofield Plateau (i.e., into the northwest boundary of the Navy model domain). Any such inflow would ultimately contribute to discharges that occur at springs along the shores of Pearl Harbor, which in many or all of the Navy models appear to be fed almost entirely by a combination of flow originating at the upslope dyke area, together with recharge accrued between this upslope area and the springs, and – in models with a high southeastern inflow – via the direction of Moanalua Valley. If a significant proportion of the discharge occurring at harbor area springs arises from the northwest boundary, this may substantially alter flow patterns within the AOI.

> ***Recommendation(s)***: An attempt should be made to obtain volumetric budgets useful for developing boundary inflow estimates from Rotzoll's Model, other suitable regional-scale models, flow-nets, or via SME concurrence. This effort should include discussions with Agency SMEs regarding the potential for inflows at the southeast and northwest boundaries.

Calibration Data Concerns and Inconsistencies between Observed Data and Simulated Results

In several places in the GWFMR and other deliverables and Navy presentations, concern has been expressed about the quality of the data available for flow model calibration. While the density in space and time of groundwater monitoring data at RHBSF is – in relative terms and given the large scale of the site – less than at many other underground storage facilities, concerns about data *quality* expressed in the GWFMR and Navy presentations appear exaggerated. Two examples are provided to highlight this.

Example 1: The GMFMR (Section 3.1) states:

> "*Also, the apparent gradients at the shallow Facility basalt wells are not consistent (can be uphill or downhill) whe*(b)(3) *is pumping. When* (b)(3) *is not pumping, the apparent gradients in shallow Facility basalt wells all point uphill toward RHM on Figure 3.1-5a. On Figure 3.1-5b, these apparent gradients all point away from RHM in all directions as though*

that was an area of high recharge. Therefore, the Facility well water level differences should not be overinterpreted, due to the very small difference values that are within the error limits of water level measurements at any one well."

The excerpt as written conflates two related but separate issues: the presence of flat and difficult-to-discern gradients (due to small-valued measured water level differences) versus interpretive value. The presence of consistently small water level differences, leading to difficult-to-discern hydraulic gradients and flow directions, is information. Measured head differences may be small, but they are not necessarily erroneous. Groundwater flow models that exhibit large head differences in areas where the data indicate small head differences are therefore inconsistent with the data, and contradict the evidence presented by the data that head differences and thus gradients are flat and uncertain. This concept is illustrated schematically in **Figure C-9** which depicts two probability density functions (PDFs). In this figure, the PDF on the left is narrow and has a well-defined peak; conceptually, this peak represents the model output which suggests consistent and large-valued head differences. The PDF on the right is wide and has a poorly defined peak; conceptually, this peak represents the measured water level data which suggest low-valued and at times indeterminate head differences. Even though the PDF on the right (representing the data) is wide, reflecting uncertainty and the fact that the resulting hydraulic gradients and flow directions are not known with confidence based on measured head differences, the PDFs differ distinctly and the model PDF does not correspond to the data PDF.

Example 2: The interpretation that small-valued head differences (and resulting flat gradients) have limited interpretive value leads the Navy to develop a method for weighting certain observation data in the model calibration that deemphasizes them. As a result, the calibration emphasizes matching regional head differences and gradients at the cost of reasonably reproducing head differences and gradients at RHBSF. This is not immediately evident in the figures presented in the GWFMR (for example **Figure C-10**) but can be visualized using plots that focus on RHBSF. For example, during stress period three, five of the eight facility wells compared to RHMW-01 exhibit simulated head differences that are in the opposite direction in every Navy model (**Figure C-11**): the observed head difference between (b)(3) and (b)(3) while the [redacted] is not pumping was -0.19 feet, yet the range of simulated differences was between 0.14 and 0.29 feet. This difference is not an issue of data quality; rather, as illustrated by the schematic PDFs shown in **Figure C-9**, it represents a systematic difference between the models and the field data.

Recommendation(s): In the absence of demonstrated errors, it is important to accept the data and not conflate small differences in value with error and lack of interpretive value. Although the small differences between observed and simulated results are within the limits of measurement error (and might be given smaller weight during calibration), when differences exceed reasonable limits, they should be penalized accordingly. As a partial mitigation of this issue, the Navy should incorporate data obtained February through March 2019 – which covered a planned shutdown-and-rebound test at RHBSF – into the calibration. Doing so is likely to provide substantial value for understanding groundwater flow and hydraulic containment dynamics close to RHBSF.

Pathline Figures for Depicting and Comparing Capture Zones

Particle tracking figures presented in the GWFMR to delineate the extent of hydraulic containment (capture) developed by [redacted], and depict potential sources of water to HS are challenging to compare and contrast and make it difficult to discern and compare the ultimate extent of capture at different rates.

***Recommendation(s)*:** The Capture Frequency Map (CFM) approach is recommended for depicting hydraulic containment (capture) and the sources of water to supply wells. This is illustrated in **Figure C-12**. To create this figure, forward particle tracking models developed by the Navy that simulate [redacted] as pumping were used together with a regular grid of particles (i.e., 99 columns by 73 rows with equal spacing of 100 ft) to delineate capture. After the initial simulations were completed using [redacted] pumping rates from the Navy models, the pumping rate was reduced from (b)(3) [redacted] to (b)(3) [redacted] nd then to (b)(3) [redacted] o assess the extent of capture corresponding to the reduced pumping. A CFM was created for each of three pumping rates by summing the particles captured at [redacted] at each particle starting location and dividing by the total number of models (i.e., 12). The image more completely depicts and contrasts the extent of capture under these varying conditions and rates, using the Navy models. (*Note: these figures are provided only to illustrate the application of the CFM approach using the Navy models. The extents of capture depicted in these figures do not represent an opinion of the Agencies or their SMEs as to the probable extents of capture of* [redacted].)

Relative Weighting of Alternate Models

The highest-weighted models presented in the GWFMR Table 5-7 *Summary of Multimodel Applicability for Risk-Based Decision Making* are those that simulate heterogeneous basalts using the pilot point method. In concept, the representation of heterogeneous basalts using pilot points is more consistent with the CSM than a presumption of homogeneity; however, the relative-weighting or ranking rests too heavily on the improved calibration fit obtained using pilot points. Such an improvement in fit statistics would be expected by the introduction of a much larger number of parameters to the calibration process, but should not necessarily be interpreted as improved reliability, because of the greatly increased parameterization of those models.

***Recommendation(s)*:** if using calibration statistics for multi-model ranking, more comprehensive methods should be considered that incorporate the concept of calibration or residual standard error, degrees of freedom, and parameterization, such as those described by Poeter and Anderson (2005), among others. Inclusion and representation of FEPs should, however, also be included in the weighting, ranking, and consideration of the plausibility of models.

Additional Comments

The following is a brief list of additional noteworthy comments:

- Model bottom elevation: the base elevation of freshwater in the model is based upon a simulated saltwater lens that appears to suggest that Pearl Harbor is freshwater rather than saltwater.
- Transfer Function Noise (TFN) analysis: the use of the TFN technique with analytical expressions to derive clean response functions at monitoring wells to include in the calibration of complex numerical models is appropriate. However, two concerns arise with the results and presentation:
    - The use of analytic expressions that assume anisotropic homogeneous conditions to derive response functions should not be conflated with the interpretation that the subsurface can be reasonably represented as an anisotropic homogeneous one for purposes of flow and F&T modeling.
    - The TFN provides a “clean” drawdown-recovery response, which is important to the estimation of bulk aquifer properties. However, estimation of the extent of hydraulic

containment (capture) developed by pumped wells, shafts, or tunnels also requires that the groundwater model reasonable reproduce measured groundwater elevations and head differences (gradients).

- Verification modeling: the verification results provide little inference regarding the absolute o relative performance of the various models. Reasons for this include: (1) Simplification of pumping cycles in the verification simulations obscures differences and similarities between simulated and observed responses. Simulated stress periods do not represent the pumping / non-pumping cycles (short-duration cycles, and one longer-duration cycle that results in extended recovery, are not modeled). (2) Graphical depiction of the simulation results which appears to incorporate vertical "offsets" between the simulation outputs and measured data. As noted above, correspondence with groundwater elevations and head differences is also necessary.
- Graphics comparing model output with measured data: many of the graphs in the GWFMR are prepared at a scale that makes it difficult to evaluate model performance. For example, GWFMR Figure 3.3-1 illustrates results for all wells on a single figure using the same color for each group of wells. This method of presentation obscures potentially meaningful differences between well groups and between individual wells within each group, so that very little meaningful inference can be made from the plot regarding the performance of the models.
- Observation data used for calibration: GMFMR Section 4.5 states: *"The water level differences were initially provided unit weighting for calibration because they are indicative of gradients that govern flow magnitude and direction, which are a primary objective for the model."* It appears from the model files that regional head differences were given unit weighting, while weights at RHBSF were often an order of magnitude less than unit weighting. This may be a contributing factor to the poor fit to head differences at the facility. There may also be inconsistencies in depicted observation locations: for example, GWFMR Figure 3.1-1b illustrates well locations used for calibration, yet there is no reference to most of these wells in the calibration files.
- Parameter values estimated during calibration: in several models, hydraulic conductivity values for one or more HSUs were estimated at their upper or lower limits and in some cases estimated values appear greater than maximum values presented in Table 4-1 of the GWFMR. In addition, parameter ranges listed in GWFMR Table 4-1 do not appear to match those listed in the calibration input files, nor to match GWFMR Table 5-2. There also appear to be parameters listed in GWFMR Table 5-2 that are not listed in GWFMR Table 4-1 nor appear in the model files. These apparent discrepancies may, however, arise from version differences between the model files reviewed and those depicted in the GWFMR.

Conclusions

The main conclusions from this review were provided at the commencement of this comment letter. I hope you find the foregoing review helpful. If you have any questions or comments regarding the contents of this review letter, please do not hesitate to contact me.

(b)(6)
(b)(6)
[redacted]

References

Beven, K. 2019. Towards a Methodology for Testing Models as Hypotheses in the Inexact Sciences: Proceedings of the Royal Society A 475: 19.

Beven, K. and Freer, 2000. Equifinality, data assimilation, and uncertainty estimation in mechanistic modelling of complex environmental systems using the GLUE methodology.

Beven, K., and A. Binley. 2014. GLUE: 20 Years On: Hydrological Processes 28: 5897-5918.

Beven, K., and J. Freer. 2001. Equifinality, Data Assimilation, and Uncertainty Estimation in Mechanistic Modelling of Complex Environmental Systems Using the GLUE Methodology: Journal of Hydrology 249: 11-29.

Department of the Navy (DON). 2019. Conceptual Site Model, Investigation and Remediation of Releases and Groundwater Protection and Evaluation, Red Hill Bulk Fuel Storage Facility, Joint Base Pearl Harbor-Hickam, Oʻahu, Hawaiʻi; June 30, 2019, Revision 01. Prepared by AECOM Technical Services, Inc., Honolulu, HI. Prepared for Defense Logistics Agency Energy, Fort Belvoir, VA, under Naval Facilities Engineering Command, Hawaii, JBPHH HI.

Department of the Navy (DON). 2020a. Groundwater Flow Model Report, Red Hill Bulk Fuel Storage Facility, Joint Base Pearl Harbor-Hickam, Oʻahu, Hawaiʻi; March 25, 2020, Revision 00. Prepared by AECOM Technical Services, Inc., Honolulu, HI. Prepared for Defense Logistics Agency Energy, Fort Belvoir, VA, under Naval Facilities Engineering Command, Hawaii, JBPHH HI

Department of the Navy (DON). 2020b. Investigation and Remediation of Releases Report, Red Hill Bulk Fuel Storage Facility, Joint Base Pearl Harbor-Hickam, Oʻahu, Hawaiʻi; March 25, 2020, Revision 00. Prepared by AECOM Technical Services, Inc., Honolulu, HI. Prepared for Defense Logistics Agency Energy, Fort Belvoir, VA, under Naval Facilities Engineering Command, Hawaii, JBPHH 30 HI.

Grueber, C.E., S. Nakagawa, R.J. Laws, and I.G. Jamieson. 2011. Multimodel Inference in Ecology and Evolution: Challenges and Solutions: Journal of Evolutionary Biology 24: 699-711.

LaVenue, M., and de Marsily, G., 2001, Three-dimensional interference test interpretation in a fractured aquifer using the pilot-point inverse method: Water Resources Research, v. 37, no. 11, p. 2659–2675, doi:10.1029/2000WR000289.

Poeter, E., and D. Anderson. 2005. Multimodel Ranking and Inference in Ground Water Modeling: Ground Water 43, no. 4: 597-605. Doherty, J., 2003, Groundwater model calibration using pilot-points and regularization: Ground Water, v. 41, no. 2, p. 170–177, doi:10.1111/j.1745-6584.2003.tb02580.x.

White, J. T., Doherty, J., & Hughes, J. 2014. Quantifying the predictive consequences of model error with linear subspace analysis. Water Resources Research, 50(2), 1152-1173. https://doi.org/10.1002/2013WR014767

Figures

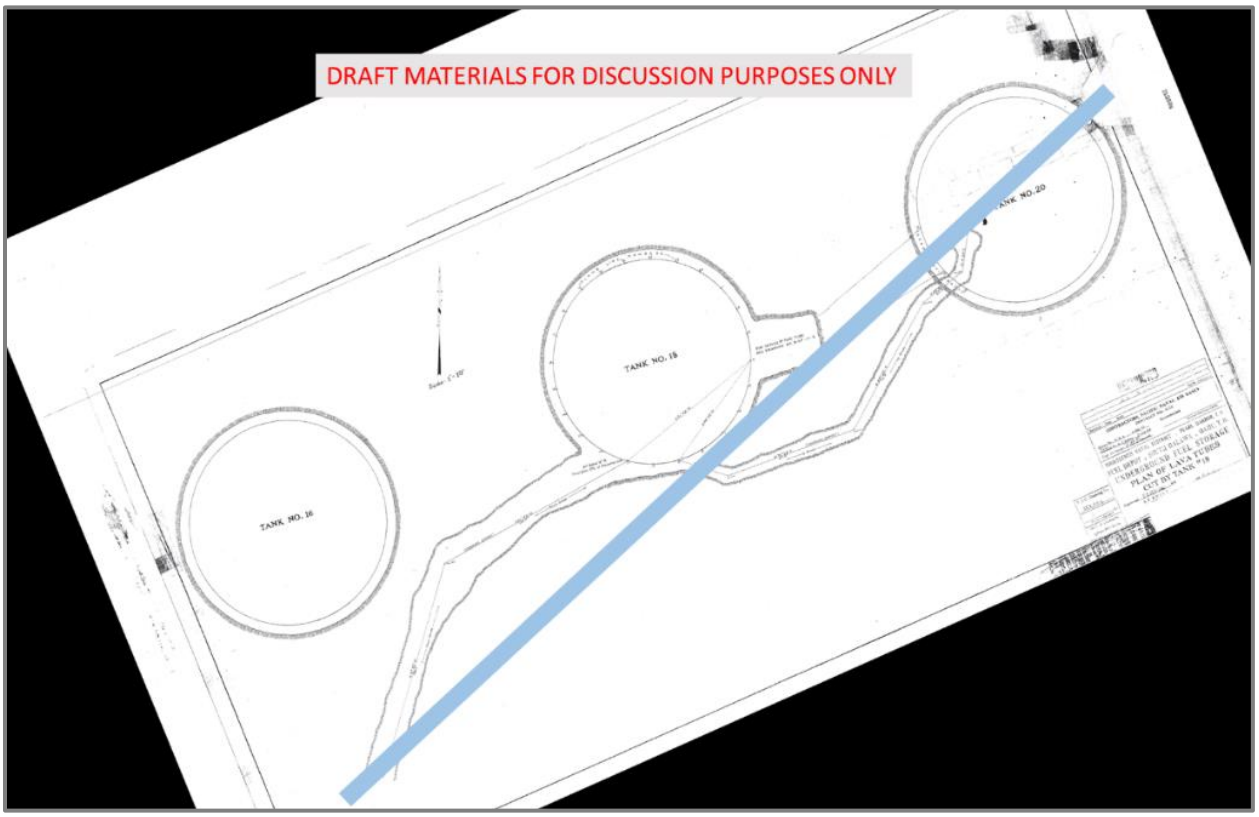

Figure C-1: Illustration of Mapped Lava Tube from CSM Report

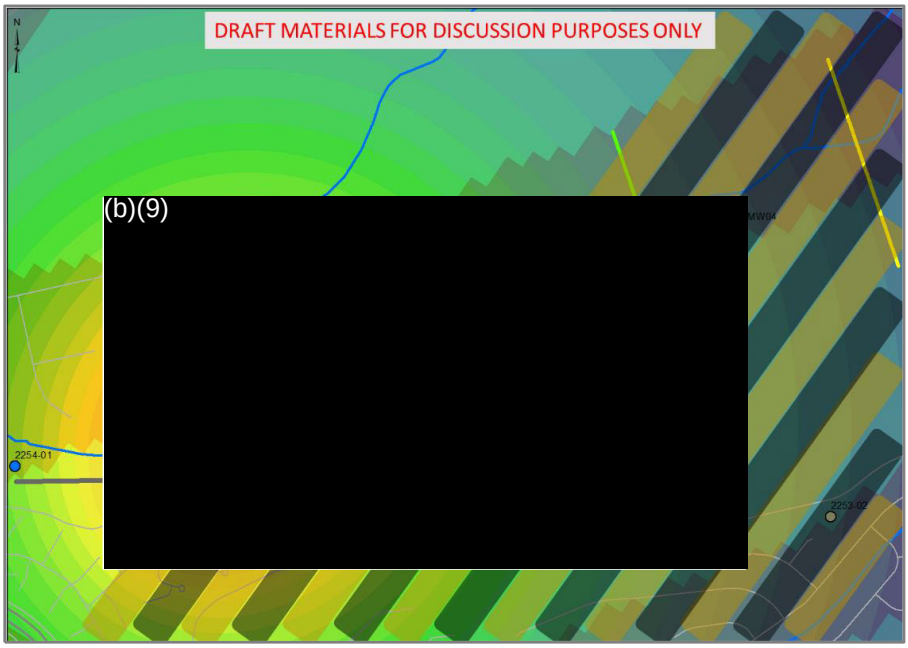

Figure C-2: Gross Schematic of Bedrock Fabric and Orientation of any Preferential Pathways

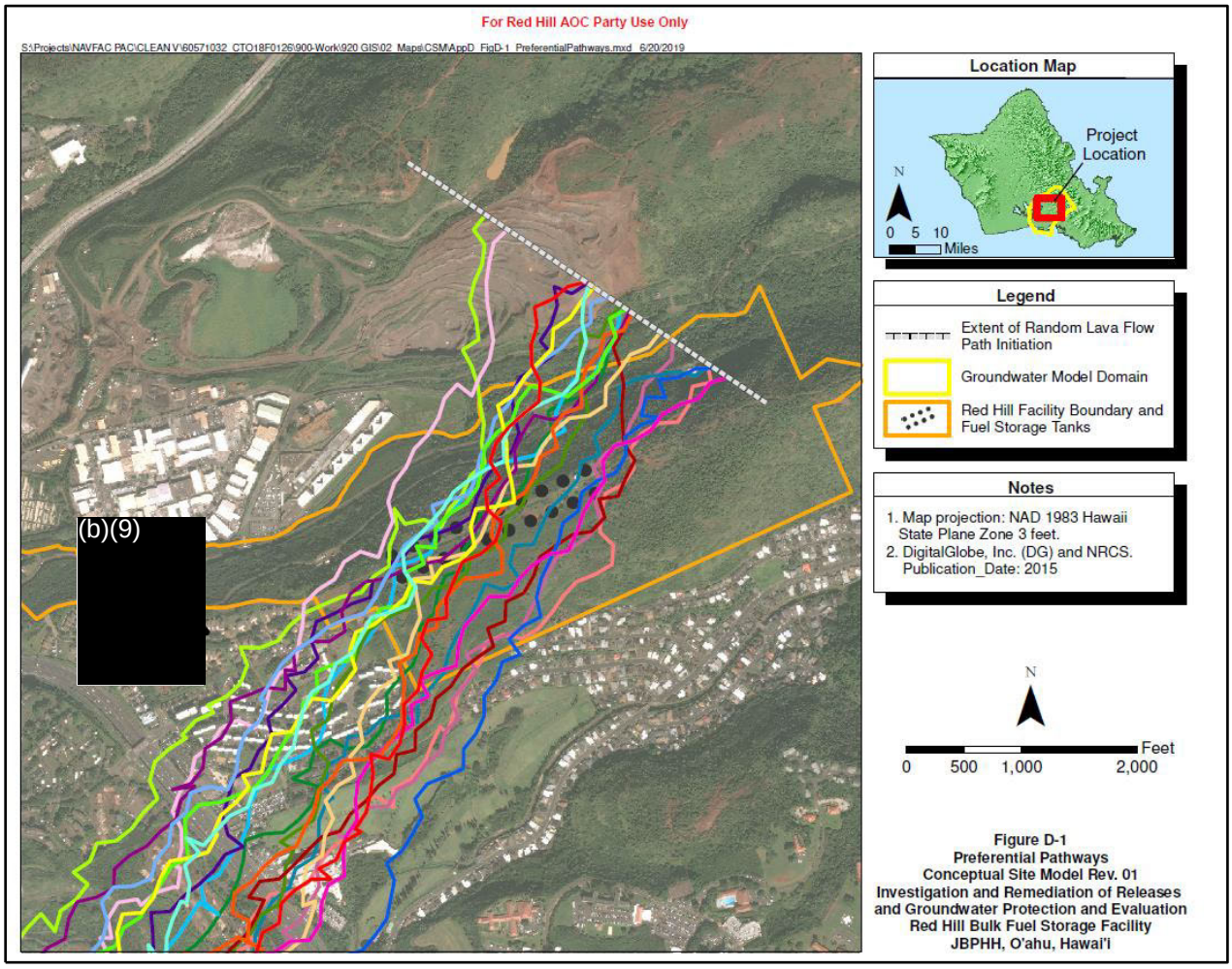

Figure C-3: Results of Structure-Imitating Stochastic Lava Simulations

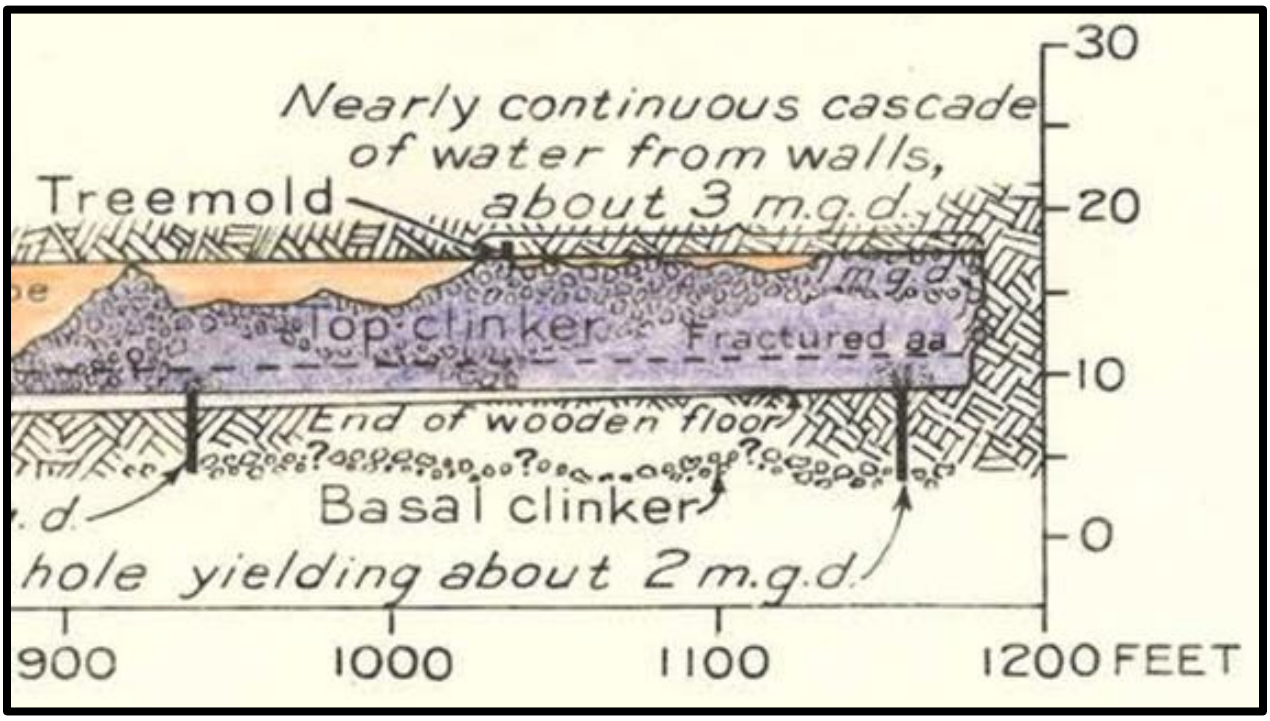

Figure C-4: Extract from Boring log for Red Hill Tunnel

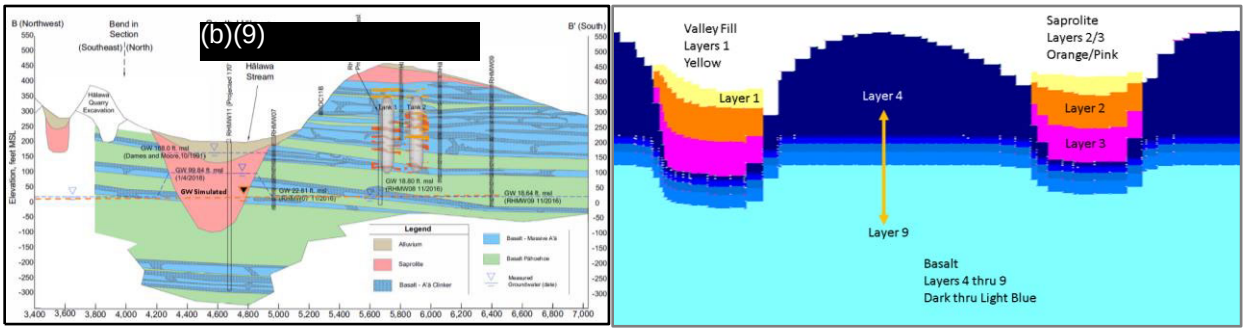

Figure C-5: Conceptual Model for Saprolite-Basalt (Left) and Simulated Representation (Right)

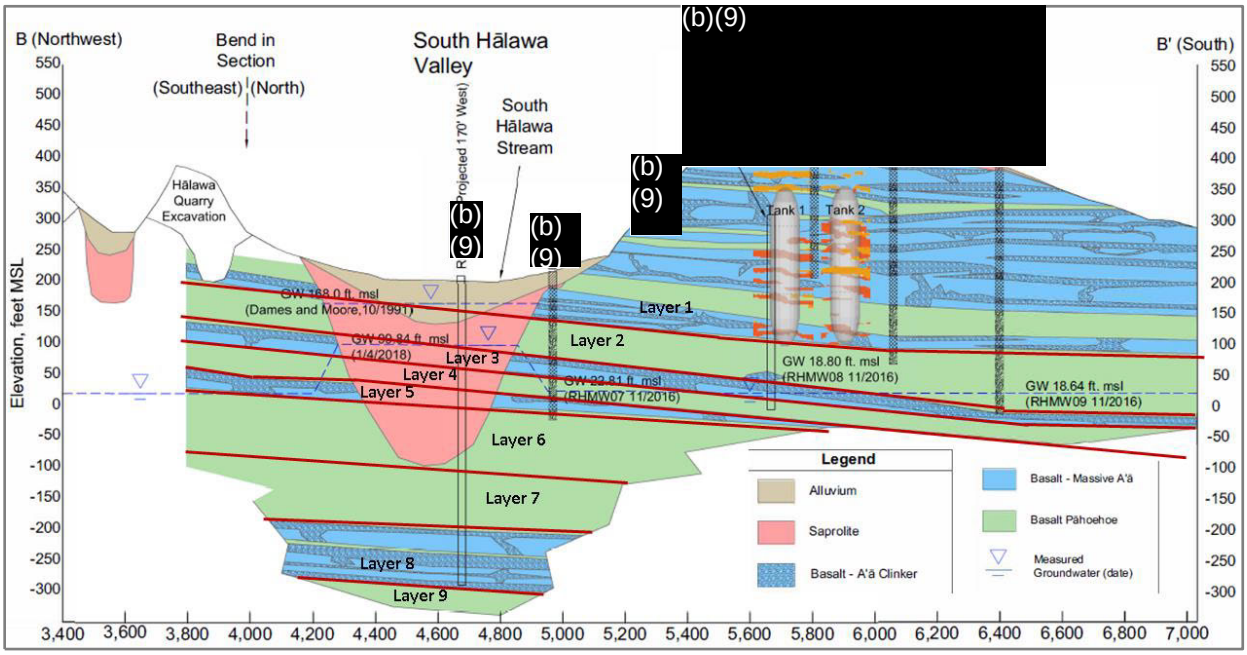

Figure C-6: Alternative Representation of Saprolite-Basalt Relationships

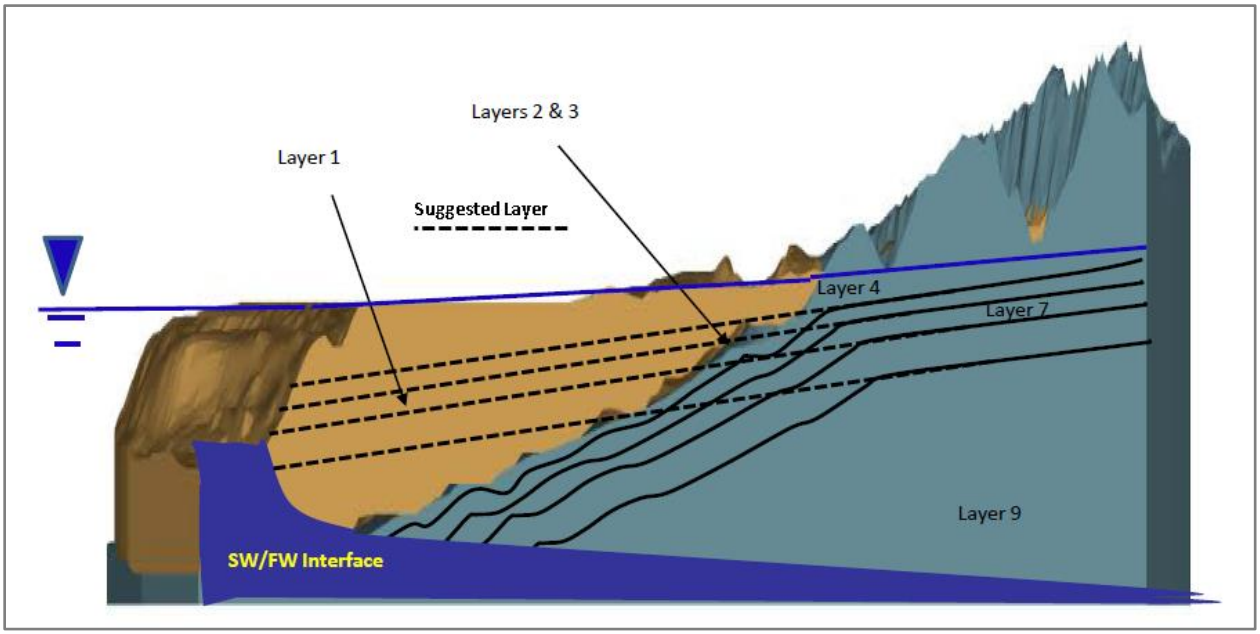

Figure C-7: Alternative Representation of Basalt-Caprock

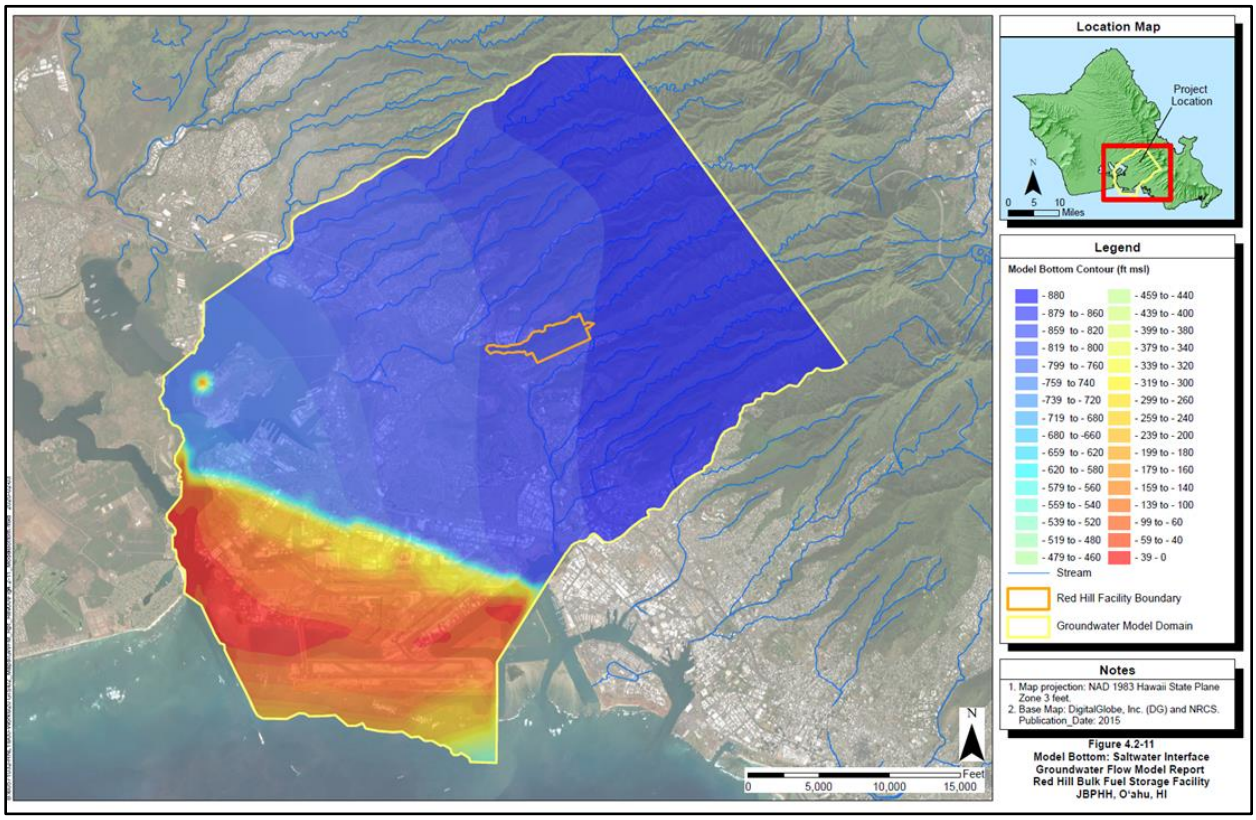

Figure C-8: Representation of Freshwater-Saltwater Interface

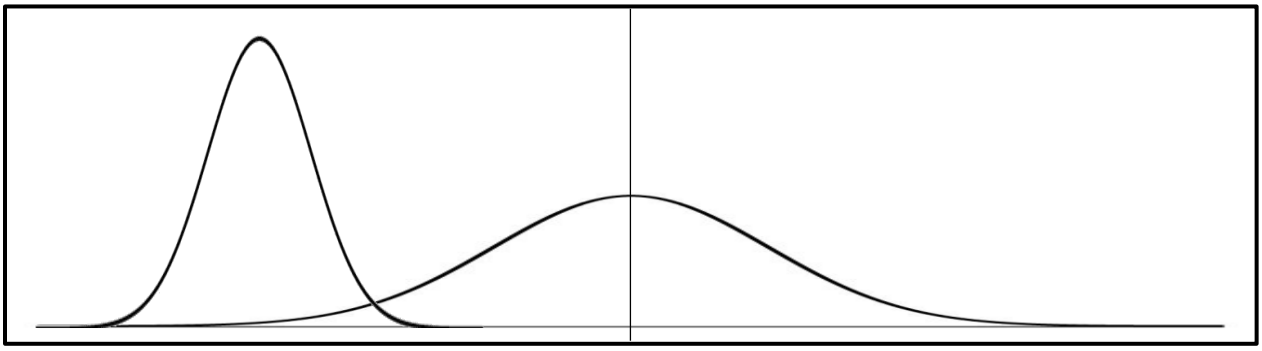

Figure C-9: Schematic Illustration Comparing Two Different Probability Density Functions (PDFs)

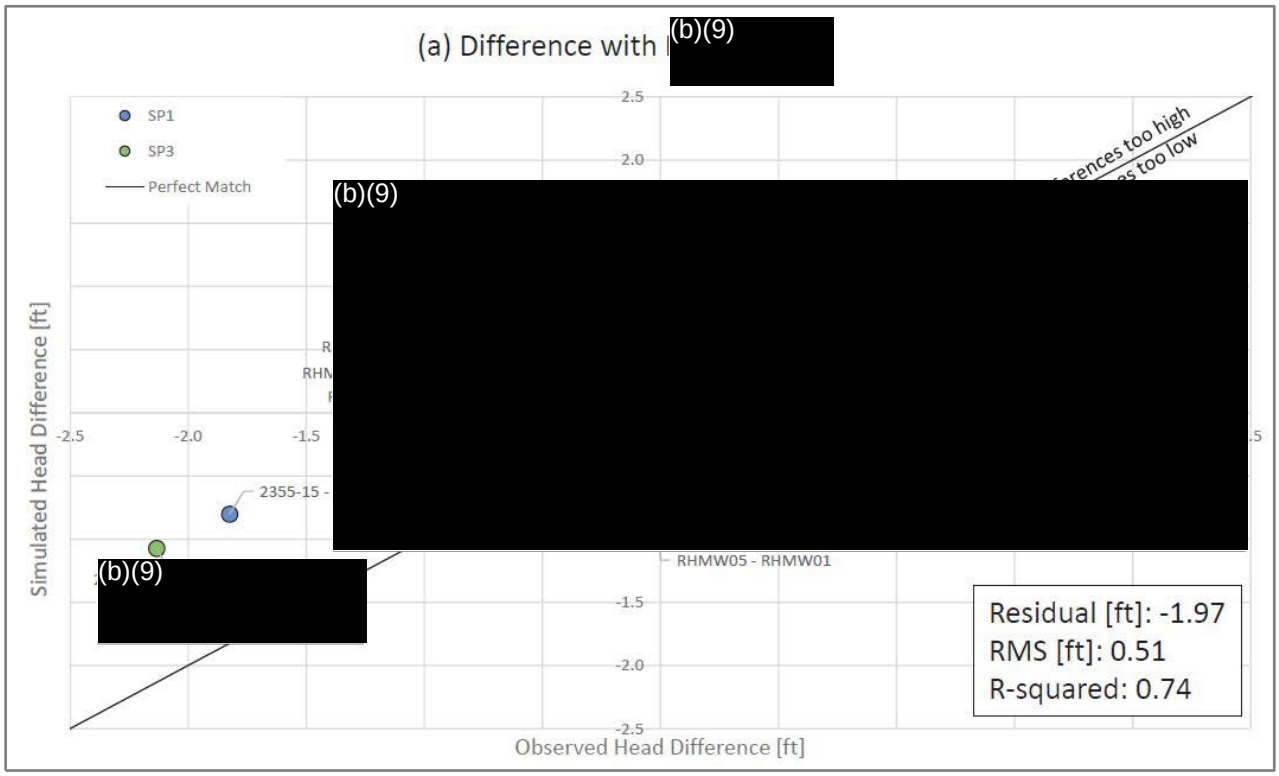

Figure C-10: Example Graphical Depiction of Simulated and Observed Head Differences

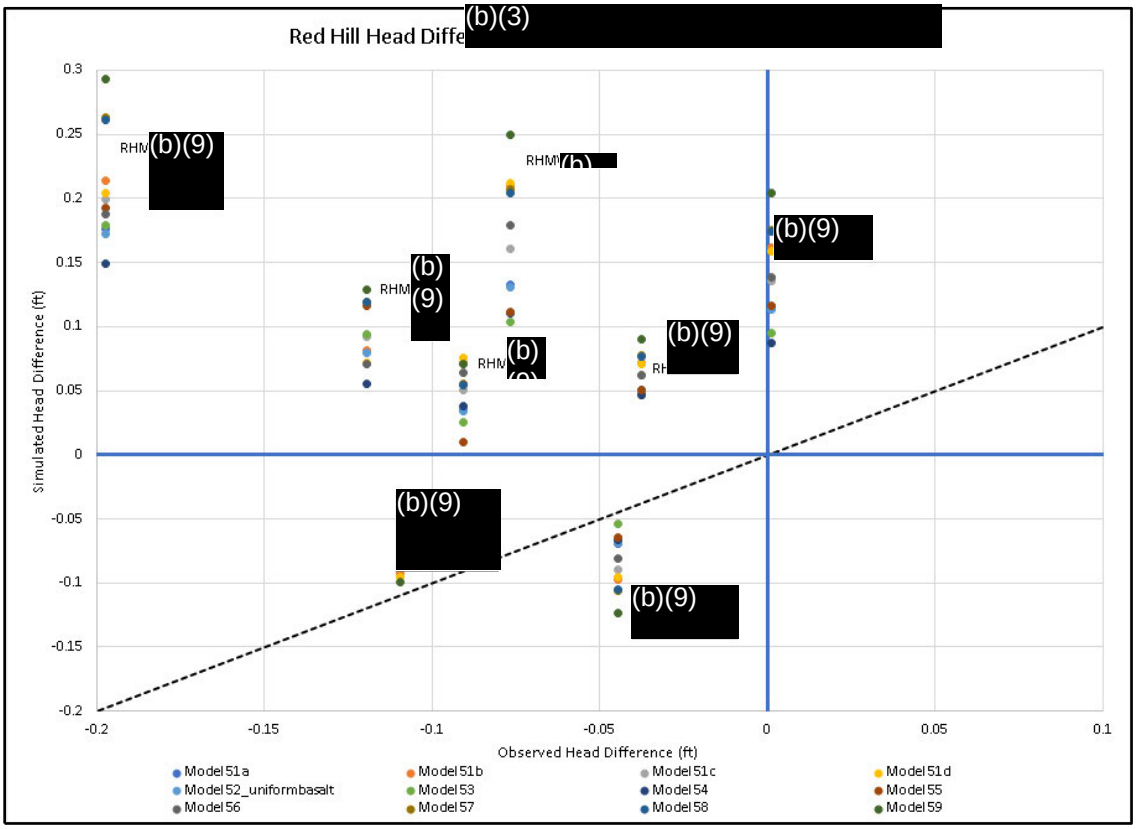

Figure C-11: Alternative Graphical Depiction of Simulated and Observed Head Differences

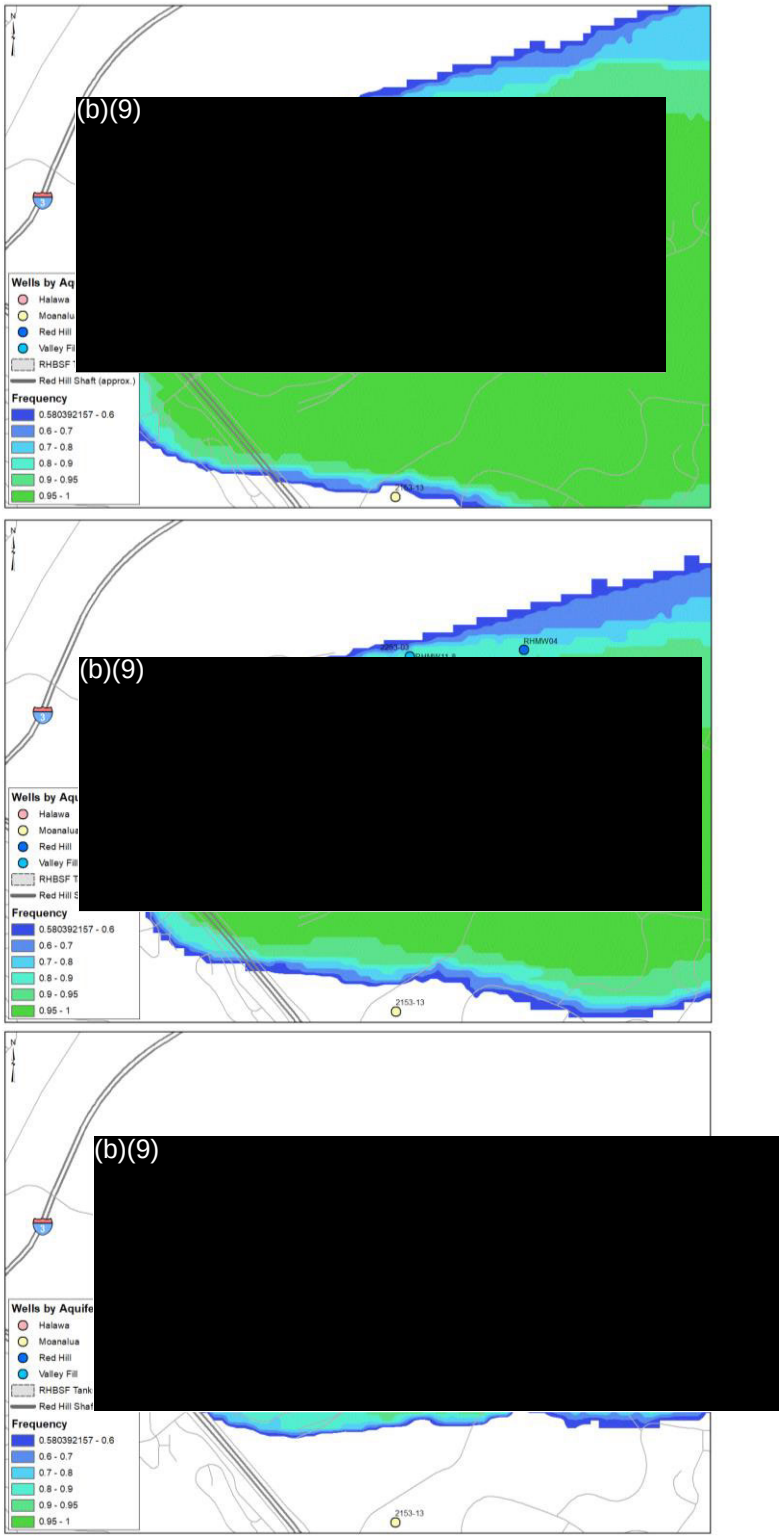

Figure C-12: Example Capture Frequency Maps at Three Alternate Pumping Rates for (b)(3)

Tables

Table C-1: List of Parameter Literature Values and Estimated Values

(Bold indicates estimated value at/above max/min)

Parameter	Minimum Literature Value	Maximum Literature Value	Minimum Estimated Value	Maximum Estimated Value	Average Estimated Value	Percentage at or below Minimum	Percentage at or above Maximum
Caprock Kh (marine)	500	2500	**2500**	**5000**	**4808**	0.0%	100.0%
Caprock Kv (marine)	0.001	15	0.18	11.87	9.3	0.0%	0.0%
Caprock Kh (alluvial)	0.1	20	**0.1**	**20**	18.5	7.7%	92.3%
Caprock Kv (alluvial)	0.001	2	0.09	**20**	**13.8**	0.0%	69.2%
Valley fills, Kh	2	200	**1**	**200**	16.3	92.3%	7.7%
Valley fills, Kv	0.01	10	0.001	3.37	0.26	92.3%	0.0%
Saprolite under valley fill, Kh	0.1	10	4.81	**10**	5.7	0.0%	7.7%
Saprolite under valley fill, Kv	0.001	0.1	0.002	**0.8**	0.072	0.0%	7.7%
Saprolite under caprock, Kh	0.1	10	0.8	**10**	4.7	0.0%	7.7%
Saprolite under caprock, Kv	0.001	0.1	0.002	**0.8**	0.084	0.0%	7.7%
Tuff overlying marine, Kh	0.01	200	**200**	**500**	**477**	0.0%	100.0%
Tuff overlying marine, Kv	0.01	15	**0.01**	3.17	0.30	69.2%	0.0%
Tuff overlying alluvial, Kh	0.01	200	10	20	10.8	0.0%	0.0%
Tuff overlying alluvial, Kv	0.01	15	**0.001**	0.18	0.031	69.2%	0.0%
Tuff cone, Kh	0.01	50	**0.001**	0.089	**0.008**	92.3%	0.0%
Tuff cone, Kv	0.001	5	**0.001**	0.008	0.002	92.3%	0.0%
Basalt, Kh	500	20000	1814	8280	3657	0.0%	0.0%
Basalt, Kv	2	200	44.54	**200**	136	0.0%	23.1%

Table C-2: List of Estimated Vertical Anisotropies

Vertical Anisotropy	Maximum	Minimum	Average
Caprock (marine)	13889	421	1531
Caprock (alluvial)	222	1	49
Valley fills	1000	59	928
Saprolite under valley fill	2500	6	737
Saprolite under caprock	2500	6	596
Tuff overlying marine	50000	158	35429
Tuff overlying alluvial	10000	100	7002
Tuff cone	11	1	2
Basalt	151	9	48

DOH Review:
Navy Groundwater Flow Models & Related Issues with the Navy CSM for the Red Hill Facility

By:

(b)(6)

GWFM - Drinking Water Risk Concerns

1. GWFMs boundary conditions have uncertainty
   a) Chosen BCs are reasonable for primary models
   b) Data indicate other boundary conditions are probable
2. Validation doesn't ensure the model adequately replicates groundwater flow trajectories
   a) Currently used comparative data – g.w. gauging
   b) Verification simulations appear not to match elevations
   c) Alternative verification data sets
3. Model conclusions and data contrasts are problematic
   a) Critical question: Do the model results support the conclusions in the IRR Report?
   b) And future CF&T (Part II discussion)

Critical Drinking Water Risk Evaluation Questions

- Does pumping the (b)(3)(b)(3)(b)(3)(b)(3) (b)(3)(b)(3)(b)(3)(b)(3) mobilize groundwater from beneath all tanks toward the (b)(3)(b)(3)(b)(3)(b)(3) (b)(3)(b)(3)(b)(3)(b)(3)?
- Is there an unobstructed hydraulic pathway from beneath the tanks to the Halawa Shaft?
- Over-arching question:
  - Is the model informative for answering either or both of those questions?
  - Can the models adequately inform CF&T (Part II)?

GWFM Boundary Conditions

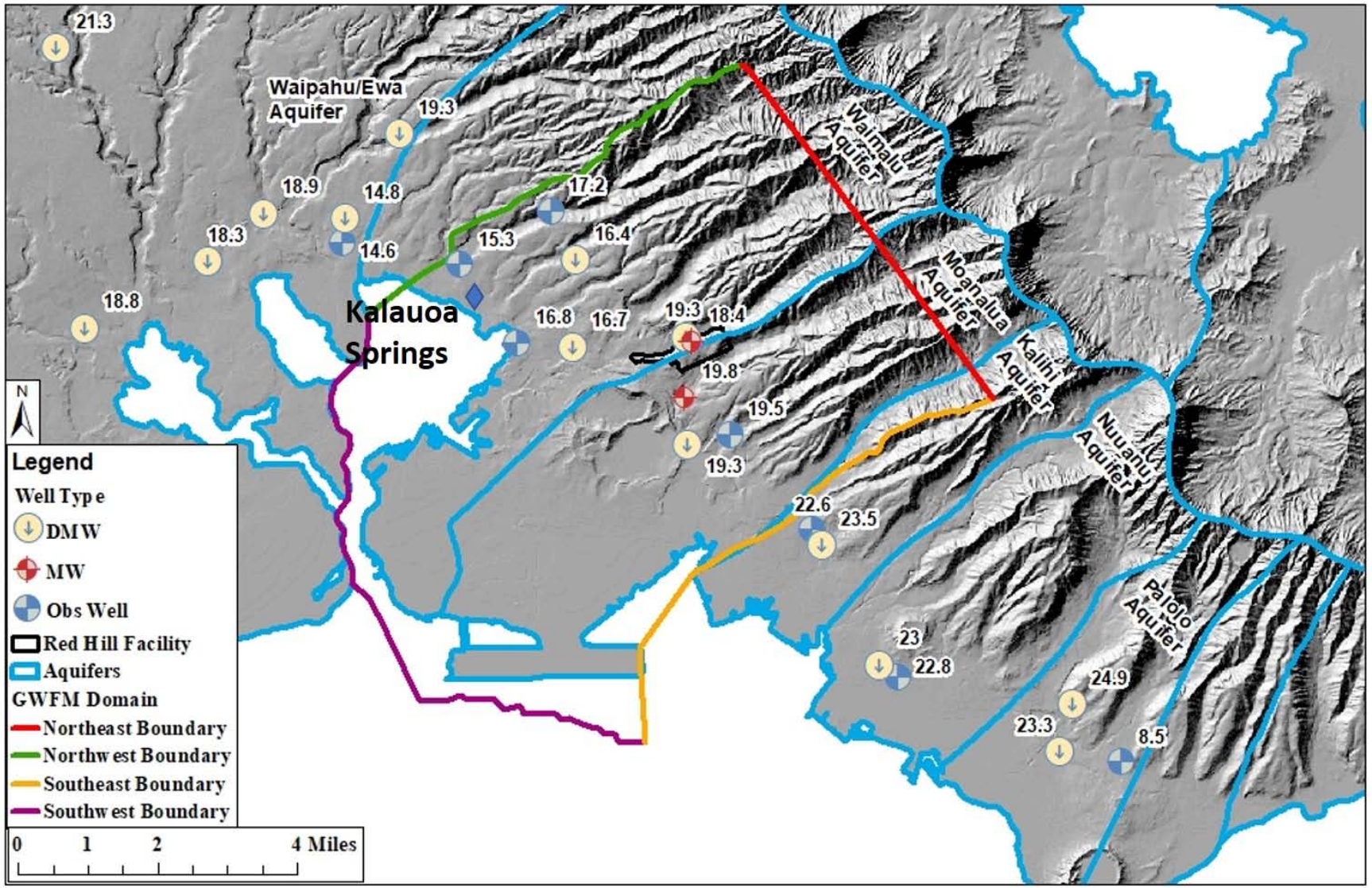

Model Validation – Compare to Site Data

1. Methods & data currently used
   a) Groundwater elevations
   b) Transient responses
   c) Others
2. Concern with current comparative data
   a) Mis-match between modeled and measured gradients
   b) Groundwater elevations have low accuracy (Part II review)
3. Alternative groundwater behavior data
   a) Chloride and other natural tracers

Regional Water Levels

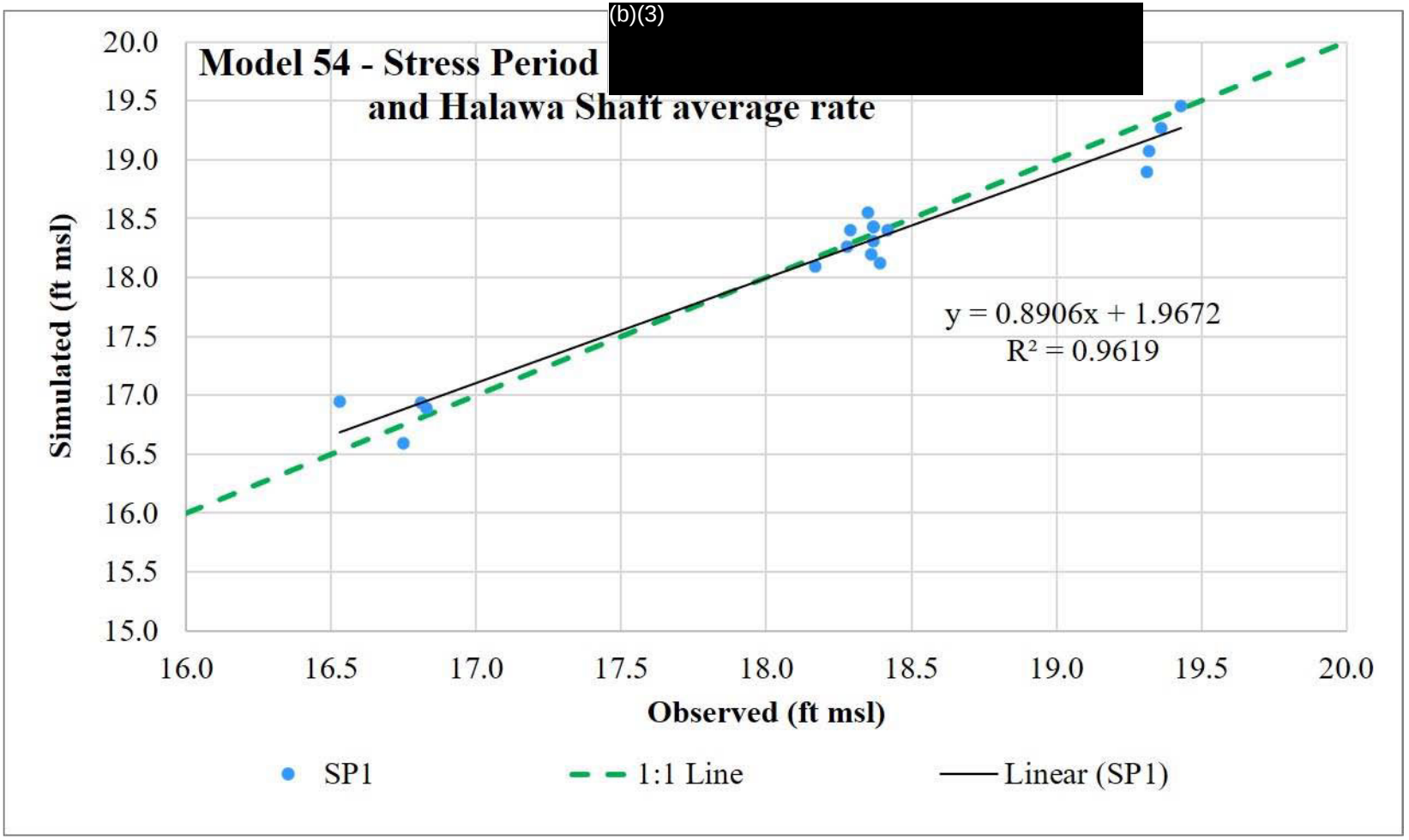

Local Water Levels

(Navy GWFMs do not match local data)

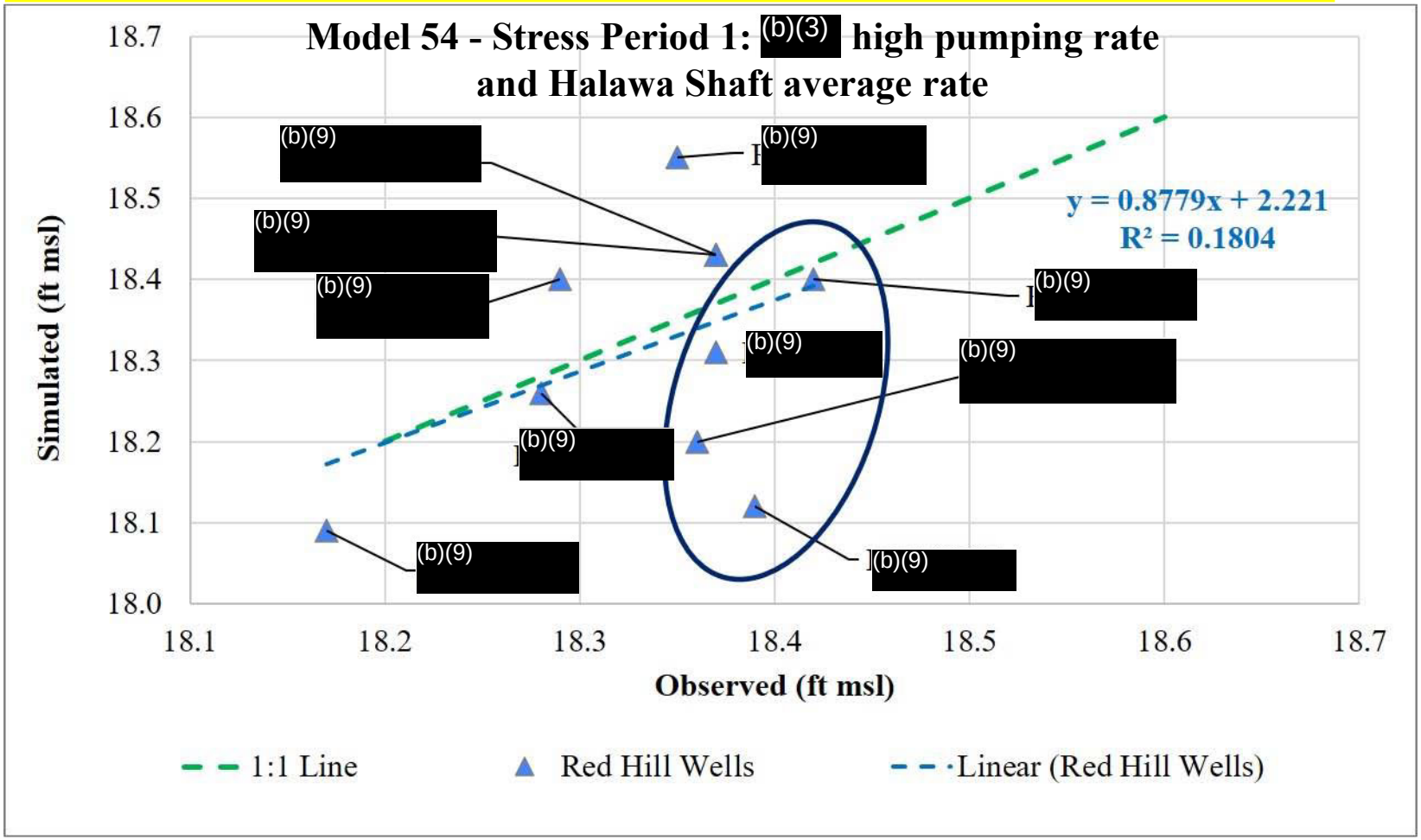

Gradient beneath and downslope of the tanks
(output from Navy GWFMs)

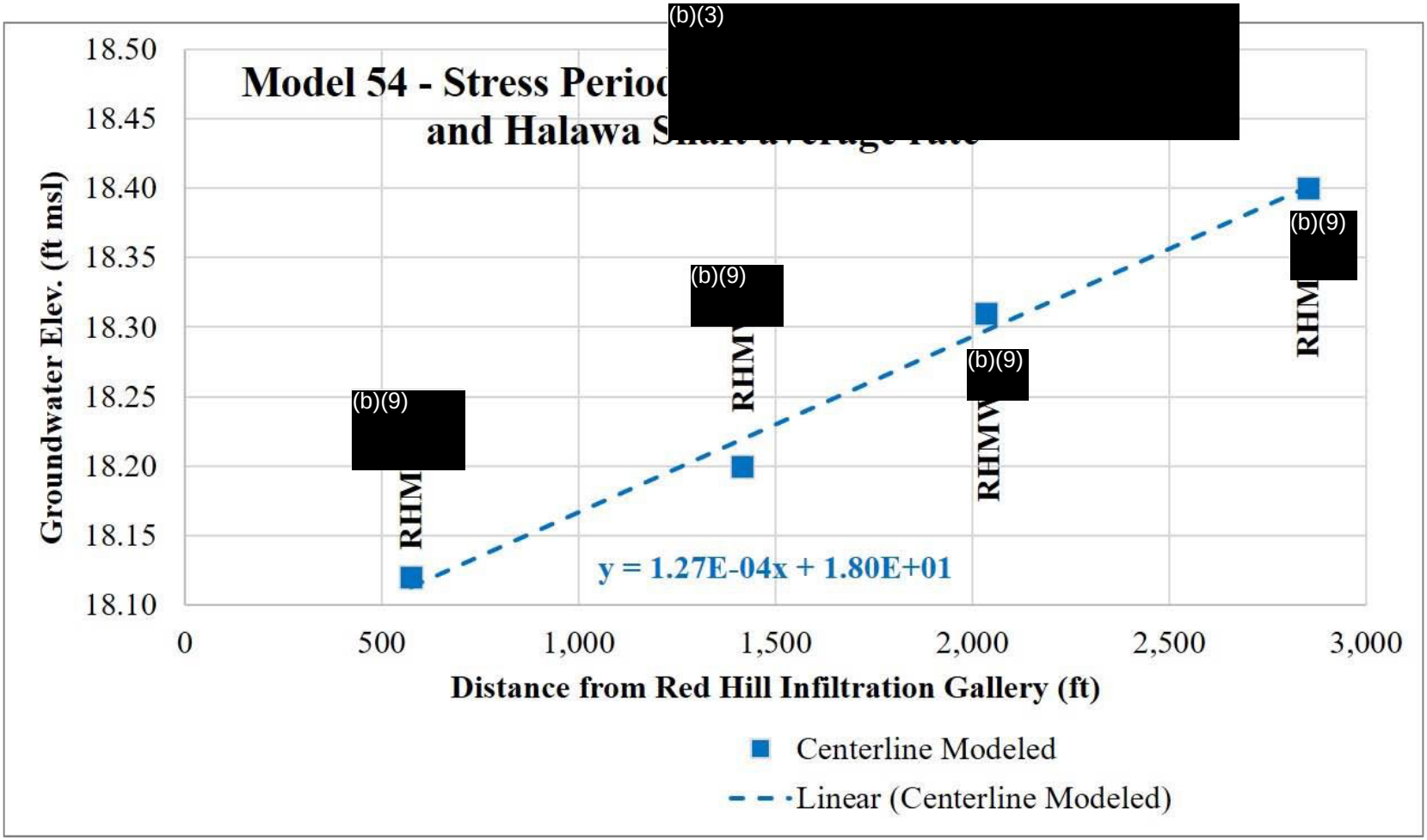

Measured vs. Modeled RH Ridge Gradients
(Gradient beneath and downslope of the tanks)

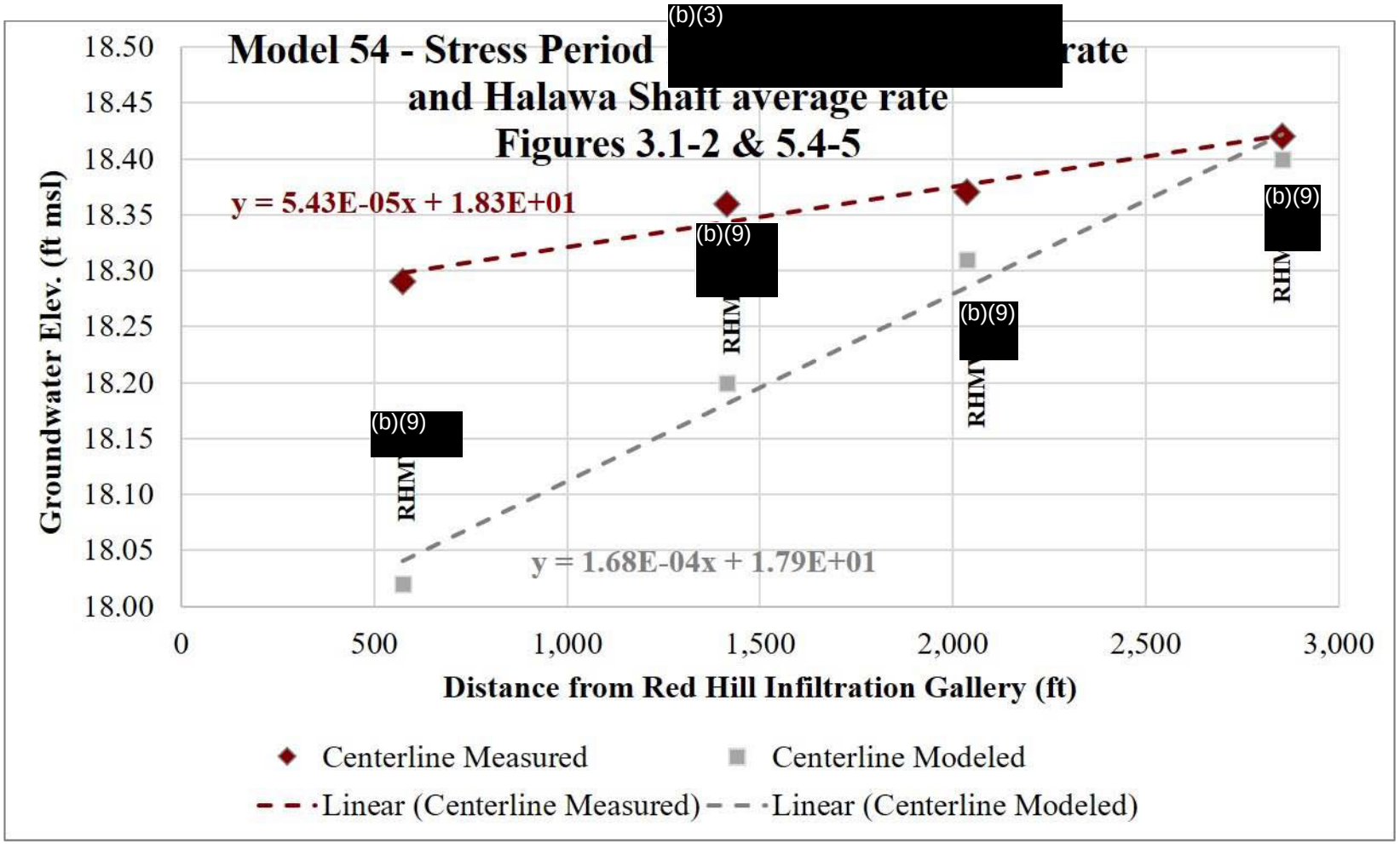

Red Hill Ridge gradient - under three different pumping conditions

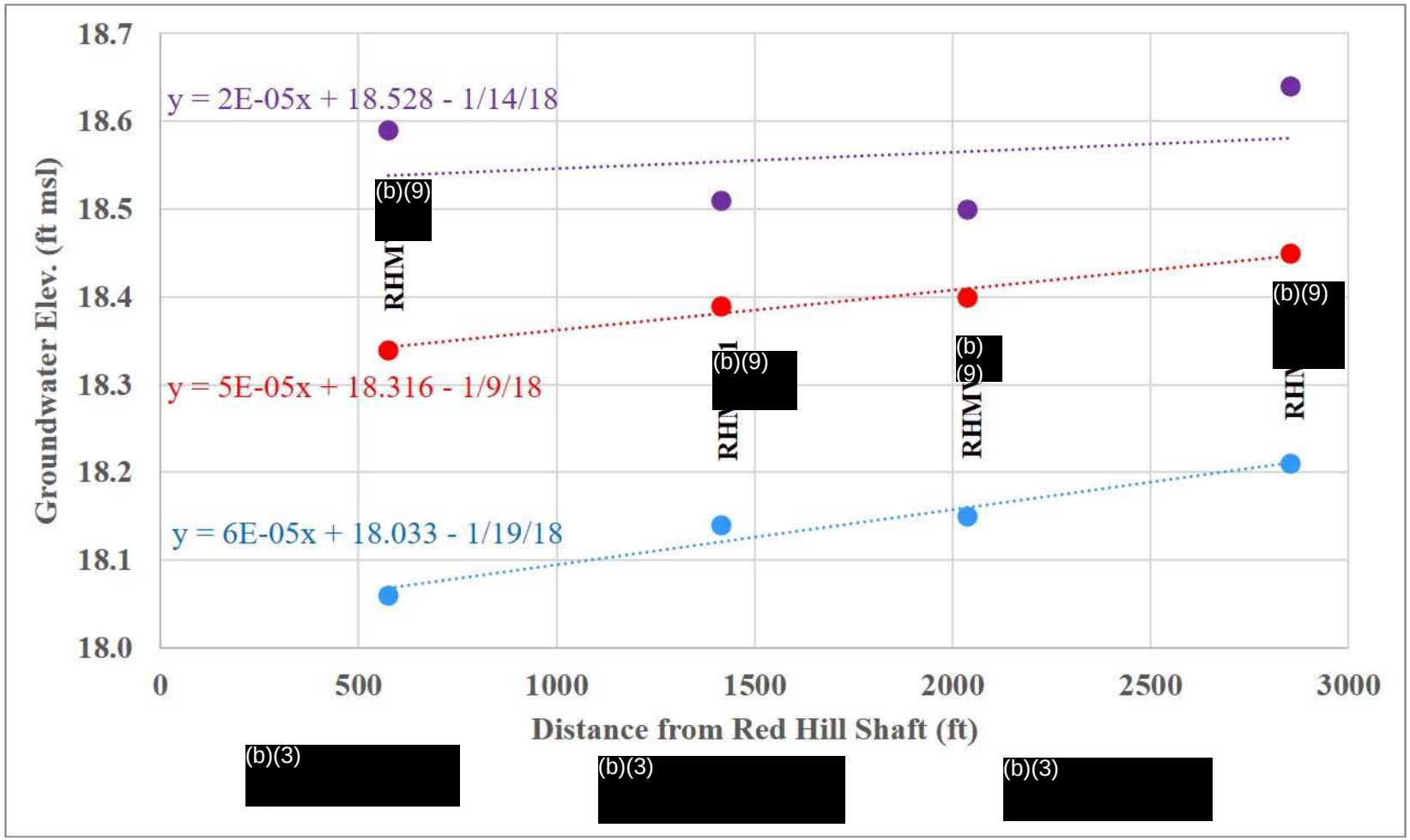

Reliability of GW Elevation Data

~~For Red Hill AOC Party Use Only~~

magnitude and direction, which are a primary objective for the model. However, the measurements of absolute water levels or gradients between well pairs may incur errors due to datum measurements and borehole gyroscopic tape corrections for the reasons previously discussed. The spring fluxes at Pearl Harbor Spring at Kalauao and Kalauao Spring were also calibration targets with target values shown in Table 3-2. Weighting on these targets was determined after preliminary PEST simulations such that the flux magnitudes did not overwhelm water level targets in the objective function. Finally, the extraction rates at pumping wells were also included in the PEST multi-objective function to ensure that pumping did not reduce with bottom-hole conditions during calibration.

9. Groundwater Data

Chemistry shows indication of a poorly mixed system

- Chloride conc. vary from ~40->1000 mg/L
- Southeast very different from northwest
- Northwest chlorides still highly variable
- A large flux of groundwater down the Red Hill ridge should show better mixing

Estimated Chloride Conc. in Recharge

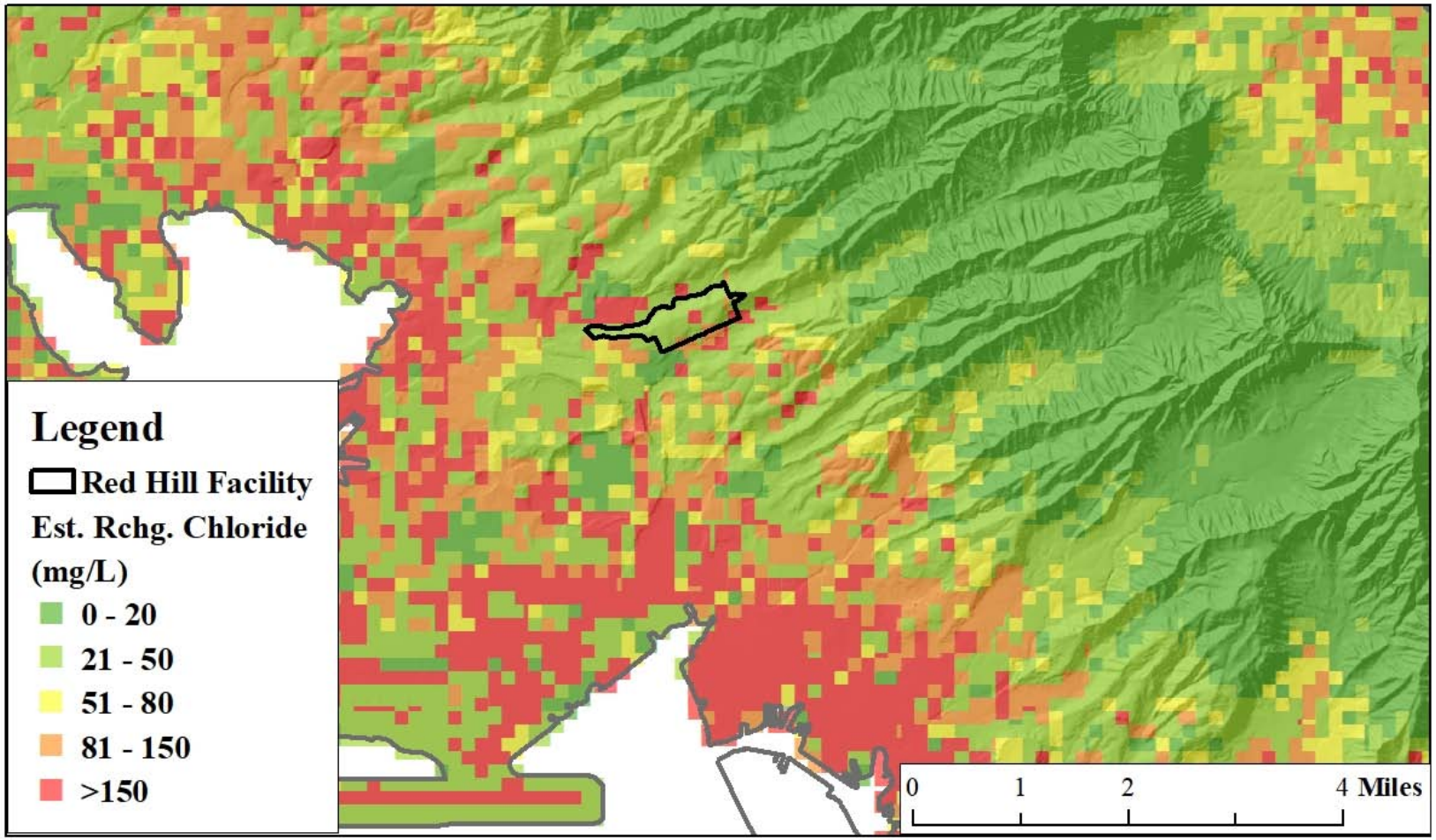

- Chloride in recharge estimated using the chloride mass balance approach
- Chloride concentration at the Facility <50 mg/L
  - Except for one pixel

Using Geochemistry to Refine Models
(without needing explicit CF&T simulations)

- Mixing Equation
  - $C_{mix}=(C_1*Q_1+C_2*Q_2+C_3*Q_3)/(Q_1+Q_2+Q_3)$
  - 93 mg/L = 2%*28 + 38%*37 + 59%*133
- (b)(3)(b)(3)(b)(3) average chloride conc. ~ 95 mg/L
  - Chloride concentration is weighted Cl sum from the source areas

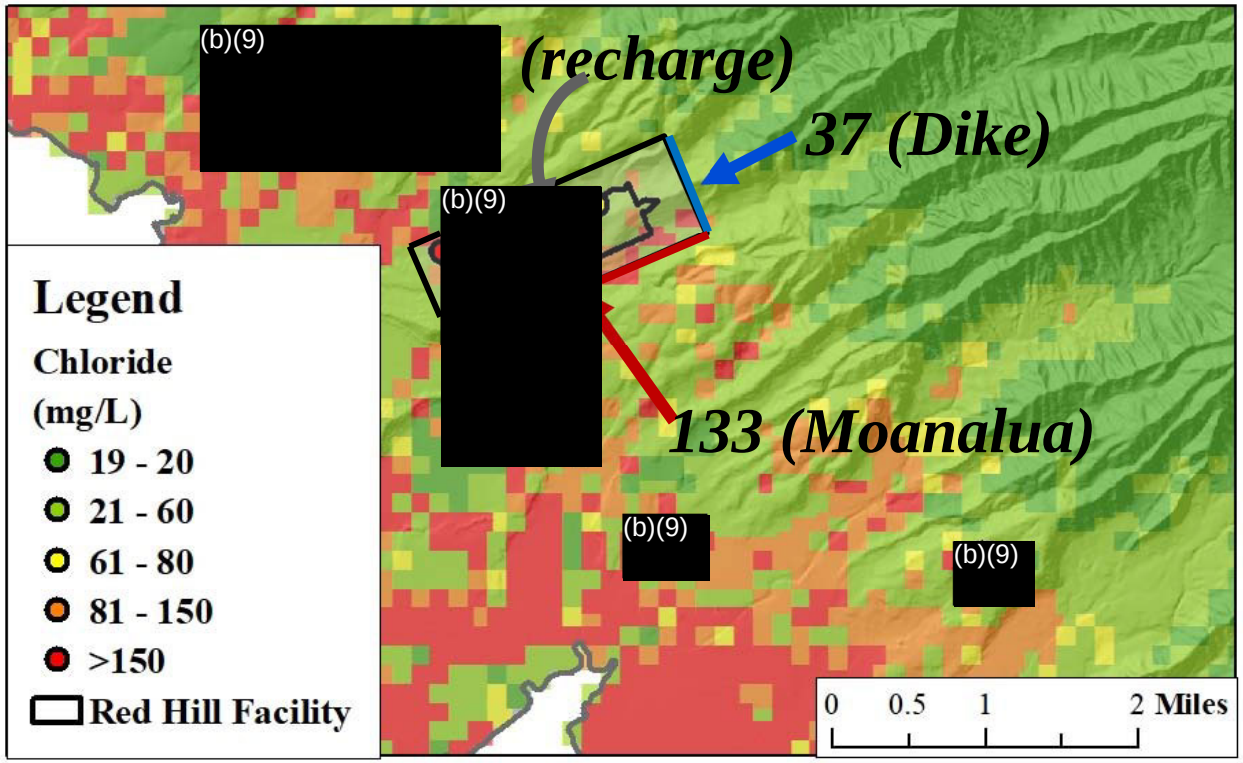

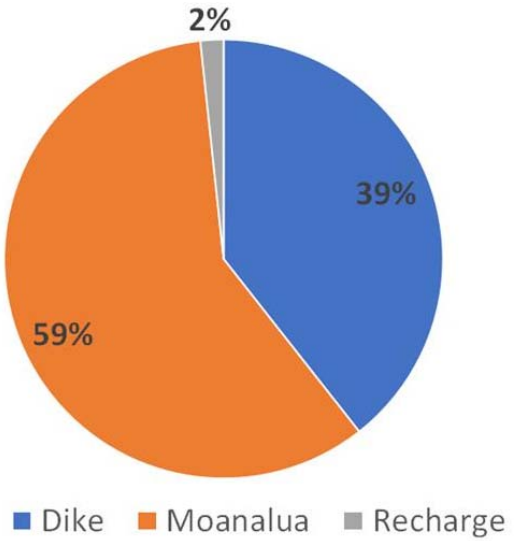

Numbers denote assumed chloride concentration

It is unlikely that chlorides originating in the Halawa region elevated the chloride concentration in the (b)(3) (b)(3)

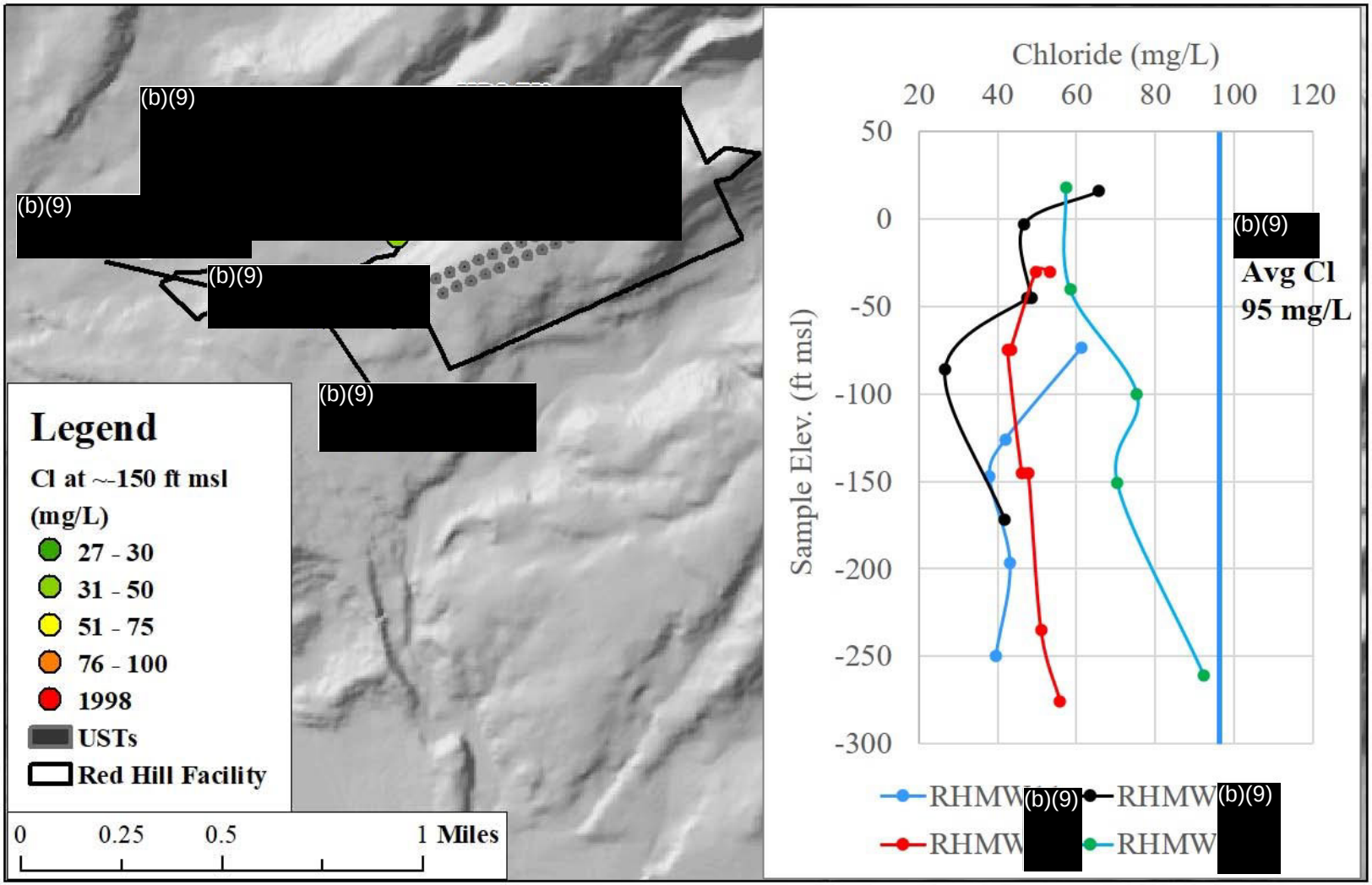

Application of model conclusions

2.3.2 Overview of Preliminary Capture Zone Analyses

The GWFM Report (DON 2020b) is published concurrently with this IRR Report. The GWFM Report describes the various models that are part of the multimodel approach, including capture zone analyses that pertain to each model (including certain variations for specific models). The reverse and forward particle track analyses presented in the report are related only to potential groundwater flow relative to the assumptions in a particular model, and do not relate to potential contaminant flow; contaminant flow will be determined as part of the CF&T modeling effort. Certain conclusions based on model capture zones and associated particle tracks are provided below:

- All available capture zones indicate that when (b)(3) is pumping at slightly below its permitted rate of [redacted] million gallons per day [mgd]) and (b)(6) is pumping at slightly above its permitted rate of (b)(9) mgd, the (b)(3) capture zone extends across the entire tank farm. As such, potential releases from any tank would be contained in the Red Hill Shaft capture zone.

- Investigation and Remediation of Releases Report; Page 2-18
- Issues previously discussed cast doubt on the assumption the Red Hill Shaft will contain the offsite migration of any contaminant plume
- The model results are currently not informative for developing release response plans
  - Questions regarding the ability of the (b)(3) to capture a contaminant plume and the risk the (b)(3)(b)(3)(b)(3) remain unanswered

Further GWFM & CSM Review Items

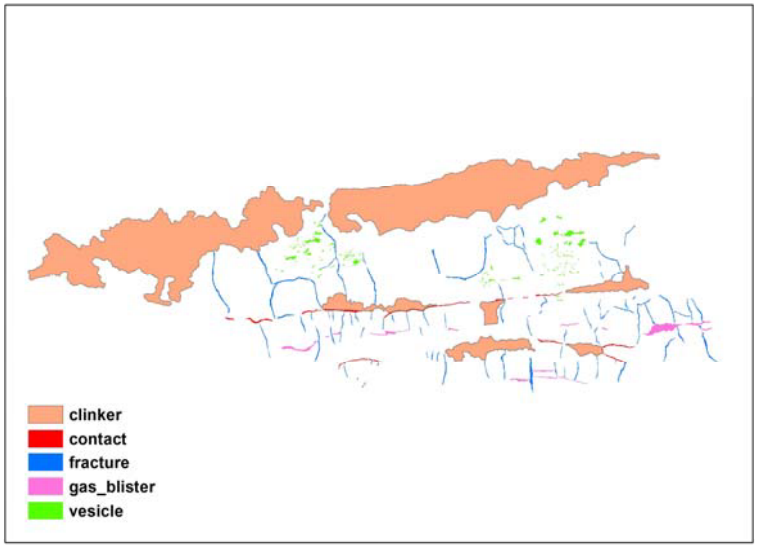

DOH Technical Team:

(b)(9)

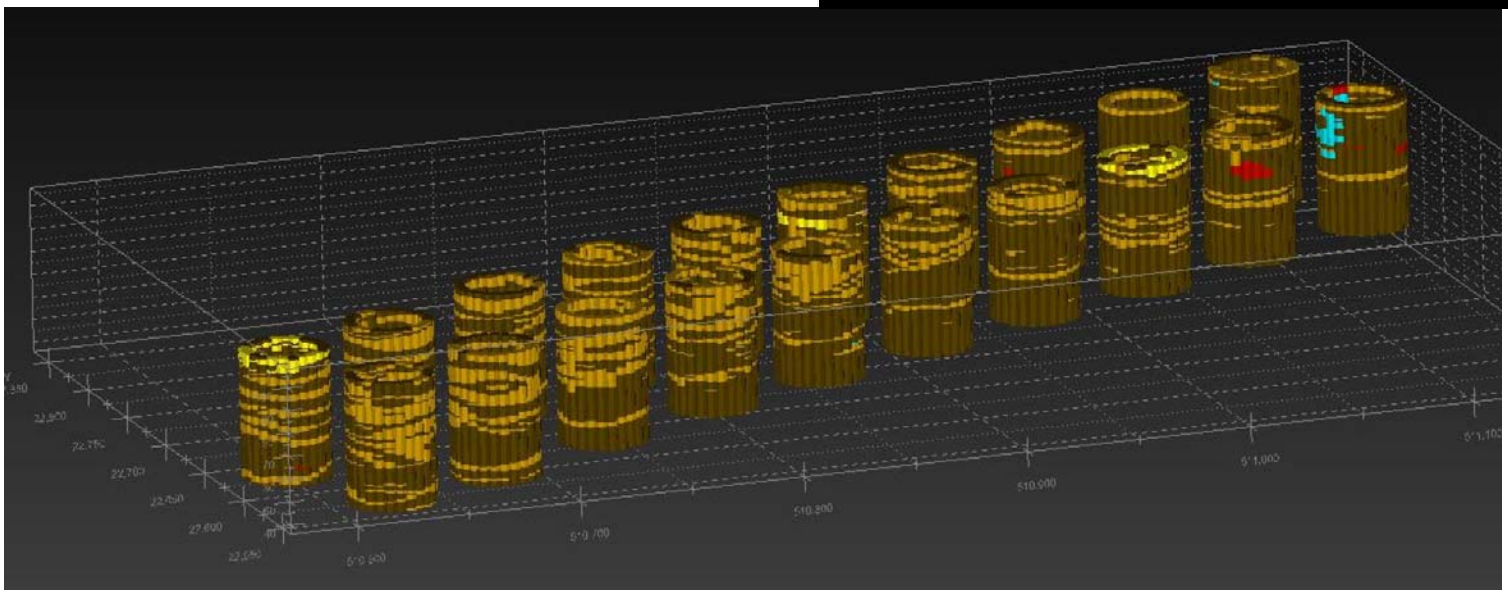

Key Groundwater Model Objective

- The purpose of this deliverable is to refine the existing groundwater flow model and improve the understanding of the direction and rate of groundwater flow within the aquifers around the Facility (AOC, 2015)
  - *To do this, the underlying hydrogeologic conditions must be refined and better understood in light of new data not available to prior modeling*

The Navy Has Delivered Multiple Models

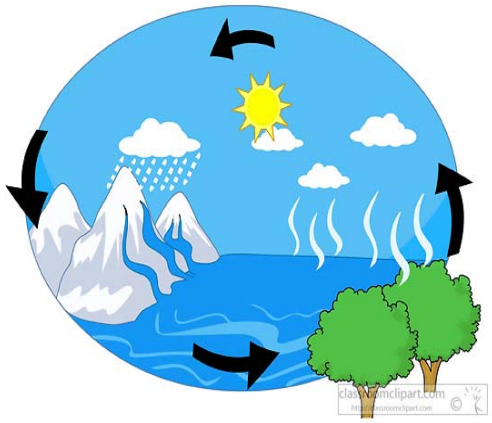

- Key review questions:
  - Do the models represent local heads?
  - Gradients?
  - Transient aspects?
    - Pumping from Red Hill & Halawa shafts
    - Monitoring well response “groupings”
  - Do transient simulations better past models?
  - Are models consistent with geochemistry?
    - And with dissolved-phase patterns?
  - Are models parameters appropriate?
- Will the model(s) inform risk estimates?
  - Most uncertain aspect is NAPL
    - Where is it presently & in what state?
    - How far/fast could releases travel?
  - What are the key processes?
  - Are those adequately described & demonstrated?

General Area/Model Map

(Halawa Shaft On, [redacted]

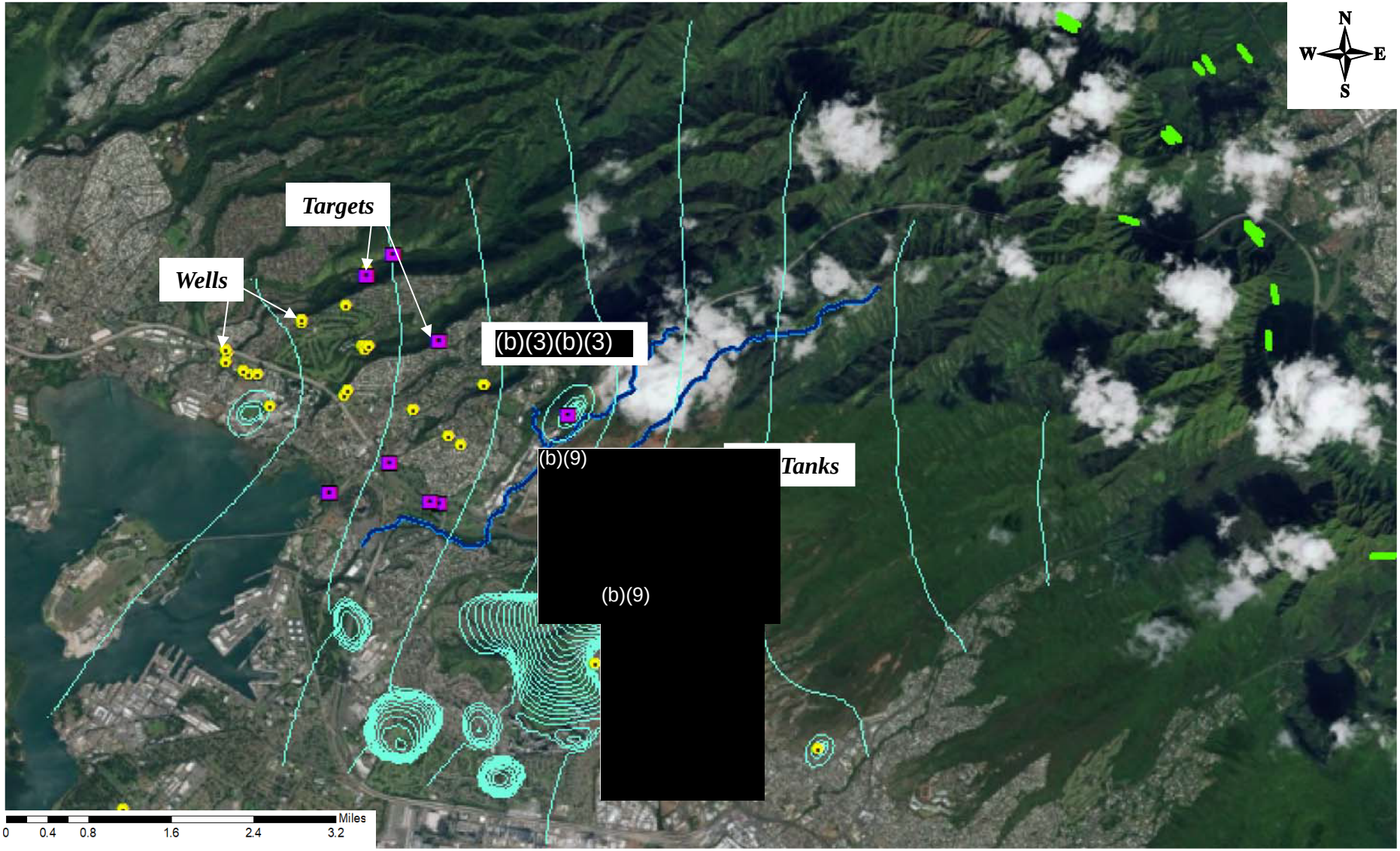

The Primary Issue with the Prior Model

(calibrated to drawdown, but not to heads; complexity)

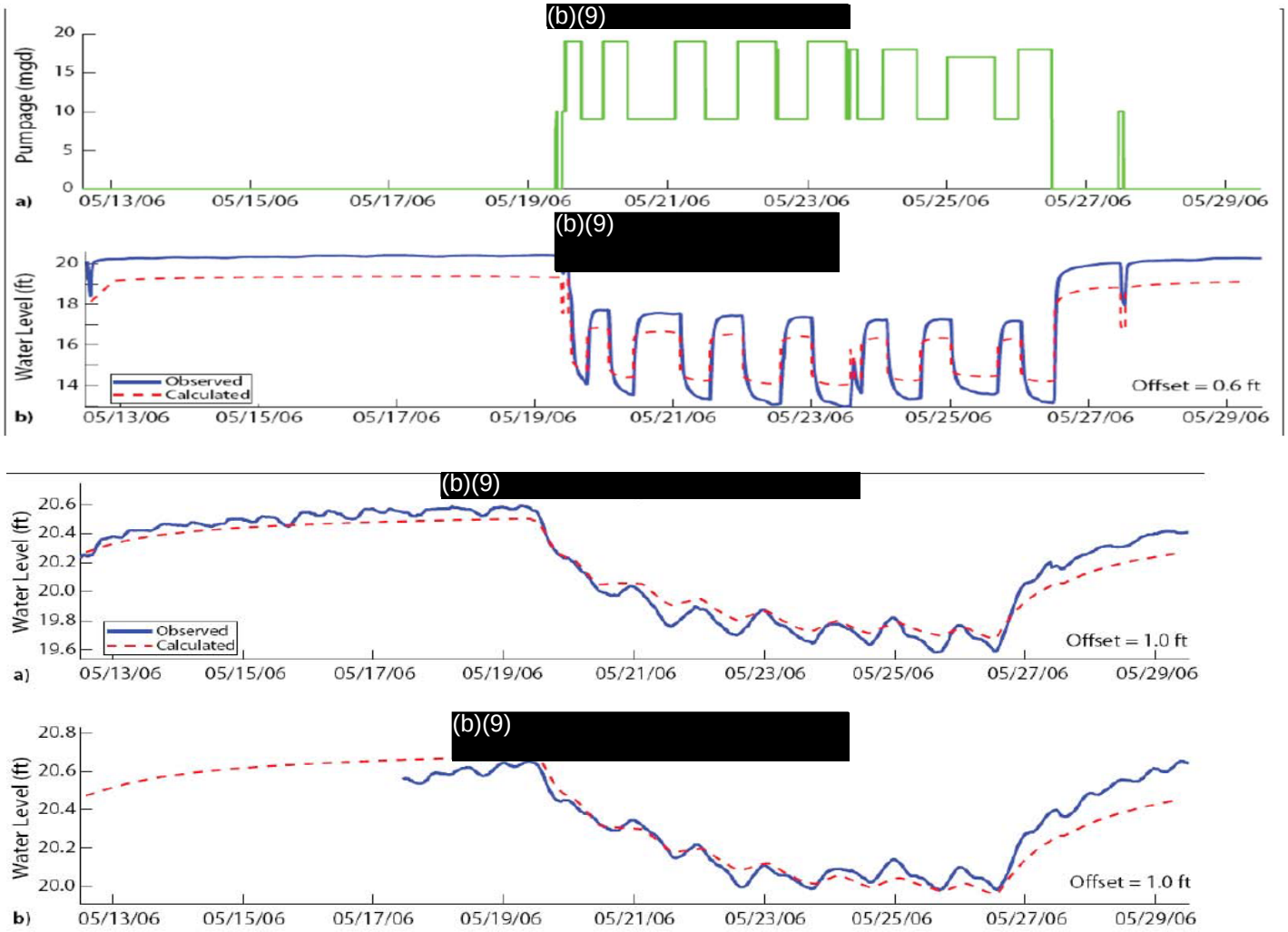

Kolja Rotzoll and Aly I. El-Kadi, 2007

Objectives of Verification Models
(GWFMs apparent mismatch to g.w. elevations)

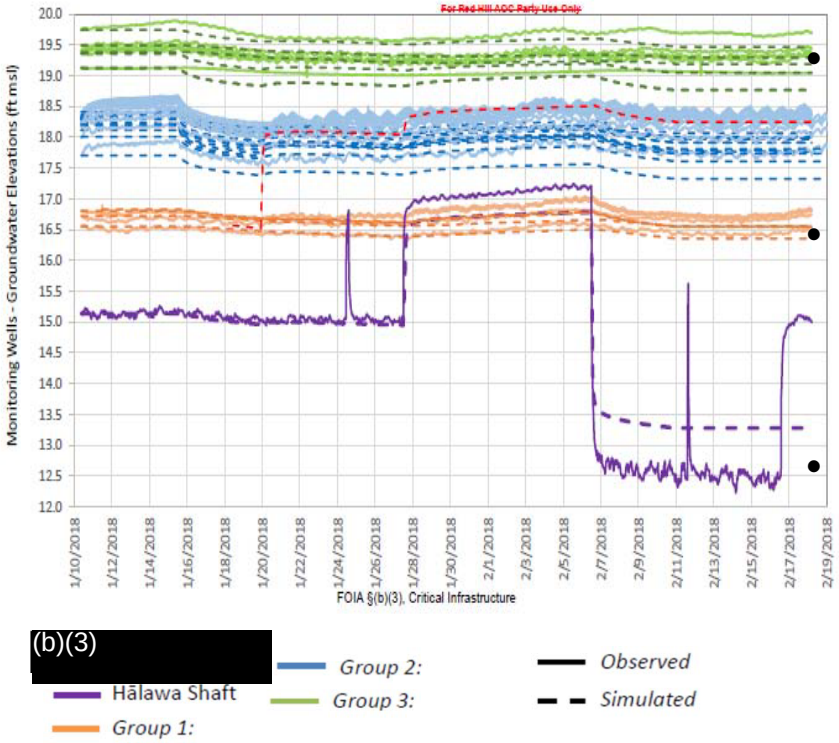

Abbreviated legend

Figure 5.1.1-7, Redacted GWFM Rept, Mar 2020

- Verification means just that
  - A "blind" test of the GWFMs predictions
  - How well do they agree with elevation data?
- How is this typically implemented?
  - Calibrate main models
  - Run against site data from another time
  - See how well each model reflects the data
- Purpose
  - Identify deficiencies in main models
  - Identify which are "best fits"
  - Consider transient implications
  - Consider compartmental responses (& others)
- Issue, we cannot replicate the reported results
  - Plots do not agree with modeled output
  - May be a superposition (drawdown upon measured)
- The g.w. elevation offset was prior model issue
  - Recall primary AOC objective

Example Hydrographs; M51a Verification

(charts are direct model output – GWV)

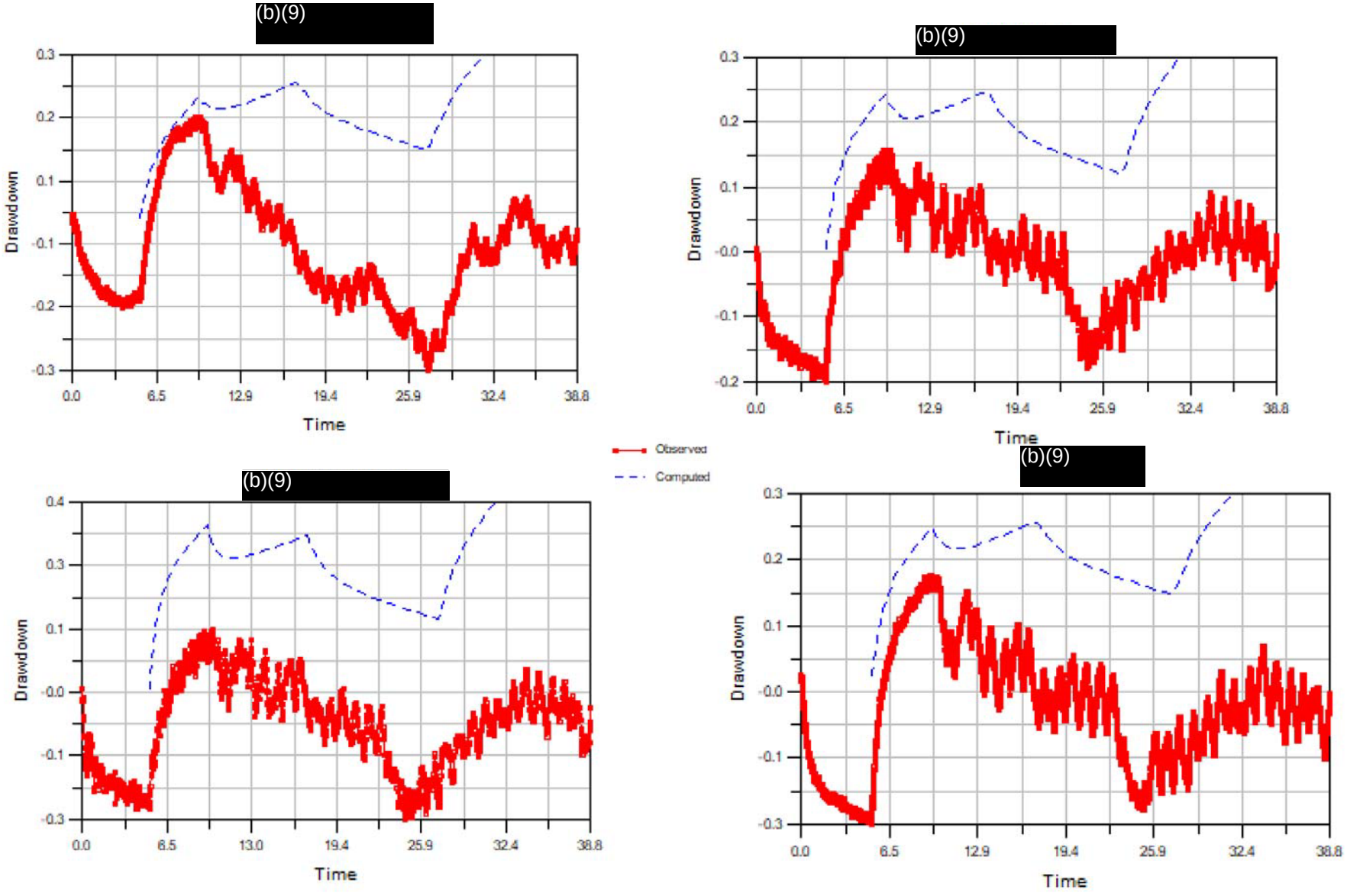

GW Elevation Variance – Transient Models

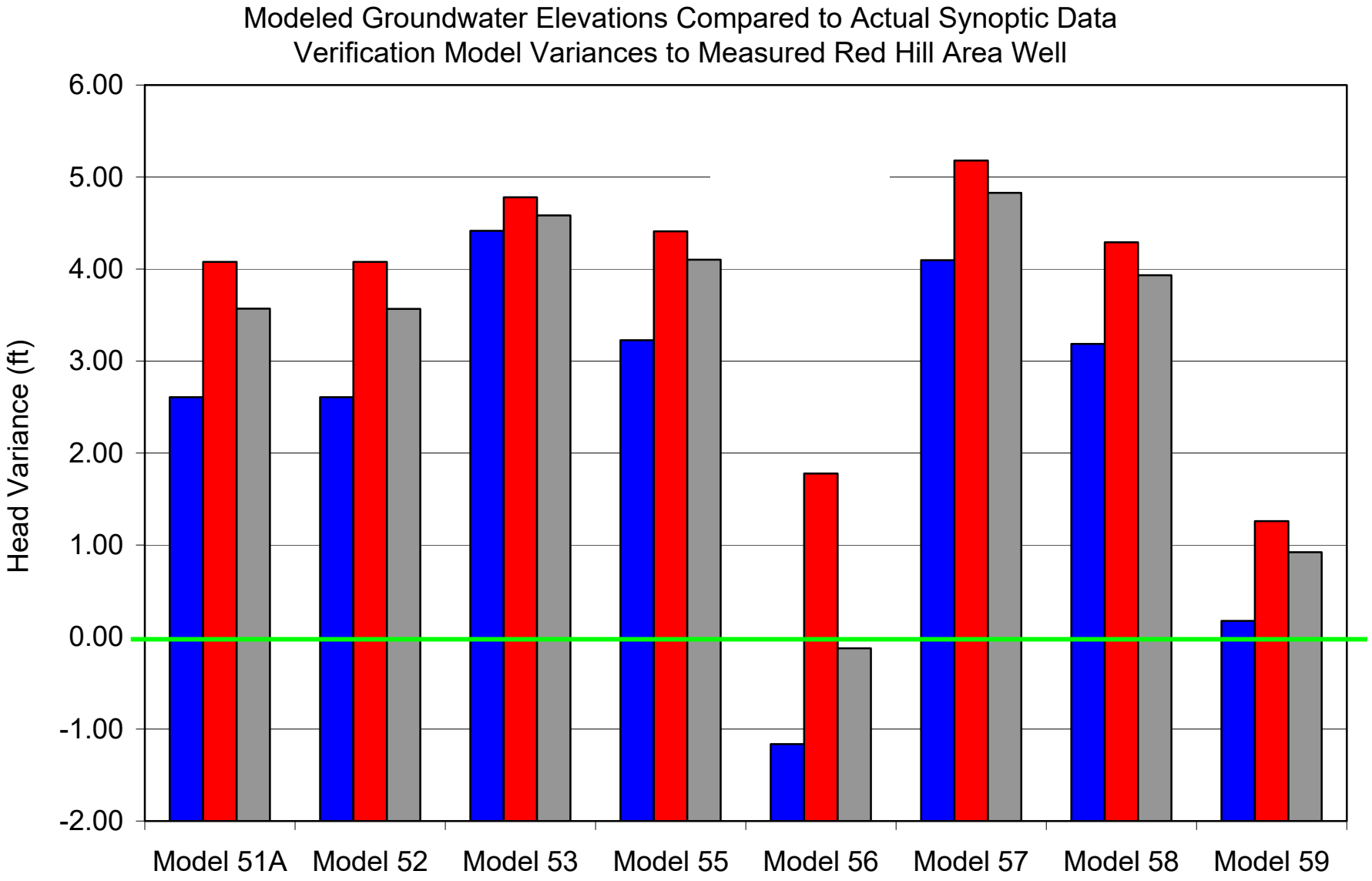

Non-Uniform Distance Drawdown Behavior

(indicates complexities not captured by models)

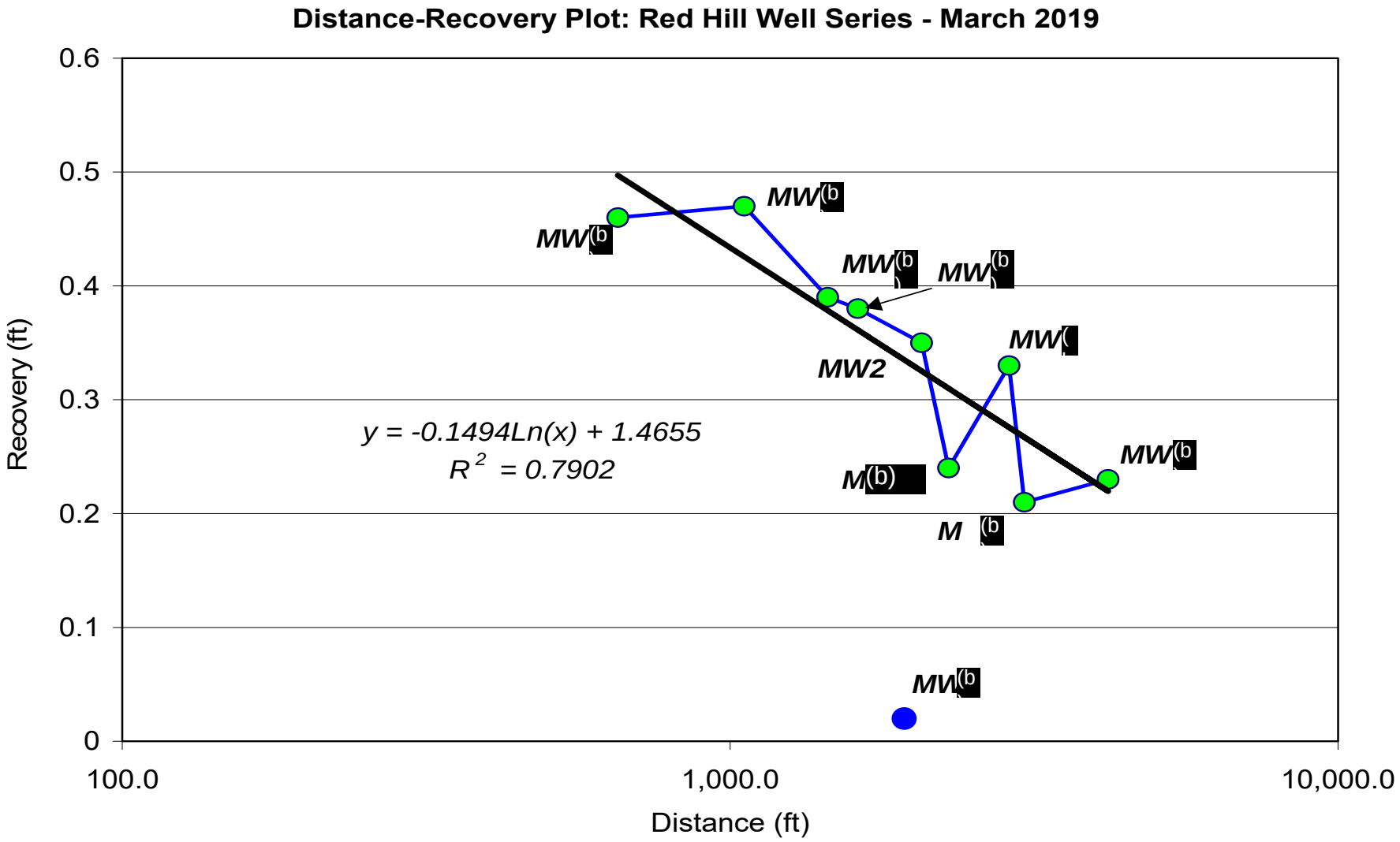

Prior Key Parameters v. Navy Models

(ranges are inconsistent & w/o explanations)

	Oki, 2005			Navy GWFM - avgs		
Hydrostratigraphic Unit	Kv	Kt	Kl	Kv	Kt	Kl
Volcanic-rock aquifer	7.5	1,500	4,500	65	1,000	2,999
Caprock, upper-limestone unit	25	2,500	2,500	0.01	500	500
Caprock, low-permeability unit						
Above Waianae Volcanics	0.3	0.3	0.3	0.01	1	1
Above Koolau Basalt, west of Waiawa Stream	0.01	0.01	0.01	0.01	1	1
Above Koolau Basalt, east of Waiawa Stream	0.6	0.6	0.6	0.01	1	1
Valley-fill barriers	0.058	0.058	0.058	0.01	1	1

Key Model Review Observations

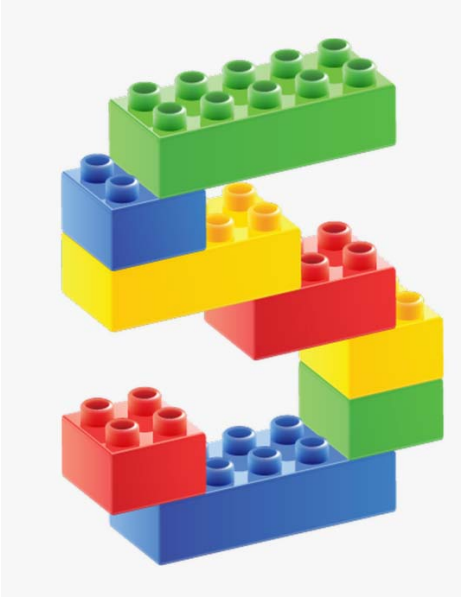

- GWFMs do not match heads, diminishing reliability
  - Particularly in transient verification runs
  - Similar issue as in prior modeling (2007)
- GWFMs use atypical parameters for Hawaii aquifer
  - If retained, in-depth justification needed
- GWFMs do not use CSM geologic details – SSPA work
  - Impact of heterogeneity needs detailed evaluation
- GWFMs do not comport with natural g.w. tracers
  - Complex distributions may imply multiple source waters
- GWFMs capture zones not supported by field data at pumping rates similar to those modeled
  - Approaches used may overestimate capture potential
  - Gradient issues & complexity not covered
- The current GWFMs are not reliable for decisions
  - For CF&T, risk analyses and mitigation decisions
- Modifications will be needed (SSPA work follows)

Ongoing Issues with the Navy CSM

The CSM being the fundamental basis for the Navy GWFMs, future CF&T/Risk Evaluations and the overall key conditions at the Red Hill Bulk Fuel Storage Facility

The Hawaii Hard Rock Release Experience

Sourc (b)(6) [redacted]

- Fuel releases often move quickly
  - Typically in complex pathways
    - Primary & secondary transport
  - Often difficult to characterize
- Fast-track/other geologic features exist
  - Lava tubes, voids, fractures, clinkers
  - Confining beds & non-volcanics
  - Preferred & random orientation scales
  - Often sparse distribution, large effect
- Weathering of rock is complex
  - Bulk rock properties may not apply
- For Red Hill
  - How is the architecture arranged?
  - How will fuel behave within that?
  - Effects on capture/remediation?
  - All relates to g.w. protection goals
    - And sole source aquifer preservation

Overview – Unresolved CSM Issues

Source (b)(6)

- Red Hill is under-characterized
  - Compared to similar sites
  - Results in high uncertainty in the CSM
- Complex geology is noted in CSM
  - But, simplified in GWFMs
  - Insufficient basis for appropriate CF&T
  - G.W. & CF&T behavior appears more complex
- Data indicate TPH beyond RH Ridge
  - CSM interprets these as artifacts (generally)
- CSM interprets LNAPL migration to SW
  - But available data indicate otherwise
- CSM indicates fuel retained ~ 30-ft depth
  - Not supported by available data
- Fuel retention characteristics are unknown
  - Fuel/NAPL parameters inapplicable
  - Geometry unconstrained by data
  - Dynamics are critical to g.w. protection
- Many other issues remain
- In total, CSM is not reliable for g.w. protection

Example Navy CSM Cross-Section

(schematic rendering, but details are not in GWFMs)

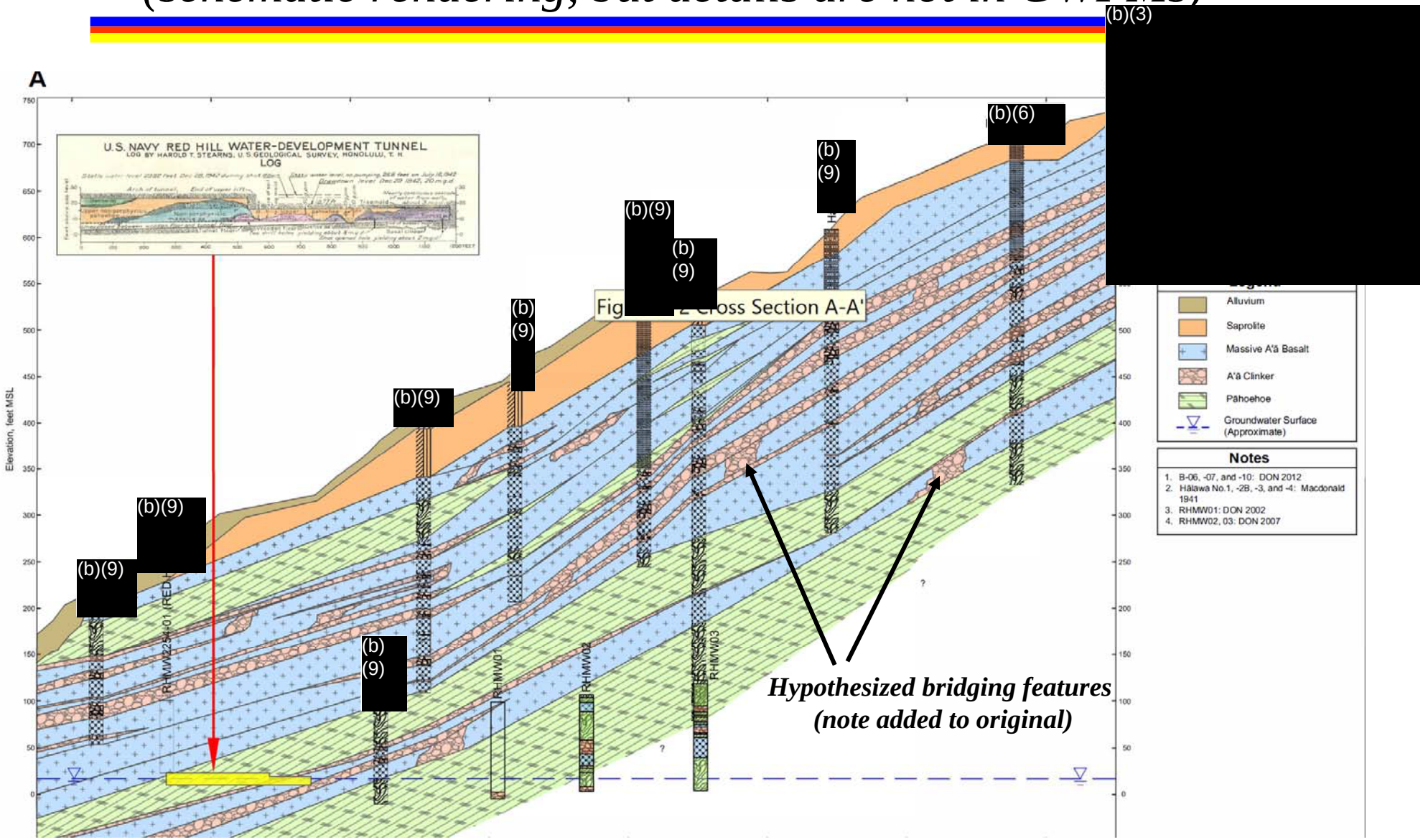

Source: Red Hill Conceptual Site Model Report, Rev 01, June 2019

Navy 3D Lithologic Model – Barrel Logs

(same issue, (b)(6) will address)

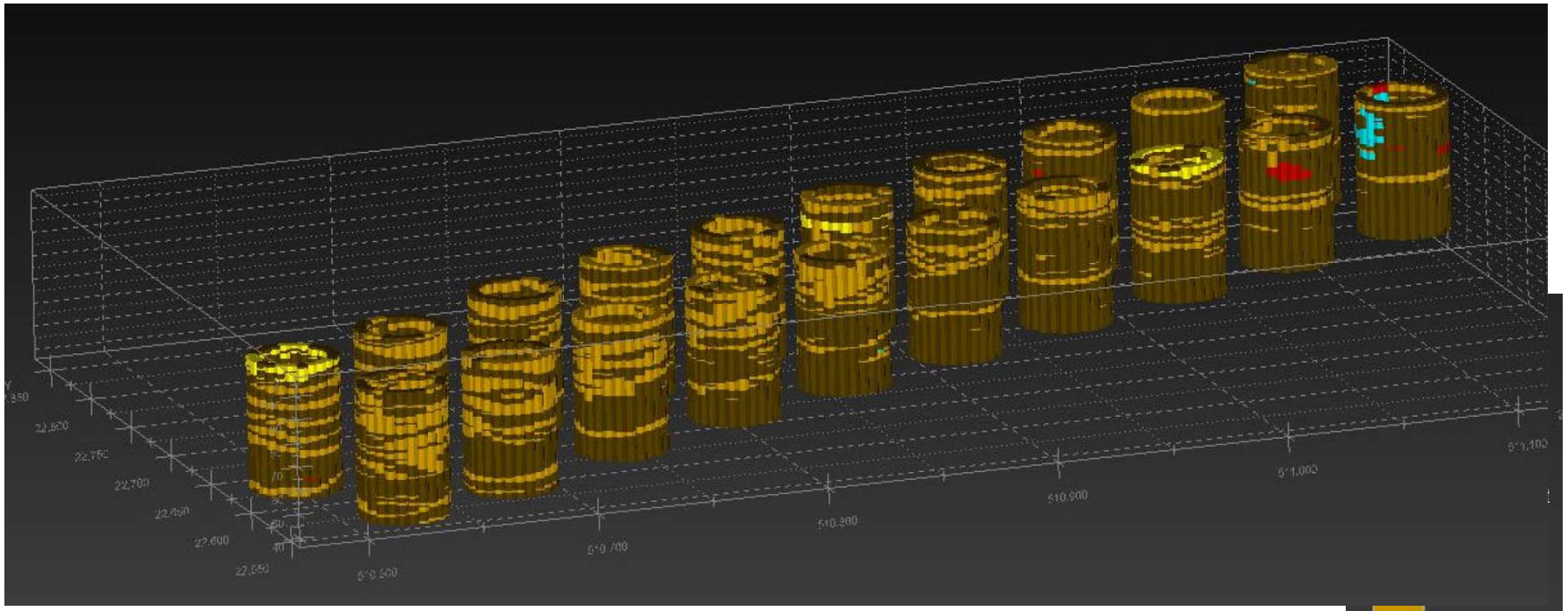

Source: Red Hill Conceptual Site Model Report, Rev 01, June 2019

Outcrop Interpretation – (b)(9) (UH)

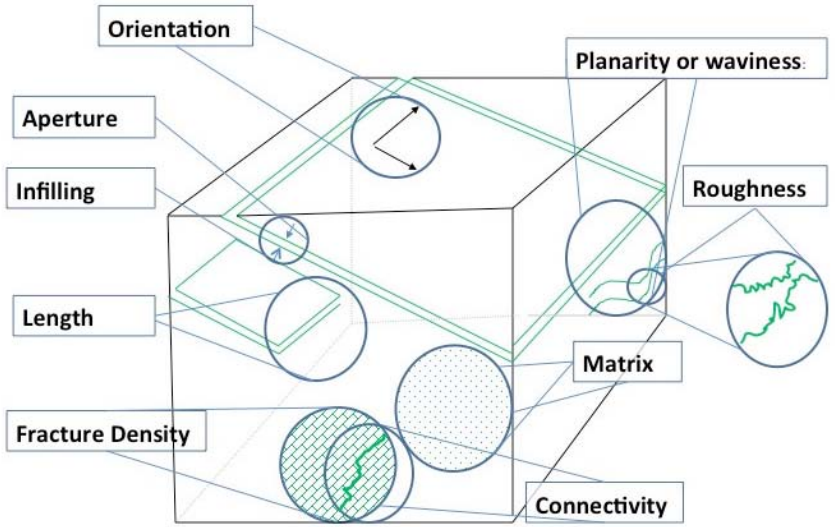

Source: ITRC, 2017

Complex NAPL Distribution in a Fracture

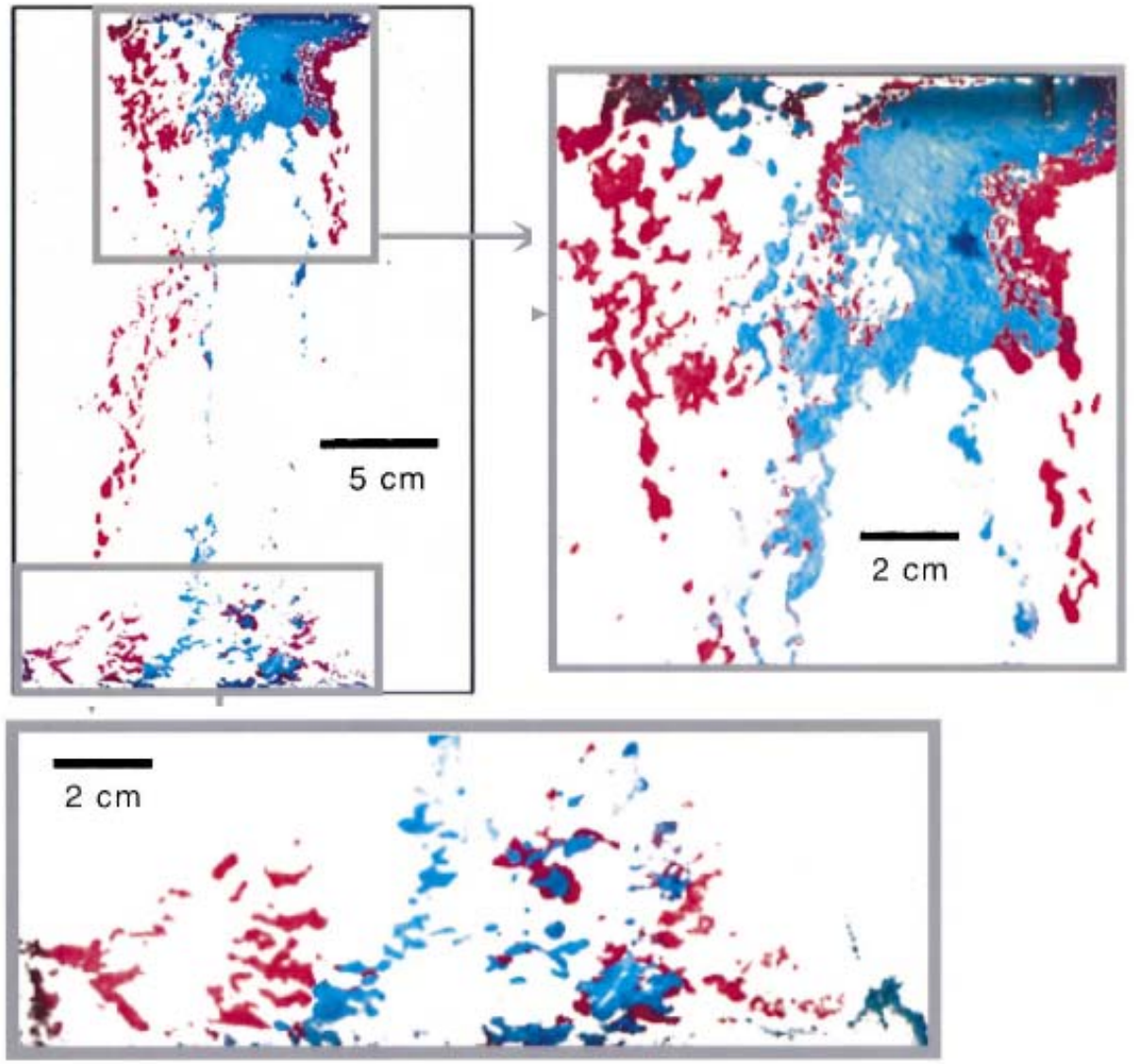

Geller et al., 2000

Lab vs. Field Scale – Permeability

(Site lab data are not comparable to field scale)

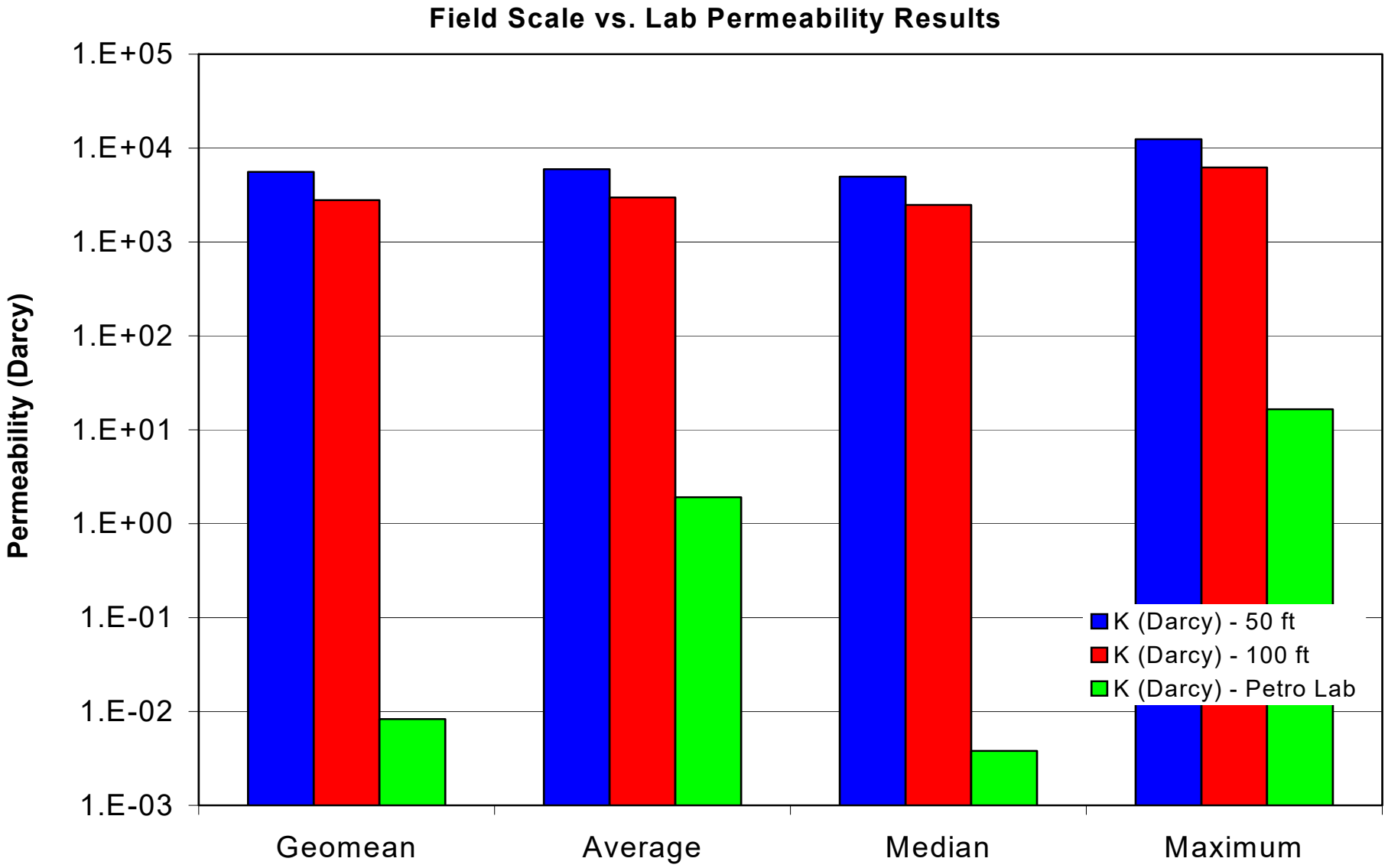

Data source: Conceptual Site Model, June 2019, Rev 01

Summary of CSM Review (to date)

(broad issues, other details pertain)

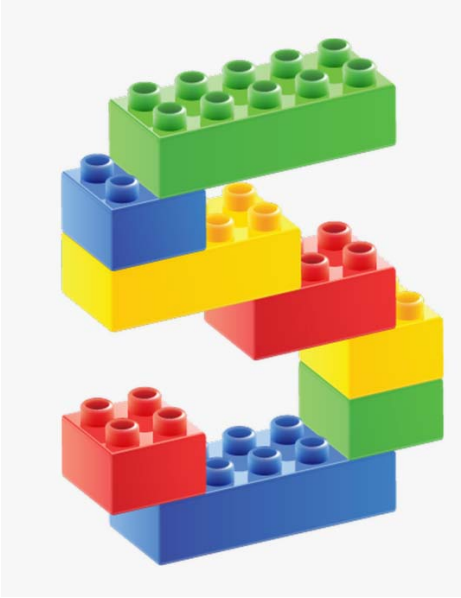

- Issues have been ongoing, unresolved by new data
  - Or interpretations unconstrained by available data
- The site is not well characterized – (safety concerns)
  - Fate of 2014 & 2021 releases are undelineated
  - Data suggest fuel has reached the water table under RH
- Geologic complexity noted in CSM
  - But not explored at the needed level of detail
  - No assessment of EPM scale or applicability
- Groundwater flow paths and behavior is uncertain
- Distal detections are considered generally valid
  - Reported by certified labs & independently validated
  - There is TPH-range mass in GCs
  - Detections are consistent with other data/patterns
- NSZD rates are likely overestimated & uncertain
  - RHM(b)(9) & RHM(b)(9), net thermal profiles, no NAPL
  - Plume size and character likely larger than estimated
- The whole of the RH Tank Farm has likely had releases
  - CSM does not account for long & variable fuel history
  - And those implications for CF&T/risk/mitigation

Implications of CSM Concerns
(relative to groundwater protection matters & TUA)

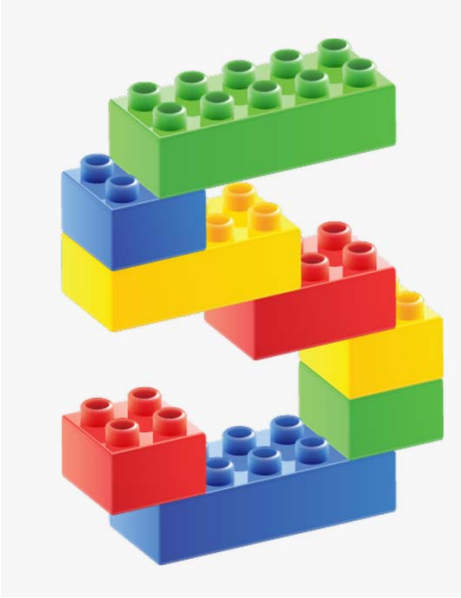

- G.W. capture of releases is not demonstrated
  - By field data or adequately by GWFMs
- NSZD may not be reliable as a cleanup method
  - RHM(b)(9) interpreted impacts remain > 20 yrs
- G.W. protection depends on several factors
  - How fuel migrates under release conditions
  - Speed and effectiveness of release detection & actions
  - Cannot be addressed by GWFMs alone
- Capture may not be an appropriate G.W. remedy
  - Fuel migration & remedy must be aligned
  - Capture is not a cleanup method – relies on uncertain NSZD
  - ***<u>However, g.w. treatment may protect water services</u>***
- (b)(3)(b)(3)(b)(3) is indicated to be at risk from releases
  - Proximity & low-level TPH detections (including July 2021)
  - Dilution & NSZD make this both surprising & concerning
- Risk evaluations must be connected to a conservative CSM
  - Presently, there is insufficient conservatism in the CSM
  - Along with high uncertainty that is not addressed

Appendix C: Responses to Regulator Comments and Correspondence from Regulators

- Responses to Regulator Comments, 2024-04-16
- Responses to DOH Comments, 2024-08-20
- DOH letter: Insufficient Time to Review Draft GWM Report, 2024-08-20
- EPA letter: Deferral of Review of Draft GWM Report, 2024-08-20

Response to Regulatory Agency Comments on Navy Proposal To Use Total Petroleum Hydrocarbon as Diesel Fuel (TPH-d) as a Model Calibration Metric, dated April 16, 2024

1. General: The presentation is a useful discussion of TPH and other fuel constituent data. The discussions and comments provided here are intended to be constructive and help continue the discussion.

Navy Response: We appreciate the comments provided and value the input of additional technical expertise in interpreting these complex data sets.

2. General: Given the recently completed defueling, emphasis in terms of the conceptual site model (CSM), long term monitoring (LTM), and risk should be on change vs. mobilization vs. migration. For example, some changes may represent remobilization but not migration.

Navy Response: We agree that future groundwater quality data collection and interpretation, coupled with prospective modeling, should focus on changes in chemical occurrence and other site conditions that could indicate movement of current potentially mobile LNAPL and/or dissolution and subsequent migration of LNAPL constituents.

3. General: The fate and transport (F&T) scenario described under Item 10, below is a useful exercise for which the Navy should perform an objective investigation. Data currently presented by the Navy show inconsistencies in the interpretation, and the use of processed data for model calibration masks important features of the apparent breakthrough curves. This proposed scenario requires further work and discussion.

Navy Response: We agree that additional investigative work to support the conceptual model provided in the presentation is needed. The purpose of the presentation was to frame the issue of using TPH-d for model calibration, and we anticipate additional discussion and analysis. As explained below, the simulations of TPH-d described in this report have already had an effect on the conceptual model. Because of the scheduled deadlines, we have proceeded to use these TPH-d data for model calibration for the simulations in this report, but we remain open to alternative explanations for the observed TPH-d data and the use of other physically consistent datasets for model calibration should they be identified.

4.May/November 2021 Comparison: Comparison of the May and November 2021 events and data is valuable and appropriate. However:

- ***a. With regard to the May 2021 release: the chance o(b)(3) ying on a migration path is negligible, and it seems implausible for the documented net-to-ground mass of the May release to have created these responses.***
- ***b. Regarding increases post-November 2021 a(b)(3) n particular: ascribing most to lab issues suggests historical data values ranging from 1,000 to 5,000 are potentially rendered "the same," presenting challenges to interpretation of breakthroughs/transport. There may be more plausible explanations.***

Navy Response:

a. The current conceptual model of quasi-down-ridge flow of groundwater carrying TPH to RHM(b) and RHM(b) from a release at RHM(b) is a working hypothesis, although the simulations described in this report have demonstrated its likelihood. As DOH indicates in comment 3 above, there is additional investigative work to be

performed to verify the conceptual model. In fact, simulations with the current flow model documented here suggest a source other than release to groundwater at a single well-defined area near RHM(b) . Those mechanisms include transport of TPH in vapor with subsequent dissolution into groundwater, preferential flow paths of the (b) to the water table, entrainment and/or dissolution of (b) in wash water used in the cleanup, and mobilization of dissolved TPH by precipitation events from existing residual LNAPL. At this time, it is not clear how the apparent TPH pulse seen at the three tank farm wells originated.

The somewhat simultaneous breakthrough curves at RHM(b) and RHM(b) , and their respective concentrations support the concept that they are either attributed to LNAPL and/or wash water which reached the water table at various point along the axis between RHM(b) and RHM(b) . In our opinion, the most likely indication of saturated zone transport is the subsequent breakthrough curves at RHM(b) and RHM(b) , which is supported by their timing and the consistency of the chromatograms. The CF&T modeling focused on these two wells for calibration.

We should clarify that we do not maintain that these three wells lie directly downgradient from each other on a single flow line (migration path). Wells can be impacted by a source even if they do not lie directly on a downgradient flow path. Dispersion, changing groundwater gradients, and preferential flow paths all cause spreading of chemicals in groundwater that can cause impacts to wells that are oblique to the average advective flow path. Note that prior to the November 2021 release, (b) cycled on and off one or more times most days. This cycling would have frequently shifted gradients. The current flow model predicts that there is a significant component of flow that occurs generally down the Red Hill Ridge, but this flow path is somewhat oblique to the line that extends through the three tank farm wells. Model simulations results indicate that a plume at RHM(b) would migrate to the northwest of RHM(b) and not likely appear at the well, whereas a plume passing through RHM(b) would likely pass through RHM(b) , but travel slightly off axis from the two wells.

The exact volume of LNAPL that was released in the May 6, 2021 release is not known. While the current estimate is that it is small and cannot be calculated, additional factors such as use of surfactants in cleanup, contact of wash water with residual LNAPL already in the subsurface, and vapor migration can cause even a small release volume to create detectable groundwater impacts. For example, our calculations indicate that there is sufficient soluble TPH mass in a relatively small, 100-gallon volume of (b) to create the observed concentrations, as detailed below.

One hundred gallons of (b) contains approximately 4.4 kg of soluble (b) components. This soluble component mass could have been supplemented by dissolution of residual LNAPL by surfactant-containing wash water used in the cleanup following the release. A 4.4-kg mass is sufficient to create an average TPH concentration of approximately 8,000 µg/L in a groundwater plume 200 ft long, 100 ft wide, and 10 ft deep with a porosity of

0.1. If dissolution of degradation products or slightly soluble components of LNAPL constituents outside of the TPH-d range are added to the soluble (b) fraction, concentrations in a plume of these dimensions could be higher. Therefore, it is possible for even the limited release of (b) to result in the observed changes in groundwater concentrations.

Of course, both the true volume of LNAPL released and the dimensions of the affected part of the aquifer are not known. But this simple calculation does indicate that a relatively small (b) release has the potential to impact a volume of groundwater that is of the same order of magnitude as a likely "pulse" plume that would have resulted from a release using the current conceptual model.

A second method of assessing whether the (b) release could have caused the observed impacts is to integrate the breakthrough curve. Again assuming a 100-ft wide, 10-ft deep volume of groundwater present in the formation with a specific discharge of 10 ft/d, approximately 0.55 kg of additional TPH appeared in RHM(b) between May 6, 2021 and December 15, 2021. This mass is approximately 12% of the 4.4-kg soluble component fraction, and again indicates that it is possible for a 100-gallon release of (b) to create the concentrations observed in the tank farm wells, and at RHM(b) in particular.

b. To clarify, the increase in concentrations at RHM(b) following the November 2021 release are not ascribed to laboratory issues, but to potential leaching of in-place LNAPL by precipitation. We do agree that the post November 2021 changes in TPH concentrations within the tank farm wells are unlikely to have been caused by the May 6, 2021 (b) release or the November 2021 release in the release in the (b)(3) Tunnel. We are currently investigating other explanations for the increase in TPH-d in tank farm wells following the November Adit 3 Tunnel release. We agree that it is likely that this increase, and similar increases in the past, are the result of a different, yet to be identified mechanism(s). At this time, our best theory is that the increases are the result of precipitation events that mobilized degraded LNAPL constituents in residual LNAPL in the vicinity of the well.

5. Slides 24, 65, 85, and 86: Only Slide No. 24 shows TPH-d for RHM(b), RHM(b), and RHM(b) on the same graph and makes comparison of non-normalized concentrations difficult. The displayed concentrations are not consistent with other graphs showing non-normalized concentrations (Slide Nos. 65, 85, and 86).

Navy Response: There is an error on the display of TPH-d for RHM(b) on slide 24. The TPH-d after silica gel cleanup was inadvertently plotted instead of the TPH-d concentration. We apologize for the error and any confusion that it may have caused.

6. Slide 24: The attached figure compares Slide No. 24 graph (a) with graph (b) which was generated by the RAs and corrects the TPH-d concentrations for pre-release concentrations.

Response to Regulatory Agency Comments on Navy Proposal To Use Total Petroleum Hydrocarbon as Diesel Fuel (TPH-d) as a Model Calibration Metric, dated April 16, 2024

a. Graph (a) and the subsequent graphs with the normalized TPH data fail to provide critical information needed to assess TPH at a tracer for model validation.

b. Graph (b), if presented, would have raised serious questions about the value of TPH for model validation/calibration.

i. These serious questions should have been addressed prior to presenting to the RAs.

ii. A more comprehensive internal review of products prior to delivering to the RAs will shorten the regulatory review time, not to mention the overall project schedule.

a.)

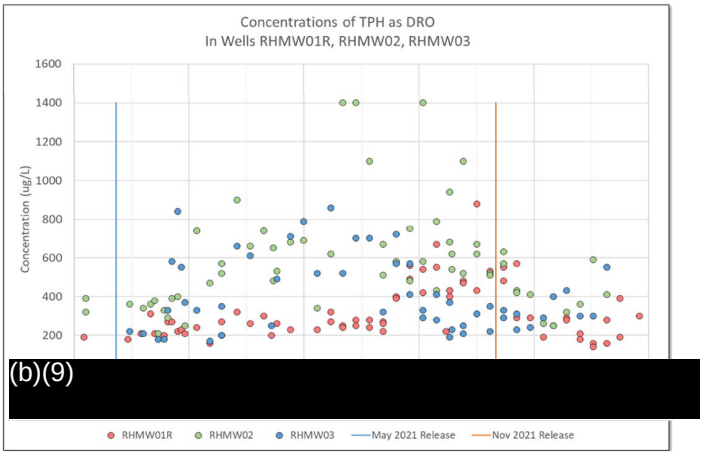

b.)

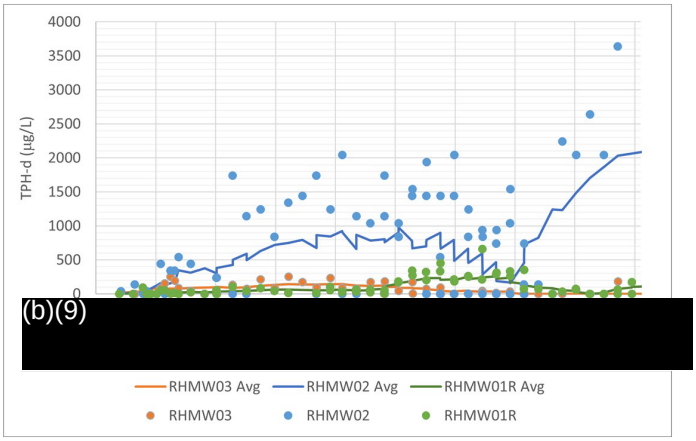

Navy Response: We concur that the plot created by the RAs is the correct representation of the TPH-d data in wells RHM(b) , RHM(b) , and RHM(b) . But we believe that this error does

not affect the interpretation of the data. As acknowledged by the EPA in comment 5, the correct concentrations of TPH-d were plotted on slides 65, 85, and 86. The correct concentrations are also shown in numerous other slides, including slides 32, 33, 46, 52, 64, 69, 75, and 78.

We strongly disagree that the incorrect plot on slide 24 fails to provide critical information needed to assess TPH as a tracer for model validation. The salient point of slide 24 is that the breakthrough curves for these three wells are difficult to discern because the concentrations are both highly variable and of a different magnitude. The correct RA plot makes the problem of comparing concentrations of different magnitudes much more apparent than the incorrect plot on slide 24, and provides an even stronger rationale for normalizing and smoothing the data by plotting moving averages.

The normalized concentrations were used only to compared timing of the breakthrough curves and were not used as calibration targets. Normalized breakthrough curves allowed for assessment of the timing, which eventually led to the conclusion that the sources at RHM(b) and RHM(b) were likely either a dispersed source from the same release or related to separate source. This concept was later supported with model simulations that showed TPH concentrations at RHM(b) either attenuating through advection/dispersion or migrating to the northwest of RHM(b).

We also strongly disagree that serious questions are raised by the RA plot. As explained in the presentation and in the comment responses herein, there is considerable uncertainty regarding the cause of the TPH-d signals observed in the three tank farm wells. Because the exact cause and migration mechanisms are unknown, the timing of these apparent breakthrough curves is the salient observation, particularly in associating saturated zone transport with the breakthrough curves between 02 ad (b).

As EPA indicated in comment 4a above, it is unlikely that the three wells lie directly on the same flow path, so that differences in the magnitude of concentrations are expected. TPH is carried to wells that are further away from the central flow line by dispersion and/or other factors, and would naturally exhibit much lower concentrations than wells that are more directly in the path of average migration.

As stated in the presentation verbally and on slides 31, 37, 42, and 49, evidence is mixed as to whether TPH-d concentrations in any of the tank farm wells are related to each other and to the May 6, 2021 release. Recent additional analyses explained in this report suggest that the TPH-d in RHM(b) may be from a separate source than the TPH-d in wells RHM(b) and RHM(b). Nevertheless, the timing of the breakthrough curves seen at wells RHM(b) and RHM(b), and possibly at RHM(b), do suggest TPH-d migration from an event that can be used to assist in calibrating certain parameters in the mass transport model.

We regret that the incorrect plot was shown on slide 24 and that it extended regulatory review time. EPA's suggestion of additional data QA/QC is appreciated. We suggest that in the future, the RAs contact the Navy experts directly to resolve apparent discrepancies of this type, as they may be easily rectified.

7. Slide 92: Initial Navy Comment: Do you agree that the apparent breakthrough curves are consistent with down-ridge TPH migration from the May 6, 2021, release and can be used for model calibration? This is currently the only dataset that we have identified that is suitable for model calibration. Are there other datasets that you would suggest are suitable for model calibration?

RAs' Response: *There are many challenges with using the TPH-d data to calibrate a model. Primarily these are:*

a. *The apparent contaminant mass in the plume is greater than the "small (not calculable)" mass stated in Slide No. 23 for the May 6, 2021 release. If mobilization of pre-existing contamination is used to explain the mass differential, then the point of release is no longer that which occurred on May 6, 2021, but where that re-mobilized contamination was located which could be down dip in the vadose zone.*

b. *To expand on the statement above, the mode of transport, time, and point of impact with water table are unknowns. How is the plume migration to be partitioned between vapor phase transport, light non-aqueous phase liquid (LNAPL) transport, vadose zone dissolved phase transport (all the preceding can't be simulated with the Best Available Model (BAM)), and groundwater dissolved transport (which can be simulated with the BAM)?*

c. *Normalization of the data in Slide No. 27 masks an important consideration in plume assessment. The relative peaks TPH-d concentrations need to be considered when evaluating whether the TPH-d traces indicate movement of a contaminant plume from the point of release at the upper part of the tank farm down to and including RHM(b)). Typically, a plume's maximum concentration would decrease while the length of the plume would increase with down gradient movement due to dispersion and degradation. Adjusted for pre-plume arrival the maximum TPH-d concentration at RHM(b) is about 130 micrograms per liter (µg/L) much less than the 310 µg/L maximum at RHM(b)). RHM(b) adjusted maximum concentration is about 1,100 µg/L. These relative plume maxima are inconsistent with the Navy's hypothesis of a plume reaching the water table upslope of RHM(b) then migrating down ridge to RHM(b)).*

d. *The Navy's conclusion that the increased rate of TPH-d detections in the perimeter wells was not associated with either the May 6th or the November 21st releases needs to be revisited. If the TPH-d data for RHM(b) were graphed using the same methodology as shown on Slide No. 27, an apparent breakthrough curve would result for this well. For several perimeter wells, there was a significant increase in the rate of TPH-d detections following the May 6th release. If these detections are unrelated to the release, then a credible alternative needs to be provided.*

e. *The uncertainties described above make any meaningful model calibration very challenging. The post May 6th TPH-d data are not well enough constrained for model*

calibration. It needs to be one of the lines of evidence considered in the modeling process but is not solid enough to be the primary calibration metric.

f. There appear to be multiple breakthrough curves at some locations, staggered in time and by other characteristics (e.g., bailer samples vs low-purge vs silica gel clean-up [SGC]).

g. Use of a moving average may confuse "true" versus "apparent" artefactual breakthroughs.

Smoothing gives the impression of classic migration-related breakthrough via lateral transport, but averaging combines high peaks and non-detects (NDs).

Navy Response:

a. As explained in the response to comment 4 above, the exact quantity of LNAPL released is unknown. Based on a hypothetical 100-gallon release of (b) , sufficient soluble TPH-d components would be present to create the observed concentration in RHM(b) , which exhibited the highest concentrations. Sufficient mass notwithstanding, we agree that it is certainly possible that LNAPL remobilization, or more likely, dissolution of components from residual LNAPL, is responsible for the observed TPH-d breakthrough curves, especially at RHM(b) .

   We also agree that the point of introduction of TPH-d into the groundwater may not coincide with the original (b) release location. The mass transport modeling described in this report seems to indicate that the location of TPH-d introduction to groundwater may have been further from RHM(b) than initially assumed. The source location has a strong impact on the concentrations at generally downgradient wells, and the source location could be responsible for the considerable variability in tank farm well TPH-d concentrations.

b. We agree that the mode of transport, timing, and point of impact are unknown. However, explicit simulation of LNAPL and vapor transport is not necessary for mass transport model calibration in the saturated zone. The TPH-d breakthrough curve at RHM(b) may not be the result of groundwater transport. However, the breakthrough curves at RHM(b) and RHM(b) appear consistent with solute transport of TPH-d from a location near RHM(b) and onward to RHM(b) . We base this conclusion on the similarity of constituents, the fact that vapor concentrations were very low at RHM(b) , and the timing of the breakthrough curves.

   The result of the mass transport simulations described herein indicate that groundwater transport alone can explain the part of the TPH-d concentrations observed at RHM(b) and RHM(b) immediately following the May 6, 2021 release that was the focus of the SPM presentation. As noted in the presentation on slide 87, the goal is to calibrate the groundwater transport model, so that TPH-d migration that was more likely to be caused

by vapor transport, LNAPL transport, or phenomena other than transport in groundwater are not explicitly simulated.

c. We agree that the relative concentrations at RHM(b) , RHM(b) , and RHM(b) are not consistent with a release directly upgradient of RHM(b) with subsequent flow to RHM(b) and RHM(b) along a direct flow path. The low TPH-d concentrations in RHM(b) suggest one or more of the following scenarios:

- The surface release occurred upgradient or cross-gradient of RHM(b) , but subsequent migration of the jet fuel and/or wash water in the vadose zone largely bypassed RHM(b) on its way to the groundwater.
- The relatively low TPH-d concentrations in RHM(b) , which is closest to the release's location, are caused by vapor partitioning into groundwater near or upgradient of the well and are not caused by transport of TPH-d in groundwater.
- Jet fuel released at the surface migrated in the vadose zone to a point downgradient of RHM(b) .

Because the relationship of TPH-d concentrations at RHM(b) to concentrations at the other two tank farm wells is equivocal, two separate conceptual models were used: one with an elongated source between RHM(b) and RHM(b) , and another with two separate sources. These two conceptual models exhibit similar saturated zone behavior between RHM(b) and RHM(b) , and account for several potential conceptual models which cannot be directly simulated. TPH-d data from only RHM(b) and RHM(b) , which appear to be more chemically similar, is sufficient to assist in the calibration of certain transport parameters. For calibration purposes, knowledge of the exact cause of the concentration breakthrough curves is desirable but not necessary. The only requirement for the TPH-d data to be useful in calibration is that its occurrence at two locations be related through solute migration from a specific release event in time.

d. There are very significant differences in the pattern of TPH-d detections between the tank farm wells and the perimeter wells, including RHM(b) . To help illustrate this point, TPH-d concentrations in the three tank farm wells and RHM(b) are plotted on Figure C-1 (attached). In wells RHM(b) and RHM(b) , TPH-d concentrations in the period that is suggested for calibration (June 2021 to December 2021 for RHM(b) ; October and November 2021 for RHM(b)) are nearly all detections, with a few J-values. With the exception of a single low J-value in RHM(b) , the TPH-d concentrations show a distinct pattern of continuous elevated concentrations. The concentrations in RHM(b) are less consistent, but still show a distinct period of elevated concentrations preceded and followed by lower concentrations.

On the other hand, concentrations of TPH-d in RHM(b) are mostly non-detects or J-values that are significantly less than the detection limit. The two detections in January 2022 are separated from earlier TPH-d detections by at least fifteen non-detects. These

January 2022 detections do not represent any kind of obvious breakthrough curve. The two detections in December 2021 (two of the data points represent duplicate samples) are separated by 1 week, and are preceded and followed by much lower J-values and non-detects. It is possible that these two detections, and the low J-values before and after them, are a very weak signal of the May 2021 release. However, the low magnitude and number of detections in RHM(b) make the data reliability difficult to ascertain, so that they are much less useful for model calibration. The nearly random detections of TPH-d in other wells indicate that the TPH-d detections are unrelated to the May 2021 release, although some could be related to past fuel releases at the tank farm.

Professional judgment must be used to determine if a smoothing method such as moving averages is appropriate for each individual dataset. Moving average plots of TPH-d in the three tank farm wells and RHM(b) are provided in Figure C-2 (attached). Because of the uniformity and persistence of detections in the calibration period for the tank farm wells, the moving averages plot as relatively smooth curves. The curves incorporate a period in which nearly all of the concentrations were either detections or elevated J-values. The moving average plot of RHM(b), on the other hand, cannot be plotted because it incorporates sparse detections that are widely separated in time from the two detections following the November 2021 release. The moving average plots are representative of the TPH-d data from the tank farm wells, but the trend in TPH-d detections in RHM(b) is not well-represented by a moving average, so using a moving average to draw conclusions about TPH-d breakthrough in this well is not appropriate.

Although we disagree that TPH-d concentrations in any of the perimeter wells represent breakthrough curves that can be confidently attributed to the May 2021 (b) release, we acknowledge that the cause(s) of the sporadic detections of TPH-d in the perimeter wells is not known. There is a possibility that the sporadic detections are related to recent or historical LNAPL releases at the tank farm. However, because these sporadic detections occur at many different distances and directions from the tank farm, and cannot be simulated as resulting from groundwater transport without invoking numerous hypothetical source boundary conditions, the perimeter well TPH-d data was not used for model calibration.

There are literally thousands of potential causes of TPH detections unrelated to petroleum releases, including the possible sources listed on slides 64 and 80 of the presentation. Given the non-specific nature of TPH analyses and the large number of possible sources, it is not possible to definitively explain every TPH-d detection in perimeter wells. Instead, the Navy is following a more practical approach by examining each TPH-d detection in perimeter wells to determine if the TPH-d detections are attributable to releases of petroleum products from the tank farm using multiple lines of evidence. These lines of evidence include, but are not limited to the following:

- Whether the characteristics of the TPH-d analysis chromatogram are consistent with a release of the types of petroleum products stored at the tank farm, including the

effects of weathering and conversion of raw fuel components to polar degradation products.

- Identification of individual chromatogram peaks as known non-hydrocarbon products (e.g., DEET, pesticides, herbicides, cleaning products).
- Whether there is a feasible migration pathway for the detected TPH-d to reach the perimeter location (these pathways include vapor transport, LNAPL transport through preferential pathways, and transport in the vadose zone pore water, among others).
- Conditions near the time of the detection that could have contributed to the detection (e.g., following a release, following a precipitation event, other elevated detections in nearby wells).

e. We agree that there are many uncertainties regarding the TPH-d data. However, we disagree that the data are not sufficiently constrained for use in model calibration. Although the source of TPH-d is uncertain, the tank farm wells, with the possible exception of RHM(b) , clearly show a pulse of TPH-d in the groundwater. This pulse is consistent with travel in groundwater from RHM(b) to RHM(b) . To calibrate a model, the specific cause of the concentration pulse is not required; only the timing. The exact sources and subsurface travel paths are never known with certainty in mass transport modeling, and the TPH-d dataset at RHM(b) and RHM(b) is the only dataset yet identified that can be used to calibrate a groundwater transport model. The simulations described in this report demonstrate that calibration using the TPH-d dataset leads to realistic values of dispersivity and effective porosity. While the calibration cannot be said to be unique, it is a reasonable initial calibration that can continue to be refined as additional data become available. Additional lines of evidence to determine the validity of the TPH-d data for model calibration will continue to be investigated.

f. We agree that other characteristics such as sampling method can cause variation in TPH-d concentrations that add challenges to the data interpretation. The tank farm wells show multiple periods of elevated TPH-d concentrations, but with the exception of the increased TPH-d concentrations at RHM(b) following the November 2021 release, these concentrations are not as consistent as the breakthrough curves following the May 2021 release. Elevated concentrations during other time periods are interspersed with non-detect and low J-values that are not consistent with a pulse of TPH-d migrating in groundwater. The cause of other periods of elevated TPH-d concentrations in tank farm wells is the subject of on-going analysis. The most likely cause identified to date is dissolution of residual LNAPL and/or its more soluble degradation products in the vadose zone by infiltrating water after precipitation events .

g. The moving average concentrations are simply a tool used mainly to detect breakthrough curves that are less apparent from unsmoothed data. The moving averages are relatively faithful to breakthrough time because they are central moving averages rather than

leading or trailing moving averages. We acknowledge that moving averages are not a perfect reflection of the underlying data because samples were not collected at uniform intervals. Nevertheless, they are extremely useful for identifying concentration trends and comparing breakthrough curves of different magnitudes. It should be noted that the transport models inherently smooth the concentrations spatially and temporally, so that simulated concentrations can often match smoothed data better than individual data points.

The moving averages at RHM(b) and RHM(b) in the periods used for model calibration include J-values and detections, but no non-detects. Although J-values are an imperfect substitute for actual detections, the J-values tended to follow the same trend as the detections in these two wells and are considered representative. The RHM(b) data moving average is less rigorous, and includes one non-detect as well as many J-values. The many J-values in the breakthrough curve in RHM(b) are another reason why this dataset is less useful for model calibration.

8. Slide 92 Initial Navy Comment: Given the sparsity of specific chemical data, do you think that other chemicals are better than TPH-d for CF&T simulations?

RAs' Response: *The RAs have previously suggested using general and isotopic chemistry to better constrain the model boundary fluxes. Attempts to date by the Navy to implement this suggestion have been insufficient. We suggest you consider this approach; while it will not "calibrate" the model this approach will fall in the "to be considered" recommendation that we are making for using the TPH-d data.*

Furthermore, the following data may be useful to screen data suitable for model "collaboration" from data that are not useful for this purpose:

- *Temperature*
- *Dissolve Oxygen (DO)/Oxidation-Reduction Potential (ORP)/pH*
- *Chlorides/conductivity*
- *Nitrite/Nitrate*

Navy Response: General and isotopic chemistry are useful for flow model calibration, but do not provide information needed for contaminant fate and transport modeling. To be useful for CF&T modeling, concentration observations must be tied to a specific event in time, even if the exact nature of the event is uncertain.

We appreciate the suggestion of temperature, DO/ORP, chlorides/conductivity, and nitrite/nitrate for model calibration. However, like isotopes, these parameters are not introduced into the aquifer from a source that is well-defined space and time, and so cannot be used directly for model calibration. They can, however, be used to assess the usefulness of other data for calibration as suggested. For example, the DO/ORP data can be used to characterize the type of

biodegradation (or the lack thereof) that could explain differences in the nature of TPH-d at specific locations. Depletion of nitrite/nitrate and increases in temperature may similarly suggest on-going TPH transformations that can be considered.

9. Slide 92 Initial Navy Comment: Do you have suggestions on what other factors may be contributing to the observed concentration increases and sporadic detections in perimeter wells?

RAs' Response: *The following is a partial list of factors under consideration by the RA SMEs:*

- *Sheen/film transport of product (primarily from any fresh releases),*
- *Undocumented releases and other hydrocarbon sources, including oil waste and bunker fuel,*
- *Entrainment of other organics under high precipitation events (well integrity?),*
- *Infiltration of drilling fluids/grout (pH v. TPH correspondence),*
- *Further analysis of DO and other indicators obtained via the multi-parameter dataloggers may help identify transport/relative mass, e.g.:*
  - *Background DO - vapor/local recharge impacts, low mass, quick degradation.*
  - *Depressed DO - substantial mass present/migrating, consistent detections.*

Navy Response: We agree that the sources listed above are potential causes of TPH in perimeter wells. We would add to this list other anthropogenic and non-anthropogenic sources of compounds that elute as TPH-d in wells, including the following:

- Petroleum carriers for pesticides or herbicides
- Propellants in spray products
- Cosmetic products
- Incidental spillage of gasoline or diesel from commercial equipment (e.g., landscaping)
- Compounds associated with sampling equipment
- Naturally occurring organic matter (e.g., humic acids)

10. Slide 92 Initial Navy Comments:

a. May 6, 2021, release caused rapid vapor migration down Red Hill ridge.

RAs' Response: *Then early arrivals could not be used to calibrate saturated zone model parameters.*

b. Released jet fuel mixed with existing LNAPL in the vadose zone, and some may have reached the water table fast.

RAs' Response: *This may have been enhanced via cleanup efforts/flushing activities.*

c. The released jet fuel was subject to rapid weathering through degradation and evaporation.

RAs' Response:

- *Some newly released LNAPL may have been mobilization by a large precipitation event.*
- *Perhaps, although post-SGC values fell after precipitation, and it is possible that rain may also result in dilution.*

d. TPH-d and total petroleum hydrocarbons as oil (TPH-o) migrated in groundwater down the Red Hill ridge.

RAs' Response: *Perhaps, but the net mass-to-ground mass reported for the May 2021 release appears insufficient to cause the observed breakthrough after the significant volatilization and degradation noted above.*

Navy Response:

a. We agree that early arrivals potentially caused by rapid vapor migration, LNAPL transport, or mechanism other than flow in groundwater cannot be used for model calibration. As indicated on slide 87, we recognize that the current model cannot simulate vapor transport so that modeling is focused on the center of mass in the saturated zone and not the early arrival of TPH-d.

b. We agree that rapid transport of (b) constituents may have been exacerbated by surfactants used in the cleanup effort. Surfactant-containing water may also have either partially mobilized residual LNAPL or caused dissolution of sparingly soluble (b) compounds and/or degradation products in the vicinity of the release.

c. It is possible that newly released LNAPL was mobilized by one or more large precipitation events, or that historical residual LNAPL was dissolved by these same events. These events may be a cause for recurring elevated TPH observed in the tank farm and perimeter wells. We are currently investigating that possibility.

Although dilution in either the vadose zone or in the saturated zone likely resulted in lower concentrations of TPH-d appearing in the tank farm wells, dilution itself is not an indication of weathering. On the other hand, the TPH-d concentrations before and after SGC are clear indications of weathering by biodegradation because there is very little non-polar material in fresh (b). TPH-d-SGC concentrations averaged about 25% of TPH-d in RHM(b) samples during the calibration period. The TPH-d-SGC

concentration average is about 20% in the RHM(b)) calibration period, indicating a similar degree of weathering. These data suggest extensive weathering of LNAPL, whether it was sourced from fresh product that underwent rapid weathering, or mobilization of polar constituents from residual historically released LNAPL.

d. As noted in response to comment no. 4 above, our calculations indicate that even a small amount of (b) (100 gal) could have resulted in the concentrations observed in the tank farm wells. Mobilization of degraded residual LNAPL by wash water could have provided additional influx of TPH-d and TPH-o (especially polar material) to the groundwater that appeared in the tank farm wells in the TPH-d range.

11. Slide 92 Initial Navy Comment: Do you believe that precipitation could be a major factor in either the observed breakthrough curves along Red Hill ridge or in perimeter wells?

RAs' Response: *The relationships are well-specific, non-linear, and/or threshold dependent. We suggest the Navy consider other water quality indicators that may help in this regard (DO, ORP, pH, alkalinity). Further, consider the range of responses such as sporadic large-volume events may cause occasional detections in outlying wells or may cause short-term dilution within the tank farm. Also, consider the cumulative impact of rain. Cumulative departures may cause more persistent signatures in residual (heavy-end) fractions that are separate from the lighter-end fractions representing lateral migration.*

Navy Response: We agree that the effect of precipitation is likely different at each well location and is a complex function of local geology, precipitation intensity, precipitation duration, and subsurface moisture redistribution. Other water quality indicators may prove very useful in this evaluation, and we appreciate the suggestion to use those to evaluate TPH-d mobilization by precipitation events at both the tank farm wells and the perimeter wells. DO and chloride, in particular, may be indications of mixing of infiltrating precipitation with basal groundwater.

12. Slide 92 Initial Navy Comment: If you believe that TPH detections in perimeter wells are related to the Red Hill Tank Farm, how would you endeavor to simulate those detections?

RAs' Response:

a. Due to the complexity of conditions, processes, and residual impacts, it is doubtful the TPH data can be "matched" using a transport model. Impacts at outlying wells may represent a combination of vapor, LNAPL, and saturated transport, together with other miscellaneous organics.

b. An approach that has previously been suggested by RA SMEs is to use multiple lines of evidence that for this question may include:

i) Whether each location was impacted persistently, often, occasionally, or never;

ii) What processes are considered plausible to describe the impacts that occurred; and

iii) From the above answers, define regions of impacts via each process.

This also applies to the scenario development presented with Question 11, above.

Navy Response:

a. We agree that the complexities cited make it doubtful that TPH data at all locations can be matched with a transport model.

b. We agree that a multiple lines of evidence approach to determining the cause of perimeter well TPH detections is appropriate, and we are considering factors such as detection frequency and plausible physical processes that could cause the TPH detections. We are also considering the chemical characteristics of the TPH-d and other potential sources of chemicals that elute in the TPH-d range. These factors, along with potential migration scenarios, are being assessed for their ability to cause the TPH-d detections observed in the perimeter wells.

13. General/Concluding Thoughts: Doing a Relative Percent Difference analysis to evaluate whether changing laboratories impacted the data quality is problematic. Instead, we suggest doing this both for the TPH analysis and TPH-SGC analysis. Consider lagged recession analysis from other factors such as precipitation. That is, are the differences between labs post-SGC? Some apparent differences between labs may just be lagged recession from ongoing changes such as precipitation or reduced (b) pumping.

Navy Response: We agree that RPD is problematic for directly evaluating the effect of changing laboratories. Our RPD analysis was not used directly to assess the impact of changing laboratories. Rather, the RPD analysis examined the variability in duplicate samples collected at the same time. The analysis of duplicate samples provides an indication of the baseline intra-laboratory variation in TPH-d results. Changes in TPH-d concentration in individual wells after laboratory changes that are less than this baseline variation are than less likely to be caused by the laboratory change.

By comparing this baseline laboratory variability to the variability of concentrations observed over time, we can assess whether a TPH-d concentration change after switching laboratories could be caused by simple analytical variation. Our conclusion is that the variability in TPH-d concentrations after switching laboratories is not significantly different than the baseline intra-laboratory analytical variation in duplicate samples, so that laboratory changes are unlikely to be the cause of variability in TPH-d concentrations observed in wells.

Response to Hawaii Department of Health Comments on July 22, 2024
Draft Groundwater Model Report, dated August 20, 2024

General: On July 22, 2024, the Hawai'i Department of Health (DOH) received the following submissions from the Navy Closure Task Force – Red Hill (NCTF-RH), hereinafter collectively referred to as the Draft Groundwater Model Report (GWM Report):

- ***Draft Groundwater Model Report, Red Hill Bulk Fuel Storage Facility, Volume 1: Main Report, Appendices A-C, dated July 17, 2024, which included the: o Draft Groundwater Model Technical Memorandum;***
  - ***Draft Vadose Zone Model Technical Memorandum; and***
  - ***Draft Contaminant Fate and Transport Technical Memorandum;***
- ***Draft Groundwater Model Report, Red Hill Bulk Fuel Storage Facility, Volume 2: Appendices D-H, dated July 17, 2024; and***
- ***A hard drive of model files.***

On August 9, 2024, we also received a revised version of GWM Report, Volume 1 because the original submission on July 22, 2024 was missing Appendix C, Responses to April 16, 2024 Regulator Comments.

As the GWM Report consists of approximately 12,000 pages with more than six terabytes of accompanying model files and the original submission was incomplete, the DOH is unable to conduct a thorough review by the requested date of August 20, 2024. Moreover, the NCTF-RH states in the GWM Report that it plans to refine the models at a later time by incorporating results from ongoing field studies, such as the geophysics, in-well testing, and tracer testing conducted by the University of Hawai'i (UH), as we have suggested previously. We believe the forthcoming real-world data will provide a more accurate understanding of site-specific subsurface conditions at Red Hill, which the U.S. Department of the Navy (Navy) has struggled to reflect in previous models. Although we recognize that substantial revisions have been made since we required the Navy to submit its "Best Available Model" in June 2023, for these reasons, we have completed a cursory review at this time and have the following general comments.

Navy Response: The Navy understands that DOH "completed a cursory review" and that a more detailed review will be completed after the NCTF-RH refines the models with results from ongoing field studies.

1. General: The DOH recognizes the models presented are much more thorough and have substantially better calibration characteristics than the 2020 Navy modeling effort. However, the models still do not appear to reflect key elements observed in the aquifer and transport related site-specific data sets that have been collected over the past two decades. Below are two examples.

a. The 2021 fuel releases indicated a contaminant migration to the northwest. This plume trajectory is consistent with the regional and cross-ridge hydraulic gradient to the northwest that is not captured by the groundwater model.

b. The model indicates a hydraulic pathway from the Red Hill Facility to beneath the Department of Agriculture Animal Quarantine Station in Hālawa and eventually passing beneath 'Aiea Bay ultimately being captured by Kalauao Springs (Figure 2-20). However, the recently installed groundwater monitoring well NM(b) indicates there is little flow in this zone as shown in initial hydraulic testing done by the NCTF-RH and colloidal borescope testing conducted by UH. Therefore, the model should be revised to reflect this result from NM(b) .

Similarly, the forward particle flow paths shown in Figures 2-17 through 2-19, which show flow directly down Red Hill Ridge with some divergence to the northwest side of the ridge, do not appear to capture the variability noted in Figure 4-10 of the Final Report of Findings, Red Hill Shaft Flow Optimization Study dated September 19, 2023. Prior to the next modeling iteration, it would be useful to overlay the modeled gradients on Figure 4-10, as the calibration charts provided are not gradient triplets, but rather head with distance.

Navy Response: The Navy appreciates that DOH recognizes that the models are much more thorough and have substantially better calibration characteristics then the 2020 model. The current model has very good calibration statistics compared to the field data.

Regarding the two examples:

1a. In the January 31, 2024, Special Purpose Meeting, the Navy presented its analysis of data, suggested that downridge flow after the May 2021 release was the best data set for model calibration and requested feedback from the RAs if they felt some other data set could be used. None was provided.

The May 2021 release occurred near Tank 17. Apparent COC concentration increases were observed in RHM(b) , RHM(b) , and RHM(b) (the "tank farm wells" located along the Red Hill ridge) following the release, and possibly in RHM(b) . These wells are located southwest or west-southwest of the release location. There were no patterns of increases in total petroleum hydrocarbon (TPH) concentrations in other wells that are reasonably attributable to the May 2021 release. It is true that there were a few TPH detections in wells north of the tank farm, but as discussed in the Special Purpose Meeting, there was no evidence of a persistent plume that could be simulated using the model based on continuity. The increases in concentrations in the tank farm wells may indicate groundwater flow approximately down the Red Hill ridge but does not indicate transport to the northwest.

As to the statement that, "the regional and cross-ridge hydraulic gradient to the northwest is not captured by the groundwater model," please see Figures 3-10 through 3-13, which show that this hydraulic gradient is in the model. Other parameters, such as geologic structure and anisotropy result in groundwater flow that is not orthogonal to the hydraulic gradient.

1b. Data from NM(b) (when well installation is complete), other UH studies, and other Navy investigations that are finalized after the cut-off date for this report, can be incorporated in future models.

Flow Optimization Study.

With regard to portion of this comment related to the 3-point problems on Figure 4-10 of the *Final Report of Findings,* (b)(3)(b)(3) *Flow Optimization Study* (FOS) dated September 19, 2023, the flow model was calibrated to and is compared against the same underlying data set as Figure 4-10. As mentioned in the FOS Report, 3-point solutions are challenging in areas with extremely flat gradients and we recommend comparing the model results to the underlying data set, rather than any particular interpretation of that data.

2. General: While the use of parameter values that deviate from those used by previous modelers or published literature is not in itself incorrect, sufficient basis should be provided and modeled results should reflect field data; in this case the model results do not conform with data collected. Therefore, the values of the parameters should be re-evaluated. Below are some examples.

- ***a. Basalt hydraulic conductivity – The NCTF-RH model uses a value of 9,310 feet per day (ft/d), while literature values range from 500-5,000 ft/d (Hunt, 1996) with a value of 4,500 ft/d used by the U.S. Geological Survey in its Pearl Harbor Aquifer model (Oki, 2005).***
- ***b. Basalt vertical anisotropy – The NCTF-RH model uses a value of 66, while literature provides a value of 600 (Oki, 2005; Rotzoll and El-Kadi, 2007).***
- ***c. Basalt horizontal anisotropy – The NCTF-RH model uses a value of 10, while literature provides a value of 3 (Oki, 2005).***

Navy Response: The Navy respectfully disagrees with the statement that the model results do not agree with the field data. Extensive calibration as performed to ensure that the model does conform with the field data.

In addition, the parameter values used in the literature sources referenced this comment, are mostly if not all values used by other models, not field-measured data. As such, these literature parameter values are not necessarily more valid than the parameter values used in the current model. Because most models are non-unique and are created on different scales for different objectives, different sets of parameters may create similar results in terms of groundwater flow patterns.

Reasons why the specific parameters used in the current model differ from literature sources include:

- The current model has a much higher density of underlying field data, than any of the other models in the literature.
- The model domains of the literature models differ from the model domain of the current model.

- The data sets used for model calibration are different.
- The structures of the models are different in terms of discretization, local grid refinement, and incorporation of local heterogeneities. Most if not all of the other models simply modeled the basalt as a uniform equivalent porous media; the current model by contrast and in response to extensive Regulatory Agency comments models the basalt in the area of interest using detailed advanced heterogeneous modeling techniques.

Contrary to the comment above, the current model does conform to the data collected. The model was specifically calibrated using these data, and the final parameters reflect the best match of the model simulations to the measurements. The validity of a model is judged by how well the simulations match the measured data, and not whether they match the results of other models.

3. General: Although fuel/vadose zone modeling was not explicitly specified as an item in the 2015 Administrative Order on Consent, this element is foundational to contaminant transport, risk, and cleanup. The modeling conducted by the NCTF-RH does not allow for an understanding of where remaining fuel mass may reside in the subsurface and whether it can act as a potential source for future transient impacts. For example, the total petroleum hydrocarbons as oil, polar compounds, and polycyclic aromatic hydrocarbons that were primarily mobilized following the May 2021 release do not appear to be represented by the NCTF-RH's modeling suite.

Navy Response: The Navy agrees that the AOC did not require detailed vadose zone modeling; rather, the goal is "to improve the understanding of the direction and rate of groundwater flow."

Accurate simulation of fuel mass location and migration requires a more detailed characterization of the site than is currently available. For example, there are very few indications of product in the vadose zone in any of the wells or borings advanced outside the tank farm and Adit 3 area. Unlike groundwater in the saturated zone, migration of fuels in the unsaturated zone follows heterogeneities that exist on the scale of centimeters, while many of these small-scale heterogeneities are averaged out in groundwater flow. As a general rule, the complexity of models should be consistent with the quality of data needed to parameterize them. The deterministic VZM technique selected for this iteration of the models is consistent with the lack of detailed data delineating the presence of LNAPL in the vadose zone. In future model updates, stochastic techniques could be employed to estimate the presence of LNAPL in the vadose zone.

The current VZM was initially developed to generate hypothetical impacts at the groundwater surface that could have developed during defueling. Currently, the primary use of the VZM is the partitioning module that predicts the concentrations of fuel constituents based on their content in the fuel and local groundwater flow rates.

4. General: There appears to be an absence in the document of the 3-D lithologic model(s) that served as part of the hydrogeologic framework/parameter distributions in the groundwater and contaminant transport models. While the report notes that geologic fabric explorer coupled with the lava flow simulator were used to create lithologic distributions, there

do not appear to be specifics on how this approach was used, nor were any visualizations provided. In future iterations, critical elements, such as site-specific geologic cross-sections from the 3-D lithologic renderings, should be provided as figures and expanded on in the text of the main document.

Navy Response: The 3-D lithologic model was documented in the *Conceptual Site Model Appendix E Addendum: Geological Modeling Framework Technical Memorandum* dated January 20, 2023. The documentation of the geologic fabric explorer methodology and resulting realizations is documented in Section 3 of the report. Visualizations are also included in figures associated with Section 3 of the report. In addition, Appendix F further explains how heterogeneity was created using the software tools and how these data were incorporated into the model grid. The actual model files were also provided to the RAs as requested.

5. General: The chosen method to calculate anisotropy assumes a single point source and a spatially expansive aquifer, which differs from conditions at Red Hill (two-line sources and an aquifer that is confined along two sides). This likely leads to a calculated anisotropy that is not representative of the conditions at the site.

Navy Response: While it is true that (b)(3)(b)(3) is a linear feature, most of the water produced (60%) enters the shaft in the easternmost 150–200 feet of the shaft through a clinker layer (see report Figure 3-3). Although the treatment of this section of the shaft as a point feature is not strictly accurate, the error introduced by this assumption is likely not large considering the size of the drawdown ellipses used to estimate anisotropy. Similarly, the distance to the GHBs that define the limits of the groundwater basin are too far from the ellipses used to estimate anisotropy to have a significant effect on the results.

6. General: Some tables that have been provided in the text contain errors. Revise the tables and provide the correct information. For example, Table 2-11 contains errors in reporting the row names, and some variables do not match what is provided in Volume 2, Appendix D.

Navy Response: The inconsistencies between Table 2-11 and Volume 2, Appendix D have been addressed.

JOSH GREEN, M.D.
GOVERNOR OF HAWAIʻI
KE KIAʻĀINA O KA MOKUʻĀINA ʻO HAWAIʻI

KENNETH S. FINK, MD, MGA, MPH
DIRECTOR OF HEALTH
KA LUNA HOʻOKELE

STATE OF HAWAIʻI
DEPARTMENT OF HEALTH
KA ʻOIHANA OLAKINO
P. O. BOX 3378
HONOLULU, HI 96801-3378

In reply, please refer to:

August 20, 2024

(b)(6)

Dear (b)(6)

SUBJECT: **Insufficient time provided to review Draft Groundwater Model Report Volume 1, Volume 2, and hard drive; dated July 17, 2024**

On July 22, 2024, the Hawaiʻi Department of Health (DOH) received the following submissions from the Navy Closure Task Force – Red Hill (NCTF-RH), hereinafter collectively referred to as the *Draft Groundwater Model Report* (GWM Report):

- Draft Groundwater Model Report, Red Hill Bulk Fuel Storage Facility, Volume 1: Main Report, Appendices A-C, dated July 17, 2024, which included the:
  - Draft Groundwater Model Technical Memorandum;
  - Draft Vadose Zone Model Technical Memorandum; and
  - Draft Contaminant Fate and Transport Technical Memorandum;
- Draft Groundwater Model Report, Red Hill Bulk Fuel Storage Facility, Volume 2: Appendices D-H, dated July 17, 2024; and
- A hard drive of model files.

On August 9, 2024, we also received a revised version of GWM Report, Volume 1 because the original submission on July 22, 2024 was missing Appendix C, Responses to April 16, 2024 Regulator Comments.

As the GWM Report consists of approximately 12,000 pages with more than six terabytes of accompanying model files and the original submission was incomplete, the DOH is unable to conduct a thorough review by the requested date of August 20, 2024. Moreover, the NCTF-RH states in the GWM Report that it plans to refine the models at a later time by incorporating results from ongoing field studies, such as the geophysics, in-well testing, and tracer testing conducted by the University of Hawaiʻi (UH), as we have suggested previously. We believe the forthcoming real-world data will provide a more accurate understanding of site-specific

subsurface conditions at Red Hill, which the U.S. Department of the Navy (Navy) has struggled to reflect in previous models. Although we recognize that substantial revisions have been made since we required the Navy to submit its "Best Available Model" in June 2023, for these reasons, we have completed a cursory review at this time and have the following general comments.

1. The DOH recognizes the models presented are much more thorough and have substantially better calibration characteristics than the 2020 Navy modeling effort. However, the models still do not appear to reflect key elements observed in the aquifer and transport related site-specific data sets that have been collected over the past two decades. Below are two examples.
    a. The 2021 fuel releases indicated a contaminant migration to the northwest. This plume trajectory is consistent with the regional and cross-ridge hydraulic gradient to the northwest that is not captured by the groundwater model.
    b. The model indicates a hydraulic pathway from the Red Hill Facility to beneath the Department of Agriculture Animal Quarantine Station in Hālawa and eventually passing beneath 'Aiea Bay ultimately being captured by Kalauao Springs (Figure 2-20). However, the recently installed groundwater monitoring well NM(b) indicates there is little flow in this zone as shown in initial hydraulic testing done by the NCTF-RH and colloidal borescope testing conducted by UH. Therefore, the model should be revised to reflect this result from NM(b).

    Similarly, the forward particle flow paths shown in Figures 2-17 through 2-19, which show flow directly down Red Hill Ridge with some divergence to the northwest side of the ridge, do not appear to capture the variability noted in Figure 4-10 of the *Final Report of Findings,* (b)(3)(b)(3) *Flow Optimization Study* dated September 19, 2023. Prior to the next modeling iteration, it would be useful to overlay the modeled gradients on Figure 4-10, as the calibration charts provided are not gradient triplets, but rather head with distance.

2. While the use of parameter values that deviate from those used by previous modelers or published literature is not in itself incorrect, sufficient basis should be provided and modeled results should reflect field data; in this case the model results do not conform with data collected. Therefore, the values of the parameters should be re-evaluated. Below are some examples.
    a. Basalt hydraulic conductivity – The NCTF-RH model uses a value of 9,310 feet per day (ft/d), while literature values range from 500-5,000 ft/d (Hunt, 1996) with a value of 4,500 ft/d used by the U.S. Geological Survey in its Pearl Harbor Aquifer model (Oki, 2005).
    b. Basalt vertical anisotropy – The NCTF-RH model uses a value of 66, while literature provides a value of 600 (Oki, 2005; Rotzoll and El-Kadi, 2007).
    c. Basalt horizontal anisotropy – The NCTF-RH model uses a value of 10, while literature provides a value of 3 (Oki, 2005).

3. Although fuel/vadose zone modeling was not explicitly specified as an item in the 2015 Administrative Order on Consent, this element is foundational to contaminant transport, risk, and cleanup. The modeling conducted by the NCTF-RH does not allow for an

understanding of where remaining fuel mass may reside in the subsurface and whether it can act as a potential source for future transient impacts. For example, the total petroleum hydrocarbons as oil, polar compounds, and polycyclic aromatic hydrocarbons that were primarily mobilized following the May 2021 release do not appear to be represented by the NCTF-RH's modeling suite.

4. There appears to be an absence in the document of the 3-D lithologic model(s) that served as part of the hydrogeologic framework/parameter distributions in the groundwater and contaminant transport models. While the report notes that geologic fabric explorer coupled with the lava flow simulator were used to create lithologic distributions, there do not appear to be specifics on how this approach was used, nor were any visualizations provided. In future iterations, critical elements, such as site-specific geologic cross-sections from the 3-D lithologic renderings, should be provided as figures and expanded on in the text of the main document.

5. The chosen method to calculate anisotropy assumes a single point source and a spatially expansive aquifer, which differs from conditions at Red Hill (two-line sources and an aquifer that is confined along two sides). This likely leads to a calculated anisotropy that is not representative of the conditions at the site.

6. Some tables that have been provided in the text contain errors. Revise the tables and provide the correct information. For example, Table 2-11 contains errors in reporting the row names, and some variables do not match what is provided in Volume 2, Appendix D.

(b)(6)

(b)(6)

References:

Hunt Jr., C.D, 1996. *Geohydrology of the Island of Oahu, Hawaii*. Professional Paper 1412-B. Regional Aquifer-System Analysis – Oahu, Hawaii. U.S. Geological Survey.

Oki, 2005. *Numerical Simulation of the Effects of Low-Permeability Valley-Fill Barriers and the Redistribution of Ground-Water Withdrawals in the Pearl Harbor Area, Oahu, Hawaii.* Scientific Investigations Report 2005-5253. U.S. Geological Survey.

Rotzoll, K and A.I. El-Kadi, 2007. *Numerical Ground-Water Flow Simulation for Red Hill Fuel Storage Facilities, NAVFAC Pacific, Oahu, Hawaii*. August 2007.

(b)(6)

REGION 9

SAN FRANCISCO, CA 94105

August 20, 2024

(b)(6)

0

Subject: Deferral of U.S. Environmental Protection Agency Review of *Draft Groundwater Model Report, Red Hill Bulk Fuel Storage Facility, Joint Base Pearl Harbor Hickam, Hawaii*, dated July 2024

(b)(6)

Thank you for the submittal of the *Draft Groundwater Model Report, Red Hill Bulk Fuel Storage Facility, Joint Base Pearl Harbor Hickam, Hawaii*, on July 22, 2024. The submittal was provided in accordance with the 2015 Administrative Order on Consent and included a report, responses to regulatory comments, and approximately 3.5 terabytes of model files (collectively, Draft 2024 GWFM). The Navy requested EPA's expedited comments by close of business on August 20, 2024.

EPA will defer commenting on the July 22nd submittal, given time constraints and the Navy's indication that it will submit a newer version of the groundwater flow model in September 2024. Thorough and constructive review of the Red Hill groundwater flow model is important to EPA. We strive to provide comments on each iteration that the Navy can use to develop a more representative model.

EPA met with the Hawai'i Department of Health and the Navy for a Special Purpose Meeting related to the groundwater flow model on January 31, 2024. We provided comments and responses to questions posed by Navy and its contractors on April 16, 2024. We hope that feedback helped the Navy improve the Draft 2024 GWFM.

Please submit the planned September 2024 version of the model as Supplement 4 to the Phase 2 Closure Plan, Groundwater Flow Model in accordance with the 2023 Administrative Consent Order. EPA will review the September files and provide comments that the Navy shall use to improve the model for a future submittal.

(b)(6)

(b)(6)